Synthesis and characterization of new liquid crystalline compounds derived from novel aromatic ring structures

by
Irla Siva Kumar

A thesis submitted to the Jawaharlal Nehru University
for the degree of

Doctor of Philosophy

2022

Raman Research Institute
Bangalore 560080
India

Dedicated to my lecturer CV Sairam, family members & friends

DECLARATION

I hereby declare that this thesis is composed independently by me at Raman Research Institute, Bangalore, under the supervision of Prof. Arun Roy and Prof. Sandeep Kumar. The subject matter presented in this thesis has not previously formed the basis of the award of any degree, diploma, associateship, fellowship or any other similar title. I also declare that I have run it through the **Turnitin** plagiarism software.

Signature of the Student
Irla Siva Kumar

Signature of the Supervisor

Prof. Arun Roy
Raman Research Institute
Bangalore 560080

Signature of the Co-supervisor

Prof. Sandeep Kumar
Raman Research Institute
Bangalore 560080

CERTIFICATE

This is to certify that the thesis entitled **Synthesis and characterization of new liquid crystalline compounds derived from novel aromatic ring structures** submitted by Irla Siva Kumar for the award of degree DOCTOR OF PHILOSOPHY of Jawaharlal Nehru University is his original work. This has not been published or submitted to any other university for any other degree or diploma.

Signature of the Supervisor

Prof. Arun Roy
Raman Research Institute
Bangalore 560080

Signature of the Co-supervisor

Prof. Sandeep Kumar
Raman Research Institute
Bangalore 560080

Signature of the Director

Prof. Tarun Sauradeep
The director,
Raman Research Institute,
Bengaluru- 560080.

Acknowledgments

My sincere gratitude and thanks to Prof. Sandeep Kumar for his valuable guidance and support. I really enjoyed working with him. He gave me enough freedom to choose my research problems and always motivated me to execute them to completion, and encouraged me to apply to international programs. Ph.D. Life would not have been the same without him.

I would like to thank Prof. Arun Roy for his support and guidance and for taking responsibility for finishing my Ph.D.

I am thankful to Prof. Tarun Sauradeep, present director of Raman Research Institute, and Prof. Ravi Subrahmanyan, former director of Raman Research Institute, for research facilities to complete my Ph.D. work.

I take this opportunity to thank Prof. V. A Raghunathan for being on the doctoral committee. Also, his keen interest and valuable suggestion in interpreting XRD data and giving very thoughtful ideas to extend my work in unprecedented phenomena of flow-induced transient chirality. His patience and ability to explain things straightforwardly encouraged me greatly.

I am grateful to my doctoral committee members, Prof. Reji Philip and Prof. Promod, for their support, motivation, and valuable input. I would like to thank all faculty members, Prof. N.V. Madhusudana, Prof. V. Lakshminarayanan, Prof. R. Pratibha, Prof. Ranjini, Dr. Sayantan, Dr. Gautam Soni, Prof. Yasodhan, Prof. Shivsethi, Prof. Sadiq Rangwala, prof. Sumathi Surya. I thank my course work faculty Prof. S. Ramakrishna, Prof. Uday Maitra, Prof. Kavirayani R. Prasad, Prof. Prabhu, Prof. Erode N. Prabhakaran, and Prof. Santanu Mukherjee.

I would like to thank Dr. Reji Varghese for giving me a chance in my research career at an early stage. I thank other faculty members at IISER-TVM, Prof. Kana M. Sureshan, Prof. Mahesh Hariharan, Dr. Sukhendu Mandal, Dr. Vinesh Vijayan, and Dr. R. S. Swathi, Dr. Ajay Venugopal, Dr. A Thirumurugan for their support during my JRF position. Special thanks to Dr. Vennapusa Sivaranjana Reddy from IISER-TVM for his support during my JRF and Ph.D. career and for helping in the DFT calculations. Prof. Subi J. George, JNCASR, Prof. C. V.

Yelamaggad, CeNS. Dr. Dharmendra Pratap Singh ULCO. France, Dr.Upendra Kumar Pandey, SNU., for their support and discussion during my Ph.D.

I thank Vasudha, Dr. Srinivas, Dhason, Mani, and Yadhu's technical assistance, for allowing me to complete this work efficiently. Vasudha mam deserves special recognition for her excellent time management and technical abilities. Her aid is critical for each of us in our lab, and also the way she showed concern and care about me and listened to all my complaints, worries, and research problems. Thank you, ma'am, once again.

I would like to extend my gratitude to administrative officers Mr. C. S. R. Murthy and Mr. Naresh for all the academic and administrative help. I am thankful to Mr. Radhakrishna, Ms. Marisa, Ms. Radha, Ms. Vidya, and Mr. G. Manjunatha, Amuda, and Chaitanya for all the help with the paperwork.

Thanks to all the library staff for maintaining an excellent collection in the library. I would like to thank Ms. Meera B. M, Mr. Nagaraju, Mr. Manjunath K., Mr. M. Manjunath, and Ms. Vani for keeping the library a peaceful place to study and for their help with my Ph.D., and special thanks to Mr. Manjunath K.

Thanks to the staff of the computer department and workshop for their help. I am thankful to the purchase and account departments for their help with travel and buying lab equipment.

I would like to thank lab attender Rame Gowda, Venkatesh, Raja, and Murali for helping with all the necessary things for the lab.

I am grateful to all canteen staff and cooks at Vyalikaval hostel who serve food and all the security staff and drivers.

I am grateful to have a lab mate like Dr. Swamynathan. Thanks for all his support with experiments and discussions. He was always ready to help me professionally and personally. Thanks to Marichandran V for all his help, support, and discussions. I would like to thank Alakananda and Vanishree for their support in the lab and also for helping correct my thesis. Thanks to Dr. Vinaya Kumara, Dr. Avinash, Dr. Ashwath, and Manish. I would like to thank our projects students Dinesh Ram, Pruthvi, Kavita Rathod, Anu Vashishtha, Najiya, Shikha, Tripti, Priyanka, smriti, Litwin, Hari, Deepika, Suraksha, Shaina, Femi, Shalaka, Vaibhav.

I thank Dr. Madhu Babu Kanakala and Dr. Sachin Bhat from CeNS, who helped me record CD measurements, and other friends fromCeNS.

I am happy to have Adit Raj, Arpit, Nishanth, Saichand, Nancy, Adwith, Arsalan, Akash, Subhadeep, Aditi, Sanhita, Silpa, Maheswar, Subhajit, and Koushik as batchmates, Thanks to all of them for a wonderful time during the Ph.D. Special thanks to Nancy for the help with fluorescence measurements and Arsalan for his help with the graphical abstract for one of the projects.

I thank Dr. S. Madhukar, Dr. A. Jayakumar, Jaggu, Surya, Niranjan, Sumanth, Meera, Sreeja Asha, Chandan, Sanjay, Anindya, and Nomaan; they were kind enough to be with me all the time. I would like to thank all the SCM students for the excellent discussions I had with them. Thanks to Ayush, Dubey, Deepshika, Vishnu, Deepak Patra, Swarnak, Ashish, Sukhweer, Deepak M, Puja, Palak, Chandu, Rajkumar, Vaibhav, Yogesh, Anson, Sourabh, Sukanya, Sebanthi, Abhishek, Sachitanand, Swarnadeep, and other friends Sreyas, Arun, Vardhan, Bapan, Sagar, Anand, Subhod, Pradosh, Manami, Gunjan, Hemanth, Sandeep M, Archana for their valuable time at RRI.

Here comes the moment to remember the care and concern that enabled me to finish this beautiful endeavor. First and foremost, I would like to express my deep sense of gratitude to Dr. Hari Veera Prasad Thelu, who has given me the way for my research career, support, and care. I would like to thank Dr. Shine K Albert for her support during my research career. Special thanks to Dr. Nithiyanandan, who taught me synthesis and experimental techniques. I am thankful for all my lambastes at IISER-TVM, Dr. Murali Golla, Dr. Atchim Naidu, Dr. D. Perumal, Dr. Swathi, and Dr. Dileep. Whole-hearted thanks to them for providing an enthusiastic and scientific working atmosphere. Thanks to all the other project students, Mr. Sai Praveen, Ms. Hanna, Ms. Soma Choudhary, Mr. Nagarjuna, Mr. Vishnu Raj, and Ms. Theja. Mr. Deepak, for extending never-ending care and concern. Special Thanks to Mr. Adarsh for teaching me the NMR instrument and Mr. Aneesh, Mr. Alex, and Mr. Nibith for all the technical support.

Thanks to all my IISER friends for their encompassing support. Dr. Jaise Jose, Dr. Dhamodhar reddy, Dr. Shinaj, Dr. Atchutha Rao, Dr. Vidya Sagar and Dr. Rijo Mrs. Reshmi, Dr. Jiji, Dr. Shabnam, Dr. Subila,Dr. Asha, Dr. Anoop, Dr. Priya Kumari, Dr. Gireesh, and Dr. Pratap Zalake. Dr. Kalaivanan, Dr. Purnachandra Rao, Dr. Putta Sivashankar, Dr. Eswar Reddy, Dr. Prabhu, Mrs. Hema, Ms. Hemna, Ms. Arthi, Ms. Swathi, Ms. Elizabeth, Mr. Pratap, Mr.

Sanoop, Mr. Rafeeque, Mr. Arun, Mr. Sujith, Mr. Manoj, Dr. Abbey, Dr. Selva Kumar, Ms. Jobha, Ms. Anjana, Mr. Rajesh,

It's time to acknowledge my friends who made my life memorable and cheerful. They accepted me as I am and supported me throughout my stay in Bangalore. Special thanks to Rahmat, Ajay, Yougant, Sonali, Heena, Pradipta, Vikas, and other IISC friends Ravi, Rathod, Sandeep, Raghavaram, Dipen, Sunit, Sruthi, Amarnath reddy, etc.

It's my pleasure to thank all my college friends, Swamy, Yesu Babu, Girish, Jhony, Baghya Raju, Satyanarayana, Murthi, Nagaraju, Manga, Devi, Padma, Dhana, Veera Babu, Subhash, Aparna, Sravanthi, Nagaraju, Malli and special thanks to Nageswra Rao, Yelamanda, Swamy, for all their care and support. I thank Koti reddy, Pavan kumar, Vasu, Ashok, Chenna, Mahesh, Chenna Reddy, Bhaskar, Riyaz, Nagarjuna Reddy, pera reddy

I am incredibly grateful to CV Sairam, sir, who molded me to become a researcher, and for his support and motivation to live life.

I would like to thank Navita, Jeba, Bhargavi

My family is always a source of inspiration and great moral support for me in perceiving my Education. I am really fortunate to have a great family comprised of my mother, father, sister, brother, sister-in-law, wife, nephew and grandparetnts. Without them, I am nothing. I would like to extend my gratitude to my in-law's family for their care and support.

Above all, finally, I would like to thank my beloved wife, Dr. Sreeja Sasidharan, for her love, concern, care, and constant unconditional support. Thank you for being my muse, editor, proofreader, soulmate, and best friend, but above all, thanks for being in my life and making my life better. I owe you everything. You are the best thing that ever happened to me.

SYNOPSIS

Synthesis and characterization of new liquid crystalline compounds derived from novel aromatic ring structures.

The research on non-covalent interactions has become an important area of research due to their significance in biological functions, drug delivery applications, material properties and the device fabrication. Supramolecular assemblies of complex structure have been found in natural and artificial systems, which arises as a result of multiple non-covalent interactions among small structural motifs and molecular sub-units(*1*). With this broad area of supramolecular science, research on the properties and applications of liquid crystals have caught increasing attention in the last two decades(*2*). Liquid crystals (LCs) are functional soft materials which possess both order and mobility(*3*) ranging from the molecular to macroscopic level(*4*) . These liquid crystals are classified into thermotropic LCs (temperature dependent) and lyotropic LCs (mesophase is obtained by varying concentration and /or temperature). Based on the shape of the mesogenic molecules, thermotropic LCs are classified into three groups: (a) calamitic (rod-like), (b) bent-core (bad rods, boomerang, banana-like) and (c) discotic (disk-like) LCs (**Figure1).**

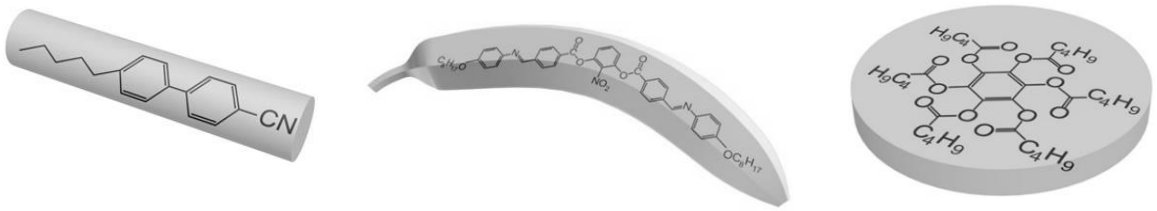

a. Calamitic (rod-like) **b. Bent-core (banana like)** **c. Discotic (disk-like)**

Figure 1. Schematic representation of types of thermotropic liquid crystals.

LCs formed by disc-shaped molecules were realized in 1977 and they are now commonly known as discotic liquid crystals (DLCs)(*5*–*7*) . It consists of a central rigid core surrounded by flexible aliphatic chains connected to the core directly or via linking atom or a group. A general template of discotic LC molecules is shown in **Figure 2**.

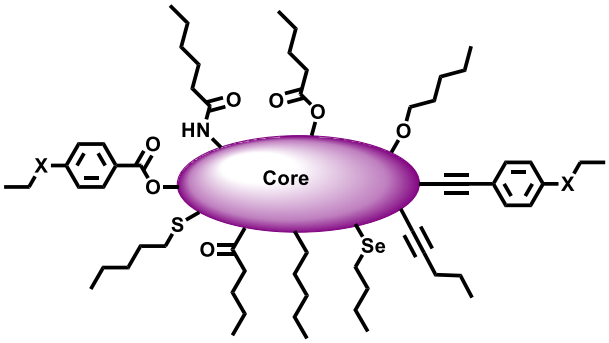

Figure 2. General template for DLC molecular architecture.

Disc-shaped molecules self-assemble into nematic (having only orientational order) or columnar (having both orientational and positional order) phases on appropriate substitutions (**Figure 2**). The polymerized films formed by discotic nematic LCs have already been commercialized as optical compensation films to enlarge the viewing angle of typical LCDs. Also their use as an active component in LCDs has been discussed(*8*). However, the majority of DLCs (about 95%) form columnar phases as they are mainly derived from polycyclic aromatic cores(*9*, *10*) which possess strong π-π interactions and, therefore they prefer stacking one on the top of other to form molecular columns.

Synthesis of different columnar LCs should be driven by the optimum balance between the structure–functional properties of the molecule. For this, distinct molecular concepts need to be explored. These include: the chemical structure, the symmetry and size of the rigid core, properties of the connecting groups between the conjugated core and the flexible side chains and phase behavior and transitions by variations of the rigid core and connected substituents(*11–16*). Further modifications on structural, mesomorphic and physical properties of the discotic molecules(*17*, *18*) lead to their usage as an organic semiconductor in organic field-effect transistors (OFETs), organic light emitting diodes (OLEDs) and organic photovoltaic devices (OPVs)(*19*, *20*). DLC systems have been well explored and many review articles have appeared in the literature (*21*, *22*). About sixty central cores have been exploited to prepare more than 3500 DLCs. Most of these are electron-rich (p-type semiconductors) materials and only a few electron-deficient DLCs (n-type semiconductors) are known. Our research group has previously invented some of the discotic molecules like decacyclene(*23*), tricycloquinazoline(*24*), dibenzo[g,p]-chrysene(*25*), phenanthro[a]- and phenanthro[b]-phenazines (*26*, *27*) which show liquid crystalline properties on proper chemical modifications. Based on the literature, our interest is mainly to focus on the design and synthesis of new

aromatic ring structures as discotic liquid crystals (DLCs). With this objective, we have designed and synthesized new π-conjugated aromatic ring structures as a central core for discogenic systems. The synthesized derivatives have been characterized for their liquid crystallinity using polarizing optical microscopy, differential scanning calorimetry and X-ray diffractometry. This thesis contains the following chapters.

Chapter 1: Introduction

This chapter deals with the brief history of liquid crystals followed by the discussion about lyotropic liquid crystals and thermotropic liquid crystals and their classification. Different characterization techniques are also briefly outlined. Since this thesis mainly deals with discotic liquid crystals, the discussion on discotic liquid crystals and details about the columnar mesophases formed by respective mesogens is incorporated in this chapter. A short discussion about the chirality in liquid crystalline materials and liquid crystalline dendrimers is followed thereafter.

Chapter 2: Rubicene, an Unusual Contorted Core for Discotic Liquid Crystals

In this chapter, we have synthesized rubicene derivatives (**Figure 3**). Rubicene, an unusual contorted polycyclic aromatic hydrocarbon, was realized to function as a novel core fragment for discotic liquid crystals. The central π-conjugated motif was prepared from dialkoxyiodobenzene via Sonagashira coupling, followed by pentannulation and Scholl cyclodehydrogenation. The synthesized rubicene derivatives were found to be thermally stable and exhibit enantiotropic columnar mesophases. The columnar arrangement of these derivatives has been validated using polarising optical microscopy, differential scanning calorimetry & small-angle X-ray scattering.

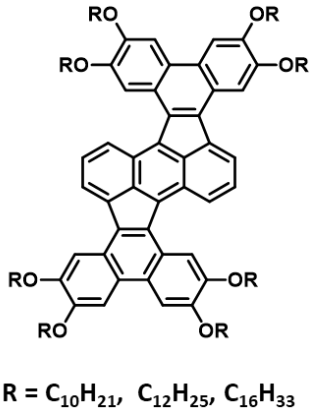

$R = C_{10}H_{21}, C_{12}H_{25}, C_{16}H_{33}$

Figure 3: Structure of rubicene derivatives.

Chapter 3: Design and synthesis of extended pyrene based discotic liquid crystalline materials.

In this chapter we have designed new liquid crystalline materials derived from novel core generated from pyrene molecule. Herein new class of polycyclic aromatic hydrocarbons (PAHs) containing a five-membered ring with 1, 6 dibromo pyrene as a discotic core have been designed and synthesized via palladium-catalyzed cyclopentannulation followed by Scholl reaction. The synthesis and characterization of these novel materials (**Figure 4**) is presented here. All the compounds show good thermal stability. The mesomorphic properties of all the compounds were determined using a combination of polarized optical microscopy (POM), differential scanning calorimetry (DSC) and X-ray diffractometry. The synthesized molecules exhibit preferred homeotropic alignment in their columnar phase regime. Pyrene derivatives have been widely used in various devices and therefore, these novel supramolecular materials may find application in several opto-electronic devices.

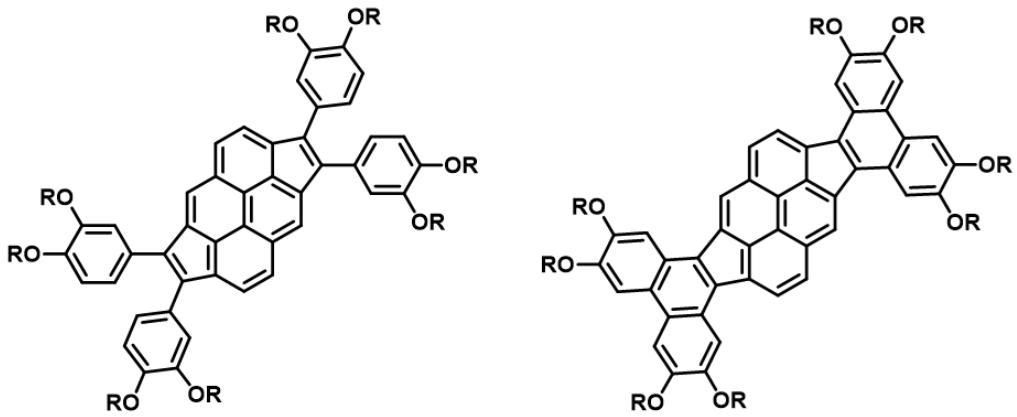

Figure 4: Structure of new liquid crystalline materials derived from novel core generated from pyrene molecule.

Chapter 4: Columnar mesomorphism in heptazine discotics

In this chapter, we report on the design and synthesis of C_3- symmetry columnar liquid crystals in which the heptazine core is flanked by six alkoxy chains. These novel derivatives (**Figure 5**) show hexagonal and rectangular columnar liquid-crystalline (LC) phases over a wide range of temperatures. All the compounds exhibit a columnar hexagonal phase (Col_h) at high temperatures, among which two compounds with lower alkoxy chains show a rectangular phase

at lower temperatures. The mesomorphic properties of all the compounds are confirmed by polarizing optical microscopy, differential scanning calorimetry, and X-ray diffractometry.

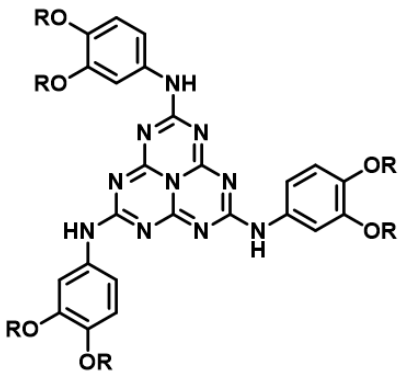

R = C_6H_{13}, C_8H_{17}, $C_{10}H_{21}$, $C_{12}H_{25}$, $C_{16}H_{33}$

Figure 5: Structure of heptazine discotic liquid crystals.

Chapter 5: Supramolecular self–assembly of Hydrogen-bonded dendritic-benzotri (imidazole) derivative architectures.

Dendrimers represent a special class of synthetic macromolecules, which has a significant interest in fields such as material science, nanoscience and nanotechnology, and biomedical sciences. In this chapter, we have synthesized carboxylic acid-functionalized dendrimers like 1st and 2nd generations (**Figure 6**). These compounds were prepared by copper-catalyzed azide-alkyne ‘‘click’’ cycloaddition. The formed dendrimers are found to be mesomorphic in nature and H-bonded supramolecular complexation with benzotri (imidazole) derivatives of the same was studied. Such stable hydrogen-bonded complexes (**Figure 6**) also show mesomorphism. The formation of these complexes and dendrimers was investigated through FT-IR, NMR studies and elemental analysis. The mesomorphic properties of all the compounds werecharacterized using polarized optical microscopy (POM), differential scanning calorimetry (DSC) and X-ray diffraction (XRD) studies.

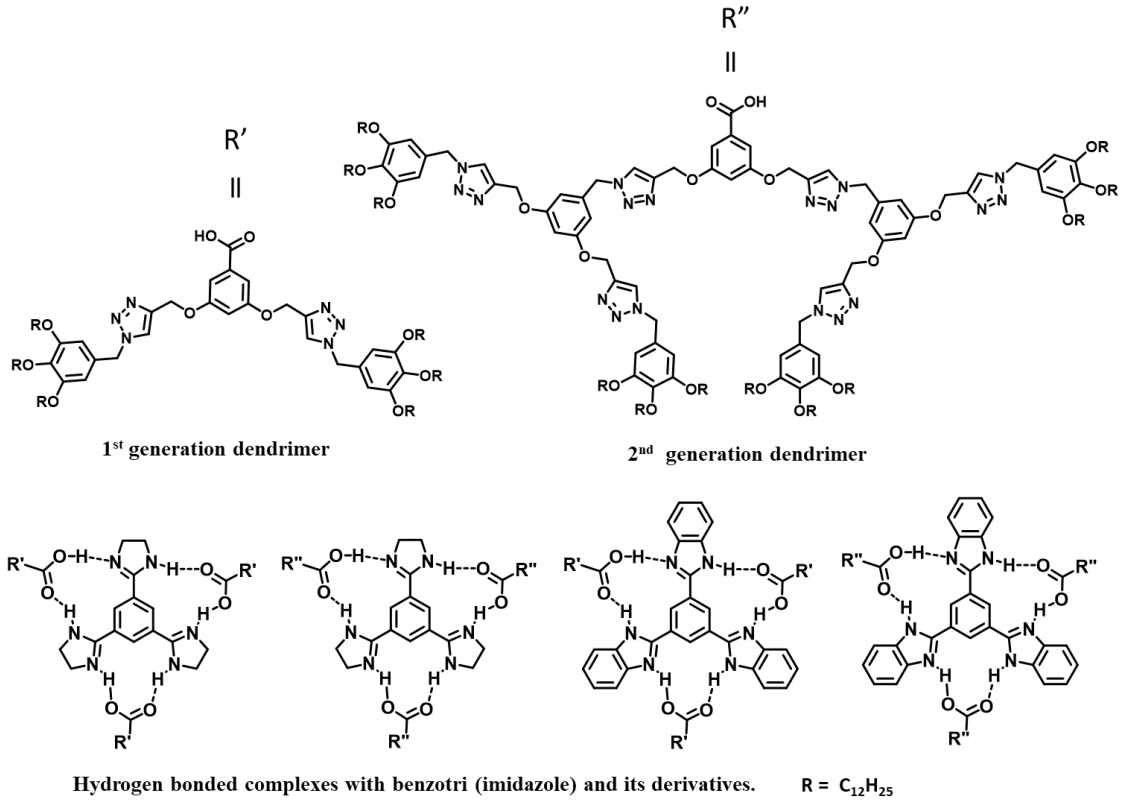

Figure 6: Structure of the dendrimers and corresponding hydrogen bonded complexes with benzotri (imidazole) and its derivatives.

Chapter 6: Synthesis and mesomorphic behavior of cyanostar precursors.

In this chapter we have synthesized precursors (**Figure 7**) for the cyanostar. Interestingly these precursors are found to be mesomorphic and exhibit columnar mesophase. All precursors show good thermal stability which was confirmed using thermal gravimetric analysis. Mesomorphic behavior of the compounds was characterized by different experimental techniques such as polarized optical microscopy (POM), differential scanning calorimetry (DSC). The self-assembly of these compounds in the columnar phase was confirmed by X-ray diffraction (XRD) studies. These precursors are potential molecules to generate the novel DLCs namely cyanostar.

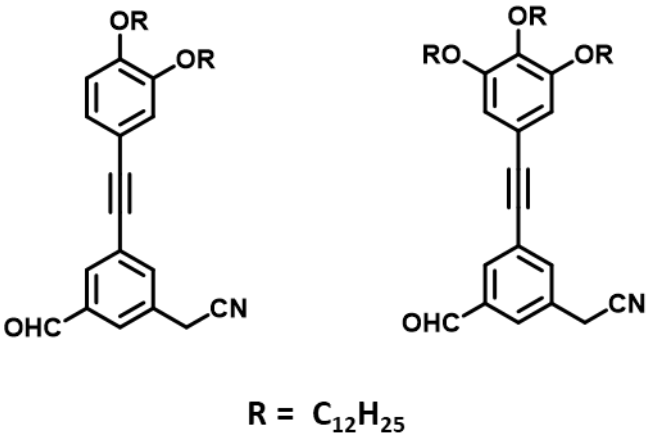

Figure 7: Structure of the cyanostar precursors.

Chapter 7: Summary

This chapter summarizes some of the important results and conclusions obtained from this thesis work, which deals with the "*Synthesis and characterization of new liquid crystalline compounds derived from novel aromatic ring structures*". Also we briefly explain the divergent possibilities and scope for the future work obtained from our experimental work.

References:

1. J. W. Steed, J. L. Atwood, *Supramolecular Chemistry* (John Wiley & Sons, Ltd, Chichester, UK, 2009.
2. J. M. Lehn, From supramolecular chemistry towards constitutional dynamic chemistry and adaptive chemistry. *Chem. Soc. Rev.* **36**, 151-160, (2007).
3. E. T. Samulski, A review of: "Handbook of Liquid Crystal Research," Editors in Chief: P.J. Collings and J. S. Patel; Oxford University Press, New York, Oxford, 1997
4. H. K. Bisoyi, S. Kumar, Discotic nematic liquid crystals: Science and technology. *Chem. Soc. Rev.* **39**, 264-285 (2010).
5. S. Chandrasekhar, B. K. Sadashiva, K. A. Suresh, Liquid crystals of disc-like molecules. *Pramana*. **9**, 471–480 (1977).
6. S. Kumar, Self-organization of disc-like molecules: Chemical aspects. *Chem. Soc. Rev.*

35, 83-109, (2006).

7. Sandeep Kumar, *Chemistry of Discotic Liquid Crystals: From Monomers to Polymers* CRC Press, Boca Raton, FL, 2011 (2011).
8. S. Kumar, S. K. Varshney, A Room-Temperature Discotic Nematic Liquid Crystal. *Angew. Chemie.* **39**, 3140–3142 (2000).
9. A. Gowda, M. Kumar, S. Kumar, Discotic liquid crystals derived from polycyclic aromatic cores : from the smallest benzene to the utmost graphene cores. *Liq. Cryst.* **00**, 1–28 (2017).
10. M. Kumar, A. Gowda, S. Kumar, Discotic Liquid Crystals with Graphene: Supramolecular Self-assembly to Applications. *Part. Part. Syst. Charact.* **34**, 1700003 (2017).
11. E. F. Gramsbergen, H. J. Hoving, W. H. de Jeu, K. Praefcke, B. Kohne, X-ray investigation of discotic mesophases of alkylthio substituted triphenylenes. *Liq. Cryst.* 397- 400 (1986),
12. R. J. M. Nolte, J. F. van der Pol, E. Neeleman, J. W. Zwikker, R. J. M. Nolte, W. Drenth, J. Aerts, R. Visser, S. J. Picken, Liquid-crystalline phthalocyanines revisited. *Liq. Cryst.* **33**, 1373–1387 (2006).
13. P. Herwig, C. W. Kayser, K. Müllen, H. W. Spiess, Columnar mesophases of alkylated hexa-peri-hexabenzocoronenes with remarkably large phase widths. *Adv. Mater.* **8**, 510–513 (1996).
14. N. B. McKeown, *Phthalocyanine materials: synthesis, structure, and function.* (1998).
15. D. Markovitsi, S. Marguet, J. Bondkowski, S. Kumar, Triplet excitation transfer in triphenylene columnar phases. *J. Phys. Chem. B.* **105**, 1299-1306 (2001).
16. M. Lehmann, G. Kestemont, R. Gómez Aspe, C. Buess-Herman, M. H. J. Koch, M. G. Debije, J. Piris, M. P. de Haas, J. M. Warman, M. D. Watson, V. Lemaur, J. Cornil, Y. H. Geerts, R. Gearba, D. A. Ivanov, High Charge-Carrier Mobility in π-Deficient Discotic Mesogens: Design and Structure-Property Relationship. *Chem. - A Eur. J.* **11**, 3349–3362 (2005).
17. P. A. Heiney, Structure and Physical Properties of Columnar Liquid Crystals. *Handb. Liq. Cryst.*, 1–47 (2014).

18. R. J. Bushby, N. Boden, Responses of Discotic Liquid Crystals to Mechanical, Magnetic, and Electrical Fields in *Handbook of Liquid Crystals* (Wiley-VCH Verlag GmbH & Co. KGaA, Weinheim, Germany, 2014.

19. W. Pisula, K. Müllen, Discotic Liquid Crystals as Organic Semiconductors. *Handbook of Liquid Crystals* (Wiley-VCH Verlag GmbH & Co. KGaA, Weinheim, Germany) 1–47 (2014).
20. S. Sergeyev, W. Pisula, Y. H. Geerts, Discotic liquid crystals: a new generation of organic semiconductors. *Chem. Soc. Rev.* **36**, 1902 (2007).
21. S. K. Pal, S. Setia, B. S. Avinash, S. Kumar, Triphenylene-based discotic liquid crystals: recent advances. *Liq. Cryst.* **40**, 1769–1816 (2013).
22. T. Wöhrle, I. Wurzbach, J. Kirres, A. Kostidou, N. Kapernaum, J. Litterscheidt, J. C. Haenle, P. Staffeld, A. Baro, F. Giesselmann, S. Laschat, Discotic Liquid Crystals. *Chem. Rev.* **116**, 1139–1241 (2016).
23. E. Keinan, S. Kumar, R. Moshenberg, R. Ghirlando, E. J. Wachtel, Trisubstituted decacyclene derivatives: Bridging the gap between the carbonaceous mesophase and discotic liquid crystals. *Adv. Mater.* **3**, 251–254 (1991).
24. S. Kumar, E. J. Wachtel, E. Keinan, Hexaalkoxytricycloquinazolines: New Discotic Liquid Crystals. *J. Org. Chem.* **58**, 3821-3827 (1993).
25. S. Kumar, S. K. Varshney, Dibenzo [g , p] chrysene , a Novel Core for Discotic Liquid. *Mol. Cryst. Liq. Cryst.*, **378**, 59-64, (2002)
26. S. Kumar, M. Manickam, Synthesis of phenanthro [a] phenazine derivatives : a novel ring structure forming discotic liquid crystals. *Liq. Cryst.* **26**, 1097–1099 (1999).
27. T. Section, A. M. Crystals, S. Kumar, M. Manickam, Synthesis of phenanthro [b] phenazine , a novel heterocyclic ring structure for discotic liquid crystals. *Mol. Cryst. Liq. Cryst.*, **338**, 175-179, (2000).

List of Publications:

1. **Irla Sivakumar**, V. A. Raghunathan, Sandeep Kumar, "Columnar Mesomorphism in Heptazine Discotics." ***Journal of Molecular Liquids***, 314, **2020**, 113631, https://doi.org/10.1016/j.molliq.2020.113631.

2. **Irla Sivakumar**, Pruthvi Mahesh, V. A. Raghunathan, and Sandeep Kumar. "Design and synthesis of extended pyrene based discotic liquid crystalline dyes" ***Dyes and pigments,*** 194, **2021**, 109574. https://doi.org/10.1016/j.dyepig.2021.109574
3. **Irla Sivakumar**, K. Swamynathan, Dinesh Ram, V. A. Raghunathan, Sandeep Kumar, "Rubicene, an unusual contorted core for discotic liquid crystals" ***Chemistry: An Asian Journal***, 2022, e202200073. https://doi.org/10.1002/asia.202200073.
4. **Irla Sivakumar**, K. Swamynathan, Dinesh Ram, V. A. Raghunathan, Sandeep Kumar, "Flow-induced Transient Chirality in a Columnar Liquid Crystal" (Submitted to Angewandte Chemie).
5. **Irla Sivakumar**, V. A. Raghunathan, and Sandeep Kumar. "Supramolecular self – assembly of Hydrogen-bonded dendritic - benzotri (imidazole) derivative architectures." (manuscript under preparation).

The present author was involved in other projects as well but the results obtained are not described in this thesis and published in the following journals.

6. Marichandran Vadivel, **Irla Sivakumar**, K Swamynathan, V. A. Raghunathan, and Sandeep Kumar. "Novel Annulated Triphenylene Discotic Liquid Crystals Generated by Pictet-Spengler Cyclization." ***Chemistry Select***, 3, **2018**, 8763–8769, https://doi.org/10.1002/slct.201801738.
7. Shine K. Albert, **Irla Sivakumar**, Murali Golla, Hari Veera Prasad Thelu, Nithiyanandan Krishnan, Joseph Libin, K. L Ashish and Reji Varghese, "DNA-Decorated Two-Dimensional Crystalline Nanosheets." ***J. Am. Chem. Soc.*** 139, **2017**, 17799−17802, https://doi.org/10.1021/jacs.7b09283.
8. Gokanapalli Anusha , Meenigalndira, **Irla Sivakumar**, Loka Subramanyam Sarma, Kakarla Raghava Reddy, Peddiahgari Vasu Govsrdhana Reddy, Tejraj M. Aminabhavi. "Synthesis of bis-1,3-(benz)azoles catalyzed by palladium-PEPPSI complex-based catalysts and the study of photophysical properties." ***Chemosphere***, 301, **2022**, 134751, 10.1016/j.chemosphere.2022.134751
9. K. Swamynathan, **Irla Sivakumar**, V. A. Raghunathan and Sandeep Kumar. "Synthesis and Mesomorphism Anthraquinone Based Bolaamphiphiles." (manuscript under preparation).

10. K. Swamynathan, **Irla Sivakumar**, V. A. Raghunathan and Sandeep Kumar. "Synthesis and Characterization of Cholesteryl Functionalized Amphiphilic Anthraquinones." (manuscript under preparation).

Signature of Student
Irla Siva Kumar

Signature of Supervisor

Prof. Arun Roy
Raman Research Institute
Bengaluru 560080

Signature of Co-Supervisor

Prof. Sandeep Kumar
Raman Research Institute
Bengaluru 560080

TABLE OF CONTENTS

Chapter-2 Rubicene, an Unusual Contorted Core for Discotic Liquid Crystals

Chapter-3 Design and synthesis of extended pyrene based discotic liquid crystalline materials

Chapter-7 Summary

Chapter - 1

Introduction

Abstract

This chapter deals with the brief history of liquid crystals, followed by the discussion about lyotropic and thermotropic liquid crystals and their classifications. Different characterization techniques are also briefly outlined. Since this thesis mainly deals with thermotropic discotic liquid crystals, the discussion of the same and details about the columnar mesophases formed by respective mesogens are incorporated in this chapter, along with a short discussion about the objective thereafter.

1.1 Introduction

Supramolecular chemistry is a multidisciplinary field of science that studies the chemical, physical, and biological properties of chemical entities. Supramolecular chemistry is a scientific area that focuses on studying noncovalent interactions within and between molecules.[1] Chemists are concentrated on understanding how covalent and ionic bonds hold atoms and ions together. And also how these bonds are connected and break during the chemical reactions. On the other hand, they also study the noncovalent interaction that is weaker and reversible, such as hydrogen bonding, metal coordination, hydrophobic forces, Van der Waals forces, π-π interactions, and electrostatic effects.

Supramolecular chemistry has been used to discover new organic materials, medication delivery systems, pharmaceuticals, sensors, polymers and CAT scan contrast agents. It is also essential for designing catalysts, solid-state processes, and radioactive waste remediation. In addition to this, noncovalent interactions are also crucial for understanding various biological systems and processes, including cell structure and vision. The desire to learn more about biological systems typically drives supramolecular chemical research. Supramolecular chemistry has adopted many scientific fields that include molecular self-assembly, molecular recognition, molecular folding, molecular recognition, mechanically-interlocked molecular architectures, host-guest chemistry, and dynamic covalent chemistry.[2] Among these supramolecular chemistry concepts, molecular self-assembly plays an essential role in forming nanostructures. This refers to either (1) the folding of the individual molecules which is called intramolecular self-assembly, or (2) the formation of nanostructures containing two or more molecules using noncovalent interactions called as intermolecular self-assembly. The molecules are said to "self-assemble" since the structures are generated based on the inherent features of the molecules involved, rather than any external management (other than the provision of a suitable environment).

Molecular self-assembly confesses for the construction of macroscopic structures such as membranes, micelles, vesicles, liquid crystals and also it is crucial for crystal engineering. The template self-assembly allows for precise control of size, periodicity, and structure to create a wide range of novel nanomaterials. The template for the production of these nanomaterials can be hard or soft. Some of the hard templates are silica[3,4] and carbon.[5] Soft templates are biomolecules[6] and polymers.[7–10] These soft templates show the ability to self-assemble into

transferable superstructures. Liquid crystals (LCs) are one of the fascinating soft templates in this field, and they have been frequently used to create nanostructure.[11–14]

1.2 Liquid crystals

On heating any organic crystalline substance goes from crystal to fluid transition, and it loses the orientational and positional order at once. Some compound transitions occur through one or more intermediate states where the position or orientation order is gradually lost. These phases are called plastic crystals and mesomorphic states of matter. Liquid crystals are a state of matter with qualities that fall between liquids and solid crystals. Liquid crystals may flow like a liquid, and their molecules may orient in a crystal manner and are therefore defined as a mesophase (from the ancient Greek word "mesos," which means "intermediate"). It is sometimes referred to as the "fourth state of matter."[15–21] Mesomorphic compounds are materials that have LC characteristics. Mesomorphism is another term for LC behavior. Mesogenic groups are molecular fragments that can be used to induce LC behavior in a structure. Several aromatic rings are frequently found in such groups. The high order characteristic of crystalline solids is partially diminished in an LC phase, giving the molecules some mobility and rendering the substance fluidic or plastic. The schematic representation of crystals to isotropic and intermediate phases is shown in **Figure 1.1.**

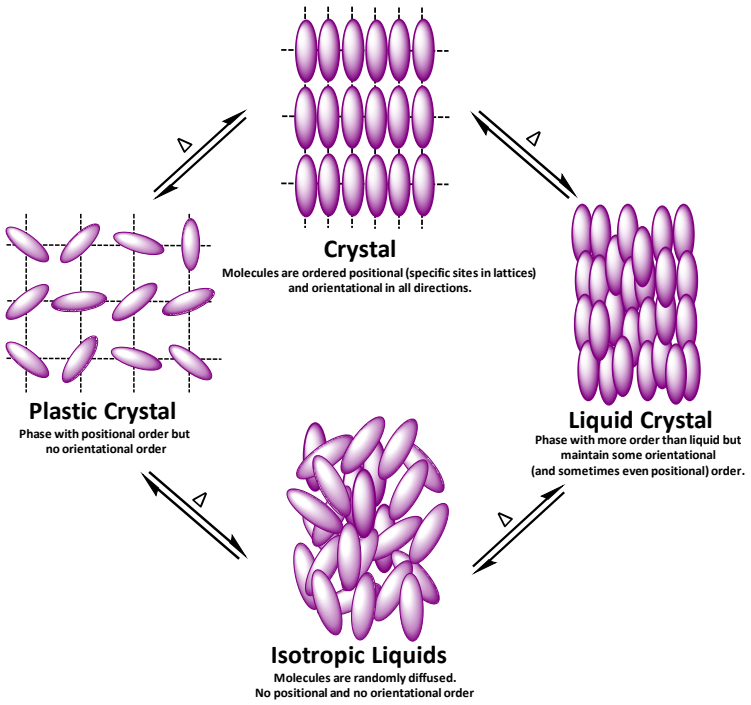

Figure 1.1: General schematic representation of crystal to isotropic and intermediate phases

1.3 History of liquid crystals

It is the 134th year since liquid crystals were discovered.[22] Liquid crystals have found their way into so many products we use today that life would be incomprehensible without them. Almost no other high-tech material has gained such widespread use so quickly. The millions of users who own a tablet computer are fascinated by its fantastic display, oblivious of the liquid crystals sandwiched between the glass plates and polarizers.

W.Heintz, a German biochemist, reported the synthesis of a triglyceride in 1850, which exhibited cloudy liquid on the heating before turning to clear liquid. Stearin melted from solid to cloudy liquid at 52°C and changed from 58°C to an opaque at 62.5°C to a clear liquid, but he could not understand what was happening. The structure of stearin is shown in **Figure 1.2**.[23]

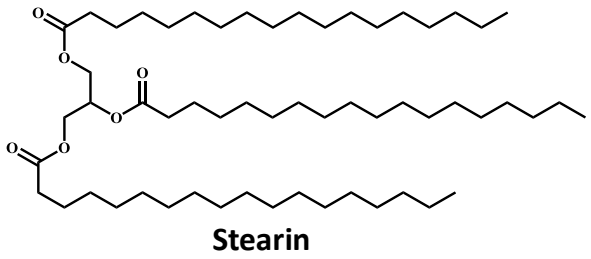

Figure 1.2: Structure of Stearin.

The story behind liquid crystals is about Friedrich Reinitzer, 1888 botany and technical microscopy professor at Technical University in Prague. He was working on cholesterol derivatives.[24] In the case of Cholesterol and cholesterol benzoate, which he had extracted from carrot, and measured the melting point of the cholesterol benzoate was (**Figure 1.3a**) at 145.5 °C; however, he found a second melting point at 178.5 °C, and between the two transitions, a milky liquid phase was observed, and above 178.5 °C, the phase was clear. Under the polarised optical microscopy, he observed distinct violet and blue color phenomena at both phase transitions (double melting). However, cholesteryl acetate (**Figure 1.3b**) behaved similarly to cholesterol benzoate with a monotropic cholesteric phase. Later, he contacted physicist otto Lehmann, an expert in the physical isomerism of crystals. Lehmann had a polarizing microscope with a hot stage and was thus able to investigate more precisely than Reinitzer. The German physicist Otto Lehmann explained the existence of "double melting," a curious

phenomenon. He referred to them as "soft crystals" first, then "crystalline fluids." He began to refer to the opaque phase as "liquid crystals" as he became more convinced that it was a homogeneous phase of matter with properties similar to liquids and solids. The discovery of liquid crystals, like today's science and technology of liquid crystals, also required an interdisciplinary approach. It's worth noting that researchers were working with liquid crystals as early as the 1850s, but they hadn't recognized how unique the phenomenon was. As a result of very lively correspondence between Lehmann and Reinitzer, In 1889, Lehmann had a publication on *About flowing crystals.* As a result, Reinitzer, a biologist, is credited with discovery of liquid crystals, while Lehmann, a physicist, is credited with finding liquid crystal research.[22]

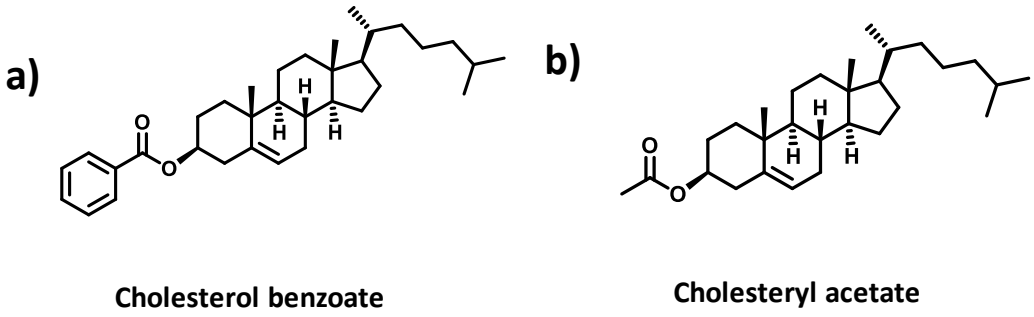

Figure 1.3: Structure of Cholesterol benzoate.[25]

Afterward, in the early twentieth century, Daniel Vorländer, a chemistry professor at the University of Halle, began a systematic synthetic work in order to determine the structure-mesophase relation, and by 1935, he had synthesized over 1100 liquid crystalline substances in his laboratory alone.[26] He pointed out that all compounds with mesophases possessed elongated (rod-like) molecules, which are today known as calamitic molecules (**Figure 1.4**).

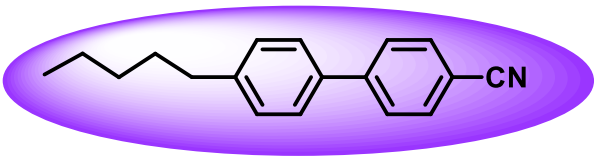

Figure 1.4: Representation of a calamitic liquid crystal.

In 1923, Vorlander, a pioneer in liquid crystal research, proposed disc-shaped molecules with packing arrangements comparable to voltas columns while examining triphenylene and perylene.[27] Because of the lack of flexible chains, he could not detect any mesomorphic fingerprints. His article also stated that leaf-shaped molecules do not form any liquid crystals. Later, however, triphenylenes and perylenes with flexible periphery were essential reports in discotic literature. However, in 1977, Chandrasekhar and his colleagues at Raman Research Institute discovered for the first time that flat disc-shaped molecules (**Figure 1.5**) do form liquid crystalline phases. They synthesized a series of benzene hexaesters and described a novel class of LCs, using optical, thermal, and X-ray diffraction techniques.[28] This finding caught the attention of chemists all over the world, resulting in the birth of a fascinating new branch of discotic liquid crystal study.

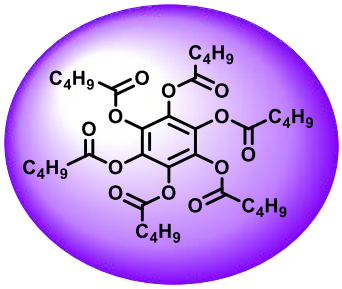

Figure 1.5: Representation of a disc-shaped liquid crystal.

Banana-shaped molecules (**Figure 1.6**)[29] are the most recent addition to the liquid crystal family. An angular central unit, two stiff linear cores, and terminal chains make up their molecular structure. The finding of ferroelectricity in non-chiral banana-shaped molecules prompted a surge of study. So far, over a thousand bent molecular form compounds have been created. Mesophases with polar order and supramolecular chirality can be reached using bent-shaped molecules.

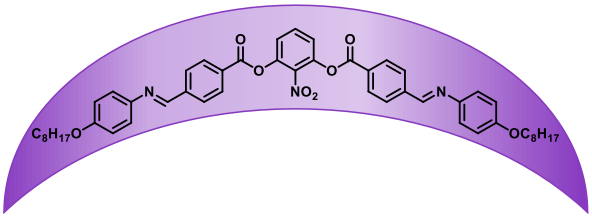

Figure 1.6: Representation of a bent-shaped liquid crystal.

1.4 Classification of liquid crystals.

A variety of factors can be used to categorize liquid crystals. For example, based on the molecular weight of constituent molecules, such as low molecular mass liquid crystals (monomers and oligomers) and high molecular mass liquid crystals (polymers). Based on how mesophase forms, such as by adding a specific solvent (lyotropic) and changing the temperature (thermotropic). Based on constituent molecules' nature (organic, inorganic, and organometallic) and also based on constituent molecule's shape (calamitic, discotic & bent-core). The flow chart in **Figure 1.7** depicts the classification of liquid crystals. However, the most popular variety of LCs can be divided into three groups:

(i) Thermotropic liquid crystals – mesophase formation is temperature-dependent.

(ii) Lyotropic liquid crystals – mesophase formation is solvent and concentration-dependent.

(iii) Amphotropic liquid crystals exist when the component molecules exhibit thermotropic and lyotropic liquid crystalline phases.

Despite the fact that this thesis is only concerned with thermotropic liquid crystals, a small introduction to lyotropic liquid crystals is provided below due to their importance in living systems.[30]

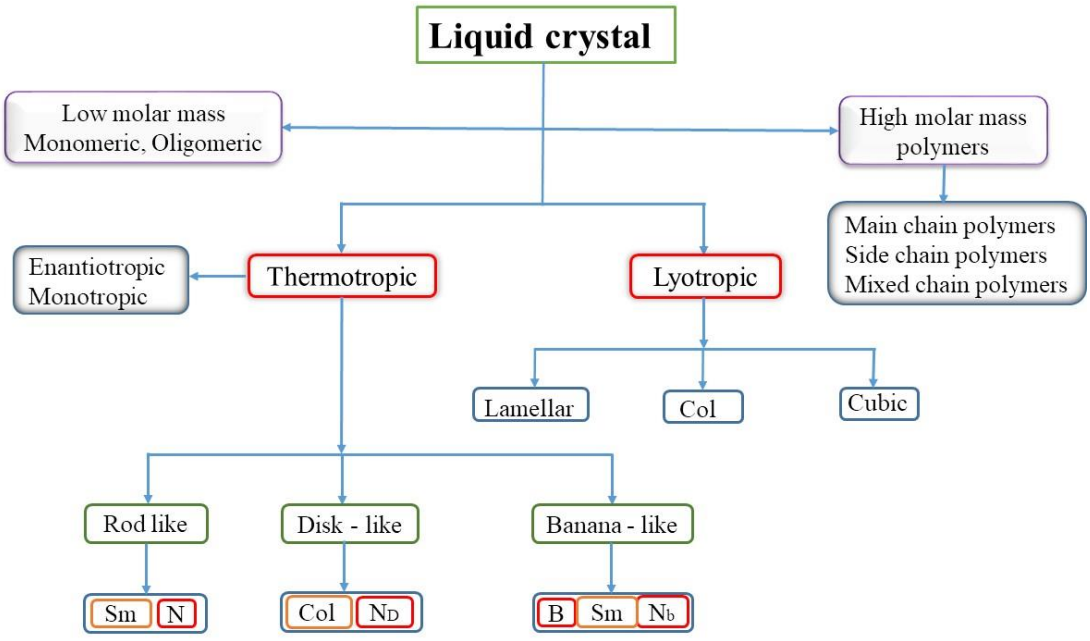

Figure 1.7: Classification of liquid crystals.

1.5 Lyotropic liquid crystals:

Amphiphiles are the molecules that contain both hydrophilic and hydrophobic segments because of the incompatibility of these different segments with the surrounding medium. Amphiphiles are well known to self-assemble into diverse nanostructures using supramolecular interactions such as hydrogen bonding, Van der Waals interactions, hydrophobic interactions, etc. These nanostructures may exhibit mesophase properties. Concentration and/or temperature control the formation of mesophases in lyotropic liquid crystals.[31] Typical examples of lyotropic liquid crystals are soaps in water and various phospholipids. One of the well-reviewed amphiphilic self-assembling systems is the self-assembly of phospholipids with phosphate as the hydrophilic domain and a fatty acid chain attached to it as the hydrophobic domain to form a bilayer. The polar head group is exposed to the aqueous medium, while hydrophobic interactions between the alkyl chain drive self-assembly to form a bilayer with a hydrophobic segment embedded inside (**Figure 1.8**). Numerous amphiphilic systems self-assemble into soft nanomaterials with tailored functional properties which have been reported in the literature.[32] Below are the descriptions of a few representative systems. According to their molecular architecture, a series of amphiphiles with rod-coil topology are self-assembled into diverse nanostructures such as lamellar, vesicles, micelles, and cylindrical micelles[33], hexagonal columnar, and the cubic phases. X-ray diffraction techniques have classified these mesophase structures.[34,35] The schematic representation of lyotropic liquid crystalline self-assembly is shown in **Figure 1.9.**

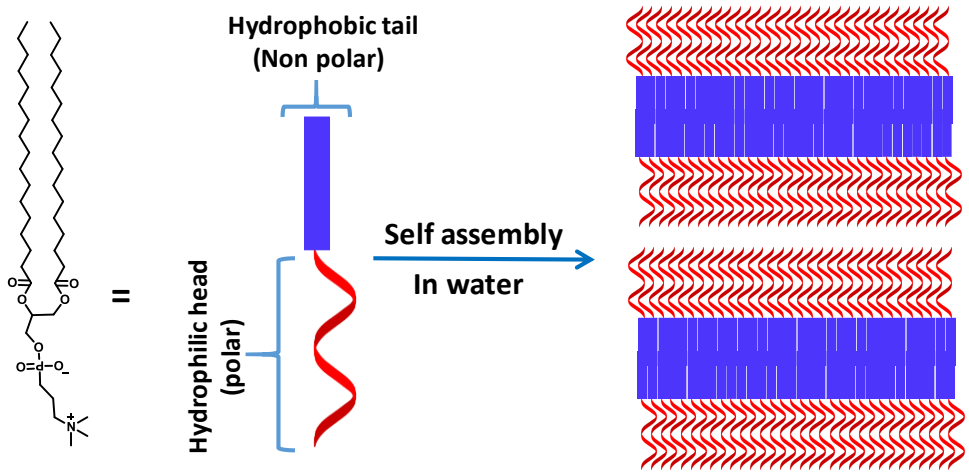

Figure 1.8: Schematic showing the self-assembly of phospholipids in an aqueous medium into a bilayer.

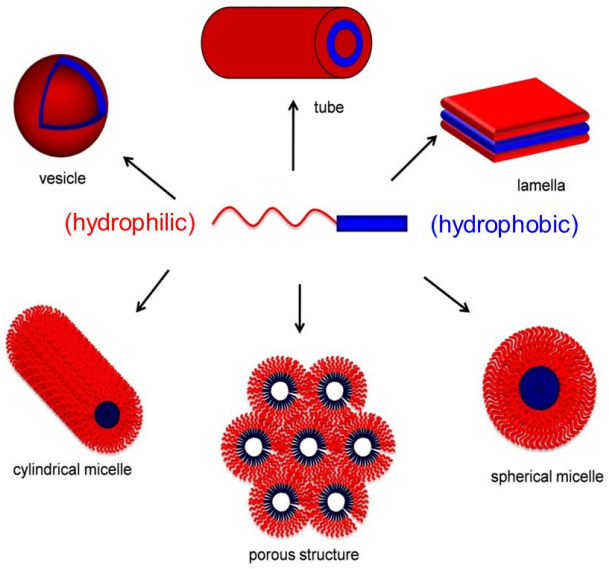

Figure 1.9: Lyotropic liquid crystalline self-assembly.

1.6 Thermotropic liquid crystals

The liquid crystalline phases formed by changing the temperature of the compounds are known as thermotropic liquid crystals. The mesophase can be obtained by heating a solid or cooling an isotropic liquid. The melting point is the temperature at which a crystal transitions to a mesophase, while the clearing point is the temperature at which a mesophase transitions to an isotropic liquid. Thermotropic LCs are classified into two types. Enantiotropic phases can be obtained by heating and cooling stable materials. If the mesophase is obtained solely by cooling the isotropic liquid it is called a monotropic phase. It is a metastable mesophase, with the mesophase transition occurring below the melting point.[36] The schematic representation of enantiotropic and monotropic mesophase is shown in **Figure 1.10.**

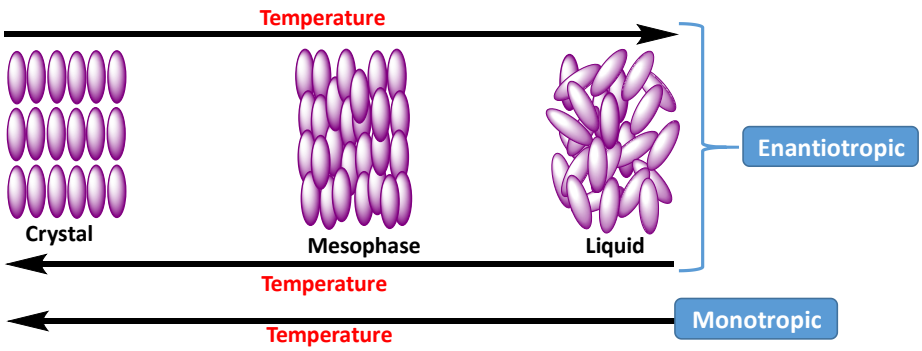

Figure 1.10: Representation of enantiotropic and monotropic mesophases.

A structure consisting of a central core (often aromatic) and a flexible peripheral moiety (generally aliphatic chains) is required for a molecule to be a thermotropic liquid crystal. Furthermore, interaction anisotropy, geometric anisotropy, and microsegregation are driving parameters for mesophase formation. The molecular shape is a significant factor in constructing liquid crystal phases. Three distinct species can be identified based on the rotational volumes of the molecules: spheroid, ellipsoid, and discoid. Spheroid mesomorphic materials like adamantane generally give rise to plastic crystals with long-range positional order but rapid reorientation motion about their lattice sites. Calamitic liquid crystals are formed by ellipsoid or rod-like molecules. They include nematic (N, nematos, Greek for thread-like), lamellar smectic liquid crystals (S, smectos, Greek for soap-like), and anisotropic plastic crystals. Nematic-discotic and columnar discotic liquid crystals are produced by discoid materials (D, disc-like). Materials containing molecules with a combination of these shapes can also be mesomorphic such as phasmidic, bowlic, or pyramidal mesophases, bent-core, or banana phases, Ionic materials, commonly dyes, with board-like or sanidic architectures are often found to exhibit chromonic liquid crystal mesophases.[37] **Figure 1.11** depicts a variety of molecular templates for the formation of various liquid-crystalline mesophases.

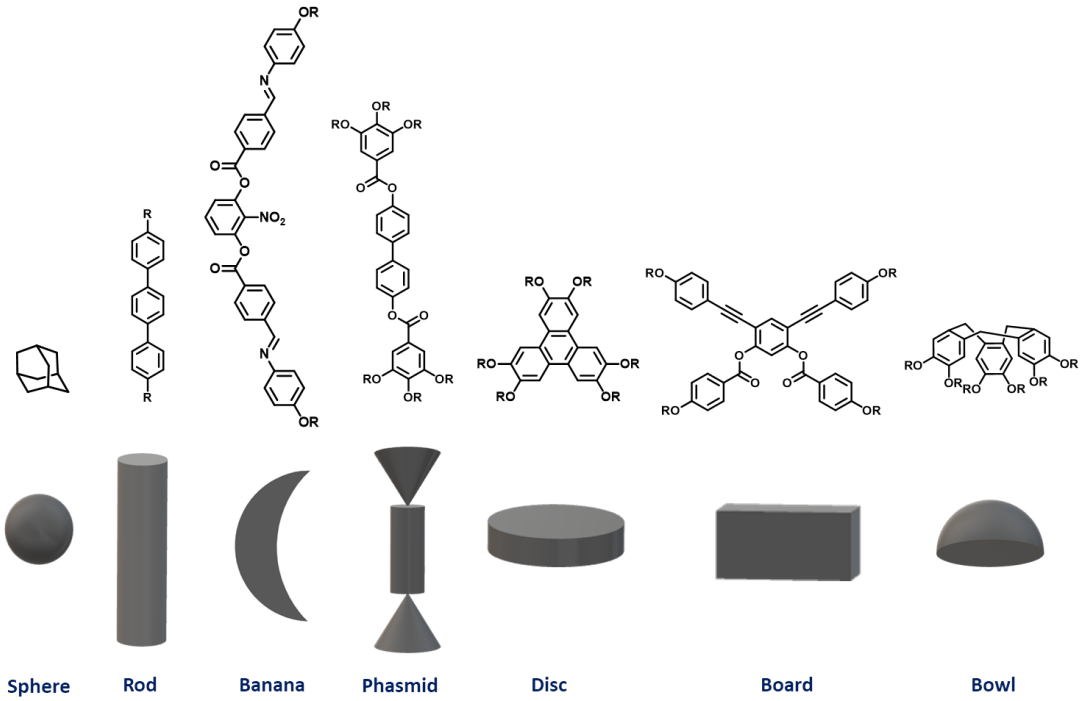

Figure 1.11: Topologies of materials exhibiting mesomorphic behavior and examples of typical low-molar-mass liquid crystals.

The above-mentioned molecular structures, known as thermotropic liquid crystals, are divided into three classes.

(a) Calamitic (rod-shaped) liquid crystals

(b) Discotic (disc-shaped) liquid crystals

(c) Bent-core (banana-shaped) liquid crystals

1.7 Calamitic (rod-like) liquid crystals

Rod-like molecules are the most common type of molecules that form thermotropic mesophase. As shown in **Figure 1.12,** these molecules have an elongated shape in which the molecular length (l) is significantly greater than the molecular breadth (b).

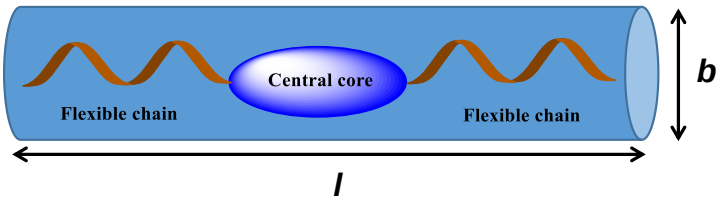

Figure 1.12: Representation of a calamitic LC molecule where $l \gg b$.

In calamitic LCs, geometric shape anisotropy combined with interaction anisotropy and microsegregation of incompatible parts, results in a variety of mesophase morphologies. The majority of calamitic liquid crystalline compounds are made up of two or more ring structures bonded together directly or via linking groups. They typically have terminal hydrocarbon chains as well as lateral substituents. The general template, as shown in **Figure 1.13,** can represent the typical chemical structure of these molecules, where **A** and **B** are core units (benzene, naphthalene, biphenyl, etc.), **R** and **R′** are flexible moieties such as normal and/or branched alkyl groups, and **M** and **N** are generally small lateral substituents (–Cl, –Br, $–NO_2$, $–CH_3$, $–OCH_3$, –CN, etc.). **Y** is a linking group to the core units, and **X** and **Z** are terminal chains and core unit linking groups. The central core, linking groups, and lateral substituents significantly impact the mesophase morphology and physical properties of calamitic LCs. Calamitic LCs have two types of mesophases: (a) nematic and (b) smectic.

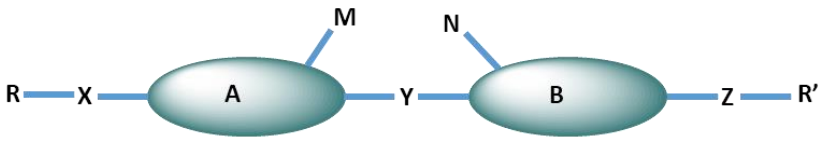

Figure 1.13: The general template for calamitic LC molecules.

1.8 Banana or bent-core liquid crystals

Vorlander and Matsunaga reported the bent-core LCs in the early 1990s and studied mesogenic properties and low thermal stability of the mesophase compared to straight core analogs.[38] But they did not realize the physical significance of the molecules until the discovery of polar switching in these compounds. Bent-shaped molecules were considered "bad" molecules for forming LC phases because if such molecules freely rotate about their long molecular axes, the excluded volume increases, and the ability to develop mesophase is violated; thus, only a few bent-core molecules have been synthesized. Niori et al. reinvented these molecules as banana LCs in 1996 and demonstrated ferroelectric switching in these achiral molecules.[39] The discovery of polar order in non-chiral banana-shaped molecules sparked a surge in research activity. So far, hundreds of bent molecular shape compounds have been synthesized. Despite the mesogens being achiral, bent-shaped molecules allow access to mesophase with polar order and supramolecular chirality.[40–43] Their molecular structure is typically composed of three units: an angular central core, two rigid linear cores, and terminal chains **(Figure 1.14).** The bent angle is around 120–140º in these molecules. Numerous new mesophases have been discovered using bent-core molecules. According to the order of discovery, there are eight phases designated as B1, B2, B3, B4, B5, B6, B7, and B8, where B stands for "bent-core," "banana," "bow," and so on, and is not to be confused with the smectic B phases of calamitic LCs. The optical textures, different characteristic X-ray diffraction diagrams and the electro-optical responses are used to differentiate the bent-core phases. Some of the mesophase structures proposed have columnar order, while others have lamellar order. Bent-core LCs form conventional nematic and smectic phases in addition to the fascinating B phases. Bent-core mesogens are the first thermotropic LCs with an unambiguously determined biaxial nematic (N_b) phase.[44,45] In addition to the polarity, another aspect of fundamental interest is the chirality of the layers. The combination of director tilt and polar order in the Sm_{CP} phase leads

to a chirality of the smectic layers, even though the constituent molecules are achiral; this can be regarded as a "superstructural chirality." The three vectors, layer normal, tilt direction, and polar axis of a layer, can make up an orthogonal coordinate system, which may be left- or right-handed, and left- and right-handed systems are mirror images of one another. The layers are chiral **(Figure 1.15).**[41]

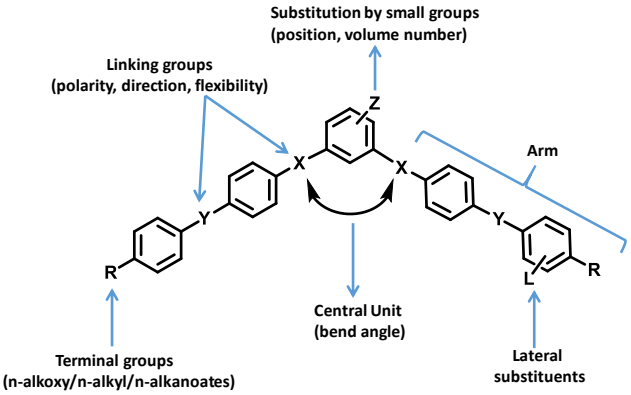

Figure 1.14: General template for banana LC molecules.

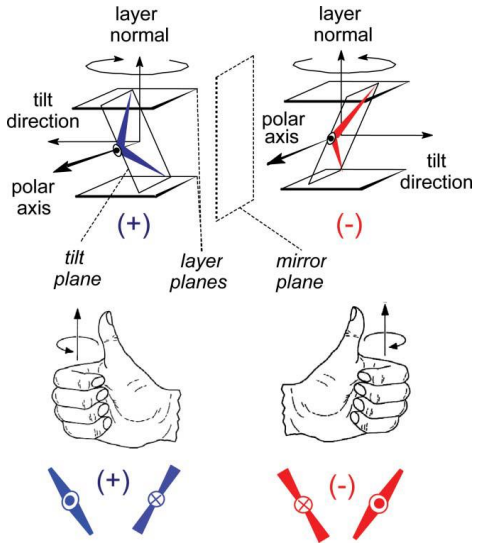

Figure 1.15: Origin of the superstructural (layer) chirality within the smectic phases of bent-core molecules.[41] Copyrights also applied to thesis

1.9 Discotic liquid crystals

The debate over discotic liquid crystals began in 1923 when Vorländer proposed the possibility of liquid crystalline phases with packing behavior similar to "Voltas columns" while studying the flat molecules such as triphenylene and perylene. Unfortunately, he could not observe any mesomorphism for these compounds, which were later recognized as the archetypal core units of many discotic molecules. The experimental breakthrough occurred in 1977 when Chandrasekhar published his observations on the mesomorphic features of benzene-hexa-n-alkanoates and their self-assembly into the columnar hexagonal phase **(Figure 1.16)** which were studied using differential scanning calorimetry (DSC), polarising optical microscopy (POM), and X-ray diffraction (XRD).[28] This is now regarded as the birth of discotic liquid crystals.

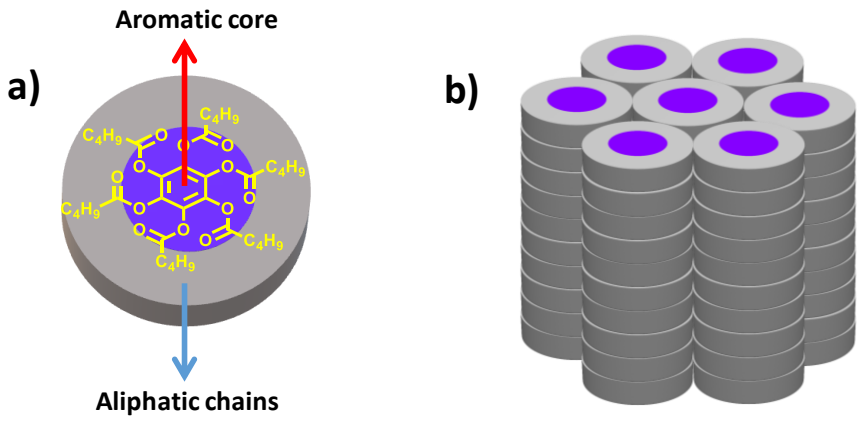

Figure 1.16. a) Structure of benzene-hexa-alkonates b) columnar structure

Since the invention of the first discotic mesogens, many efforts have been directed toward understanding the nature of the molecular parameters that favor the formation of mesophases and control their phase transition. It is well recognized that the molecules in DLCs are usually made up of a central core and substituted with saturated aliphatic chains of three or more carbon atoms. These materials frequently have rotational symmetry of two, three, four, or six-fold. There are several exceptions, and materials with low symmetry, a nonplanar, nonaromatic core, and fewer chains are also documented. The microsegregation of the two dissimilar constituents causes the liquid crystalline phase: the crystalline character is attributed to the interaction of

the conjugated cores, while the fluid character is induced by the melting of the saturated alkyl chains in the mesophase. A general template for discotic mesogens is shown in **Figure 1.17.**

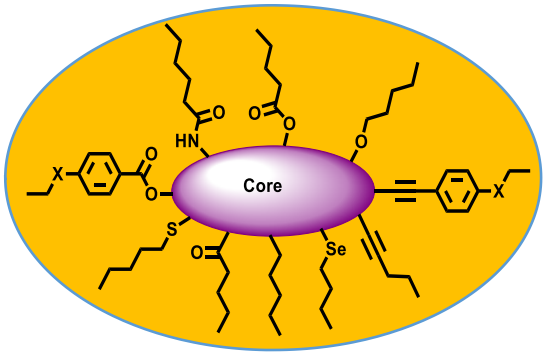

Figure 1.17: A general template for discotic mesogens.

1.10 Characterization of Discotic Liquid Crystal Phases

The thermotropic phase behavior of DLCs, is typically studied using differential scanning calorimetry (DSC), polarised optical microscopy (POM), small- and wide-angle X-ray scattering[46] and solid-state NMR.[47,48] POM easily detects the fluid character of the sample and mesophases, in many cases, the characteristic textures. DSC is used to find the phase transition temperature as well as the enthalpy changes associated with each transition. DSC is always used in conjunction with optical microscopy to detect the presence of LC phases by detecting the enthalpy change associated with a phase transition. This technique, however, cannot determine the type of LC phase, but the magnitude of enthalpy change does provide some information about the degree of molecular ordering within a mesophase. X-ray diffraction, specifically 2D X-ray scattering of macroscopically oriented samples, can be used to study the supramolecular organization and the corresponding packing parameters in each phase in great detail. The majority of discotic mesogens have columnar phases, but there are few examples of polymorphism.[27,49–52] There are four types of mesophases formed by discotic mesogens: 1) Nematic phase, 2) Columnar phase, 3) Cubic phase, 4) Smectic phase

Nematic phase

Nematic phases are the most straightforward liquid crystalline phases to form because they only have long-range orientational order (of molecules, columns, etc.) and no degree of long-range translational order. There are four types of nematic phases in disk-like molecules

depending on the molecular arrangements: (1) discotic nematic (N_D), (2) chiral nematic (N_D*), (3) columnar nematic (N_{Col}), and (4) nematic lateral (N_L). **Figure 1.18** depicts the structure of these nematic phases.[53]

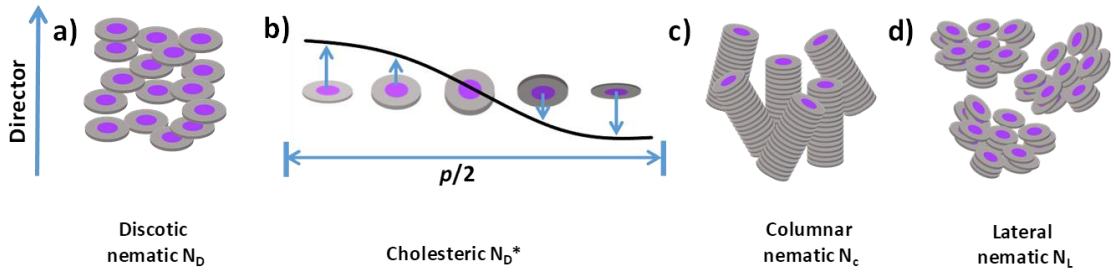

Figure 1.18: Structure of various nematic phases exhibited by discotic mesogens: (a) discotic nematic, (b) chiral nematic, (c) columnar nematic, and (d) nematic lateral.

The nematic phase in a discotic nematic mesophase N_D (**Figure 1.18a**) is made up of single flat molecules with complete translational and orientational freedom around their principal short axes.[54] The cholesteric phase N_D* (**Figure 1.18b**) is a chiral variant of the discotic nematic phase that can be formed by chiral discotic mesogens or by adding a chiral dopant to an achiral discotic nematic phase. Columns are building blocks for the columnar nematic mesophase N_c (**Figure 1.18c**).[55] This mesophase was observed in the presence of an electron donor doped with an electron acceptor.[56] Because of charge-transfer interactions, ordered columns are formed here. The use of molecules with significantly different side chain lengths prevents the formation of a 2D lattice. The columns are now parallel to each other in a columnar nematic mesophase, exhibiting short-range positional and long-range orientational order. Besides these two nematic phases, the lateral nematic phase N_L was observed in these nematic phases.[57] The lateral nematic phase consists of aggregates formed by multiple discotic mesogens. These supramolecular aggregates then organize into a nematic phase (**Figure 1.18d**).

Lamellar Mesophase.

The uneven distribution of peripheral chains causes smectic organization in discotic molecules. The discs are layered and separated by a sublayer of peripheral chains. Because of the

restriction of molecular rotation along the axes, the possibility of biaxiality in these phases is quite strong (**Figure 1.19**).[58] Smectic phases are uncommon in discotic systems.

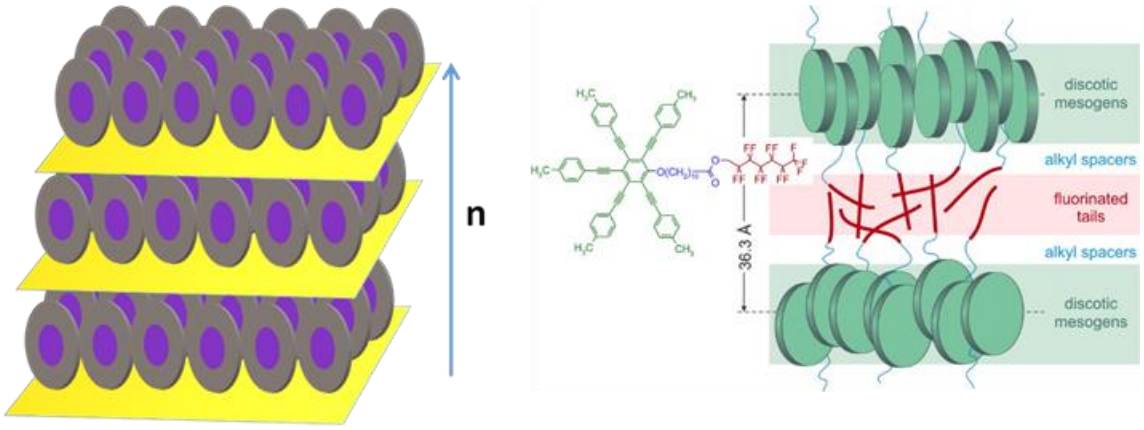

Figure 1.19: Arrangement of discotic lamellar phase

Columnar phases of discotic mesogens:

Since the π-fused central units often constitute discotic liquid crystals, they have strong π-π interactions among themselves. The most distinctive class of DLCs, the family of columnar mesophases, is formed due to significant π-π interaction. Discotic molecules stack one on top of the other, leading to column formation (**Figure 1.20**). These columns can be "disordered columns" with irregular stacking of discs and "ordered columns" where the molecules are regularly stacking. Molecules can also be tilted at an angle to their columnar axis, resulting in the formation of "tilted columns." These columns then occupy a variety of 2D lattices in which the columns are arranged parallel to one another. Columnar mesophases are classified into six classes based on the degree of order in the molecular stacking, the orientation of molecules along the columnar axis (orthogonal, tilted, helical, etc.), the dynamics of the molecules within the columns, and the 2D lattice symmetry of the columnar packing.[36] The classification is shown below.

(i) Columnar hexagonal mesophase (Col_h),
(ii) Columnar rectangular mesophase (Col_r),
(iii) Columnar oblique phase (Col_{ob}),
(iv) Columnar plastic phase (Col_p),

(v) Columnar helical phase (H),

(vi) Columnar square (tetragonal) phase (Col_{tet}),

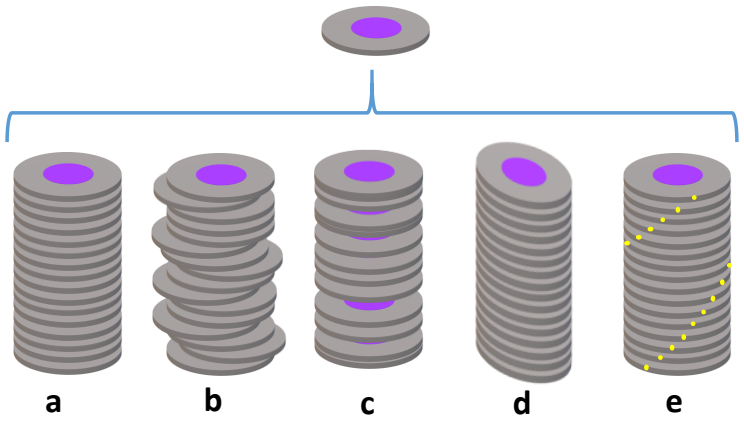

Figure 1.20: (a) ordered column, (b) & (c) disordered columns, (d) tilted column (e). helical column, These self-assembled columns self-organize into different types of 2D columnar lattices.

Columnar hexagonal mesophase (Col_h).

Most of the discotic liquid crystals exhibit the columnar hexagonal mesophase (Col_h). X-ray diffraction (XRD) studies are widely used to characterize the presence of various columnar mesophases.[59] **Figure 1.21** depicts a schematic representation of the molecular arrangement in Col_h and a typical 2D X-ray diffraction pattern of the Col_h phase, which contains many sharp reflections in the small-angle regime and two broad diffused peaks in the wide-angle regime. The typical reflections of the small-angle region, with d-spacings in the characteristic ratio of 1:1/√3:1/√4:1/√7... according to the following equation shown in **Figure 1.21**. '*a*' is the lattice parameter. The broad diffuse peak in the wide-angle region represents the liquid-like order of molten alkyl chains. A second relatively narrow peak appears due to the columns' regular packing of cores. Due to shape anisotropy, liquid-crystalline phases are birefringent in nature under crossed polarizers. As a result of a combination of symmetry-dependent elasticity, defect formation, and sample surface conditions, each mesophase type has a distinct texture in POM. The **Figure 1.22** depicts typical textures of the Col_h phase.

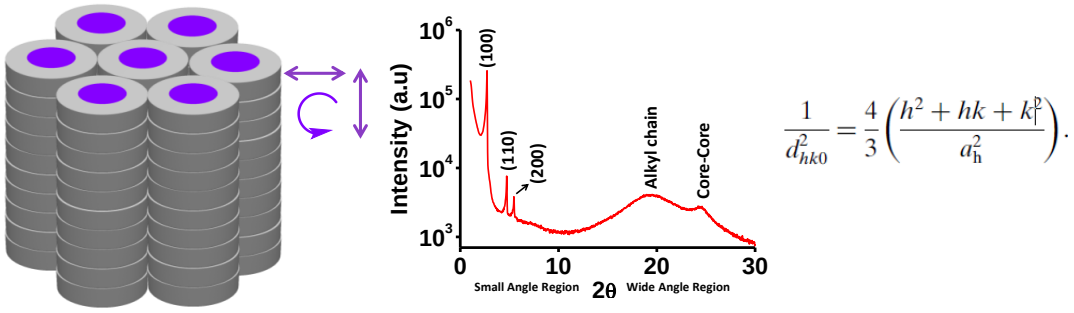

Figure 1.21: Schematic representation of hexagonal columnar phase structure, X-ray diffractograms and equation.

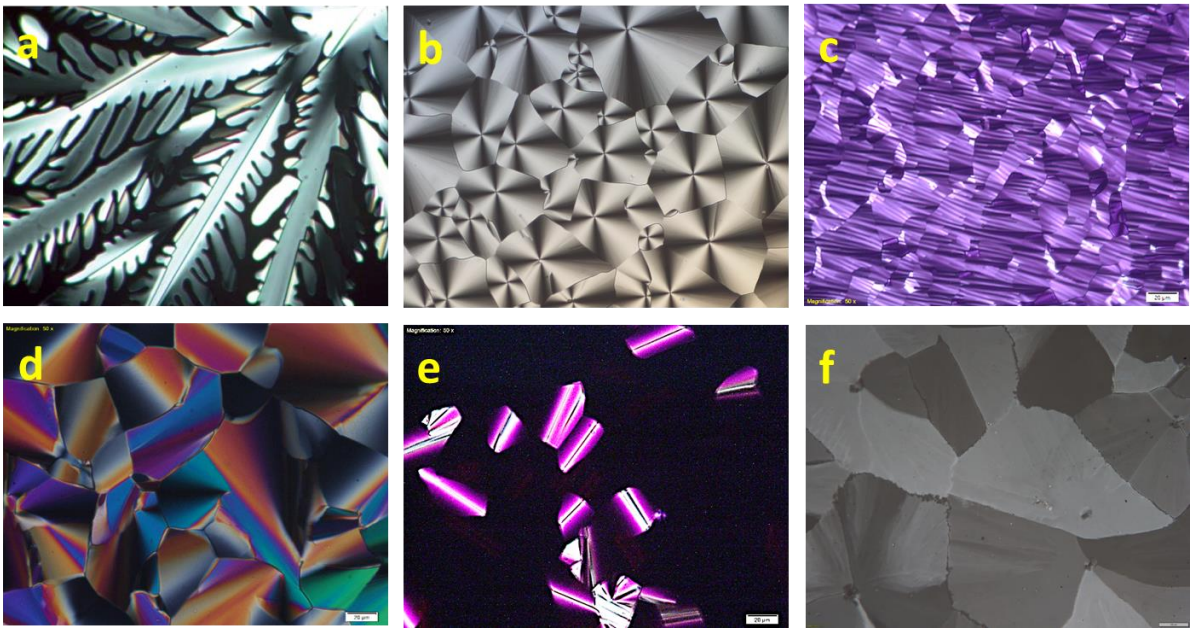

Figure 1.22: POM Images of Col_h mesophases. a) Dendritic b) Focal conic c) Undulating texture d) Pseudo focal conic e) Mosaic textures with rectilinear defects f) Plate-like texture

The rectangular columnar mesophase (Col_r).

The molecules in the rectangular columnar mesophase (Col_r) are tilted with regard to the columnar axis, resulting in an elliptic cross-section of molecules, and these columns occupy the rectangular lattice. Rectangular phases are also known as pseudohexagonal phases. There are several symmetry groups in the Colr family of rectangular columnar mesophases. The Levelut group distinguished three distinct Col_r mesophases using the planar space groups $P2_1/a$, P2/a, and C2/m, corresponding to the plane groups p2gg, p2mg, and c2mm (**Figure 1.23a**).

Tschierske described a fourth columnar rectangular phase with the plane group p2mm (**Figure 1.23b**).[60] Stronger core-core interactions are required in Col_r phases than in hexagonal phases because the tilt angle and the tilt direction must be correlated from one column to the next. With increasing chain length, this frequently results in a transition from the Col_r to the Col_h phase.

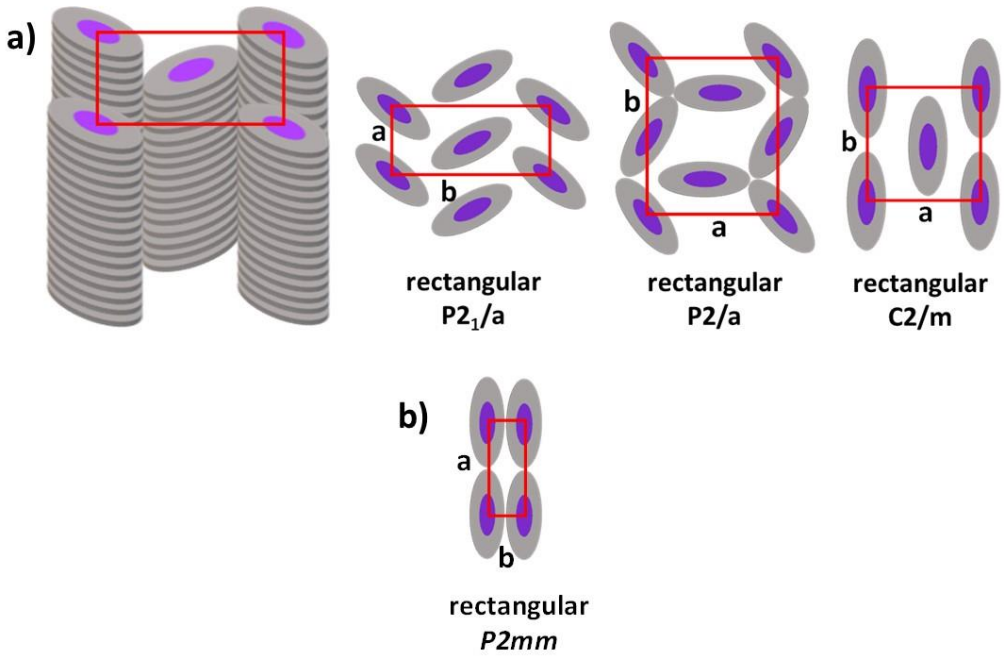

Figure 1.23: The molecular arrangement and different types of rectangular columnar mesophase.

Columnar oblique phase (Col_{ob}).

Columnar oblique (Col_{ob}) mesophase with tilted columns represented by elliptic cross-sections is shown in **Figure 1.24.** The P1 space group corresponds to the symmetry of this 2D lattice. Due to the strong core-core interactions, the compounds showing columnar oblique mesophases are rare.[46,61] Because P1 is a primitive planar space group, there are no reflection conditions, such as columnar hexagonal and rectangular phases, so all peaks are permitted. This phase is very uncommon in discotic.

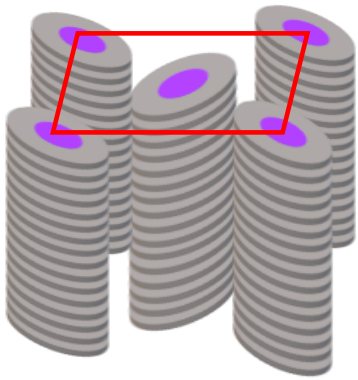

Figure 1.24. Schematic representation of columnar oblique phase structure,

Columnar square (tetragonal) phase (Col_{tet}).

The columnar square phase is also referred to as the tetragonal phase (Col_{tet}). **Figure 1.25** shows the structure of the columnar square phase. The columns are upright and arranged in a square lattice in this mesophase. Like the columnar hexagonal phase, this phase exhibits spontaneous homeotropic alignment of the columns. Sugar molecules, phthalocyanines, and supramolecular fluorinated liquid crystals exhibit this phase. Identifying this mesophase from optical texture is difficult. However, X-ray diffraction studies have always been used to determine the phase structure, with the diffraction pattern displaying (10) and (11) reflections in the small-angle region with a reciprocal spacing ratio of 1:√2.[62,63]

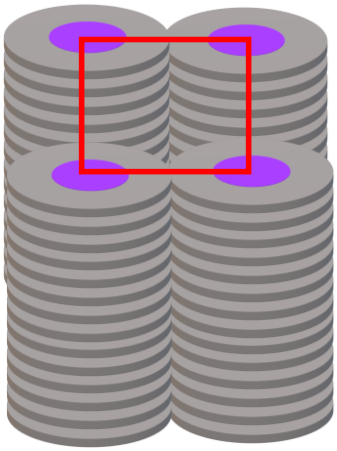

Figure 1.25: Structure of columnar tetragonal (square) phase.

Columnar plastic phase (Col_p),

This phase is denoted as Col_p and was noticed in discotic liquid crystals.[59,64] The plastic phase has three-dimensional crystal-like order, but the columns are organized in two-dimensional hexagonal lattices, as shown in **Figure 1.26**. The diffraction pattern contains small-angle peaks that can be indexed into a hexagonal, rectangular, or oblique lattice (recently reported). The wide-angle region, around 3.4Å, shows two sharp reflections, which are thought to be a typical signature for a plastic phase. The presence of an alkyl chain fluidity peak distinguishes the plastic phase from the crystal phase. Hexabutyloxy-triphenylene (H4TP) and its derivatives were reported for their plastic nature of mesophase, making them one of the most studied compounds. Correlation length calculated from X-ray diffraction studies can confirm the variations between plastic and hexagonal phases.

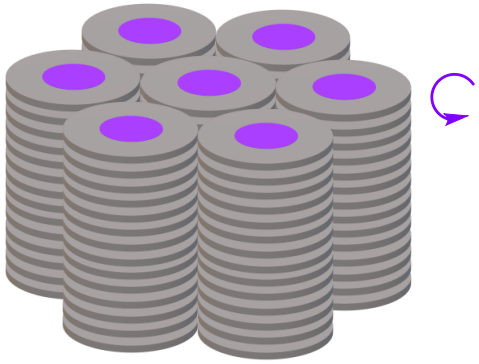

Figure 1.26: Structure of columnar plastic phase, the curved arrow indicates the rotational disorder of the molecules in the columns. Note that the axial and lateral displacements of the molecules are not present in this phase.

Columnar helical (H) phase.

Triphenylene derivatives, especially hexahexylthiotriphenylene(HHTT), have demonstrated a unique mesophase structure with helical order. Helical columns develop by interdigitating in groups of three columnar stacks during the so-called H phase. The triphenylene cores are stacked helicoidally within each column, with the helical period being incompatible with the intermolecular (intracolumnar) spacing. The third column in the superlattice is vertically

displaced by half an intracolumnar distance from the other two columns. **Figure 1.27** depicts the H phase of HHTT.[65,66][67]

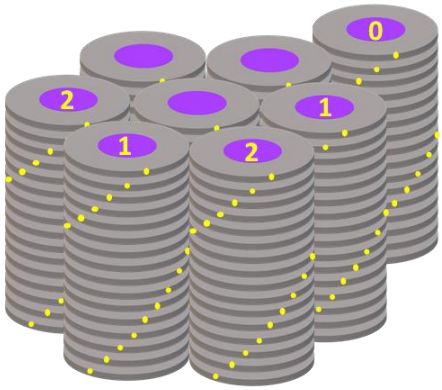

Figure 1.27: Structures of columnar helical phase.

Cubic mesophase

In lyotropic systems, cubic phases are frequently observed. There have been reports of cubic arrangement in phthalocyanines and triphenylene-containing discotic compounds.[68,69] They produce bicontinuous phases in general. To the naked eye, they will appear very viscous. These phases are isotropic in terms of optical properties. Diffraction is the only method for confirming this phase. Based on space-group symmetry, cubic phases can be classified into three types. The extinction rules and the ratio of d spacings are shown below in **Figure 1.28**

Symmetry	Formula		Selection Rules
$Pn\bar{3}m$	$d = \frac{a}{\sqrt{h^2+k^2+l^2}}$	=1/√2:1/√3:1/√4:1/√6:1/√8:1/√9: 1/√10:1/√11:1/√12:1/√14:1/√16: 1/√17…	0*kl* : *k*+*l* = 2*n* *h*00: *h* = 2*n*
$Im\bar{3}m$	$d = \frac{a}{\sqrt{h^2+k^2+l^2}}$	=1/√2:1/√4:1/√6:1/√8:1/√10:1/√12:1/√14:1/√16:1/√18:1/√20:1/√22:1/√24:1/√26…	*hkl* : *h*+*k*+*l* = 2*n* 0*kl* : *k*+*l* = 2*n* *hhl* : *l* = 2*n* *h*00: *h* = 2*n*
$Ia\bar{3}d$	$d = \frac{a}{\sqrt{h^2+k^2+l^2}}$	=1/√6:1/√8:1/√14:1/√16:1/√20:1/√22:1/√24:1/√26:1/√32:1/√38:1/√42:1/√46:1/√48:1/√50:1/√52:1/√54:1/√56…	*hkl* : *h*+*k*+*l* = 2*n* 0*kl* : *k*, *l* = 2*n* *hhl* : 2*h*+*l* = 4*n* *h*00: *h* = 4*n*

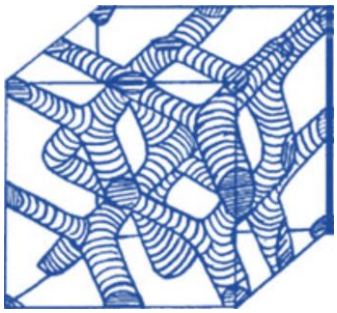

Figure 1.28: Structure of the cubic phase exhibited by DLCs.

In the formation of columnar mesophases, the molecules need not be disc-shaped. Any shape molecules that favor the supramolecular interactions (hydrogen bonding, dipole interaction, metal coordination, hydrophobic forces, π-πinteractions, etc.) leads to columnar mesophase. Some of the examples are shown in **Figure 1.29.**[70]

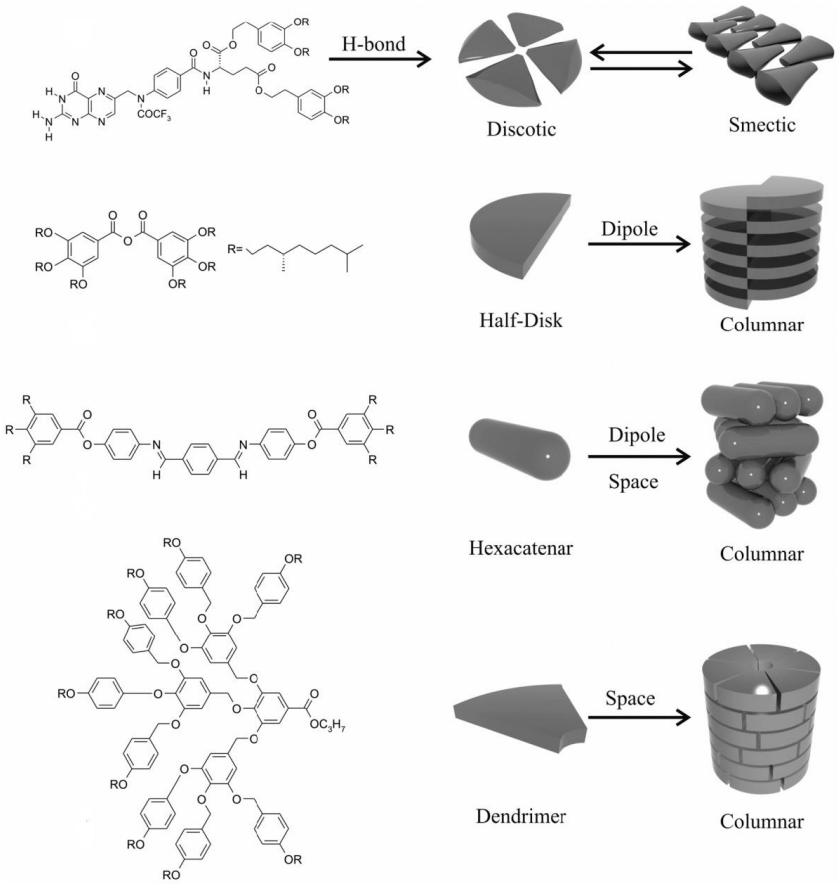

Figure 1.29: Schematic representation of columnar and smectic mesophase from different shapes of molecules.

1.11 Alignment of discotic liquid crystals

As previously discussed, the ability of the discotic molecules to self-assemble into columnar superstructures, combined with the self-healing of structural defects in liquid crystalline columnar mesophases, suggests that they have great potential for use as semiconductors in organic electronic devices.[70] However, a significant challenge is to create a suitable processing technique for synthesizing a defect-free long-range oriented discotic materials. The degree of structural order is critical to the performance of semiconducting devices. Controlling the molecular stacking of DLCs to form a highly ordered columnar phase is essential for achieving good device performance. Thus a thorough understanding of the mechanisms underlying DLC molecular stacking is essential.[49] Discotic molecules can have two distinct orientations, planar alignment and homeotropic alignment.

Planar alignment and Homeotropic alignment

DLCs can form uniaxial alignment of horizontal columns on various substrates by employing the proper processing techniques such as zone casting, friction transferred, pre-oriented poly(tetrafluoroethylene) PTFE, Langmuir–Blodgett (LB) technique, crystalline surfaces, zone melting, magnetic field, field-force alignment, circularly polarised infrared radiation, etc.

DLCs with face-on homeotropic alignment have been achieved either between two substrates or on a single substrate, and the alignment can be obtained from isotropic melt or from solution using various solution processing techniques through chemical modifications of the molecules. Homeotropically aligned samples do not show birefringence in the POM between crossed polarizers since the optical axis, in this case, coincides with the columnar axes. Planar alignment samples exhibit the birefringence textures in the POM between the crossed polarizes. In order to distinguish between the homeotropically and planar aligned columnar mesophase and the isotropic phase, additional experiments are necessary; x-ray diffraction is one of the best methods, which also precisely confirms the alignment.[71–74] The schematic representation of homeotropic alignment and planar alignment are shown in **Figure 1.30.**

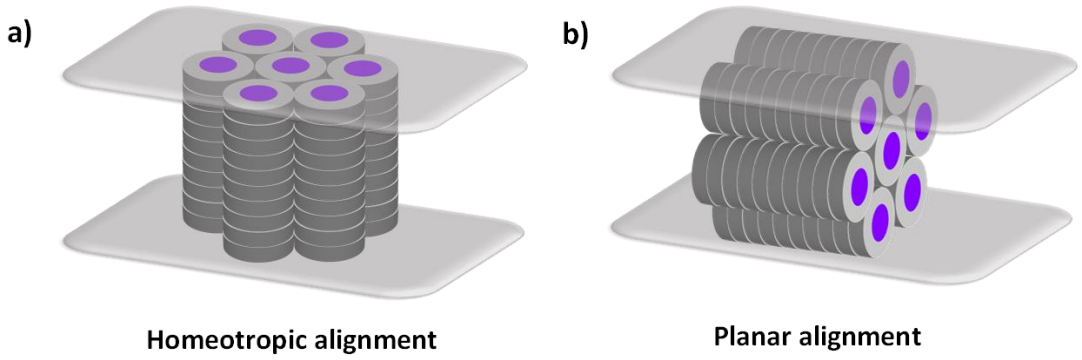

Figure 1.30: Schematic representation of (a) homeotropic and (b) planar alignment configurations of discotic columnar phases.

1.12 Liquid crystals characterization techniques.

Polarized optical microscopy (POM), differential scanning calorimetry (DSC), and powder X-ray diffraction (XRD) are commonly used to investigate the bulk properties of liquid crystalline materials. Along with these, solid-state NMR is also used for the characterization of liquid crystals. These techniques help us understand the nature of self-assembly, stability, phase transition temperatures, and enthalpy associated with discotic mesogen transitions.

Polarized optical microscopy (POM).

Polarised optical image illumination techniques are most commonly used for birefringent materials, where the polarised light interacts strongly with the sample, resulting in contrast with the background. In optical mineralogy, polarised light microscopy is commonly used. This microscopy is also frequently used to characterize liquid crystals because they are one of the anisotropic materials. When light passes through a birefringent material, it splits into two components: a fast component known as the ordinary ray (o) and a slow component known as the extraordinary ray (e). These two components move through the sample at different speeds and become out of phase. Because of the phase difference, when both rays recombine as they leave the birefringent material, the plane of polarization of the light is altered. The sample is placed between two glass slides and loaded onto a microscope stage with a variable temperature controller in the POM experiment. Liquid crystalline phases are anisotropic fluids that exhibit optical birefringence and a characteristic pattern (textures) when viewed through crossed polarizers. Texture characteristics in the mesophase range are characteristics of a specific LC

phase. The LC phase's symmetry-dependent elasticity causes the textures in combination with defects and surface conditions. However, the birefringent is absent in homeotropically aligned samples, leaving only a dark field. Crystals are also optically anisotropic and birefringence under POM, but due to the fluid nature of the mesophase, they can be distinguished from LCs. When liquid crystals with low viscosity melt from the crystalline phase, they begin to flow. When they cool from the isotropic phase, they form textures, which change the texture of the mesophase when pressed. On the other hand, crystals do not change in texture or they form cracks with defined edges when the glass slide is pressed. Schlieren and thread-like textures are frequently associated with nematic liquid crystals, whereas fan-shaped structures, mosaic, and dendritic textures are common in columnar mesophase. Straight linear defects are common in the textures of the ordered columnar mesophase.

Differential scanning calorimetry (DSC).

Differential scanning calorimetry (DSC) is a thermoanalytical technique that measures the difference in heat required to raise the temperature of a sample and a reference as a function of temperature. The sample and reference are kept at nearly the same temperature throughout the experiment. The basic idea behind this technique is that when the sample undergoes a physical transformation, such as phase transitions, more or less heat must flow to it than to the reference in order to keep both at the same temperature. The amount of heat that must be transferred to the sample depends on whether the process is exothermic or endothermic. For example, as a solid sample melts to a liquid, more heat must be applied to the sample in order to raise its temperature at the same rate as the reference. This is due to the sample absorbing heat during the endothermic phase transition from solid to liquid. Similarly, as the sample goes through exothermic processes (such as crystallization), less heat is required to raise the sample temperature. Differential scanning calorimeters can measure the amount of heat absorbed or released during such transitions by observing the difference in heat flow between the sample and the reference. DSC can also detect more minor physical changes, such as glass transitions. Because of its utility in evaluating sample purity and studying polymer curing is widely used in industrial settings as a quality control instrument. DSC is a technique used to investigate liquid crystals. Some types of matter pass through a third state as they transition from solid to liquid, displaying properties from both phases. This anisotropic liquid is classified as crystalline liquid or mesomorphous liquid. DSC can detect the small energy changes that occur

when matter transitions from a solid to a liquid crystal and from a liquid crystal to an isotropic liquid. The typical DSC thermogram is plotted as heat flow (mW) versus temperature (°C), with the peaks corresponding to phase transition temperatures and the area under the curve corresponding to the associated enthalpy change. The transition from crystal to LC phase usually results in a significant enthalpy change (20-100 kJ/mol) as it moves from a highly ordered crystalline state to a less ordered (or short-range ordered) LC phase. The LC phase to the isotropic phase transition, on the other hand, involves much lower enthalpy values (below 10 kJ/mol). The DSC thermogram reveals the number of mesophase transitions and the structural ordering of the LC phases. Although DSC does not provide any concrete evidence of the liquid crystallinity of the material, it acts as a complementary technique to POM.

Powder X-ray diffraction

X-ray diffraction is a powerful tool for the structural characterization of most materials. It is possible to determine an exact and usually unique structure for atomic or molecular arrays with three-dimensional periodicity. In contrast, only a time-averaged or statistical distribution can be established for liquids, where the constituent atoms are in constant motion. This technique can be used to study the supramolecular organization of liquid crystalline phases into various lattices and corresponding packing parameters in each phase. The XRD technique works on the principle of Bragg's law, and the equation is $n\lambda = 2d \sin\theta$. For practical reasons, the Bragg's law will be used to convert all diffraction angles (2θ) into interplanar spacing distances. Where λ is the X-ray wavelength, d is the interplanar spacing generating the diffraction, θ is the diffraction angle, h, k, l are the Miller indices of the associated reflection, and n is an integer. Hereafter, all diffractions will be considered as their distance equivalents instead of their diffraction angles. The mesophase of the XRD pattern clearly shows two different angle regions small-angle region (from $2\theta = 0$ to 12-15°) and a wide-angle region (from $2\theta >$ 12-15°). The latter is distinguished by a broad halo produced by the slow motion of the flexible molten alkyl chains. The columnar phase in the wide-angle region exhibits the two peaks: molten alkyl chain and π- π core stacking (core-core distance) that differentiates the mesophase from "true" crystals. The core-core separation is usually in the order of 3-4 Å. In the small-angle region, sharp reflection peaks are observable relative to the intercolumnar dhkl distances. The small-angle area usually shows a few sharp peaks that are indexed to a specific mesophase structure, such as Col_h, Col_r, and Col_{ob}. The XRD profile of a mesophase provides structural

symmetry information and data on (i) the ordering of the peripheral hydrocarbon chains and the central core, (ii) the core-core correlation length along the columnar axis, and (iii) the intercolumnar distance and lattice parameters.

Solid-state NMR

The solid-state NMR helps in the investigation of the molecular dynamics in the liquid crystalline mesophase. This technique can investigate the rotation of the core in relation to its neighbors or the peripheral mobility of alkyl chains. The various electronic environments of the aromatic protons in the intracolumnar packing and the tilted arrangement of the discs in the solid phase can be determined. All of these complementary experimental methods must be used in order to obtain a clear, comprehensive, and unambiguous picture of the self-assembling behavior of discotic mesogens.

A mesogen transition from crystalline to liquid crystalline phase is accompanied by an increase in molecular dynamics, such as axial and lateral displacement of discs and rotation of discs around the columnar axis, among other things. The centers of gravity of the mesogens in the columnar mesophases are located along the column axis, and the peripheral chains induce fluidity and allow the column to slide concerning each other, resulting in self-healing behavior.

1.13 Liquid-crystalline packing and charge transport.

Solar cells (photovoltaics), light-emitting diodes (LEDs), and field-effect transistors (FETs) all rely on the transport of electrical charges between two electrodes. Inorganic semiconductors with relatively high charge carrier mobility, such as crystalline silicon, are widely used as charge carrier components. However, processing crystalline silicon is costly, and preparing flexible electronic components from the hard material is difficult. Hence, an alternative to this "softer" semiconductive organic materials is used to produce flexible and cheaper devices because they are soluble in organic solvents and can be easily deposited on a substrate.

To produce highly efficient, cheaper, and easily processable organic semiconductors and increase the charge transport of these materials to achieve fast response in devices, researchers have made intensive efforts. However, the primary contest is to find a balance between the mobility and processability of these materials. For example, single crystals,[75] known for high mobilities, suffer from inherent fragility and flexibility, which limit their usability in devices. Similarly, in polymeric systems,[76–78] inadequate solubility, low purity, and structural and

energetic disorder have curbed their charge transport properties. To overcome these challenges, discotic liquid crystals (DLCs),[79] comprising a central rigid aromatic core substituted with a mantle of flexible alkyl chains, are currently in the spotlight of material scientists.[80] Strong π–π interactions among rigid aromatic cores arrange the discogens in a columnar fashion, and thus, charge transport in these materials is expected to be quasi-one dimensional. Besides that, the supramolecular columnar architecture is advantageous in terms of providing the right balance between mobility and processability.[81,82] and that is why discotic liquid crystals are essential for organic electronics.

The two-dimensional chemical structure of columnar liquid crystals is a fascinating area of research. Due to the intense π-π interactions of polyaromatic cores, the majority of discotic liquid crystals form columnar mesophases. In a columnar mesophase, the core-core (intra-columnar) separation is usually of the order of 3-4 Å, resulting in a significant overlap of π-orbitals between two neighboring discs. Long, flexible alkyl chains surround the core; the inter-columnar distance is usually in the range of 20- 40 Å, depending on the lateral chain length and number of lateral chains. To form columnar mesophase, the alkyl chains surrounding the aromatic core range from 3 to 8. As a result, interactions between neighboring mesogens within the same column are much stronger than interactions between neighboring columns. This results in anisotropic liquid crystal behaviour, with charge migration in these discotic materials being quasi-one-dimensional. In columnar mesophases, conductivity along the director is several orders of magnitude greater than in the perpendicular direction. As shown in **Figure 1.31**, discotic liquid crystals, also known as molecular wires, have to conduct through aromatic cores surrounded by insulating aliphatic chains in the columnar phase. During the past decade, self-assembled supramolecular structures formed by disc-shaped molecules have attracted tremendous interest due to their potential applications in wide-viewing liquid crystal displays sensors, photovoltaic solar cells, light-emitting diodes, thin-film transistors, etc.[49]

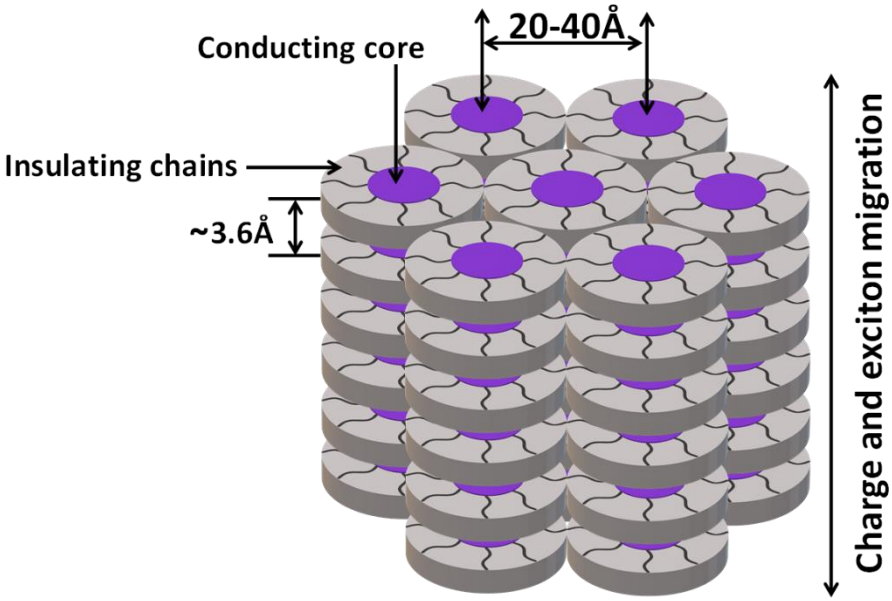

Figure 1.31: Energy and charge migration in discotic liquid crystals

1.14 Functional liquid-crystalline assemblies

A new design of molecules and self-assembled structures from the nano to the macro scale is required to increase the functional capabilities of LCs.[83,84] The idea of supramolecular chemistry[85] has broadened our horizon in LC design, and since 1989, supramolecular liquid-crystalline phases with well-defined structures have been formed by employing intermolecular hydrogen bonding (**Figure 1.32**).[86]

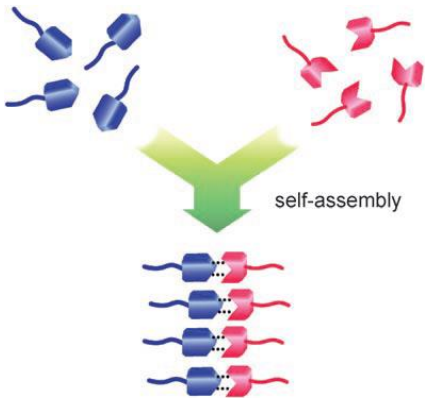

Figure 1.32: Supramolecular assembly of liquid-crystal complexes via noncovalent interactions.

Covalent bonding was used in the conventional design of liquid-crystal molecules to synthesise mesogenic molecular structures.[17] Specific intermolecular interactions, such as hydrogen bonds, were not recognized as being very important in conventional covalent approaches to the preparation of functional materials. Because it was thought that the molecular interaction sites would disrupt the performance and durability of such materials. The supramolecular approach provides us with another tool for creating more dynamic liquid-crystal molecules.[86,87] Formalized paraphrase specific molecular interactions such as hydrogen bonds, ionic bonds, and charge-transfer interactions, can be used to construct these new liquid-crystal assemblies. Hydrogen bonding has also been used to create a wide range of self-assembled systems.[88–90]These non covalent approaches have increased the possibility of incorporating chemical processes into materials, such as molecular recognition and molecular self-assembly. These approaches have been identified as critical in the development of new dynamically functional materials.[86]

1.15 Objective of the thesis.

Many liquid crystals, such as calamitic, bent-core, and discotic, have been investigated extensively since their discovery.These liquid crystals are used in many devices we use today. These liquid crystal devices, most of them are in calamitic liquid crystals. As a result, the chemistry and physics of calamitic liquid crystals are well understood. However, recently discovered discotic and banana-shaped LCs have not yet been thoroughly investigated for their structure-property relationship and device applications. New materials are required to understand the structure-property relationship of these intriguing materials and to consider their application. The main objective of this thesis is to synthesize and characterize new liquid crystalline compounds derived from novel aromatic ring structures. We have synthesized the new molecular materials for discotic liquid crystals using different core moieties such as **pyrene**, **heptazine**, **rubicene**, **cyanostar.** We have investigated their mesophase behavior and photophysical properties. We have also synthesized carboxylic acid-functionalized dendrimers by click chemistry, which usually form a stable hydrogen-bonded complex with benzotri-imidazole. The formation of the mesophases and supramolecular assemblies are confirmed with different instrumental techniques.

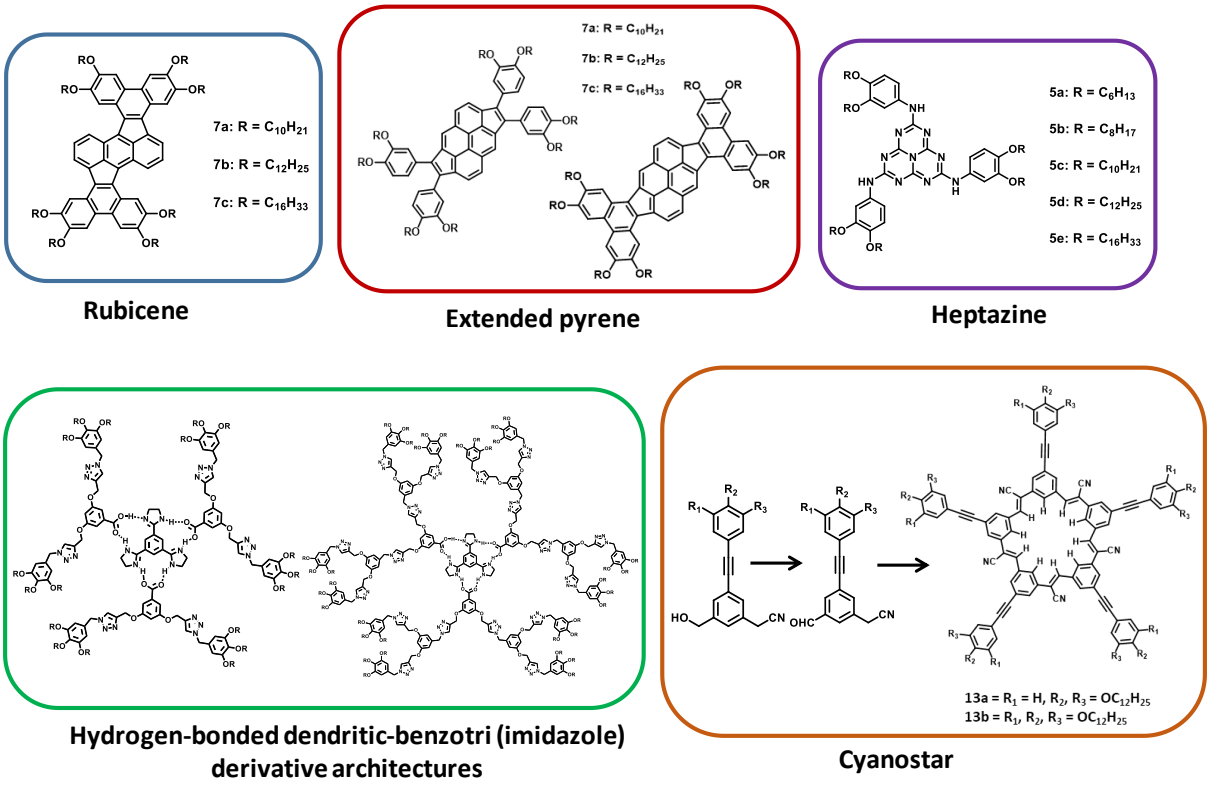

1.16 References:

[1] J. M. Lehn, *Science* **1993**, *260*, 1762–3.

[2] G. V. Oshovsky, D. N. Reinhoudt, W. Verboom, *Angew. Chem. Int. Ed. Engl.* **2007**, *46*, 2366–93.

[3] L. F. Giraldo, B. L. López, L. Pérez, S. Urrego, L. Sierra, M. Mesa, *Macromol. Symp.* **2007**, *258*, 129–141.

[4] A. Thomas, F. Goettmann, M. Antonietti, *Chem. Mater.* **2008**, *20*, 738–755.

[5] K. Zhu, J. Sun, H. Zhang, J. Liu, Y. Wang, *J. Nat. Gas Chem.* **2012**, *21*, 215–232.

[6] N. Pal, A. Bhaumik, *Adv. Colloid Interface Sci.* **2013**, *189–190*, 21–41.

[7] D. Papapostolou, S. Howorka, *Mol. Biosyst.* **2009**, *5*, 723–32.

[8] B. Liu, Y. Yao, S. Che, *Angew. Chem. Int. Ed. Engl.* **2013**, *52*, 14186–90.

[9] B. Liu, Y. Yao, S. Che, *Angew. Chemie* **2013**, *125*, 14436–14440.

[10] Z. Huang, Y. Yao, S. Che, *Chemistry* **2014**, *20*, 3273–6.

[11] L. Han, S. Che, *Chem. Soc. Rev.* **2013**, *42*, 3740–52.

[12] H. Yang, N. Coombs, I. Sokolov, G. A. Ozin, *Nature* **1996**, *381*, 589–592.

[13] G. S. Attard, J. C. Glyde, C. G. Göltner, *Nature* **1995**, *378*, 366–368.

[14] C. G. Goltner, M. Antonietti, *Adv. Mater.* **1997**, *9*, 431–436.

[15] M. Kléman, *Acta Crystallogr. Sect. A* **1981**, *37*, 607–608.

[16] J. W. Goodby, G. W. Gray, J. W G Goodby, *Smectic Liquid Crystals: Textures and Structures*, Leonard Hill, Leonard Hill: Glasgow, London, **1991**.

[17] D. Demus, J. Goodby, G. W. Gray, H. -W. Spiess, V. Vill, in *Handb. Liq. Cryst. Set*, Wiley, Weinheim, **1998**.

[18] D. Demus, J. Goodby, G. W. Gray, H.-W. Spiess, V. Vill, *Physical Properties of Liquid Crystals*, Wiley, Wiley-VCH: Weinheim, **1999**.

[19] P. Collings, in *Liq. Cryst. Nature's Delicate Phase Matter*, Princeton University Press: Princeton, NJ, **2002**.

[20] I. Dierking, in *Textures Liq. Cryst.*, Wiley, Weinheim, **2003**.

[21] A. Jákli, A. Saupe, *One- and Two- Dimensional Fluids: Properties of Smectic, Lamellar and Columnar Liquid Crystals*, Taylor & Francis:, London, **2006**.

[22] T. Geelhaar, K. Griesar, B. Reckmann, *Angew. Chemie Int. Ed.* **2013**, *52*, 8798–8809.

[23] H. Kelker, *Mol. Cryst. Liq. Cryst.* **1973**, *21*, 1–48.

[24] F. Reinitzer, *Liq. Cryst.* **1989**, *5*, 7–18.

[25] V. N. Kozhevnikov, B. Donnio, D. W. Bruce, *Angew. Chemie Int. Ed.* **2008**, *47*, 6286–6289.

[26] D. Vorländer, *Kristallinisch-Flüssige Substanzen*, Enke, Stuttgart, **1908**.

[27] S. Laschat, A. Baro, N. Steinke, F. Giesselmann, C. Hägele, G. Scalia, R. Judele, E. Kapatsina, S. Sauer, A. Schreivogel, et al., *Angew. Chemie Int. Ed.* **2007**, *46*, 4832–4887.

[28] S. Chandrasekhar, B. K. Sadashiva, K. A. Suresh, *Pramana* **1977**, *9*, 471–480.

[29] J. W. Goodby, I. M. Saez, S. J. Cowling, V. Görtz, M. Draper, A. W. Hall, S. Sia, G. Cosquer, S.-E. Lee, E. P. Raynes, *Angew. Chemie Int. Ed.* **2008**, *47*, 2754–2787.

[30] I. Dierking, A. Martins Figueiredo Neto, *Crystals* **2020**, *10*, 604.

[31] G. Tiddy, *Phys. Rep.* **1980**, *57*, 1–46.

[32] D. Lombardo, M. A. Kiselev, S. Magazù, P. Calandra, *Adv. Condens. Matter Phys.* **2015**, *2015*, 1–22.

[33] B.-S. Kim, D.-J. Hong, J. Bae, M. Lee, *J. Am. Chem. Soc.* **2005**, *127*, 16333–16337.

[34] R. Zana, *Dynamics of Surfactant Self-Assemblies*, CRC Press, **2005**.

[35] C. Fong, T. Le, C. J. Drummond, *Chem. Soc. Rev.* **2012**, *41*, 1297–322.

[36] Sandeep Kumar, *Chemistry of Discotic Liquid Crystals: From Monomers to Polymers*,

2011.

[37] J. W. Goodby, I. M. Saez, S. J. Cowling, in *Supramol. Chem.*, John Wiley & Sons, Ltd, Chichester, UK, **2012**.

[38] D. Vorländer, A. Apel, *Berichte der Dtsch. Chem. Gesellschaft (A B Ser.* **1932**, *65*, 1101–1109.

[39] T. Niori, T. Sekine, J. Watanabe, T. Furukawa, H. Takezoe, *J. Mater. Chem.* **1996**, *6*, 1231.

[40] C. Tschierske, G. Dantlgraber, *Pramana* **2003**, *61*, 455–481.

[41] R. A. Reddy, C. Tschierske, *J. Mater. Chem.* **2006**, *16*, 907–961.

[42] M. B. Ros, J. L. Serrano, M. R. de la Fuente, C. L. Folcia, *J. Mater. Chem.* **2005**, *15*, 5093.

[43] Link, Natale, Shao, Maclennan, Clark, Korblova, Walba, *Science* **1997**, *278*, 1924–7.

[44] B. R. Acharya, A. Primak, S. Kumar, *Phys. Rev. Lett.* **2004**, *92*, 145506.

[45] L. A. Madsen, T. J. Dingemans, M. Nakata, E. T. Samulski, *Phys. Rev. Lett.* **2004**, *92*, 145505.

[46] C. Destrade, P. Foucher, H. Gasparoux, N. H. Tinh, A. M. Levelut, J. Malthete, *Mol. Cryst. Liq. Cryst.* **1984**, *106*, 121–146.

[47] I. Fischbach, F. Ebert, H. W. Spiess, I. Schnell, *Chemphyschem* **2004**, *5*, 895–908.

[48] M. Lehmann, I. Fischbach, H. W. Spiess, H. Meiert, *J. Am. Chem. Soc.* **2004**, *126*, 772–784.

[49] S. Sergeyev, W. Pisula, Y. H. Geerts, *Chem. Soc. Rev.* **2007**, *36*, 1902.

[50] S. Kumar, *Chem. Soc. Rev.* **2006**, *35*, 83–109.

[51] S. Kumar, *Liq. Cryst.* **2009**, *36*, 607–638.

[52] S. Chandrasekhar, *Liq. Cryst.* **1993**, *14*, 3–14.

[53] T. Wöhrle, I. Wurzbach, J. Kirres, A. Kostidou, N. Kapernaum, J. Litterscheidt, J. C. Haenle, P. Staffeld, A. Baro, F. Giesselmann, et al., *Chem. Rev.* **2016**, *116*, 1139–1241.

[54] H. K. Bisoyi, S. Kumar, *Chem. Soc. Rev.* **2010**, *39*, 264–285.

[55] S. Kohmoto, E. Mori, K. Kishikawa, *J. Am. Chem. Soc.* **2007**, *129*, 13364–5.

[56] L. Y. Park, D. G. Hamilton, E. A. McGehee, K. A. McMenimen, *J. Am. Chem. Soc.* **2003**, *125*, 10586–10590.

[57] P. H. J. Kouwer, W. F. Jager, W. J. Mijs, S. J. Picken, *Macromolecules* **2001**, *34*, 7582–7584.

[58] P. H. J. Kouwer, S. J. Picken, G. H. Mehl, *J. Mater. Chem.* **2007**, *17*, 4196.

[59] S. Krishna Prasad, D. S. Shankar Rao, S. Chandrasekhar, S. Kumar, in *Mol. Cryst. Liq. Cryst.*, **2003**, pp. 121–139.

[60] C. Tschierske, *Angew. Chemie Int. Ed.* **2013**, *52*, 8828–8878.

[61] B. Donnio, B. Heinrich, H. Allouchi, J. Kain, S. Diele, D. Guillon, D. W. Bruce, *J. Am. Chem. Soc.* **2004**, *126*, 15258–15268.

[62] T. Yasuda, H. Ooi, J. Morita, Y. Akama, K. Minoura, M. Funahashi, T. Shimomura, T. Kato, *Adv. Funct. Mater.* **2009**, *19*, 411–419.

[63] T. Vlad-Bubulak, J. Buchs, A. Kohlmeier, M. Bruma, D. Janietz, *Chem. Mater.* **2007**, *19*, 4460–4466.

[64] J. Simmerer, B. Glüsen, W. Paulus, A. Kettner, P. Schuhmacher, D. Adam, K.-H. Etzbach, K. Siemensmeyer, J. H. Wendorff, H. Ringsdorf, et al., *Adv. Mater.* **1996**, *8*, 815–819.

[65] E. Fontes, P. A. Heiney, W. H. de Jeu, *Phys. Rev. Lett.* **1988**, *61*, 1202–1205.

[66] P. Davidson, M. Clerc, S. S. Ghosh, N. C. Maliszewskyj, P. A. Heiney, J. Hynes, A. B. Smith, *J. Phys. II* **1995**, *5*, 249–262.

[67] S. H. J. Idziak, P. A. Heiney, J. P. Mccauley, P. Carroll, A. B. Smith, *Mol. Cryst. Liq. Cryst. Sci. Technol. Sect. A. Mol. Cryst. Liq. Cryst.* **1993**, *237*, 271–275.

[68] K. Hatsusaka, K. Ohta, I. Yamamoto, H. Shirai, *J. Mater. Chem.* **2001**, *11*, 423–433.

[69] M. Ichihara, A. Suzuki, K. Hatsusaka, K. Ohta, *Liq. Cryst.* **2007**, *34*, 555–567.

[70] R. J. Bushby, O. R. Lozman, *Curr. Opin. Colloid Interface Sci.* **2002**, *7*, 343–354.

[71] T. Bjørnholm, T. Hassenkam, N. Reitzel, *J. Mater. Chem.* **1999**, *9*, 1975–1990.

[72] O. Karthaus, H. Ringsdorf, V. V. Tsukruk, J. H. Wendorff, *Langmuir* **1992**, *8*, 2279–2283.

[73] O. Y. Mindyuk, P. A. Heiney, *Adv. Mater.* **1999**, *11*, 341–344.

[74] S. Kurnar, *Chemistry of Discotic Liquid Crystals:From Monomers to Polymers*, CRC Press, New York, **2011**.

[75] V. C. Sundar, J. Zaumseil, V. Podzorov, E. Menard, R. L. Willett, T. Someya, M. E. Gershenson, J. A. Rogers, *Science* **2004**, *303*, 1644–1646.

[76] I. Kang, H. J. Yun, D. S. Chung, S. K. Kwon, Y. H. Kim, *J. Am. Chem. Soc.* **2013**, *135*, 14896–14899.

[77] M. Kim, S. U. Ryu, S. A. Park, K. Choi, T. Kim, D. Chung, T. Park, *Adv. Funct. Mater.* **2020**, *30*, 1904545.

[78] M. Nikolka, K. Broch, J. Armitage, D. Hanifi, P. J. Nowack, D. Venkateshvaran, A. Sadhanala, J. Saska, M. Mascal, S.-H. Jung, et al., *Nat. Commun.* **2019**, *10*, 2122.

[79] S. Kumar, *Chem. Soc. Rev.* **2006**, *35*, 83–109.

[80] T. Kato, M. Yoshio, T. Ichikawa, B. Soberats, H. Ohno, M. Funahashi, *Nat. Rev. Mater.* **2017**, *2*, 17001.

[81] W. Pisula, M. Zorn, J. Y. Chang, K. Müllen, R. Zentel, *Macromol. Rapid Commun.* **2009**, *30*, 1179–1202.

[82] H. Iino, J. Hanna, *Adv. Mater.* **2011**, *23*, 1748–51.

[83] T. Kato, *Science* **2002**, *295*, 2414–8.

[84] M. Muthukumar, C. K. Ober, E. L. Thomas, *Science* **1997**, *277*, 1225–1232.

[85] J.-M. (Jean-M. Lehn, *Supramolecular Chemistry : Concepts and Perspectives*, VCH, Weinheim, Germany, **1995**.

[86] T. Kato, N. Mizoshita, K. Kishimoto, **2006**, 38–68.

[87] T. Kato, *Liquid Crystalline Functional Assemblies and Their Supramolecular Structures*, Springer Berlin Heidelberg, Berlin, Heidelberg, **2008**.

[88] L. J. Prins, D. N. Reinhoudt, P. Timmerman, *Angew. Chemie Int. Ed.* **2001**, *40*, 2382–2426.

[89] J.-M. Lehn, *Science* **2002**, *295*, 2400–2403.

[90] J. C. MacDonald, G. M. Whitesides, *Chem. Rev.* **1994**, *94*, 2383–2420.

Chapter – 2

Rubicene, an Unusual Contorted Core for Discotic Liquid Crystals

Abstract

Rubicene, an unusual contorted polycyclic aromatic hydrocarbon, was realized to function as a novel core fragment for discotic liquid crystals. The central π-conjugated motif was prepared from dialkoxyiodobenzene via Sonagashira coupling, followed by pentannulation and Scholl cyclodehydrogenation. The synthesized rubicene derivatives were found to be thermally stable and exhibit enantiotropic columnar mesophases. The columnar arrangement of these derivatives has been validated using polarising optical microscopy, differential scanning calorimetry & small-angle X-ray scattering.

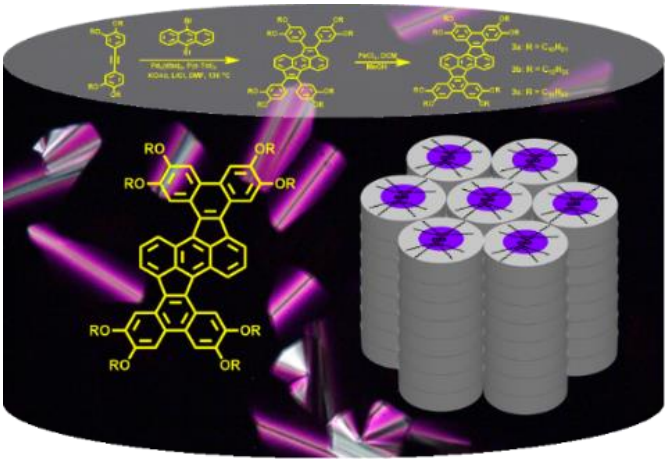

2.1 Introduction

Polycyclic aromatic hydrocarbons (PAHs) are unique compounds composed of fused conjugated aromatic rings with no heteroatoms or substituents.[1] These PAHs are mainly formed by incomplete combustion of carbon-containing fuels such as coal, diesel, wood, fat, tobacco, tar, etc. [2,3] Individual PAHs distributions vary depending upon combustion, which can lead to isomers. As a result, those created by coal combustion differ from those produced by motor fuel combustion and also distinct from those produced by forest fires. PAHs are two-dimensional graphite segments made up entirely of all-sp^2 carbons. These are divided into two categories: 1) light PAHs contain up to four rings, and 2) heavy PAHs exist as more than four rings. Due to the abundance of small PAHs, the majority of research has focused on those with up to six rings of PAH. Heavy PAHs are more stable and toxic than light PAHs. **Figure 2.1** depicts a few instances of well-known PAHs.

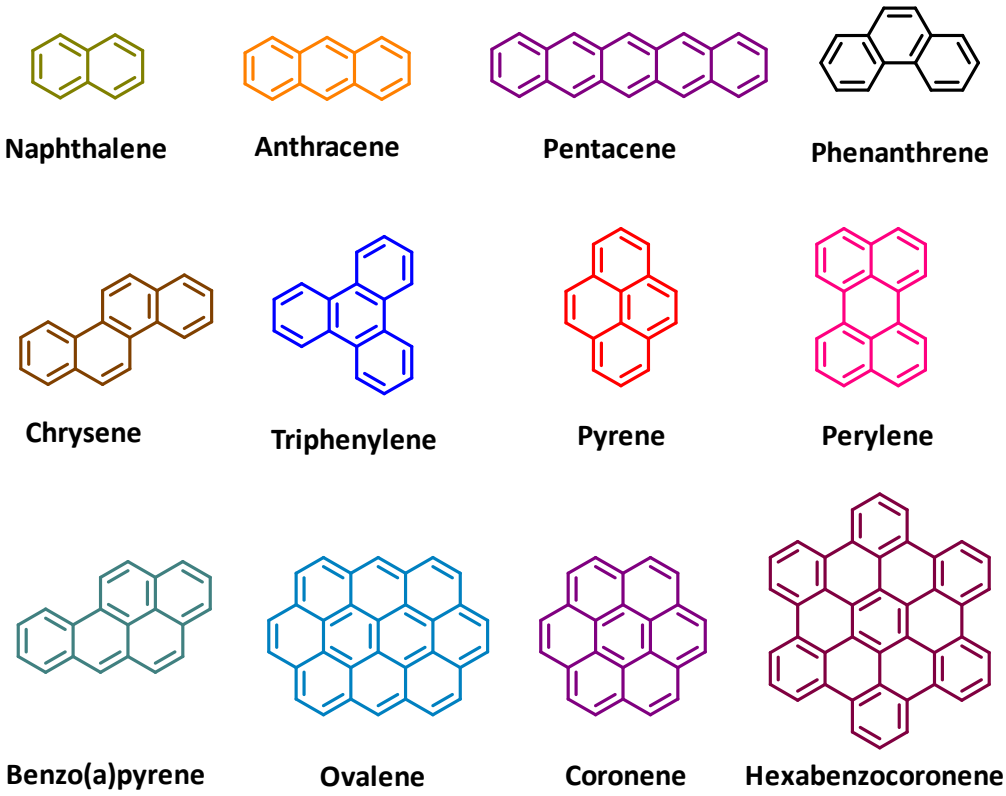

Figure 2.1: Examples of prominent PAHs.

Graphenes are 2D sheets constructed from extended PAHs motifs. These can be called graphene or graphitic segments, and these represent one of the most extensively studied compounds in synthetic chemistry and material science. Many scientists reported the systematic study on PAHs and their applications in material science. R. Scholl, E. Clar, and M. Zander made groundbreaking contributions to the guided synthesis and characterization of polycyclic aromatics using oxidation reaction.[4–6] Advances in analytical techniques aided the development of synthetic technology, allowing for the selective synthesis of various PAHs under benign conditions.[7]

One of the distinct properties of PAHs is aromaticity. This property has attracted many researchers in theoretical chemistry,[8] using different theoretical methods to find out the electronic properties of graphite based on PAHs with increasing size and varying topologies. PAHs' electronic and optoelectronic properties have received immense interest in organic semiconductors. Substitution of hydrogen, alkyl, and different functional groups on small and large PAH molecules leads to excellent electronic properties. These can be used in various organic electronic devices such as light-emitting diodes (LEDs), field-effect transistors (FETs), photovoltaic cells, and sensors.

Intensive efforts have been made for the rational design of new soft materials in order to create highly efficient, economically processable organic semiconductors. To achieve quick response in devices, researchers are focusing on improving the charge transport properties of these materials[9]. However, the main challenge is to find out the sophisticated balance between mobility and the processibility of semiconductor materials. Some examples have been reported in the literature for their high mobility using single crystals.[10] Still, it has disadvantages like inadequate solubility, low purity, structural and energetic disorder, limiting their usability in devices. Similar observations have been observed in polymeric systems.[11,12] The current research has concentrated on small organic molecules to answer these issues, which can be free of defects, solution-processed films with high chemical purity.

In this regard, material researchers are currently interested in designing and synthesizing soft materials like discotic liquid crystalline (DLCs) materials, which consist of the central aromatic core and are surrounded by flexible alkyl chains. The central aromatic cores are rigid. It leads

to crystalline packing, and flexible aliphatic chains cause a liquid-like nature. These two non-compatible parts lead to microphase segregation, which shows the mesomorphic property. The spontaneous self-assembly of rigid aromatic cores in one-dimensional stacks of columns, owing to strong π–π interactions of polycyclic aromatic cores (PAC), exhibits one-dimensional charge and energy transport. Most of the discotic liquid crystals self-assemble into columnar and nematic mesophase. This supramolecular columnar architecture provides the balance between mobility and processability. Several approaches have been reported in the literature to achieve the charge carrier mobility, such as increasing the intra columnar order within the disks, including directional H-bonding interactions in the cores, and so on. Another approach to increase charge carrier mobility is the alignment of columns macroscopically in one direction to the substrate surface. Many review articles have extensively summarized the discotic liquid crystals chemistry, self-organization, and applications.[13–22] Literature reports suggest that about sixty central cores have been exploited to prepare about 3000 discotic liquid crystals. Most of these are electron-rich (p-type semiconductors) materials. We have reported some of the new discotic liquid crystals, based on decacyclene,[23] tricycloquinazoline,[24] dibenzo[g,p]-chrysene,[25] phenanthro[a]- and phenanthro[b]-phenazines,[26,27] as a central core. As described above, the extensive π-π interactions between the cores facilitate the columnar organization. The larger aromatic core may enhance columnar stability and influence their charge transport properties.[28] The literature reports suggest most of the reported central cores are flat-shaped and exhibit liquid crystalline behavior on functionalization with flexible tails[29]. Some of the flat-shaped discotic cores are given in **Figure 2.2.** Along with flat-shaped cores, some twisted molecules also exhibit liquid crystalline properties. These contorted polycyclic aromatic molecules have rarely been explored for liquid crystalline properties.

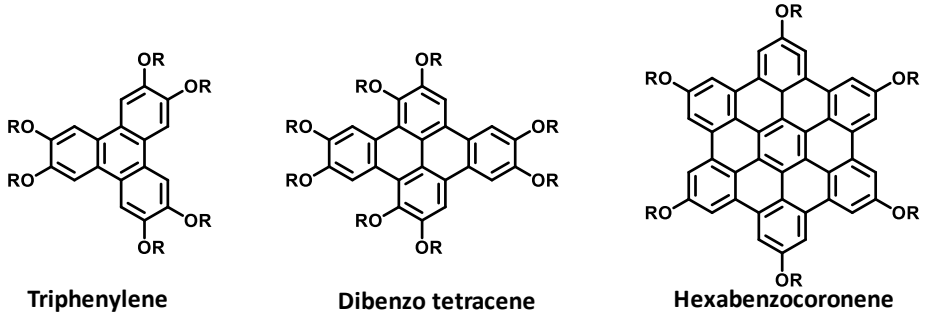

Figure 2.2: Examples of Sheet-shaped discotic liquid crystals.

Here we focus on the design, synthesis, and self-assembly of molecular materials made from strained polycyclic aromatic molecules. The aromatic molecules are substantially distorted away from planarity due to the tension in the molecular subunits. These molecules are contorted (away from the planarity or contain a twist). The main advantage of the contorted molecules is the consequences on the material's essential physical characteristics. Compared to flat aromatics, the intermolecular interactions in crystals and polycrystalline films are more varied. Hence, their charge transport properties in organic materials-based devices can be improved. Also, it offers solubility benefits, spontaneous aggregation, solution-based processing of materials. In addition, nonplanar molecules exist in the form of a concave surface that can recognize the convex surfaces of the fullerene. They help to construct atomically specified p-n junctions in organic photovoltaics because of this manner of self-assembly. Benzophenanthrene is one of the best examples of contorted molecules, also known as [4]-helicene. It is a nonplanar molecule with a splay angle of 19.9° and a barrier for inversion between the two helices of 7.6 kcal/mol. Benzophenanthrene structure and the isomers are shown in **Figure 2.3**, along with helicene nonplanar molecules. Over the last decade, there have been numerous reports in the literature on distorted PAH's synthesis and physical characteristics. Some of the contorted molecules are shown in **Figure 2.4**.

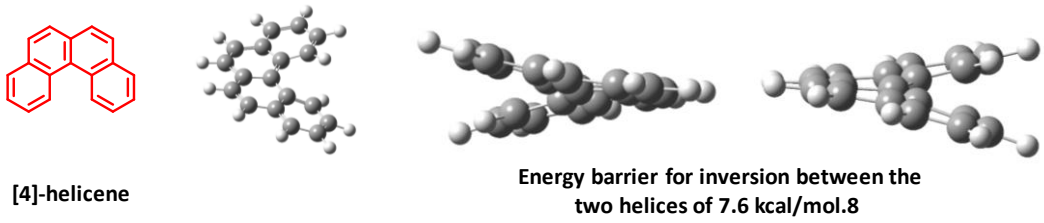

Figure 2.3: [4]-helicene and it's M and P isomers.

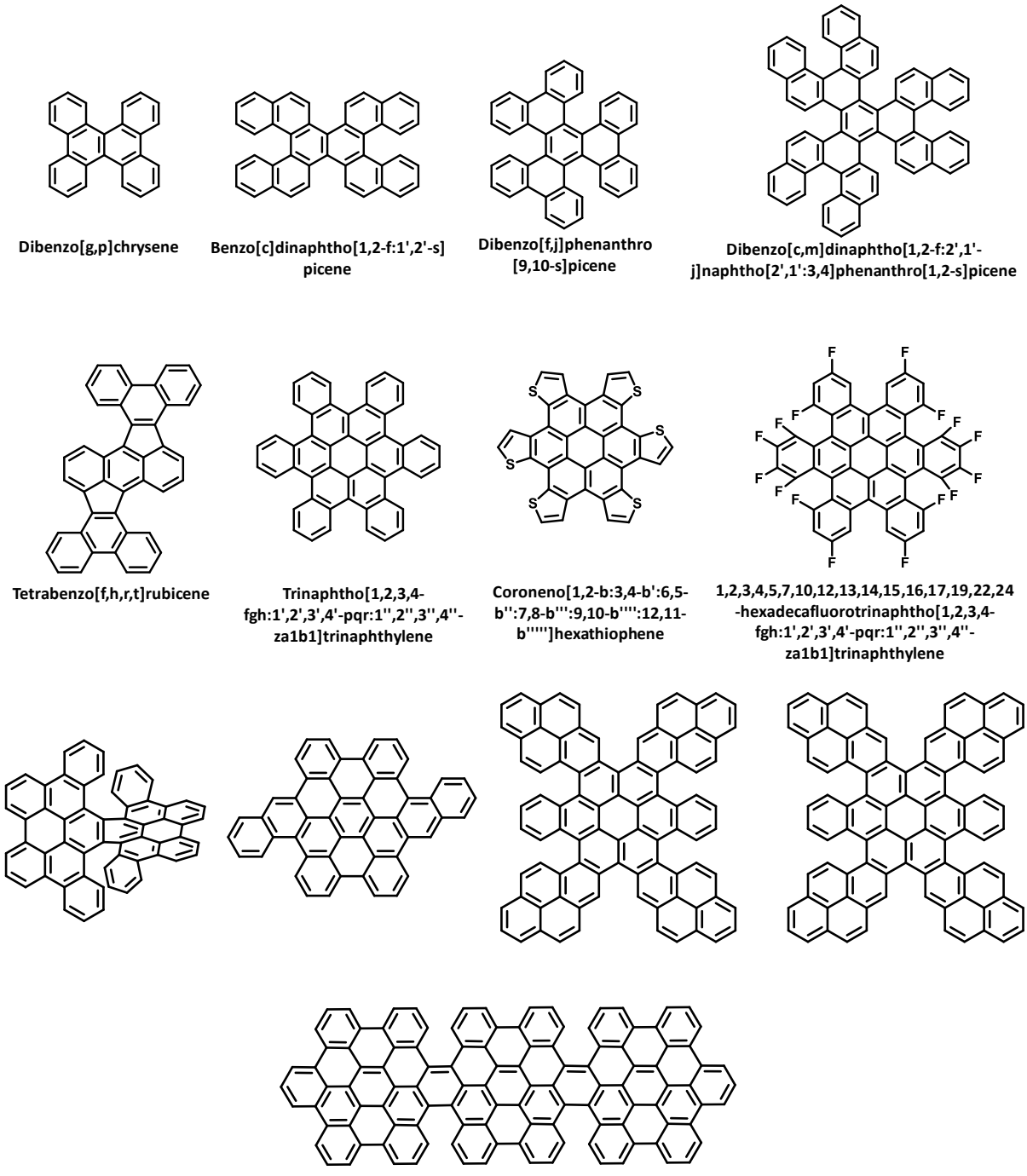

Figure 2.4: Some of the examples of contorted molecules.

Among the various contorted molecules, very few have been explored in the liquid crystals field, and they have been used in optoelectronic devices, and some of the examples have been mentioned here. Kumar et al. have reported the dibenzo[g,p], shown in **Figure 2.5**. These molecules are not perfect for exhibiting the columnar mesophase. However, charge transfer complexation with an electron acceptor TNF (2,4,7-Trinitro-9H-fluorine-9-one) immediately induces the columnar mesophase.[25] Afterward, Takazoi group have reported a series of chiral and achiral octaalkoxydibenzo[g,p]chrysene derivatives and studied their mesomorphic properties.[30] In **Figure 2.6**, they have shown the energy minimized structure that exhibits the flat molecule from the top view, and the side view of the molecule clearly shows the propeller structure. The propeller structure of the core could be the reson why the octasubstituted ether derivatives are non-mesogenic. According to these two reports, the molecule appears to be nonchiral. Takezo and co-workers reports quantum chemical calculations of dibenzo[g,p]chrysene, which exists in the form of a propeller-like twist, and it is a more stable conformation. They have concluded that this molecule is chiral and confirmed the chiral property using quantum calculations and vibrational ECD spectra[31]. The energy diagram for the transition of two chiral conformations and ECD spectra in the columnar phase at room temperature is shown in **Figure 2.7.**

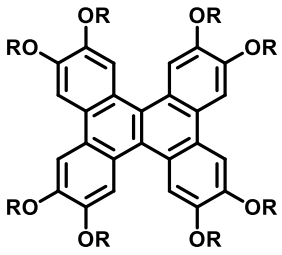

R = C_5H_{11} and C_8H_{17}

Figure 2.5: Octaalkoxydibenzo[g,p]chrysene derivatives

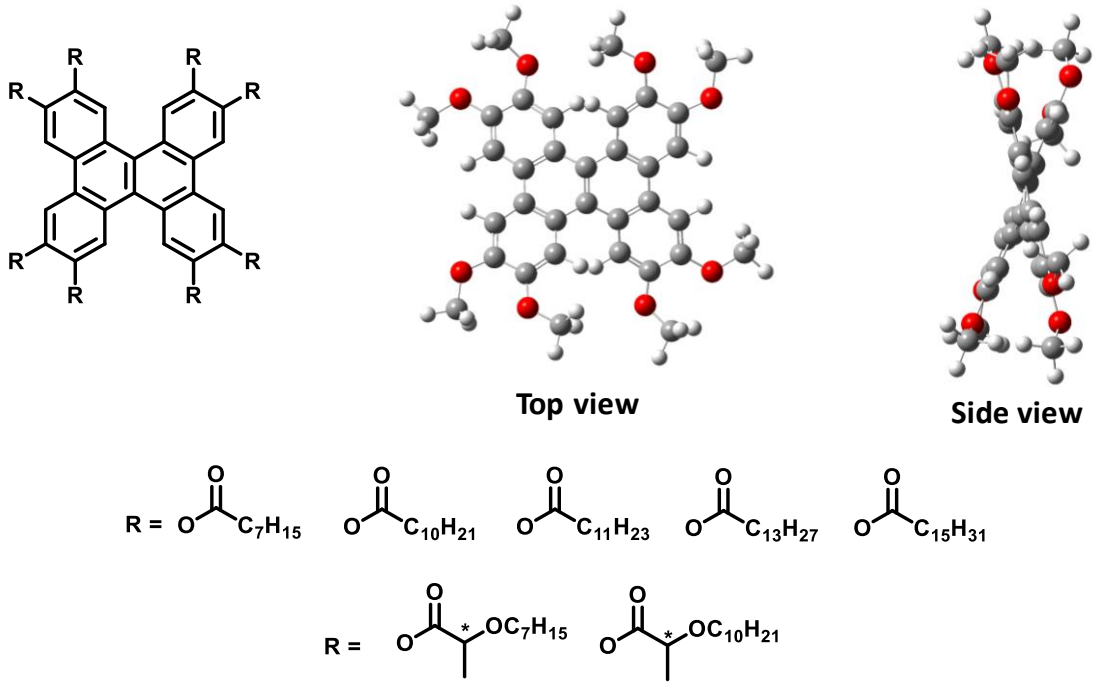

Figure 2.6. Octafunctionalised benzo[g,p]chrysene derivatives.

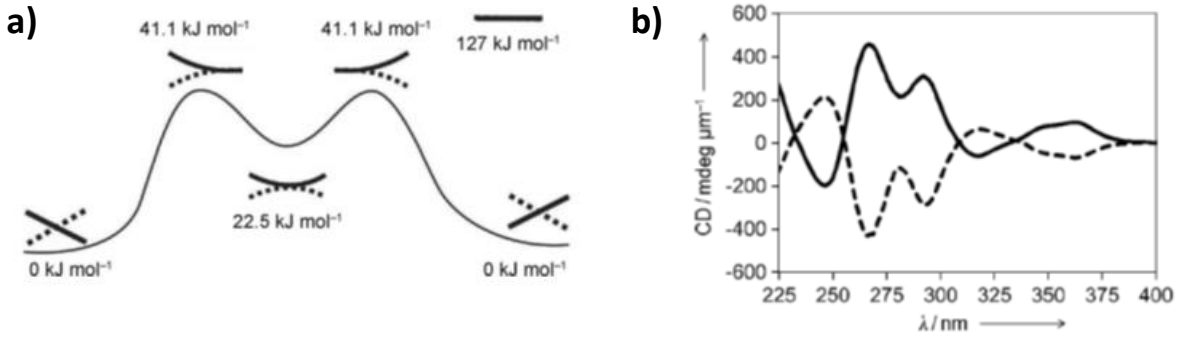

Figure 2.7: a) Energy diagram for the transition of two chiral conformations. b) ECD spectra in the columnar phase at room temperature.

Thomas J. Katz et al. reported the non-racemic helicene-based liquid crystals exhibiting the hexagonal columnar mesophase at room temperature. The structure non-racemic helicene is shown in **Figure 2.8a**.[32] The mesophase was confirmed using X-ray diffraction. The columnar organization was established using circular dichroism, specific rotations, fluorescence emission shifts, and ^{1}H NMR shieldings. Afterward, Thomas J. Katz and his group have reported electro-optical studies using helicene-dodecane mixtures. They have found that at a

concentration of < 5 vol%, it shows the columnar hexagonal liquid crystalline phase, and at >30 vol%, it shows the discotic nematic liquid crystalline phase with positive dielectric anisotropy. The POM images are shown in **Figures 2.8b** and **c**.[33] They also looked at the aggregation of a conjugated helical molecule[34] and macroscopic liquid crystalline fibers, which are made up of 50-200 nm wide and barely 10 nm tall layers.[35]

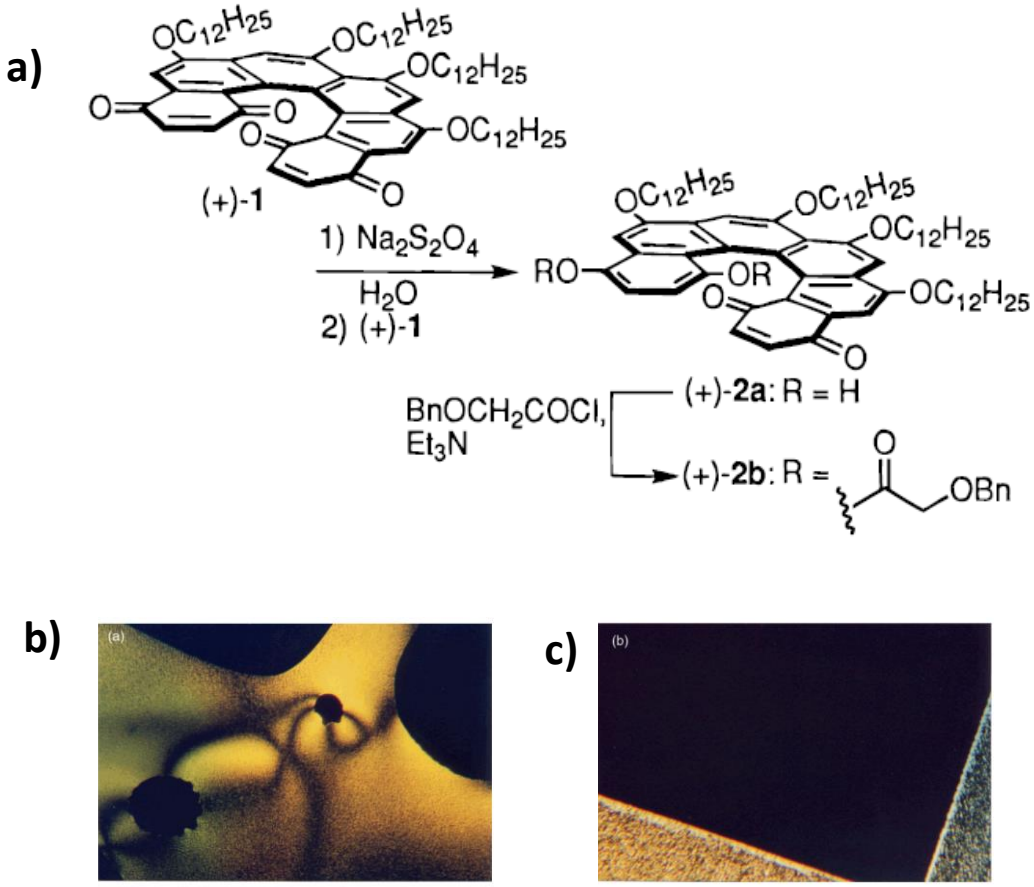

Figure 2.8: a) Synthesis of non-racemic helicene liquid crystals **b)** POM image of compound **2b** cooled from the clearing temperature **c)** POM image of 17 wt % solution of 2b in dodecane.

Colin Nuckolls and his group have reported that a new class of nonplanar hexabenzocoronene can form the columnar liquid-crystalline phases with proper substitution.[36] The molecular structure is shown in **Figure 2.9a**. The three pentacene moieties present in the molecule lead to the contorted system are shown in **Figure 2.9b.** They have studied the electrical properties of hexabenzocoronene in thin-film transistors. Here the mobility values are much higher than

those of flat hydrocarbons since the π surfaces of constrained molecules can approach and arrange themselves in various ways. These molecules tend to align parallel to the surface, which was confirmed using POM (**Figure 2.9c).** The same group has synthesized the octa-substituted derivatives of the HBCs, shown in **Figure 2.10a.** This material self-assembles into molecular stacks. Further, these stacks organize into cables or fibers. These self-organized individual fibers are placed in the device using elastomer, as shown in **Figures 2.10b** and **2.10c.**

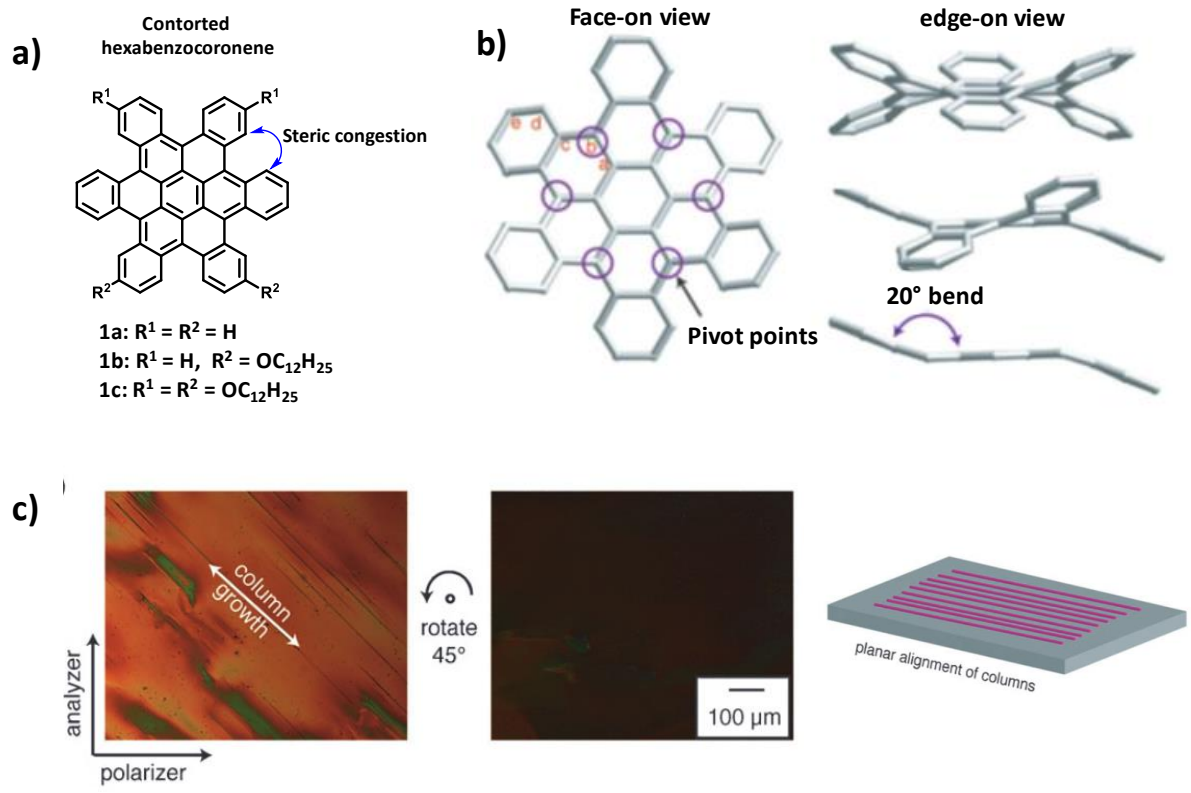

Figure 2.9: a) Molecular structure of hexabenzocoronene **b)** Crystal structure of **1a c)** POM image of compound **2b** cooled from the clearing temperature **c)** POM image of **1c,** which shows the planar alignment under cross polarizers and schematic representation of columns aligned to the surface.

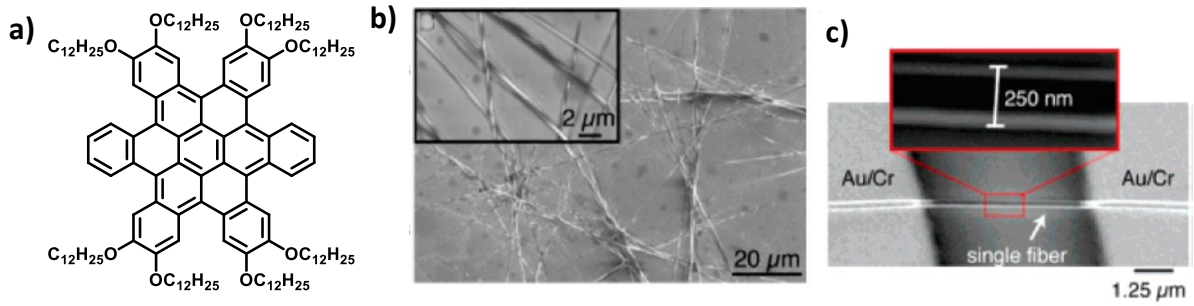

Figure 2.10: a) Molecular structure of octa-substituted hexabenzocoronene **b)** SEM images of octa-substituted HBC into nanoscale cables **c)** An elastomeric stamp could be used to place individual cables into devices.

The same group looked into making effective field-effect transistors out of polycyclic aromatic hydrocarbon monolayers that can sense and respond to their chemical environment. As we mentioned above, liquid crystalline characteristics and self-assembly of distorted molecules have been reported in the literature, and also it has a great interest in materials science due to their structural variety[37] and unique optical, electronic[38], and photophysical properties[39] with excellent intermolecular charge transport.[40–42] In the literature, co-assembly involving curved π-fused systems and electron-deficient systems displays a promising photovoltaic effect have been reported.[43–45] The contorted π-conjugated molecules have been identified as ideal receptors of molecular recognition.[46] Rubicene ($C_{26}H_{14}$) is an aromatic polycyclic hydrocarbon consisting of five benzene rings with three linearly fused rings, and one benzene ring at each diagonal side as shown in **Figure 2.11a.**[47,48] Rubicene is a promising organic semiconductor material with strong electrical properties in organic field-effect transistors.[49] Also, rubicene has a red hue, yellow fluorescence, a high rate of intersystem crossing (ISC),[50] and electrochemically generated luminescence.[51] It can be used as a chemical sensor for metal cations,[52] and extensively studied in optoelectronics and organic lasers diodes.[53] Adolf Winkler and his group reported and studied the film growth of the conjugated organic molecule rubicene on silicon dioxide. The schematic representation of rubicene on silicon dioxide is shown in **Figure 2.11b**. It is a planar molecule[54], but substitution's steric effect can lead to the contorted structure.[55] Several research groups have synthesized rubicene derivatives using different methods,[56–59] and in recent years, cyclo pentannulation has been extensively used to

synthesize the rubicene derivatives. Many research groups reported many rubicene derivatives as mentioned below using cyclo pentannulation followed by Scholl dehydrogenation.

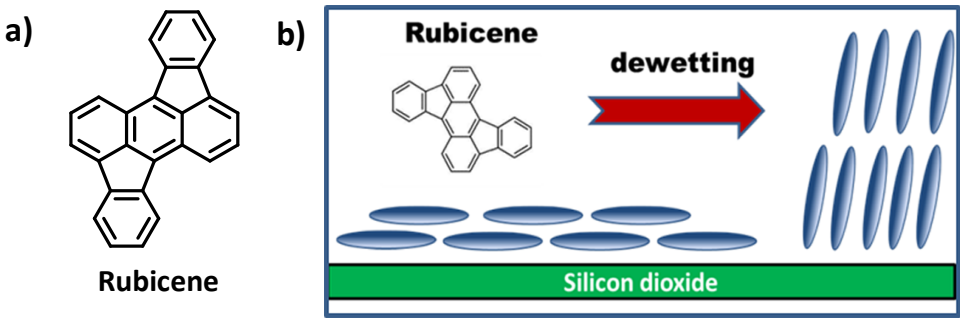

Figure 2.11: a) Structure of rubicene **b)** Rubicene on silicon dioxide

Rai-Shung Liu and his group synthesized the dibenzo rubicene and tetrabenzo rubicene using the annulation reaction are shown in **Figure 2.12**. and also studied their photophysical and electronic properties.[60]

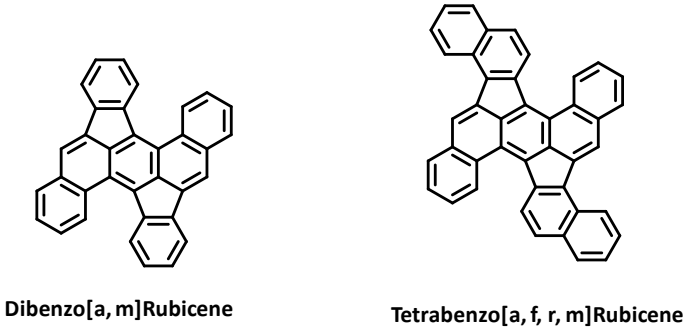

Figure 2.12: Structure of Dibenzo[a,m]rubicene, Tetrabenzo[a,f,r,m]Rubicene

Klaus Mullen and his group demonstrate (**Figure 2.13**.) an efficient bottom-up strategy toward a novel bowl-shaped polycyclic aromatic hydrocarbons (PAH) C_{34} with two pentagons. These bowl-shaped molecules are a fragment of the fullerene C_{70} containing two five-membered rings. By using single-crystal X-ray, dynamic NMR, UV-vis absorption, and CV analyses, the geometric and optoelectronic character of the resulting buckybowl is thoroughly explored.[61]

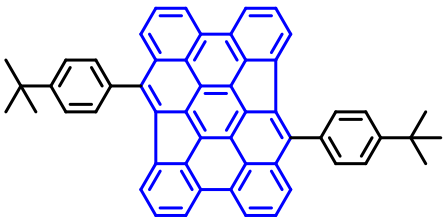

Figure 2.13: Structure of 4,11-bis(4-(tert-butyl)phenyl)dinaphtho[1,2,3,4,5-ijklm:1',2',3',4',5'-uvwxa]rubicene

Kyle N. Plunkett and his group reported the first cyclopentannulation-based rubicene compounds using dibromoanthracene and dibromopyrene. **Figure 2.14** depicts a new class of contorted polycyclic aromatic hydrocarbons (PAHs) with five-membered rings that emerged in 2015. The [4] helicene and [5] helicene fragments are present in these compounds. The compound-containing [5] helicene fragments form a twisted shape, and [4] helicene fragments form a planar structure. Planar and twisted structures were confirmed by X-ray crystallography.[62]

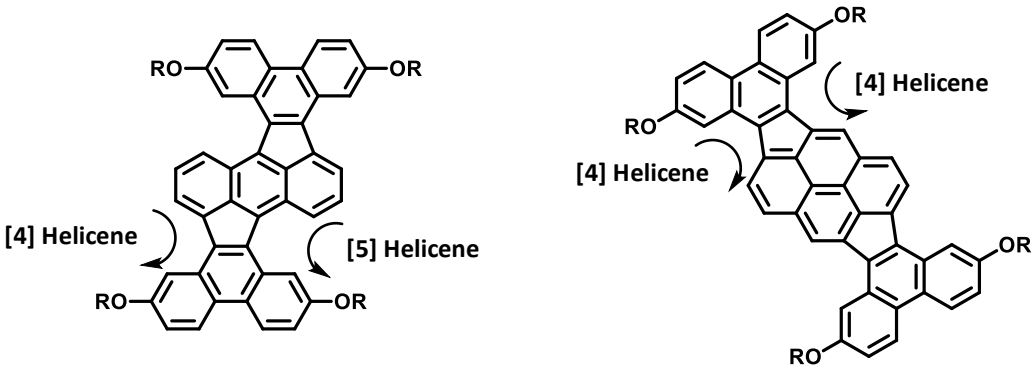

Figure 2.14: Structure of rubicene derivatives synthesized from anthracene and pyrene.

In 2018, the same group reported the contorted aromatics with large splay angles, low optical gaps, and low LUMOs. This molecule was prepared using 5,11-dibromo-2,8-dihexylanthra[2,3-b:76-b0]dithiophene treated with disubstituted alkyne using cyclopentannulation reaction. A subsequent Scholl cyclodehydrogenation reaction resulted in constrained aromatics and was studied using X-ray diffraction. The constrained chemical structure is shown in **Figure 2.15**.[63]

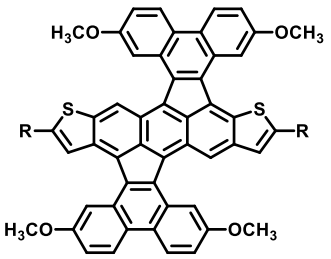

R= C_6H_{13}

Figure 2.15: Chemical structure of 2,14-dihexyl-5,10,17,22 tetramethoxytetrabenzo [4,5:6,7:11,12:13,14]rubiceno[2,3-b:10,9-b']dithiophene.

A new class of CP-PAHs with benzodithiophene appendages is shown in **Figure 2.16**. Anthracene, pyrene, and perylene dibromo derivatives undergo a simple metal-catalyzed cyclopentannulation reaction with 1,2-bis(5-hexylthiophen- 3-yl)ethyne. These products can be further converted via a Scholl cyclodehydrogenation reaction to get the contorted structures. These newly synthesized CP-PAHs have broad absorbance, low LUMOs, and twisted structures. Among these three compounds, when examined in an organic field-effect transistor, the anthracene-based CP-PAH was shown to be a p-type semiconductor.[64]

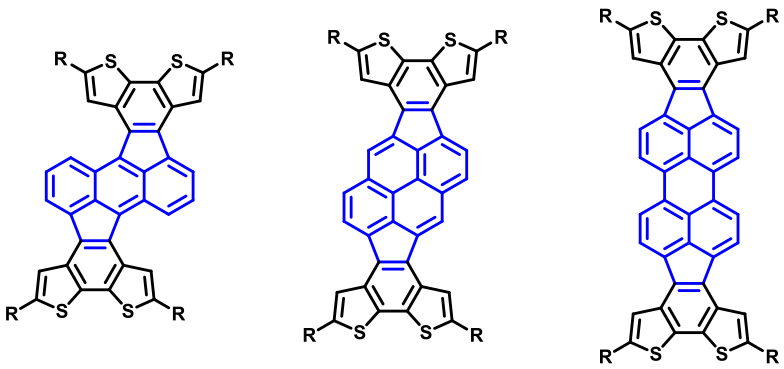

Figure 2.16: Chemical structure of new cyclopenta-fused polyaromatic hydrocarbon (CP-PAH) incorporating fused benzodithiophene subunits.

The rubicene based polymers using pentannulation have shown their immense potential in organic thin-film transistors (OTFTs) in recent years, and also low bandgap polymers were synthesized using cyclopentannulation. Kyle N. Plunkett and his colleagues also described a unique approach for synthesizing D−A copolymers (**Figure 2.17)** through a

postpolymerization cyclopentannulation of poly(arylene ethynylene)s. The polymer backbone undergoes significant structural changes due to the palladium-catalyzed annulation, which has low bandgaps and LUMO values that are low lying.[65]

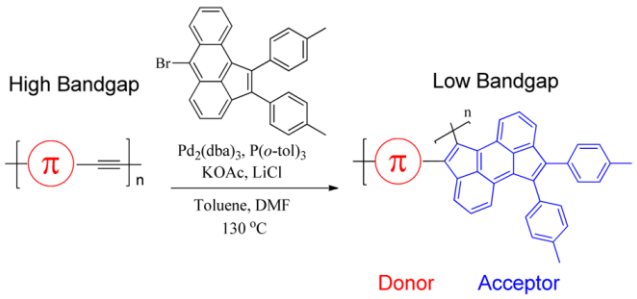

Figure 2.17: Synthetic route for D−A copolymers.

The same group has shown a novel synthetic approach for obtaining sophisticated rigid ladder polymers from simple, widely available, and non-metallated monomers are shown in **Figure 2.18**. The complex of donor-acceptor type polymers with relatively high molecular weights is produced by palladium-catalyzed annulation chemistry, which can be further treated with $FeCl_3$ to synthesize rigid ladder-type polymers. The resultant polymers have minimal optical gaps, low LUMO levels, and p-type semiconductors in OFETs.[66]

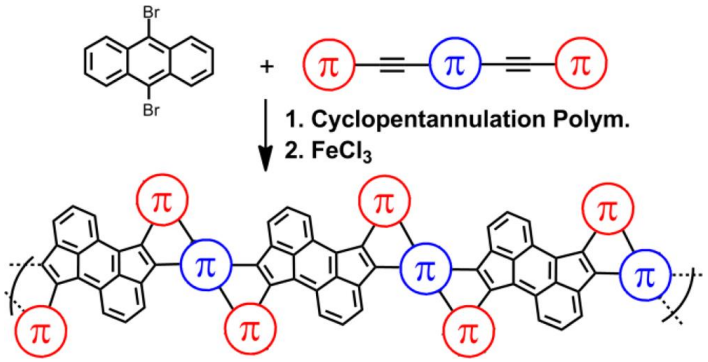

Figure 2.18: Structure of rigid ladder polymer.

Surprisingly, no liquid crystalline analog of the rubicene molecule has been developed so far. Substituted rubicene has a contorted core that is semiconducting and has a wide range of uses, as noted previously. Although its derivatives could be used as advanced materials in optoelectronics, the field of DLCs has yet to be investigated. The molecular structure and unique photophysical properties of rubicene prompted us to explore it as a central core to

prepare various novel DLCs. Here, we report the synthesis of a series of rubicene based discotic liquid crystals by varying the alkoxy chains in the periphery of the rubicene core as shown in **Figure 2.19a**. These derivatives self-assemble into columnar hexagonal mesophase. The columnar hexagonal arrangement of these derivatives can be attributed to π – π interactions between the rubicene cores.

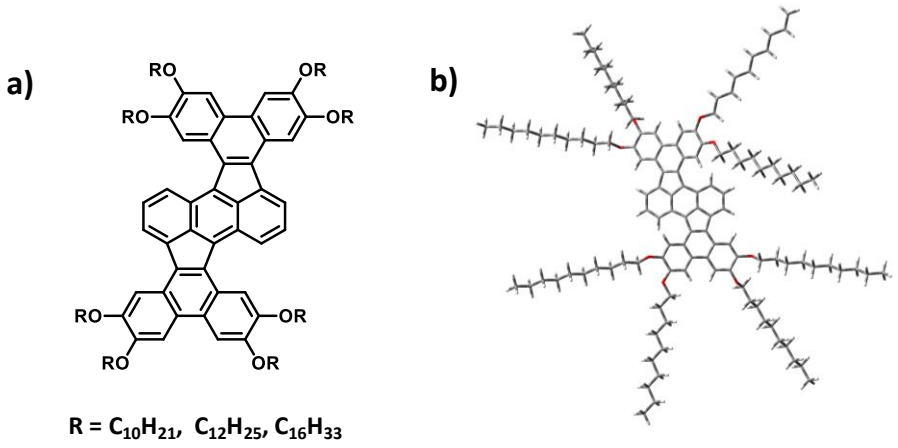

Figure 2.19: a) Structure of rubicene derivatives **7a-c** b) Energy minimized structure of **7a**.

2.2. Results and discussion:

2.2.1 Synthesis:

The synthetic route of all the intermediates and final compounds is shown in **Scheme 1.** The disubstituted alkynes were prepared from dialkoxyiodobenzene via Sonogashira coupling using the reported literature[67]. The synthesis of prefinal (**6a-c**) and final compounds (**7a-c)** was achieved via palladium-catalyzed pentannulation followed by Scholl cyclodehydrogenation. Pentannulation of 9,10-dibromoanthracene with 1,2-bis(3,4-bis(alkoxy)phenyl) ethyne to give 1,2,6,7-tetrakis(3,4-bis(alkoxy)phenyl) cyclopenta [hi] aceanthrylene. To close the fused aryl groups, we used Scholl cyclodehydrogenation, resulting in a satisfactory yield of 2,3,6,7,13, 14, 17, 18-octakis(alkoxy)-tetrabenzo [f, h, r, t]-rubicene (70 to 80%). The final compounds show the arrangement of the fused ring system with two [4] helicene-like and two [5] helicene-like fragments that resembled the previous report.[68] The purity and structure of all the compounds were characterized by ^{1}H NMR, ^{13}C NMR, MALDI-TOF, and elemental analysis, which were in good consent with the molecular structure.

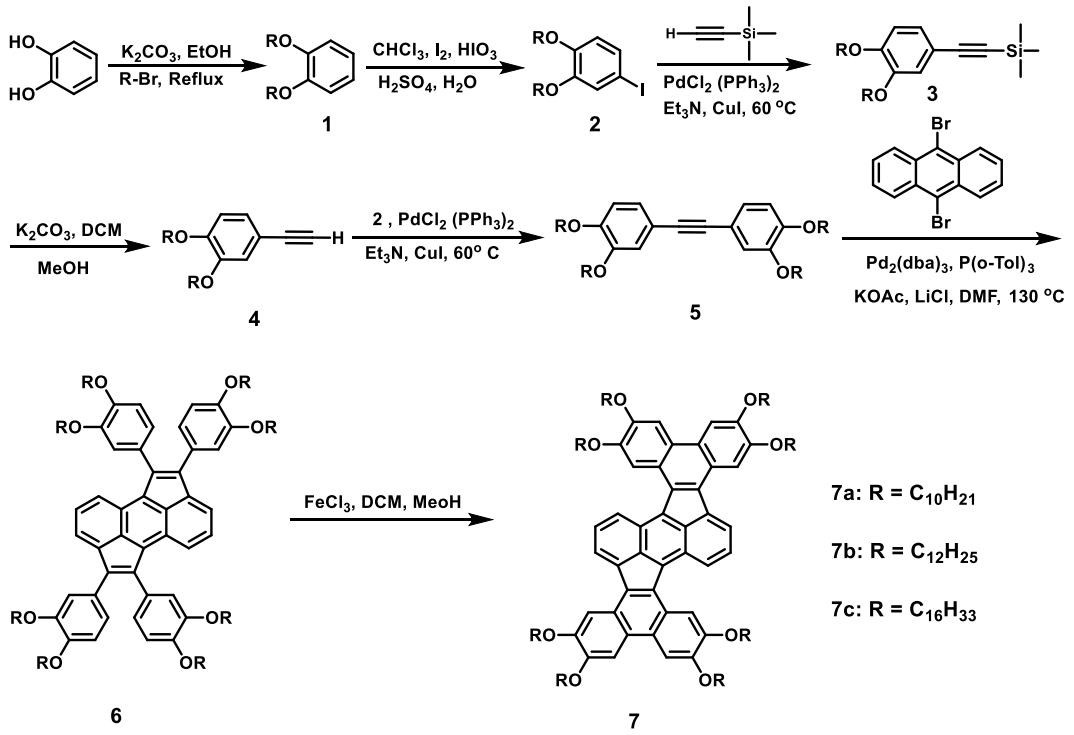

Scheme 1: Synthesis of rubicene derivatives.

2.2.2 Density functional theory studies:

We have studied the energy minimized structure of substituted rubicene using density functional theory (DFT) calculations done by GAUSSIAN-09 program at the Becke's three-parameter functional and Lee, Yang, and Parr correlation functional (DFTB3LYP) by using 6-31G (d, p) as basis set. The energy minimized structure is given in **Figure 2.19b.** The energy minimized structure had [4] helicene-like and [5] helicene-like fragments, and the splay angels that is, the dihedral angle (a-b-c-d) = A= 5.67, A' = 3.42, and (e-f-g-h) = B = 41.07, B' = 42.25 of **7a** were calculated from energy minimized structure**.** The top view and side view of energy minimized structure are shown in **Figure 2.20.** We concluded that the rubicene core has a twisted confirmation based on energy minimized structure deduced from DFT calculations**.** Further, we have visualized the contour plots of the highest occupied molecular orbital (HOMO), and the lowest unoccupied molecular orbital (LUMO) are shown in **Figure 2.21**. The energy gap was found to be around 2.23 eV. The optical band gap (Eg) in eV was calculated to be 1.56 (according to the equation Eg = 1240 / λ_{onset}, where λ_{onset} was resolved as the intersection of the extrapolated tangent of the longest wavelength absorption peak and the x-axis).

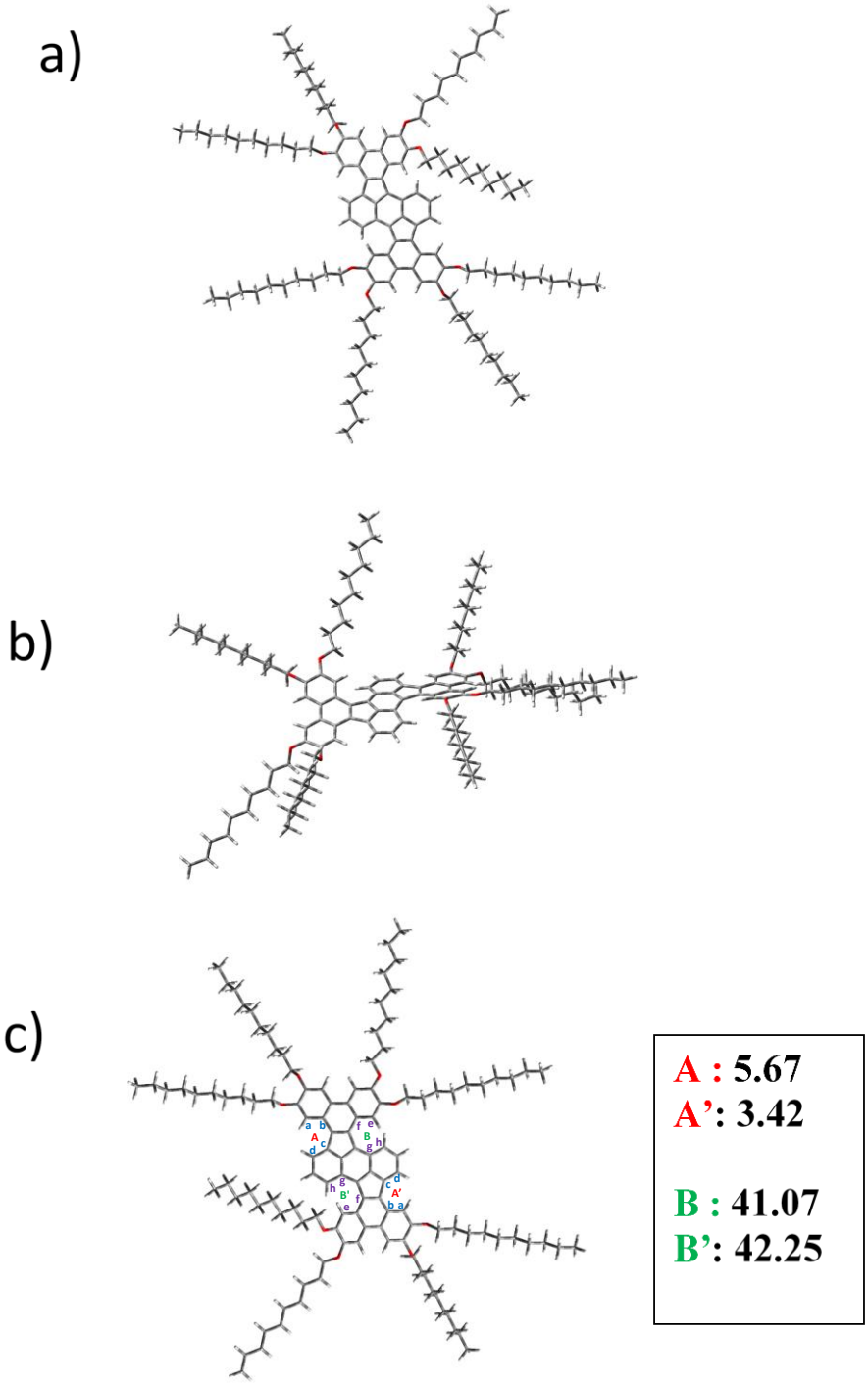

Figure 2.20: Energy-minimized structure of rubicene derivative **7a** at the **B3LYP / 6-31g (d, p)** level. **a)** Top view **b)** Side view **c**) top view with splay angles.

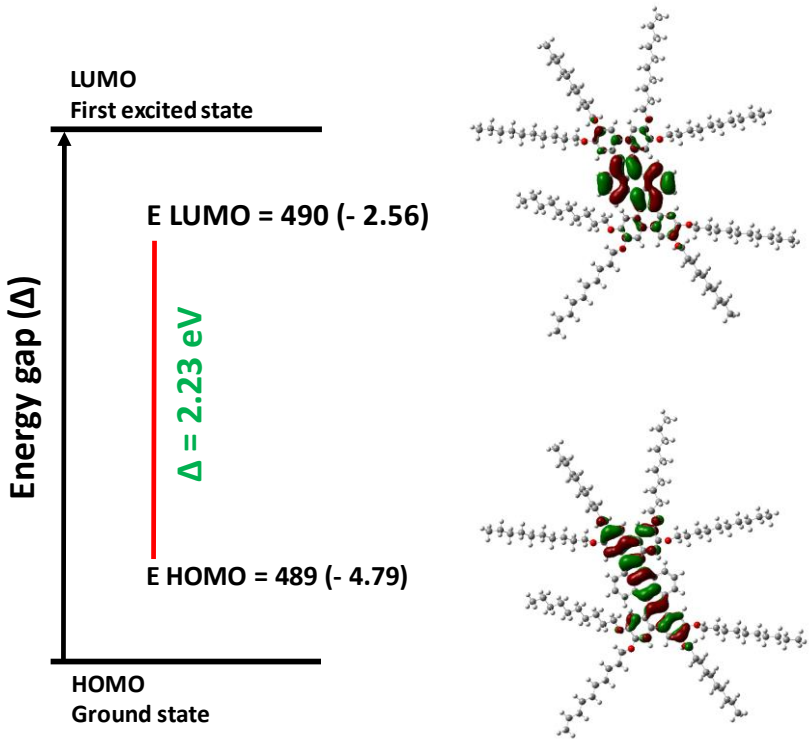

Figure 2.21: HOMO and LUMO contours of rubicene derivative **7a** calculated using **B3LYP** employing the **6-31G(d)** basis set.

2.2.3 Optical properties:

The optical properties (absorption and emission) of **7a-c** recorded in chloroform solution (3 x 10^{-6} M) are shown in **Figure 2.22**. Absorption spectra shows broad absorption peaks extending from 200 nm to 800 nm with prominent absorption features at 263 nm, 295 nm, 360 nm, 400 nm, 545 nm, 676 nm and 739 nm. Emission spectra exhibited a less intense shoulder peaks at 468 nm and two intense vibrationally resolved peaks at 411 nm, and 434 nm for **7a** (λ_{ex} = 360 nm, ε_{360nm} = 1.85 X 10^4 M^{-1} $cm^{-1)}$, **7b** (λ_{ex} = 360 nm, ε_{360nm} = 1.96 X 10^4 M^{-1} cm^{-1}), and **7c** (λ_{ex} = 360 nm, ε_{360nm} = 2.23 X 10^4 M^{-1} $cm^{-1)}$. The Stokes shift of 51 nm was observed between the absorption and emission maxima of **7a, 7b** and **7c.**

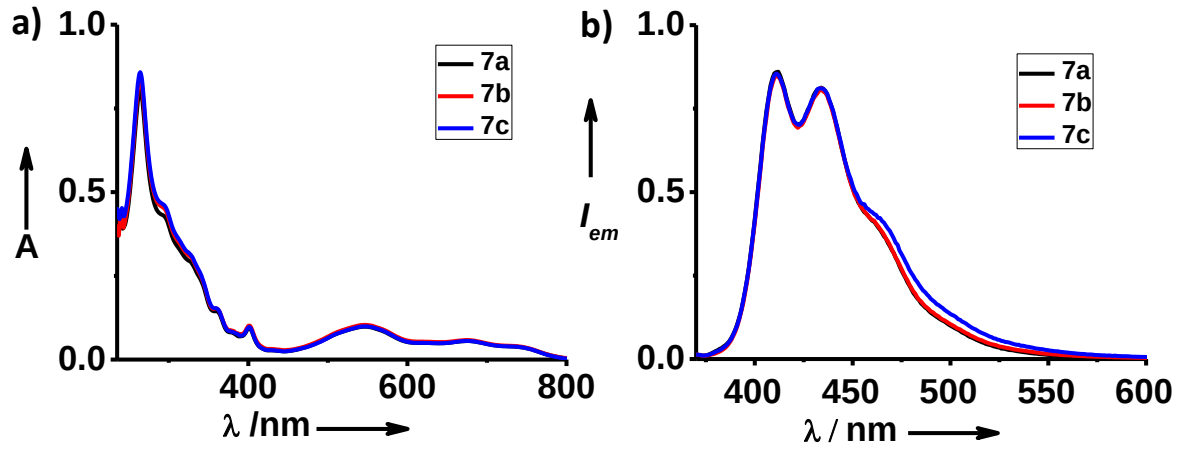

Figure 2.22: Absorption a) and emission b) spectra of **7a, 7b** and **7c**.

2.2.4 Thermal Stability:

The thermal stability of all liquid crystalline compounds was investigated using thermal gravimetric analysis. All the three compounds are (**7a-c**) placed in a heat scan of 10 °C min^{-1} under a nitrogen atmosphere. Compounds **7a**, **7b,** and **7c** show no weight loss up to 350 °C and the initial weight loss was observed at 370 °C. The thermal stability was studied till 800 °C, as shown in **Figure 2.23.** The decomposition temperature of these DLCs materials is much higher than the isotropic temperatures. It shows that these rubicene derivatives show excellent thermal stability.

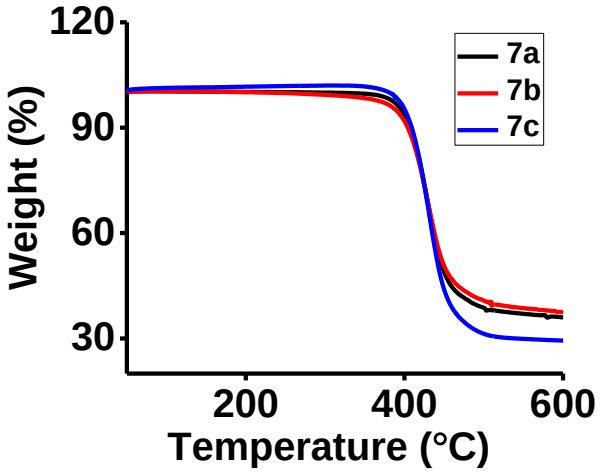

Figure 2.23. TGA spectra of **7a-c** show good thermal stability of the three compounds.

2.2.5 Mesomorphic characteristics:

The monotropic mesomorphic properties of the compounds **6a-c** were determined using a combination of polarized optical microscopy (POM) and differential scanning calorimetry (DSC). Under POM, upon heating, the compounds **6a-c** became isotropic at 81.5 ºC, 91.0 ºC, and 95.2 ºC, respectively. While cooling from the isotropic phase, the mesophase displays typical mosaic textures of a columnar phase, with the magnifications of 500x are shown in **Figure 2.24.** The phase transition temperatures of the liquid crystalline compounds observed under POM were validated using DSC measurements. Upon heating, for compounds **6a** and **6c**, crystal-crystal transitions was observed at 48.2 ºC and 53.7 ºC and became isotropic at 79.0 ºC and 92.0 ºC respectively. The isotropic temperature of compound **6b** was found to be 84.8 ºC. After cooling from the isotropic phase, the columnar phase transition appears for compounds **6a-c** at 64.9 ºC, 61.8, and 51.8 ºC, respectively. Compound **6c** crystallizes at 43.8 ºC. However, **6a** and **6b** compounds remained in mesophase down to room temperature. The DSC thermograms of **6a-c** are given in **Figure 2.25**. The phase transition temperatures and corresponding enthalpy values of all compounds are shown in **Table 2.1**

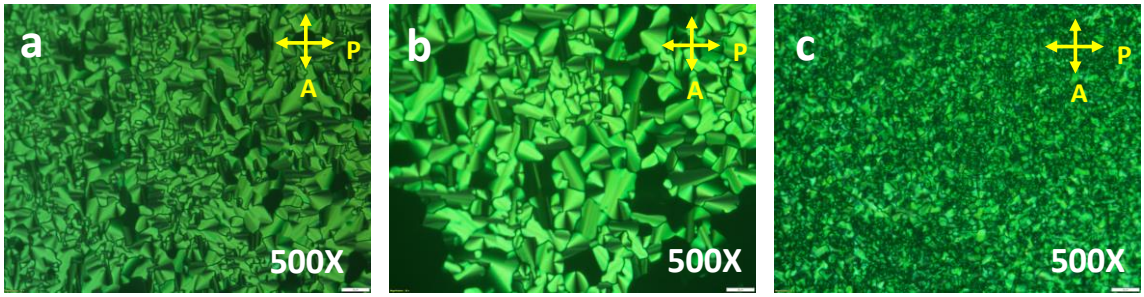

Figure 2.24. Mosaic textures were observed under POM for a compound a) **6a** at 50 °C**;** b) **6b** at 42 °C; and c) **6c** at 49 °C

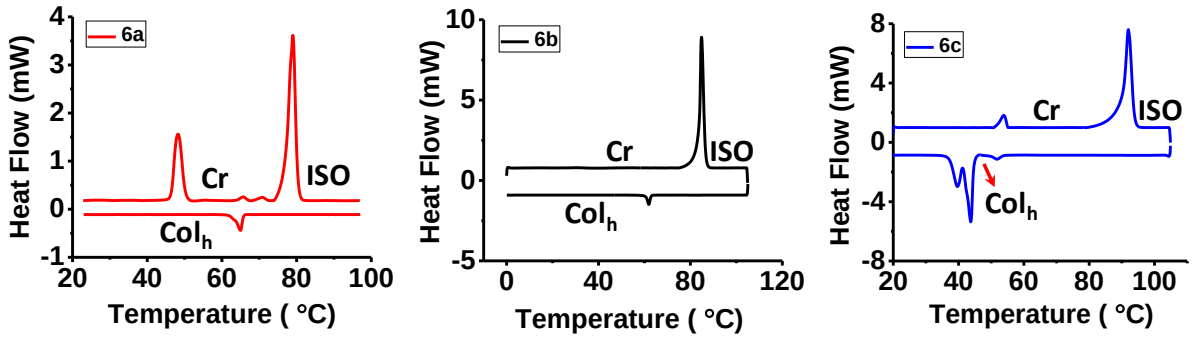

Figure 2.25. DSC thermograms were obtained for **6a-c** on heating and cooling cycles at a scan rate of 5 °C/min

Table 2.1. Phase transition temperatures (in ºC) and enthalpy changes (J g $^{-1}$) of **6a**, **6b** and **c** in the time of heating and cooling.

Cr – Crystalline phase; Col_h – Columnar hexagonal phase; I – Isotropic

Compound	Heating	Cooling
6a	Cr 79.0 (41.0) I	I 64.9 (3.2) Col_h
6b	Cr 84.8 (53.7) I	I 61.8 (2.6) Col_h
6c	Cr 92.0 (66.0) I	I 51.8 (2.0) Col_h 43.8 (47.5) Cr

The mesophase features of synthesized rubicene derivatives were investigated using polarized optical microscopy (POM), differential scanning calorimetry (DSC), and X-ray diffractometry. All the compounds exhibit enantiotropic mesomorphism with typical mosaic textures of a columnar phase under crossed polarizers upon cooling from the isotropic phase. The POM images of **7a**, **7b,** and **7c** recorded at 150.2 °C, 182 °C, and 120.2 °C, respectively, with the magnifications of 200x are shown in **Figure 2.26.** The polarized optical microscopy images revealed that these materials tend to orient columns vertically (homeotropically aligned) to the surface. The homeotropic alignment of the columns is essential for device applications.

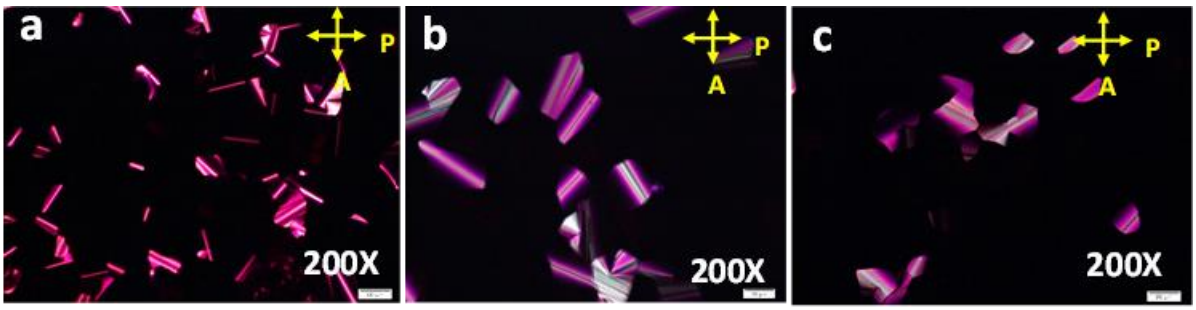

Figure 2.26: Mosaic textures were observed under POM for a compound a) **7a**; b) **7b**; and c) **7c**.

The differential scanning calorimetry (DSC) analysis was carried out to validate the phase transitions observed through POM. The compounds **7a**, **7b**, and **7c** exhibited two endothermic phase transitions on heating. At lower temperatures, compound **7a** melts at 100.3 °C, **7b** melts at 77.0 °C and **7c** melts at 41.4 °C, correspond to the crystal to mesophase transition. At higher temperatures, the isotropic (clearing) transitions were found to be around 207.7 °C, 189.1 °C, and 172.6 °C for **7a**, **7b**, and **7c**, respectively. Upon cooling from the isotropic liquid state to room temperature, compounds **7a**, **7b** and **7c** exhibited a small exothermic peaks at 207.7 °C, 184.7 °C and 170.9 °C, respectively which corresponds to the transitions from the isotropic liquid to the liquid crystalline phase. On further cooling, these materials crystallise at -26.1 °C (**7a**), 0.2 °C (**7b**), and 37.6 °C (**7c)**. The DSC thermograms of **7a-c** are given in **Figure 2.27**. The phase transition temperatures and corresponding enthalpy values of all compounds are shown in **Table 2.2**

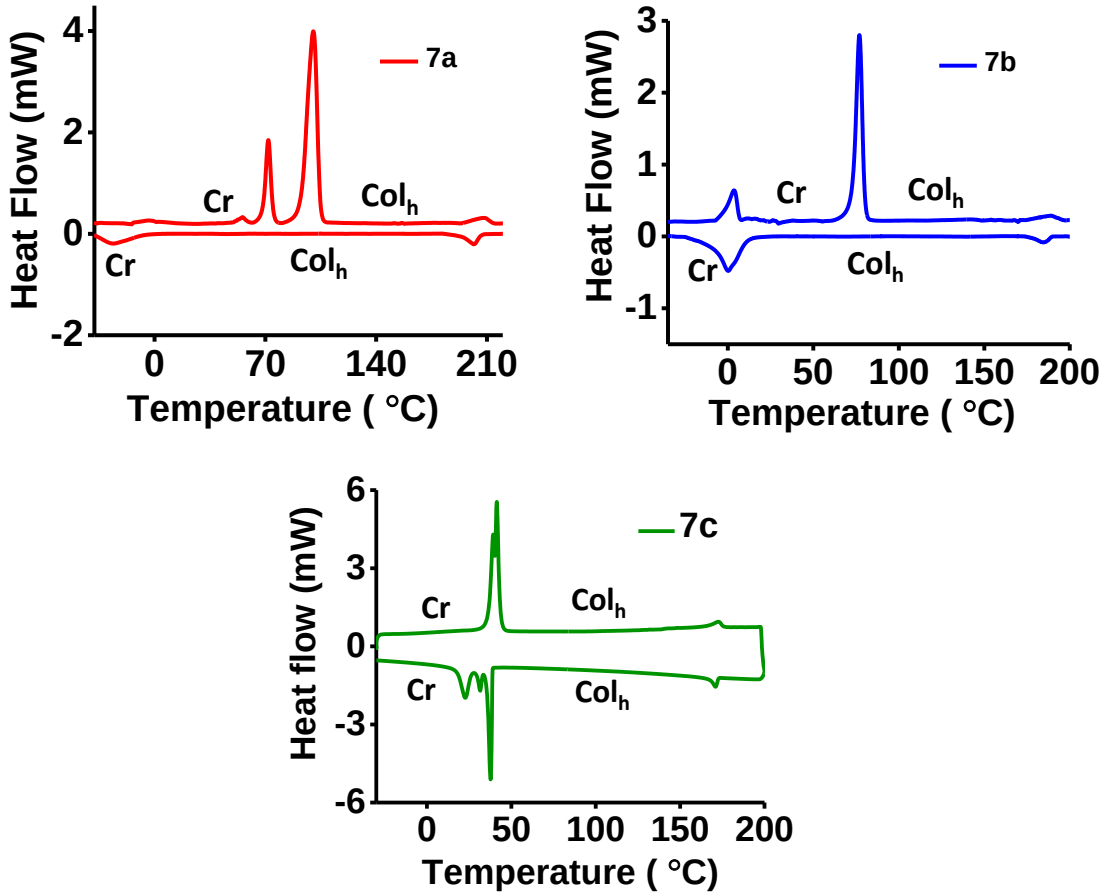

Figure 2.27: DSC thermograms were obtained for **7a-c** on heating and cooling cycles at a scan rate of 10°C/min.

Table 2.2. Phase transition temperatures (in ºC) and enthalpy changes (J g $^{-1}$) of **7a**, **7b** and **7c** in the time of heating and cooling.

Cr – Crystalline phase; Col_h – Columnar hexagonal phase; I – Isotropic

Compound	Heating	Cooling
7a	Cr 100.3 (55.8) Col_h 207.7 (2.5) I	I 207.7 (2.6) Col_h -26.1 (2.4) Cr
7b	Cr 77.0 (42.4) Col_h 189.1 (1.5) I	I 184.7 (1.4) Col_h 0.2 (17.2)Cr
7c	Cr 41.4 (55.5) Col_h 172.6 (2.9) I	I 170.9 (2.9) Col_h 37.6 (48.7) Cr

Further elucidation of the mesophases of **7a-c** was carried out using X-ray diffraction (XRD) studies. Diffraction patterns of **7a**, **7b** and **7c** compounds at a few temperatures are given in **Figure 2.28**. All the compounds are found to exhibit the hexagonal columnar (Col_h) phase as evident from the presence of sharp peaks in the small-angle region, whose spacings (d) are in the ratio 1: 1/√3: 1/2: 1/√7. In the wide-angle region, the diffraction patterns show two broad peaks at d = 4.50 Å and d = 3.61 Å, corresponding to the molten alkyl chains and the core-core separation along the column axis, respectively. The lattice parameter (a) is 31.32 Å, 33.77 Å and 37.35 Å for **7a, 7b** and **7c**, respectively. From the lattice parameter, the number of molecules spanning each column is estimated to be 1. Observed spacings in the mesophase of the three compounds are given in **Table 2.3.** A schematic of the molecular arrangement in columnar hexagonal mesophases deduced from the diffraction data is shown in **Figure 2.29.**

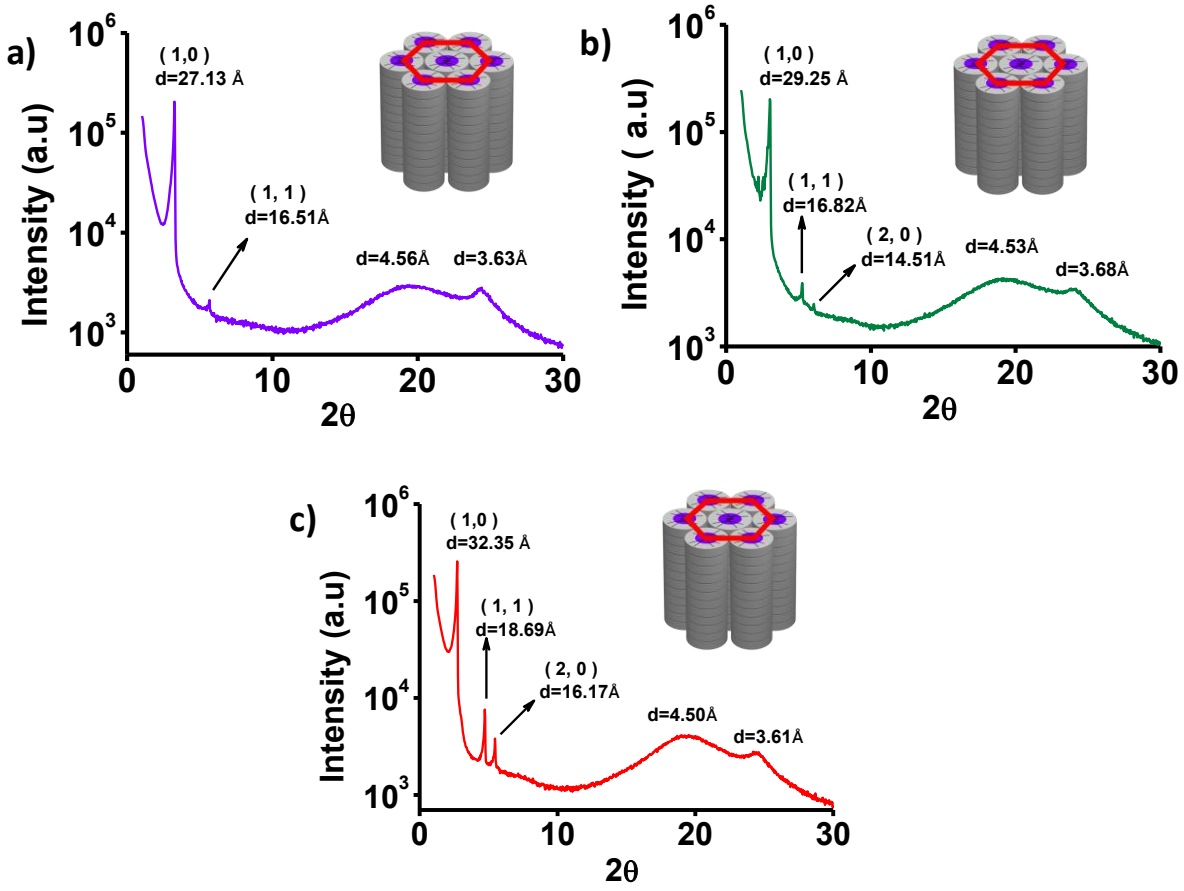

Figure 2.28: The one-dimensional intensity versus 2θ profile is derived from X-ray diffraction. **a) 7a** at 105 ºC, **b) 7b** at 140 ºC and **c) 7c** at 90 ºC**.**

Table 2.3. Layer spacing obtained from XRD for **7a, 7b,** and **7c. (a** = lattice parameter = √ (4/3) × d_{10}; lattice area $S_h = a^2\sin60^o$; lattice volume $\mathbf{V_h} = a^2 \sin60^o \times h_c$ (**h_a** if **h_c** is not observed); No of molecules per slice of column (**Z**) = $(\sqrt{3}\times N_a \times P \times a^2 \times h)/2M$; $\mathbf{N_a}$ = Avogadro number; **P** = Density in Kg/m^3; **a**=lattice parameter; **h_c**=core core peak (**h_a** if core core is not observed); **M** = molecular weight in Kg/m^3).

Compounds	**T (°C)**	**d-spacing(Å)**	**Phase**	**Parameters**
7a	105	27.13(10), 15.55 (11), 4.56, 3.63	Col_h	**a** = 31.32 Å **S_h** =849.521 $Å^2$ **V_h** = 3083.76$Å^3$ **Z** =1.04

7b	140	29.25 (10), 16.82 (11), 14.51 (20) 4.53, 3.68	Col_h	**a** = 33.77Å $\mathbf{S_h}$ =987.626 $Å^2$ $\mathbf{V_h}$ = 3634.46 $Å^3$ **Z** =1.09
7c	90	32.35 (10), 18.69 (11), 16.17 (20), 4.5, 3.61	Col_h	**a** = 37.35 Å $\mathbf{S_h}$ = 1208.12 $Å^2$ $\mathbf{V_h}$ = 4361.31 $Å^3$ **Z** =1.07

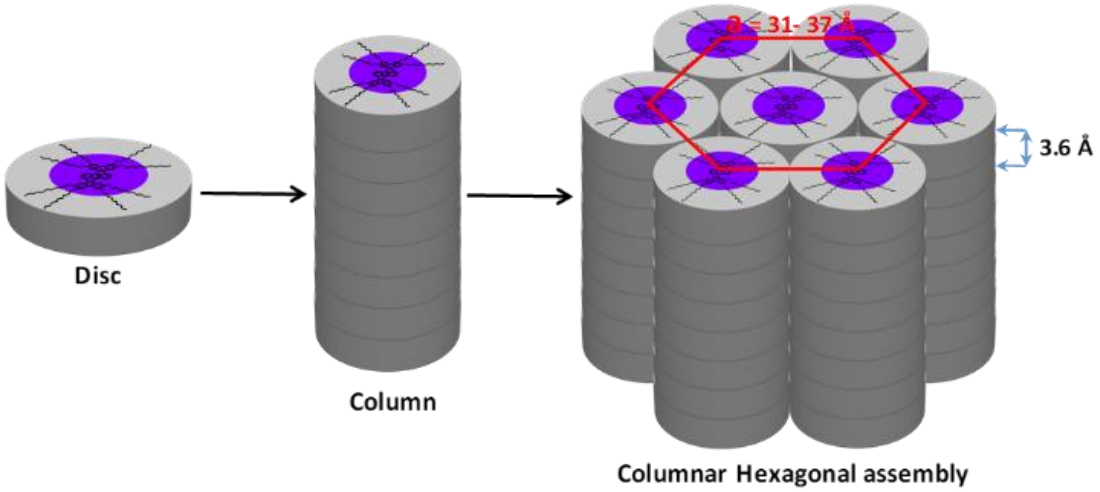

Figure 2.29: Schematic representation of the self-assembled columnar hexagonal mesophase in rubicene discotic mesogens.

2.3. Conclusions:

In summary, we discovered that rubicene, a contorted molecule displays liquid crystalline properties upon appropriate peripheral substitution. Three new compounds have been prepared and they all show hexagonal columnar phase with a wide range of temperatures. Here our theoretical studies (Gaussian) suggested that rubicene derivatives employed twist structure where the difference in the splay angels results in a contorted arrangement. All three compounds reveal excellent thermal stability, and POM confirms the formation of the aligned structures. These aligned materials with interesting optical properties are highly attractive for various device applications such as photovoltaic solar cells, light-emitting diodes, etc. The device fabrication and studies on the liquid crystalline nature of other rubicene derivatives are under progress.

2.4 Experimental section:

Materials and Methods

All the chemicals and reagents are AR-grade quality and purchased from Sigma-Aldrich, TCI, Spectrochem, Avara. The solvents were dried and distilled using standard protocols. The intermediate and final compounds were purified by column chromatography using silica gel (100–200) mesh and recrystallization from the suitable solvent. The spectral and elemental analysis confirmed the structure and purity of all compounds. ^{1}H Nuclear magnetic resonance spectroscopy (NMR) and ^{13}C NMR were recorded on Bruker 500 MHz machine using deuterated chloroform ($CDCl_3$) as a solvent, and chemical shifts are recorded in ppm from tetramethylsilane as internal standard ($CDCl_3$: ^{1}H NMR: $\delta = 7.23$; ^{13}C NMR = 77.0). Data were reported as: s = singlet, d = doublet, t = triplet m = multiplet, bd = broad doublet. Elemental analysis was carried out using Elementary Vario MICRO Select instrument. The microscopic textures were recorded on a sample placed between ordinary glass slides using an Olympus BX51 polarising optical microscope (Olympus, Tokyo, Japan) in conjunction with Mettler FP82HT hot stage and Mettler FP90 central processor. The phase transition temperature and associated enthalpies of the liquid crystalline samples were determined by the Mettler Toledo DSC instrument using 2–4 mg samples and a scan rate of 10°C min^{-1}. Further detailed examination of liquid crystalline mesophase structure is done by X-ray diffraction using Panalytical (Empyrean) Cu-Kα (1.54 Å) X-ray diffractometer. Thermal stability was established by the Perkin Elmer TGA4000 analyzer. UV-Vis Spectra was measured by Thermo Scientific™ NanoDrop 2000c. Emission spectra were recorded by Cary Eclipse fluorescence spectrophotometer. Mass spectra were recorded on Bruker Daltonics flexAnalysis.

2.5 Synthesis and characterization:

Synthesis and Characterization of Rubicene Core Liquid Crystal

7a, 7b, 7c were synthesized in multistep reactions as shown in Fig. S1[62,66,69,70]. All the final products and intermediates were purified and characterized by various spectroscopic techniques like IR, ^{1}H NMR, ^{13}C NMR, and elemental analysis.

General Procedure for the synthesis of 1a, 1b & 1c.

In a round bottom flask, 1,2- dihydroxy Benzene (Pyro Catechol) (1eq) was dissolved in ethanol / DMF, K_2CO_3 (6eq) was added to it and stirred for 15 minutes. 1-Bromo Alkane (2.2 eq) was added to it, and the mixture was refluxed overnight. Then it was cooled to room temperature, and ethanol/DMF was evaporated. The reaction mixture was extracted with $CHCl_3$ organic layer was dried over anhydrous Na_2SO_4, and the solvent was evaporated. The crude product was purified by column chromatography using petroleum ether and dichloromethane as eluent and dried under a high vacuum to get the desired product.

Compound 1a: 1,2- dihydroxy Benzene (10g, 90.82 mmol, 1eq), ethanol 500 mL, K_2CO_3 (75.31g, 544.95mmol, 6eq), 1-Bromo decane (44.19g, 199.81 mmol, 2.2eq) Yield: 83% ; M.P. 39 ºC; ^{1}H NMR (500 MHz, $CDCl_3$): δ (ppm) = 0.90 (t, *J* = 7.0 Hz, 6H), 1.29 – 1.38 (m, 24H), 1.45 – 1.51 (m, 4H), 1.80 – 1.86 (m, 4H), 4.01 (t, *J* = 6.50 Hz, 4H), 6.91 (s, 4H); ^{13}C NMR (125 MHz, $CDCl_3$): δ ppm = 14.14, 22.72, 26.09, 29.39, 29.48, 29.63, 29.68, 31.95, 69.29, 114.13, 121.01, 149.27; Elemental analysis: C, 79.94; H, 11.87 calculated (%): C, 79.88; H, 12.29 (expt. %).

Compound 1b: 1,2- dihydroxy Benzene (10g, 90.82mmol, 1eq), ethanol 500 mL, K_2CO_3 (75.31g, 544.95mmol, 6eq), 1-Bromo dodecane (49.30g, 199.81mmol, 2.2eq) Yield: 90% ; M.P. 45 ºC; ^{1}H NMR (500 MHz, $CDCl_3$): δ (ppm) = 0.88 (t, *J* = 7.0 Hz, 6H), 1.26 – 1.34 (m, 32H), 1.43 – 1.49 (m, 4H), 1.78 – 1.83 (m, 4H), 3.98 (t, *J* = 6.5 Hz, 4H), 6.88 (s, 4H); ^{13}C NMR (125 MHz, $CDCl_3$): δ ppm = 14.12, 22.71, 26.07, 29.38, 29.46, 29.65, 29.67, 29.72, 31.94, 69.31, 114.17, 121.01, 149.27; Elemental analysis: C, 80.65; H, 12.18 calculated (%): C, 80.46; H, 12.64 (expt. %).

Compound 1c: 1,2- dihydroxy Benzene (10g, 90.82mmol, 1eq), ethanol 500 mL, K_2CO_3 (75.31g, 544.95mmol, 6eq), 1-Bromo hexadecane (61.00g, 199.81mmol, 2.2eq) Yield: 87% ; M.P. 61 ºC; ^{1}H NMR (500 MHz, $CDCl_3$): δ (ppm) = 0.90 (t, *J* = 6.50 Hz, 6H), 1.28 – 1.38 (m, 48H), 1.46 – 1.51 (m, 4H), 1.80 – 1.86 (m, 4H), 4.01 (t, *J* = 6.50 Hz, 4H), 6.91 (s, 4H); ^{13}C NMR (125 MHz, $CDCl_3$): δ ppm = 14.14, 22.72, 26.08, 29.37, 29.39, 29.47, 29.67, 29.69, 29.74, 31.96, 69.29, 114.13, 121.01, 149.26; Elemental analysis: C, 81.65; H, 12.62 calculated (%): C, 81.63; H, 12.93(expt. %).

General Procedure for the synthesis of 2a, 2b & 2c.

A mixture of 1a/1b/1c (1eq), Iodine (0.38 eq), glacial acetic acid, water, concentrated sulphuric acid, and Iodic acid (0.25eq) in chloroform. The reaction mixture was heated to 40^{o}C for 14 hrs. After completion of the reaction, then cooled to room temperature and 10% aqueous Na_2SO_3 solution (100ml) and chloroform (100ml) were added to the mixture and was stirred for 0.5 hrs. The phases were separated, and the layer was extracted with chloroform. The combined organic layer dried over anhydrous Na_2SO_4 and concentrated under pressure. The crude product was purified by column chromatography using petroleum ether and dichloromethane as eluent and dried under a high vacuum to get the desired product.

Compound 2a: **1a** (10g, 25.59mmol, 1eq), Iodine (2.46g, 9.72mmol, 0.38eq), glacial acetic acid (26mL), H_2O (9mL), Concentrated H_2SO_4 (0.5ml) and Iodic acid (1.12g, 6.39mmol, 0.25eq), chloroform 50mL Yield: 92%; M.P. 50 ºC; ^{1}H NMR (500 MHz, $CDCl_3$): δ (ppm) = 0.90 (t, *J* = 7.0 Hz, 6H), 1.29 – 1.35 (m, 24H), 1.46 – 1.47 (m, 4H), 1.78 – 1.85 (m, 4H), 3.96 (t, *J* = 6.5 Hz, 4H), 6.63 (d, *J* = 8.0 Hz, 1H), 7.14 (s, 1H), 7.19 (d, *J* = 8.50 Hz, 1H); ^{13}C NMR (125 MHz, $CDCl_3$): δ ppm = 14.14, 22.72, 26.00, 29.20, 29.21, 29.38, 29.41, 29.42, 29.60, 29.64, 31.94, 69.36, 69.43, 82.53, 115.72, 122.67, 129.82, 149.25, 150.14; Elemental analysis: C, 60.46; H, 8.78 calculated (%): C, 60.33; H, 8.9 (expt. %).

Compound 2b: 1b (10g, 22.36mmol, 1eq), Iodine (2.15g, 8.50mmol, 0.38eq), glacial acetic acid (26mL), H_2O (9mL), Concentrated H_2SO_4 (0.5ml) and Iodic acid (0.98g, 5.59mmol, 0.25eq), chloroform 50mL Yield: 89 %; M.P. 56 ºC; ^{1}H NMR (500 MHz, $CDCl_3$): δ (ppm) = 0.90 (t, *J* = 6.50 Hz, 6H), 1.28 -1.35 (m, 32H), 1.45 – 1.46 (m 4H), 1.78 – 1.84 (m 4H), 3.96 (t, *J* = 6.50 Hz, 4H), 6.63 (d, *J* = 8.50 Hz, 1H), 7.14 (s, 1H), 7.19 (d, *J* = 8.50 Hz, 1H); ^{13}C NMR (125 MHz, $CDCl_3$): δ ppm = 14.14, 22.71, 25.99, 29.18, 29.19, 29.39, 29.41, 29.46, 29.63, 29.67, 29.71, 31.94, 69.36, 69.43, 82.51, 115.72, 122.66, 129.80, 149.24, 150.14; Elemental analysis: C, 62.92; H, 9.33 calculated (%): C, 63.18; H, 9.84 (expt. %).

Compound 2c: 1c (10g, 17.89mmol, 1eq), Iodine (1.72g, 6.79mmol, 0.38eq), glacial acetic acid (26mL), H_2O (9mL), Concentrated H_2SO_4(0.5 ml) and Iodic acid (0.78g, 4.47mmol, 0.25eq), chloroform 50 mL Yield: 95% ; M.P. 68 ºC; ^{1}H NMR (500 MHz, $CDCl_3$): δ (ppm) = 0.90 (t, *J* = 6.5 Hz, 6H), 1.28 (m, 48H), 1.46 (m, 4H), 1.78 – 1.83 (m, 4H), 3.96 (t, *J* = 6.0 Hz, 4H), 6.63 (d, *J* = 8.50 Hz, 1H), 7.10 (s, 1H), 7.19 (d, *J* = 8.50 Hz, 1H); ^{13}C NMR (125 MHz, $CDCl_3$): δ ppm = 14.14, 22.71, 26.00, 29.18, 29.20, 29.39, 29.41, 29.64, 29.69, 29.74, 31.95,

69.36, 69.43, 82.52, 115.72, 122.66, 129.81, 149.25, 150.14; Elemental analysis: C, 66.64; H, 10.16 calculated (%): C, 66.44; H, 10.16 (expt. %)

General Procedure for the synthesis of 3a, 3b & 3c.

A solution of 2a/2b/2c (1eq) in dry triethylamine was degassed using nitrogen/argon for 15 mins. To this solution $PdCl_2(PPh_3)_2$ (0.02eq) and then stirred for 15 minutes. Later, CuI (0.01eq) was added. Trimethyl silylacetylene (2eq) was added by syringe. A black precipitate appeared after 30 mins of stirring at room temperature. The reaction mixture was refluxed under N_2 atmosphere for overnight. After the completion of the reaction, the reaction mixture was cooled to room temperature, and triethylamine was evaporated using rota vapor. The resulting black colored solid was dissolved in dichloromethane. The dichloromethane solution was washed with water, 10% HCl solution, and water. The organic phase was dried over anhydrous Na_2SO_4, and dichloromethane was removed under vacuum. The crude product was purified by column chromatography using petroleum ether and dichloromethane as eluent and dried under a high vacuum to get the desired product.

Compound 3a: 2a (10g, 19.35mmol, 1eq), dry triethyl amine (30 mL), $PdCl_2(PPh_3)_2$ (0.278g, 0.39mmol, 0.02eq), CuI (0.0564g, 0.296 mmol, 0.015eq), trimethylsilylacetylene (3.80g, 38.71mmol, 2eq) Yield: 93%; ^{1}H NMR (500 MHz, $CDCl_3$): δ (ppm) = 0.26 (s, 9H), 0.90 (t, *J* = 6.50 Hz, 6H), 1.29 – 1.36 (m, 24H), 1.44 – 1.48 (m, 4H), 1.80 – 1.85 (m, 4H), 3.98 – 4.01 (m, 4H), 6.78 (d, *J* = 8.0 Hz, 1H), 6.98 (s, 1H), 7.05 (d, *J* = 8.0 Hz, 1H); ^{13}C NMR (125 MHz, $CDCl_3$): δ ppm = 14.04, 22.62, 25.93, 29.11, 29.15, 29.29, 29.34, 29.51, 29.55, 29.56, 31.85, 68.99, 69.10, 91.93, 105.43, 112.93, 113.01, 115.11, 116.84, 117.04, 125.35, 125.42, 148.48, 149.78; Elemental analysis: C, 76.48; H, 11.18 Calculated (%): C, 76.27; H, 10.90; (expt. %)

Compound 3b: 2b (6.6g, 11.59mmol, 1eq), dry triethyl amine (20mL), $PdCl_2(PPh_3)_2$ (0.166g, 0.237mmol, 0.020eq), CuI (0.033g, 0.177mmol, 0.015eq), trimethylsilylacetylene (2.27g, 23.19mmol, 2eq) Yield: 89% ; M.P. 44 ºC; ^{1}H NMR (500 MHz, $CDCl_3$): δ (ppm) = 0.23 (s, 9H), 0.88 (t, *J* = 7.0 Hz, 6H), 1.26 – 1.34 (m, 32H), 1.43 – 1.46 (m, 4H), 1.77 – 1.83 (m, 4H), 3.95 – 3.99 (m, 4H), 6.76 (d, *J* = 8.0 Hz, 1H), 6.96 (s, 1H), 7.02 (d, *J* = 8.0 Hz, 1H); ^{13}C NMR (125 MHz, $CDCl_3$): δ ppm = 14.04, 22.63, 25.93, 25.94, 31.86, 69.02, 69.13, 91.95, 105.43, 112.98, 115.12, 116.89, 125.36, 125.44, 148.50, 149.80; Elemental analysis: C, 77.42; H, 11.51 calculated (%): C, 77.56; H, 11.84 (expt. %).

Compound 3c: 2c (10g, 14.60mmol, 1eq), dry triethyl amine (30mL), $PdCl_2(PPh_3)_2$ (0.210g, 0.2993mmol, 0.020eq), CuI (0.042g, 0.2234mmol, 0.015eq), trimethylsilylacetylene (2.86g, 29.20mmol, 2eq) Yield:90%; M.P. 51 ºC ; ^{1}H NMR (500 MHz, $CDCl_3$): δ (ppm) = 0.26 (s, 9H), 0. 90 (t, *J* = 6.5Hz, 6H), 1.28 – 1.39 (m, 48H), 1.45 – 1.48 (m, 4H), 1.79 – 1.85 (m, 4H), 4.0 (t, *J* = 5.50 Hz, 4H), 6.78 (d, *J* = 8.0 Hz, 1H), 6.98 (s, 1H), 7.05 (d, *J* = 8.50 Hz, 1H); ^{13}C NMR (125 MHz, $CDCl_3$): δ ppm = 14.05, 22.63, 25.92, 25.93, 29.10, 29.14, 29.31, 29.34, 29.56, 29.60, 29.65, 31.87, 69.01, 69.11, 91.95, 105.42, 112.94, 115.09, 116.84, 125.34, 148.48, 149.78; Elemental analysis: C, 78.83; H, 12.0 calculated (%): C, 78.89; H, 12.23 (expt. %).

General Procedure for the synthesis of 4a, 4b & 4c.

3a/3b/3c was dissolved in dichloromethane and methanol (6:4 ratio). To the above solution, K_2CO_3 (5eq) was added. The reaction mixture was stirred overnight at room temperature. After completion of the reaction, the solvent was concentrated under reduced pressure. The crude product was extracted with dichloromethane. The organic layer dried over anhydrous Na_2SO_4 and concentrated under pressure. The crude product was purified by column chromatography using petroleum ether and dichloromethane as eluent and dried under a high vacuum to get the desired product.

Compound 4a: 3a (8g, 14.02mmol, 1eq), dichloromethane (90mL), methanol (60mL), K_2CO_3 (9.7g, 70.11mmol, 5eq) Yield: 91%; M.P. 32 ºC; ^{1}H NMR (500 MHz, $CDCl_3$): δ (ppm) = 0.75 (t, *J* = 6.0 Hz 6H), 1.14 – 1.24 (m, 24H), 1.30 – 1.35 (m, 4H), 1.65 – 1.71 (m, 4H), 2.85 (s, 1H), 3.83 – 3.87 (m, 4H), 6.66 (d, *J* = 8.0 Hz, 1H), 6.86 (s, 1H), 6. 93 (d, *J* = 8.50 Hz, 1H); ^{13}C NMR (125 MHz, $CDCl_3$): δ ppm = 14.12, 22.70, 26.01, 29.18, 29.20, 29.36, 29.41, 29.59, 29.63, 29.72, 31.93, 69.11, 69.25, 75.42, 83.98, 113.10, 114.07, 117.12, 125.51, 148.65, 150.08; Elemental analysis: C, 81.1; H, 11.18 calculated (%): C, 80.60; H, 11.61 (expt. %).

Compound 4b: 3b (5.33g, 9.82mmol, 1eq), dichloromethane (60mL), methanol (40mL), K_2CO_3 (6.79g, 49.14mmol, 5eq) Yield:88%; M.P. 43 ºC; ^{1}H NMR (500 MHz, $CDCl_3$): δ (ppm) = 0.88 (t, *J* = 7.0 Hz, 6H), 1.26 – 1.34 (m, 32H), 1.42 – 1.48 (m, 4H), 1.78 – 1.83 (m, 4H), 2.98 (s, 1H), 3.95 – 4.0 (m, 4H), 6.78 (d, *J* = 8.0 Hz, 1H), 6.98 (s, 1H), 7.05 (d, *J* = 8.50 Hz, 1H); ^{13}C NMR (125 MHz, $CDCl_3$): δ ppm = 14.12, 22.71, 26.02, 29.19, 29.22, 29.39, 29.42, 29.65,

29.69, 29.72, 31.95, 69.12, 69.26, 75.42, 83.97, 113.13, 114.12, 117.16, 125.52, 148.68, 150.09; Elemental analysis: C, 81.64; H, 11.56; calculated (%): C, 81.55; H, 12.17 (expt. %)

Compound 4c: 3c (7.2g, 6.80mmol, 1eq), dichloromethane (80mL), methanol (54mL), K_2CO_3 (4.70g, 34.01mmol, 5eq) Yield: 96%; M.P. 59 ºC; ^{1}H NMR (500 MHz, $CDCl_3$): δ (ppm) = 0.80 (t, *J* = 6.0 Hz, 6H), 1.18 – 1.27 (m, 48H), 1.35 – 1.39 (m, 4H), 1.70 – 1.76 (m, 4H), 2.90 (s, 1H), 3.88 – 3.93 (m, 4H), 6.71 (d, *J* = 8.0 Hz, 1H), 6.91 (s, 1H), 6.98 (d, *J* = 8.0 Hz, 1H); ^{13}C NMR (125 MHz, $CDCl_3$): δ ppm = 13.10, 21.69, 24.99, 28.16, 28.18, 28.38, 28.40, 28.63, 28.68, 28.72, 30.93, 68.07, 68.21, 74.39, 82.94, 112.05, 113.08, 116.08, 124.47, 147.63, 149.04; Elemental analysis: C, 82.41; H, 12.1 calculated (%): C, 82.24; H, 12.38 (expt. %)

General Procedure for the synthesis of 5a, 5b & 5c.

Compound 4a/4b/4c (1eq) and 2a/2b/2c (1.2eq) in dry trimethylamine degassed for 15 mins using nitrogen. To this solution $PdCl_2(PPh_3)_2$ (0.02eq) and CuI (0.015) were added. The reaction mixture was refluxed under N_2 atmosphere overnight. After the reaction mixture was cooled to room temperature, triethylamine is removed under reduced pressure. The crude product was extracted with dichloromethane. The organic phase was dried over anhydrous Na_2SO_4, and dichloromethane was removed under reduced pressure. The crude product was purified by column chromatography using petroleum ether and dichloromethane as eluent and dried under a high vacuum to get the desired product.

Compound 5a: 4b (5.40g, 13.03mmol, 1eq), 2b (7.40g, 14.34mmol, 1.2eq), triethyl amine (35mL), $PdCl_2(PPh_3)_2$ (0.187g, 0.267mmol, 0.02eq) , CuI (0.037g, 0.199mmol, 0.015eq) Yield: 81% ; M.P. 98 ºC; ^{1}H NMR (500 MHz, $CDCl_3$): δ (ppm) = 0.81 (t, *J* = 6.0 Hz, 12H), 1.20 – 1.28 (m, 48H), 1.36 – 1.40 (m, 8H), 1.72 – 1.76 (m, 8H), 3.92 (t, *J* = 6.50 Hz, 8H), 6.74 (d, *J* = 8.50 Hz, 2H), 6.95 (s, 2H), 6.99 (d, *J* = 8.50 Hz, 2H); ^{13}C NMR (125 MHz, $CDCl_3$): δ ppm = 14.13, 22.71, 26.03, 29.24, 29.25, 29.37, 29.44, 29.60, 29.60, 29.65, 29.72, 31.94, 69.16, 69.22, 87.98, 113.30, 115.67, 116.57, 124.74, 148.72, 149.46; Elemental analysis: C, 80.74; H, 11.29 calculated (%): C, 80.59; H, 11.50 (expt. %)

Compound 5b: 4a (4.91g, 10.43mmol, 1eq), 2a (6.57g, 11.48mmol, 1.2eq), triethylamine (40mL), $PdCl_2(PPh_3)_2$ (0.150g, 0.214mmol, 0.020eq), CuI (0.030g, 0.159mmol, 0.015eq) Yield: 77% ; M.P. 101 ºC ; ^{1}H NMR (500 MHz, $CDCl_3$): δ (ppm) = 0.88 (t, *J* = 7.0 Hz, 12H), 1.26 – 1.35 (m, 64H), 1.43 – 1.49 (m, 8H), 1.79 – 1.84 (m, 8H), 3.99 (t, *J* = 7.0 Hz, 8H), 6.81

(d, *J* = 8.0 Hz, 2H), 7.02 (s, 2H), 7.06 (d, *J* = 8.0 Hz, 2H); ^{13}C NMR (125 MHz, $CDCl_3$): δ ppm = 14.12, 22.70, 26.02, 26.03, 29.23, 29.24, 29.38, 29.43, 29.64, 29.67, 29.71, 31.94, 69.18, 69.24, 87.97, 113.34, 115.67, 116.61, 124.75, 148.73, 149.47; Elemental analysis: C, 81.34; H, 11.67 calculated (%): C, 81.50; H, 11.24 (expt. %).

Compound 5c: 4c (6.02g, 10.34mmol, 1eq), 2c (8.49g, 12.40mmol, 1eq), triethyl amine (100 mL), $PdCl_2(PPh_3)_2$ (0.148g, 0.212mmol, 0.02eq), CuI (0.030g, 0.158mmol, 0.015eq) Yield: 85%; M.P. 104 ºC; ^{1}H NMR (500 MHz, $CDCl_3$): δ (ppm) = 0.80 (t, *J* = 6.0 Hz, 12H), 1.18 – 1.28 (m, 96H), 1.36 – 1.40 (m, 8H), 1.72 – 1.77 (m, 8H), 3.92 9t, *J* = 6.5 Hz, 8H), 6.74 (d, *J* = 8.50 Hz, 2H), 6.95 (s, 2H), 6.99 (d, *J* = 8.50 Hz, 2H); ^{13}C NMR (125 MHz, $CDCl_3$): δ ppm = 14.13, 22.71, 26.02, 26.04, 29.23, 29.24, 29.38, 29.44, 29.65, 29.68, 29.73, 31.94, 69.17, 69.23, 87.97, 113.30, 115.66, 116.57, 124.74, 148.72, 149.46; Elemental analysis: C, 82.18; H, 12.20 calculated (%): C, 82.57; H, 12.47(expt. %).

General Procedure for the synthesis of 6a, 6b & 6c.

A mixture of 5a/5b/5c (2.2eq) and 9,10-dibromo anthracene (1eq), $Pd_2(dba)_3$, (0.1eq) $P(o\text{-}Tol)_3$, (0.1eq) KOAc, (5eq) LiCl (2eq) in DMF and Toluene (1:1) was stirred overnight in the presence of inert gas at 130ºC. The reaction mixture was cooled to room temperature and poured into methanol green color precipitate was observed. The filtrate was filtered using Buchner Funnel. The resulting solid was washed with methanol and acetone to give the final product. The crude product was purified by column chromatography using petroleum ether and chloroform as eluent and dried under a high vacuum to get the desired product.

Compound 6a: 5a (2.62g, 3.27mmol, 2.2eq), 9, 10-dibromoanthracene (0.500g, 1.487mmol, 1eq), $Pd_2(dba)_3$ (0.136g, 0.148mmol, 0.1eq), $P(o\text{-}Tol)_3$ (0.045g, 0.148mmol, 0.1eq), KOAc (0.730g, 7.43mmol, 5eq), LiCl (0.126g, 2.97mmol, 2eq), DMF (20mL), Toluene (20mL) Yield: 79%; M.P. 82 ºC ; ^{1}H NMR (500 MHz, $CDCl_3$): δ (ppm) = 0.77 – 0.83 (m , 24H), 1.17 – 1.37 (m, 104H), 1.38 – 1.47 (m, 8H), 1.60 – 1.70 (m, 8H), 1.72 – 1.78 (m, 4H), 1.8 – 1.87 (m, 4H), 3.67 (t, *J* = 6.50 Hz, 4H), 3.82 (bs, 4H), 3.93 (t, *J* = 6.50 Hz, 4H), 4.0 (bs, 4H), 6.78 (d, *J* =

8.0 Hz, 2H), 6.82 (s, 2H), 6.88 (d, *J* = 8.0 Hz, 2H), 6.93 – 7.01 (m, 6H), 7.34 (t, *J* = 7.5 Hz, 2H), 7.72 (d, *J* = 8.0 Hz, 4H); $^{13}C\{^{1}H\}$ NMR (125 MHz, $CDCl_3$): δ ppm = 14.14, 22.71, 22.73, 26.05, 26.10, 26.12, 26.20, 29.22, 29.25, 29.40, 29.43, 29.45, 29.48, 29.52, 29.60, 29.62, 29.64, 29.69, 29.73, 29.76, 31.96, 31.98, 68.99, 69.16, 69.18, 69.30, 113.25, 113.51, 115.71, 116.39, 122.81, 123.23, 124.90, 125.73, 126.19, 127.88, 127.93, 128.26, 130.05, 137.90, 138.00, 138.68, 140.65, 148.15, 148.50, 148.52, 148.75; Elemental analysis: C, 82.28; H, 10.53 calculated (%): C, 82.26; H, 10.88 (expt. %).

Compound 6b: 5b (1.198g, 1.309mmol, 2.2eq), 9, 10-dibromoanthracene (0.200g, 0.5951mmol, 1eq), $Pd_2(dba)_3$ (0.054g, 0.059mmol, 0.1eq), $P(o\text{-}Tol)_3$ (0.018g, 0.0595mmol, 0.1eq), KOAc (0.29g, 2.97mmol, 5eq), LiCl (0.050g, 1.19mmol, 2eq), DMF (10mL), Toluene (10mL) Yield:80% ; M.P. 84ºC; ^{1}H NMR (500 MHz, $CDCl_3$): δ (ppm) = 0.87 (m, 24H), 1.24 – 1.26 (m, 120H), 1.39 (m, 16H), 1.47 – 1.52 (m, 8H), 1.70 – 1.74 (m, 8H), 1.82 – 1.89 (m, 8H), 3.74 (bs, 4H), 3.89 (bs, 4H), 4.00 (bs, 4H), 4.07 (bs, 4H), 6.85 – 6.89 (m, 4H), 6.94 – 6.96 (bd, *J* = 7.50 Hz, 2H), 7.01 – 7.08 (m, 6H), 7.41 (t, *J* = 8.0 Hz, 2H), 7.79 – 7.80 (d, *J* = 8.0 Hz, 4H); $^{13}C\{^{1}H\}$ NMR (125 MHz, $CDCl_3$): δ ppm = 13.09, 21.68, 25.01, 25.06, 25.07, 25.16, 28.18, 28.21, 28.36, 28.38, 28.44, 28.48, 28.56, 28.65, 28.69, 28.70, 28.73, 28.76, 30.92, 67.95, 68.14, 68.28, 112.24, 112.49, 114.69, 115.36, 121.76, 122.19, 123.85, 124.68, 125.14, 126.83, 126.89, 127.21, 129.01, 136.85, 136.95, 137.64, 139.61, 147.11, 147.47, 147.481, 147.72; Elemental analysis: C, 82.66; H, 10.96 calculated (%): C, 82.32; H, 10.94 (expt. %).

Compound 6c: 5c (1.49g, 1.30mmol, 2.2eq), 9, 10-dibromoanthracene (0.200g, 0.595mmol, 1eq), $Pd_2(dba)_3$ (0.054g, 0.059mmol, 0.1eq), $P(o\text{-}Tol)_3$ (0.018g, 0.059mmol, 0.1eq), KOAc (0.292g, 2.97mmol, 5eq), LiCl (0.050g, 1.19mmol, 2eq), DMF (10mL), Toluene (10mL) Yield:83% ; M.P. 94 ºC; ^{1}H NMR (500 MHz, $CDCl_3$): δ (ppm) = 0.80 (bs 24 H), 1.16 – 1.18 (m, 180H), 1.29 – 1.32 (m, 20H), 1.37 – 1.47 (m, 8H), 1.60 – 1.68 (m, 8H), 1.73 – 1.82 (m, 8H), 3.66 (t, *J* = 6.50 Hz, 4H), 3.81 (bs, 4H), 3.93 (t, *J* = 6.50 Hz, 4H), 4.0 (bs, 4H), 6.77 – 6.82 (m, 4H), 6.88 (d, *J* = 8.0 Hz, 2H), 6.94 – 7.01(m, 6H), 7.34 (t, *J* = 8.0 Hz, 2H), 7.73 (d, *J* = 8.0 Hz, 4H); $^{13}C\{^{1}H\}$ NMR (125 MHz, $CDCl_3$): δ ppm = 14.14, 22.71, 26.05, 26.10, 26.11, 26.20, 29.21, 29.24, 29.40, 29.49, 29.51, 29.53, 29.61, 29.70, 29.76, 31.96, 68.98, 69.16, 69.30, 113.25, 113.50, 115.70, 116.38, 122.79, 123.22, 124.89, 125.72, 126.18, 127.87, 127.92,

128.24, 130.04, 137.88, 137.98, 138.67, 140.63, 148.13, 148.49, 148.51, 148.74; Elemental analysis: C, 83.2; H, 11.58 calculated (%): C, 83.31; H, 11.89 (expt. %)

General Procedure for the synthesis of 7a, 7b & 7c.

6a/6b/6c was dissolved in dichloromethane. To this solution, $FeCl_3$ in CH_3NO_2 was added dropwise under argon. The reaction mixture was stirred at room temperature overnight. Methanol was added and the mixture was stirred for 20 min. The product was filtered using Büchner Funnel and the resulting solid was washed with methanol and acetone, the crude product was purified by column chromatography using petroleum ether: chloroform (v/v 7:3) as eluent and dried under high vacuum to get the desired product.

Compound 7a: 6a (1g, 0.562mmol, 1eq), dichloromethane (200 mL), $FeCl_3$ (0.730 g, 4.50mmol, 8eq), CH_3NO_2 (6mL) Yield: 92%; M.P. 207 ºC; ^{1}H NMR (500 MHz, $CDCl_3$): δ (ppm) = 0.75 – 0.82 (m, 24H), 1.17- 1.55 (m, 112H), 1.84 – 1.96 (m, 16H), 4.15 (t, *J* = 6.50 Hz, 4H), 4.21 – 4.25 (m, 12H), 7.59 (t, *J* = 7.0 Hz, 2H), 7.83 (s, 4H), 8.05 (s, 2H), 8.26 (s, 2H), 8.28 (d, *J* = 8.0 Hz, 2H), 8.69 (d, *J* = 8.0 Hz, 2H); ^{13}C{^{1}H} NMR (125 MHz, $CDCl_3$): δ ppm = 14.11, 14.15, 22.70, 22.74, 26.23, 26.28, 26.32, 29.33, 29.40, 29.44, 29.50, 29.63, 29.65, 29.69, 29.72, 29.76, 29.78, 31.93, 31.98, 69.00, 69.17, 69.61, 69.71, 106.59, 106.68, 110.23, 123.18, 124.05, 124.49, 124.55, 125.85, 126.02, 126.95, 127.77, 130.99, 134.13, 134.37, 137.46, 139.30, 148.77, 148.91, 149.05, 149.74; Elemental analysis: C, 82.47; H, 10.33 calculated (%): C, 82.60; H, 10.39 (expt. %); MALDI-TOF: 1776.39 (calculated); 1776.03 (experimental)

Compound 7b: 6b (0.800g, 0.399mmol, 1eq), dichloromethane (150mL), $FeCl_3$ (0.51g, 3.19mmol, 8eq), CH_3NO_2 (5mL) Yield: 92%; M.P. 195 ºC; ^{1}H NMR (500 MHz, $CDCl_3$): δ (ppm) = 0.83 – 0.88 (m, 24H), 1.22 – 1.28 (m, 97H), 1.44 – 1.46 (m, 16H), 1.57– 1.62 (m, 16H), 1.95– 2.01 (m, 16H), 4.24 (t, *J* = 6.0 Hz, 4H), 4.30 – 4.32 (m, 12H), 7.70 (t, *J* = 7.5 Hz, 2H), 7.93 (s, 4H), 8.16 (s, 2H), 8.37 (s, 2H), 8.40 (d, *J* = 6.5 Hz, 2H), 8.81 (d, *J* = 8.50 Hz, 2H); ^{13}C{^{1}H} NMR (125 MHz, $CDCl_3$): δ ppm = 14.13, 22.68, 22.71, 26.22, 26.26, 26.31, 29.38, 29.38, 29.41, 29.48, 29.60, 29.68, 29.72, 29.76, 31.92, 31.96, 69.02, 69.21, 69.65, 69.75,

106.74, 110.26, 123.22, 124.12, 124.59, 125.89, 126.05, 126.99, 127.85, 131.02, 134.18, 134.41, 137.52, 139.35, 148.83, 148.96, 149.11, 149.79; Elemental analysis: C, 82.83; H, 10.78 calculated (%): C, 82.80; H, 10.61 (expt. %); MALDI-TOF: 2000.64 (calculated); 2000.70 (experimental)

Compound 7c: 6c (1.5g, mmol, 1eq), dichloromethane (300mL), $FeCl_3$ (0.794g, 4.89mmol, 8eq), CH_3NO_2 (9mL) Yield:95%; M.P. 175 ºC; ^1H NMR (500 MHz, $CDCl_3$): δ (ppm) = 0.77 – 0.81 (m, 24H), 1.14 – 1.55 (m, 208H), 1.85 – 1.97 (m, 16H), 4.16 (t, *J* = 6.0 Hz, 4H), 4.21 – 4.24 (m, 12H), 7.61 (t, *J* = 7.0 Hz, 2H), 7.84 (s, 4H), 8.07 (s, 2H), 8.28 (s, 2H), 8.31(d, *J* = 6.5 Hz, 2H), 8.72 (d, *J* = 8.5 Hz, 2H); $^{13}C\{^1H\}$ NMR (125 MHz, $CDCl_3$): δ ppm = 14.14, 22.72, 26.24, 26.28, 26.33, 29.33, 29.41, 29.50, 29.63, 29.71, 29.77, 29.79, 31.96, 69.01, 69.17, 69.62, 69.72, 106.59, 106.70, 110.24, 123.20, 124.07, 124.52, 124.57, 125.86, 126.03, 126.97, 127.80, 131.00, 134.16, 134.39, 137.49, 139.33, 148.80, 148.93, 149.07, 149.76; Elemental analysis: C, 83.34; H, 11.44 calculated (%): C, 83.39; H, 11.77 (expt. %). MALDI-TOF: 2449.14 (calculated); 2449.28(experimental)

2.6 MALDI-TOF Spectra

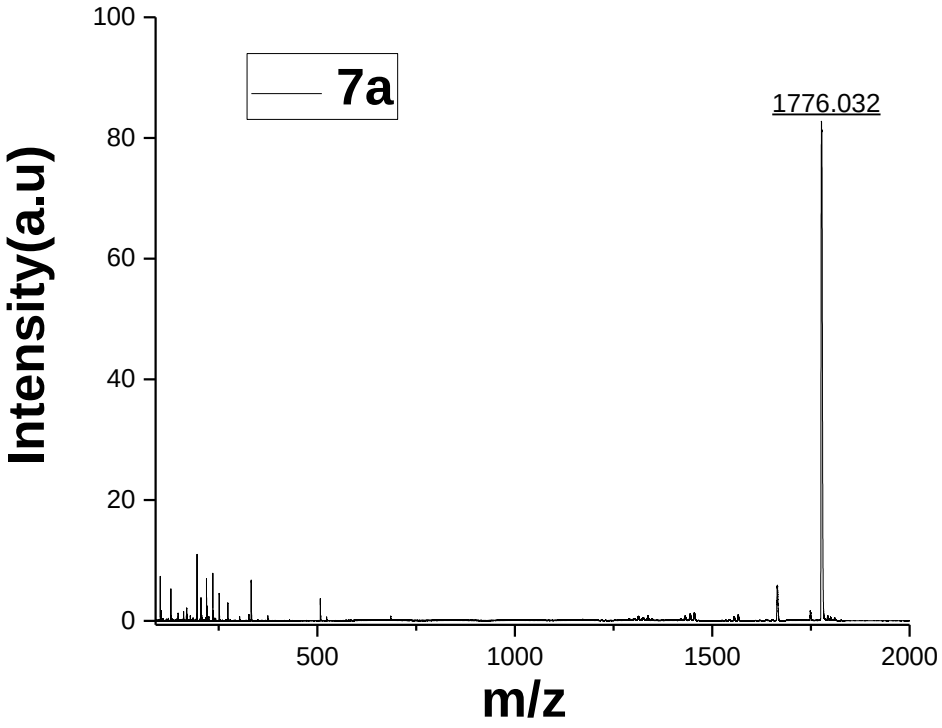

Figure 2.30: Mass spectra of **7a**

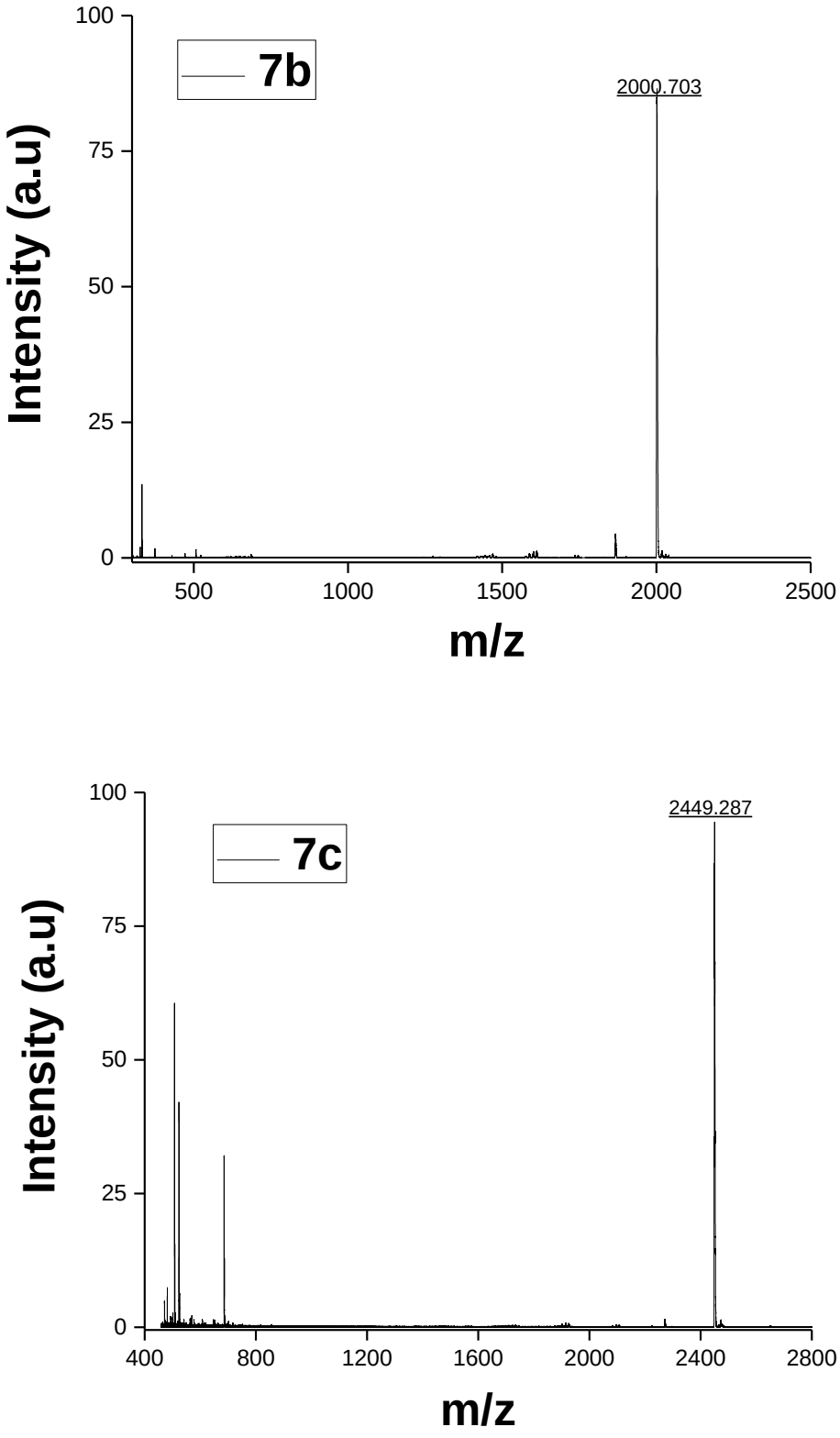

Figure 2.31: Mass spectra of **7b** (above) and **7c** (below)

2.7. NMR Spectra

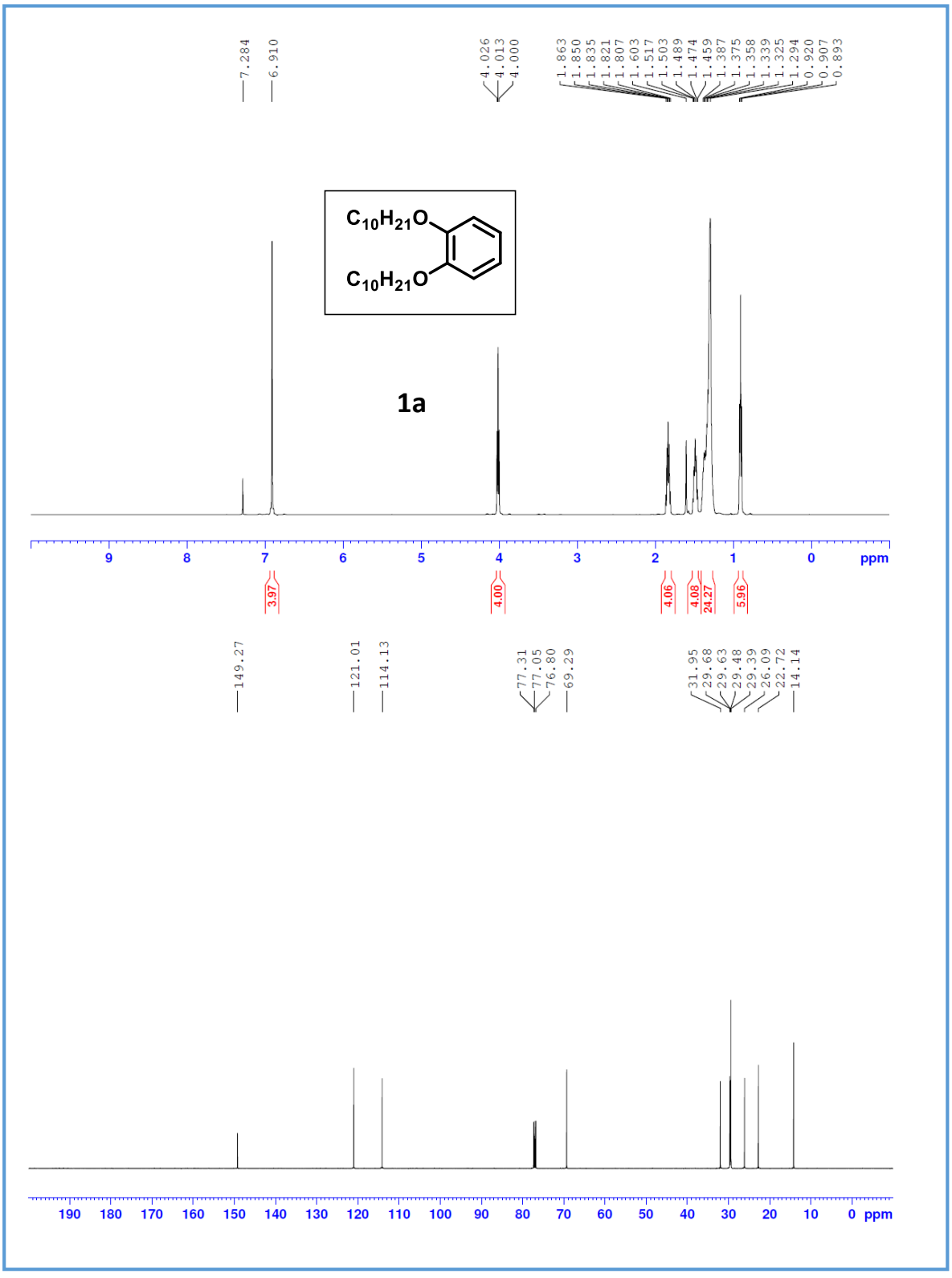

Figure 2.32: ^{1}H (top) and ^{13}C-NMR (bottom) spectra of **1a**.

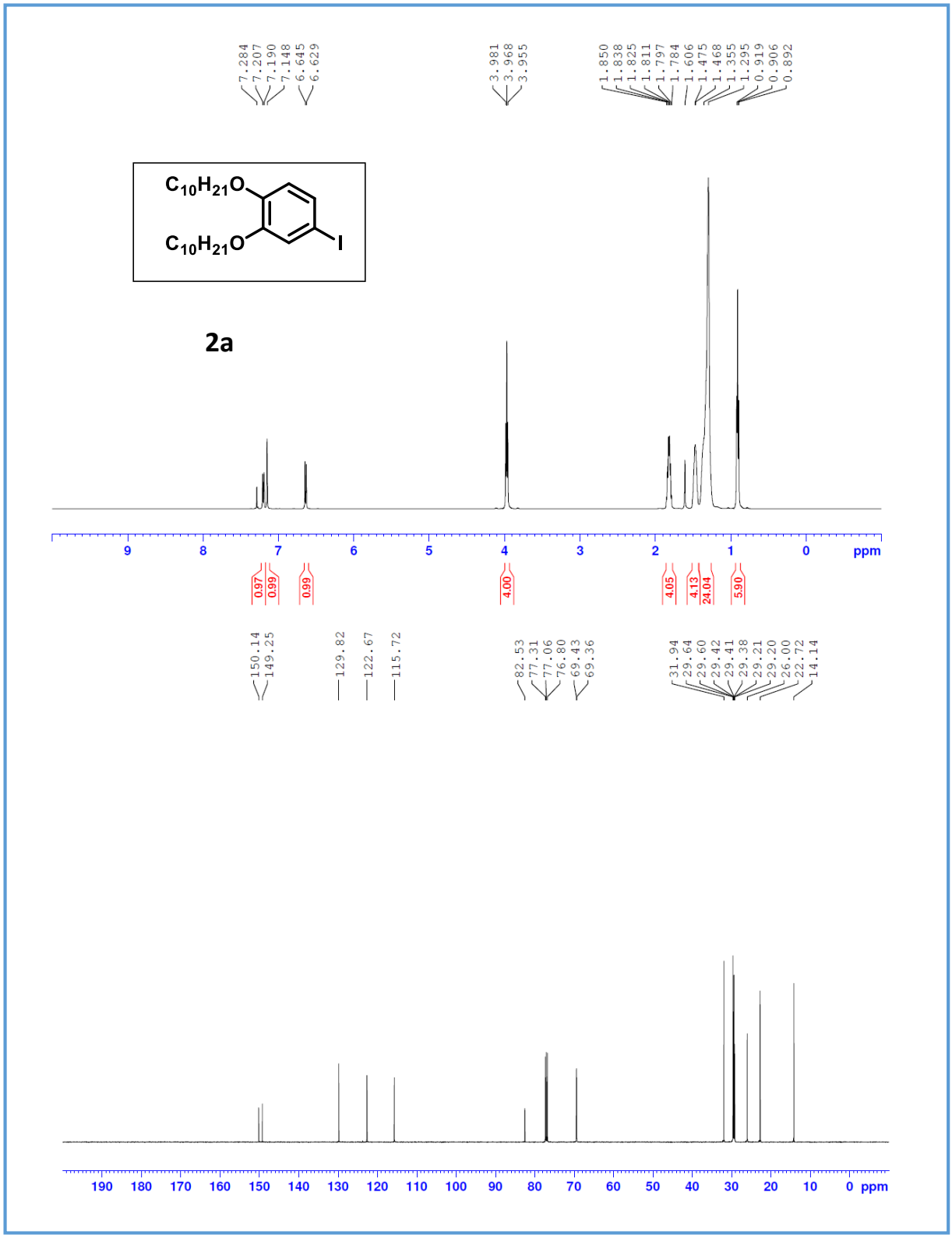

Figure 2.33: ^{1}H (top) and ^{13}C-NMR (bottom) spectra of **2a**.

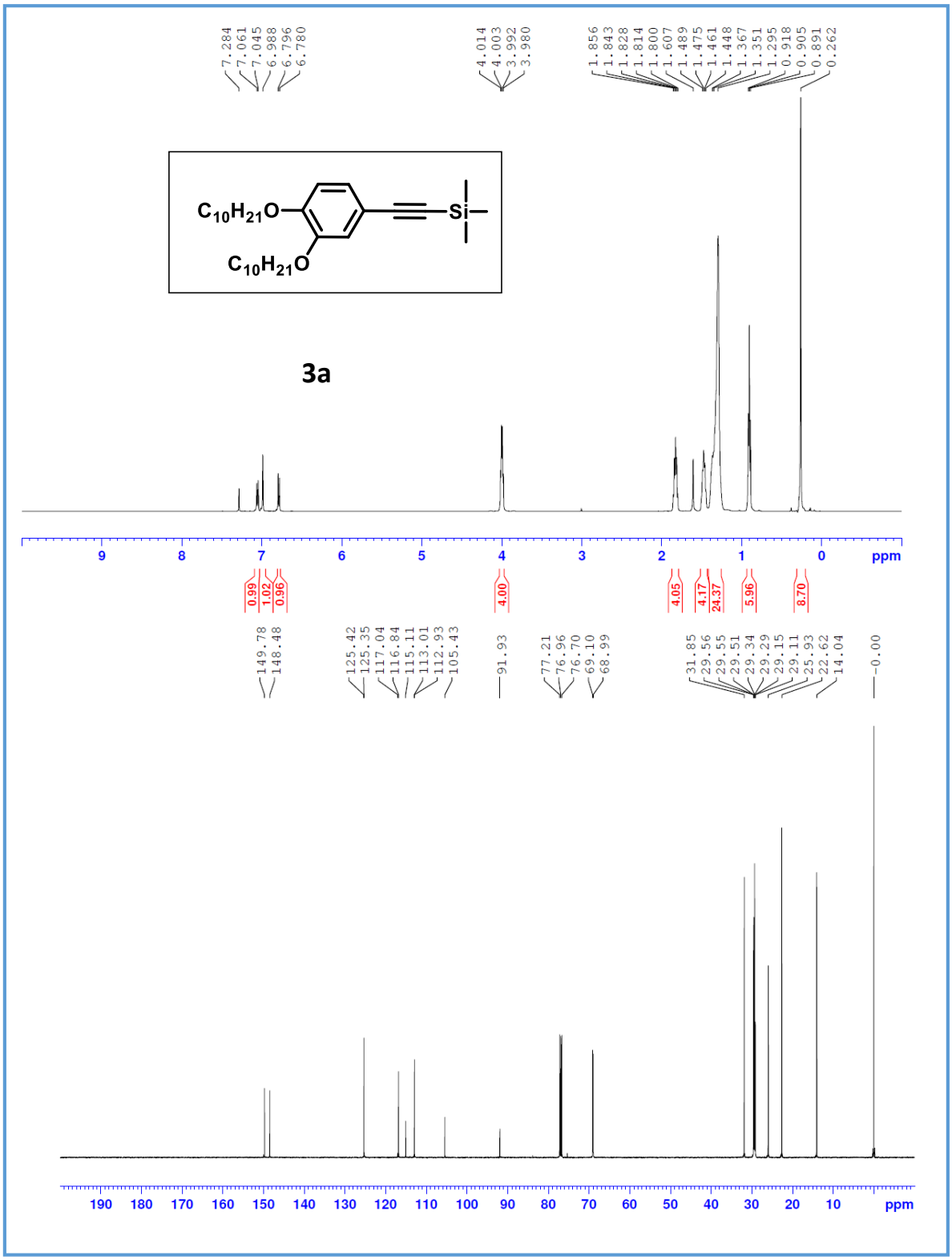

Figure 2.34: ^{1}H (top) and ^{13}C-NMR (bottom) spectra of **3a**.

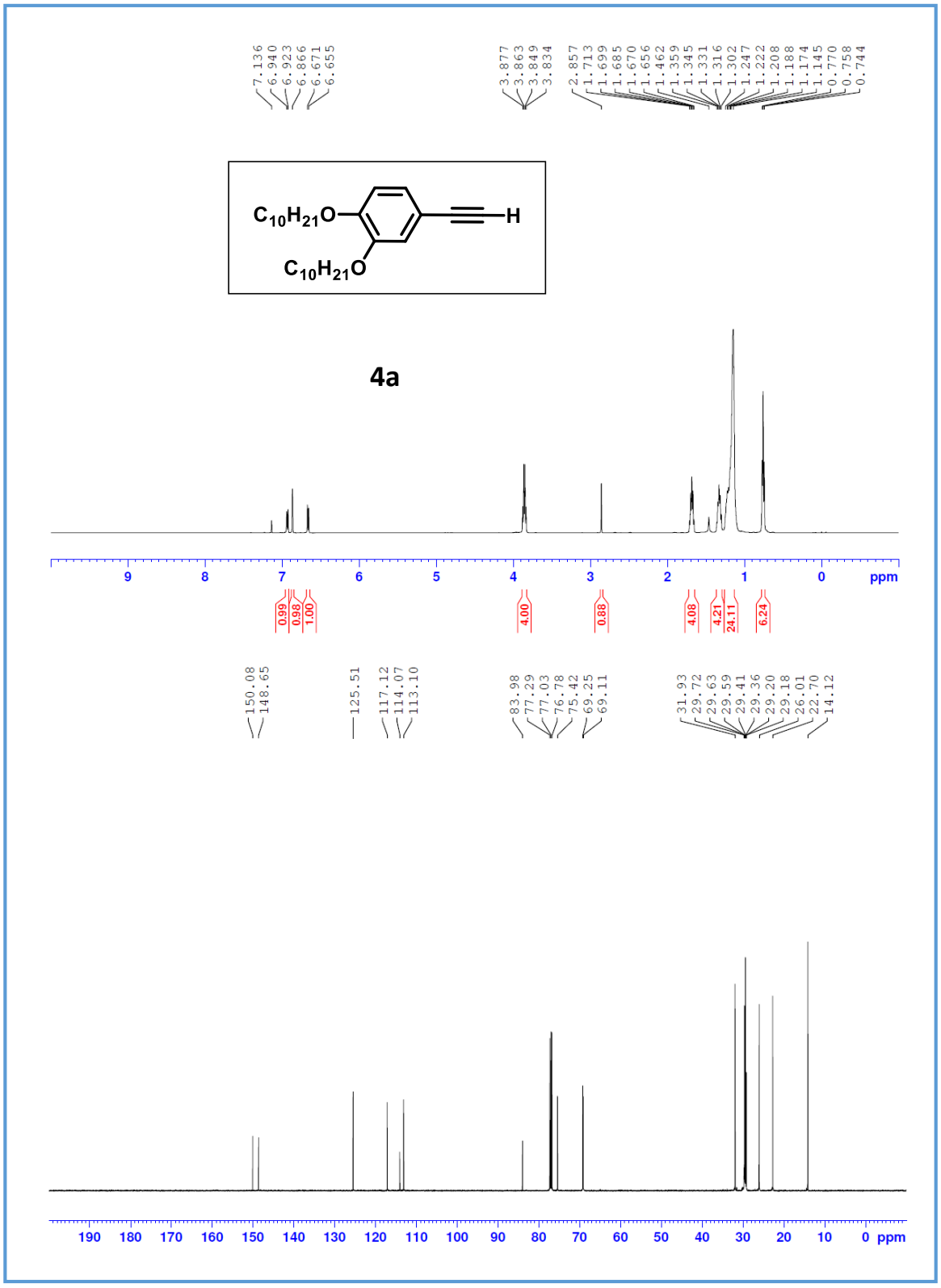

Figure 2.35: ^{1}H (top) and ^{13}C-NMR (bottom) spectra of **4a**

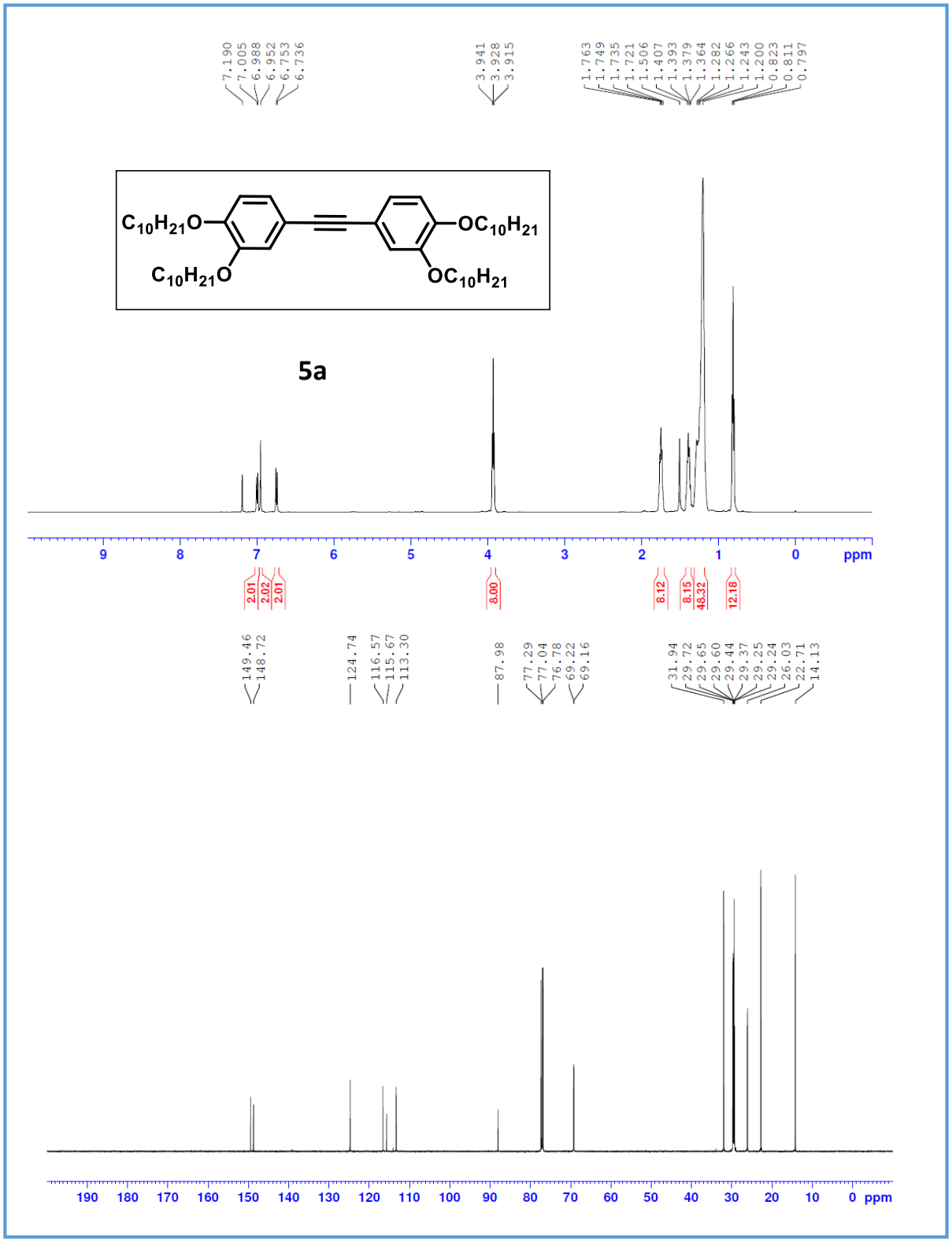

Figure 2.36: ^{1}H (top) and ^{13}C-NMR (bottom) spectra of **5a**

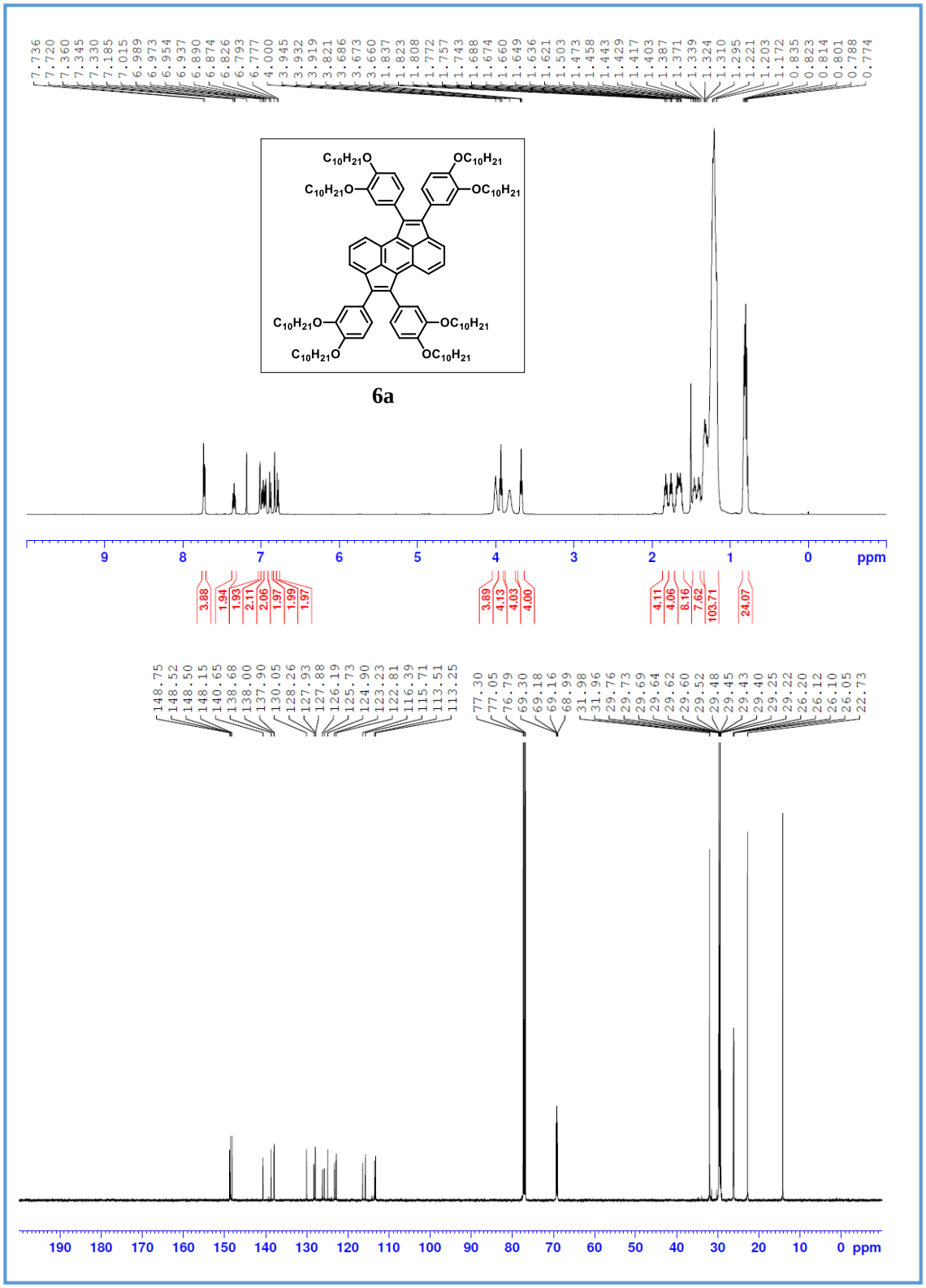

Figure 2.37: ^{1}H (top) and ^{13}C-NMR (bottom) spectra of **6a**

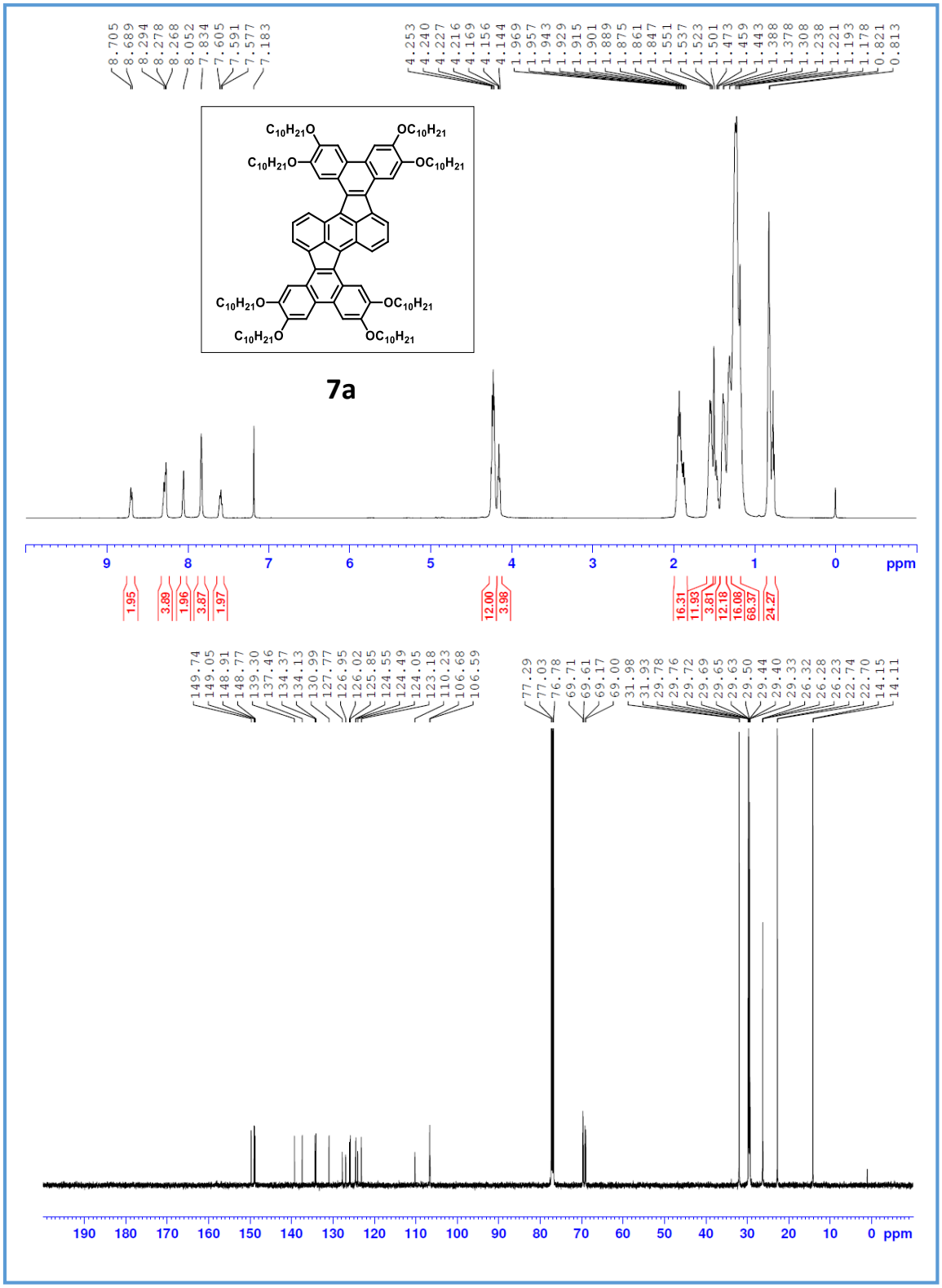

Figure 2.38: ^{1}H (top) and ^{13}C-NMR (bottom) spectra of **7a**

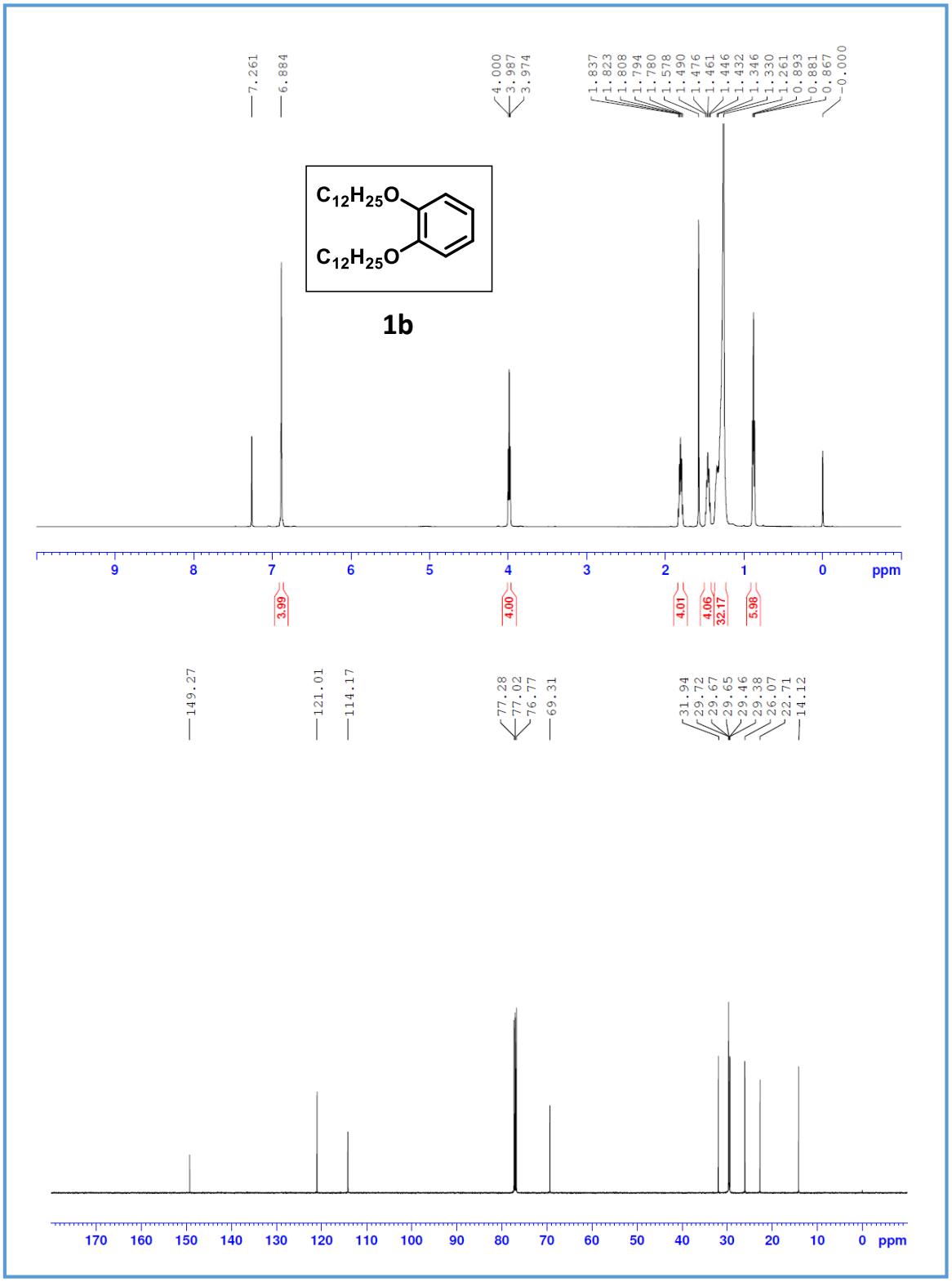

Figure 2.39: ^{1}H (top) and ^{13}C-NMR (bottom) spectra of **1b**

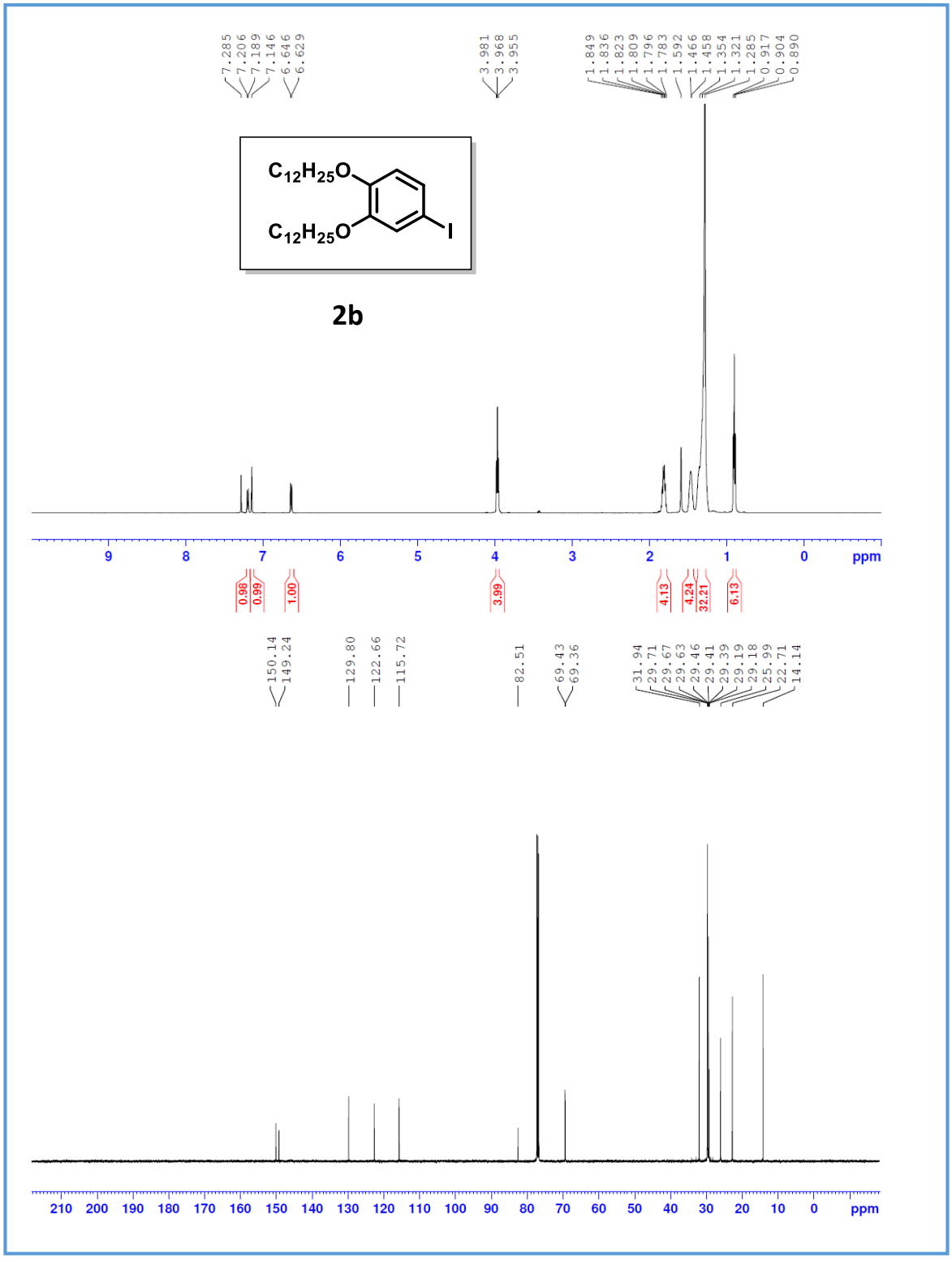

Figure 2.40: ^{1}H (top) and ^{13}C-NMR (bottom) spectra of **2b**

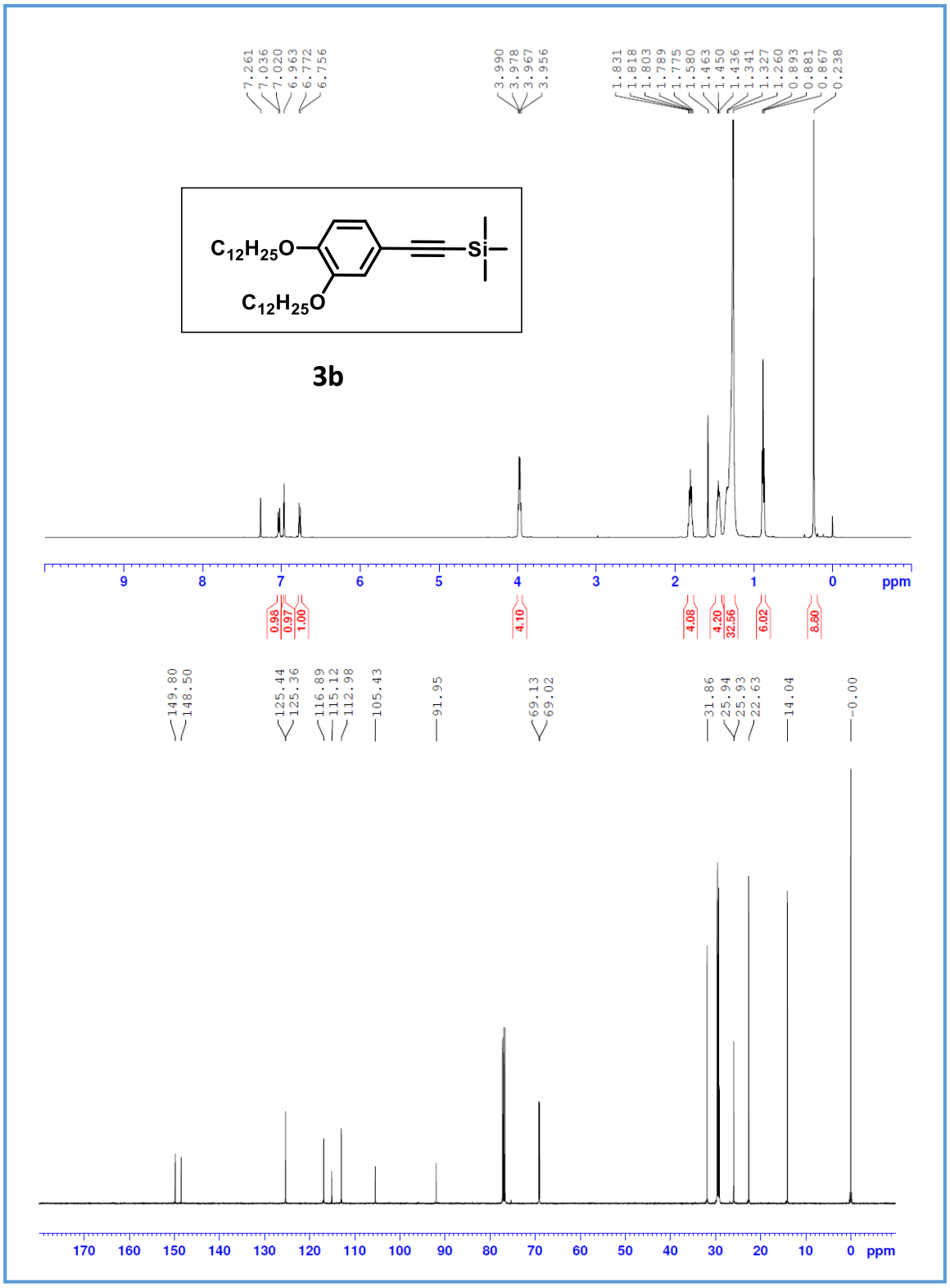

Figure 2.41: ^{1}H (top) and ^{13}C-NMR (bottom) spectra of **3b**

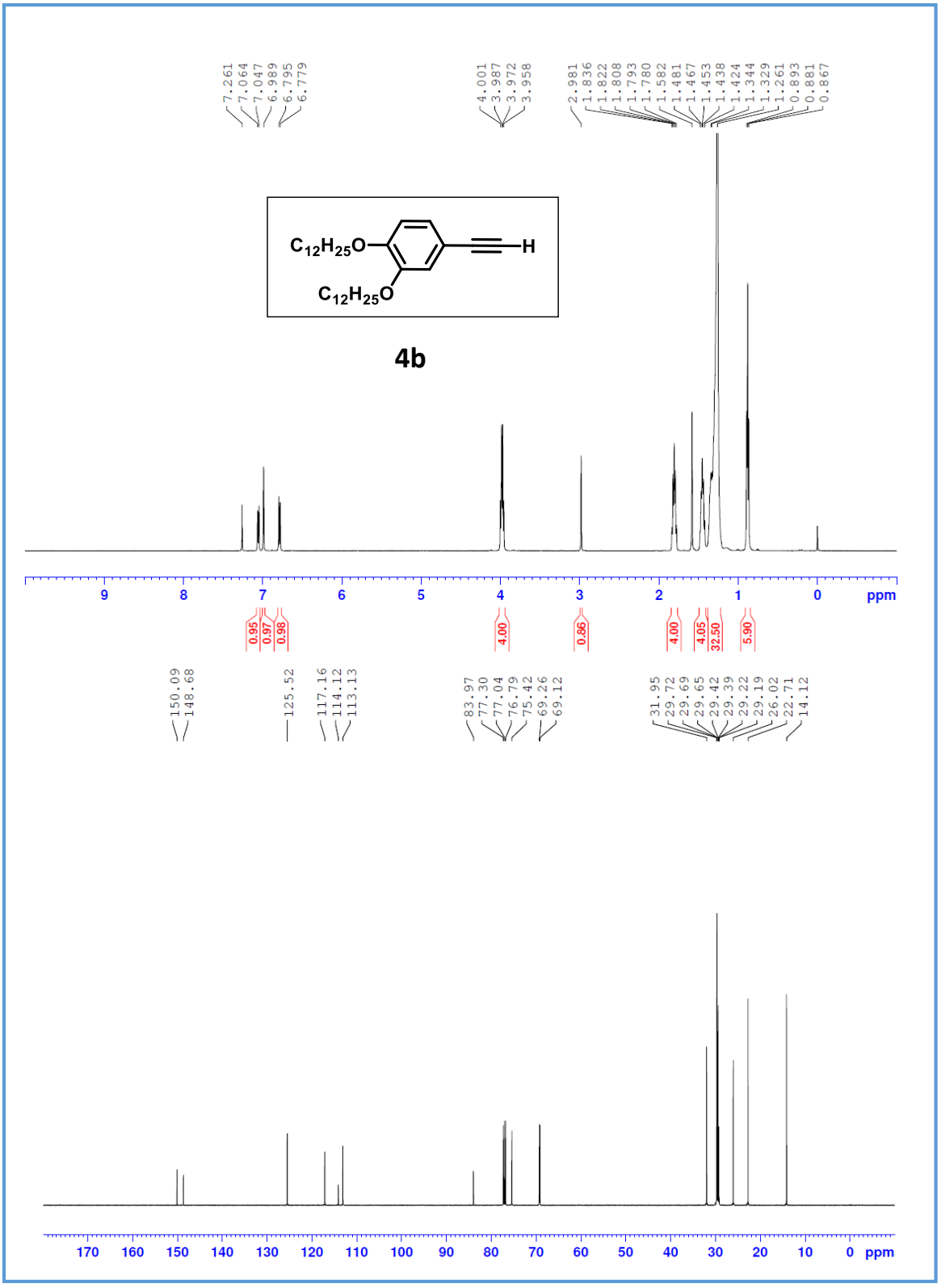

Figure 2.42: ^{1}H (top) and ^{13}C-NMR (bottom) spectra of **4b**

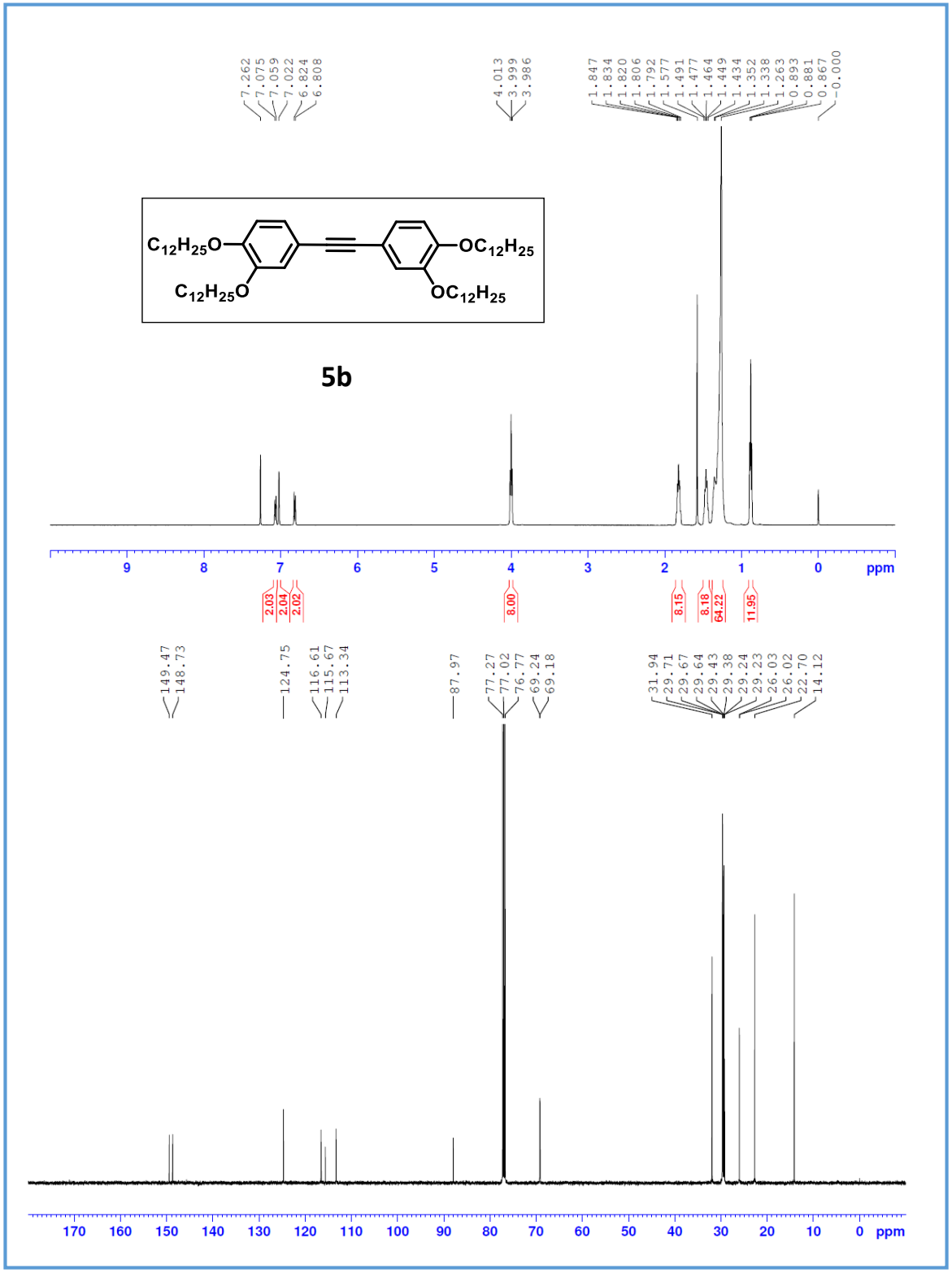

Figure 2.43: ^{1}H (top) and ^{13}C-NMR (bottom) spectra of **5b**

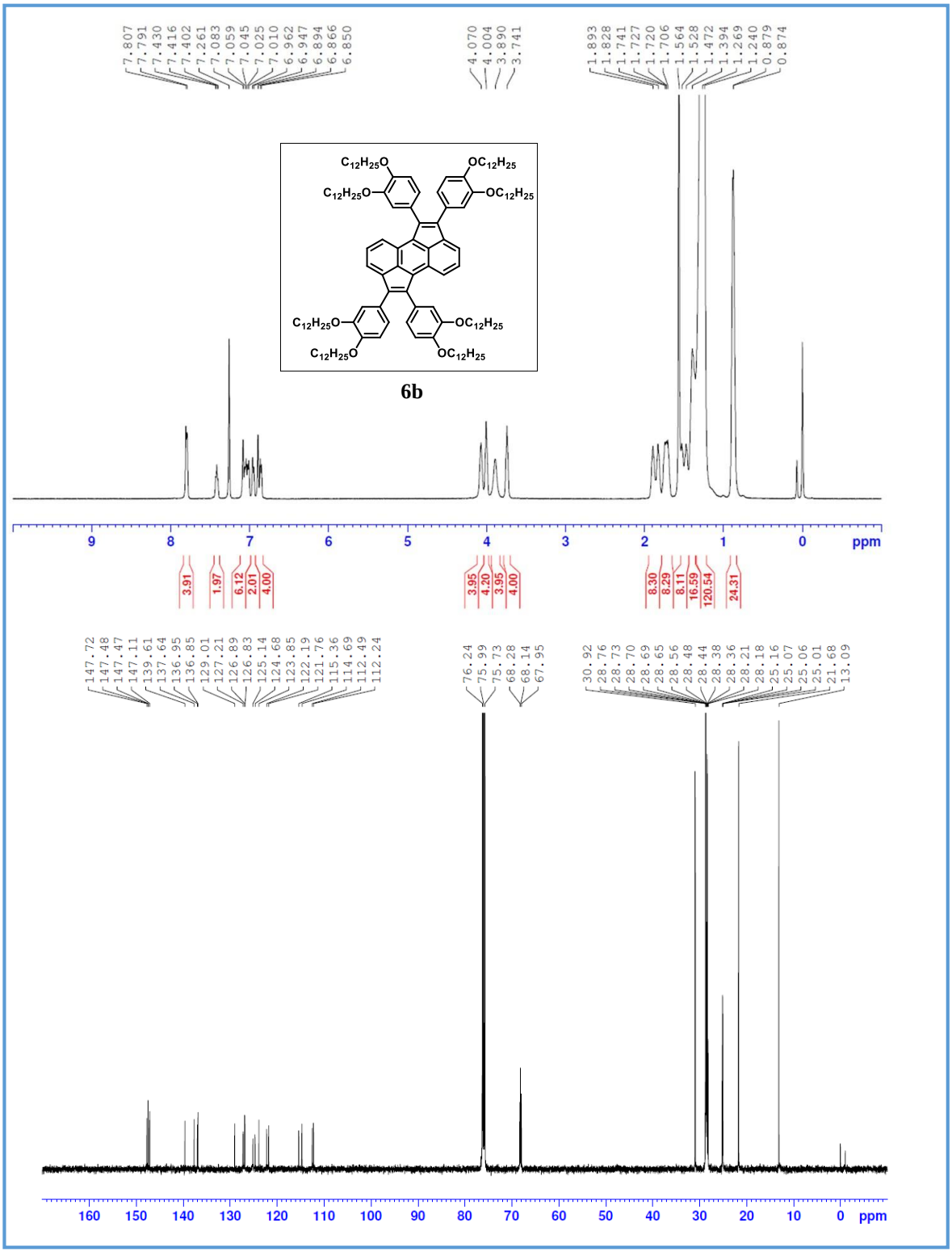

Figure 2.44: ^{1}H (top) and ^{13}C-NMR (bottom) spectra of **6b**

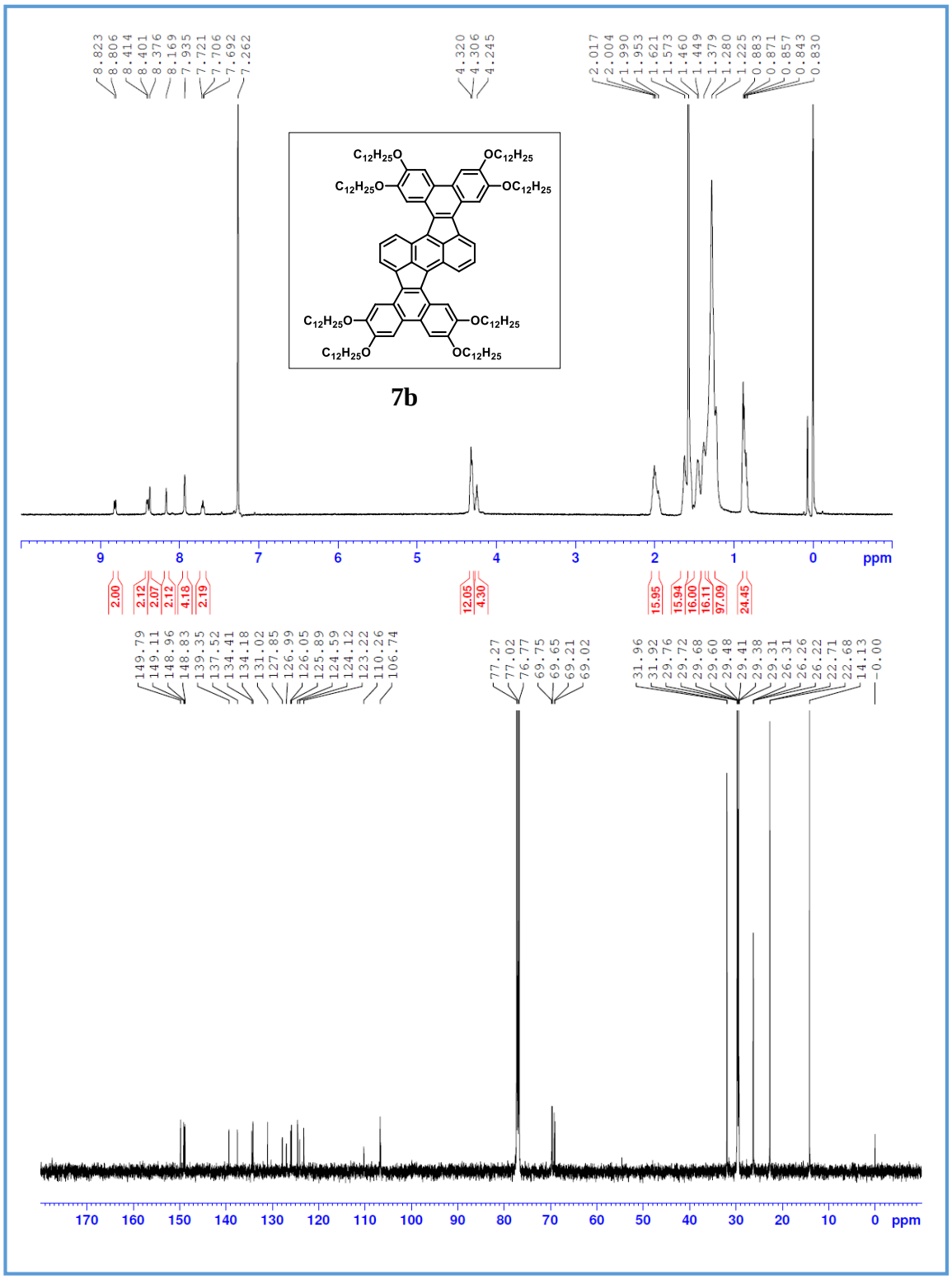

Figure 2.45: ^{1}H (top) and ^{13}C-NMR (bottom) spectra of **7b**

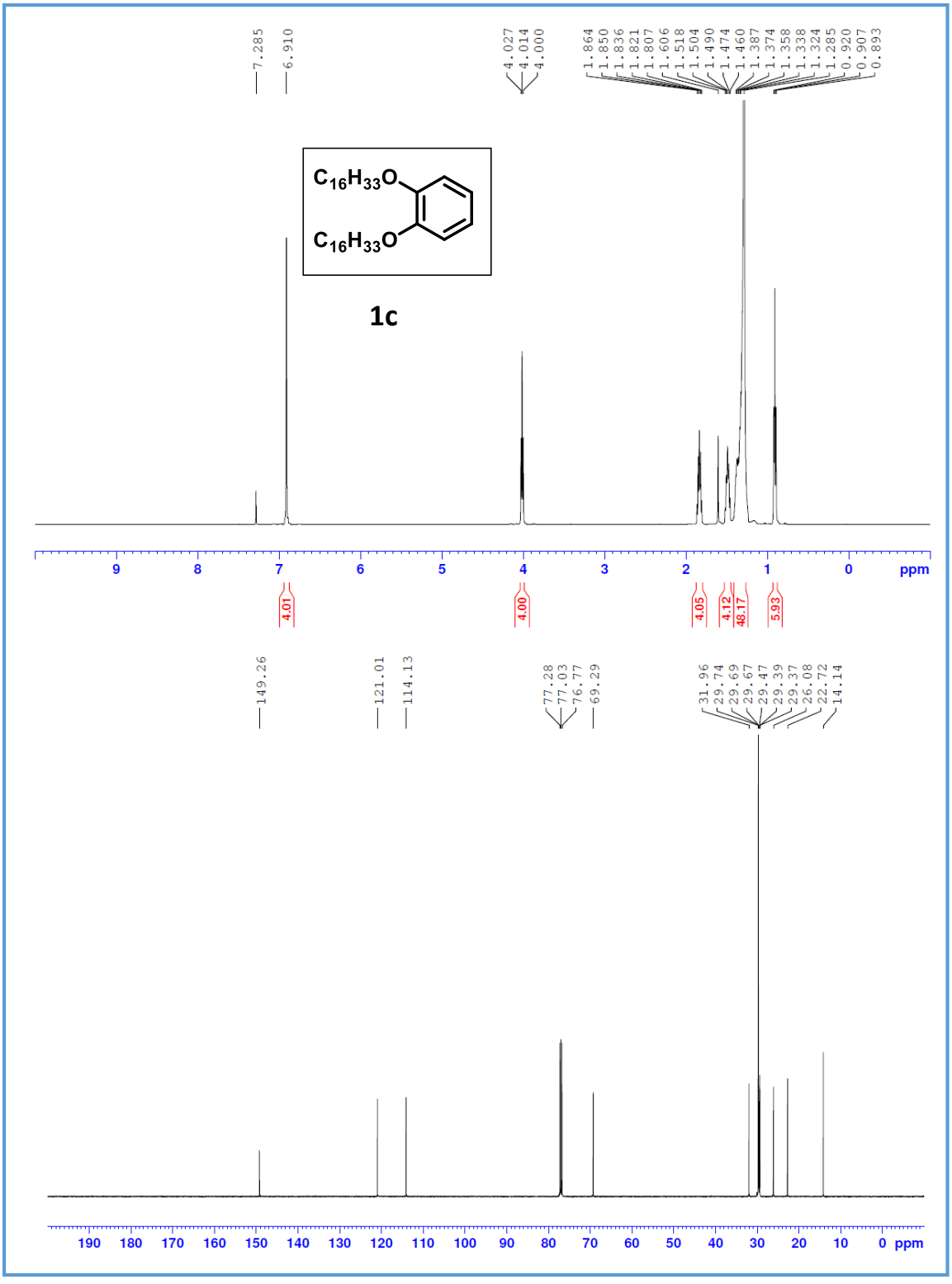

Figure 2.46: ^{1}H (top) and ^{13}C-NMR (bottom) spectra of **1c**

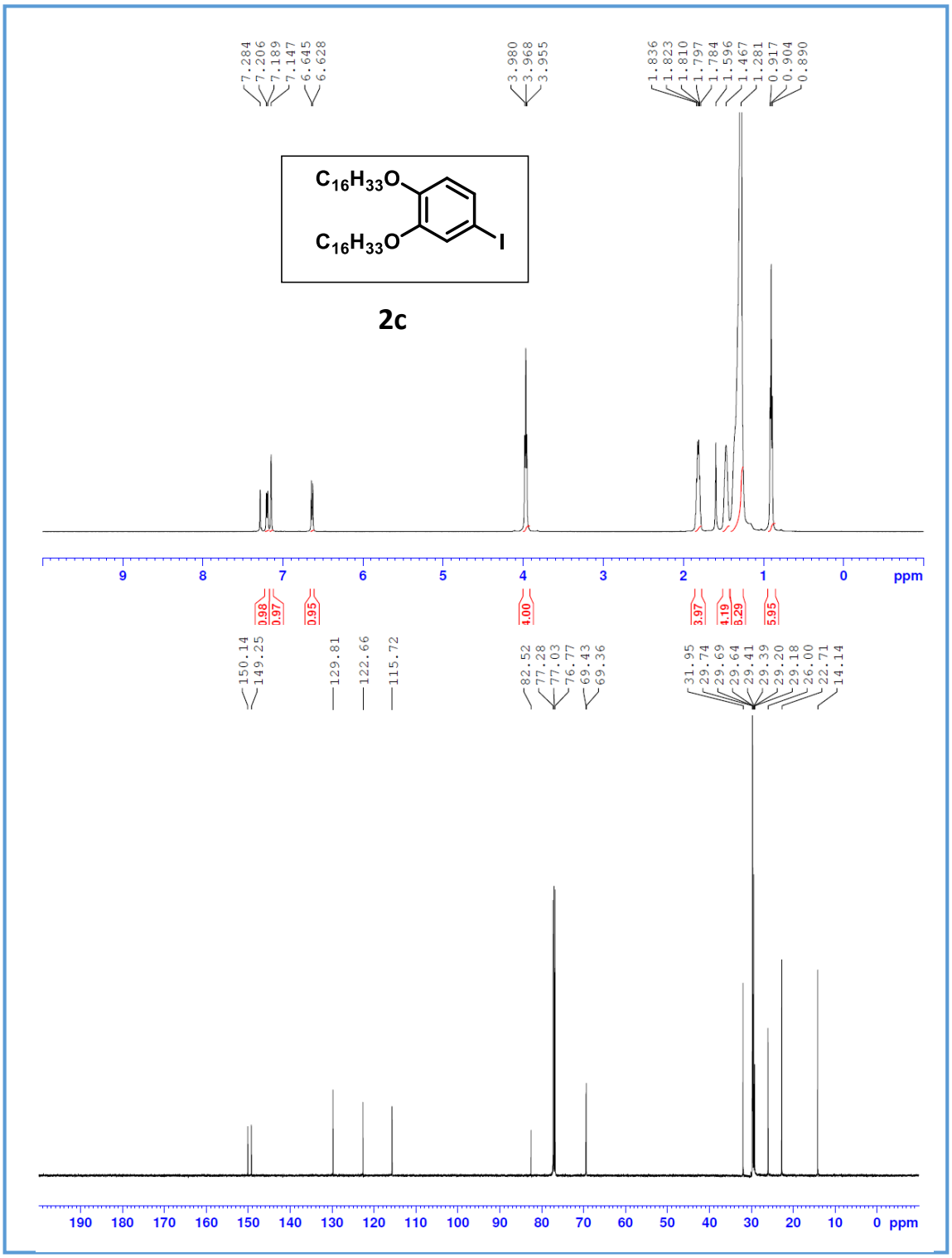

Figure 2.47: ^{1}H (top) and ^{13}C-NMR (bottom) spectra of **2c**

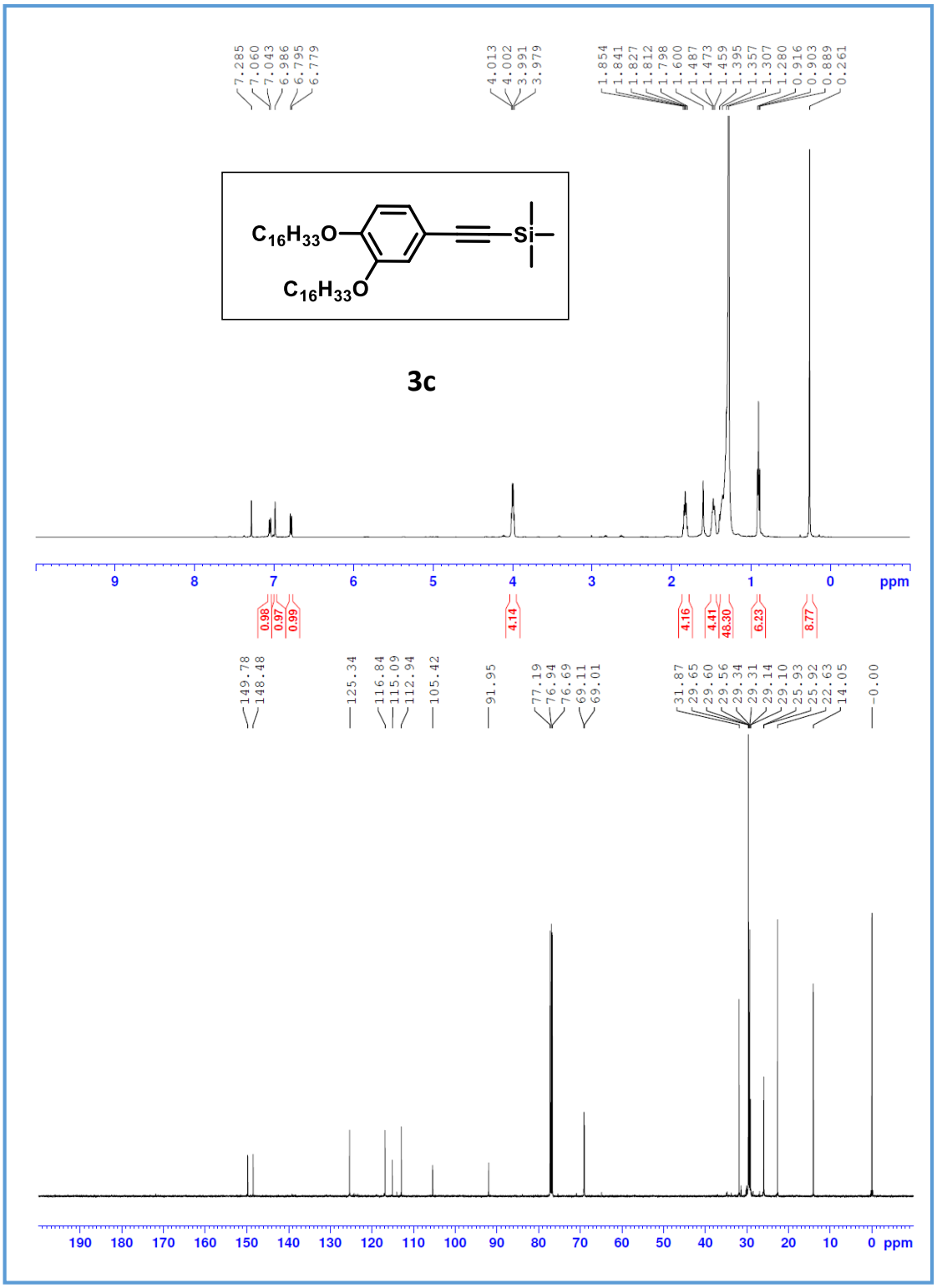

Figure 2.48: ^{1}H (top) and ^{13}C-NMR (bottom) spectra of **3c**

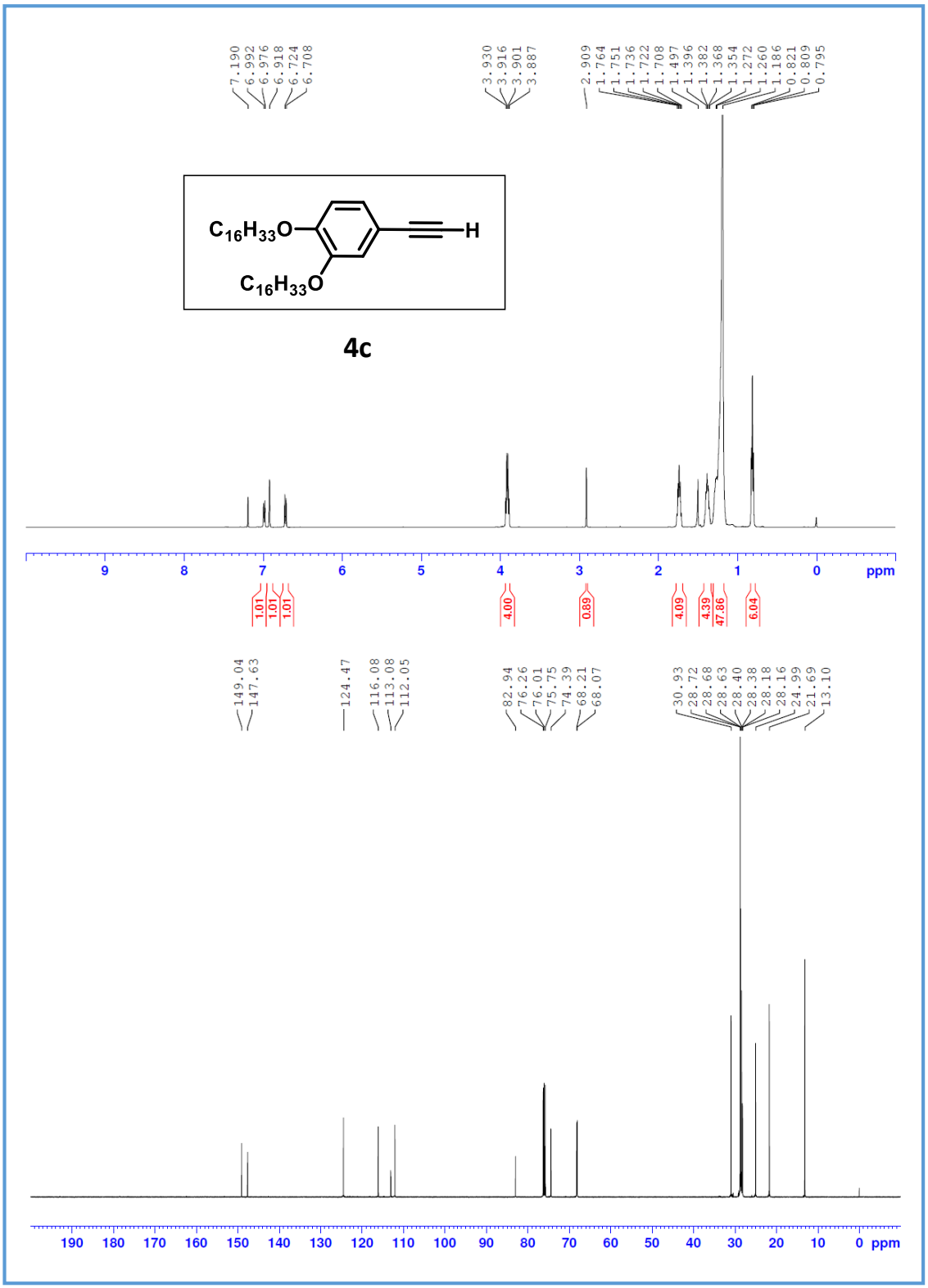

Figure 2.49: ^{1}H (top) and ^{13}C-NMR (bottom) spectra of **4c**

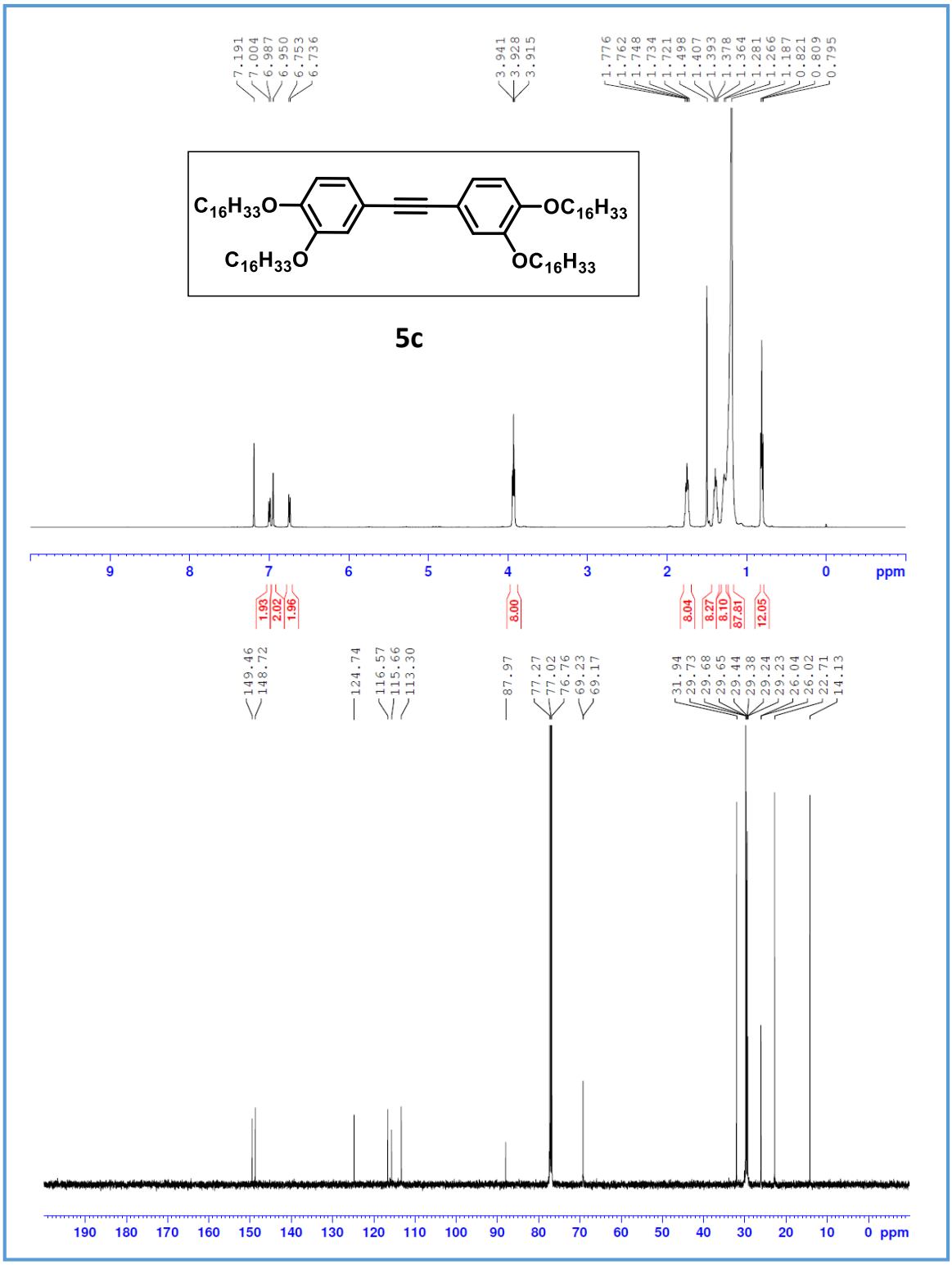

Figure 2.50: ^{1}H (top) and ^{13}C-NMR (bottom) spectra of **5c**

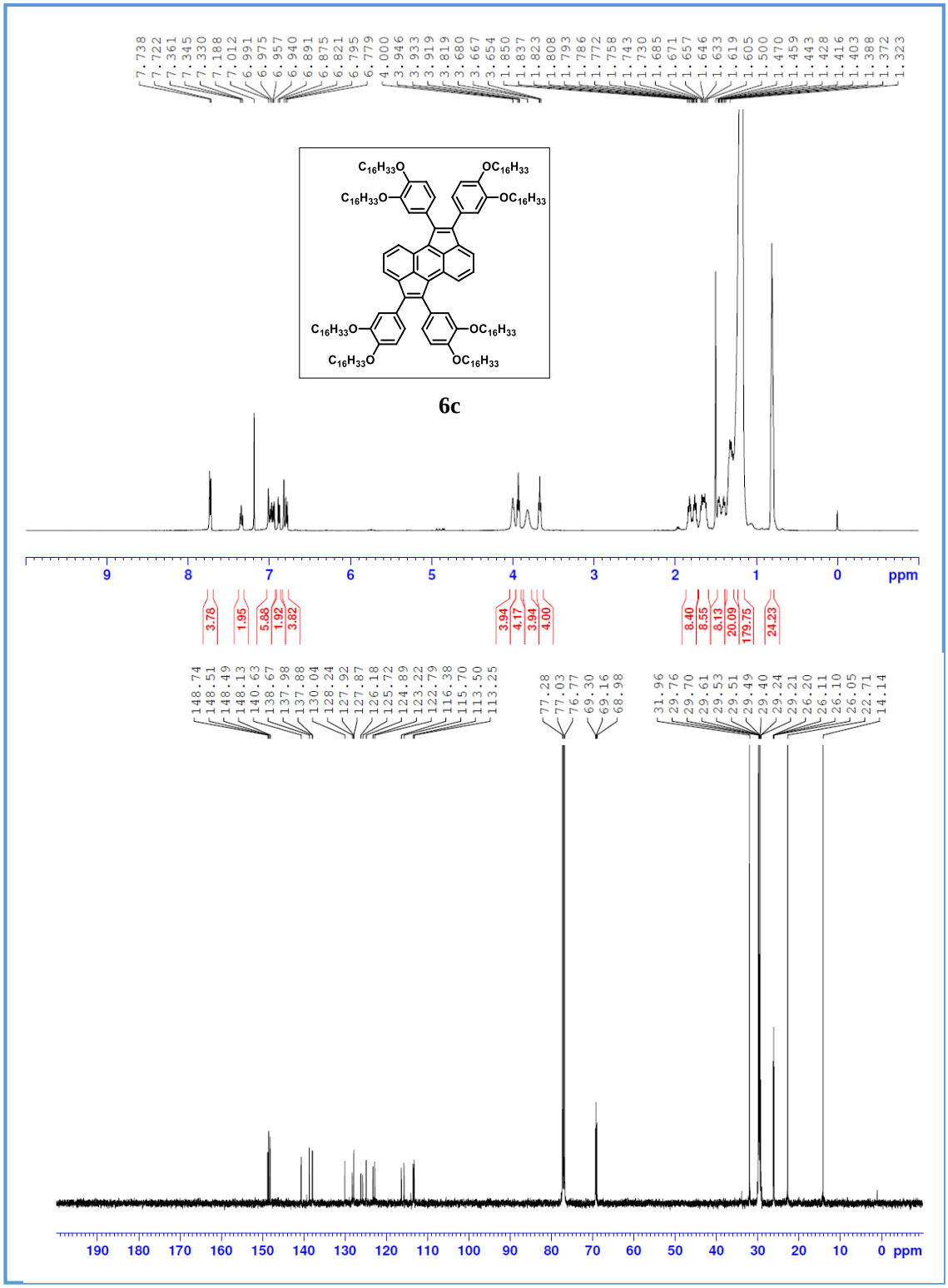

Figure 2.51: ^{1}H (top) and ^{13}C-NMR (bottom) spectra of **6c**

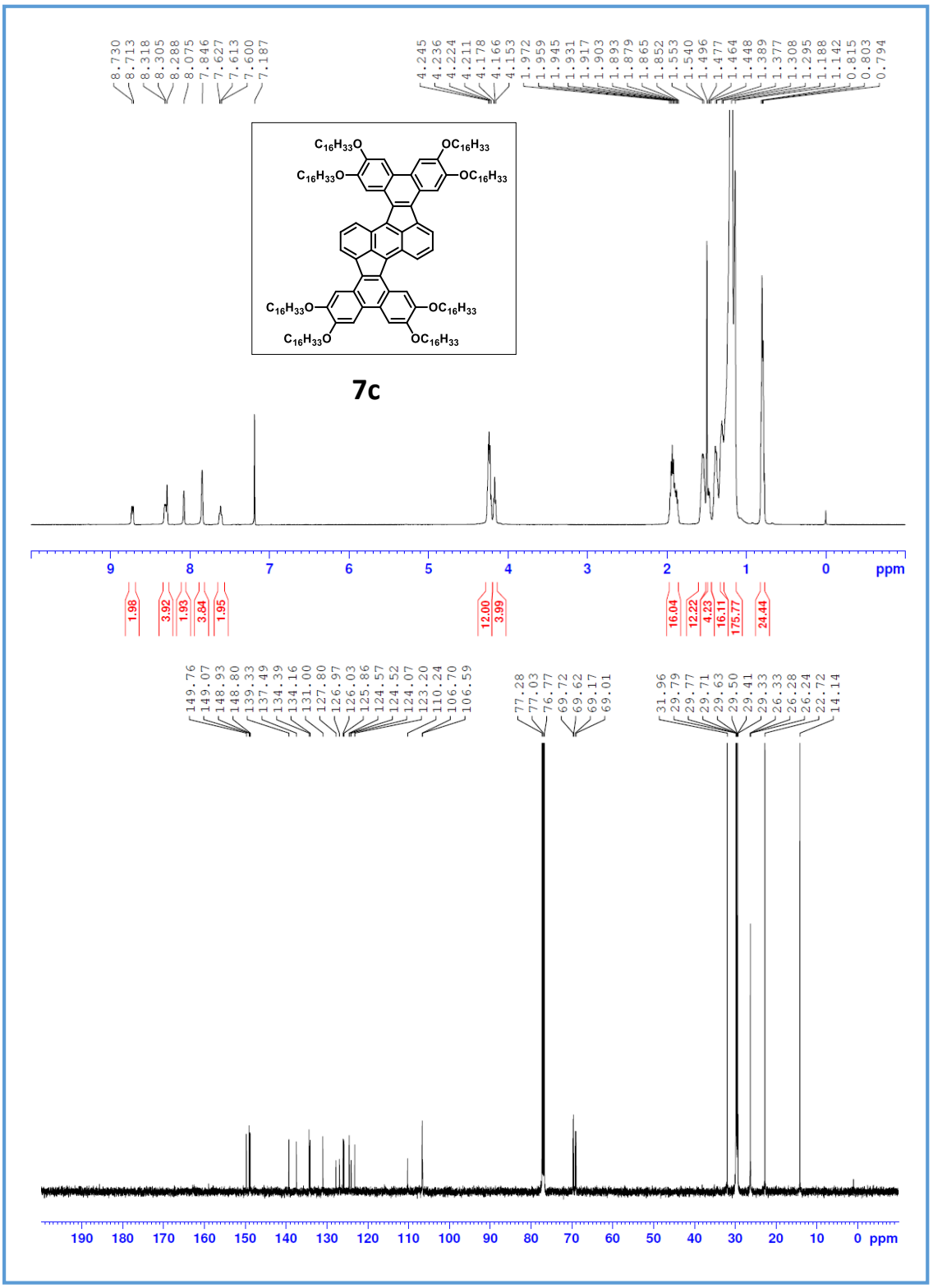

Figure 2.52: ^{1}H (top) and ^{13}C-NMR (bottom) spectra of **7c**

2.8. References:

[1] J. C. Fetzer, *Polycycl. Aromat. Compd.* **2007**, *27*, 143–162.

[2] K. F. Lang, M. Zander, *Chem. Ber.* **1964**, *97*, 2860–2863.

[3] K. F. Lang, H. Buffleb, *Chem. Ber.* **1962**, *95*, 1049–1051.

[4] R. Anschütz, M. E. Scholl, *Justus Liebig's Ann. der Chemie* **1911**, *379*, 333–350.

[5] R. Scholl, J. Mansfeld, *Berichte der Dtsch. Chem. Gesellschaft* **1910**, *43*, 1734–1746.

[6] R. Koch, *Acta Hydrochim. Hydrobiol.* **1985**, *13*, 258–258.

[7] S. Hagen, H. Hopf, Springer, Berlin, Heidelberg, **1998**, pp. 45–89.

[8] P. von R. Schleyer, *Chem. Rev.* **2001**, *101*, 1115–1118.

[9] M. Mas-Torrent, C. Rovira, *Chem. Rev.* **2011**, *111*, 4833–56.

[10] V. C. Sundar, J. Zaumseil, V. Podzorov, E. Menard, R. L. Willett, T. Someya, M. E. Gershenson, J. A. Rogers, *Science* **2004**, *303*, 1644–1646.

[11] I. Kang, H. J. Yun, D. S. Chung, S. K. Kwon, Y. H. Kim, *J. Am. Chem. Soc.* **2013**, *135*, 14896–14899.

[12] M. Kim, S. U. Ryu, S. A. Park, K. Choi, T. Kim, D. Chung, T. Park, *Adv. Funct. Mater.* **2020**, *30*, 1904545.

[13] S. Kumar, *Liq. Cryst.* **2009**, *36*, 607–638.

[14] S. Kumar, *Chem. Soc. Rev.* **2006**, *35*, 83–109.

[15] A. Gowda, M. Kumar, S. Kumar, *Liq. Cryst.* **2017**, 1–28.

[16] T. Wöhrle, I. Wurzbach, J. Kirres, A. Kostidou, N. Kapernaum, J. Litterscheidt, J. C. Haenle, P. Staffeld, A. Baro, F. Giesselmann, et al., *Chem. Rev.* **2016**, *116*, 1139–1241.

[17] S. Laschat, A. Baro, N. Steinke, F. Giesselmann, C. Hägele, G. Scalia, R. Judele, E. Kapatsina, S. Sauer, A. Schreivogel, et al., *Angew. Chemie Int. Ed.* **2007**, *46*, 4832–4887.

[18] R. J. Bushby, N. Boden, in *Handb. Liq. Cryst.*, Wiley-VCH Verlag GmbH & Co. KGaA, Weinheim, Germany, **2014**, pp. 1–33.

[19] R. J. Bushby, O. R. Lozman, *Curr. Opin. Colloid Interface Sci.* **2002**, *7*, 343–354.

[20] J. Sakuda, T. Yasuda, T. Kato, *Isr. J. Chem.* **2012**, *52*, 854–862.

[21] M. Funahashi, H. Shimura, M. Yoshio, T. Kato, in *Liq. Cryst. Funct. Assem. Their Supramol. Struct.*, Springer Berlin Heidelberg, Berlin, Heidelberg, **2007**, pp. 151–179.

[22] T. Kato, N. Mizoshita, K. Kishimoto, **2006**, 38–68.

[23] E. Keinan, S. Kumar, R. Moshenberg, R. Ghirlando, E. J. Wachtel, *Adv. Mater.* **1991**, *3*, 251–254.

[24] S. Kumar, E. J. Wachtel, E. Keinan, *J. Org. Chem.* **1993**, *58*, 3821–3827.

[25] S. Kumar, S. K. Varshney, *Mol. Cryst. Liq. Cryst.* **2002**, *378*, 59–64.

[26] S. KUMAR, M. MANICKAM, *Liq. Cryst.* **1999**, *26*, 1097–1099.

[27] S. Kumar, M. Manickam, *Mol. Cryst. Liq. Cryst. Sci. Technol. Sect. A. Mol. Cryst. Liq. Cryst.* **2000**, *338*, 175–179.

[28] S. Krishna Prasad, D. S. Shankar Rao, S. Chandrasekhar, S. Kumar, in *Mol. Cryst. Liq. Cryst.*, **2003**, pp. 121–139.

[29] S. Sergeyev, W. Pisula, Y. H. Geerts, *Chem. Soc. Rev.* **2007**, *36*, 1902.

[30] S. K. Varshney, H. Nagayama, H. Takezoe, V. Prasad, *Liq. Cryst.* **2009**, *36*, 1409–1415.

[31] H. Nagayama, S. K. Varshney, M. Goto, F. Araoka, K. Ishikawa, V. Prasad, H. Takezoe, *Angew. Chemie* **2010**, *122*, 455–458.

[32] C. Nuckolls, T. J. Katz, *J. Am. Chem. Soc.* **1998**, *120*, 9541–9544.

[33] C. Nuckolls, R. Shao, W.-G. Jang, N. A. Clark, D. M. Walba, T. J. Katz, *Chem. Mater.* **2002**, *14*, 773–776.

[34] C. Nuckolls, T. J. Katz, G. Katz, P. J. Collings, L. Castellanos, *J. Am. Chem. Soc.* **1999**, *121*, 79–88.

[35] A. J. Lovinger, C. Nuckolls, T. J. Katz, *J. Am. Chem. Soc.* **1998**, *120*, 264–268.

[36] S. Xiao, M. Myers, Q. Miao, S. Sanaur, K. Pang, M. L. Steigerwald, C. Nuckolls, *Angew. Chemie Int. Ed.* **2005**, *44*, 7390–7394.

[37] S. Nobusue, K. Fujita, Y. Tobe, *Org. Lett.* **2017**, *19*, 3227–3230.

[38] Y. Chen, T. Marszalek, T. Fritz, M. Baumgarten, M. Wagner, W. Pisula, L. Chen, K. Müllen, *Chem. Commun.* **2017**, *53*, 8474–8477.

[39] M.-J. Lin, Á. J. Jiménez, C. Burschka, F. Würthner, *Chem. Commun.* **2012**, *48*, 12050.

[40] M. Ball, Y. Zhong, Y. Wu, C. Schenck, F. Ng, M. Steigerwald, S. Xiao, C. Nuckolls, *Acc. Chem. Res.* **2015**, *48*, 267–276.

[41] S. Pola, C. H. Kuo, W. T. Peng, M. M. Islam, I. Chao, Y. T. Tao, *Chem. Mater.* **2012**, *24*, 2566–2571.

[42] W. Pisula, X. Feng, K. Müllen, *Chem. Mater.* **2011**, *23*, 554–567.

[43] S. J. Kang, J. B. Kim, C.-Y. Chiu, S. Ahn, T. Schiros, S. S. Lee, K. G. Yager, M. F. Toney, Y.-L. Loo, C. Nuckolls, *Angew. Chemie Int. Ed.* **2012**, *51*, 8594–8597.

[44] N. C. Davy, G. Man, R. A. Kerner, M. A. Fusella, G. E. Purdum, M. Sezen, B. P. Rand, A. Kahn, Y. L. Loo, *Chem. Mater.* **2016**, *28*, 673–681.

[45] N. J. Tremblay, A. A. Gorodetsky, M. P. Cox, T. Schiros, B. Kim, R. Steiner, Z. Bullard, A. Sattler, W.-Y. So, Y. Itoh, et al., *ChemPhysChem* **2010**, *11*, 799–803.

[46] S. R. Peurifoy, T. J. Sisto, F. Ng, M. L. Steigerwald, R. Chen, C. Nuckolls, *Chem. Rec.* **2019**, *19*, 1050–1061.

[47] J. V. Braun, *Berichte der Dtsch. Chem. Gesellschaft (A B Ser.* **1934**, *67*, 214–218.

[48] A. Schönberg, K.-H. Brosowski, *Chem. Ber.* **1960**, *93*, 2149–2151.

[49] H. Lee, Y. Zhang, L. Zhang, T. Mirabito, E. K. Burnett, S. Trahan, A. R. Mohebbi, S. C. B. Mannsfeld, F. Wudl, A. L. Briseno, *J. Mater. Chem. C* **2014**, *2*, 3361–3366.

[50] R. Schmidt, *Chem. Phys. Lett.* **1988**, *151*, 369–374.

[51] M. Smet, W. Dehaen, *Molecules* **2000**, *5*, 620–628.

[52] C. Gooijer, I. Kozin, N. H. Velthorst, M. Sarobe, L. W. Jenneskens, E. J. Vlietstra, *Spectrochim. Acta Part A Mol. Biomol. Spectrosc.* **1998**, *54*, 1443–1449.

[53] Patrick Mayrhofer, Photophysical Properties of Rubicene, **2012**.

[54] W. G. Shuler, S. P. Parvathaneni, J. B. Rodriguez, T. N. Lewis, A. J. Berges, C. J. Bardeen, M. J. Krische, *Chem. – A Eur. J.* **2021**, *27*, 4898–4902.

[55] M. Moral, A. J. Pérez-Jiménez, J. C. Sancho-García, *J. Phys. Chem. C* **2017**, *121*, 3171–3181.

[56] Y.-C. Chao, S.-C. Yeh, H.-L. Hsu, B.-H. Jiang, K.-H. Sun, C.-T. Chen, C.-P. Chen, R.-J. Jeng, *Org. Electron.* **2017**, *49*, 114–122.

[57] E. A. Jackson, X. Xue, H. Y. Cho, L. T. Scott, *Aust. J. Chem.* **2014**, *67*, 1279.

[58] M. Smet, J. Van Dijk, W. Dehaen, *Synlett* **1999**, *1999*, 495–497.

[59] M. Smet, R. Shukla, L. Fueloep, W. Dehaen, *ChemInform* **2010**, *30*, no-no.

[60] H. H. Hseuh, M. Y. Hsu, T. L. Wu, R. S. Liu, *J. Org. Chem.* **2009**, *74*, 8448–8451.

[61] J. Liu, S. Osella, J. Ma, R. Berger, D. Beljonne, D. Schollmeyer, X. Feng, K. Müllen, *J. Am. Chem. Soc.* **2016**, *138*, 8364–8367.

[62] S. R. Bheemireddy, P. C. Ubaldo, A. D. Finke, L. Wang, K. N. Plunkett, *J. Mater. Chem. C* **2016**, *4*, 3963–3969.

[63] S. R. Bheemireddy, W. A. Hussain, A. Uddin, Y. Du, M. P. Hautzinger, P. V. Kevorkian, F. A. Petrie, K. N. Plunkett, *Chem. Commun.* **2018**, *54*, 14140–14143.

[64] W. A. Hussain, K. N. Plunkett, *J. Org. Chem.* **2021**, *86*, 12569–12576.

[65] X. Zhu, S. R. Bheemireddy, S. V. Sambasivarao, P. W. Rose, R. Torres Guzman, A. G. Waltner, K. H. Dubay, K. N. Plunkett, *Macromolecules* **2016**, *49*, 127–133.

[66] S. R. Bheemireddy, M. P. Hautzinger, T. Li, B. Lee, K. N. Plunkett, *J. Am. Chem. Soc.* **2017**, *139*, 5801–5807.

[67] S. Irla, M. Pruthvi, V. A. Raghunathan, S. Kumar, *Dye. Pigment.* **2021**, *194*, 109574.

[68] S. R. Bheemireddy, P. C. Ubaldo, A. D. Finke, L. Wang, K. N. Plunkett, *J. Mater. Chem. C* **2016**, *4*, 3963–3969.

[69] E. J. Foster, J. Babuin, N. Nguyen, V. E. Williams, *Chem. Commun.* **2004**, 2052–2053.

[70] D. D. Prabhu, A. P. Sivadas, S. Das, *J. Mater. Chem. C* **2014**, *2*, 7039.

Chapter - 3

Design and synthesis of extended pyrene based discotic liquid crystalline materials

Abstract

The past few years have witnessed tremendous progress towards the design of new liquid crystalline (LC) materials comprised of rigid π-conjugated molecules, particularly disc shape molecules with appropriate substitution as an active component for the electronic device applications. Herein we report a new class of polycyclic aromatic hydrocarbons (PAHs) derived from pyrene core. These molecules are synthesized with 1, 6 dibromo pyrene and di-substituted arylethynylene via palladium-catalyzed cyclopentannulation followed by Scholl reaction. All the synthesized compounds were fully characterized from their spectral data and elemental analysis. LC properties of these compounds were studied using polarizing optical microscopy, differential scanning calorimetry, and X-ray diffractometry. We found molecules preferentially align homeotropically in the columnar mesophase. Pyrene derivatives have been extensively explored as novel dyes and widely used in various device applications. Therefore, these novel self-assembling supramolecular materials may find application in several optoelectronic devices.

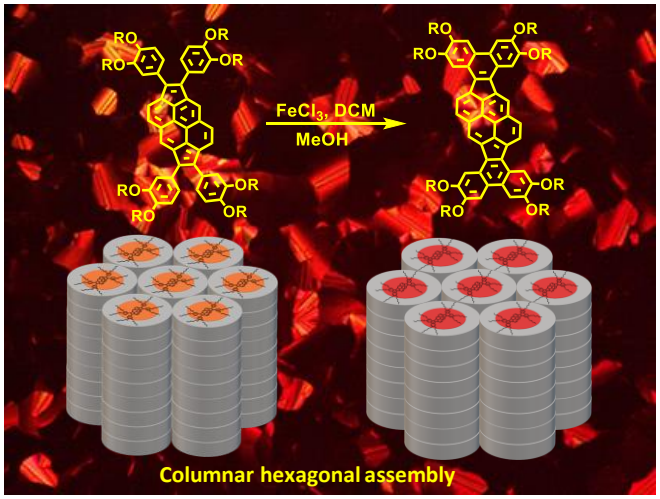

3.1 Introduction:

Pyrene belongs to the polycyclic aromatic hydrocarbon family (PAH) (**Figure 3.1**) and consists of four fused benzene rings, resulting in a large and flat aromatic system. It is a colorless or pale yellow solid and obtained from the combustion of organic materials. [1,2] It can be prepared using different pyrolytic processes, such as pyrolysis of acetylene and hydrogen,[3] pyrolysis of natural gas and destructive distillation of soft coal tar.[4] The pyrene molecule is highly symmetrical, which belongs to the point group D_{2h} *and* can also be viewed as one of the basic structure for graphite and fullerene subunits[5]. It is an aromatic compound with 16 π electrons, but disobeys the Huckels 4*n* + 2 rule of aromaticity. However, it obeys Clar's aromatic π-sextet rule [6]. Platt's ring perimeter[7] and the Randic – Herndon conjugated circuit [8–11] are the models commonly selected for the qualitative characterization of the aromaticity of PAHs.

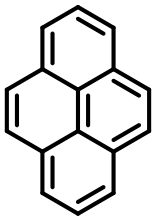

Figure 3.1: Structure of the pyrene molecule

Weizenbock and co-workers were the first to synthesize pyrene molecules in 1913 from o, o'-ditolyl[12]. Until the 1950s, several reports had been documented using different synthetic routes from the same starting compound[13]. Afterward, the distillation process of coal tar and destructive hydrogenation of hard coal methods were used for preparing pyrene molecules and other polycyclic hydrocarbons for commercial use.

3.1.1 Photochemical properties of pyrene

Pyrene is a key molecule in photochemistry. The absorption and fluorescence spectrum of pyrene in the UV-vis region is well studied in the literature[14,15]. Theoretical methods have also been employed to analyze pyrene molecules excitation and emission properties either in the gas or in solvent phases. These results are consistent with experimental data[16–18]. The UV-vis spectrum of pyrene in dichloromethane (1mM) and its fluorescence emission spectra (the

pyrene molecule excited at 337 nm) at 0.5 mM concentration in a 1M NaOH solution shown in **Figure 3.2**. [19]

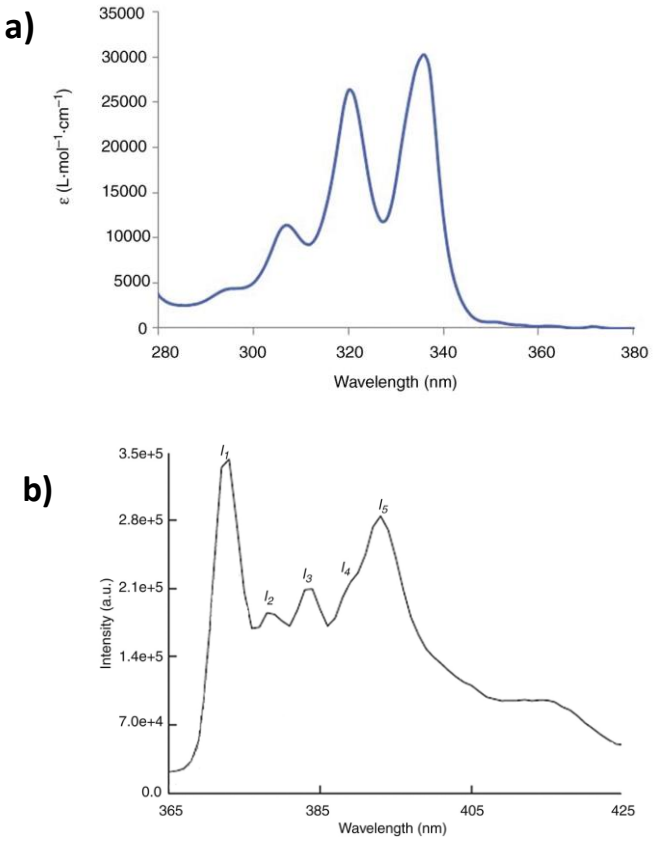

Figure 3.2: a) absorbance b) emission spectra of pyrene molecule.[20]

In the beginning, pyrene was used to prepare many dye derivatives, like pyranthrone, for the synthetic dye industry[20]. Pyrene exhibits many attractive electrochemical and photophysical attributes, which finds applications in many scientific areas[13]. The above property makes pyrene a suitable candidate for fluorescent sensors and fluorescent probes[21–26]. Forster and Kasper reported the first observation of intermolecular excimer formation in concentrated pyrene solution[27]. This excimer formation (**Figure 3.3**), associated with long-lived excited states, is also well known for its high fluorescence quantum yield[28–30] and the emission spectrum is very sensitive to the polarity of the solvents [31,32]. Except as a fluorescent sensor, there are two significant drawbacks of using pyrene as a fluorescence probe. First is the pyrene monomer absorption and emission wavelengths are confined in the UV region of 310-380 nm. The second one is pyrene can quickly form an excimer after a particular concentration

(0.1mM). For example, probing the biological membranes by fluorescence techniques, it is adorable to have a fluorophore probe that absorbs and emits in the long-wavelength region. Preferably in the visible electromagnetic spectrum, to minimize the spectral overlap of the bio-molecules intrinsic fluorescence that occurs in the UV region[19]. On the other hand, the excimer fluorescence by pyrene and its derivative is sensitive to environmental parameters, such as temperature[40], pressure[47], and pH[48]. Changes in the excimer fluorescence intensity reflect the changes in the environment. Also, it can be used to detect the guest molecules like gases (O_2 or NH_3),[33,34] organic molecules,[35–37] metals,[38–42] and other miscellaneous analytes.[43]

Theoretical [44] and experimental[45] investigations showed the tunability of pyrene electro-optical properties by conjugation with different functional groups[13]. There are some recent advancements in the synthesis and properties of pyrene derivatives in many applications, such as, pyrene labeled oligonucleotides find use in the field of DNA assay[46], biological probes[47,48], electrochemically generated luminescence[49], fluorescent dyes[50], carbon nanotube functionalization[51], supramolecular assembly[52], fluorescence chemosensors[53,54] and photonic devices[55,56].

3.1.2 General applications of pyrene and its derivatives

In addition to its use as a fluorescence probe, pyrene is an organic semiconductor that can be used in material science and only recently in the organic electronics field. In the past few decades, significant progress has been made in the synthesis of organic materials with attractive electronic and photophysical properties in optoelectronic devices.[57–59] New technologies based on organic semiconductors have extensively been promoted to devise applications such as organic light-emitting diodes (OLEDs), organic photovoltaic cells (OPV), organic field-effect transistors (OFETs), organic lasers, and memory cells[13]. They also find applications in flat-panel displays, lighting, RFID (radio frequency identification tags), electronic skin, and solar modules.

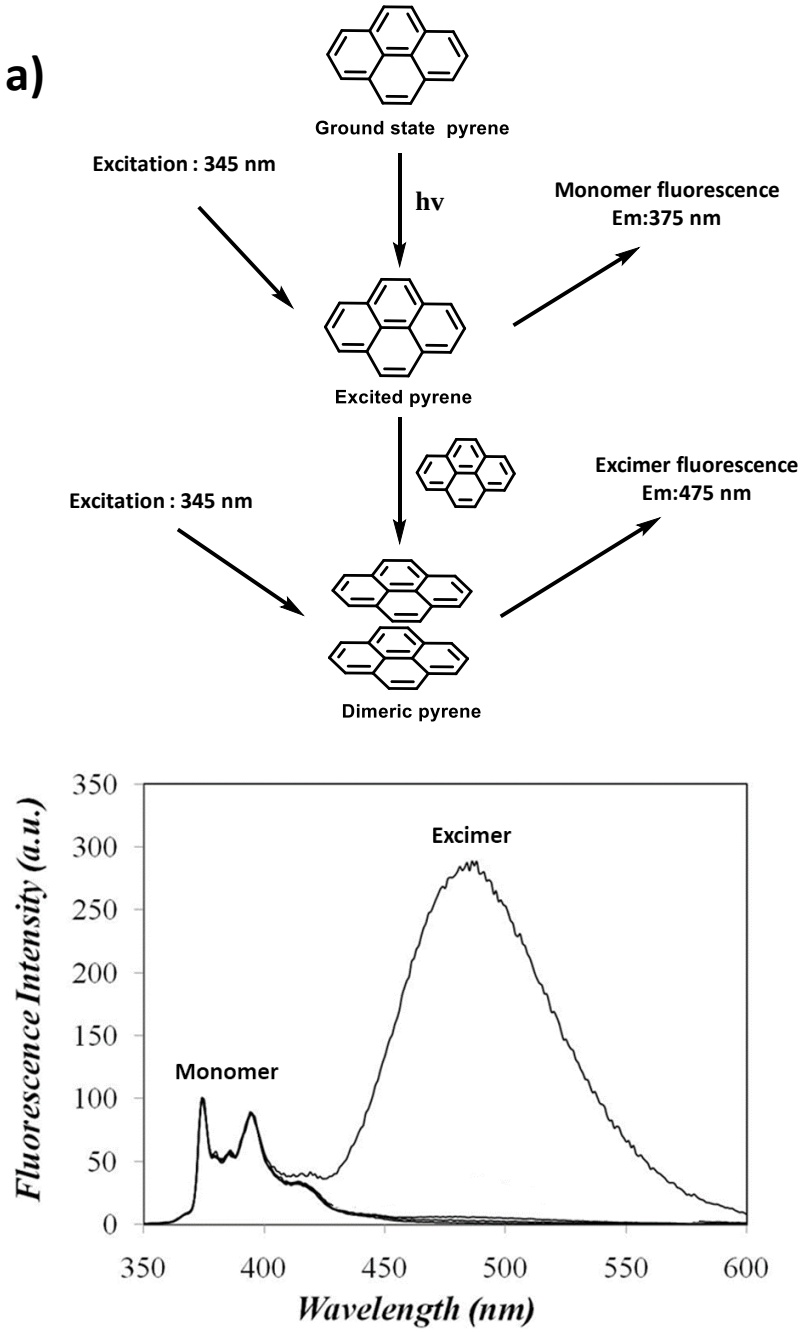

Figure 3.3: a) Schematic representation of monomer and excimer formation b) emission spectra of pyrene monomer and excimer

3.1.3 Pyrene in liquid crystal field

In the continuous search for organic semiconductors for improved electronic devices/properties, discotic liquid crystals have attracted considerable interest due to their self-organization and electronic properties. Moreover, pyrene derivatives were also found to show

liquid crystalline (LC) properties[13]. One large group of LC phases formed by disc-shaped aromatic compounds falls into discotic liquid crystals. Discotic liquid crystals (DLCs) have a particular interest because they produce one-dimensional stacks of functional materials and easily processable without using technologically advanced techniques[60–63]. Molecules forming DLCs [64] contain a flat central core with hydrogenated carbon chains disposed around the outside edge of the core[65,66]. DLCs possess the ability to self-organize into highly anisotropic and ordered self-assembled supramolecular columns. Most DLCs (about 95%) form columnar phases as they are mainly derived from polycyclic aromatic cores[67–69]. The self-assembling ability of pyrene derivatives can be designed and tuned according to the defined molecular characteristics of discotic liquid crystalline material required. In addition to its LC properties, the pyrene and its derivatives unique fluorescence can find applications in optoelectronic devices.

The fluorescence decay process/ lifetime of pyrene molecule was studied for the first time in 1969, where the pyrene molecule was incorporated into the liquid crystalline matrix (cholesterol benzoate) [70]. The use of pyrene as a discotic liquid crystal based on different functionalization at the pyrene active site (1, 3, 6, and 8 positions) using divergent synthetic methodologies was reported later[13,45,71]. The general structure of pyrene substitution is given in **Figure 3.4.** The direct electrophilic substitution of pyrene can readily produce both 1-substituted pyrenes and 1,3,6,8-tetrasubstituted pyrenes.

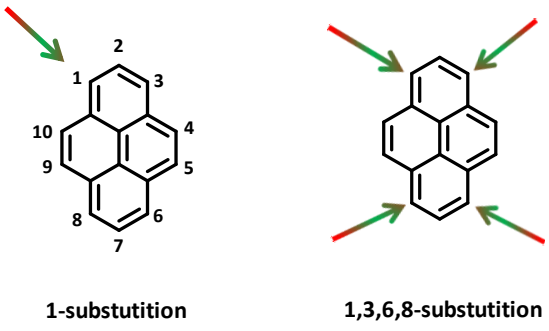

Figure 3.4: The general structure of 1-substituted and 1,3,6,8-tetrasubstituted pyrenes.

The preparation of mono and tetrasubstituted pyrene derivatives are relatively more straightforward than disubstituted pyrenes. The selective synthesis of disubstituted pyrenes is challenging. It is essential to obtain well-defined disubstituted pyrene derivatives for the

controlled synthesis of linear or cyclic oligomers and polymers. In this context, the substitution at the 1,3,6,8-positions of the pyrene aromatic system with flexible side chains represent a fascinating approach to form liquid crystalline columnar superstructures.

Pyrene can be easily substituted at 1, 3, 6 and 8 positions to prepare discotic liquid crystals. Halogenation (bromination or chlorination) of pyrene **1** provides 1,3,6,8-tetrahalopyrene **2** in excellent yield[72,73]. Compound **2,** when treated with fuming sulfuric acid followed by hydrolysis, yields 3,6-dihydroxypyrene-1,6-quinone **3**. The reductive esterification of the **3** in the presence of different acid chlorides offers various 1,3,6,8-tetraalkanoyloxypyrene derivatives **4.** The synthetic scheme is given in (**Figure 3.5**).

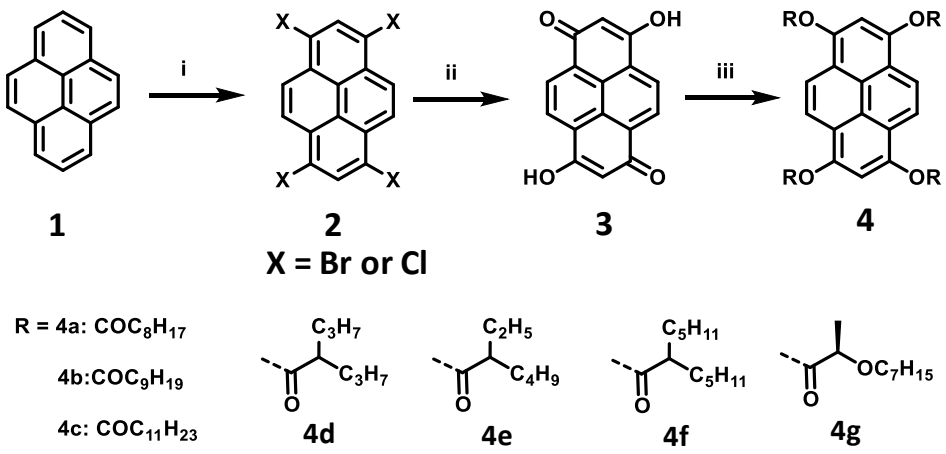

Figure 3.5: Synthesis of pyrene tetraesters: (i) Br_2, nitrobenzene or Cl_2, $C_2H_2Cl_4$; (ii) 25% H_2SO_4-SO_3; 40% H_2SO_4, H_2O; (iii) RCOCl, Zn, DMAP, THF, pyridine.

Pyrene tetra esters with long linear alkyl chains **4a–c** and branched chains **4d–f** are found to be non-mesomorphic, but when obtained via charge-transfer complexation with TNF, the columnar phases can be induced. Conversely, the chiral tetraester **4g** exhibits a monotropic columnar mesophase upon cooling below 34°C, which appears as a flower-like texture under the cross-polarized optical microscopy (POM), as shown in **Figure 3.6**[72]. The mesophase clears at 39°C on heating. This material also displays ferroelectric switching. Surprisingly, short-chain standard alkyl esters **5a**, **5b** and racemic 2-ethylhexyl ester, **5h**, are reported to be

liquid crystalline[74–76]. The chemical structure is given in **Figure 3.7.** These tetraesters have been used to fabricate an organic light-emitting diode device[75].

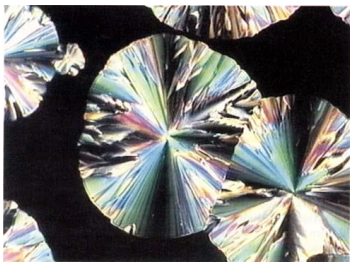

Figure 3.6: Flower-like textures are growing from the isotropic liquid upon cooling.[72]

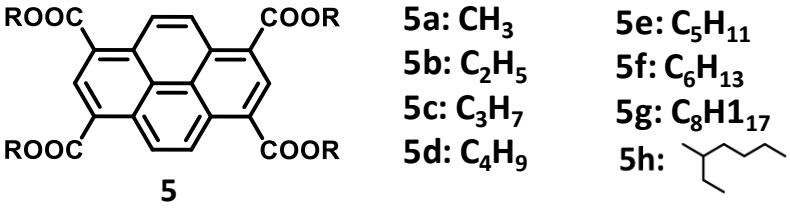

Figure 3.7: Chemical structure of pyrene-based liquid crystalline aromatic esters.

Several reports on the synthesis of the tetrasubstituted pyrene derivatives, like ethers, esters, benzoates, and thioethers, show the non-mesomorphic behavior. The chemical structure is given in (**Figure 3.8**, **6a – 6j**). The monoalkoxyphenyl-substituted derivatives (**Figure 3.8**, **6a)** were also not liquid crystalline.[77] However, dialkoxyphenyl-substituted products (**Figure 3.9, 7b**, **7c)** show the liquid crystalline behavior. It offers a small range of the Col_h phase, which quickly forms a glassy phase at ambient temperature. TOF (time of flight) measurements showed an ambipolar charge transport for **7b** with the mobilities on the order of 10^{-3} cm^2 V^{-1} s^{-1}[78].

Trialkoxyphenylethynyl substituted derivative (**Figure 3.9, 8)** is a highly fluorescent material, which shows a high quantum yield and also exhibits enantiotropic columnar mesophase phases (columnar rectangular and columnar hexagonal) over a broad range of temperature[79]. The POM texture and schematic representation of the mesophase are given in (**Figure 3.10).** This clearly demonstrates the importance of space-filling around the core in inducing mesomorphism.

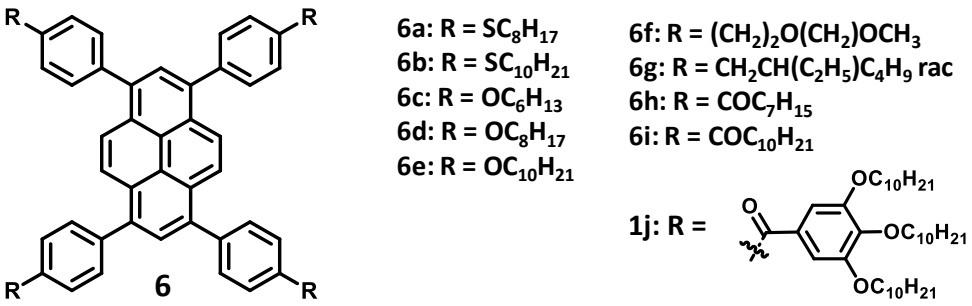

Figure 3.8: Structure of tetra aryl derivatives.[78]

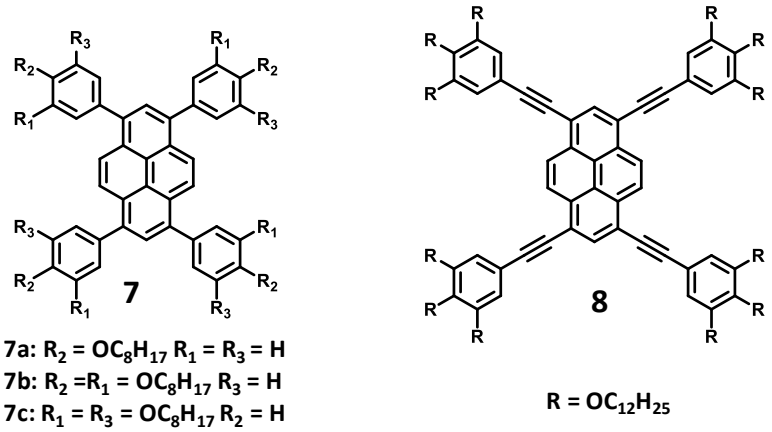

Figure 3.9: Structure of tetra aryl derivatives.[79]

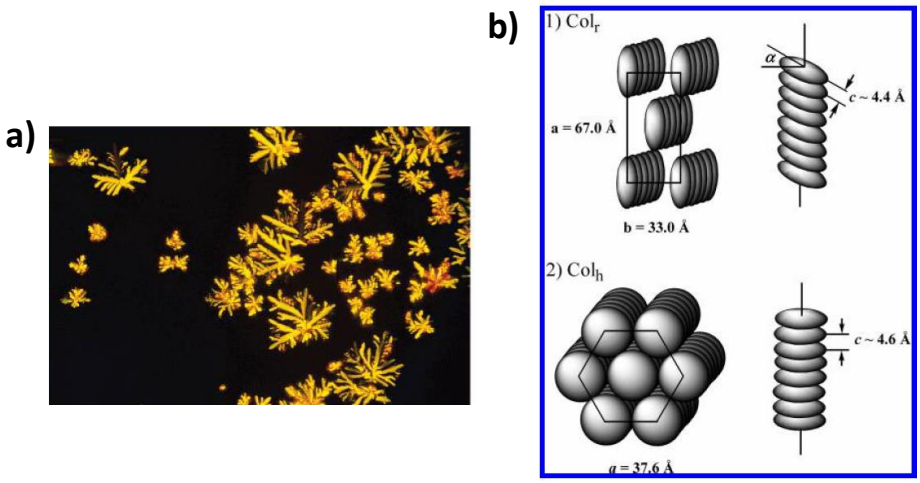

Figure 3.10: a) POM texture cooling upon isotropic phase b) schematic representation of columnar mesophases.[80]

Mikio Yasutake et al. reported two *anti*-type and three *syn*-type alkoxy pyrene derivatives, using a pyrenedione unit as a core. Short-chain derivatives (**Figure 3.11, 9a, 9b,** and **10a)** are non-mesomorphic, longer alkoxy chain derivatives (**Figure 3.11, 9c, 9d, 10b, 10c and 10d)** show the liquid crystalline phases having a terrace and band textures. These molecules are self-assembled into a discotic lamellar phase D_{L2}[80].

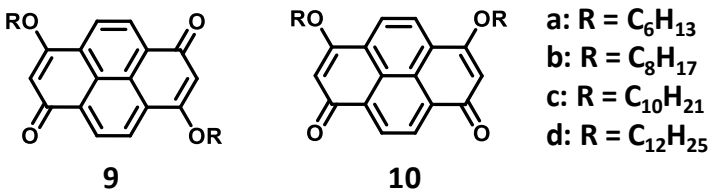

Figure 3.11: Synthesis of dialkoxy *syn*- and *anti*-pyrenediones.[80]

The majority of liquid crystals formed by the pyrene core's functionalization show hexagonal columnar mesophase[78,81,82]. Some of the discotic liquid crystals associated with the pyrene core show unusual behavior, such as different columnar phases (discotic lamellar, columnar rectangular, columnar oblique, etc). A range of dendritic groups has been reported as LC molecular components. Several reports on the monosubstituted pyrene functionalized dendrimers **(Figure 3.12)** show the columnar hexagonal mesophase[81,83–85]. It was also previously reported that dendritic H-bonded molecules with bulky substituents exhibit columnar cubic phase transitions[86,87].

Sagara and Kato reported the liquid crystalline nature of 1,6 disubstituted pyrene derivatives decorated with the fan-shaped dendron using Sonogashira coupling exhibit a liquid crystalline optically isotropic columnar cubic phase. A few reports on the pyrene-based stimuli-response luminescent liquid crystals show the shear-induced phase transition (**Figure 3.13)** (columnar cubic to columnar hexagonal) associated with the photoluminescent change[88,89]. Mobility studies of pyrene-based discotic liquid crystals have been done using time of flight (TOF)[78,90,91] and field-effect mobility[92,93] experiments. Exploring effective and convenient synthetic strategies to functionalize the pyrene core to synthesize liquid crystalline materials and pyrene-based discotic liquid crystals are emerging for future optoelectronic device

applications. Over the past decades, our group has mainly focused on synthesizing new discotic liquid crystalline materials from novel aromatic ring structures. Here, we report the synthesis and characterization of a new class of pyrene-based planar polycyclic aromatic hydrocarbons which exhibit columnar mesomorphism over a wide temperature range and interesting optical properties.

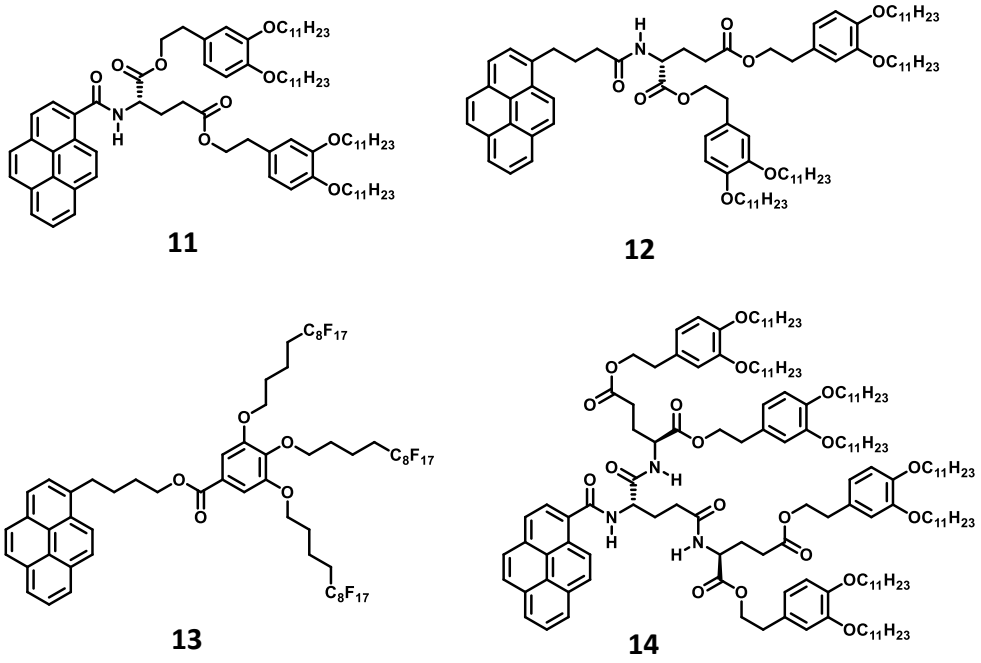

Figure 3.12: Chemical structure of monosubstituted pyrene functionalized dendrimer liquid crystal.

a)

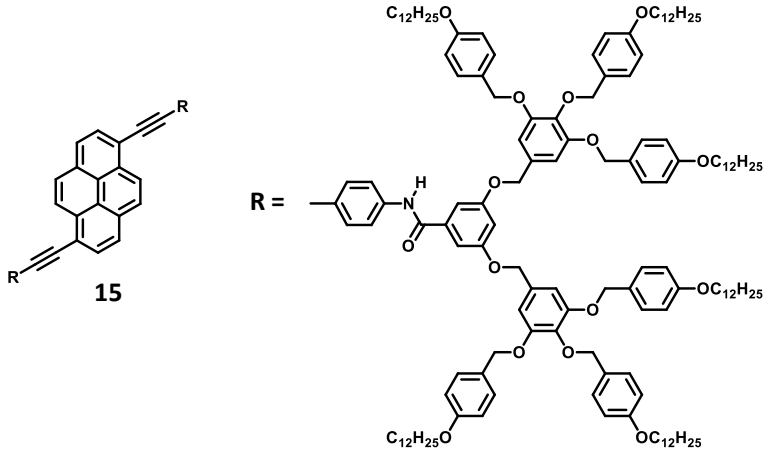

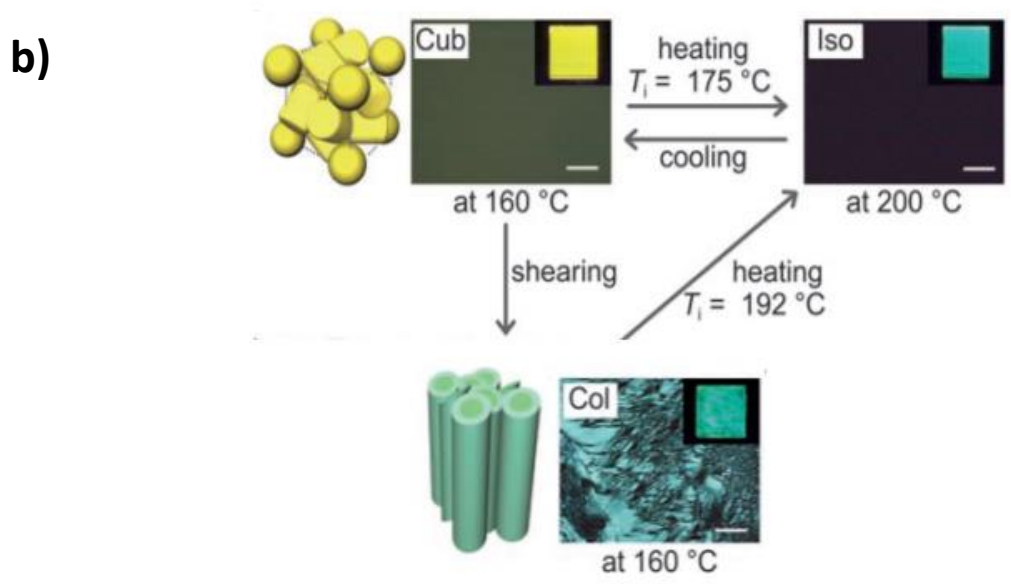

Figure 3.13: a) Chemical structure of pyrene fan-shaped liquid crystal **15.** b) POM images of columnar cubic and columnar hexagonal mesophase.[90,91]

3.2. Results and discussion:

3.2.1 Synthesis:

The synthetic route to prepare the novel discotic core **24** is depicted in **Figure 3.14.** This is prepared *via* a palladium-catalyzed cyclopentannulation followed by Scholl cyclodehydrogenation. The intermediate compound **21** was synthesized via alkylation of catechol followed by the iodination and Sonogashira reaction. The annulation chemistry was made between di-substituted arylethynylene **21** and 1,6 dibromopyrene to form **23a – 23c**, Scholl' cyclodehydrogenation was used to close the external fused aryl groups to form the π-extended core of **24a-c** as reported in the literature with some modifications.[94,95] The chemical structure of newly synthesized LC materials and intermediates were confirmed by ^{1}H-NMR, ^{13}C-NMR spectroscopy, elemental analysis and MALDI-TOF. The NMR of compounds **24a-c** could not be recorded due to their insolubility in common organic solvents such as chloroform, methanol, DMSO, DMF, etc. even at elevated temperature. We have observed broad NMR peaks for **24c** at 85 ºC in tetrachloroethane-d2. The NMR spectra of **24c** at 85 ºC

and at different temperatures are given in **Figure 3.28.** The detailed synthetic procedures and characterization data are given in the experimental section. The energy minimized structures of **23a** and **24a** are presented in **Figure 3.15.**

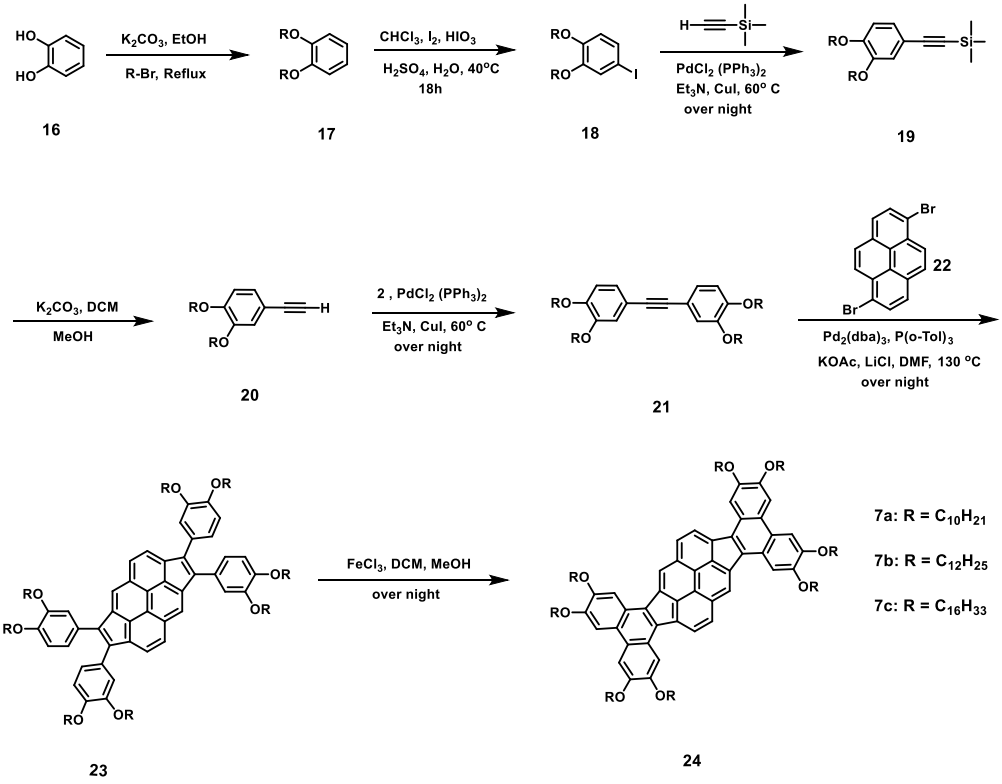

Figure 3.14: Synthesis of extended pyrene derivatives.

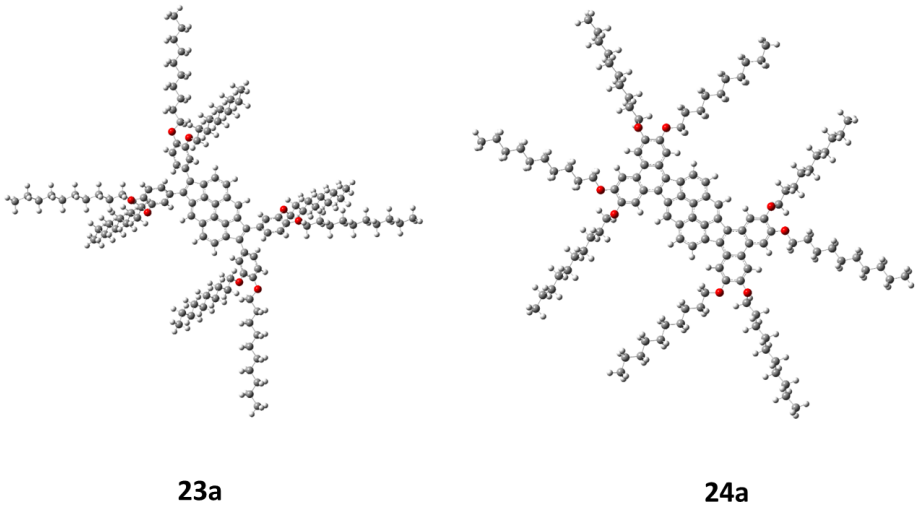

Figure 3.15: Energy minimized structure of **23a** and **24a**.

3.2.2 Thermal Stability:

The thermal stability of all the mesogenic compounds was investigated by using a TGA 4000 thermogravimetric analysis instrument. All the compounds (**23a-c** and **24a-c**) were analyzed under the scan rate of 10 °C min^{-1}. The weight loss is observed at about 400 and 380 °C, as shown in **Figure 3.16.** The decomposition temperature of all the compounds is much higher than isotropic temperatures. These results suggest that all pyrene derivatives have excellent thermal stability.

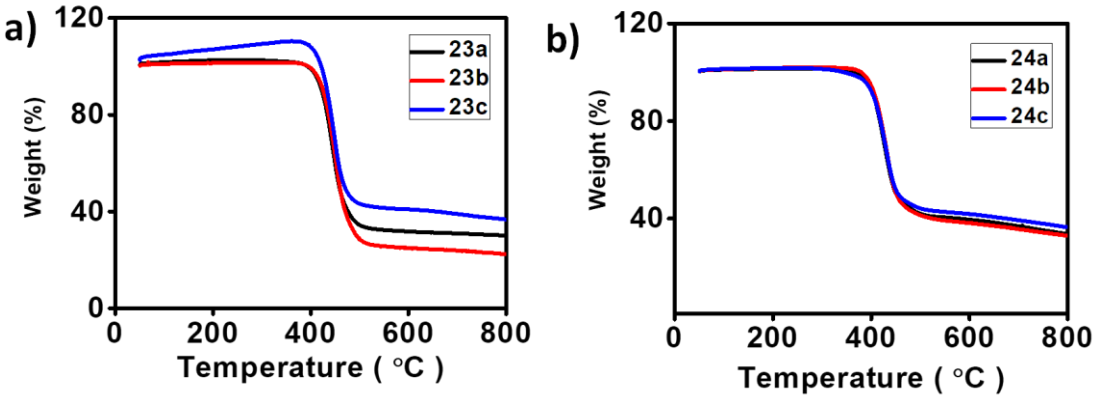

Figure 3.16: TGA spectra of **23a-c** and **24a-c** show good thermal stability of the pyrene derivatives.

3.2.3 Mesomorphic characteristics:

The thermotropic mesophase behavior of **23a-c** and **24a-c** was investigated using differential scanning calorimetry (DSC) and cross-polarized optical microscopy (POM). Additional characterization of these mesophases and the determination of the structural parameters was performed by X-ray diffractometry. Interestingly compounds **23a-c** and **24a-c** show the columnar hexagonal phase (Col_h). The formation of the mesophase was confirmed through DSC & XRD. The phase transition temperatures are given in **Table 3.1** (peak temperature in ºC) and associated enthalpy values (ΔH in kJ mol^{-1}) were acquired from the heating and successive cooling of respective mesogens at the scan rate of 10 ºC min^{-1} under nitrogen atmosphere. Compounds **23a-c** and **24a-c** show the enantiotropic columnar mesophase over a broad range of temperatures along with two endothermic phase transitions from the Cr (Crystal)

to Col_h phase at lower temperatures and Col_h to the isotropic phase at higher temperatures. The DSC thermograms are shown in the **Figure 3.17.** The POM textures (**Figure 3.18)** observed under the cross polarizers upon cooling from the isotropic phase revealed the existence of the columnar hexagonal phase.

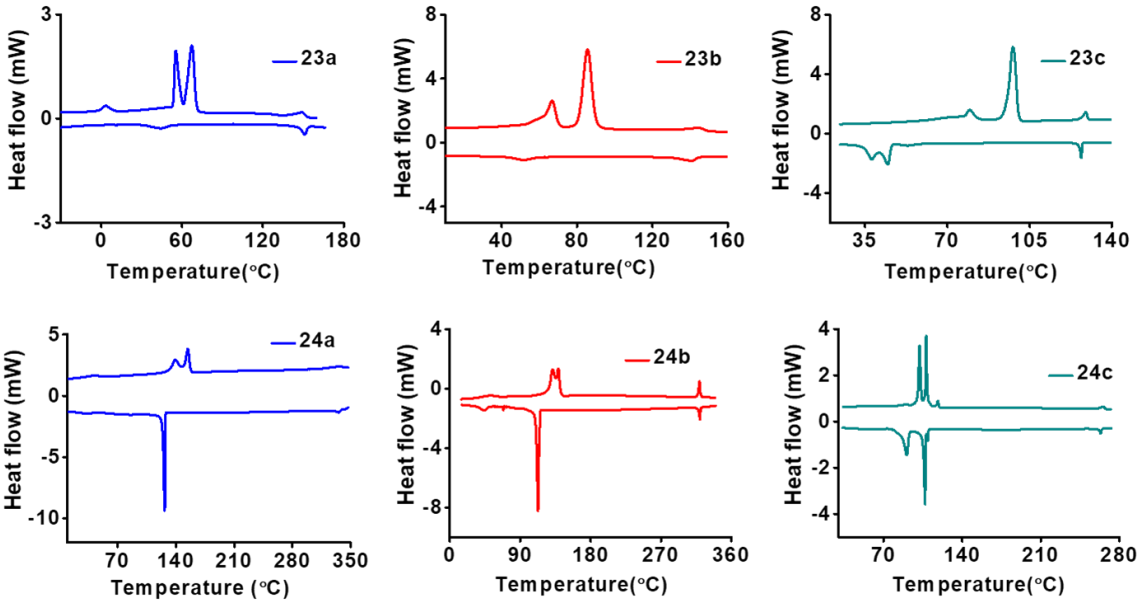

Figure 3.17: DSC thermograms were obtained for the **23a-c** and **24a-c** derivatives showing phase transitions during heating and cooling cycles at a scan rate of 5 ºC min^{-1}.

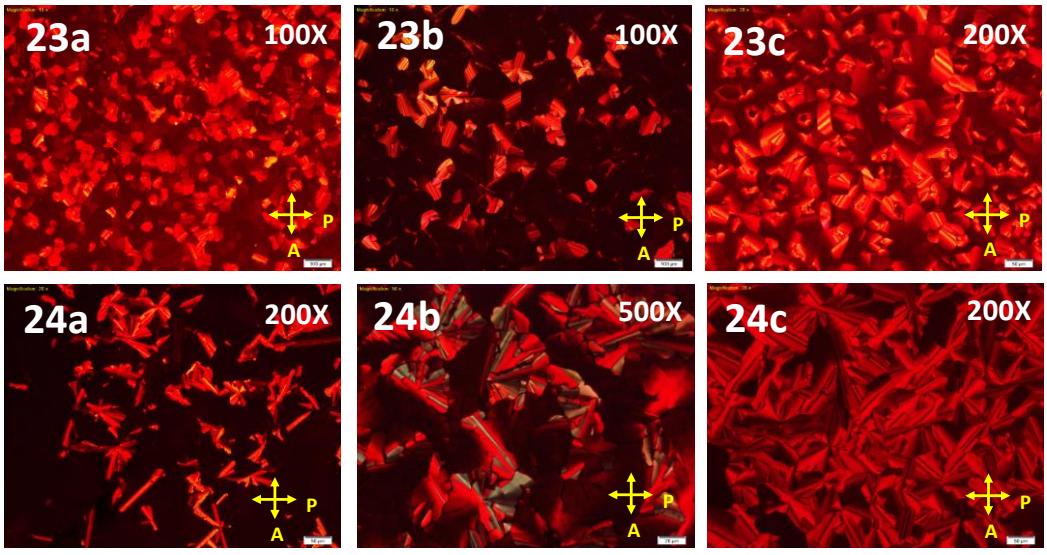

Figure 3.18: Birefringence texture observed under POM for compound **23a** at 142 °C, **23b** at 125 °C, **23c** at 110°C, **24a** at 80 °C, **24b** at 220 °C, and **24c** at 205 °C upon cooling from the isotropic phase.

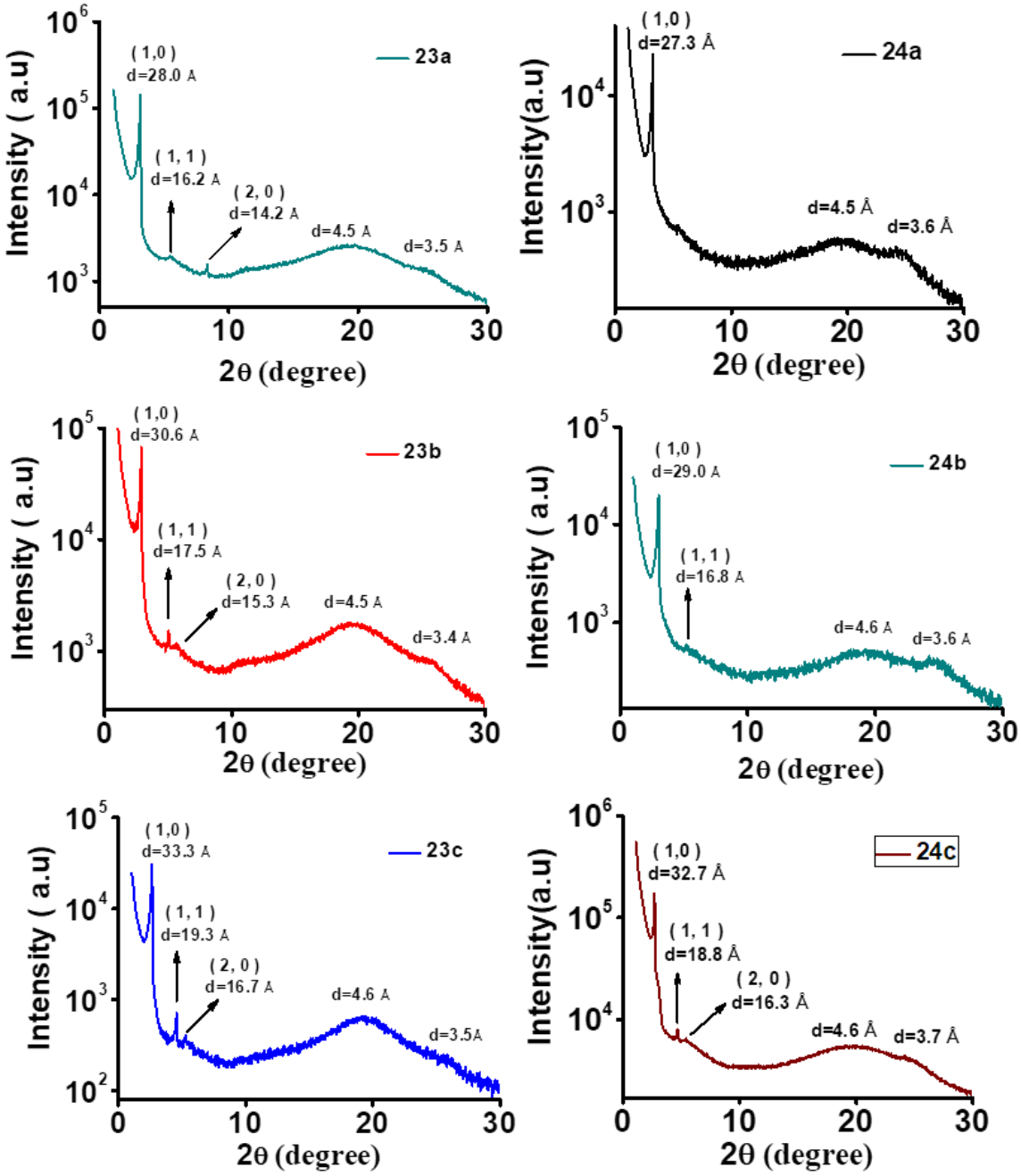

Figure 3.19: X-ray diffraction patterns of the hexagonal phase of compounds **23a-c** and **24a-c.**

X-ray diffraction experiments were done using unoriented samples to infer the mesophase structure and supramolecular organization of these compounds (**23a-c** and **24a-c**). **Figure 3.19** shows the X-ray diffraction patterns of the mesophase exhibited by compounds **23a-c** and **24a-c** upon cooling from the isotropic phase.

These patterns are consistent with a hexagonal arrangement of the columns since the spacings of the small-angle peaks are in the ratio of 1: 1/√3: 1/2. The wide-angle region shows a broad peak around d = 4.4 - 4.6Å, which corresponds to the liquid-like packing of the aliphatic chains. The d-spacings of all compounds and their Miller indices are given in the **Table 3.2**, along with their lattice parameters. The number of molecules occupying a single slice of the column was calculated from the XRD data and is found to be close to 1 for all the samples. The core-core peak, centered at about 3.4 Å, is found to be broader in compounds **23a-c**, compared to **24a-c**, indicating that the correlation length for the ordering of the molecular cores along the columns is shorter in the former set of compounds. The correlation length was estimated from the full width at half maximum (FWHM) of Gaussian functions fitted to the core-core wide-angle peaks values are given in **Table 3.3**. In agreement with the increased correlation length of **24a-c**, the optimized structures obtained from DFT calculations showed planar conformation, whereas, in the case of **23a-c** compounds, substituted phenyl rings are in staggered conformation, as shown in the **Figure 3.15.** A schematic of the molecular arrangement in the columnar hexagonal mesophases deduced from the diffraction data is shown in the **Figure 3.20.**

Table 3.1: Phase transition temperatures (in ºC) and corresponding enthalpy values (J g^{-1}) of **23a-c** and **24a-c** in the time of heating and cooling.

Compound	Heating	Cooling
23a	Cr 75.3 (20.2) Col_h 157.2 (2.3) I	I 150.9 (3.6) Col_h 44.2 (3.8) Cr
23b	Cr 85.6 (47.7) Col_h 144.2 (2.4) I	I 138.6 (2.5) Col_h 49.3 (2.4) Cr
23c	Cr 97.9 (69.7) Col_h 128.9 (5.0) I	I 127.03 (4.3) Col_h 44.5 (36.0) Cr
24a	Cr 154.2 (42.7) Col_h 337.8 (1.9) I	I 335.2 (1.9) Col_h 126.4 (36.0) Cr
24b	Cr 134.7 (37.3) Col_h 319.2 (4.2) I	I 319.7 (2.7) Col_h 112.7 (37.7) Cr
24c	Cr 118.5 (1.7) Col_h 265.5 (1.8) I	I 263.4 (1.5) Col_h 107.0 (25.9) Cr

Cr – Crystalline phase; Col_h – Columnar hexagonal phase; I – Isotropic

Table 3.2: Layer spacing obtained from XRD for **23a-c,** and **24a-c. (a** = lattice parameter = $\sqrt{(4/3)} \times d_{10}$; lattice area $S_h = a^2 \sin 60^o$; lattice volume $\mathbf{V_h} = a^2 \sin 60^o \times h_c$ (**h_a** if **h_c** is not observed); No of molecules per slice of column (**Z**) = $(\sqrt{3} \times N_a \times P \times a^2 \times h)/2M$; **$N_a$** = Avogadro number; **P** = Density in Kg/m^3; **a**=lattice parameter; **h_c**=core core peak (**h_a** if core core is not observed); **M** = molecular weight in Kg/m^3)

Compounds	T (°C)	d-spacing(Å)	Phase	Parameters
23a	140	28.07 (10), 16.22 (11), 14.23 (20) 4.55, 3.52	Col_h	**a** = 32.41 Å **S_h** =909.399 Å^2 **V_h** = 3201.08Å^3 **Z** =1.06
23b	95	30.59 (10), 17.53 (11), 15.29 (20) 4.52, 3.44	Col_h	**a** = 35.32 Å **S_h** =1080.368 Å^2 **V_h** = 3716.468Å^3 **Z** =1.09
23c	115	33.31 (10), 19.32 (11), 16.73 (20) 4.56, 3.47	Col_h	**a** = 38.43 Å **S_h** =1279.002 Å^2 **V_h** = 4438.138Å^3 **Z** =1.07
24a	205	27.31 (10), 4.48, 3.68	Col_h	**a** = 31.53 Å **S_h** =860.951 Å^2 **V_h** = 3168.30Å^3 **Z** =1.03
24b	175	29.00 (10), 16.76 (11), 4.63, 3.56	Col_h	**a** = 33.48Å **S_h** =970.736 Å^2 **V_h** = 3455.82 Å^3 **Z** =1.02
24c	110	32.73 (10), 18.85 (11), 16.33 (20), 4.60, 3.67	Col_h	**a** = 37.79 Å **S_h** = 1236.97 Å^2 **V_h** = 4539.67 Å^3 **Z** =1.1

Table 3.3: FWHM and correlation length values

Compounds	σ	FWHM = $\Delta 2\theta$ $2\sqrt{2\ ln\ 2}\ \sigma\ \approx 2.3548\ \sigma$	Correlation length (Å) $\xi = K\lambda/(\Delta 2\theta . Cos\theta)$
23a	2.34	5.52	0.25
23b	2.36	5.57	0.26
23c	2.83	6.66	0.21
24a	1.99	4.69	0.29
24b	2.06	4.86	0.28
24c	1.81	4.27	0.32

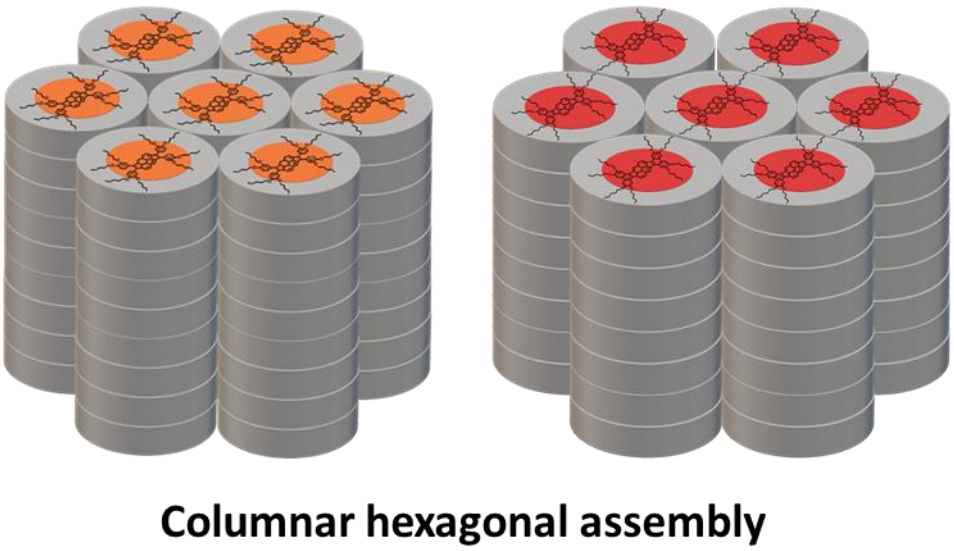

Figure 3.20: Schematic representation of the columnar hexagonal assembly of **6** and **7**

3.2.4 Density functional theory:

Density functional theory (DFT) calculations were performed using Gaussian 09 software with a B3LYP/6-311G (d, p) basis set to understand the geometrical and electronic structures of the **23a** and **24a** compounds. The energy minimized structures of **23a** and **24a** are shown in **Figure 3.15.** The HOMO of the compounds is predominantly located on the electron-rich complete π – surface, while the LUMO is distributed on the pyrene core. The energy gap was found to be

1.30 eV and 1.40 eV for **23a** and **24a**. HOMO and LUMO frontier molecular orbitals are given in **Figure 3.21**, which provides separate transporting channels for holes and electrons. The optical energy gap (Eg) in eV was calculated to be 2.03 (according to the equation Eg = $1240/\lambda_{onset}$, where onset was resolved as the intersection of the extrapolated tangent, the most extended wavelength absorption peak and the x-axis).

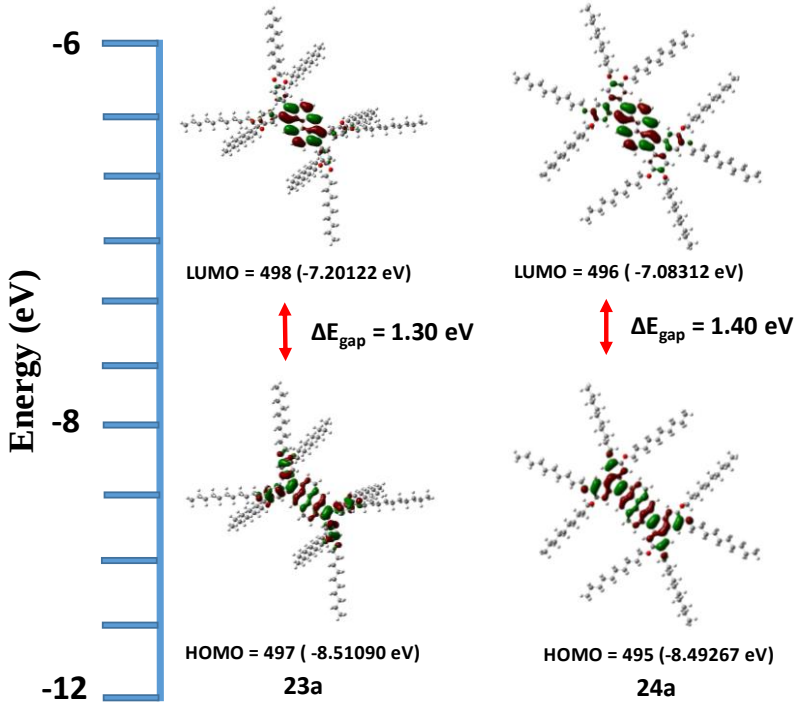

Figure 3.21: HOMO and LUMO energy level diagrams and theoretical bandgap of **23a** and **24a** calculated by using **B3LYP** was employing the **6-311G(dp)** basis set.

3.2.5 Optical properties:

Optoelectronic properties of **23a-c** derivatives were measured. The absorption and photoluminescent (PL) spectrum of these compounds were recorded in chloroform (3×10^{-6}M), as shown in **Figure 3.22.** The absorption spectra of all compounds **23a-c** are similar, with multiple absorption peaks at 247, 298, 345, 422, 448, 523 and 566 nm (ε370 = 3.3×10^{-4} (6a), 3.4×10^{-4} (6b), 3.5×10^{-4} M^{-1} cm^{-1} (6c)). The photoluminescent spectra display two intense

peaks at wavelengths of 410 nm and 434 nm, whereas the shoulder peaks is at 465 nm. The photoluminescent spectra of **23a-c** compounds are similar. The Stokes shift between the absorption maxima and emission maxima is around 40 nm, which is observed in all the compounds. These results reveal that the difference in branching at peripheral chains in pyrene discotic core has no effect on the optical properties of the liquid crystals. In the case of **24a-c**, due to the insolubility of the compounds, we could not measure the photophysical properties.

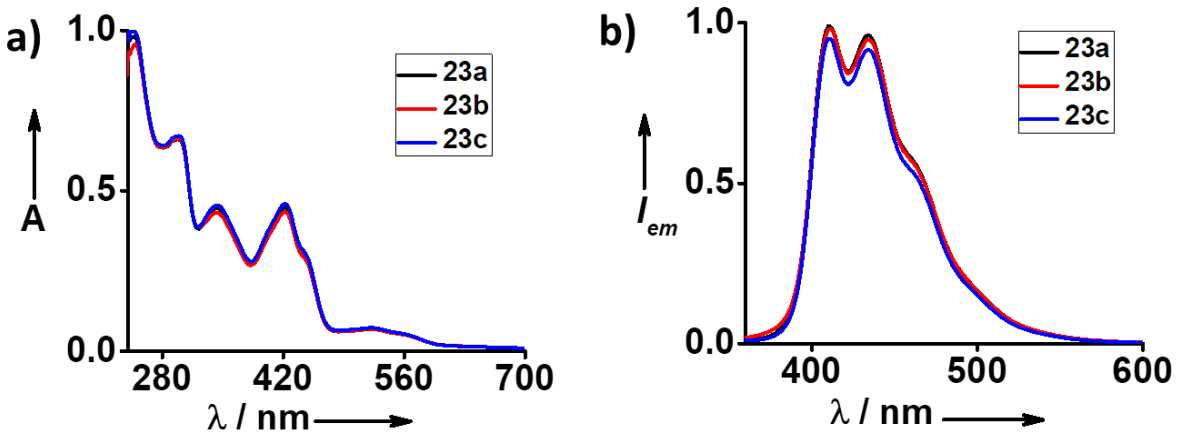

Figure 3.22: Normalized **a)** absorption and **b)** emission spectra of **23a – c** in chloroform (the path length of the cuvette is 1 cm, Concentration: 3×10^{-6} M). The excitation wavelength of all compounds at 370 nm.

3.3. Conclusions:

In conclusion, we have synthesized a novel class of extended pyrene based discotic liquid crystals. These compounds are found to be enantiotropic mesomorphic and exhibit the columnar hexagonal mesophase over a wide range of temperatures, as confirmed by POM, DSC, and the self-assembly of columnar mesophase confirmed by X-ray diffraction studies. The number of molecules occupying a single slice of the column was calculated from the XRD data and is found to be close to 1 for all the samples. The core-core distance of **24a-c** is slightly larger than the **23a-c**. These pyrene-based polycyclic aromatic hydrocarbons (PAHs) derivatives are potential candidates for the growing field of organic electronics.

3.4 Experimental section:

Materials and Methods

Referee the page number 65

3.5 Synthesis and characterization:

Synthesis and characterization of pyrene core liquid crystal

The synthetic procedure of **17a-c** to **22a-c,** NMR data and NMR spectra are given in chapter 2

23a-c and **24a-c** were synthesized in a multistep reaction, as shown in **Figure 3.14.** All the final products were purified and characterized by various spectroscopic techniques like IR, ^{1}H NMR, ^{13}C NMR, and elemental analysis, MALDI-TOF

General procedure for the synthesis of 23a, 23b & 23c.

A mixture of **21a/21b/21c** (2.3eq) and 1, 6-dibromopyrene (1eq), $Pd_2(dba)_3$, (0.1eq) $P(o\text{-}Tol)_3$, (0.1eq) KOAc, (5eq) LiCl (2eq) in DMF was stirred overnight at 130^{o}C. The reaction mixture was cooled to room temperature and poured into methanol a brown color precipitate was observed. The filtrate was filtered using Buchner funnel. The resulting solid was washed with methanol and acetone to give the final product. The crude product was purified by column chromatography using petroleum ether and chloroform as eluent and dried under a high vacuum to get the desired product.

Compound 23a: **21a** (2.05g, 2.55mmol, 2.3eq), 1, 6-dibromopyrene (0.400g, 1.11mmol, 1eq), $Pd_2(dba)_3$ (0.101g, 0.111mmol, 0.1eq), $P(o\text{-}Tol)_3$ (0.033g, 0.111mmol, 0.1eq), KOAc (0.545g, 5.55mmol, 5eq), LiCl (0.094g, 2.22mmol, 2eq), DMF (30mL), Yield: 81%; ^{1}H NMR (500 MHz, $CDCl_3$): δ (ppm) = 0.80 (t, *J* = 7.0 Hz, 24H), 1.20 – 1.31 (m, 104H), 1.40 – 1.42 (m, 8H), 1.64 (s, 8H), 1.75 – 1.79 (m, 8H), 3.72 – 3.77 (m, 8H), 3.93 – 3.96 (m, 8H), 6.78 – 6.86 (m, 8H), 6.95 (t, *J* = 9.0 Hz, 4H), 7.48 (d, *J* = 8.50 Hz, 4H), 7.64 (d, *J* = 7.50 Hz, 2H); ^{13}C NMR (125 MHz, $CDCl_3$): δ(ppm) = 13.09, 25.05, 25.09, 25.10, 28.21, 28.36, 28.39, 28.45, 28.49, 28.62, 28.66, 28.70, 30.93, 68.10, 68.22, 68.28, 112.44, 112.62, 113.95, 114.52, 120.51, 120.68, 120.83, 121.27, 123.91, 126.85, 126.96, 128.29, 129.49, 130.94, 137.87, 139.86, 139.87, 140.51, 147.61, 147.63, 147.68, 147.80; Elemental analysis: C, 82.52; H, 10.39 calculated (%): C, 82.46; H, 10.81 (expt. %). Mass (MALDI-TOF): m/z 1804.3.

Compound 23b: **21b** (1.02g, 1.27mmol, 2.3eq), 1, 6-dibromopyrene (0.200g, 0.55mmol, 1eq), $Pd_2(dba)_3$ (0.050g, 0.055mmol, 0.1eq), $P(o\text{-}Tol)_3$ (0.016g, 0.055mmol, 0.1eq), KOAc (0.272g, 2.77mmol, 5eq), LiCl (0.047g, 1.11mmol, 2eq), DMF (20mL), Yield: 85%; ^{1}H NMR (500 MHz, $CDCl_3$): δ (ppm) = 0.80 (t, *J* = 6.25 Hz, 24H), 1.18 – 1.31 (m, 136H), 1.40 – 1.42 (m, 8H), 1.64 (m, 8H), 1.76 – 1.77 (m, 8H), 3.72 – 3.77 (m, 8H), 3.92 – 3.95 (m, 8H), 6.78 – 6.85 (m, 8H), 6.95 (t, *J* = 9.25 Hz, 4H), 7.48 (d, *J* = 8.50 Hz, 4H), 7.64 (d, *J* = 8.5 Hz, 2H); ^{13}C NMR (125 MHz, $CDCl_3$): δ(ppm) = 14.11, 22.70, 26.08, 26.12, 29.22, 29.40, 29.48, 29.52, 29.52, 29.70, 29.74, 29.78, 31.95, 69.12, 69.24, 69.31, 113.45, 113.64, 114.97, 115.55, 121.54, 121.71, 121.84, 122.29, 124.94, 127.87, 127.98, 129.31, 130.52, 131.96, 138.89, 140.90, 141.54, 148.63, 148.65, 148.70, 148.82; Elemental analysis: C, 82.86; H, 10.83 calculated (%): C, 82.89; H, 11.15 (expt. %). Mass (MALDI-TOF): m/z 2028.4.

Compound 23c: **21c** (1.456g, 1.277mmol, 2.3eq), 1, 6-dibromopyrene (0.200g, 0.555mmol, 1eq), $Pd_2(dba)_3$ (0.050g, 0.055mmol, 0.1eq), $P(o\text{-}Tol)_3$ (0.016g, 0.055mmol, 0.1eq), KOAc (0.272g, 2.77mmol, 5eq), LiCl (0.047g, 1.11mmol, 2eq), DMF (20mL), Yield: 79%; ^{1}H NMR (500 MHz, $CDCl_3$): δ (ppm) = 0.80 (s, 24H), 1.17 – 1.31 (m, 200H), 1.40 – 1.41 (m, 8H) 1.64 (s, 8H), 1.76 – 1.77 (m, 8H), 3.72 – 3.75 (m, 8H), 3.94 (d, *J* = 6.0Hz, 8H), 6.78 – 6.85 (m, 8H), 6.95 (t, *J* = 9.25Hz, 4H), 7.48 (d, *J* = 8.0Hz, 4H), 7.64 (d, *J* = 7.5Hz, 2H); ^{13}C NMR (125 MHz, $CDCl_3$): δ (ppm) = 13.09, 21.68, 25.05, 25.09, 25.11, 28.20, 28.36, 28.46, 28.50, 28.67, 28.72, 30.92, 68.10, 68.21, 68.29, 112.44, 112.62, 113.94, 114.52, 120.53, 120.70, 120.81, 121.26, 123.92, 126.84, 126.95, 128.30, 129.51, 130.95, 137.88, 139.88, 140.52, 147.60, 147.68, 147.80; Elemental analysis: C, 83.36; H, 11.47 calculated (%): C, 83.78; H, 11.45 (expt. %). Mass (MALDI-TOF): m/z 2476.4.

General procedure for the synthesis of 24a, 24b & 24c.

23a/23b/23c was dissolved in dichloromethane. To this solution, $FeCl_3$ in CH_3NO_2 was added dropwise under nitrogen. The reaction mixture was stirred at room temperature overnight. Methanol was added, and the mixture was stirred for 20 min. The product was filtered using Büchner Funnel, and the resulting solid was washed with methanol and acetone. The crude product was purified by column chromatography using petroleum ether and chloroform as eluent and dried under a high vacuum to get the desired product.

Compound 24a: **23a** (0.40g, 0.22mmol, 1eq), dichloromethane (150 mL), $FeCl_3$ (0.287 g, 1.773mmol, 8eq), CH_3NO_2 (5mL) Yield: 92%; Elemental analysis: C, 82.71; H, 10.19 calculated (%): C, 82.60; H, 10.39 (expt. %); Mass (MALDI-TOF): m/z 1799.51.

Compound 24b: **23b** (0.300g, 0.14mmol, 1eq), dichloromethane (120mL), $FeCl_3$ (0.19g, 1.18mmol, 8eq), CH_3NO_2 (5mL) Yield: 89%; Elemental analysis: C, 83.03; H, 10.65 calculated (%): C, 82.48; H, 10.96 (expt. %); Mass (MALDI-TOF): m/z 2024.67

Compound 24c: **23c** (0.500g, 0.201mmol, 1eq), dichloromethane (200mL), $FeCl_3$ (0.261g, 1.61mmol, 8eq), CH_3NO_2 (6mL) Yield:95%; ^1H NMR (500 MHz, $C_2D_2Cl_4$): δ (ppm) = 2.14 (bs, 24H), 2.55 – 2.80 (m, 203H), 3.18 – 3.37 (m, 16H) 5.51 (bs, 16H), 8.99 (bs, 14H),; Elemental analysis: C, 83.50; H, 11.33 calculated (%): C, 83.39; H, 11.77 (expt. %). Mass (MALDI-TOF): m/z 2471.90

3.6 MALDI-TOF Spectra:

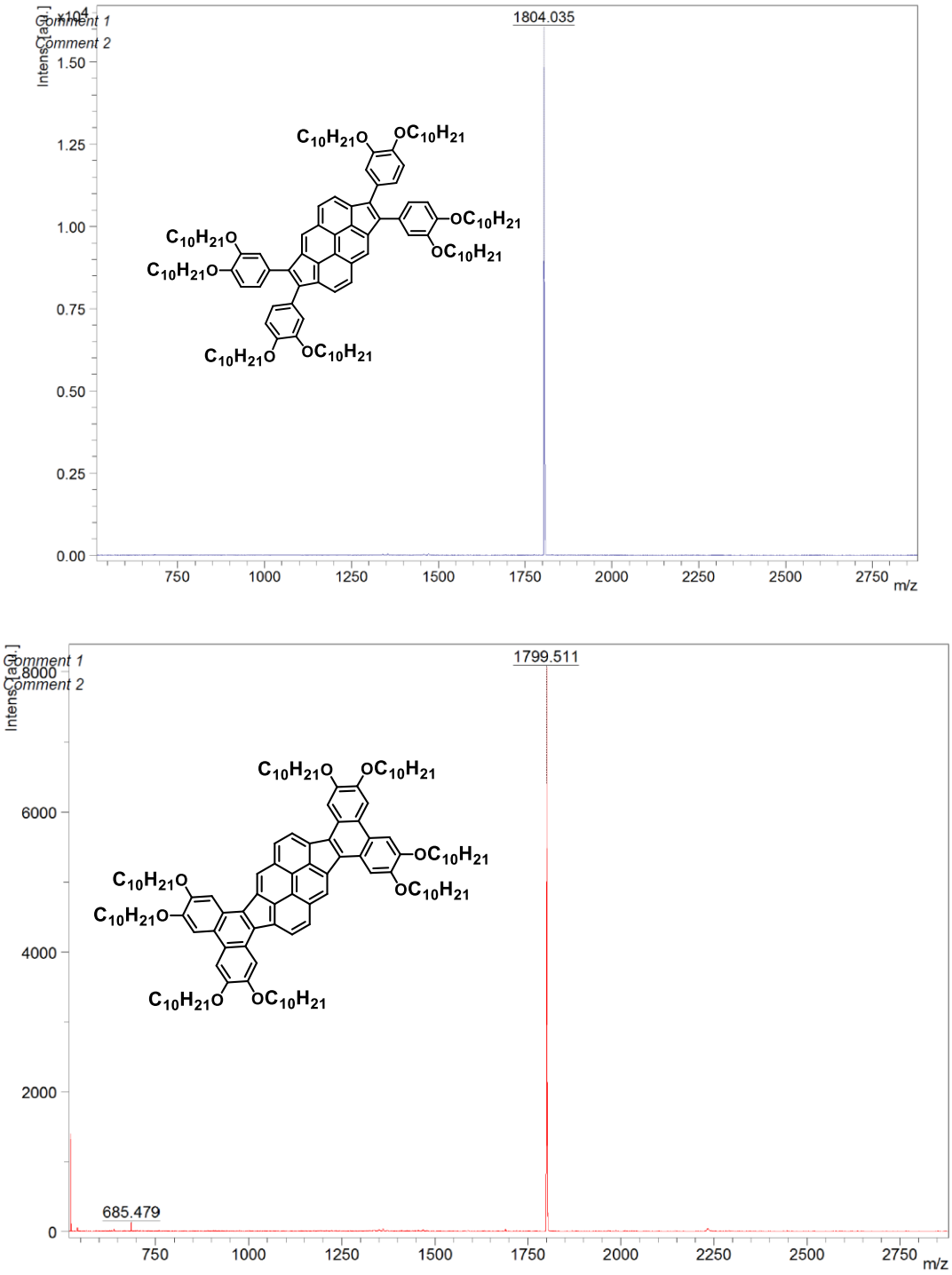

Figure 3.23: **23a** (top) and **24a** (bottom) data of MALDI-TOF.

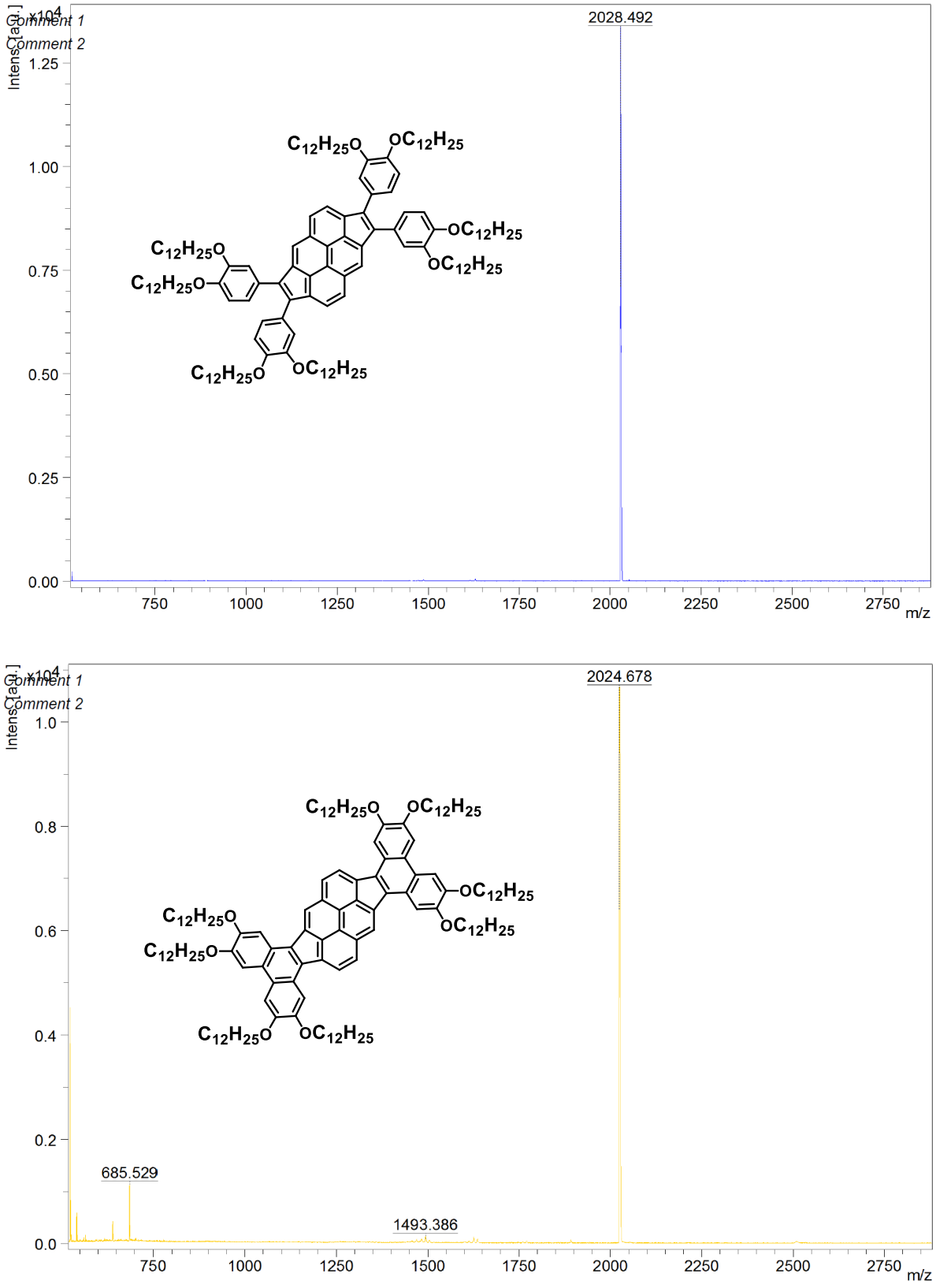

Figure 3.24: 23b (top) and **24b** (bottom) data of MALDI-TOF.

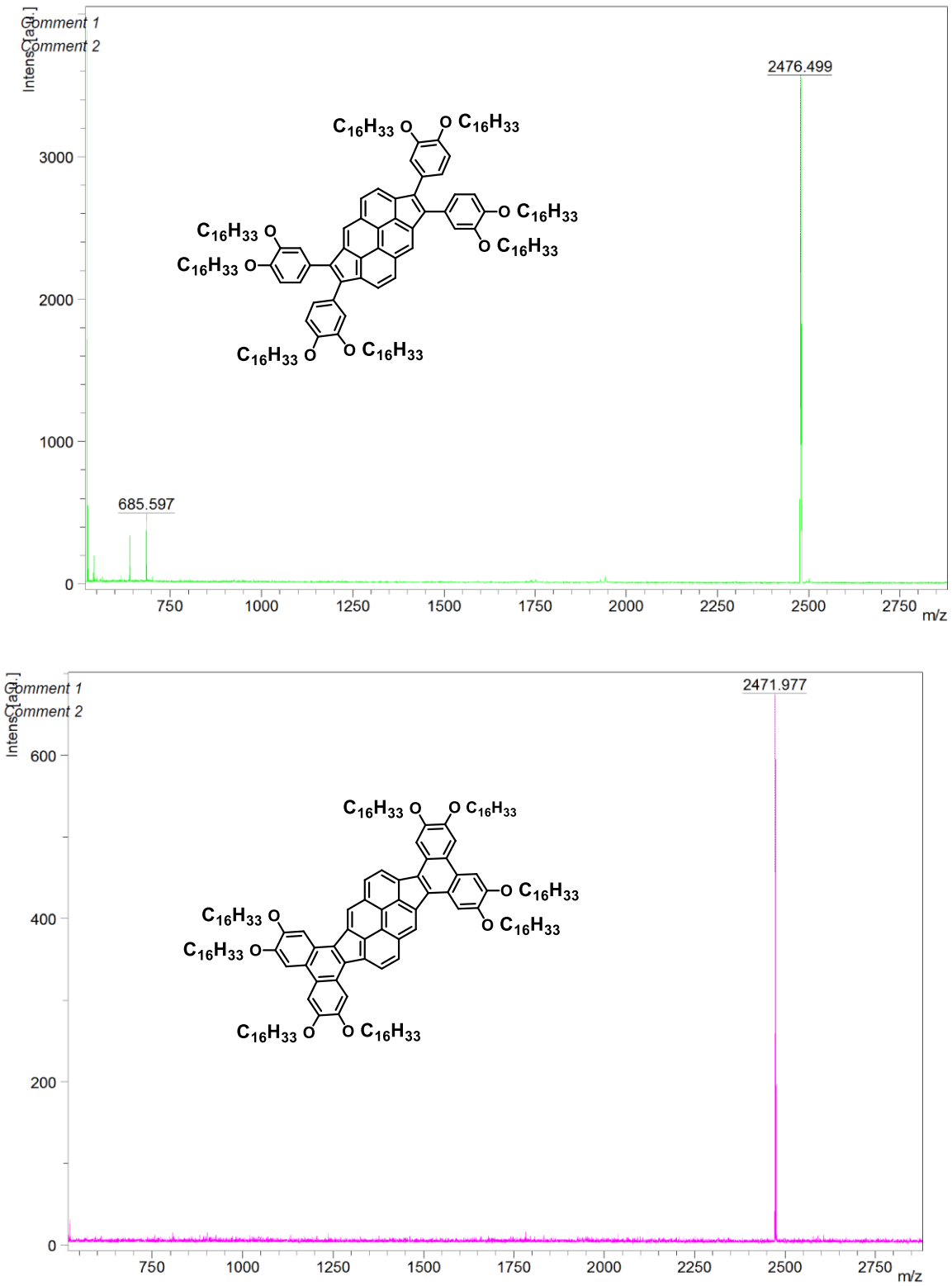

Figure 3.24: 23c (top) and **24c** (bottom) data of MALDI-TOF.

3.7. NMR Spectra:

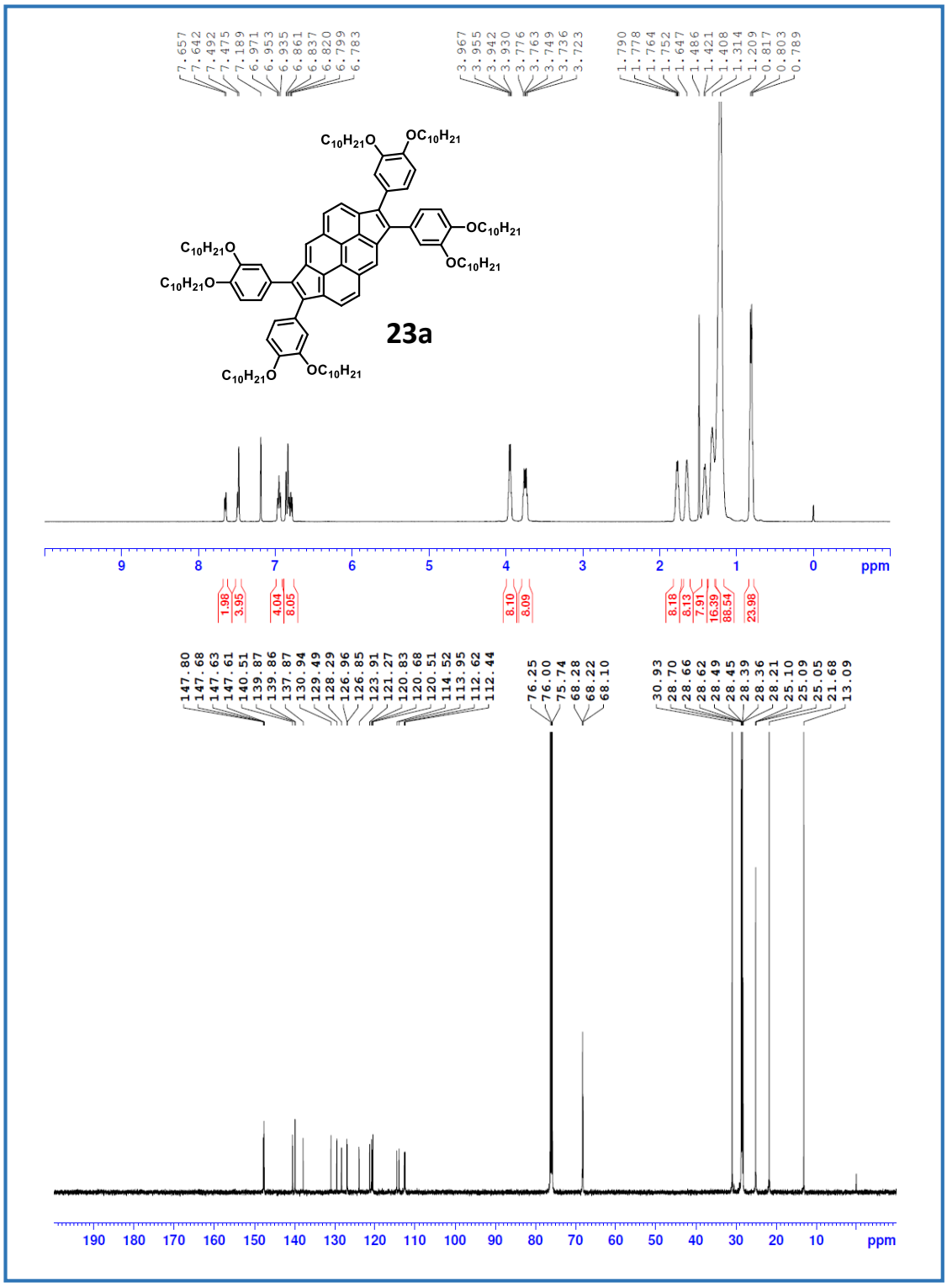

Figure 3.25: ^{1}H (top) and ^{13}C-NMR (bottom) spectra of **23a**

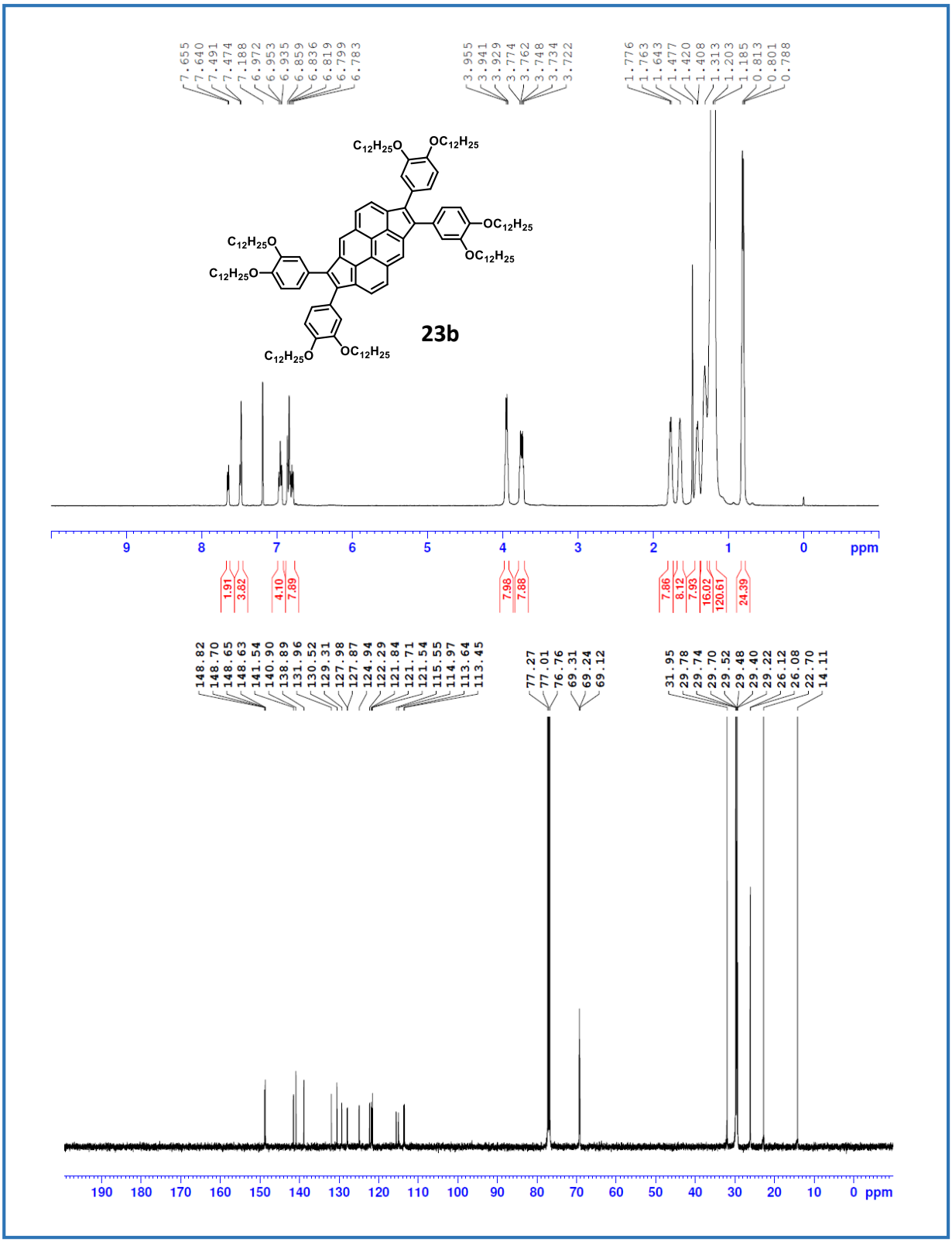

Figure. 3.26: ^{1}H (top) and ^{13}C-NMR (bottom) spectra of **23b**

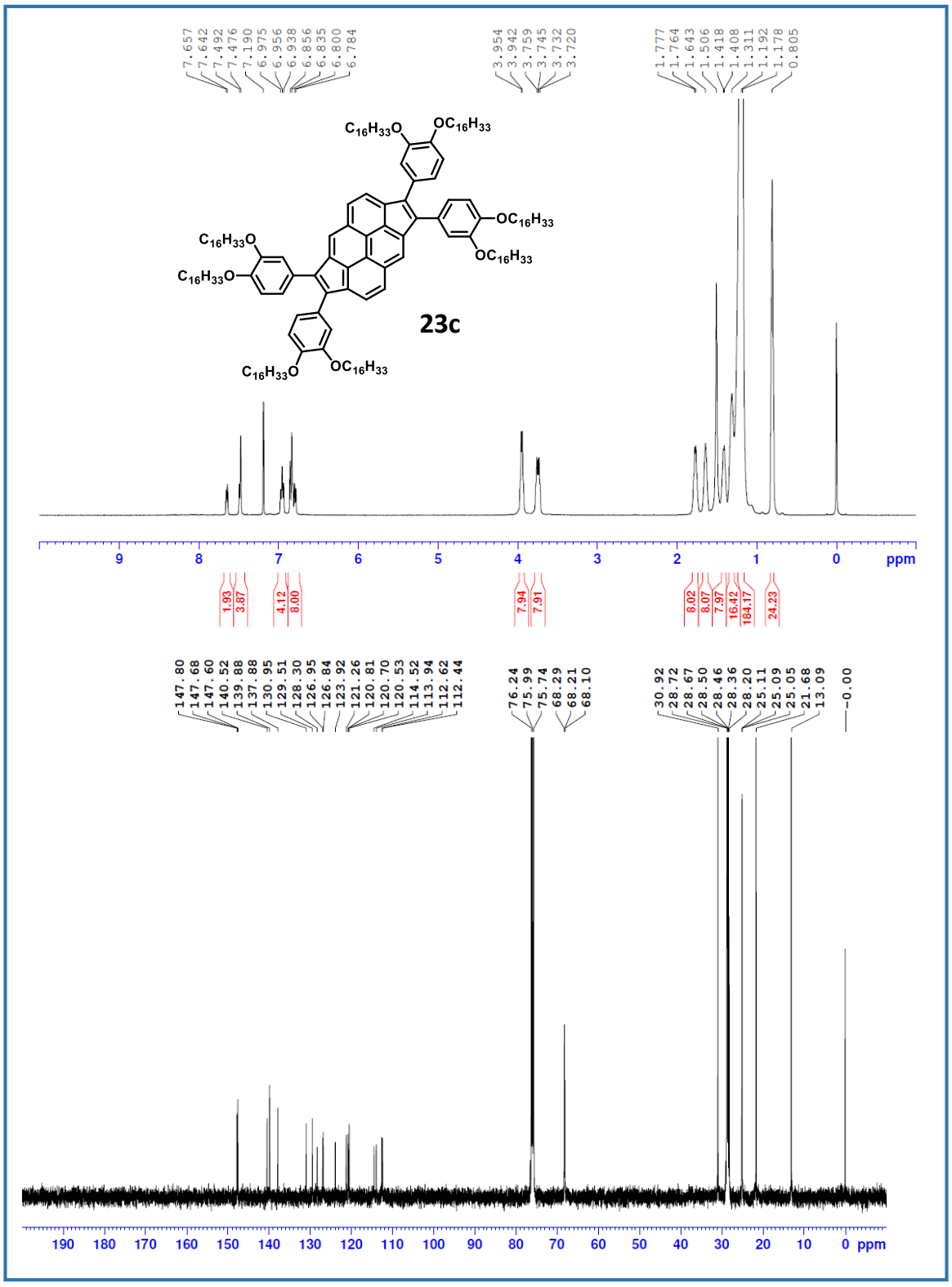

Figure 3.27: ^{1}H (top) and ^{13}C-NMR (bottom) spectra of **23c**

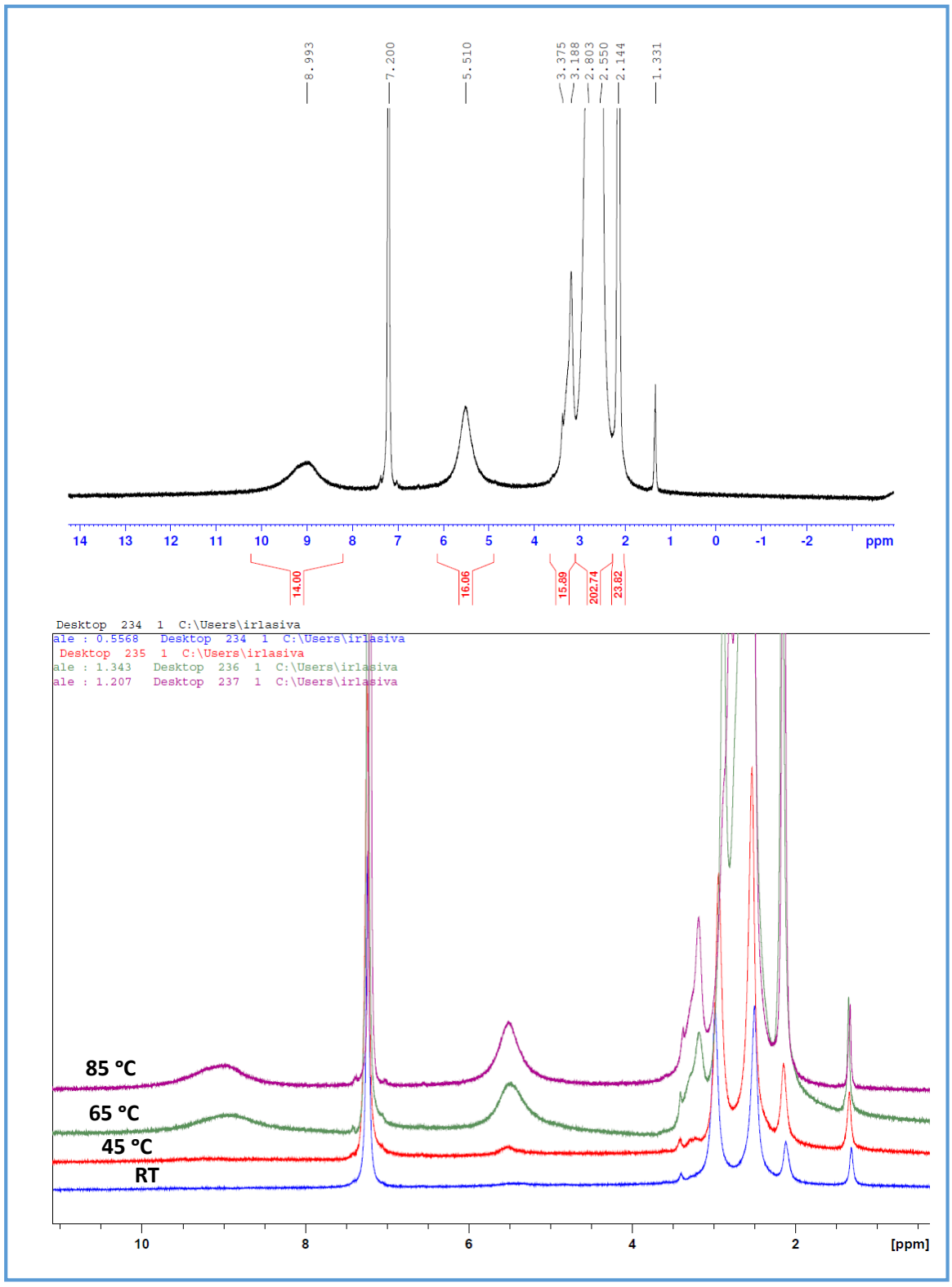

Figure 3.28. ^{1}H (top) NMR of **24c** and temperature-dependent ^{1}H (bottom) NMR spectra of **24c.**

3.8. References:

[1] L. T. Scott, *Chem. Soc. Rev.* **2015**, *44*, 6464–6471.

[2] R. Harvey, *Curr. Org. Chem.* **2004**, *8*, 303–323.

[3] R. Meyer, *Berichte der Dtsch. Chem. Gesellschaft* **1912**, *45*, 1609–1633.

[4] A. W. Campbell, N. H. Cromwell, J. J. Hager, *J. Am. Chem. Soc.* **1936**, *58*, 1051–1052.

[5] X. Lu, Z. Chen, *Chem. Rev.* **2005**, *105*, 3643–96.

[6] M. Solà, *Front. Chem.* **2013**, *1*.

[7] J. R. Platt, *J. Chem. Phys.* **1954**, *22*, 1448–1455.

[8] M. Randić, *Chem. Phys. Lett.* **1976**, *38*, 68–70.

[9] M. Randić, *Tetrahedron* **1977**, *33*, 1905–1920.

[10] M. Randic, *J. Am. Chem. Soc.* **1977**, *99*, 444–450.

[11] M. Randić, *Chem. Rev.* **2003**, *103*, 3449–3606.

[12] R. Weitzenbock, *Monatshefte for Chemie* **1913**, *34*, 193–223.

[13] T. M. Figueira-Duarte, K. Müllen, *Chem. Rev.* **2011**, *111*, 7260–7314.

[14] R. S. Becker, I. Sen Singh, E. A. Jackson, *J. Chem. Phys.* **1963**, *38*, 2144–2171.

[15] J. Tanaka, *Bull. Chem. Soc. Jpn.* **1965**, *38*, 86–102.

[16] E. A. Mangle, M. R. Topp, *J. Phys. Chem.* **1986**, *90*, 802–807.

[17] I. S. K. Kerkines, I. D. Petsalakis, G. Theodorakopoulos, W. Klopper, *J. Chem. Phys.* **2009**, *131*, 224315.

[18] Y. Bito, N. Shida, T. Toru, *Chem. Phys. Lett.* **2000**, *328*, 310–315.

[19] N. P. E. Barry, B. Therrien, in *Org. Nanoreactors*, Elsevier, **2016**, pp. 421–461.

[20] R. D. Welham, *J. Soc. Dye. Colour.* **2008**, *79*, 181–185.

[21] K. Fujimoto, H. Shimizu, M. Inouye, *J. Org. Chem.* **2004**, *69*, 3271–3275.

[22] G. T. Hwang, Y. J. Seo, B. H. Kim, *J. Am. Chem. Soc.* **2004**, *126*, 6528–9.

[23] K. Yamana, Y. Fukunaga, Y. Ohtani, S. Sato, M. Nakamura, W. J. Kim, T. Akaike, A. Maruyama, *Chem. Commun.* **2005**, 2509.

[24] G. Jones, V. I. Vullev, *Org. Lett.* **2001**, *3*, 2457–2460.

[25] L. Pu, *Chem. Rev.* **2004**, *104*, 1687–1716.

[26] R. Martínez-Máñez, F. Sancenón, *Chem. Rev.* **2003**, *103*, 4419–4476.

[27] T. Förster, K. Kasper, *Zeitschrift für Phys. Chemie* **1954**, *1*, 275–277.

[28] R. Katoh, K. Suzuki, A. Furube, M. Kotani, K. Tokumaru, *J. Phys. Chem. C* **2009**, *113*, 2961–2965.

[29] J. B. Birks, *J. Res. Natl. Bur. Stand. Sect. A Phys. Chem.* **1976**, *80A*, 389.

[30] M. Sharnoff, *J. Lumin.* **1971**, *4*, 69–71.

[31] D. C. Dong, M. A. Winnik, *Photochem. Photobiol.* **1982**, *35*, 17–21.

[32] C.-Z. Wang, X. Feng, Z. Kowser, C. Wu, T. Akther, M. R. J. Elsegood, C. Redshaw, T. Yamato, *Dye. Pigment.* **2018**, *153*, 125–131.

[33] Y. Fujiwara, Y. Amao, *Sensors Actuators B Chem.* **2003**, *89*, 58–61.

[34] E. D. Lee, T. C. Werner, W. R. Seitz, *Anal. Chem.* **1987**, *59*, 279–283.

[35] H. Ikeda, M. Nakamura, N. Ise, N. Oguma, A. Nakamura, T. Ikeda, F. Toda, A. Ueno, *J. Am. Chem. Soc.* **1996**, *118*, 10980–10988.

[36] A. Ueno, I. Suzuki, T. Osa, *Anal. Chem.* **1990**, *62*, 2461–2466.

[37] T. Aoyagi, H. Ikeda, A. Ueno, *Bull. Chem. Soc. Jpn.* **2001**, *74*, 157–164.

[38] B. Valeur, *Coord. Chem. Rev.* **2000**, *205*, 3–40.

[39] R.-H. Yang, W.-H. Chan, A. W. M. Lee, P.-F. Xia, H.-K. Zhang, L, *J. Am. Chem. Soc.* **2003**, *125*, 2884–2885.

[40] J. Strauss, J. Daub, *Org. Lett.* **2002**, *4*, 683–686.

[41] B. Bodenant, F. Fages, M.-H. Delville, *J. Am. Chem. Soc.* **1998**, *120*, 7511–7519.

[42] J.-S. Yang, C.-S. Lin, C.-Y. Hwang, *Org. Lett.* **2001**, *3*, 889–892.

[43] C. Monahan, *Chem. Commun.* **1998**, 431–432.

[44] M. Baba, M. Saitoh, Y. Kowaka, K. Taguma, K. Yoshida, Y. Semba, S. Kasahara, T. Yamanaka, Y. Ohshima, Y.-C. Hsu, et al., *J. Chem. Phys.* **2009**, *131*, 224318.

[45] X. Feng, J.-Y. Hu, C. Redshaw, T. Yamato, *Chem. - A Eur. J.* **2016**, *22*, 11898–11916.

[46] K. Yamana, T. Iwai, Y. Ohtani, S. Sato, M. Nakamura, H. Nakano, *Bioconjug. Chem.* **2002**, *13*, 1266–1273.

[47] A. Okamoto, K. Kanatani, I. Saito, *J. Am. Chem. Soc.* **2004**, *126*, 4820–4827.

[48] S. M. Langenegger, R. Häner, *Chem. Commun. (Camb).* **2004**, 2792–3.

[49] J. Strauß, J. Daub, *Adv. Mater.* **2002**, *14*, 1652–1655.

[50] B. M. de França, J. S. Bello Forero, S. J. Garden, E. S. Ribeiro, R. da S. Souza, R. S. Teixeira, R. J. Corrêa, *Dye. Pigment.* **2018**, *148*, 444–451.

[51] H. Li, R. B. Martin, B. A. Harruff, R. A. Carino, L. F. Allard, Y.-P. Sun, *Adv. Mater.* **2004**, *16*, 896–900.

[52] M. El Idrissi, S. J. Teat, P. F. X. Corvini, M. J. Paterson, S. J. Dalgarno, P. Shahgaldian, *Chem. Commun.* **2017**, *53*, 1973–1976.

[53] G. He, N. Yan, J. Yang, H. Wang, L. Ding, S. Yin, Y. Fang, *Macromolecules* **2011**, *44*, 4759–4766.

[54] W. Zhang, Y. Luo, Y. Zhou, M. Liu, W. Xu, B. Bian, Z. Tao, X. Xiao, *Dye. Pigment.* **2020**, *176*, 108235.

[55] T. Otsubo, Y. Aso, K. Takimiya, *J. Mater. Chem.* **2002**, *12*, 2565–2575.

[56] W.-L. Jia, T. McCormick, Q.-D. Liu, H. Fukutani, M. Motala, R.-Y. Wang, Y. Tao, S. Wang, *J. Mater. Chem.* **2004**, *14*, 3344.

[57] J. E. Anthony, *Angew. Chemie Int. Ed.* **2008**, *47*, 452–483.

[58] Y. Shirota, H. Kageyama, *Chem. Rev.* **2007**, *107*, 953–1010.

[59] J. Wu, W. Pisula, K. Müllen, *Chem. Rev.* **2007**, *107*, 718–747.

[60] T. Wöhrle, I. Wurzbach, J. Kirres, A. Kostidou, N. Kapernaum, J. Litterscheidt, J. C. Haenle, P. Staffeld, A. Baro, F. Giesselmann, et al., *Chem. Rev.* **2016**, *116*, 1139–1241.

[61] S. Kumar, *Liq. Cryst.* **2004**, *31*, 1037–1059.

[62] S. Kumar, **2017**, *8292*, 607–638.

[63] A. S. Achalkumar, B. N. Veerabhadraswamy, U. S. Hiremath, D. S. S. Rao, S. K. Prasad, C. V. Yelamaggad, *Dye. Pigment.* **2016**, *132*, 291–305.

[64] S. Chandrasekhar, B. K. Sadashiva, K. A. Suresh, *Pramana* **1977**, *9*, 471–480.

[65] A. Gowda, M. Kumar, S. Kumar, *Liq. Cryst.* **2017**, 1–28.

[66] S. Kumar, *Chem. Soc. Rev.* **2006**, *35*, 83–109.

[67] A. Gowda, M. Kumar, S. Kumar, *Liq. Cryst.* **2017**, *00*, 1–28.

[68] M. Kumar, A. Gowda, S. Kumar, *Part. Part. Syst. Charact.* **2017**, *34*, 1700003.

[69] A. Gowda, L. Jacob, A. Patra, A. George, R. Philip, S. Kumar, *Dye. Pigment.* **2019**, *160*, 128–135.

[70] Y. Tomkiewicz, A. Weinreb, *Chem. Phys. Lett.* **1969**, *3*, 229–230.

[71] Sandeep Kumar, *Chemistry of Discotic Liquid Crystals: From Monomers to Polymers*, **2011**.

[72] H. Bock, W. Helfrich, *Liq. Cryst.* **1995**, *18*, 707–713.

[73] T. Hirose, O. Kawakami, M. Yasutake, *Mol. Cryst. Liq. Cryst.* **2006**, *451*, 65–74.

[74] T. Hassheider, S. A. Benning, H.-S. Kitzerow, M.-F. Achard, H. Bock, *Angew. Chemie Int. Ed.* **2001**, *40*, 2060–2063.

[75] S. Keuker-Baumann, H. Bock, F. Della Sala, S. A. Benning, T. Haßheider, T. Frauenheim, H.-S. Kitzerow, *Liq. Cryst.* **2001**, *28*, 1105–1113.

[76] E. Dantras, J. Dandurand, C. Lacabanne, L. Laffont, J. M. Tarascon, S. Archambeau, I. Seguy, P. Destruel, H. Bock, S. Fouet, *Phys. Chem. Chem. Phys.* **2004**, *6*, 4167.

[77] V. de Halleux, J.-P. Calbert, P. Brocorens, J. Cornil, J.-P. Declercq, J.-L. Brédas, Y. Geerts, *Adv. Funct. Mater.* **2004**, *14*, 649–659.

[78] M. J. Sienkowska, H. Monobe, P. Kaszynski, Y. Shimizu, *J. Mater. Chem.* **2007**, *17*, 1392.

[79] A. Hayer, V. de Halleux, A. Köhler, A. El-Garoughy, E. W. Meijer, J. Barberá, J. Tant, J. Levin, M. Lehmann, J. Gierschner, et al., *J. Phys. Chem. B* **2006**, *110*, 7653–7659.

[80] M. Yasutake, T. Fujihara, A. Nagasawa, K. Moriya, T. Hirose, *European J. Org. Chem.* **2008**, *2008*, 4120–4125.

[81] Y. H. Kim, D. K. Yoon, E. H. Lee, Y. K. Ko, H.-T. Jung, *J. Phys. Chem. B* **2006**, *110*, 20836–20842.

[82] V. Percec, M. Glodde, T. K. Bera, Y. Miura, I. Shiyanovskaya, K. D. Singer, V. S. K. Balagurusamy, P. A. Heiney, I. Schnell, A. Rapp, et al., *Nature* **2002**, *419*, 384–387.

[83] V. Percec, M. Glodde, T. K. Bera, Y. Miura, I. Shiyanovskaya, K. D. Singer, V. S. K. Balagurusamy, P. A. Heiney, I. Schnell, A. Rapp, et al., *Nature* **2002**, *419*, 384–387.

[84] I. Shiyanovskaya, K. D. Singer, V. Percec, T. K. Bera, Y. Miura, M. Glodde, *Phys. Rev. B* **2003**, *67*, 035204.

[85] Y. Kamikawa, T. Kato, *Langmuir* **2007**, *23*, 274–278.

[86] T. Kato, T. Matsuoka, M. Nishii, Y. Kamikawa, K. Kanie, T. Nishimura, E. Yashima, S. Ujiie, *Angew. Chemie Int. Ed.* **2004**, *43*, 1969–1972.

[87] Y. Kamikawa, M. Nishii, T. Kato, *Chem. - A Eur. J.* **2004**, *10*, 5942–5951.

[88] Y. Sagara, T. Kato, *Angew. Chemie Int. Ed.* **2008**, *47*, 5175–5178.

[89] Y. Sagara, S. Yamane, T. Mutai, K. Araki, T. Kato, *Adv. Funct. Mater.* **2009**, *19*, 1869–1875.

[90] T. Hirose, Y. Shibano, Y. Miyazaki, N. Sogoshi, S. Nakabayashi, M. Yasutake, *Mol.*

Cryst. Liq. Cryst. **2011**, *534*, 81–92.

[91] K. P. Gan, M. Yoshio, T. Kato, *J. Mater. Chem. C* **2016**, *4*, 5073–5080.

[92] B. R. Kaafarani, L. A. Lucas, B. Wex, G. E. Jabbour, *Tetrahedron Lett.* **2007**, *48*, 5995–5998.

[93] H. Cho, S. Lee, N. S. Cho, G. E. Jabbour, J. Kwak, D.-H. Hwang, C. Lee, *ACS Appl. Mater. Interfaces* **2013**, *5*, 3855–3860.

[94] S. R. Bheemireddy, P. C. Ubaldo, A. D. Finke, L. Wang, K. N. Plunkett, *J. Mater. Chem. C* **2016**, *4*, 3963–3969.

[95] S. R. Bheemireddy, M. P. Hautzinger, T. Li, B. Lee, K. N. Plunkett, *J. Am. Chem. Soc.* **2017**, *139*, 5801–5807.

Chapter - 4

Columnar Mesomorphism in Heptazine Discotics

Abstract

In this chapter, we report the design and synthesis of C_3- symmetric columnar liquid crystals in which heptazine core is flanked with six alkoxy chains. These novel derivatives show hexagonal and rectangular columnar liquid-crystalline (LC) phases over a wide range of temperatures. All the compounds exhibit columnar hexagonal phase (Col_h) at high temperatures, among which two compounds with lower alkoxy chains show a rectangular phase at lower temperatures. The mesomorphic properties of all the compounds are confirmed by polarizing optical microscopy, differential scanning calorimetry and X-ray diffractometry.

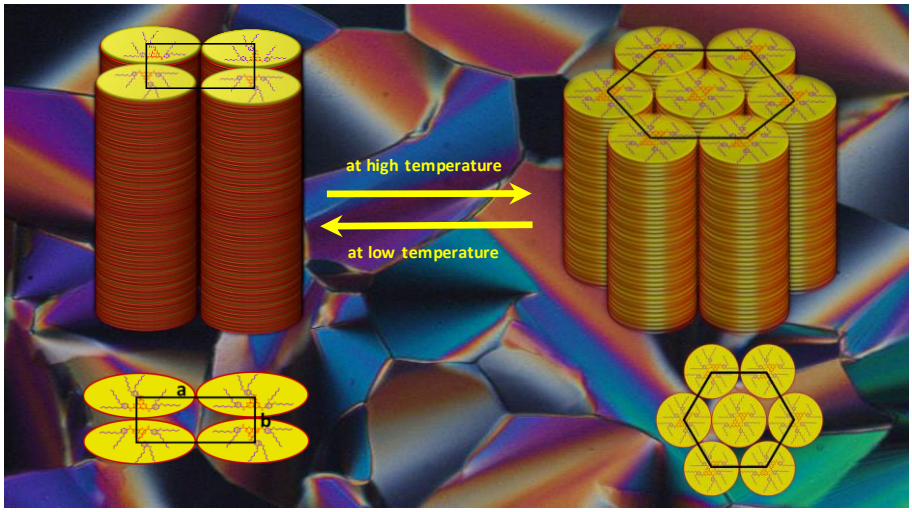

4.1 Introduction:

Semiconductors have attracted much interest in the liquid crystal field since the discotic liquid crystal was discovered in the late 20th century.[1] Graphitic carbon nitride (g-C_3N_4) (**Figure 4.1**) falls under the category of semiconducting material. C_3N_4 is one of the oldest synthetic polymers and was first reported by Berzelius and Liebig during the 1830s. It has many allotropes such as α-C_3N_4, β-C_3N_4, pseudocubic C_3N_4, cubic C_3N_4, g-h triazine and g-C_3N_4.

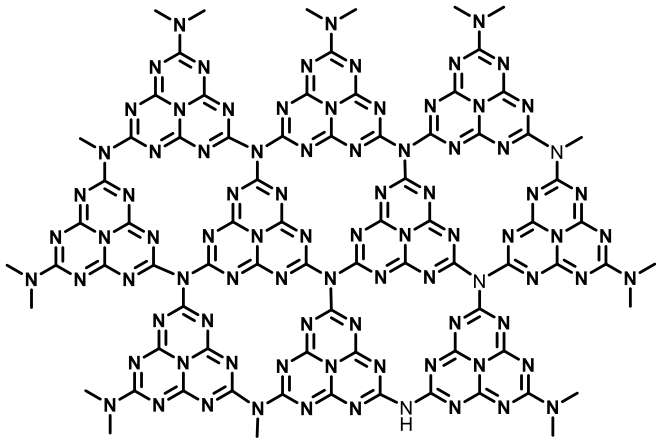

Figure 4.1: Molecular structure of graphitic carbon nitride.

Among these allotropes, graphitic carbon nitride (g-C_3N_4) has received more attention since 1989, Liu and Cohens theoretically predicted that polymorphs of hydrogen-free C_3N_4 would be a super hard material.[2] It is the most stable allotrope with unique properties of semiconductors formed from earth-abundant elements with high chemical and thermal stability.[3,4] The energy band gap of g-CN is 2.7 eV[5] and can be used as a visible light-responsive material. The energy levels of the conduction band (CB) and valence band (VB) are at 1.1 and 1.6 eV vice versa, comparable with standard hydrogen electrode (NHE). g-C_3N_4 is made up of carbon & nitrogen elements therefore, the synthesis of graphitic nitride has been discussed in the literature using different starting materials like cyanamide and dicyandiamide melamine, urea and thiourea through thermal polymerization[6] shown in **Figure 4.2.** It can also be prepared using electrodeposition on silica substrate with a saturated acetone solution of cyanuric trichloride and melamine (ratio =1:1.5) at room temperature and also through chemical vapor deposition (CVD). Moreover the choice of precursor and different pyrolysis

temperature influences the electronic structure and bandgap of g-C_3N_4, which further affects its potential applications in many fields.

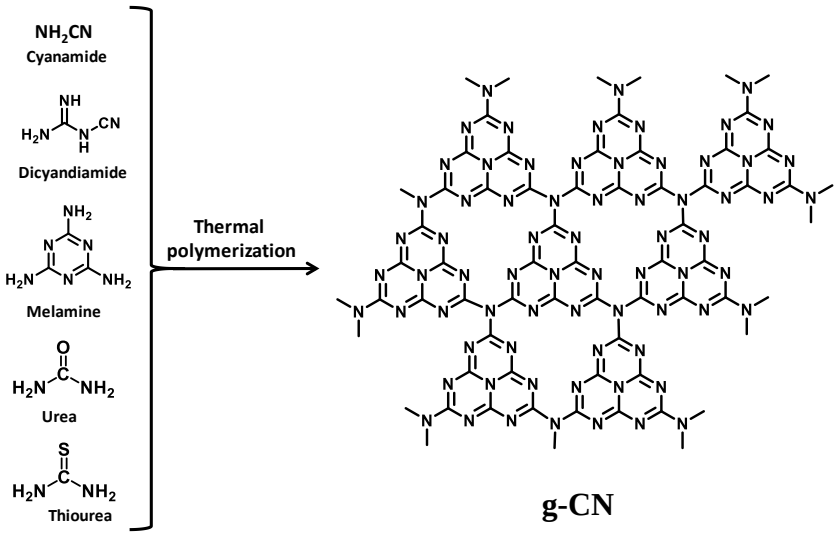

Figure 4.2: Synthesis of graphitic carbon nitride from diverse starting materials.

Melamine units (C_3N_3) and tri-s-triazine (heptazine, C_6N_7) rings have been proposed as some of the basic building blocks of g-C_3N_4. Tri-s-triazine (heptazine, C_6N_7) rings are structurally close to the melon structure and are more stable and energetically favored building blocks of g-C_3N_4 than melamine.[7] Komatsu et al. reported the characterized form of melon consisting oligomers that can be described as the condensation of melem tautomer with loss of ammonia (NH_3). In this case, X-ray diffraction data and other evidence indicate that the oligomer is planar and the triangular heptazine cores have alternating orientations, as shown in **Figure 4.3**.[8] All graphitic nitride-based derivatives can split water molecules by reducing protons to hydrogen through light excitation[5] and its schematic representation is given in **Figure 4.4**. It has been widely studied as a metal-free photo catalyst[9,10] and in the fields of supramolecular chemistry, agricultural chemistry, polymers, dyes, explosives, etc.[11] In addition to this, porous heptazine polymeric materials extend their applications to selective absorbance, sensing and biological applications.[12] Unlike s-triazine, the carbon nitride precursor s-heptazine (C_6N_7) has not been explored through some fascinating aspects, which are described in a recent comprehensive review.[6]

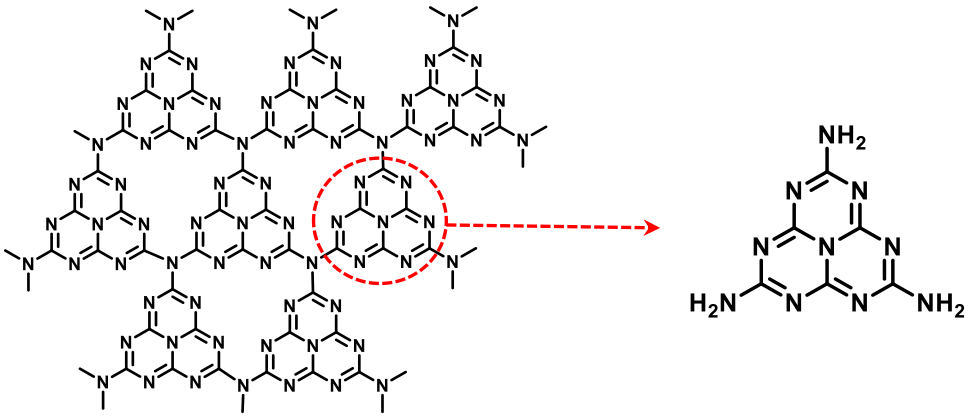

Figure 4.3: Tri-s-triazine-based connection patterns of potential g-C_3N_4 allotropes.

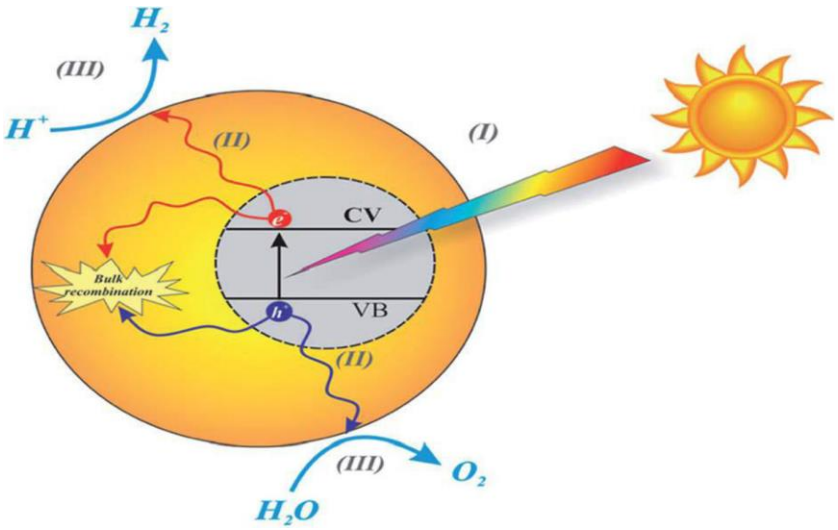

Figure 4.4: Schematic diagram of the basic mechanisms of the photocatalytic activity of water splitting.

Kroke et al. have extensively studied the s-heptazine nucleus irrespective of the heptazine precursor used in molecular and polymeric material.[6] The parent molecule of the cyamelurine is the H-substituted tri-s-triazine core shown in **Figure 4.5a,** which was first discussed using theoretical studies carried out by J. Wirz (1980), which were successfully synthesized by Leonard co-workers (1982) along with comprehensive structural analysis.[13,14] From the above

literature, it is clear that the heptazine-based compounds were known for two centuries but were less explored as an organic moiety due to difficulty in synthesis protocols and their insolubility in most organic solvents. Eventually, melem, cyameluric acid, cyameluric chloride, and triazido-s-heptazine **(Figure 4.5b–e)** were also reported in 1830–1844. However, these compounds had solubility issues; thus, characterization of these compounds is done using only elemental analysis studies.

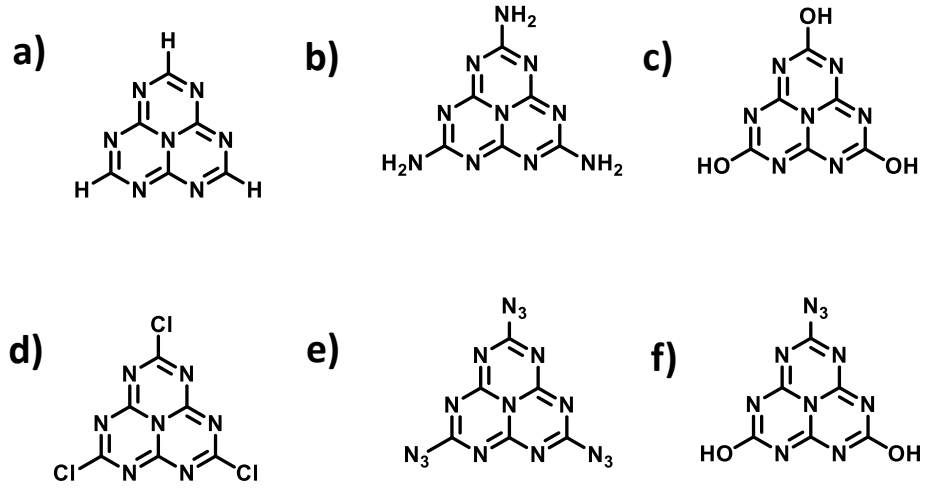

Figure 4.5: Tri-s-triazine-based derivatives

Pauling remain interested in this class of compounds as a molecular structure, 2-azido-5,8-dihydroxy-1,3,4,5,7,9,9b-hepta-azaphenalene, having a heptazine core retained on his chalkboard **(Figure 4.5f).** Until today trichloro-tri-s-triazine is a soluble member of the heptazine family. It has been extensively used to incorporate peripheral functionality using nucleophilic substitution reactions in organic solvents. The first synthesis of trichloro-s-heptazine was reported by Redemann and Lucas (1940) through a solid phase reaction by reacting K-melem / cyameluric acid with PCl_5 in a bomb tube.[15] But the synthesis and extensive characterization data was published in 2002 by Kroke. Initial investigation on trichloro-s-heptazine is based on the equal reactivity of the three chloro-groups and thus, symmetrically substituted derivatives are reported initially.[16] Unsymmetrical mono- and di-substituted chloro heptazines are challenging to synthesize till now.[16–18] The straightforward synthesis of trichloro-s-heptazine was reported by Kroke's group in 2002.[18] Nucleophilic substitution on trichloro-heptazine derivatives, which have been extensively studied in the

literature and its derivatives, has attracted attention in the material science field. The heptazine derivatives were synthesized using nucleophilic substitution reactions by several research groups.[19–21] Some of the examples are given in **Figure 4.6.**

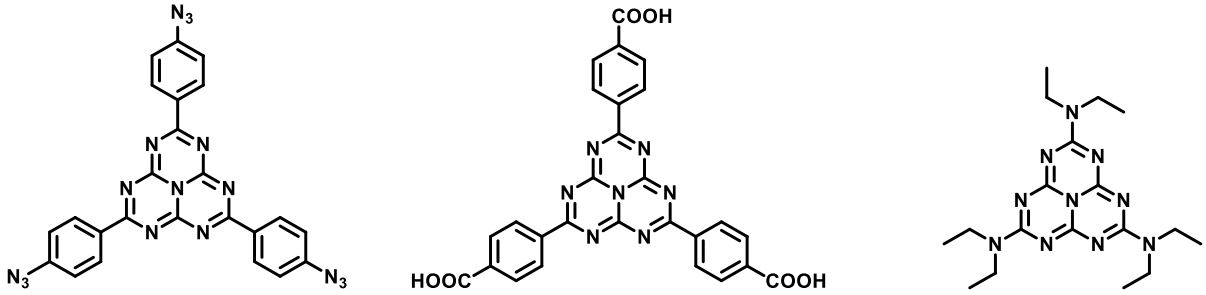

Figure 4.6: Some examples of heptazine derivatives.

Heptazine is an electron-accepting core, which has been studied in the field of organic light-emitting diodes (OLED).[22,23] Moreover, heptazine-based porous organic polymer materials have been explored for sensing, field emission, energy storage, separation and polluted water purification. The polymer structures and OLED-based heptazine derivatives are shown in **Figure 4.7**.[6,24–31]

a)

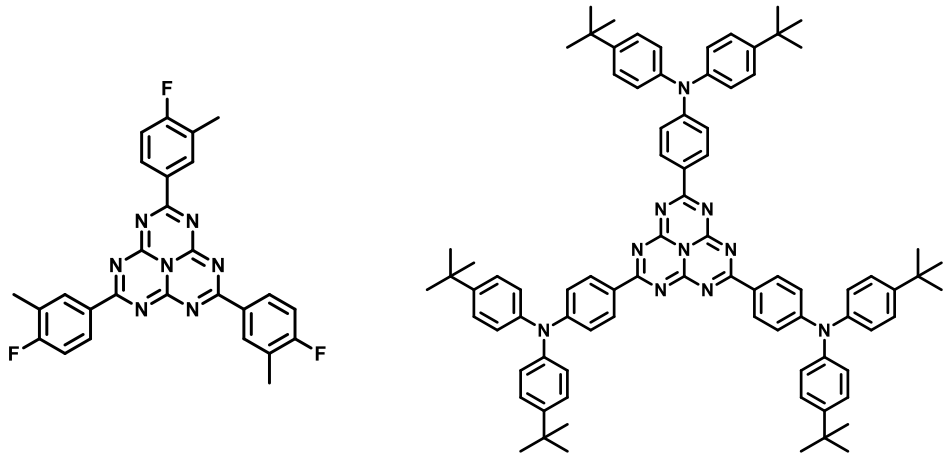

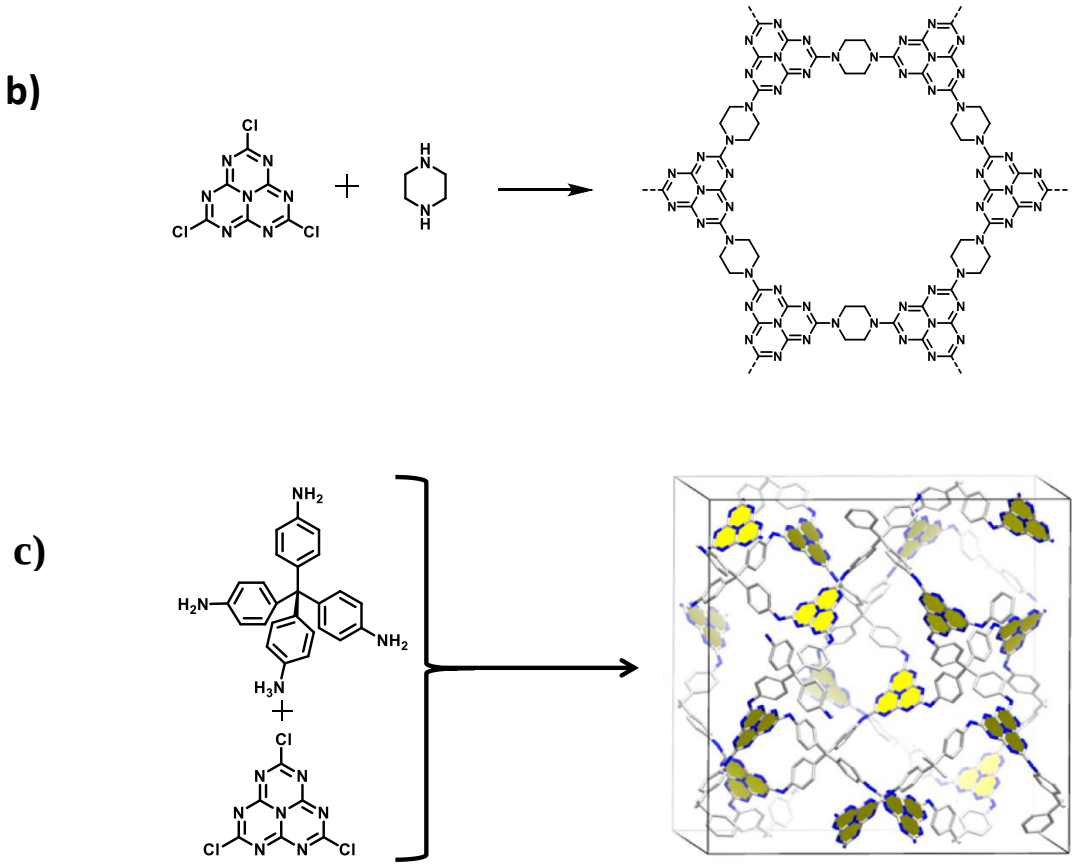

Figure 4.7: Heptazine derivatives for OLED application, b) Heptazine-based porous framework for selective CO_2 sorption, c) Luminescent porous organic polymer.

There is only one report on the liquid crystal using graphitic nitride in the graphitic nitride molecules application reported so far[29]. Zhixin Zhou et al. reported graphite-phase polymeric carbon nitride (GPPCN) has emerged as a promising metal-free material for optoelectronics and photocatalysis. This also shows the insolubility in organic solvents, except conc. H_2SO_4, the first feasible solvent so far. As a result, the first successful liquid-state NMR spectra of GPPCN were obtained, which provides a more viable method to reveal the more acceptable structure of GPPCN. They have dissolved this material in different concentrations. At higher concentrations, GPPCN shows the liquid crystal behavior. The details of the work is shown in **Figure 4.8.** This anisotropic mesophase formation shown by GPPCN significantly improved to its potential applications, such as GPPCN-based nanocomposites or assembly of macroscopic, ordered materials.

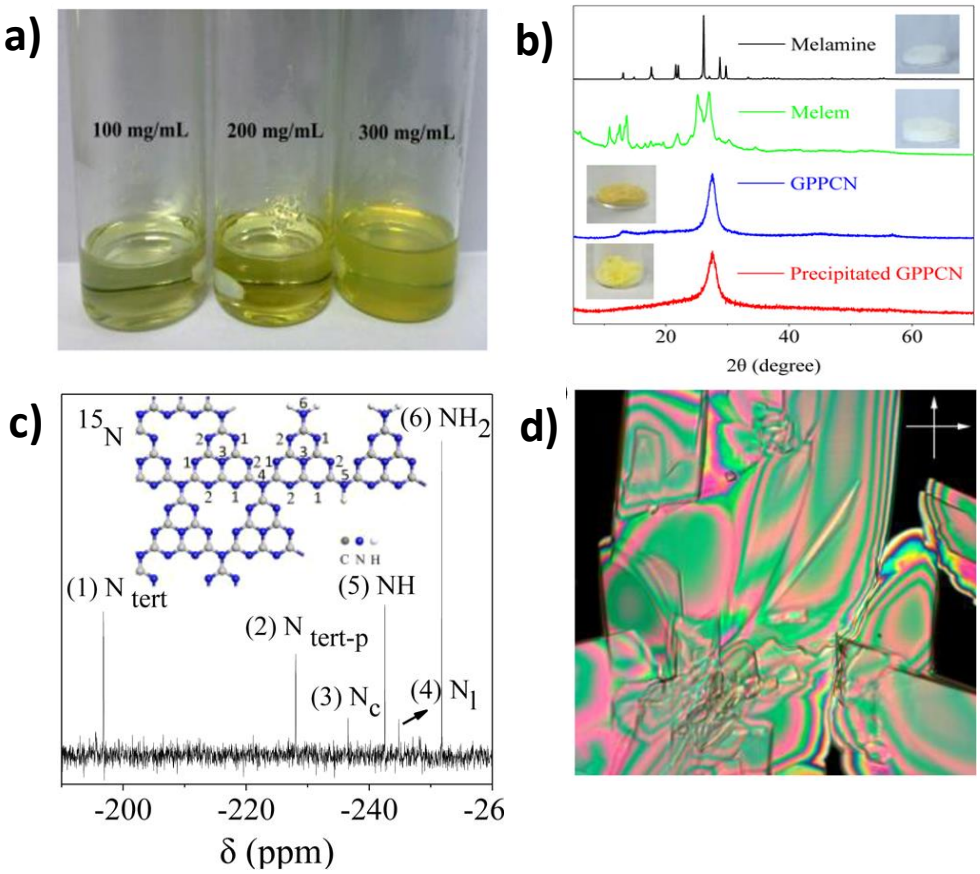

Figure 4.8. (a) GPPCN dissolved in concentrated sulfuric acid at different concentrations. (b) XRD patterns of melamine, melem, GPPCN, and the GPPCN precipitated from GPPCN/H_2SO_4 solution using methanol. c) ^{15}N liquid-state NMR spectrum of GPPCN/H_2SO_4 solution; inset: the proposed structure for GPPCN. (b) Optical textures of GPPCN/H_2SO_4 under a polarizing microscope (crossed polarizer, magnification ×20).[29]

Heptazine offers a flat disc-shaped core, semiconducting, and it shows many applications as mentioned above. Although its derivatives could be implemented as advanced materials in devices, it has not yet been well explored in the field of DLCs. Hong Yang et al. have published the first room-temperature heptazine discotic liquid crystals (HDLCs) shown in **Figure 4.9.** The condensation of cyameluric chloride and trialkoxyaniline resulted in the synthesis of novel trisubstituted heptazine derivatives. The HDLCs are self-assembled into columnar hexagonal mesophase. Detailed electro-optical properties and mesomorphic properties were studied.[32]

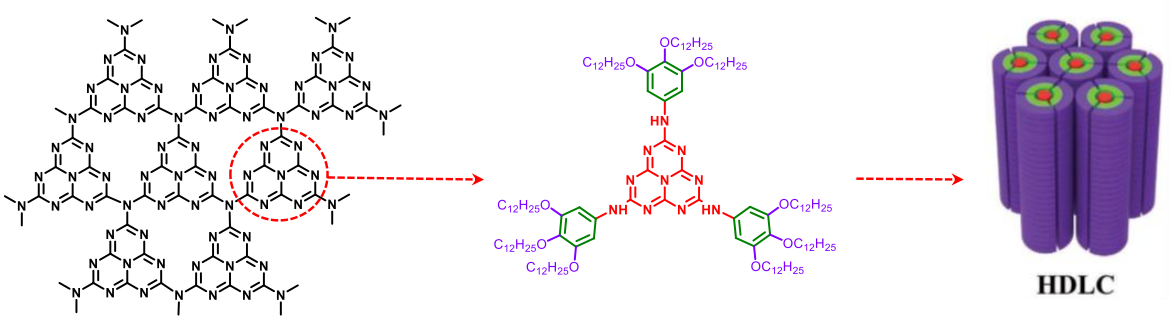

Figure 4.9: Heptazine discotic liquid crystal-forming columnar hexagonal mesophase.[32]

Pal et al. have also synthesized the HDLCs by varying the alkoxy chains.[33] The mesomorphic properties of these materials were investigated. Supramolecular assembly of the mesogenic derivatives was confirmed by X-ray scattering experiments which shows the stable Col_h phase and Sm phase at ambient temperature. The self-assembly of both the mesophases schematic representation is given in **Figure 4.10.**

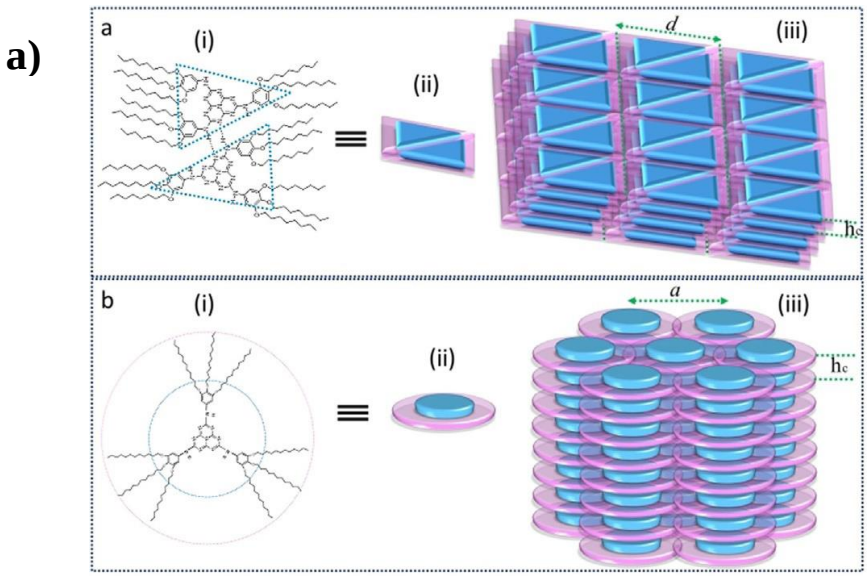

Figure 4.10: a) Schematic representation smectic phase and columnar hexagonal mesophase of heptazine discotic liquid crystals.[33]

They also reported the H-bonded heptazine complexes with 3,4,5-tri-alkoxy benzoic acids. It exhibits the enantiotropic columnar mesomorphism over a wide range of temperatures and even at room temperature. The stability of resulting H-bonded supramolecular complexes (**Figure**

4.11) was studied using temperature-dependent FT-IR and NMR studies and H–D exchange studies, and their mesomorphic behavior was confirmed by polarized optical microscopy (POM), differential scanning calorimetry (DSC) and X-ray diffraction (XRD) studies. The resulting complexes exhibit fluorescent behavior in the solution state as well as in the solid state.[34] The heptazine derivatives were found to have AIE (Aggregation-Induced Emission) properties, which leads to the fabrication of deep blue OLED.[35] Pierre Audebert et al reported the recent review on synthesis and functional applications of heptazine[36].

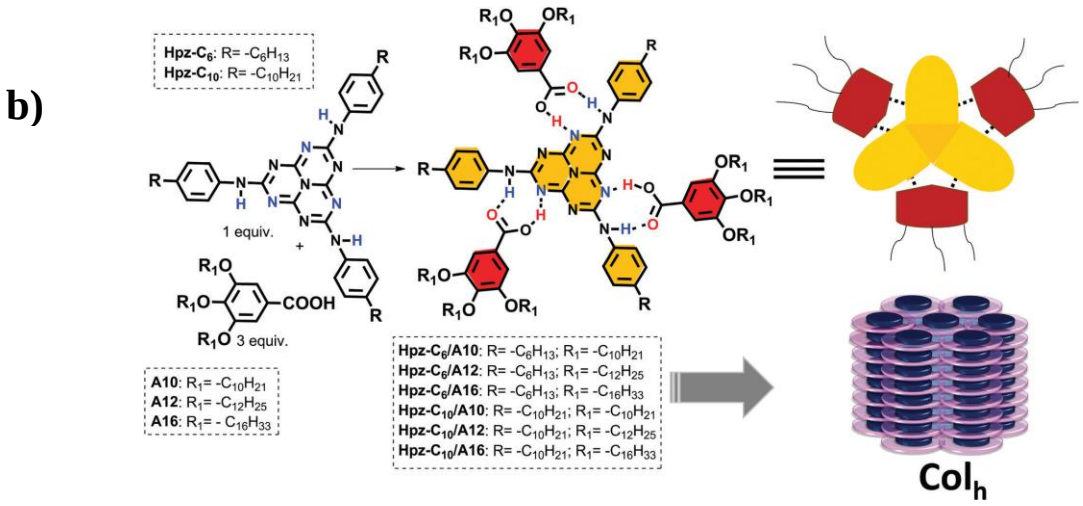

Figure 4.11: Schematic representation of H-bonded complexes between heptazine and 3,4,5-tri-alkoxy benzoic acids.[34]

4.2 Results and discussion:

4.2.1 Synthesis

Here, we present the synthesis and mesomorphic properties of some novel heptazine-based DLCs. The heptazine core is connected to dialkoxy substituted aniline derivatives with different alkoxy chain lengths. The synthesis of these novel tri-substituted heptazine derivatives is shown in **Figure 4.12.** Compounds **5a** and **5b** show two different mesophases (columnar rectangular and columnar hexagonal) at different temperatures, whereas compounds **5c-e** show columnar hexagonal mesophase**.**

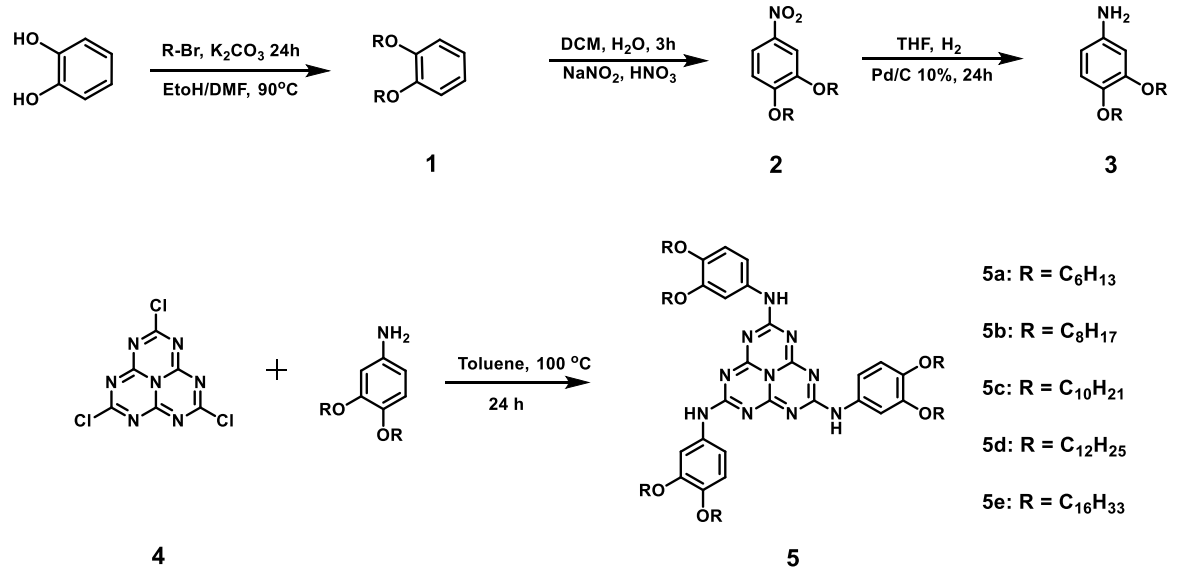

Figure 4.12: Synthesis of trisubstituted heptazine derivatives.

Dialkoxyaniline and the trisubstituted heptazine derivatives were prepared following the procedure as reported.[32,37] All the compounds were purified by using column chromatography and precipitated in methanol and further well characterized by using ^{1}H NMR, ^{13}C NMR, UV, emission spectra and MALDI-TOF. All the members of the series gave similar spectra. Spectral analysis of the compounds was in good agreement with their structures, specifying the high purity of all materials.

4.2.2 Optical properties:

The solution of the trisubstituted heptazine derivatives in chloroform (3×10^{-6}M) shows absorption and emission spectra as shown in **Figure 4.13**. The absorption spectra of all compounds **5a-5e** are similar, with two absorption peaks at 268 nm and 333 nm (ε 330 = 5.3×10^{4} (**5a**), 5.4×10^{4} (**5b**), 5.1×10^{4} (**5c**), 4.9×10^{4} (**5d**), 4.3×10^{4} M^{-1} cm^{-1} (**5e**)). The emission spectra display structured emission which shows two intense peaks at wavelengths of 411 nm and 435 nm (**5a – 5e**), whereas the shoulder peaks are at 450 nm to 530 nm. The Stokes shift between the absorption maxima and emission maxima is of around 81 nm, which was observed in all the compounds. Contrarily, trialkoxyaniline heptazine derivatives reported in the literature[33] showed a very broad emission with maxima at 490 nm. This could be attributed to the aggregation.

Emission spectra of **5a-5e** differ from that of the reported trialkoxy aniline heptazine derivatives (TAAHD). Emission spectra of **5a-5e**, as well as TAAHD, were recorded in chloroform at a concentration of 10^{-6} M. **5a-5e** showed a highly structured emission with peaks at 406, 432 and 460 nm, whereas TAAHD showed a very broad emission with maxima at 490 nm. This could be attributed to the aggregation of TAAHD at the concentration under study and can be explained by analyzing the structure of TAAHD. TAAHD has nine alkyl chain per molecule hence can non-covalently (mainly through Van der Waals interaction) interact with those of neighboring molecules to form the assembly. However, **5a-5e** having only 6 alkyl chains per molecule and hence the number of counterparts with which it can interact is lesser than that of TAAHD by virtue of which more molecules / higher concentration is required for the **5a-5e** to form aggregates. In other words, **5a-5e** exist as monomers at 10^{-6} M concentration while TAAHD aggregates. To check this possibility, taking **5a** and **5d** as a representative example, we have recorded the emission spectra at different concentrations. With a systematic increment in concentration, the structured emission at 10^{-6} M concentration is slowly diminished and a concomitant decrease in emission intensity was observed (**Figure 4.14**). This can be considered the characteristic feature of assembly formation and at 5 x10-5 M concentration, spectra became very broad and similar to that of TAAHD at 10^{-6} M concentration. In short, the reported emission spectrum of TAAHD is of aggregates and that of **5a-5e** is of monomers.

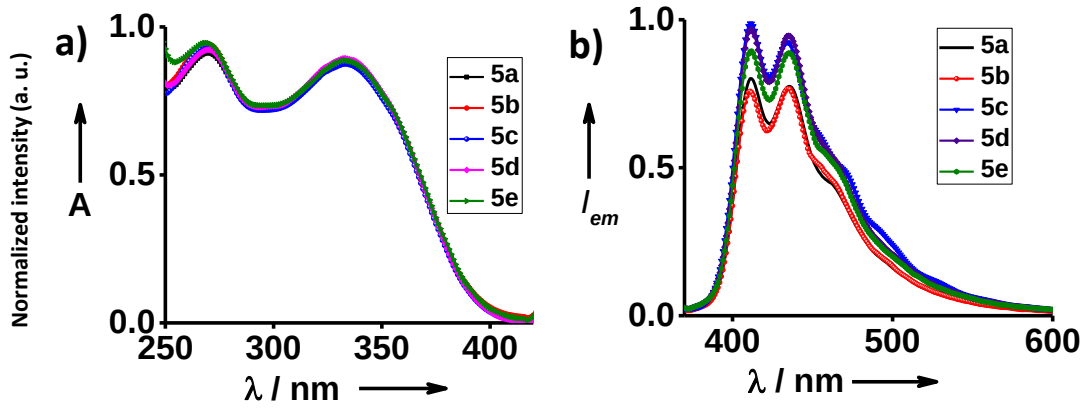

Figure 4.13: Normalized a) absorption and b) emission spectra of **5a – 5e** in chloroform (the path length of the cuvette is 1 cm, Concentration: 3×10^{-6} M). The excitation wavelength of all compounds is at 330 nm.

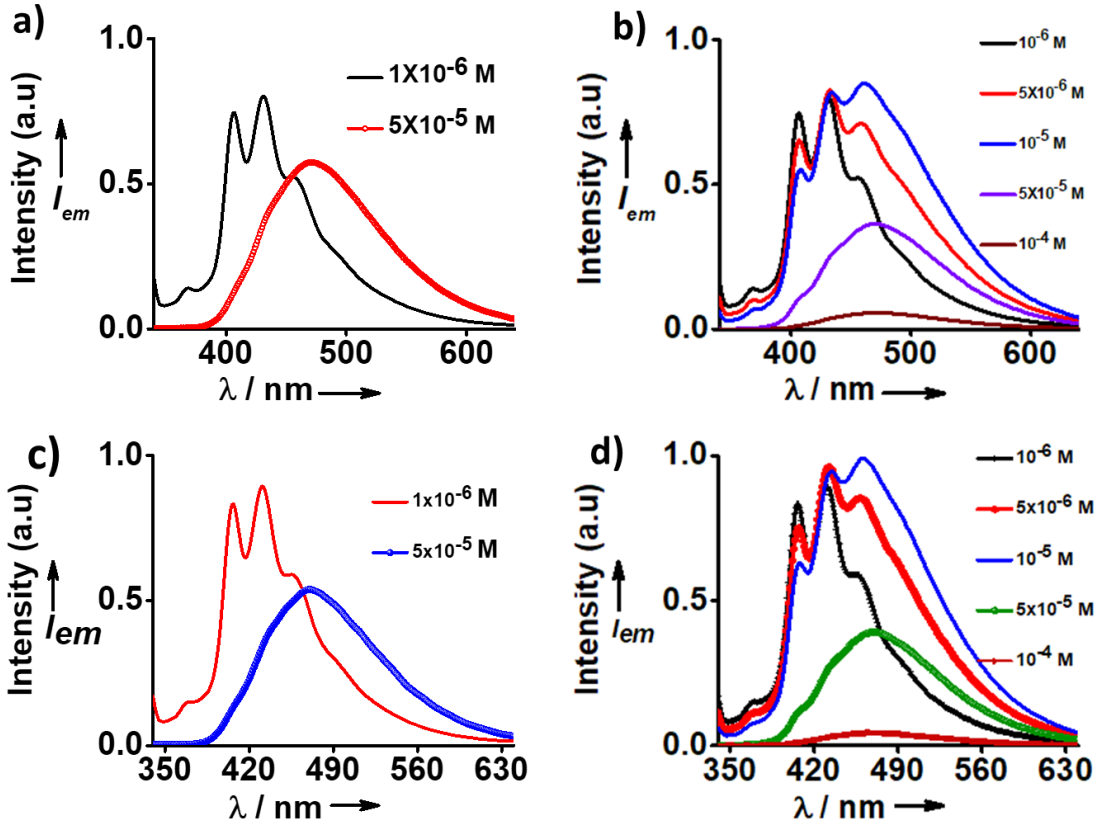

Figure 4.14: a) **5a** black curve lowest concentration red curve is the highest concentration and red curve is multiplied with a factor of 10 b) **5a** systematic study of concentration-dependent c) **5d** red curve lowest concentration blue curve is the highest concentration and blue curve is multiplied with a factor of 10 b) **5d** systematic study of concentration dependency

4.2.3 Density functional theory:

The theoretical studies were done using the GAUSSIAN-09 program at the Becke's three-parameter functional and Lee, Yang, and Parr correlation functional (B3LYP) using the 6-311G (d p) basis set. The energy-minimized structure of 5a and HOMO LUMO molecular orbitals are given in **Figure 4.15.** The theoretical energy gap found to be 3.63 eV and the optical energy gap (E_g) in eV was calculated to be 3.17 (according to the equation Eg = 1240/onset, where onset was resolved as the intersection of the extrapolated tangent of the longest wavelength absorption peak and the x-axis).

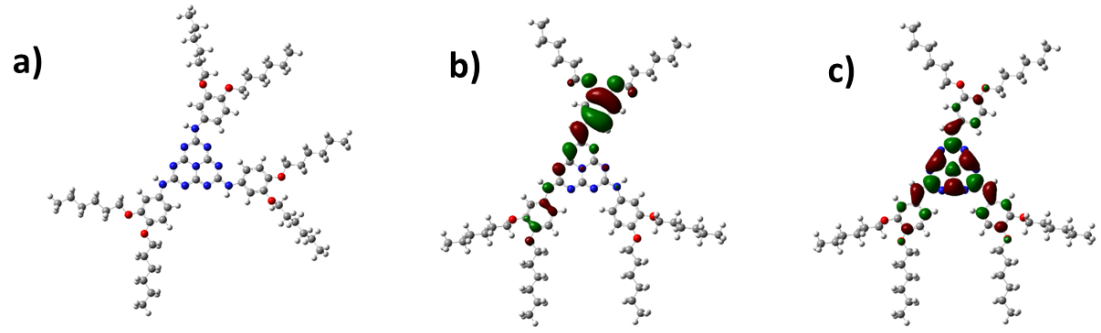

Figure 4.15: a). Energy minimized structure, **b)** and **c**) are HOMO and LUMO energy level diagrams of 5a calculated by using B3LYP employing the 6–311G (d, p) basis set.

4.2.4 Thermal Stability

The thermal stability of all the mesogenic compounds (**5a-5e**) was analyzed under the scan rate of 10 °C min^{-1}. No weight loss was observed till the temperature reaches 360 °C but the compounds start decomposing at a temperature around 390 – 490 °C as shown in **Figure 4.16.** The decomposition temperatures of all the compounds are much higher than isotropic temperatures. This indicates that all heptazine derivatives have excellent thermal stability. The thermotropic liquid crystalline properties of all the compounds were visualized by using X-ray diffraction (XRD), polarizing optical microscopy (POM) and differential scanning calorimetry (DSC). Interestingly, all the compounds **5a – 5e** found to be mesomorphic. Compounds **5a** and **5b** with lower alkyl chains display two mesophases, namely columnar rectangular and columnar hexagonal mesophases, whereas the longer alkyl chains derivatives **5c-5e** exhibit only columnar hexagonal mesophase.

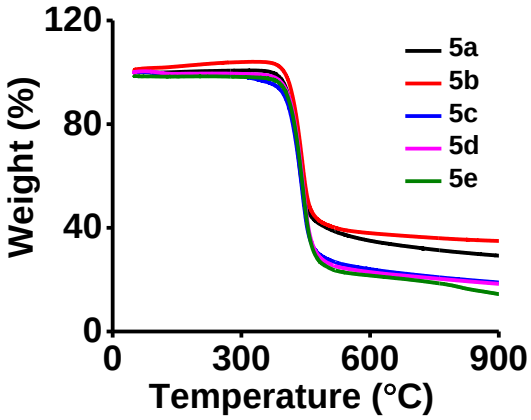

Figure 4.16: TGA spectra of **5a-e**

4.2.5 Mesomorphic characteristics

Polarized optical microscopy was considered as the standard examination method for the observation of mesophases. All the compounds (**5a – 5e**) revealed the characteristic textures of discotic LCs in their mesophase. Dialkoxy substituted heptazine derivatives **5b**, **5c** and **5d** typically demonstrate fan-shaped, pseudo focal conical, mosaic texture has been observed in the case of **5a** and **5e** shown in the **Figure 4.17**. The transition temperatures and enthalpy values of heptazine derivatives were investigated by using DSC, which was further validated from POM. DSC thermogram of compounds **5a** and **5b (Figure 4.18**) clearly shows three-phase transitions associated with the existence of two mesophases.

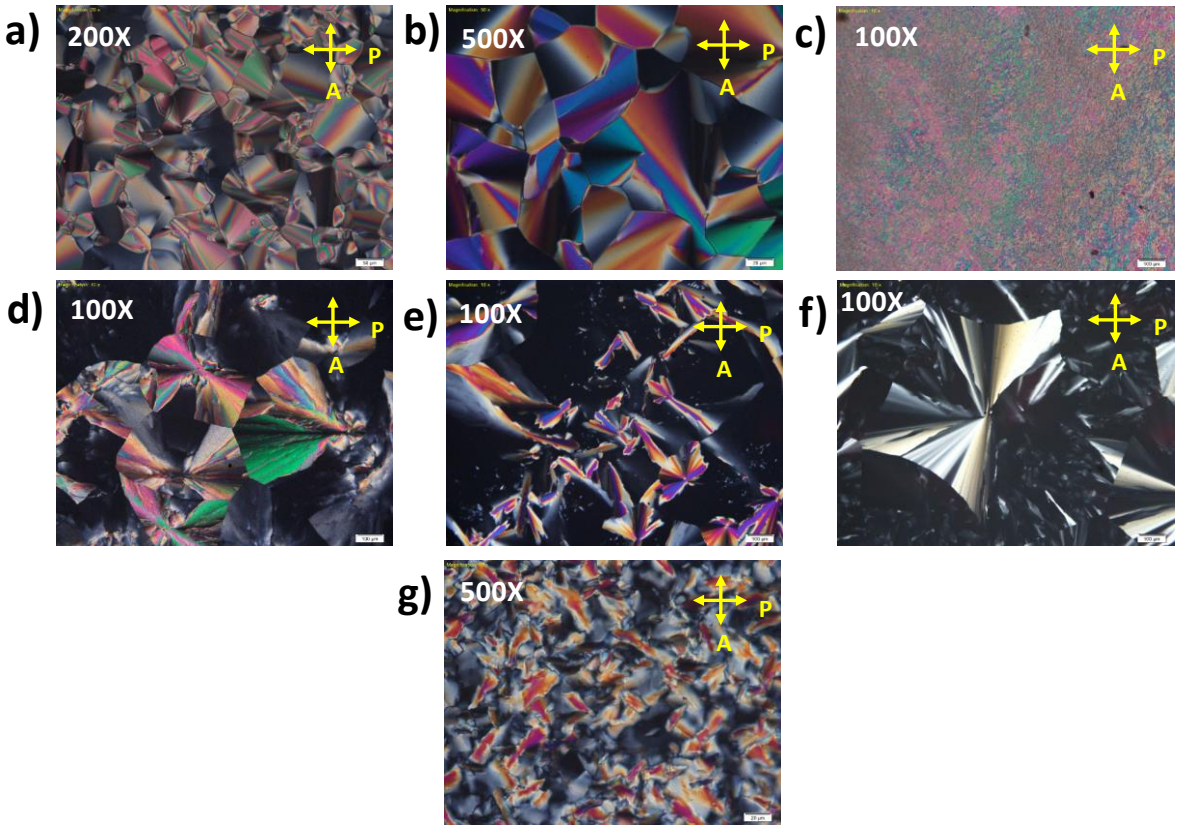

Figure 4.17: Birefringence texture observed under POM at different temperature upon cooling from the isotropic phase, a) and b) **5a** at 160 °C, and 180 °C, c) and d) **5b** at 110°C, and 180 °C, e) **5c** at 170 °C, f) **5d** at 180 °C, g) **5e** at 140 °C, POM images of (a) and (c) were recorded upon heating the sample.

These compounds melt at about 99 °C and 109 °C and columnar rectangular phase transition appears at about 173 °C and 141 °C, respectively which becomes isotropic at around 180 °C

and 193 °C. Upon cooling from an isotropic phase, the hexagonal columnar phase transition appears at 176 °C and 190°C, respectively, which converted to the columnar rectangular mesophase at around 146 °C and 116 °C and then crystallizes at around 87 °C and 96 °C, respectively. Compound **5c – 5d** melts around 98 °C and 84 °C and clearing temperature centered at about 192 °C and 182 °C, respectively. Upon cooling from the isotropic phase, columnar mesophase appears around 186 °C and 183 °C, respectively which super cool down to the room temperature. DSC thermograms of compounds **5a – 5e** are given in **Figure 4.18.** On the other hand, compound **5e** exhibits a sharp melting transition at about 40 °C and a clearing temperature peak centered at about 163 °C. Upon cooling, the isotropic phase to columnar hexagonal mesophase transition appears at 161 °C and crystallizes at 34 °C. The phase transition temperatures and enthalpy values of all the compounds (**5a – 5e**) are given in the **Table 4.1.**

Table 4.1. Phase transition temperatures (°C), enthalpy changes and the proportional enthalpies (J/g) of **5a-5e** at the time of heating and cooling obtained from DSC. Cr – Crystalline phase; Col_h – Columnar hexagonal phase; Col_{rec} – Columnar rectangular phase; I – Isotropic.

Compound	Heating	Cooling
5a	Cr 99.1 (17.2) Col_r 173.0 (15.4) Col_h 180.8 (1.5) I	I 176.8 (1.6) Col_h 146.5 (14.5) Col_r 87.4 (16.1) Cr
5b	Cr 109.4 (20.6) Col_r 141.4 (6.4) Col_h 193.4 (2.4) I	I 190.5 (2.3) Col_h 116.4 (2.3) Col_r 96.4 (16.6) Cr
5c	Cr 98.4 (34.3) Col_h 192.8 (3.2) I	I 186.3 (2.4) Col_h
5d	Cr 84.9 (31.7) Col_h 185.1 (2.6) I	I 183.2 (2.2) Col_h
5e	Cr 40.8 (29.7) Col_h 163.6 (1.8) I	I 161.8 (1.8) Col_h 34.8 (27.9) Cr

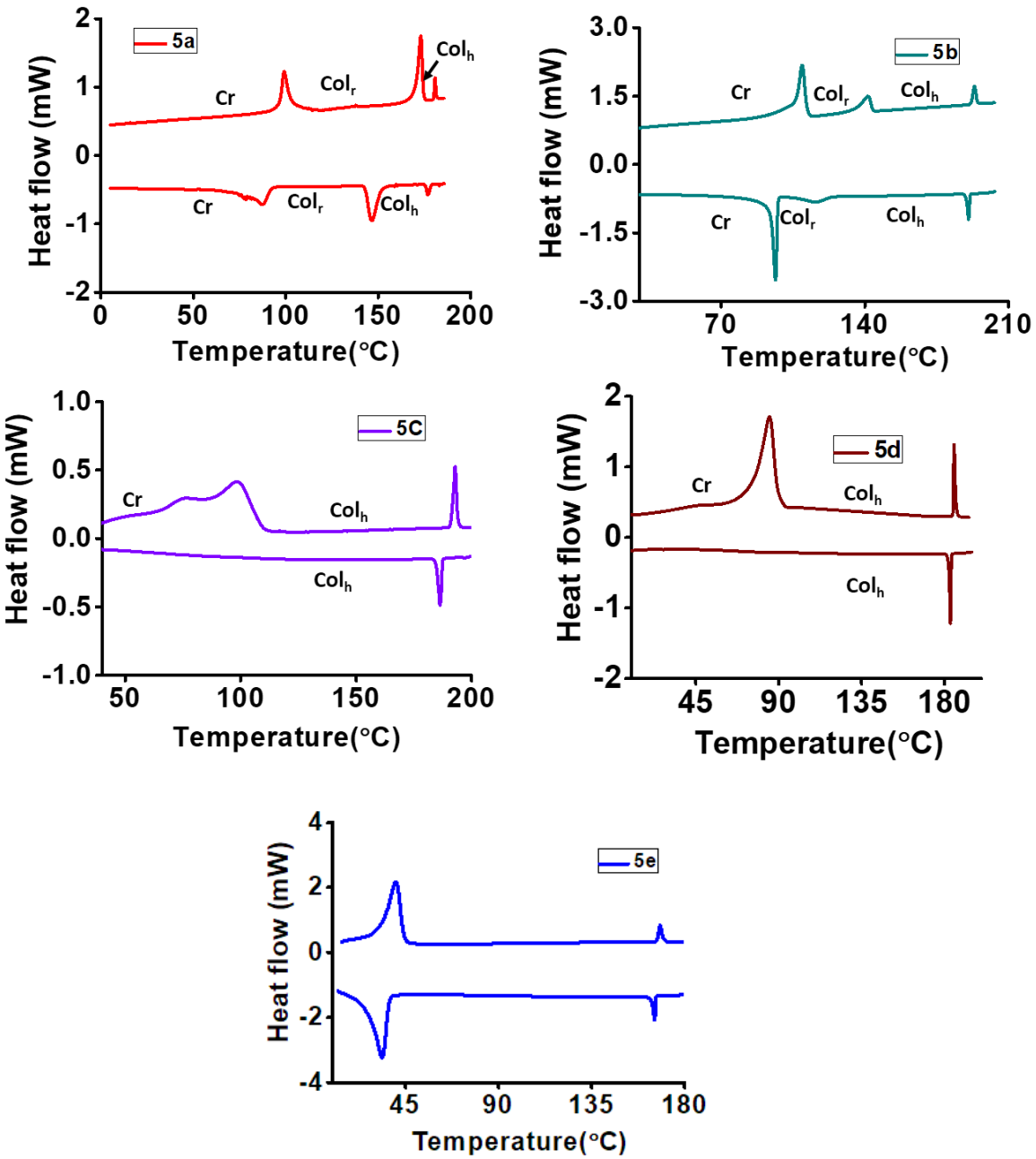

Figure 4.18. DSC thermograms were obtained for the **5a – 5e** derivatives showing phase transitions during heating and cooling cycles at a scan rate of 5 ^{o}C min^{-1}.

X-ray diffraction patterns of the mesophases of **5c, 5d** and **5e** at 110 ºC, 95 ºC, and 125 ºC, respectively, are shown in (**Figure 4.19).** Up to three sharp peaks are seen in the small-angle region, whose spacings are in the ratio 1: 1/√3: 1/2, and a broad peak is found in the wide-angle region at around 4.5 Å, corresponding to molten alkyl chains. The sharp peaks can be indexed on a two-dimensional hexagonal lattice (**Table 4.2**), and hence the mesophase in these compounds can be identified as hexagonal columnar. The lattice parameter is found to be 34.3, 37.7 and 40.9 Å for **5c, 5d,** and **5e**, respectively. The number of molecules in each layer of the column (Z) was estimated from the densities and molecular weights of the compounds. Z is found to be very close to 2 in all the three systems.

DSC data of compounds **5a** and **5b** suggest the formation of the second mesophase in these compounds. Hence X-ray scattering studies were carried out at two temperatures corresponding to the two mesophases. The high-temperature mesophase in both these compounds is again found to be hexagonal columnar, with Z = 2 (**Figure 4.20).** The lattice parameters of the two systems are 28.02 Å and 31.32 Å. The low-temperature mesophase of both the compounds give a few sharp peaks in the small-angle region and a broad peak in the wide-angle region **(Figure 4.20**). These patterns can be indexed on a two-dimensional rectangular lattice (**Table 4.2**), and hence we can identify the low-temperature mesophase in these two compounds as the rectangular columnar phase. The lattice parameters of the two systems are found to be a = 23.43Å, b = 19.75 Å and a = 29.25 Å, b = 21.41 Å respectively. The value of Z in the rectangular phase is found to be close to 1.

A schematic of the molecular arrangement in the two mesophases deduced from the diffraction data is shown in **Figure 4.24**. A similar kind of mesophase behaviour has been reported in the literature.[38] The switching of rectangular to hexagonal mesophase in triphenylene system on doping with charge-transfer complex (TNF) also has been reported.[39]

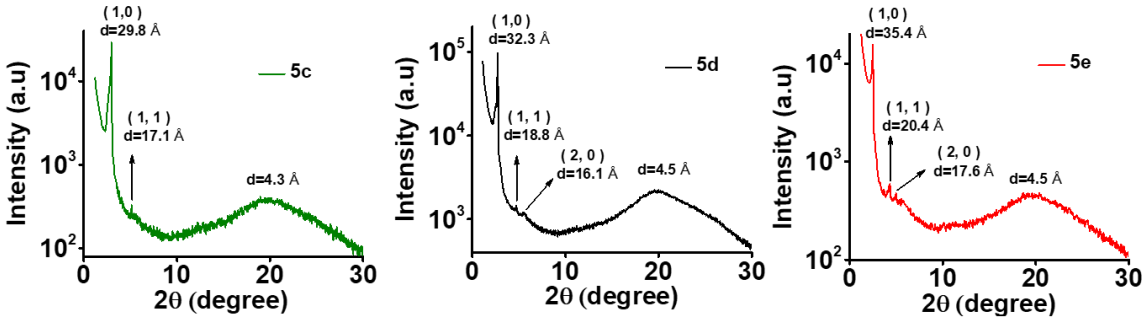

Figure 4.19. One-dimensional intensity versus 2θ profile obtained from X-ray diffraction of **5c**, **5d** & **5e** at 110 ºC, 95 ºC, and 125 ºC, respectively upon cooling from the isotropic phase.

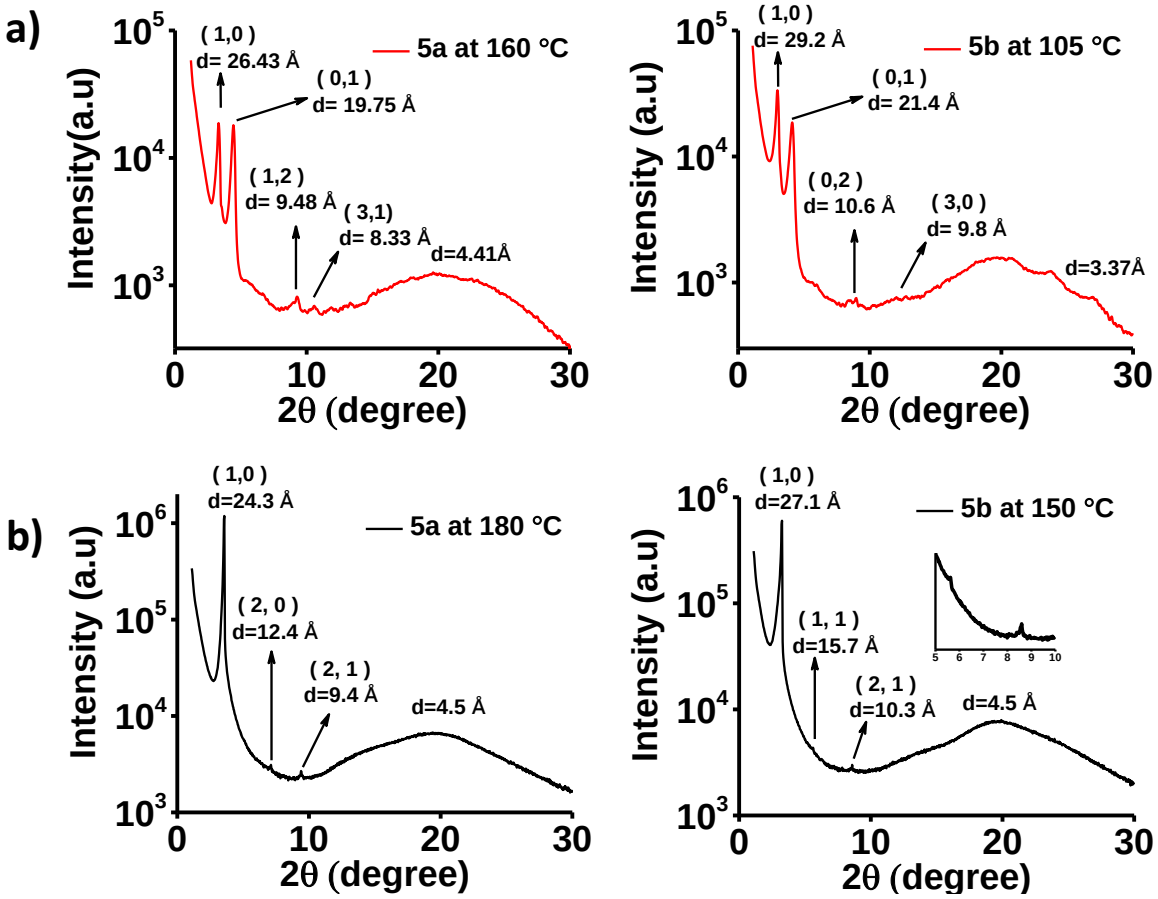

Figure 4.20. One-dimensional intensity versus 2θ profile obtained from X-ray diffraction of **5a** and **5b** upon cooling from the isotropic phase. a) at low temperatures shows the rectangular columnar phase b) at high temperatures shows the columnar hexagonal phase.

Compounds	T (°C)	d-spacing(Å)	Phase	Parameters
5a	180	24.27 (10), 12.42 (20), 9.36 (21) 4.46	Col_h	**a** = 28.02 Å S_h = 706.196 Å^2 V_h = 3142.572Å^3 **Z** = 1.8
5a	160	26.43 (1 0), 19.75 (0 1), 9.48 (1 2), 8.33 (3 1), 4.41	Col_r	**a** = 26.43 Å **b** = 19.75 Å S_h = 521.99 Å^2 V_h = 2296.76Å^3 **Z** = 1. 2
5b	180	27.13 (10), 15.69 (11), 10.27 (21) 4.46	Col_h	**a** = 31.32 Å S_h = 836.0132 Å^2 V_h = 3762.059Å^3 **Z** = 1.8
5b	105	29.25 (1 0), 21.41 (0 1), 10.56 (0 2), 9.78 (3 0), 3.37	Col_r	**a** = 29.25 Å **b** = 21.41 Å S_h = 626.24 Å^2 V_h = 2210.43Å^3 **Z** = 1.0
5c	110	29.77 (1 0), 17.14 (1 1), 4.33	Col_h	**a** = 34.37 Å S_h = 1023.03 Å^2 V_h = 4429.73Å^3 **Z** = 1.92
5d	95	32.66 (1 0), 18.85 (1 1), 16.06 (2 0), 4.52	Col_h	**a** = 37.71 Å S_h = 1231.52 Å^2 V_h = 5566.49Å^3 **Z** = 2.1
5e	125	35.42 (1 0), 20.37 (1 1), 17.60 (2 0) 4.55	Col_h	**a** = 40.90Å S_h = 1448.69Å^2 V_h = 6591.56 Å^3 **Z** = 2.1

Table 4.2. Layer spacing obtained from XRD for **5a-e, Hexagonal: (a** = lattice parameter = $\sqrt{(4/3)} \times d_{10}$; lattice area $S_h = a^2\sin 60^o$; lattice volume $V_h = a^2 \sin 60^o \times h_c$ (h_a if h_c is not observed); No of molecules per slice of column (**Z**) = $(\sqrt{3}\times N_a \times P \times a^2 \times h)/2M$; N_a = Avogadro's number; **P** = Density in Kg/m^3; **a**=lattice parameter; h_c=core core peak (h_a if core-core is not observed); **M** = molecular weight in Kg/m^3). For **columnar rectangular** (**a** and **b** are lattice parameter) lattice area $S_{rec} = a \times b$; lattice volume $V_{rec} = a \times b \times h$: no of molecules per slice of column (Z) = $(N_a \times P \times a \times b \times h)/2M$; N_a = Avogadro's number; **P** = Density in kg/m^3; **a** and **b** =lattice parameter; h_r=core core peak (h_a if core-core is not observed).

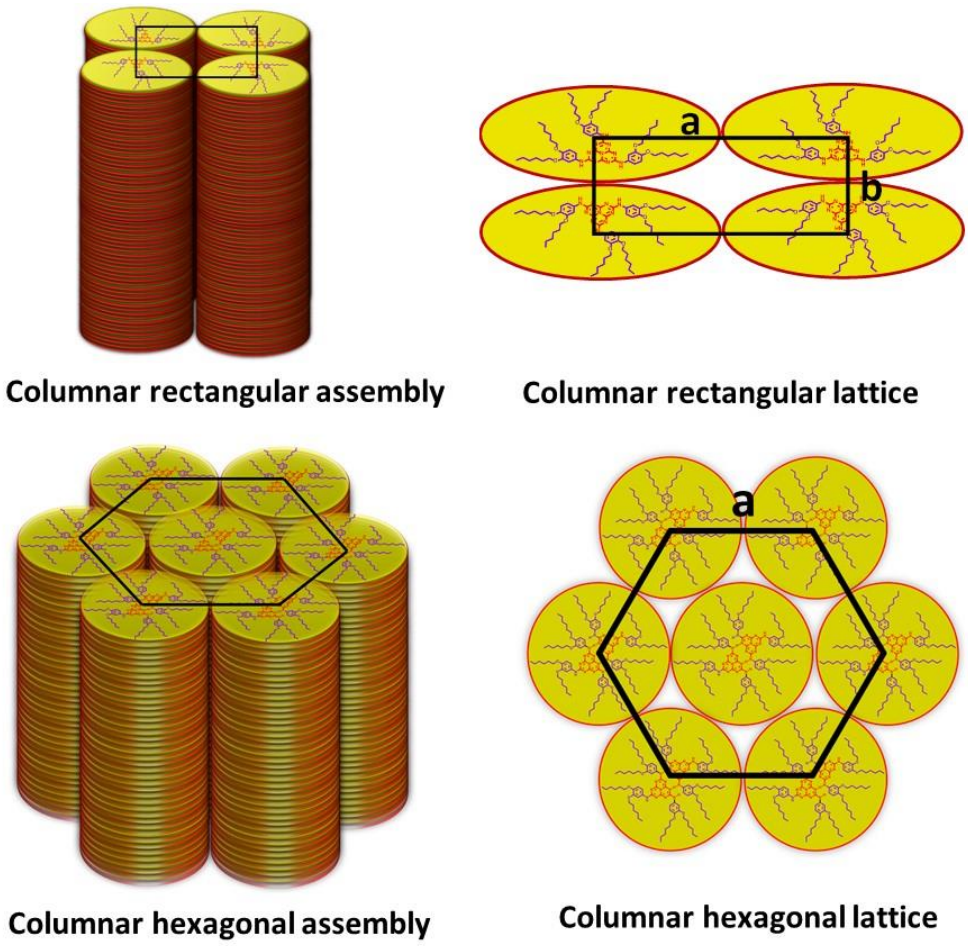

Figure 4.21. Schematic representation of the self-assembly of columnar rectangular mesophase and columnar hexagonal mesophase in heptazine discotics.

4.3 Conclusion:

In this chapter, we have described the synthesis of the heptazine derivatives with dialkoxy aniline and detailed the molecular organization of heptazine derivatives within two columnar mesophases that appear as a function of temperature. All the derivatives exhibited the columnar hexagonal phase, which was confirmed by X-ray diffraction, POM and DSC. The lower homologs of the series were found to show both rectangular and columnar hexagonal mesophase. However, there is a change in the molecular organization between the rectangular and the hexagonal mesophases which were reflected in the change in the number of molecules in the columnar section. In the Col_r phase, it was found to be one molecule per slice in the

column, whereas in the case of Col_h phase, there are two molecules per slice in the column. We have studied the effect of linear chain functionalization on mesomorphic properties of dialkoxy aniline heptazine derivatives, which showed both hexagonal and rectangular phases. Literature reports on DLCs suggest that, functionalization of branched chains and various functional groups may influence the clearing temperature which enables them for use in various applications.

4.4 Experimental section:

Materials and Methods

Referee the page number 65

4.5 Synthesis and characterization:

General procedure for the synthesis of 1a, 1b, 1c, 1d, 1e.

In a round bottom flask, 1,2- dihydroxy benzene (pyro catechol) (1eq) was dissolved in ethanol / DMF, K_2CO_3 (6eq) was added to it and stirred for 15 minutes. 1-Bromo alkane (2.2 eq) was added to it and the mixture was refluxed overnight. Then it was cooled to room temperature, and ethanol/DMF was evaporated. The reaction mixture was extracted with $CHCl_3$ organic layer was dried over anhydrous Na_2SO_4 and the solvent was evaporated. The crude product was purified by column chromatography using petroleum ether and dichloromethane as eluent and dried under high vacuum to get the desired product.

Compound 1a: 1,2- dihydroxy benzene (10g, 90.82 mmol, 1eq), ethanol 500 mL, K_2CO_3 (75.31g, 544.95mmol, 6eq), 1-Bromo hexane (29.98g, 199.81 mmol, 2.2eq) Yield: 83% ; M.P. 39 ºC; ^{1}H NMR (500 MHz, $CDCl_3$): δ (ppm) = 6.91 (s, 4H), 4.01 (t, *J* = 6.25 Hz, 4H), 1.83 (t, *J* = 6.50 Hz, 4H), 1.49 (s, 4H), 1.36 (s, 8H), 0.92 (s, 6H); ^{13}C NMR (125 MHz, $CDCl_3$): δ ppm = 149.30, 121.03, 114.20, 69.32, 31.64, 29.35, 25.74, 22.;

Compound 1b: 1,2- dihydroxy benzene (10g, 90.82 mmol, 1eq), ethanol 500 mL, K_2CO_3 (75.31g, 544.95mmol, 6eq), 1-Bromo octane (38.58g, 199.81 mmol, 2.2eq) Yield: 85% ; M.P. 39 ºC; ^{1}H NMR (500 MHz, $CDCl_3$): δ (ppm) = 6.90 (s, 4H), 4.01 (t, *J* = 6.25 Hz, 4H), 1.83 (t, *J* = 6.50 Hz, 4H), 1.49 – 1.47 (m, 4H), 1.34 – 1.30 (m, 16H), 0.91 (s, 6H); ^{13}C NMR

(125 MHz, $CDCl_3$): δ ppm = 149.31, 121.03, 114.23, 69.33, 31.85, 29.41, 29.38, 29.30, 26.07, 22.68, 14.09;

Compound 1c: 1,2- dihydroxy benzene (10g, 90.82 mmol, 1eq), acetone 500 mL, K_2CO_3 (75.31g, 544.95mmol, 6eq), 1-Bromo decane (44.19g, 199.81 mmol, 2.2eq) Yield: 83% ; M.P. 39 ºC; ^{1}H NMR (500 MHz, $CDCl_3$): δ (ppm) = 6.91 (s, 4H), 4.01 (t, *J* = 6.50 Hz, 4H), 1.80 – 1.86 (m, 4H), 1.45 – 1.51 (m, 4H), 1.29 – 1.38 (m, 24H), 0.90 (t, *J* = 7.0 Hz, 6H); ^{13}C NMR (125 MHz, $CDCl_3$): δ ppm =149.27, 121.01, 114.13, 69.29, 31.95, 29.68, 29.63, 29.48, 29.39, 26.09, 22.72, 14.14

Compound 1d: 1,2- dihydroxy benzene (10g, 90.82mmol, 1eq), ethanol 500 mL, K_2CO_3 (75.31g, 544.95mmol, 6eq), 1-Bromo dodecane (49.30g, 199.81mmol, 2.2eq) Yield: 90% ; M.P. 45 ºC; ^{1}H NMR (500 MHz, $CDCl_3$): δ (ppm) = 6.88 (s, 4H), 3.98 (t, *J* = 6.5 Hz, 4H), 1.78 – 1.83 (m, 4H), 1.43 – 1.49 (m, 4H), 1.26 – 1.34 (m, 16H), 0.88 (t, *J* = 7.0 Hz, 6H), ^{13}C NMR (125 MHz, $CDCl_3$): δ ppm = 149.27, 121.01, 114.17, 69.31, 31.94, 29.72, 29.65, 29.46, 29.38, 26.07, 22.71, 14.12;

Compound 1e: 1,2- dihydroxy benzene (10g, 90.82mmol, 1eq), ethanol 500 mL, K_2CO_3 (75.31g, 544.95mmol, 6eq), 1-Bromo hexadecane (61.00g, 199.81mmol, 2.2eq) Yield: 87% ; M.P. 61 ºC; ^{1}H NMR (500 MHz, $CDCl_3$): δ (ppm) = 6.91 (s, 4H), 4.01 (t, *J* = 6.50 Hz, 4H), 1.80 – 1.86 (m, 4H), 1.46 – 1.51 (m, 4H), 1.28 – 1.38 (m, 48H), 0.90 (t, *J* = 6.50 Hz 6H); ^{13}C NMR (125 MHz, $CDCl_3$): δ ppm = 149.26, 121.01, 114.13, 69.29, 31.96, 29.74, 29.69, 29.67, 29.47, 29.39, 29.37, 26.08, 22.72, 14.14;

General procedure for the synthesis of 2a, 2b, 2c, 2d, 2e.

In a round bottom flask **1** (1 eq) was dissolved in dichloromethane, added $NaNO_2$ (0.14 eq) and stirred. To this well-stirred suspension HNO_3 (3eq in dichloromethane) was added dropwise. This mixture was stirred at room temperature for 3h. The reaction mixture was poured into water and extracted with dichloromethane. Organic layer was washed with 5% $NaHCO_3$ solution, water and brine. Organic layer was dried over anhydrous Na_2SO_4 and the solvent was removed under reduced pressure. The crude product was purified by column chromatography on silica gel (100-200 mesh) using petroleum ether and dichloromethane (10%

dichloromethane 90% pet ether) as eluent and dried under high vacuum to get the desired product. The yield of these nitro compounds was in the range of 60-70%.

Compound 2a: **1a** (5g, 17.95 mmol, 1eq), dichloromethane 20 ml, $NaNO_2$ (0.172g, 2.514 mmol, 0.14 eq), HNO_3 (3.39g, 53.87 mmol, 3eq) Yield: 65%; ^{1}H NMR (500 MHz, $CDCl_3$): δ (ppm) = 7.89 (d, *J* = 8.50 Hz, 1H), 7.74 (s, 1H), 6.89 (d, *J* = 9.0 Hz, 1H) 4.09 (p, *J* = 6.50 Hz, 4H) 1.88 – 1.87 (m, 4H), 1.50 (bs, 4H), 1.37 (bs, 8H), 0.93 (s, 6H): ^{13}C NMR (125 MHz, $CDCl_3$): δ ppm = 154.72, 148.69, 141.19, 117.64, 111.07, 108.09, 69.48, 69.42, 31.49, 31.47, 28.92, 28.89, 25.61, 25.57, 22.56, 22.54, 13.95;

Compound 2b: **1b** (7g, 20.92 mmol, 1eq), dichloromethane 20 ml, $NaNO_2$ (0.200g, 2.92 mmol, 0.14 eq), HNO_3 (3.95g, 62.77 mmol, 3eq) Yield: 70%;^{1}H NMR (500 MHz, $CDCl_3$): δ (ppm) = 7.88 (d, *J* = 9.00 Hz, 1H), 7.74 (s, 1H), 6.89 (d, *J* = 9.0 Hz, 1H) 4.08 (p, *J* = 6.50 Hz, 4H) 1.87 (bs, 4H), 1.50 – 1.49 (m, 4H), 1.38 – 1.31 (m, 16H), 0.90 – 0.89 (m, *J* = 6.50 Hz, 6H): ^{13}C NMR (125 MHz, $CDCl_3$): δ ppm = 154.72, 148.69, 141.20, 117.63, 111.09, 108.12, 69.49, 69.43, 31.79, 31.78. 29.29, 29.27, 29.23, 29.21, 28.97, 28.94, 25.95, 25.91, 22.65, 14.05;

Compound 2c: **1c** (2.5g, 6.39 mmol, 1eq), dichloromethane 20 ml, $NaNO_2$ (0.061g, 0.89 mmol, 0.14 eq), HNO_3 (1.20g, 19.19 mmol, 3eq Yield: 65%; ^{1}H NMR (500 MHz, $CDCl_3$): δ (ppm) = 7.89 (d, *J* = 8.50 Hz, 1H), 7.74 (s, 1H), 6.89 (d, *J* = 9.0 Hz, 1H) 4.09 (p, *J* = 6.50 Hz, 4H) 1.87 (bs, 4H), 1.50 – 1.48 (m, 4H), 1.38 – 1.29 (m, 25H), 0.90 (t, *J* = 6.50 Hz, 6H): ^{13}C NMR (125 MHz, $CDCl_3$): δ ppm = 154.72, 148.70, 141.21, 117.65, 111.10, 108.13, 69.50, 69.44, 31.90, 29.59, 29.57, 29.55, 29.54, 29.32, 28.96, 28.93, 25.95, 25.91, 22.67, 14.08;

Compound 2d: (25 g, 55.96 mmol, 1eq), dichloromethane 100 ml, $NaNO_2$ (0.537g, 7.83 mmol, 0.14 eq), HNO_3 (10.57g, 167.89 mmol, 3eq Yield: 56%; M.P. 39 ºC; ^{1}H NMR (500 MHz, $CDCl_3$): δ (ppm) = 7.89 (d, *J* = 8.50 Hz, 1H), 7.74 (s, 1H), 6.89 (d, *J* = 9.0 Hz, 1H) 4.09 (p, *J* = 6.50 Hz, 4H) 1.87 (bs, 4H), 1.50 – 1.48 (m, 4H), 1.38 – 1.28 (m, 32H), 0.90 (t, *J* = 6.50 Hz, 6H): ^{13}C NMR (125 MHz, $CDCl_3$): δ ppm = 154.72, 148.70, 141.22, 117.66, 111.10, 108.14, 69.51, 69.45, 31.92, 29.68, 29.65, 29.59, 29.35, 29.32, 28.96, 28.93, 25.95, 25.91, 22.68, 14.09;

Compound 2e: (7 g, 12.52 mmol, 1eq), dichloromethane 100 ml, $NaNO_2$ (0.120g, 1.75 mmol, 0.14 eq), HNO_3 (2..36g, 37.56 mmol, 3eq) Yield: 80%; ^{1}H NMR (500 MHz, $CDCl_3$): δ (ppm) = 7.89 (d, *J* = 8.50 Hz, 1H), 7.74 (s, 1H), 6.89 (d, *J* = 9.0 Hz, 1H) 4.09 (p, *J* = 6.50 Hz, 4H)

1.87 (bs, 4H), 1.50 – 1.48 (m, 4H), 1.38 – 1.28 (m, 48H), 0.90 (t, *J* = 6.50 Hz, 6H): ^{13}C NMR (125 MHz, $CDCl_3$): δ ppm = 154.72, 148.70, 141.22, 117.65, 111.10, 108.14, 69.50, 69.44, 31.93, 29.71, 29.67, 29.60, 29.58, 29.36, 29.33, 28.97, 28.94, 25.96, 25.91, 22.69, 14.09;

General procedure for the synthesis of 3a, 3b, 3c, 3d, 3e.

In a round bottom flask, **2** (1 eq) was dissolved in dry THF, added 10% Pd-C (0.4eq) This mixture was stirred under hydrogen atmosphere (balloon) at room temperature for 24h. The reaction mixture was filtered through celite bed. THF was evaporated under reduced pressure the product was precipitated by using methanol.

Compound 3a: (4 g, 12.37 mmol, 1eq), dry THF 50 ml, Pd-C 10% (0.526g, 4.95 mmol, 0.4 eq), 89%;^{1}H NMR (500 MHz, $CDCl_3$): δ (ppm) = 6.75 (d, *J* = 8.00 Hz, 1H), 6.32 (s, 1H), 6.22 (d, *J* = 8.50 Hz, 1H) 3.93 (m, 4H), 3.28 (bs, 2H), 1.84 – 1.74 (m, 4H), 1.48 – 1.46 (m, 4H), 1.35 (m, 8H), 0.92 (bs, 6H): ^{13}C NMR (125 MHz, $CDCl_3$): δ ppm = 150.65, 141.95, 141.32, 117.41, 106.88, 102.71, 71.00, 68.97, 31.69, 31.62, 29.62, 29.33, 25.76, 22.64, 22.63, 14.03, 14.02;

Compound 3b: (9.07 g, 23.91 mmol, 1eq), dry THF 100 ml, Pd-C 10% (1.01g, 9.56 mmol, 0.4 eq), 80%;^{1}H NMR (500 MHz, $CDCl_3$): δ (ppm) = 6. 65 (d, *J* = 8.00 Hz, 1H), 6.23 (s, 1H), 6.13(d, *J* = 8.00 Hz, 1H) 3.84 (m, 4H), 2.85 (bs, 2H), 1.73 – 1.65 (m, 4H), 1.38 – 1.36 (m, 4H), 1.23 – 1.20 (m, 18H), 0.81 – 0.79 (m, 6H): ^{13}C NMR (125 MHz, $CDCl_3$): δ ppm = 150.65, 142.04, 141.16, 117.40, 106.93, 102.77, 71.01, 69.02, 31.84, 29.64, 29.45, 29.39, 29.35, 29.31, 29.29, 26.08, 22.67, 14.09;

Compound 3c: (2.12 g, 4.86 mmol, 1eq), dry THF 20 ml, Pd-C 10% (1.20g, 1.94 mmol, 0.4 eq), 80%; ^{1}H NMR (500 MHz, $CDCl_3$): δ (ppm) = 6. 75 (d, *J* = 8.50 Hz, 1H), 6.32 (s, 1H), 6.23 (d, *J* = 8.50 Hz, 1H) 3.93 (m, 4H), 3.50 – 3.48 (bs, 2H), 1.83 – 1.75 (m, 4H), 1.47 – 1.44 (m, 4H), 1.29 (m, 26H), 0.91 – 0.89 (m, 6H): ^{13}C NMR (125 MHz, $CDCl_3$): δ ppm = 150.66, 142.05, 141.17, 117.42, 106.91, 102.76, 71.01, 69.01, 31.93, 29.65, 29.61, 29.50, 29.45, 29.36, 26.09, 22.69, 14.11;

Compound 3d: (6g, 12.20 mmol, 1eq), dry THF 20 ml, Pd-C 10% (0.51g, 4.800 mmol, 0.4 eq), 90%;^{1}H NMR (500 MHz, $CDCl_3$): δ (ppm) = 6. 75 (d, *J* = 8.00 Hz, 1H), 6.32 (s, 1H), 6.22 (d, *J* = 8.00 Hz, 1H) 3.96 – 3.90 (m, 4H), 3.45 (bs, 2H), 1.83 – 1.74 (m, 4H), 1.47 – 1.44 (m, 4H), 1.28 (m, 32H), 0.91 – 0.89 (m, 6H): ^{13}C NMR (125 MHz, $CDCl_3$): δ ppm = 150.66, 142.06, 141.17, 117.43, 106.90, 102.76, 71.02, 69.03, 31.93, 29.70, 29.66, 29.65, 29.50, 29.44, 29.36, 26.08, 22.69, 14.10;

Compound 3e: (1.50g, 2.49 mmol, 1eq), dry THF 20 ml, Pd-C 10% (0.10g, 0.99 mmol, 0.4 eq), 82%; ^{1}H NMR (500 MHz, $CDCl_3$): δ (ppm) = 6. 75 (d, *J* = 8.50 Hz, 1H), 6.32 (s, 1H), 6.22 (d, *J* = 8.50 Hz, 1H) 3.96 – 3.90 (m, 4H), 3.44 (bs, 2H), 1.82 – 1.73 (m, 4H), 1.47 – 1.44 (m, 4H), 1.28 (m, 52H), 0.91 – 0.89 (m, 6H): ^{13}C NMR (125 MHz, $CDCl_3$): δ ppm = 150.66, 142.06, 141.17, 117.42, 106.90, 102.77, 71.02, 69.03, 31.93, 29.72, 29.67, 29.65, 29.50, 29.44, 29.36, 26.08, 22.69, 14.10;

General procedure for the synthesis of 5a, 5b, 5c, 5d, 5e.

A solution of **4** (1eq) and **3** (3.5 eq) in dry toluene (40ml) was refluxed for 24h under nitrogen. After 24h. The mixture was filtered to remove the suspended particles and the filtrate was concentrated under reduced pressure. The crude product was purified by column chromatography using petroleum ether: ethyl acetate (9:1) as eluent to get the desired product which was precipitated by using cold methanol and dried under the high vacuum.

Compound 5a: 4 (0.100g, 0.361mmol, 1eq), **3a** (0.360g, 1.26mmol, 3.5eq), toluene 20ml, yield: 52%, ^{1}H NMR (500 MHz, $CDCl_3$): δ (ppm) = 8.11 – 8.0 (bd, 1H), 7.66 (bs 2H), 7.22 – 7.02 (m, 6H), 6.82 (s, 3H), 3.97 (bs, 12H), 1.80 (bs, 16H), 1.47 (bs, 12H), 1.35 (bs, 24H), 0.92 (bs, 18H); ^{13}C NMR (125 MHz, $CDCl_3$): δ ppm = 162.44, 162.34, 162.17, 156.14, 155.48, 154.81, 149.28, 148.96, 146.78, 146.68, 146.60, 130.56, 130.50, 130.44, 130.21, 115.70, 115.17, 114.68, 114.32, 114.18, 113.95, 110.05, 109.72, 108.74, 108.46, 69.66, 69.60, 69.52, 69.42, 69.32, 31.65, 31.63, 29.36, 29.29, 25.78, 25.72, 25.70, 22.62, 14.02; MALDI-TOF MS for $C_{97}H_{126}N_{10}O_2$: 1047.44 (calcd.); 1046.95 (experiment).

Compound 5b: 4 (0.300g, 1.085mmol, 1eq), **3b** (1.327g, 3.79mmol, 3.5eq), toluene 20ml, yield: 60%, ^{1}H NMR (500 MHz, $CDCl_3$): δ (ppm) = 7.98 – 7.89 (bd, 1H), 7.50 (bs 2H), 7.13 – 6.92 (m, 6H), 6.73 (s, 3H), 3.89 – 3.88 (m, 12H), 1.71 – 1.65 (m, 18H), 1.37 (bs, 12H), 1.21

(bs, 49H), 0.81 – 0.80 (m, 18H); ^{13}C NMR (125 MHz, $CDCl_3$): δ ppm162.50, 162.35, 162.22, 156.19, 155.62, 155.52, 154.87, 149.39, 149.31, 149.05, 146.86, 146.68, 130.40, 130.10, 115.70, 115.08, 114.82, 114.45, 114.27, 114.03, 109.98, 109.57, 108.86, 108.51, 69.75, 69.70, 69.60, 69.54, 69.44, 69.37, 31.86, 29.45, 29.42, 29.32, 26.13, 26.05, 22.68, 14.09; MALDI-TOF MS for $C_{97}H_{126}N_{10}O_2$: 1215.77 (calcd.); 1215.42 (experiment).

Compound 5c: **4** (0.200g, 0.72mmol, 1e q), **3c** (1.027g, 2.53mmol, 3.5eq), toluene 20ml, yield: 60%, ^{1}H NMR (500 MHz, $CDCl_3$): δ (ppm) = 8.03 – 7.92 (bd, 1H), 7.50 (bs 2H), 7.13 – 6.92 (m, 6H), 6.73 (s, 3H), 3.89 – 3.88 (m, 12H), 1.71 (bs, 16H), 1.37 (bs, 13H), 1.21 (bs, 78H), 0.81 – 0.80 (m, 18H); ^{13}C NMR (125 MHz, $CDCl_3$): δ ppm = 162.50, 162.34, 162.21, 156.18, 155.61, 155.51, 154.87, 149.38, 149.32, 149.01, 146.85, 146.70, 146.65, 130.46, 130.39, 130.14, 115.75, 115.08, 114.79, 114.46, 114.26, 114.15, 114.00, 110.09, 109.64, 108.83, 108.46, 69.75, 69.70, 69.61, 69.55, 69.44, 69.36, 31.94, 29.69, 29.66, 29.62, 29.54, 29.49, 29.38, 26.15, 26.11, 26.07, 22.69, 14.10; MALDI-TOF MS for $C_{97}H_{126}N_{10}O_2$: 1384.09 (calcd.); 1385.27 (experiment).

Compound 5d: **4** (0.200g, 0.72mmol, 1eq), **3d** (1.168g, 2.53mmol, 3.5eq), toluene 20ml, yield: 52^{1}H NMR (500 MHz, $CDCl_3$): δ (ppm) = 7.77 – 7.65 (m, 3H), 7.11 – 7.05 (m, 4H), 6.97 – 6.95 (m, 2H), 6.77 – 6.73 (m, 3H), 3.92 – 3.88 (m, 12H), 1.73 – 1.72 (m, 12H), 1.51 (bs, 8H), 1.38 (bs, 12H), 1.19 (m, 102H) 0.80 – 0.79 (m, 18H); ^{13}C NMR (125 MHz, $CDCl_3$): δ ppm = 162.29, 162.14, 156.08, 155.50, 154.91, 149.45, 149.34, 149.15, 146.84, 130.47, 130.22, 115.28, 114.60, 114.50, 114.31, 114.15, 108.73, 108.49, 69.78, 69.52,69.41, 31.94, 29.69, 29.53, 29.38, 26.14, 26.07, 22.69, 14.10 ; MALDI-TOF MS for $C_{97}H_{126}N_{10}O_2$: 1552. 42 (calcd.); 1552.57 (experiment).

Compound 5e: **4** (0.300g, 1.085mmol, 1eq), **3f** (2.058g, 3.79mmol, 3.5eq), toluene 20ml, yield: 70%, ^{1}H NMR (500 MHz, $CDCl_3$): δ (ppm) = 7.87 – 7.81 (bd, 1H), 7.44 (bs, 2H), 7.10 – 6.91 (m, 6H), 6.75 – 6.73 (m, 3H), 3.89 – 3.88 (m, 12H), 1.71 – 1.64 (m, 12H), 1.51 (bs, 14H), 1.18 (bs, 163H), 0.80 (bs, 18H); ^{13}C NMR (125 MHz, $CDCl_3$): δ ppm = 162.52, 156.26, 155.69, 149.45, 149.36, 149.20, 146.96, 146.74, 130.04, 114.90, 114.53, 114.31, 114.18, 109.35, 108.93, 108.5269.78, 69.46, 31.93, 29.74, 29.68, 29.54, 29.51, 29.37, 26.10, 26.07, 22.69, 14.10; MALDI-TOF MS for $C_{97}H_{126}N_{10}O_2$: 1889.06 (calcd.); 1888.96 (experiment).

4.6 NMR Spectra:

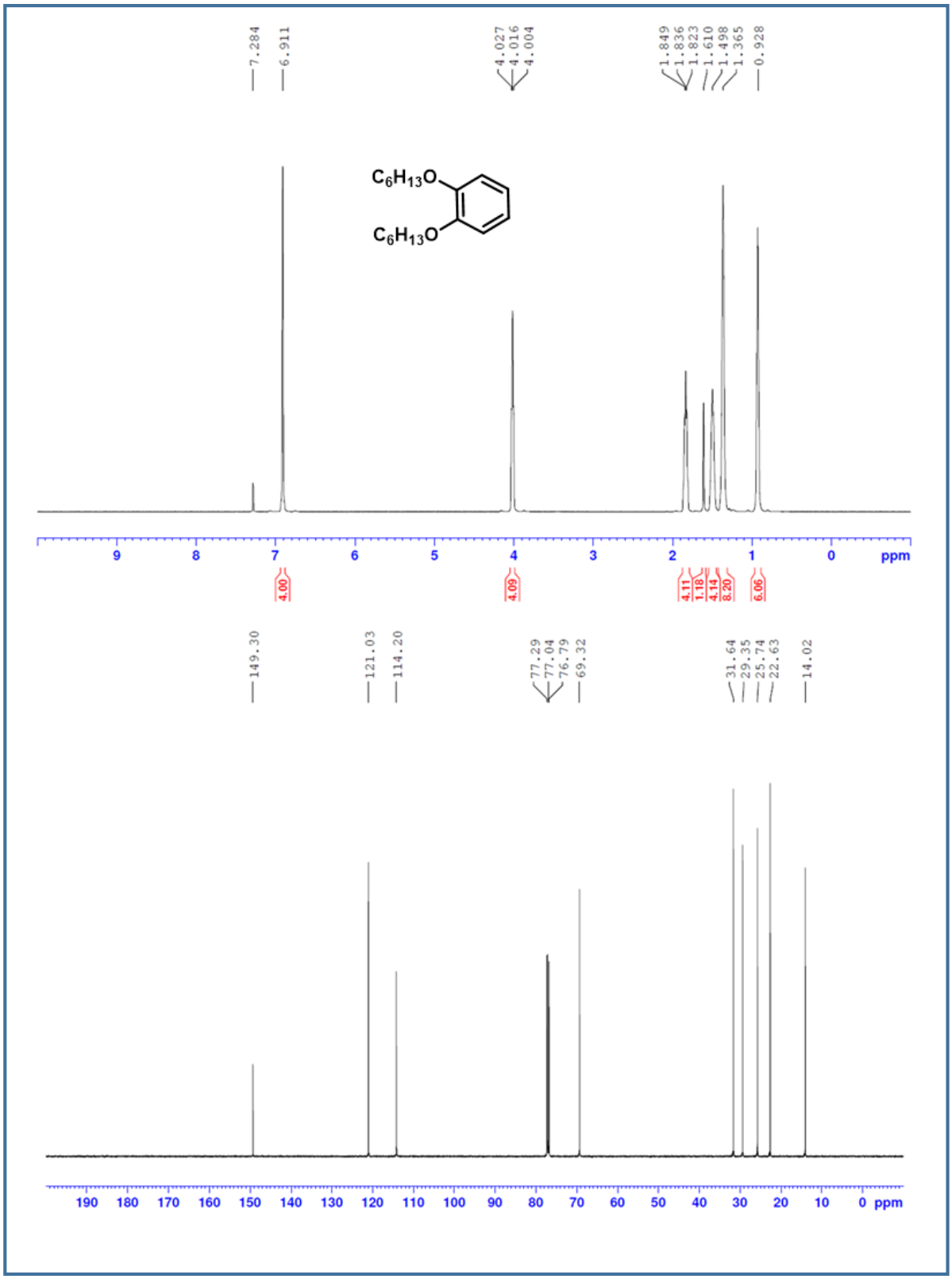

Figure 4.22: ^{1}H (top) and ^{13}C-NMR (bottom) spectra of **1a**

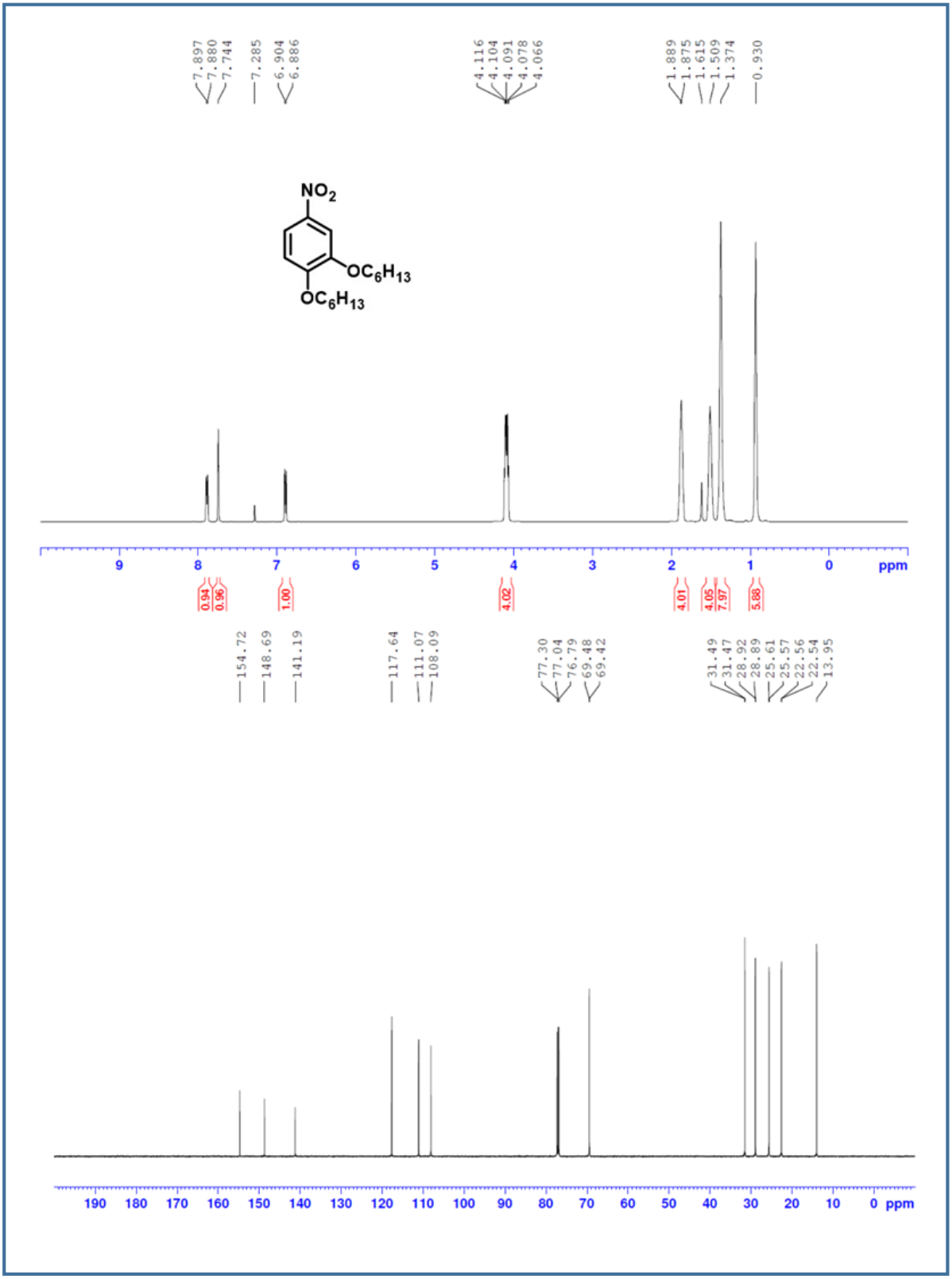

Figure 4.23: ^{1}H (top) and ^{13}C-NMR (bottom) spectra of **2a**

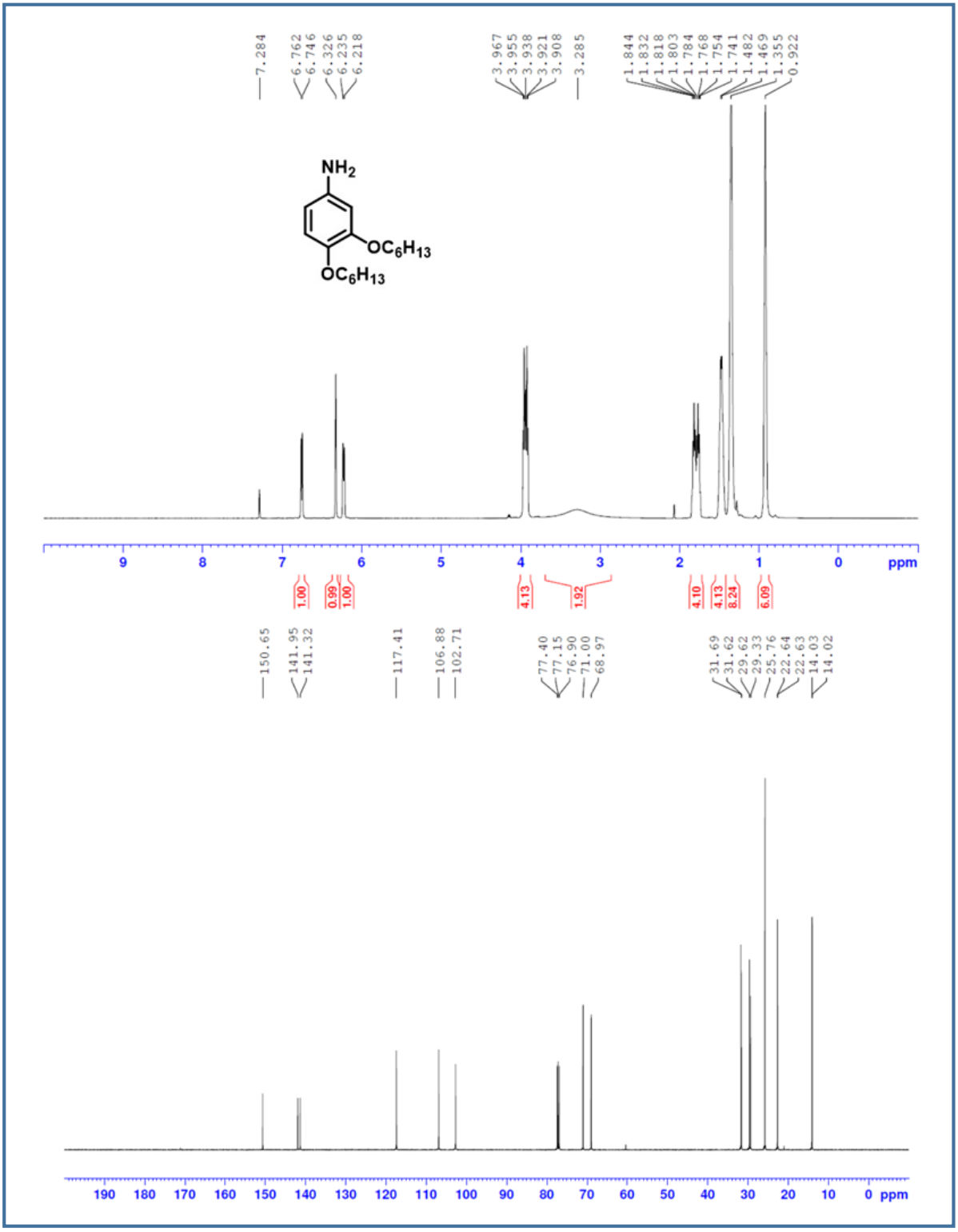

Figure 4.24: ^{1}H (top) and ^{13}C-NMR (bottom) spectra of **3a**

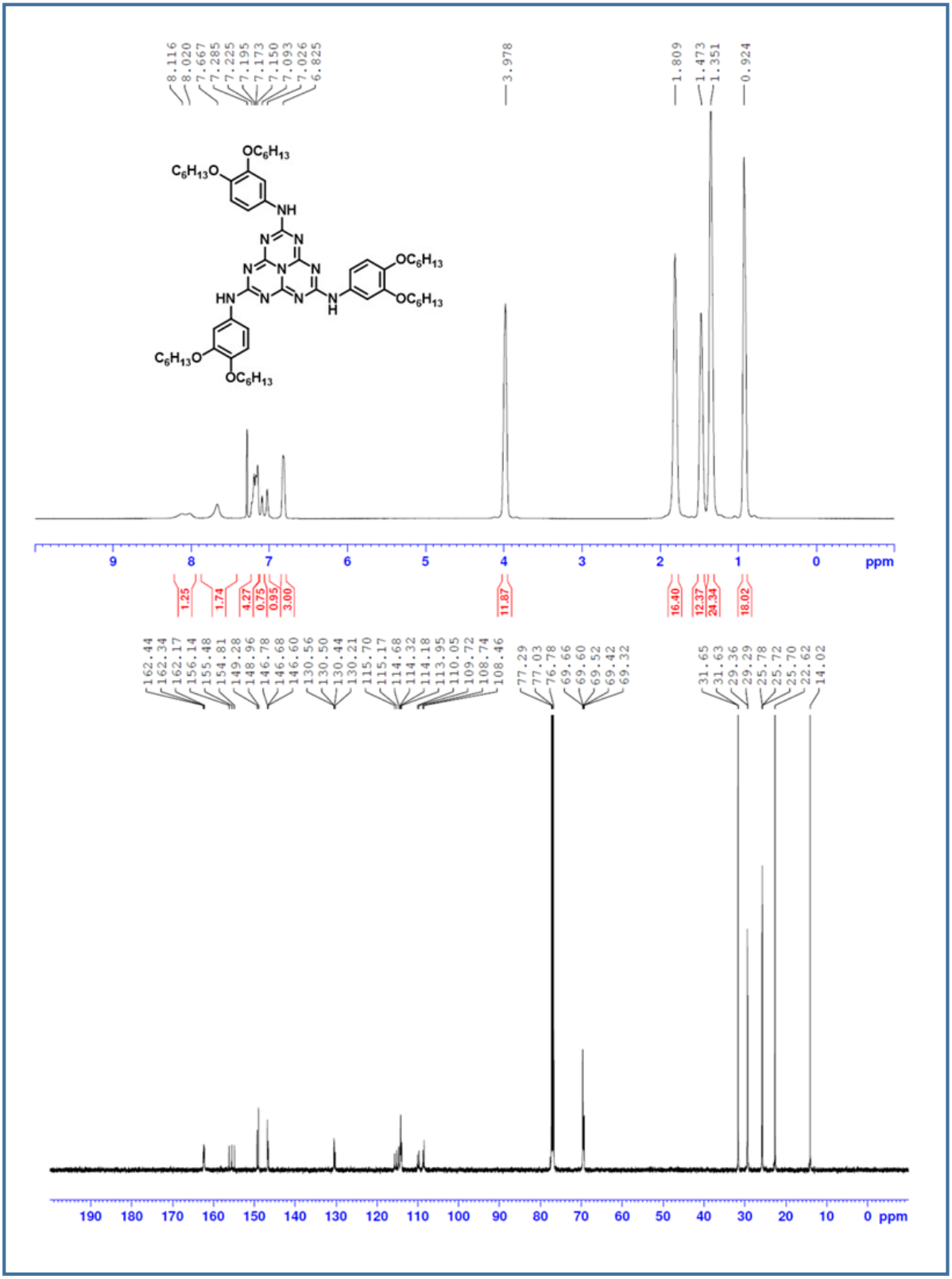

Figure 4.25: ^{1}H (top) and ^{13}C-NMR (bottom) spectra of **5a**

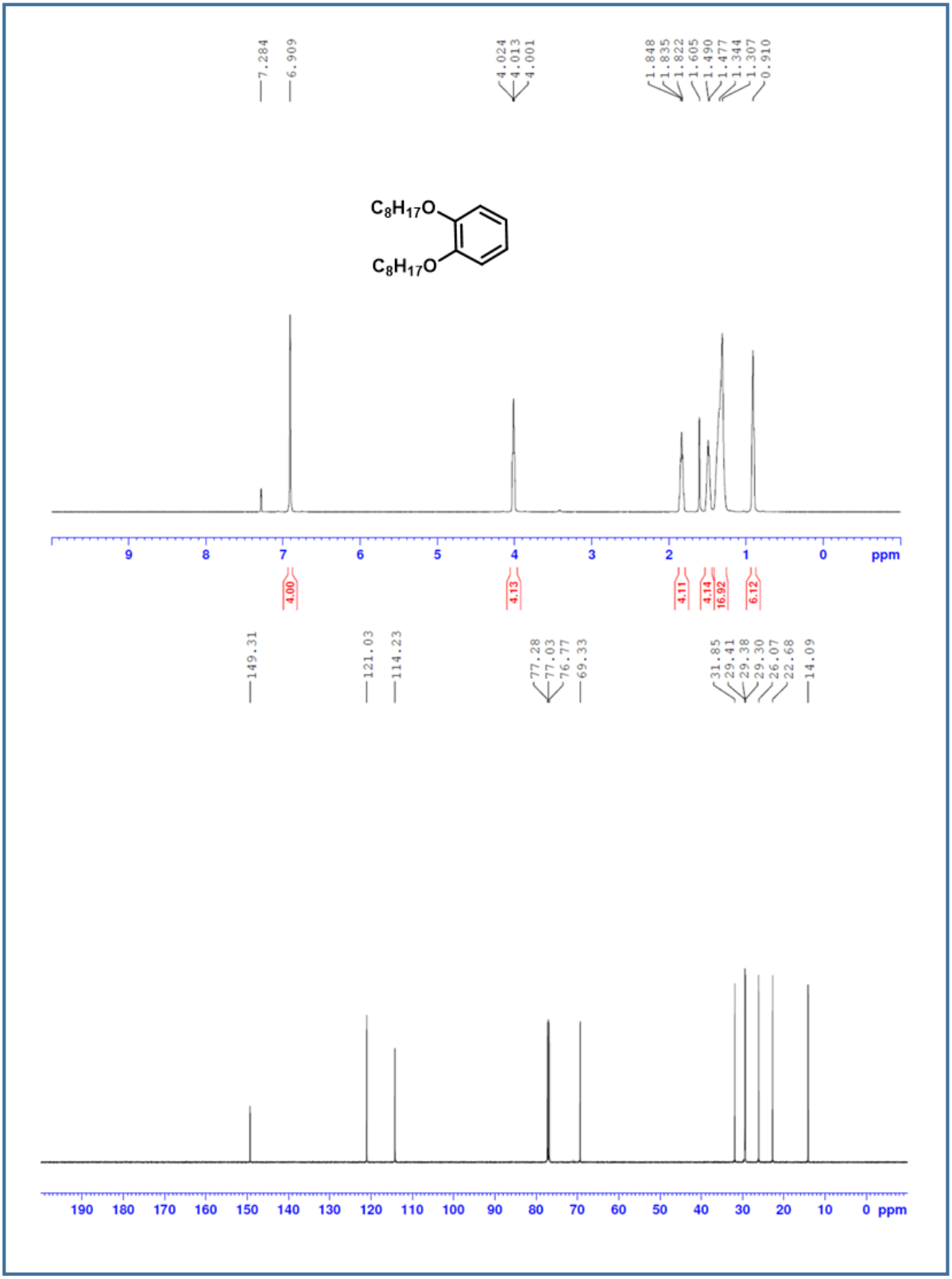

Figure 4.26: ^{1}H (top) and ^{13}C-NMR (bottom) spectra of **1b**

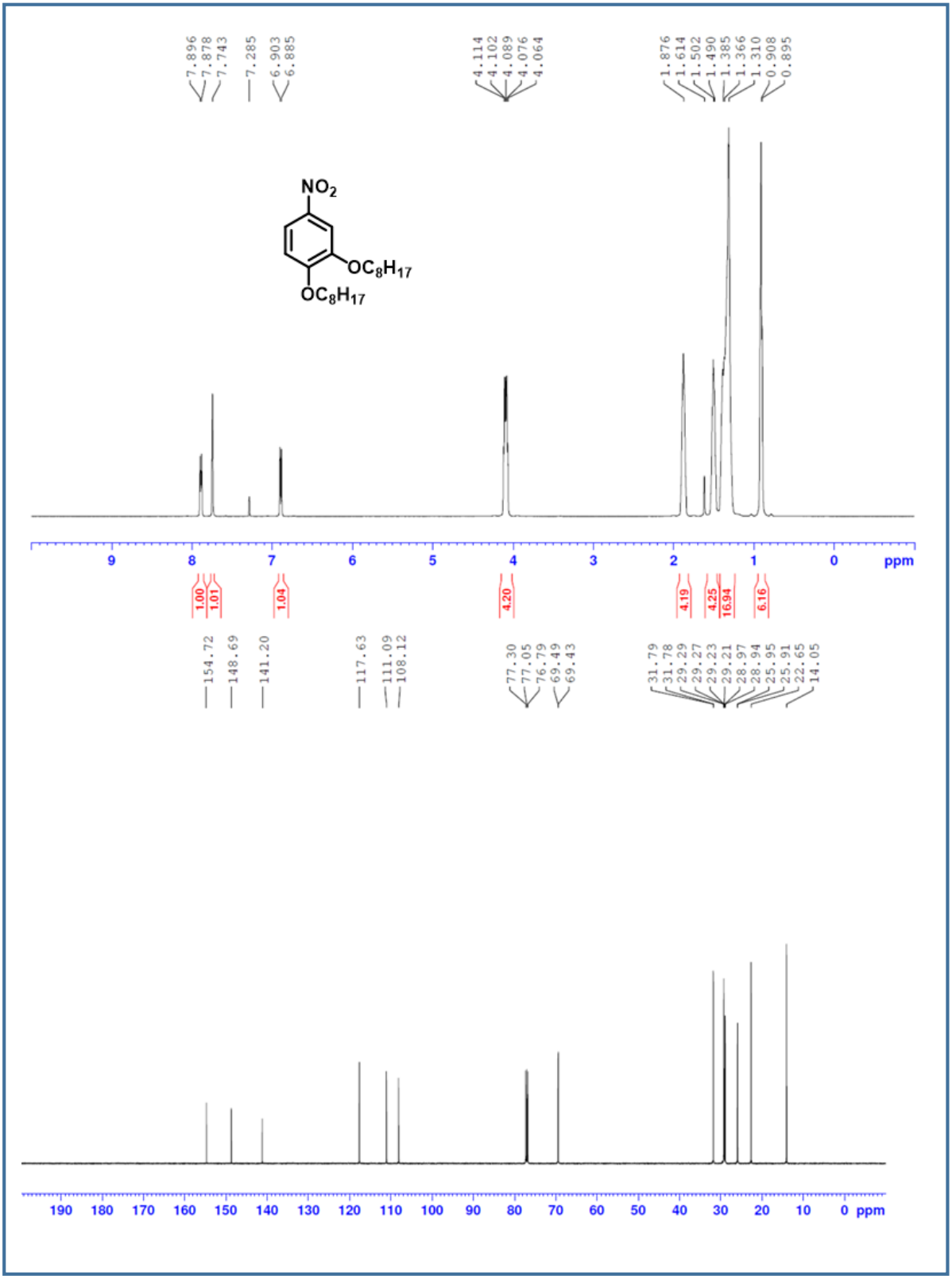

Figure 4.27: ^{1}H (top) and ^{13}C-NMR (bottom) spectra of **2b**

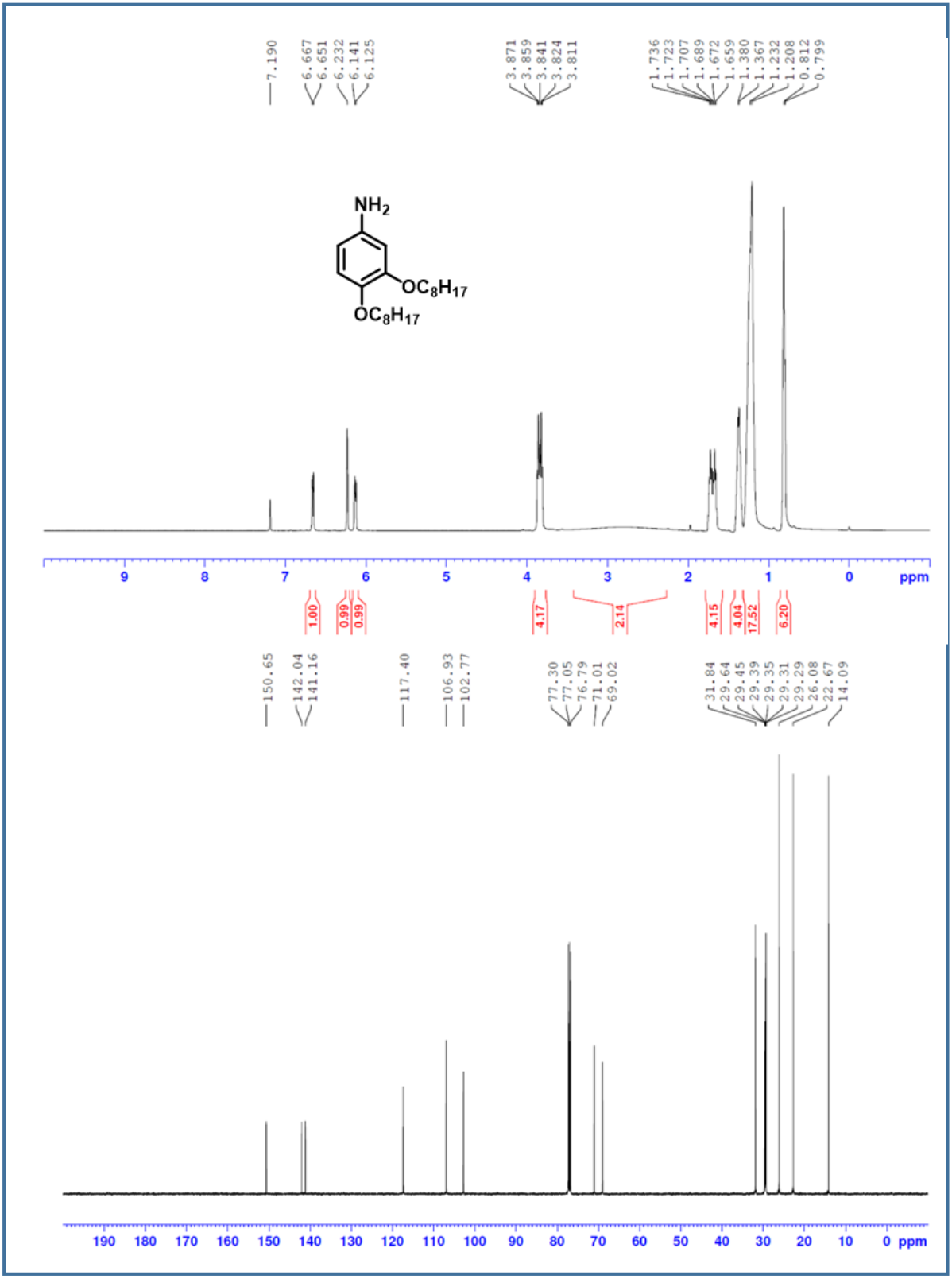

Figure 4.28: ^{1}H (top) and ^{13}C-NMR (bottom) spectra of **3b**

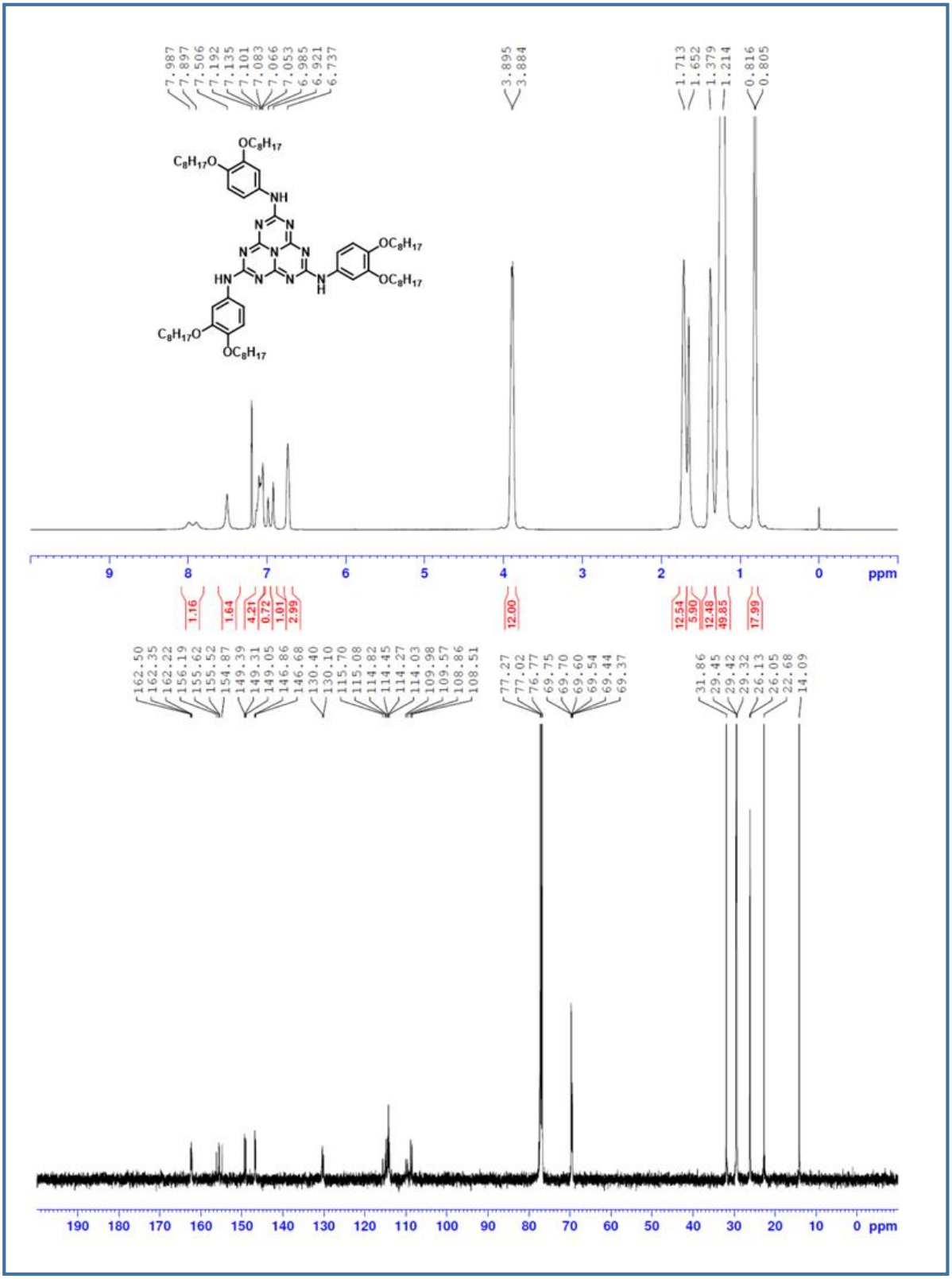

Figure 4.29: ^{1}H (top) and ^{13}C-NMR (bottom) spectra of **5b**

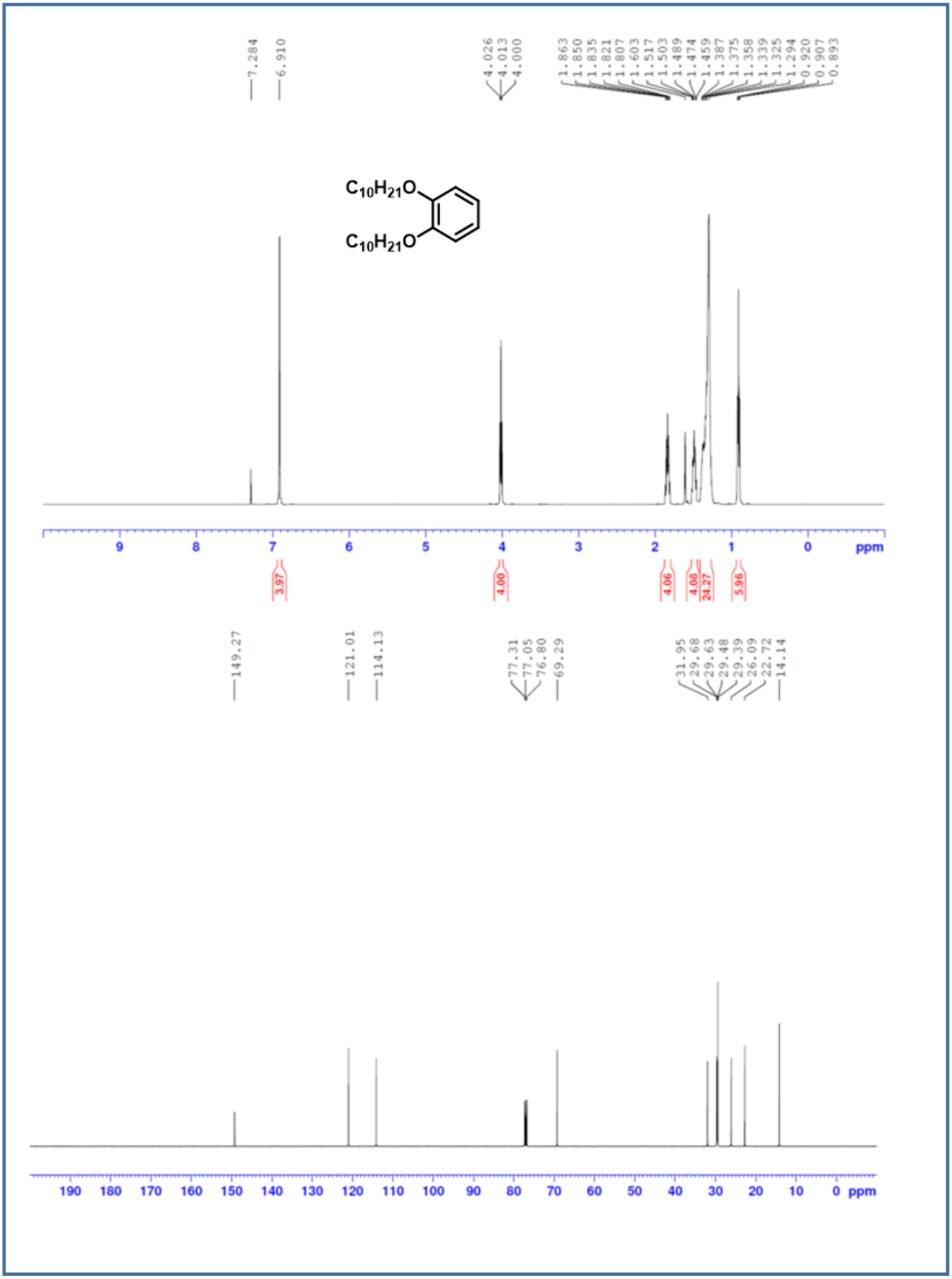

Figure 4.30: ^{1}H (top) and ^{13}C-NMR (bottom) spectra of **1c**

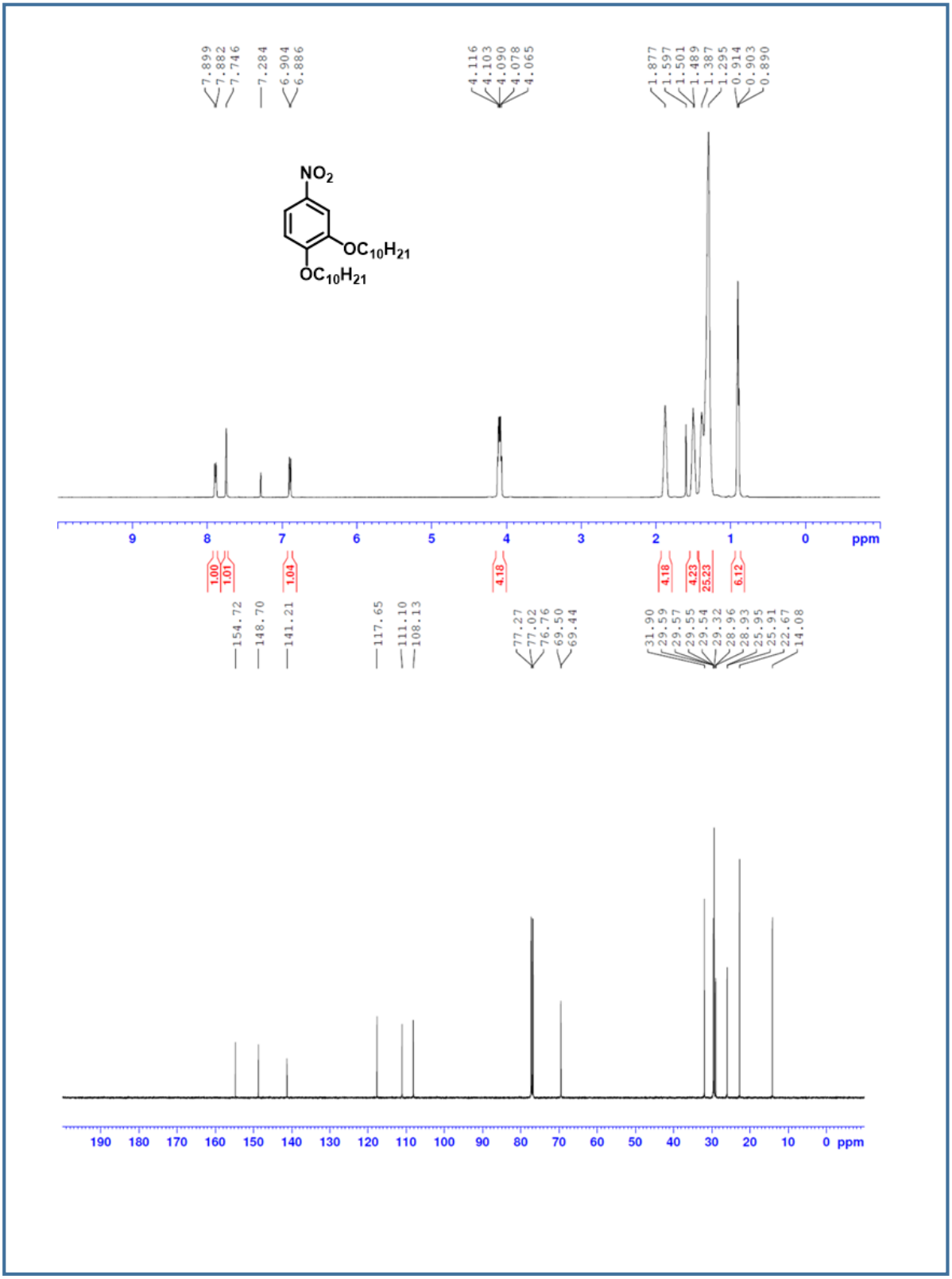

Figure 4.31: ^{1}H (top) and ^{13}C-NMR (bottom) spectra of **2c**

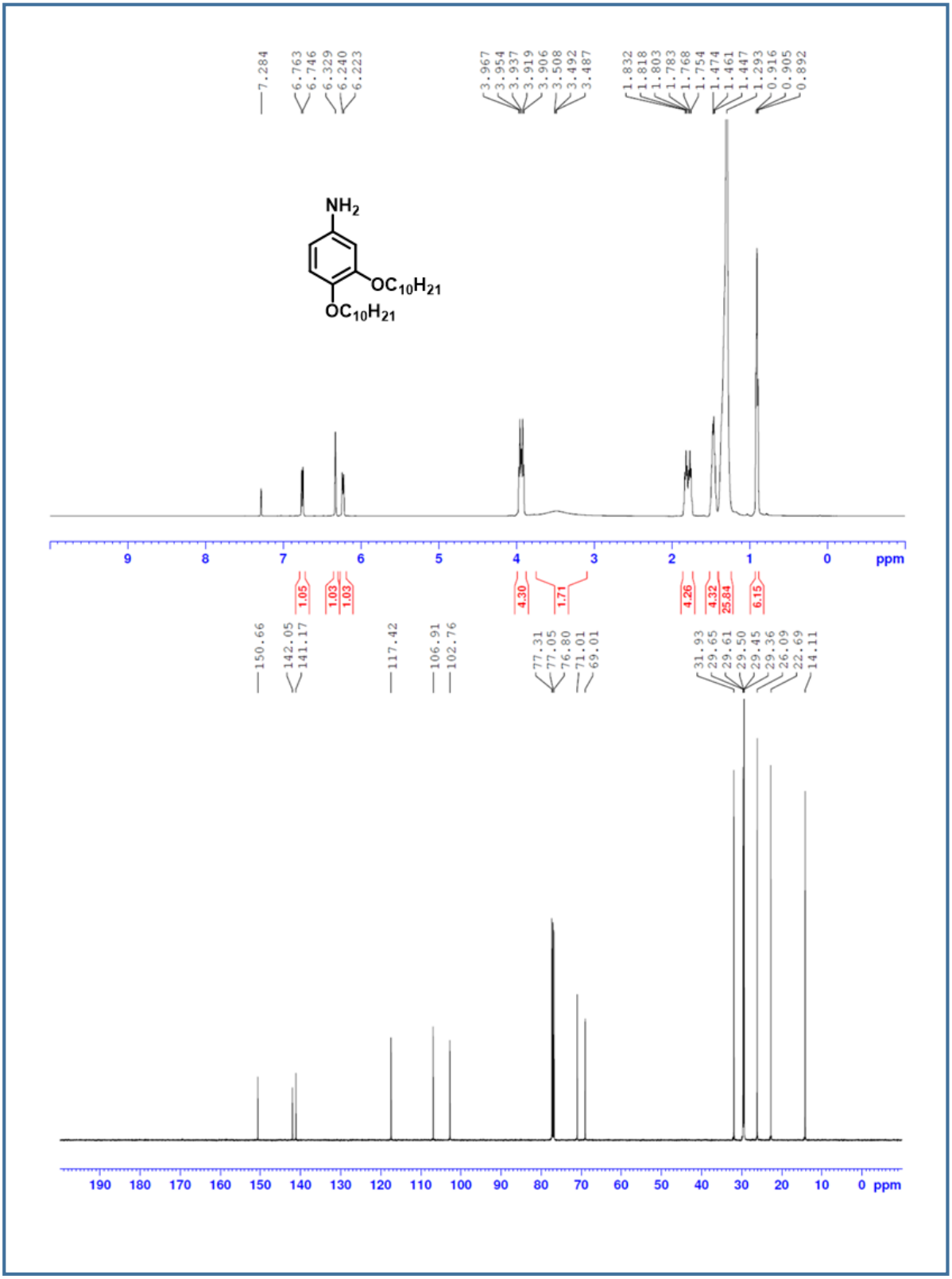

Figure 4.32: ^{1}H (top) and ^{13}C-NMR (bottom) spectra of **3c**

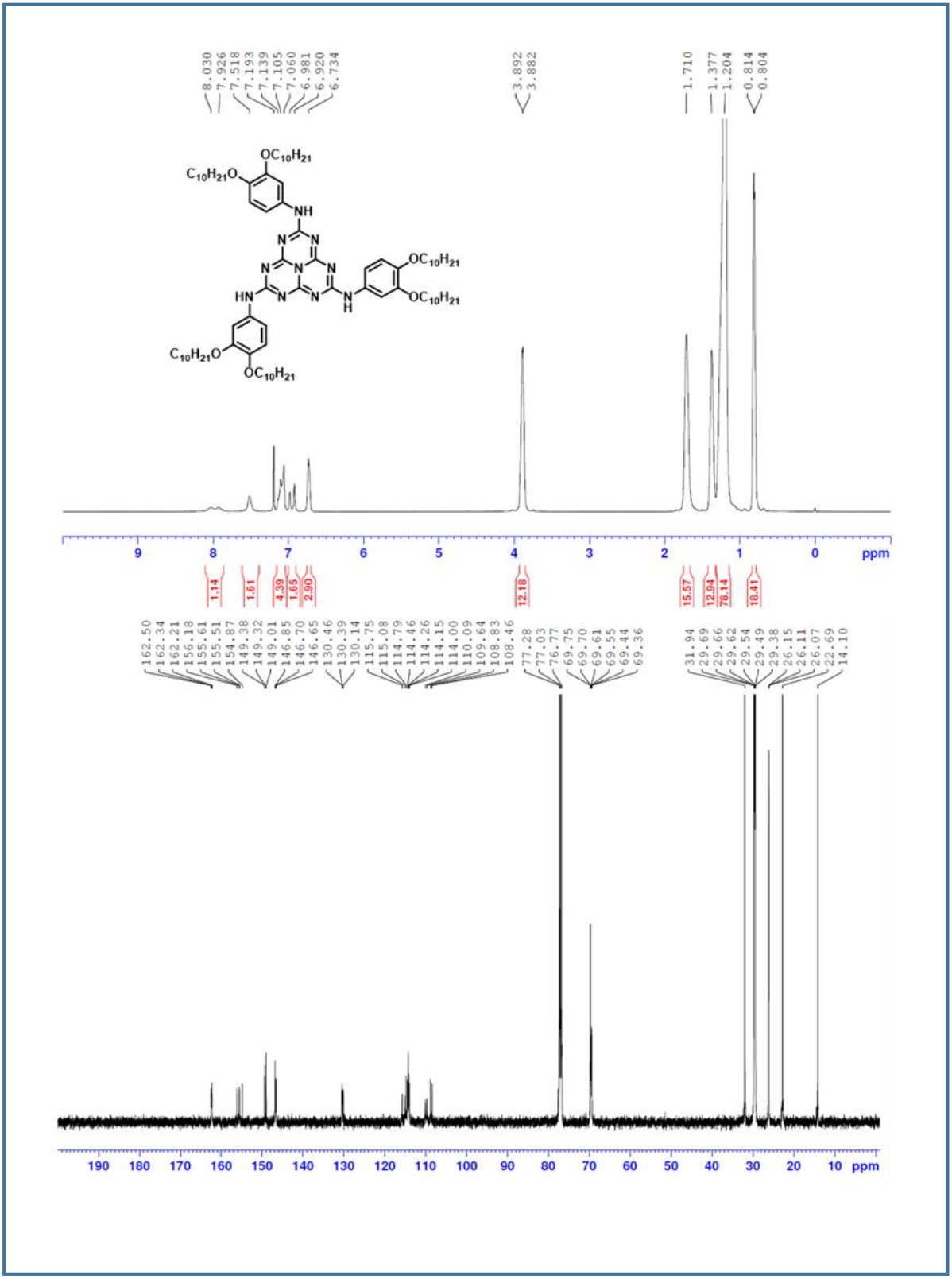

Figure 4.33: ^{1}H (top) and ^{13}C-NMR (bottom) spectra of **5c**

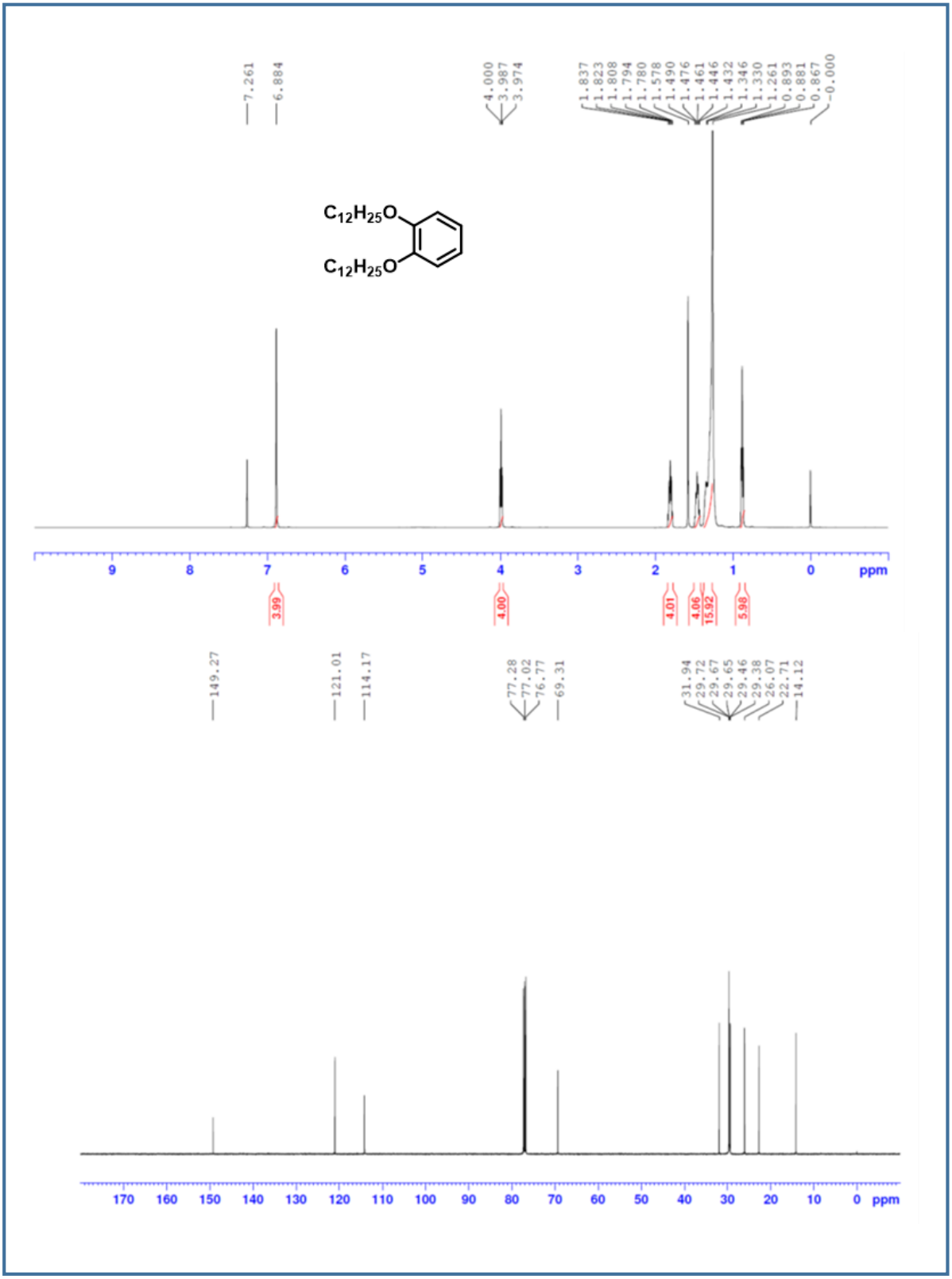

Figure4.34: ^{1}H (top) and ^{13}C-NMR (bottom) spectra of **1d**

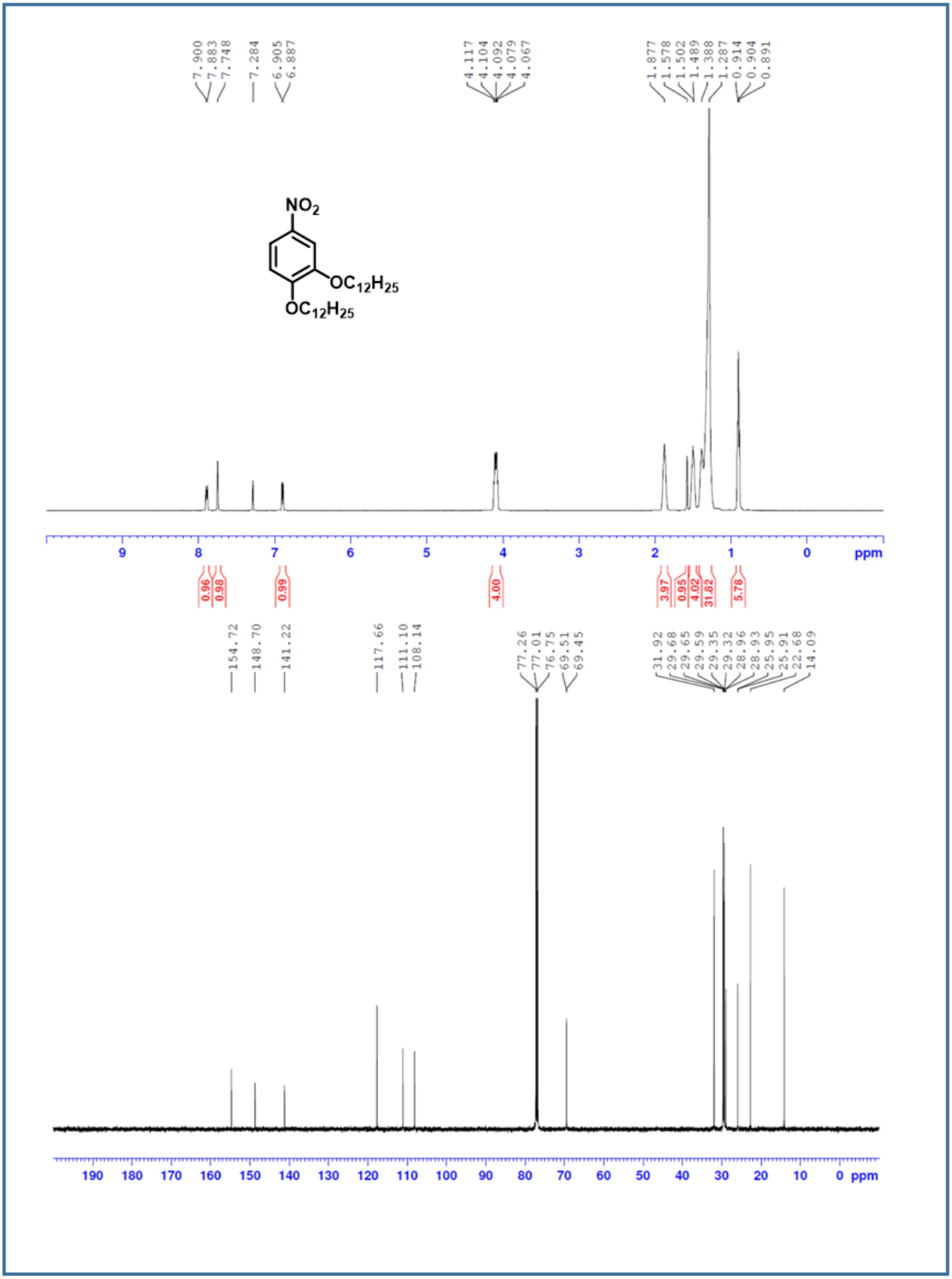

Figure 4.35: ^{1}H (top) and ^{13}C-NMR (bottom) spectra of **2d**

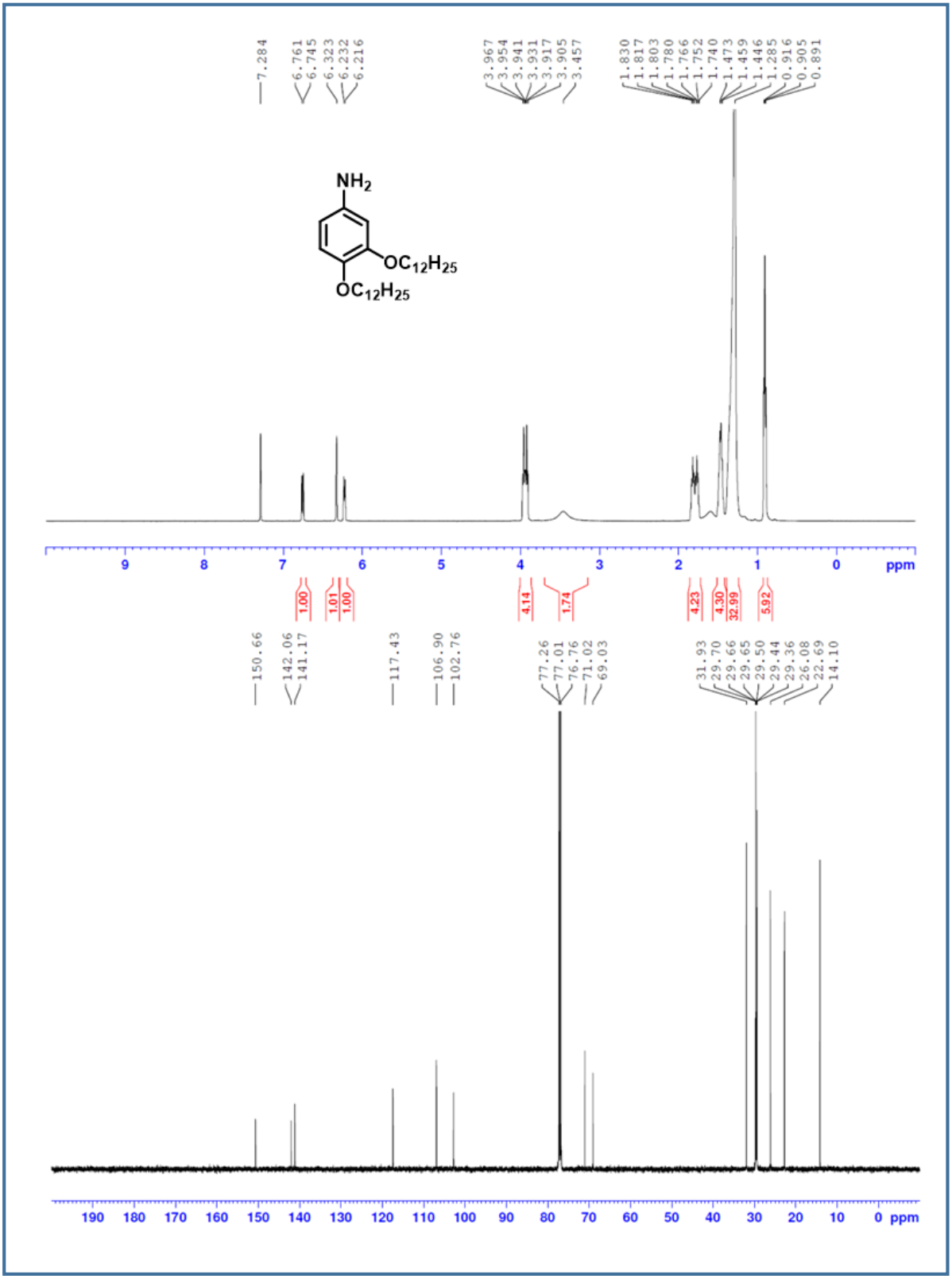

Figure 4.36: ^{1}H (top) and ^{13}C-NMR (bottom) spectra of **3d**

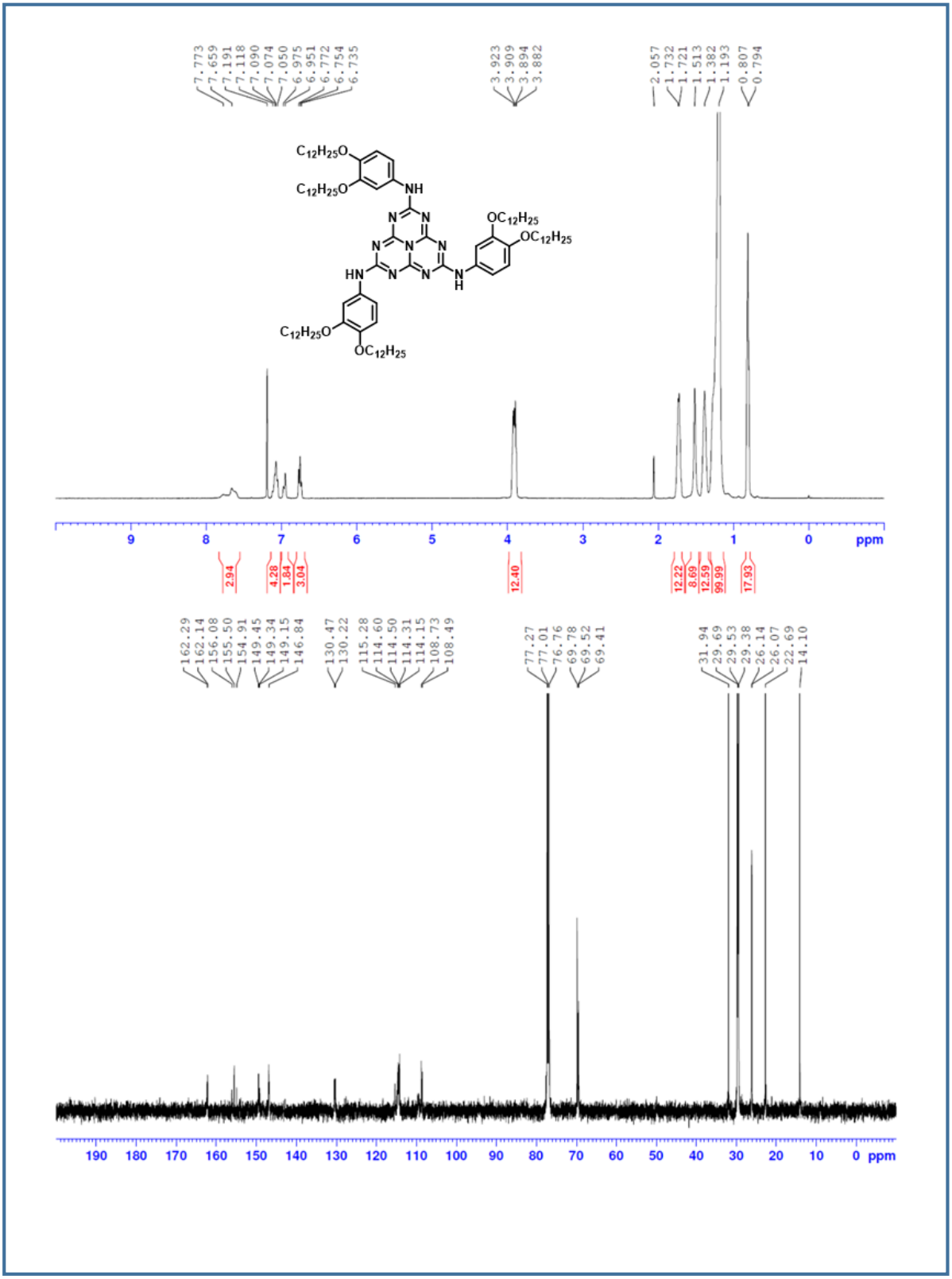

Figure 4.37: ^{1}H (top) and ^{13}C-NMR (bottom) spectra of **5d**

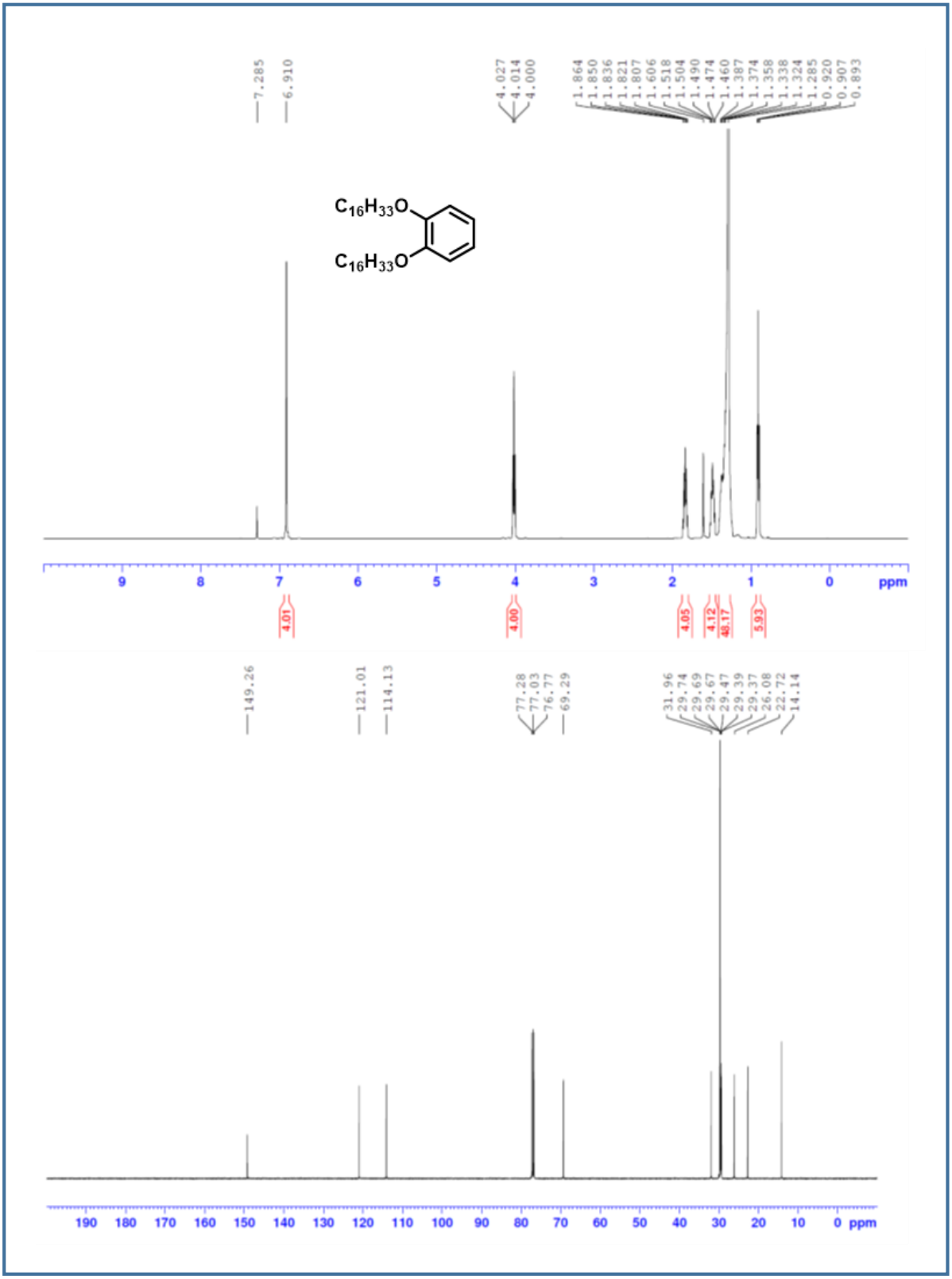

Figure 4.38: ^{1}H (top) and ^{13}C-NMR (bottom) spectra of **1e**

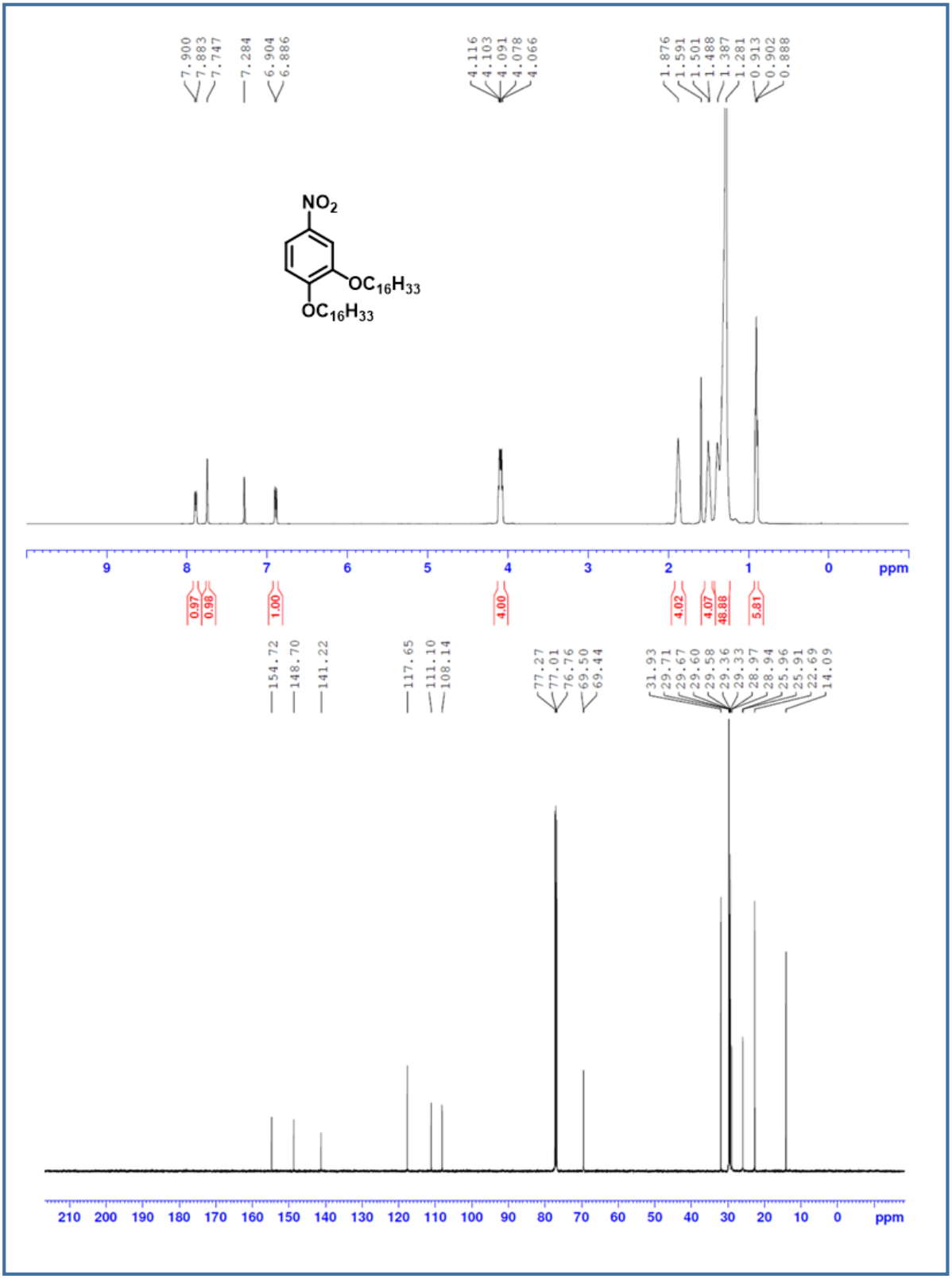

Figure 4.39: ^{1}H (top) and ^{13}C-NMR (bottom) spectra of **2e**

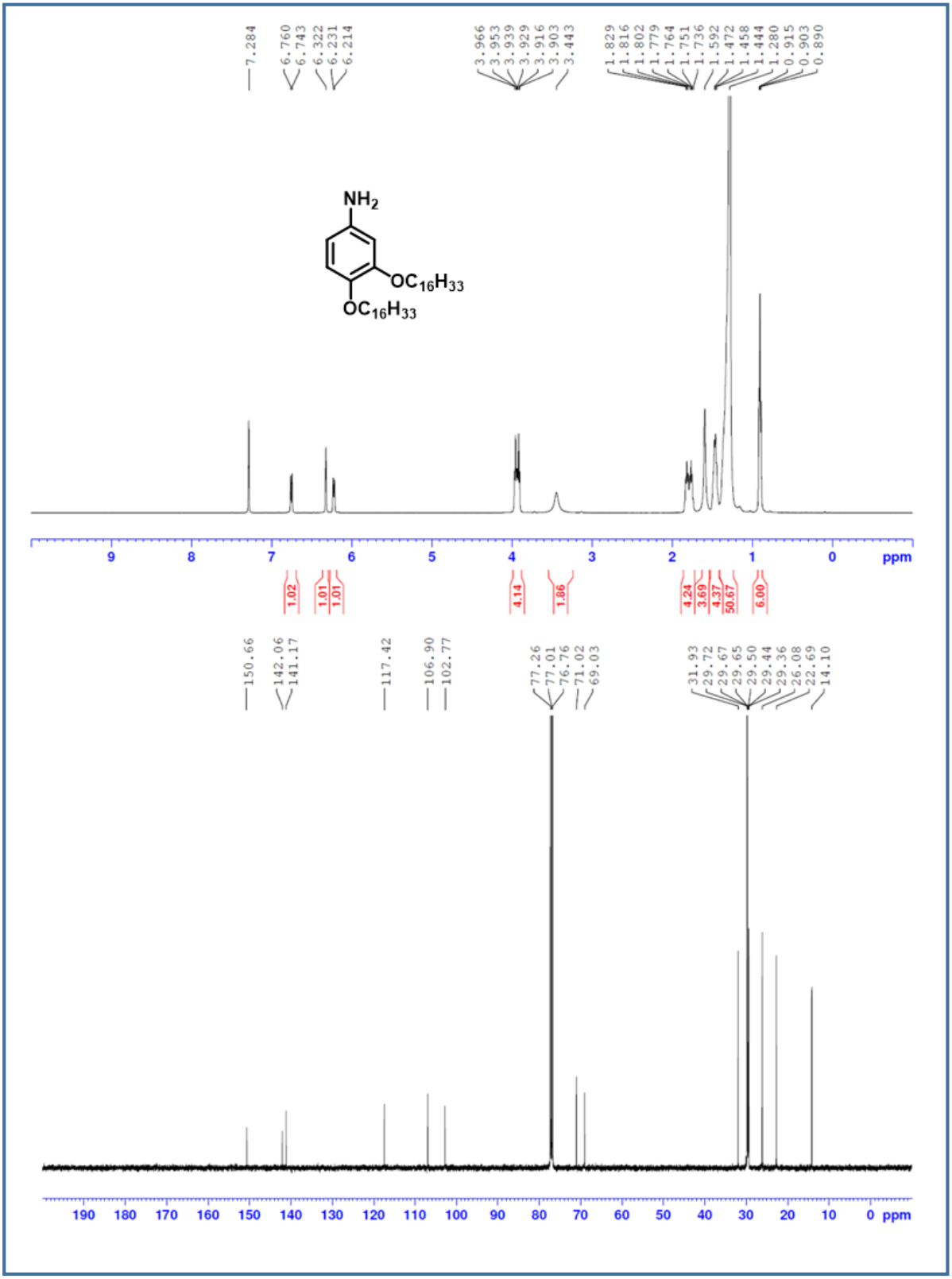

Figure 4.40: ^{1}H (top) and ^{13}C-NMR (bottom) spectra of **3e**

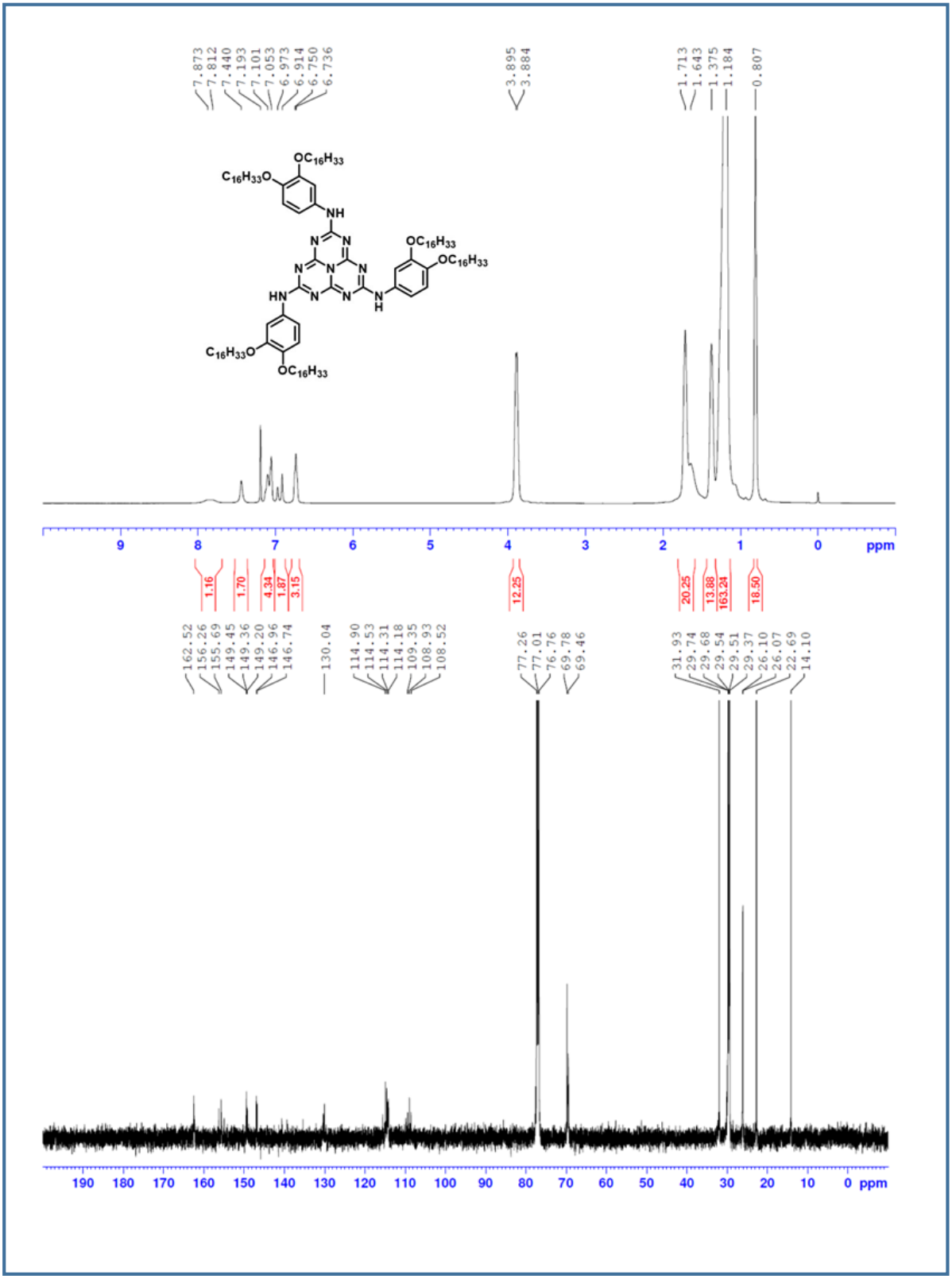

Figure 4.41: ^{1}H (top) and ^{13}C-NMR (bottom) spectra of **5e**

4.7 References:

[1] S. Chandrasekhar, B. K. Sadashiva, K. A. Suresh, *Pramana* **1977**, *9*, 471–480.

[2] A. Y. LIU, M. L. COHEN, *Science* **1989**, *245*, 841–842.

[3] J. Liu, H. Wang, M. Antonietti, *Chem. Soc. Rev.* **2016**, *45*, 2308–2326.

[4] Y. Zheng, Y. Jiao, M. Jaroniec, Y. Jin, S. Z. Qiao, *Small* **2012**, *8*, 3550–3566.

[5] X. Wang, K. Maeda, A. Thomas, K. Takanabe, G. Xin, J. M. Carlsson, K. Domen, M. Antonietti, *Nat. Mater.* **2009**, *8*, 76–80.

[6] A. Schwarzer, T. Saplinova, E. Kroke, *Coord. Chem. Rev.* **2013**, *257*, 2032–2062.

[7] A. Thomas, A. Fischer, F. Goettmann, M. Antonietti, J.-O. Müller, R. Schlögl, J. M. Carlsson, *J. Mater. Chem.* **2008**, *18*, 4893.

[8] E. Kroke, M. Schwarz, E. Horath-Bordon, P. Kroll, B. Noll, A. D. Norman, *New J. Chem.* **2002**, *26*, 508–512.

[9] C. Li, Y. Xu, W. Tu, G. Chen, R. Xu, *Green Chem.* **2017**, *19*, 882–899.

[10] I. F. Teixeira, E. C. M. Barbosa, S. C. E. Tsang, P. H. C. Camargo, *Chem. Soc. Rev.* **2018**, *47*, 7783–7817.

[11] G. Giacomelli, A. Porcheddu, L. Luca, *Curr. Org. Chem.* **2004**, *8*, 1497–1519.

[12] K. S. Lakhi, D.-H. Park, K. Al-Bahily, W. Cha, B. Viswanathan, J.-H. Choy, A. Vinu, *Chem. Soc. Rev.* **2017**, *46*, 72–101.

[13] L. Pauling, J. H. Sturdivant, *Proc. Natl. Acad. Sci.* **1937**, *23*, 615–620.

[14] W. Leupin, J. Wirz, *J. Am. Chem. Soc.* **1980**, *102*, 6068–6075.

[15] C. E. Redemann, H. J. Lucas, *J. Am. Chem. Soc.* **1940**, *62*, 842–846.

[16] H. Schroeder, E. Kober, *J. Org. Chem.* **1962**, *27*, 4262–4266.

[17] A. Schwarzer, E. Kroke, *Chem. Commun.* **2010**, *46*, 2829.

[18] A. Schwarzer, E. Kroke, *New J. Chem.* **2011**, *35*, 953.

[19] D. R. Miller, D. C. Swenson, E. G. Gillan, *J. Am. Chem. Soc.* **2004**, *126*, 5372–5373.

[20] D. R. Miller, J. R. Holst, E. G. Gillan, *Inorg. Chem.* **2007**, *46*, 2767–2774.

[21] B. Traber, T. Oeser, R. Gleiter, M. Goebel, R. Wortmann, *European J. Org. Chem.* **2004**, *2004*, 4387–4390.

[22] J. Li, H. Nomura, H. Miyazaki, C. Adachi, *Chem. Commun.* **2014**, *50*, 6174–6176.

[23] J. Li, T. Nakagawa, J. MacDonald, Q. Zhang, H. Nomura, H. Miyazaki, C. Adachi, *Adv. Mater.* **2013**, *25*, 3319–3323.

[24] Y. Qiu, L. Gao, *Chem. Commun.* **2003**, *3*, 2378–2379.

[25] M. Kawaguchi, S. Yagi, H. Enomoto, *Carbon N. Y.* **2004**, *42*, 345–350.

[26] J. L. Zimmerman, R. Williams, V. N. Khabashesku, J. L. Margrave, *Nano Lett.* **2001**, *1*, 731–734.

[27] M. Kim, S. Hwang, J.-S. Yu, *J. Mater. Chem.* **2007**, *17*, 1656–1659.

[28] Z. Zhao, W. Li, Y. Dai, G. Ge, X. Guo, G. Wang, *ACS Sustain. Chem. Eng.* **2015**, *3*, 3355–3364.

[29] Z. Zhou, J. Wang, J. Yu, Y. Shen, Y. Li, A. Liu, S. Liu, Y. Zhang, *J. Am. Chem. Soc.* **2015**, *137*, 2179–2182.

[30] Z. Lin, X. Wang, *Angew. Chemie Int. Ed.* **2013**, *52*, 1735–1738.

[31] S. Kumar, N. Sharma, K. Kailasam, *J. Mater. Chem. A* **2018**, *6*, 21719–21728.

[32] S. Mir Sayed, L.-L. Deng, B.-P. Lin, H. Yang, *Liq. Cryst.* **2017**, *44*, 2175–2183.

[33] I. Bala, H. Singh, V. R. Battula, S. P. Gupta, J. De, S. Kumar, K. Kailasam, S. K. Pal, *Chem. - A Eur. J.* **2017**, *23*, 14718–14722.

[34] I. Bala, S. P. Gupta, S. Kumar, H. Singh, J. De, N. Sharma, K. Kailasam, S. K. Pal, *Soft Matter* **2018**, *14*, 6342–6352.

[35] I. Bala, L. Ming, R. A. K. Yadav, J. De, D. K. Dubey, S. Kumar, H. Singh, J.-H. Jou, K. Kailasam, S. K. Pal, *ChemistrySelect* **2018**, *3*, 7771–7777.

[36] P. Audebert, E. Kroke, C. Posern, S.-H. Lee, *Chem. Rev.* **2021**, *121*, 2515–2544.

[37] C. V Yelamaggad, A. S. Achalkumar, D. S. S. Rao, S. K. Prasad, **2007**, 8308–8318.

[38] P. Yaduvanshi, A. Mishra, S. Kumar, R. Dhar, *J. Mol. Liq.* **2015**, *208*, 160–164.

[39] P. S. Kumar, S. Kumar, V. Lakshminarayanan, *J. Appl. Phys.* **2009**, *106*, 093701.

Chapter - 5

Supramolecular self–assembly of hydrogen-bonded dendritic-benzotri (imidazole) derivative architectures

Abstract

Dendrimers represent a special class of synthetic macromolecules which has a significant contribution in fields such as material science, nanoscience, nanotechnology, and biomedical sciences. In this chapter, we have synthesized carboxylic acid-functionalized 1st and 2nd generation dendrimers. These compounds were prepared by copper-catalyzed azide-alkyne ‘‘click’’ cycloaddition. The formed dendrimers are found to be mesomorphic in nature and H-bonded supramolecular complexation with benzotri (imidazole) derivatives of the same was studied. The stable hydrogen-bonded complexes also show mesomorphism. The formation of these complexes and dendrimers were investigated through FT-IR, NMR techniques and elemental analysis. The mesomorphic properties of all the compounds were characterized using polarized optical microscopy (POM), differential scanning calorimetry (DSC), and X-ray diffraction (XRD) techniques.

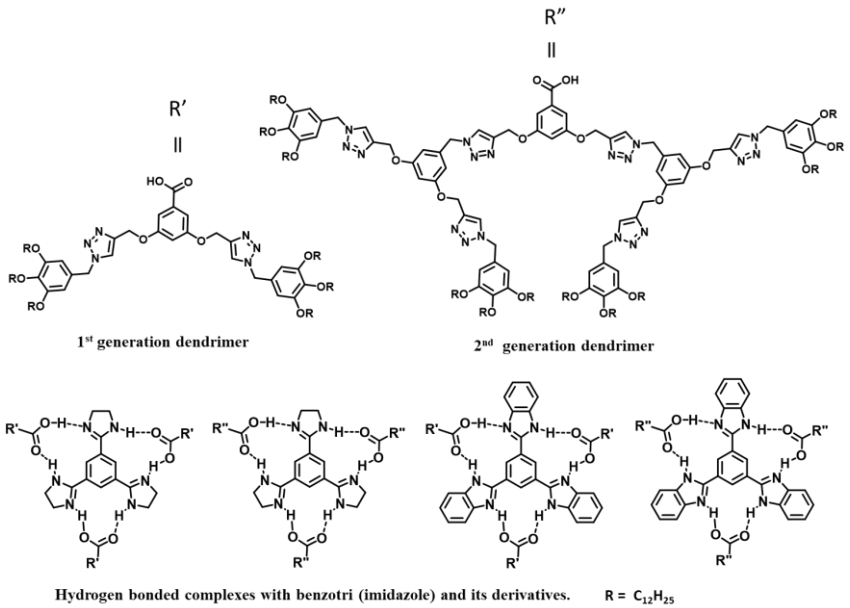

1st generation dendrimer

2nd generation dendrimer

Hydrogen bonded complexes with benzotri (imidazole) and its derivatives. R = $C_{12}H_{25}$

5.1 Introduction:

Dendritic structures are found widely in nature. The term dendrimers is derived from the Greek word dendron (meaning tree), and meros (meaning part). 'Arborols' and 'cascade' words are two synonyms for dendrimer. The dendrimers are hyper branched architectures that display the desired motif in a multivalent fashion to give synergistic enhancement of a particular function. As an example of above ground, dendritic motifs are used by trees to increase the exposure of their leaves to sunlight, which is necessary for survival and growth via photosynthesis (**Figure 5.1a**).[1] In living organisms, there are several dendritic structures present. For example, when they breath into their lungs the air flows through a massive dendritic network of bronchioles and alveoli, and the vascular network that transports blood to many organs develops into dendritic patterns.[2] The central nervous system and the brain consist of various cells forming into dendritic structures to gain the largest exchange of material (and information) with the neighboring tissue. During diseased or degenerative conditions in the brain, microglia cells serve as multifunctional helpers to the cells by generating dendritic structures (**Figure 5.1b**). Another prominent example of dendritic structures in nature discovered recently is the significant number of foot hairs on the Gecko's feet. Here the foot-hair interacts with molecules of the surface through so-called Van der Waal forces, which create the dendritic structures[3]

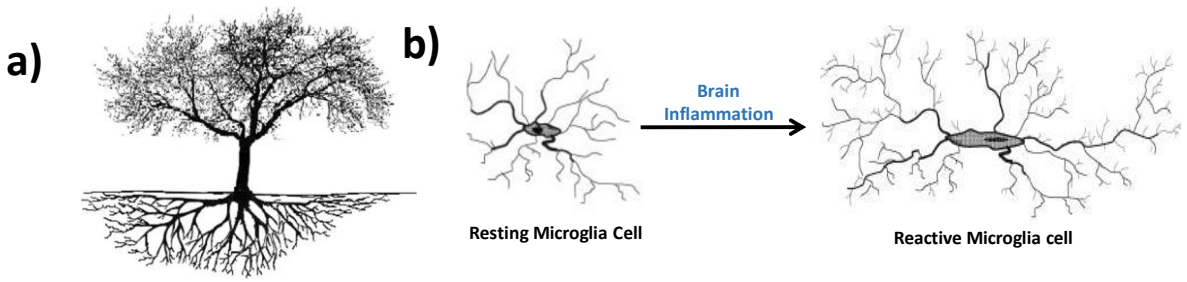

Figure 5.1: a) Dendritic structure of the tree's roots, b) Activation of a microglia cell during a pathological state in the brain.

In synthetic organic chemistry, the design and synthesis of dendritic compounds is a fascinating field. Since their discovery in the late 1970s, dendrimers have developed into a rapidly expanding area of current science[4] and massive interest in materials science[5,6] (mainly in nanoscience and nanotechnology) and biomedical sciences.[7] Dendrimers have several actual

and potential uses in health care, engineering, consumer goods, environmental sciences, electronics, optoelectronics, and other fields.[8,9]

Dendrimers and dendrimeric units (dendrons) may belong to a polymeric family with geometrically restricted structures. Because of this reason, they are one of the most adaptable, compositionally, and structurally controlled nanoscale building blocks available today. Depending on the structure and topology, dendritic polymers are classified into four main groups: dendrons, dendrimers, hyperbranched polymers (HPs), and dendrigrafts (**Figure 5.2**). Furthermore, a couple of dendritic structures can be prepared by conjugating these dendrimer structures with other synthetic scaffolds such as nanoparticles, rigid aromatic platforms, polymers, macrocycles, flexible networks, and so on.

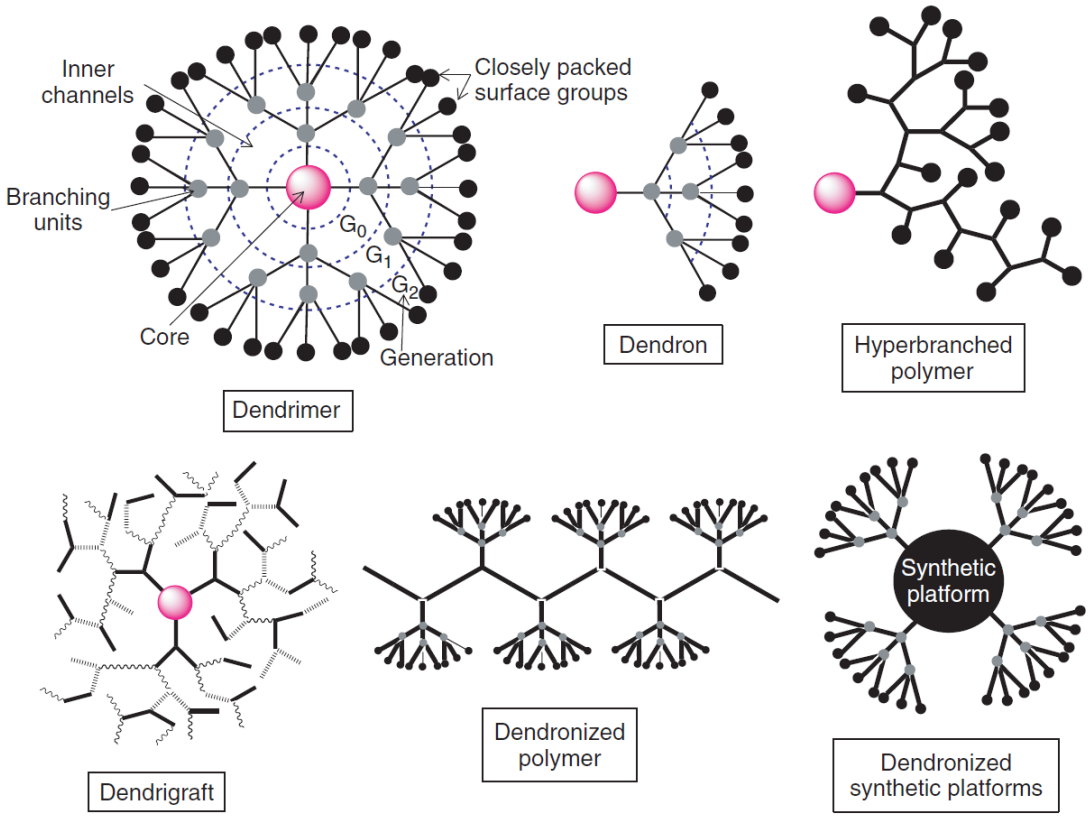

Figure 5.2: Schematic representation of a few dendritic structures.

Dendrimers and dendrons can show a singular structure developing from the focal point, and these can be prepared by convergent[10] and divergent methods.[11,12] There are few reports with the combined divergent and convergent approach.[13] Most of the dendrimers reported in the

literature are prepared using a convergent method. Schematic representation of the convergent, divergent, and combined synthesis of dendrimers have shown in **Figure 5.3.**

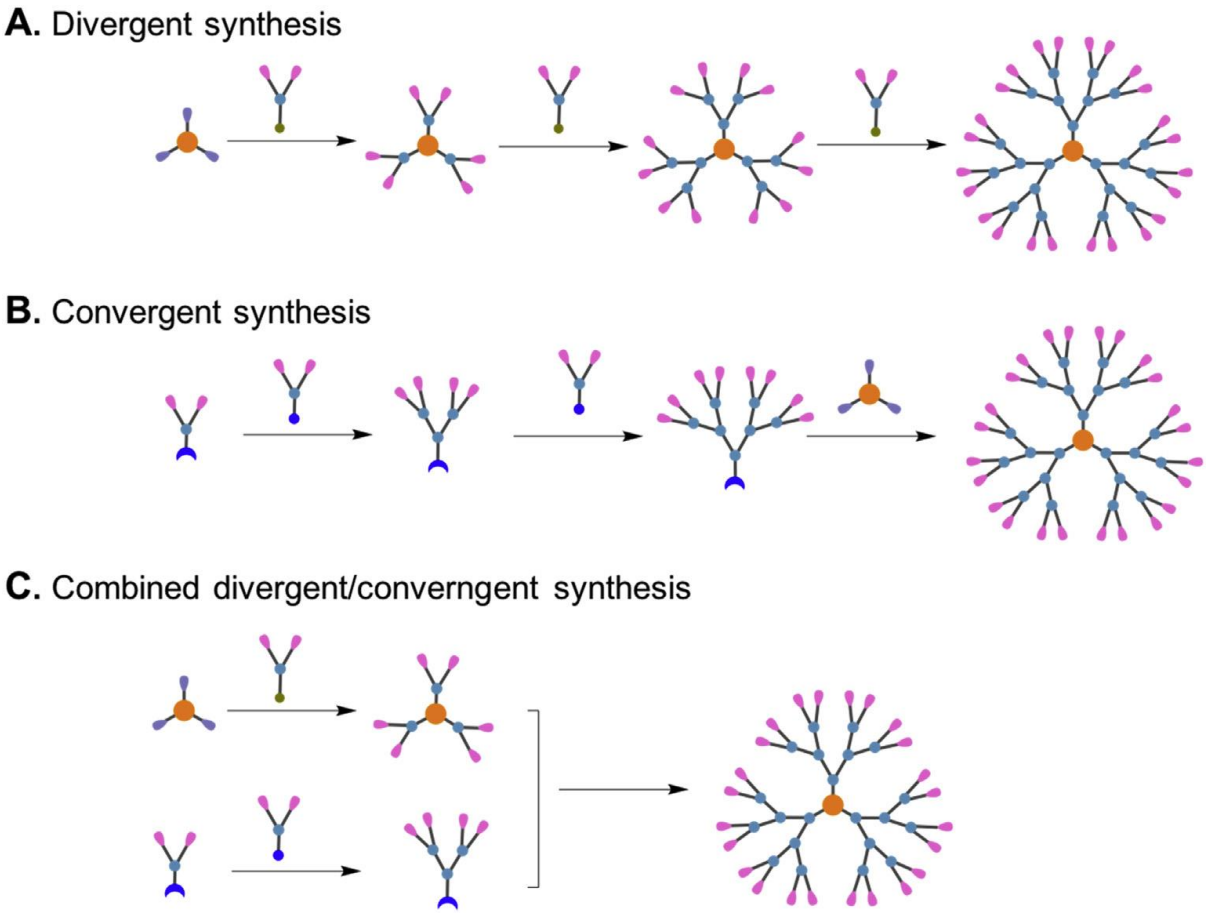

Figure 5.3: Schematic representation of the different approaches for covalent dendrimer synthesis approach.

Several methods can be used to develop liquid crystalline dendritic polymers (**Figure 5.4**). [14,15] The most common method of inducing mesophases is to functionalize dendrimers with peripheral external groups. These molecules exhibit mesophases on their own (mesogenic) or can induce liquid crystallinity with promesogenic molecules. On the other side, mesogenic dendritic polymers can self-assemble into a cylindrical shape. Instead of changing the termini, these anisotropic groups can form the polymeric branches, resulting in main-chain liquid crystalline dendritic polymers. Discotic dendritic matrices are formed when rigid rod branches are combined with conjugated junctions (most commonly aromatic junctions). The periphery

of these 'shape-persistent' liquid crystalline dendrimers can be decorated with flexible aliphatic chains to induce molecular anisotropy.[16,17] Supramolecular liquid crystalline dendrimers, also known as dendromesogens,[18] can be produced using dendritic structures attaching to the central focal point to form into round or cylindrical shape dendritic polymers.[19,20]

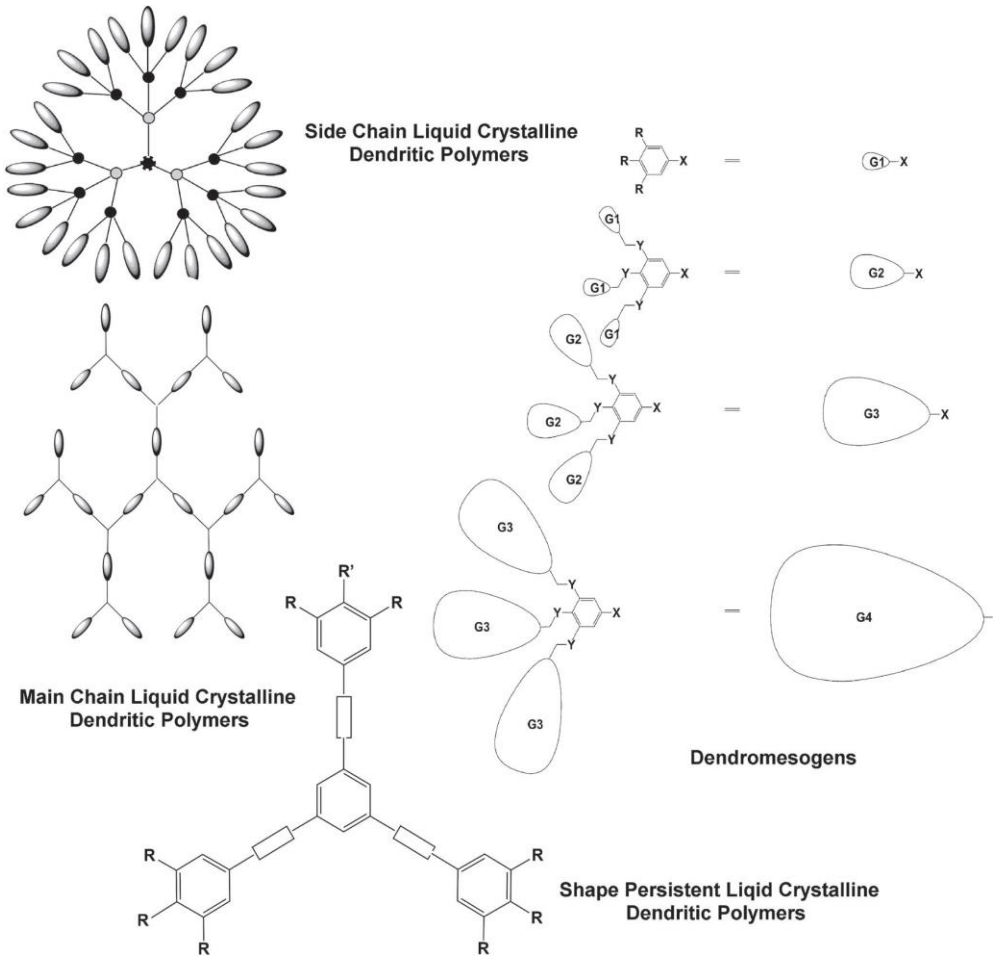

Figure 5.4: Schematic representation of the most common methods to achieve mesophase formation to dendritic polymers.

In the literature, few examples are not include in the above category. One is a dendritic polymer with a rigid discotic core[21], and the second is supramolecular linear or branched rod-coil block co dendrimers.[22] The polypedes described are one more intermediate that will not come under the category mentioned above.[14,23] These three are shown in **Figure 5.5**.

Dendrimers could have a size approximate to proteins and DNA. They have been used to mimic enzymes and drug or gene delivery vehicles.[24,25] Furthermore, they can create defined oligomeric materials with precisely defined functionalities, either in the interior micro-environment or periphery, making them valuable catalysts[26–29]and building blocks for functional assemblies in nanoscience, nanotechnology, and supramolecular chemistry.[30–34]

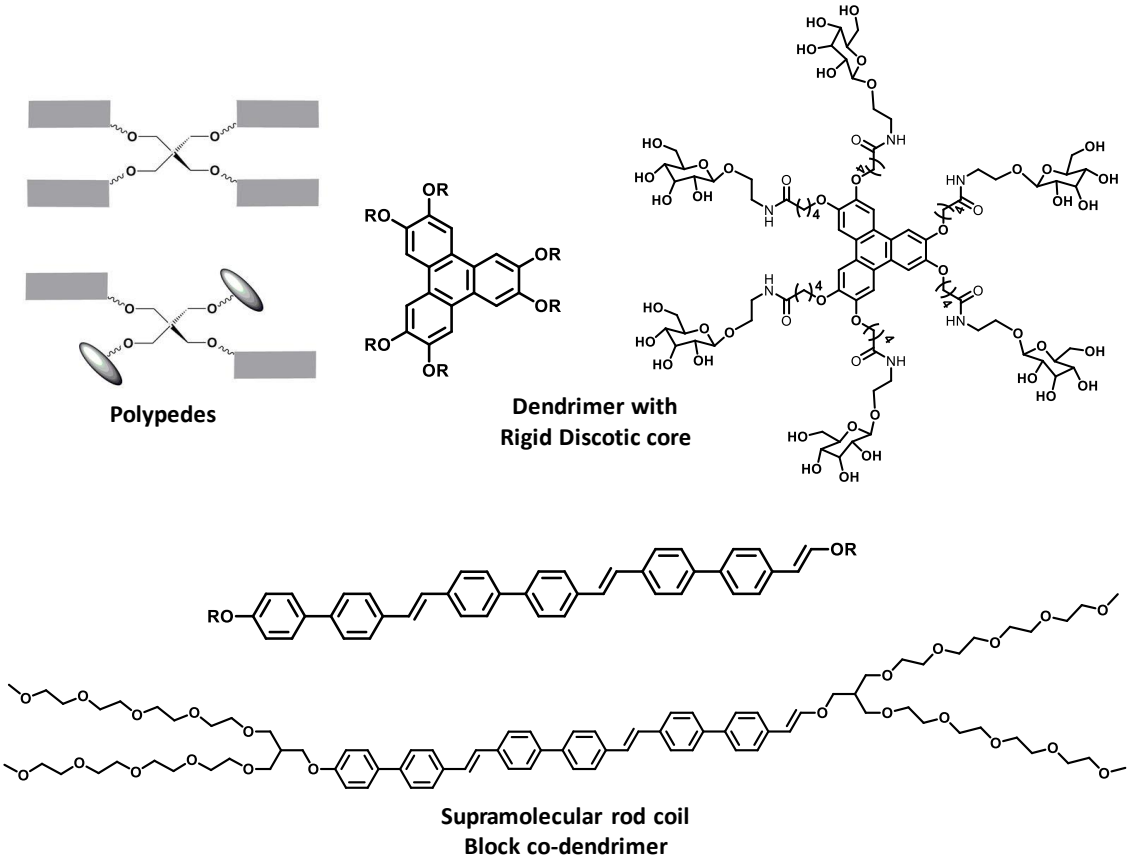

Figure 5.5: Schematic representation of polypedes and some exceptional cases of liquid crystalline dendritic polymers with rigid interior

Dendrimers and dendrons can be organized into different supramolecular architectures. These architectures produce distinct liquid crystalline (LC) phases by using various supramolecular interactions such as Van der Waals forces, ionic interactions, π-πinteractions, dipolar and quadrupolar interactions, and so on. Also, these LC phases result from the micro-segregation of incompatible structural units and the overall molecular shape, which is heavily influenced

by the topology of the branching points, and other factors.[35–38] In the literature, several mesophases have been observed in amphiphilic systems and dendrimers, such as lamellar, bicontinuous cubic, columnar, and spheroidal cubic phases. However, since the introduction of dendrimer architectures, new and unusual 3D mesophases have been discovered, such as a tetragonal P42/mnm lattice[39]and a quasi-LC phase with 12 fold symmetry, both built up by spheroidic aggregates.[40]

As mentioned above, the liquid crystalline dendrimers are formed by different supramolecular interactions. Among those supramolecular interactions, hydrogen bonding interactions are the essential noncovalent interactions in many scientific fields, particularly chemistry and biology, which is also true for liquid crystals. Hydrogen bonding exists in two ways: inter (occurring between separate molecules) and intramolecular (happening among parts of the same molecule). The hydrogen bonding significantly impacts the functionality of the external groups and shape of the dendritic structures. Furthermore, they have been responsible for the rigidity of certain parts of the mesogenic molecules, which are frequently found in the central core. The arrangement of the rigid parts leads to more ordered structures and higher thermal stability.[41] The hydrogen bond is stronger than the Van der Waals interactions and weaker than the covalent and ionic interactions.[42] As a result, they are directional, adaptable, reversible, and they enable critical biological processes like molecular recognition. Furthermore, hydrogen bonding is inherently dynamic. It provides a viable method of preparing functional materials that can adapt to minor changes in the external environment. Micro phase separation is influenced by hydrogen bonding, and also it offers many advantages for the advancement of new functional materials.

In the liquid crystal field, the liquid crystalline properties of dendritic polymers are generally induced through secondary interactions, especially hydrogen bonds. In the literature, quite a lot of concepts have been suggested. These concepts are mainly divided into two categories. One is a chemical modification on peripheral groups to form hydrogen bonds with themselves or with complementary mesogens or promesogenic molecules. Further, they have a particular shape (rigid rod, disk, flexible alkyl chain) or characteristics (polarity) that induce the liquid crystalline phase. The second one is the interaction of modified groups with mesogens containing complementary moieties in a melt or specific solvent to form supramolecular complexes.

The first hydrogen-bonded complex exhibited mesophase behavior as a result of carboxylic acid dimerization.[43,44] Gray and Jones reported liquid crystalline phases in p-n-alkoxybenzoic acids more than 45 years ago.[45] Kato et al. reported the first example (**Figure 5.6**) of intermolecular hydrogen bonding between two components that exhibit liquid crystalline behavior.[46,47] Lehn et al. thoroughly investigated the supramolecular hydrogen-bonded liquid crystalline properties.[48] After that, there have been several reports on hydrogen-bonded liquid crystals in the literature.

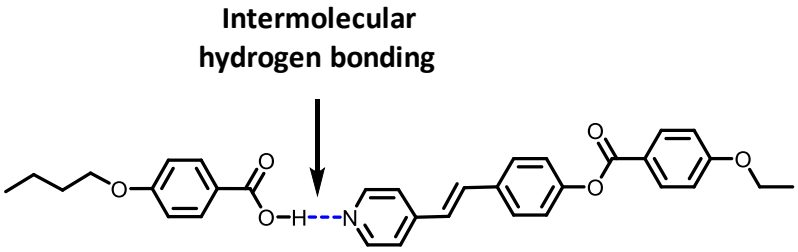

Figure 5.6: The proposed structure of the new mesogen formed by intermolecular Hydrogen bonding.

The external functional groups of liquid crystalline dendritic structures or dendritic polymers surfaces tend to form hydrogen bonding without further modification. Bitan-Cherbakovsky reported that the co-solubilized glycerol monooleate and polypropylene imine dendrimers in water develop hydrogen bonding, leading to the reverse gyroid lyotropic cubic LC phase **Figure 5.7.**[49] External amino groups induced columnar hexagonal phase with the help of hydrogen bonding.[50] Many research groups have investigated the concepts of intra (with the same molecules) and inter (with external molecules) molecular hydrogen bonding in the literature. Hydrogen bonding induces the rod and disk, star-shaped molecules through molecular recognition. Some examples are given here like rigid rod-shaped molecules,[51,52] flexible moieties,[53,54] and disc-shaped core molecules through multiple hydrogen bonds **Figure 5.8**.[55,56] In a similar way, dendrons or dendrimers are also inducing the rigid-rod or disk-shaped core through hydrogen bonding. [57–61]

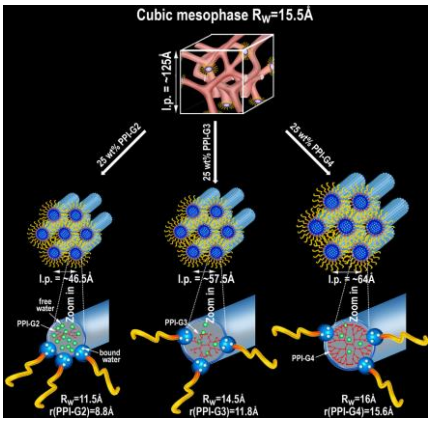

Figure 5.7: Schematic illustration of the interactions between the components, representing the solubilization of PPI dendrimers of 2nd, 3rd, and 4th generation within QG mesophase.

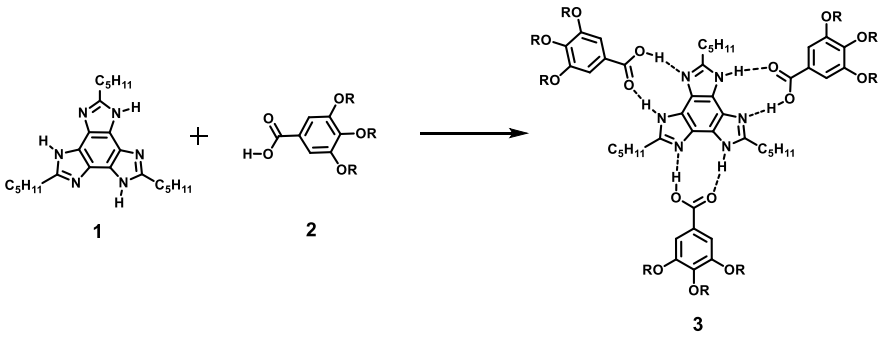

Figure 5.8: Supramolecular discotic liquid crystal **3** formed from **1**and **2**.

Tian and his colleagues investigated the role of intramolecular hydrogen bonding in induction of liquid crystalline behavior and the stabilization of mesophases.[62] They have synthesized the hydrated precursors bearing formamide (HCONH-) moieties, showing the columnar and cubic phases resulting from dimerization and polymerization via intramolecular hydrogen bonding as shown in **Figure 5.9.**

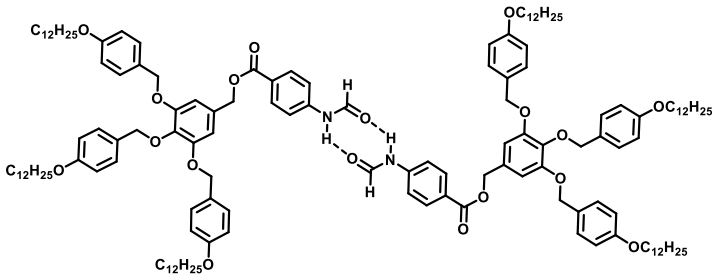

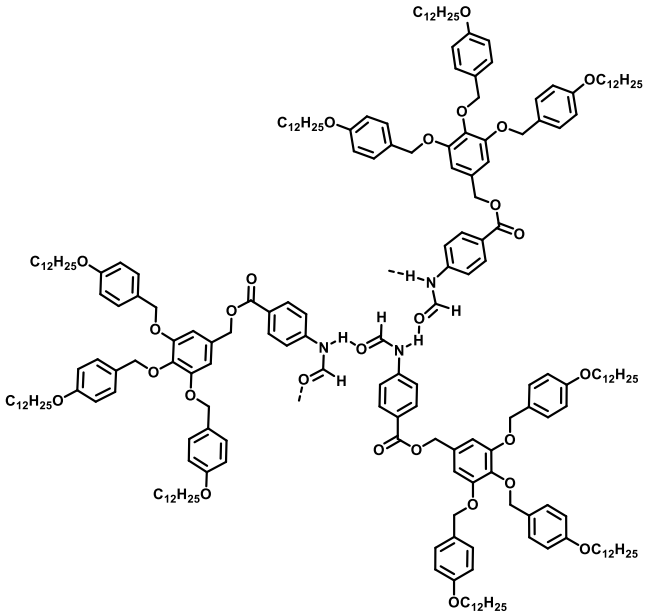

Figure 5.9: Possible hydrogen bonding patterns of formamide dendrons.

In few cases, hydrogen bonding influences the shape (for example, rigid disk or rod) of the liquid crystalline dendritic molecules and thereby diversity of the resulting mesophases. The most common example of molecular structure definition by intermolecular bonds is the formation of dimers or oligomers with specific shapes (rigid disk or rod) that favour liquid crystalline phases. Takashi Kato and his group reported the folic acid derivative, which shows hydrogen bonding layers and column patterns (**Figure 5.10).**[63] Folic acid and glutamic acid derivatives extensively studied the hydrogen-bonded liquid crystalline dendron's properties [64–67]. Further, the addition of alkali metal salts induced columnar structure due to ion-dipolar interactions.

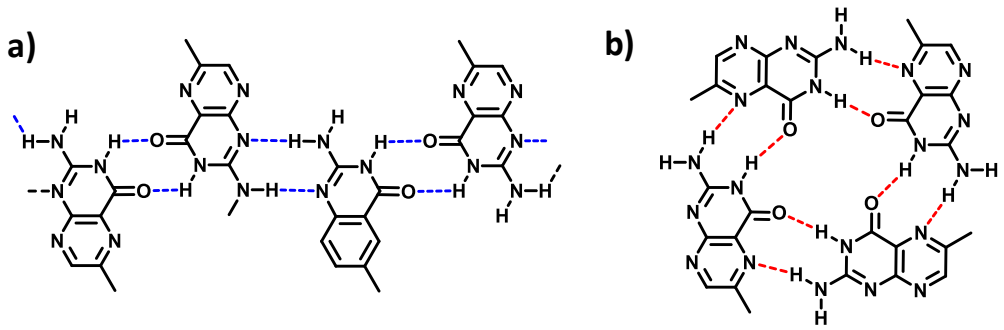

Figure 5.10: Ribbon (a) and disk (b) conformations of folic acid derivatives.

As mentioned above, literature related to the dendrimers, liquid crystalline dendrimers, and inter, intramolecular hydrogen-bonded complexes reports the various liquid crystalline phases. Among different hydrogen bonding concepts, Sierra and many other groups have reported multifunctional hydrogen bonding using two-component systems that exhibit columnar liquid crystals.[68] We are now focusing on the two-component systems using tris(imidazoline) and its derivatives and hydrogen complexes with dendrimer molecules, which results in the liquid crystalline behavior.

Hydrogen-bonded liquid crystals and porous polymer materials of tris(imidazoline) and their derivatives have been reported in the literature that has been presented below. Jin-Feng Xiong et al. reported the new kind of columnar liquid crystals (**Figure 5.11**) using hydrogen bonding between the 1,3,5-tri(1H-benzo[d]-imidazol-2-yl)benzene (T) and serial gallic acid derivatives.[69]

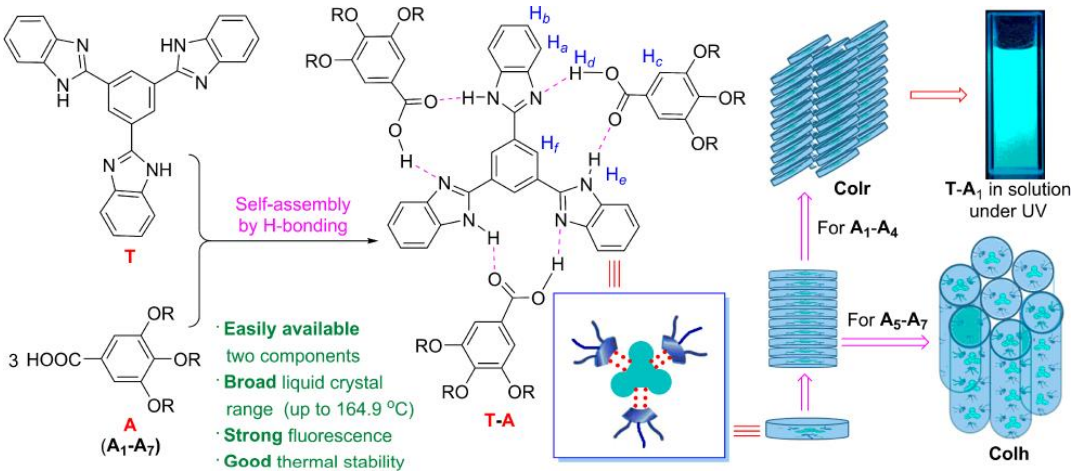

Figure 5.11: Formation of supramolecular columnar liquid crystals based on 1,3,5-Tri(1H-benzo[d]imidazol-2-yl)benzene

Jody A. M. Lugger et al. studied the polymerized hexagonal columnar liquid crystals that were used to create the nanoarchitecture porous polymer films, using the hydrogen bonding as a template between the MeTB and gallic acid derivatives of alkoxy, trimethylene glycol shown in **Figure 5.12**. Photo-initiated free-radical copolymerization was used to stabilize the homeotropic alignment liquid crystalline properties were studied using IR and POM

techniques. Further, the removal of hydrogen-bonded templates from the aligned columns creates the nanoporous network[70].

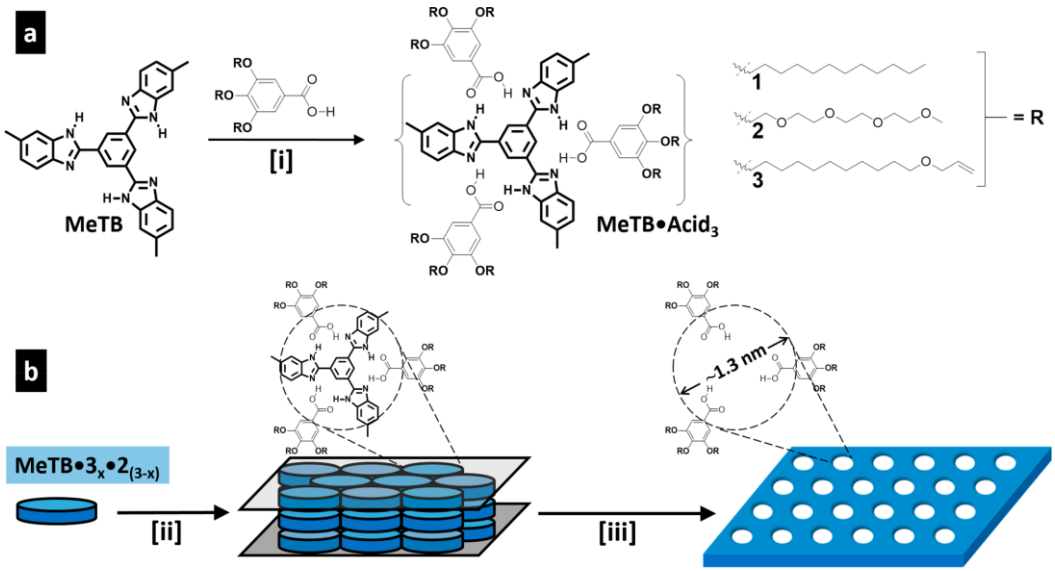

Figure 5.12: (a) Molecular representation of triply hydrogen-bonded discotic liquid crystals. (b) Homeotropic alignment of the MeTB·$Acid_3$ complex by mixing in dopant 2. and photo-initiated radical polymerization, followed by the formation of nanopores by template removal.

Subham Bhattacharjee et al. reported that the self–supporting polymer film was obtained through polymerizing an AB3-type hydrogen-bonded complex in the plastic columnar phase. The porous poly membrane was created by removing a hydrogen bonding template with a size of 1.1 and 1.6 nm. Further, they have studied the formed pore, and pore size has collapsed due to the adsorption of cations shown in **Figure 5.13**.[71]

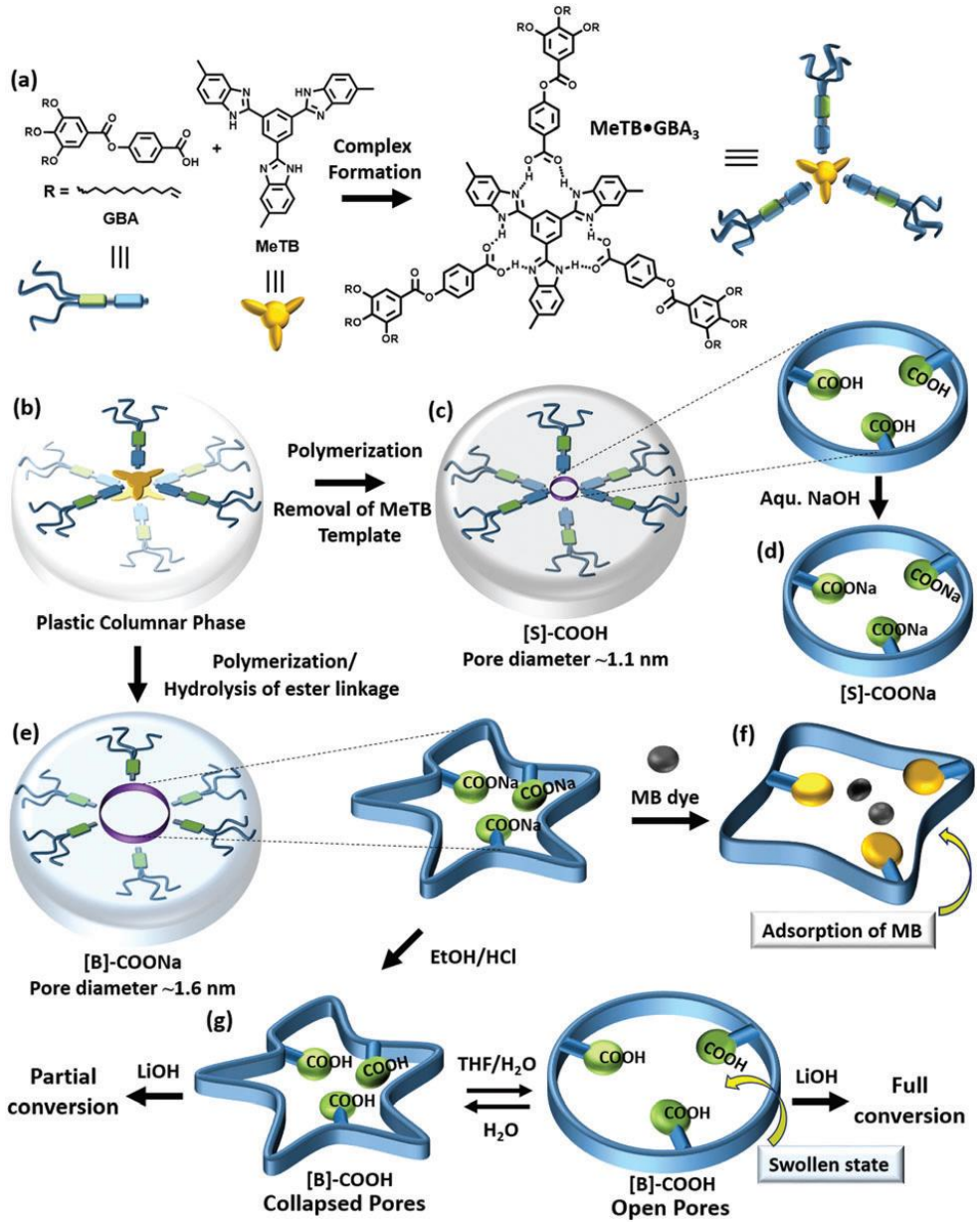

Figure 5.13: Chemical structures and schematic representations of GBA, MeTB, and MeTB-GBA3 complex and collapsed polymer pores.

Jody A. M. Lugger et al. reported the formation of columnar liquid crystals based on tris-benzoimidazolyl benzene (TBIB) and commercially available fatty acids. The hydrogen-bonded liquid crystalline complexes temperatures were tuned by increasing the length of the fatty acids shown in **Figure 5.14**.[72]

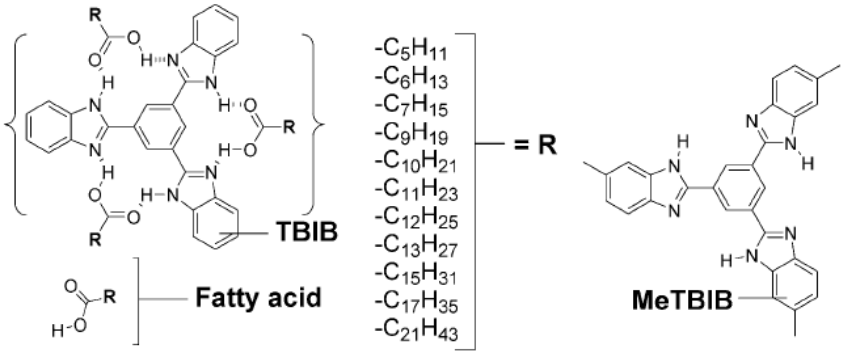

Figure 5.14: Complexation of TBIB with fatty acids.

Gerardus M. et al. developed the nanoporous materials from columnar liquid crystals using hydrogen bonding as a template, as shown in **Figure 5.15**. The complexation between the polymerizable benzoic acid derivative and 1,3,5-*tris* (1Hbenzo [d] imidazol-2-yl) benzene template molecule is described here. The hydrogen-bonded complex is self-assembled into columnar hexagonal phase, followed by polymerization resulting in the nanoporous materials. These materials are used for the cation binding selectively in the aqueous solution.[73]

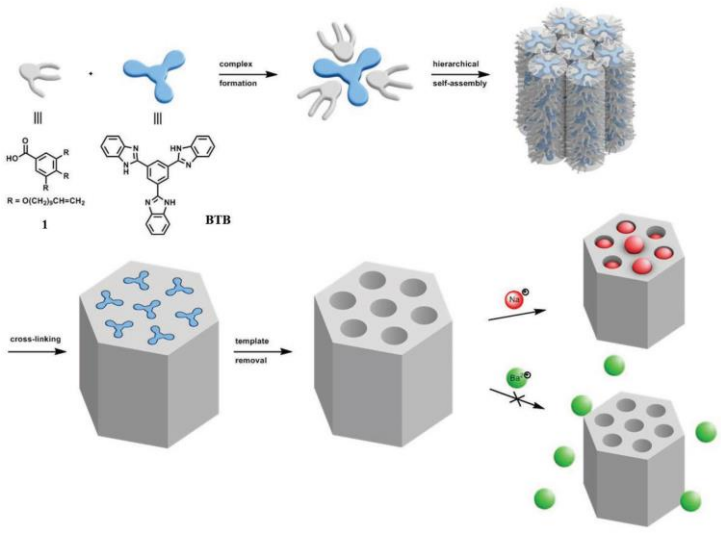

Figure 5.15: Self-assembly approach for the template-assisted development of a nanoporous material and size-selective ion binding.

Xunda Feng et al. have reported the formation of single crystals with thoroughly controlled texture over the large area in a soft mesophase of columnar discotic liquid crystals shown in

Figure 5.16. They have explored the dual-axis control in a supramolecular discogen produced by a hydrogen bonding template between a C3-symmetric tribasic core of 1,3,5-tris(4,5-dihydroimidazol-2-yl) benzene (TDIB) and a wedge-shaped gallic acid derivative, 3,4,5-tris(11' acryloyloxyundecyloxy) benzoic acid (TABA). They have studied the orientation of the columnar axis in a controlled manner using the magnetic field.

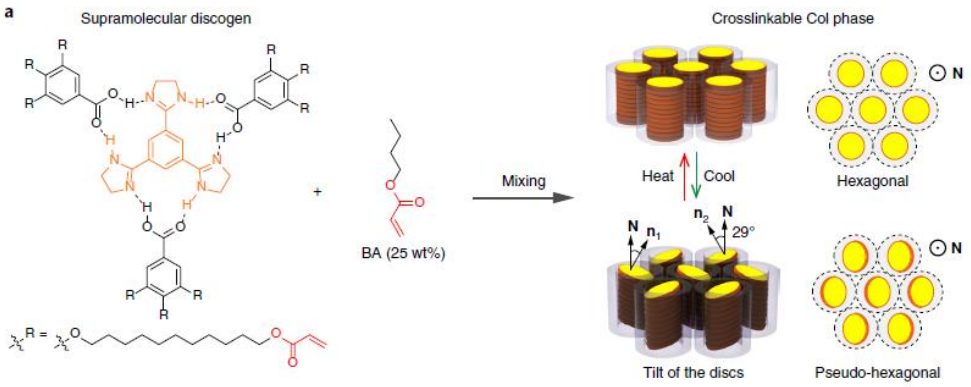

Figure 5.16: Molecular structure of a cross-linkable supramolecular discogen formed by hydrogen bonding. The illustration schematically shows non-tilted to tilted discotic Col mesophases and pseudo-hexagonal.

5.2 Results and discussion:

5.2.1 Synthesis

Herein we report the design and synthesis of a novel class of carboxylic acid-functionalized dendrimers like 1st and 2nd generations and hydrogen-bonded complexes were shown in **Figure 5.17**. These compounds were prepared by incorporation of two (5-(azidomethyl)-1,2,3-tris(dodecyloxy)benzene) units to a central resorcinol core through copper-catalyzed azide-alkyne ''click'' cyclo-addition reaction.[74] Then benzotri (imidazole) derivatives (compounds **12** and **13**) were prepared according to the literature procedures.[75,76] All compounds were purified by column chromatography on silica gel (100-200 mesh) followed by repeated recrystallization using suitable analytical grade solvents. The chemical structures of all the compounds were confirmed by ^{1}H-NMR, ^{13}C-NMR spectroscopy and elemental analysis. The detailed synthetic procedures and characterization data are given below. The hydrogen-bonded LC complexes were prepared by first dissolving the carboxylic acid derivatives and benzotri (imidazole) derivatives in a MeOH/$CHCl_3$ and stir for two hours, followed by solvent removal.

Spectroscopic and thermal characterization techniques fully confirmed the complex formation. The synthesized dendrimers are found to be mesomorphic, which shows the columnar hexagonal and cubic phases. The H-bonded complexes exhibit the hexagonal columnar mesophase at room temperatures and high temperatures indicate the columnar cubic phase.

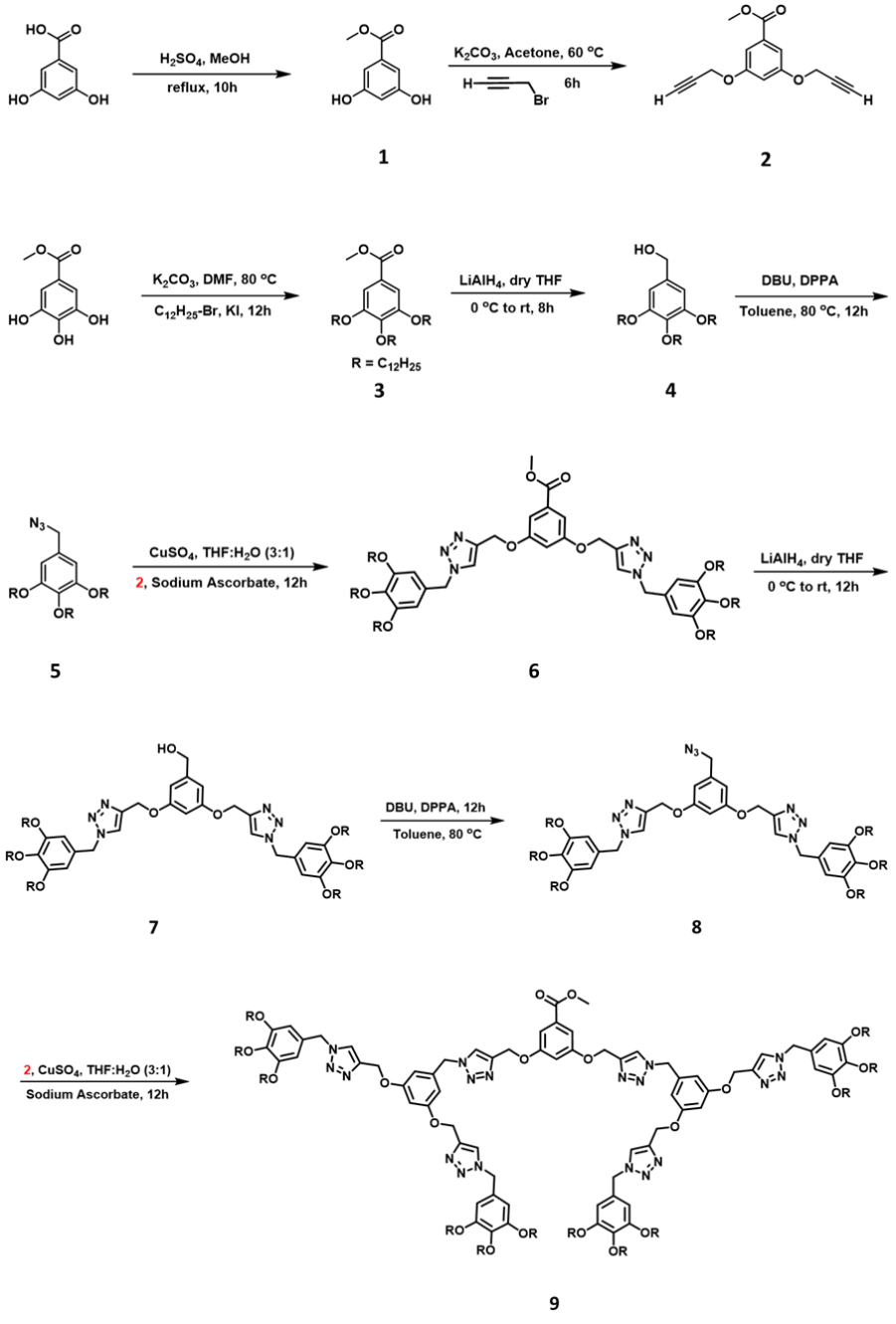

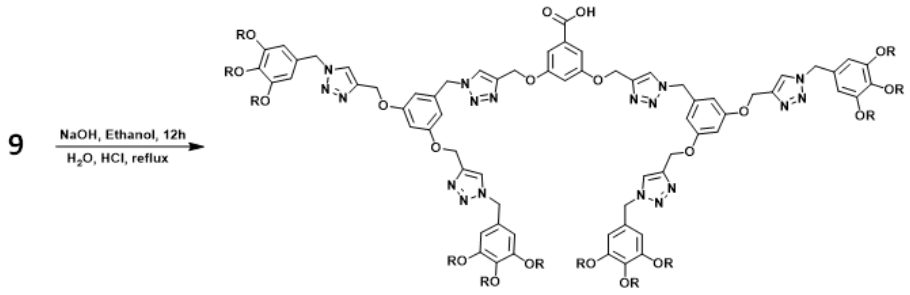
9
NaOH, Ethanol, 12h
H2O, HCl, reflux
10

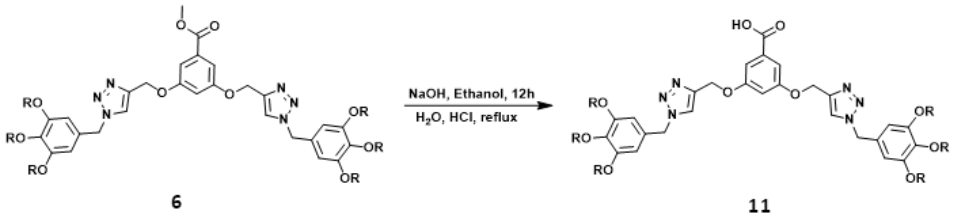
6
NaOH, Ethanol, 12h
H2O, HCl, reflux
11

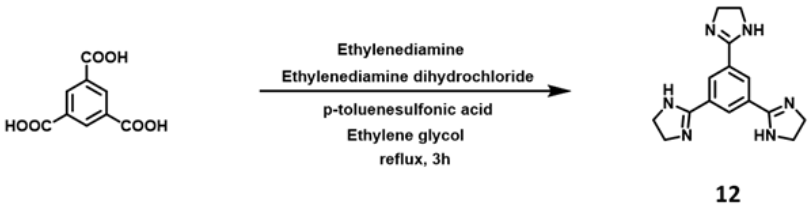
Ethylenediamine
Ethylenediamine dihydrochloride
p-toluenesulfonic acid
Ethylene glycol
reflux, 3h
12

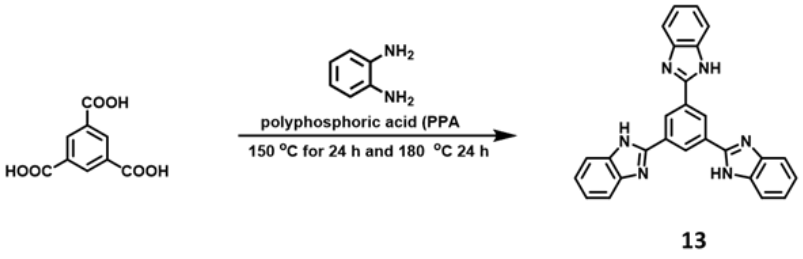
polyphosphoric acid (PPA
150 °C for 24 h and 180 °C 24 h
13

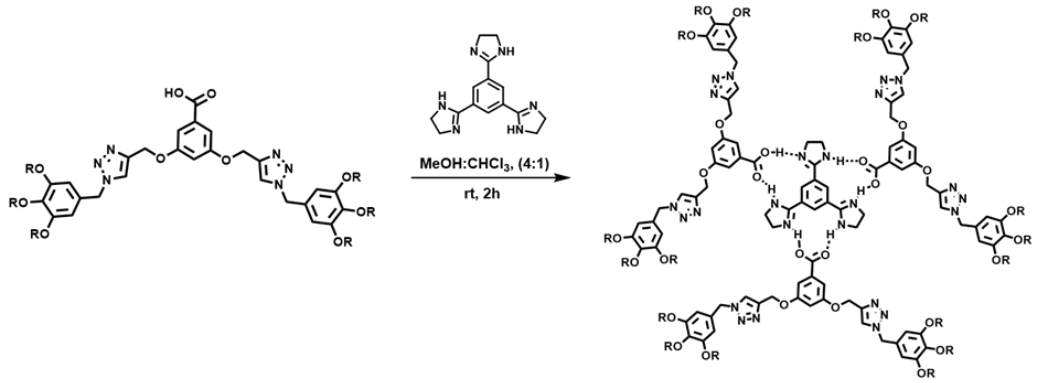

14

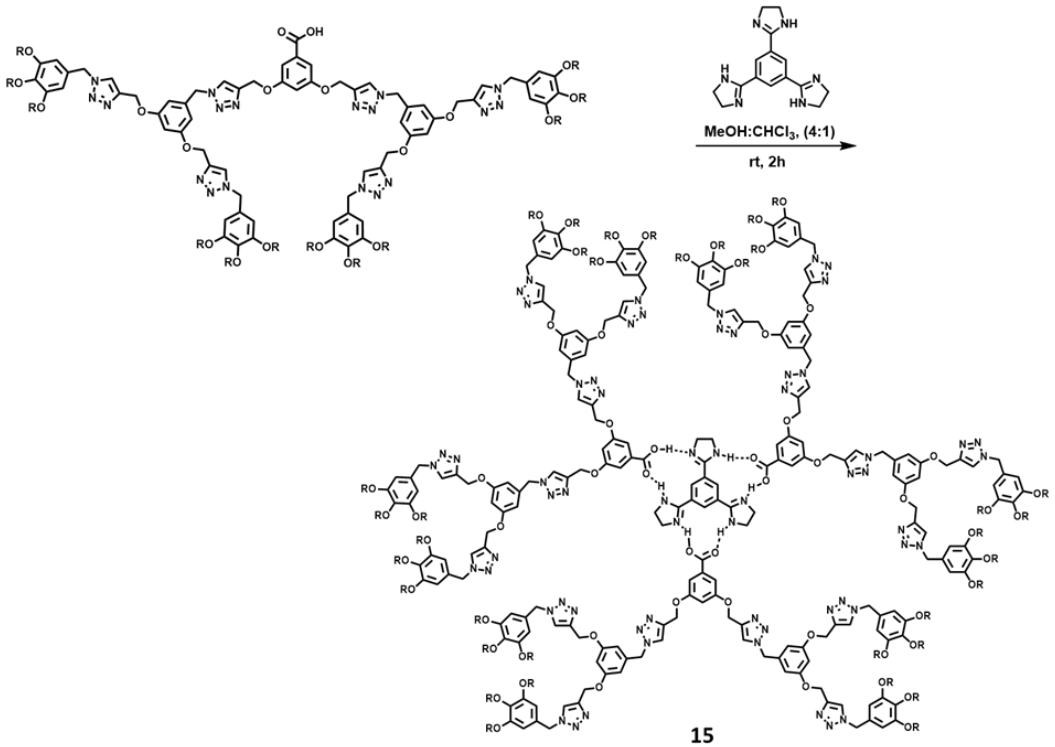

15

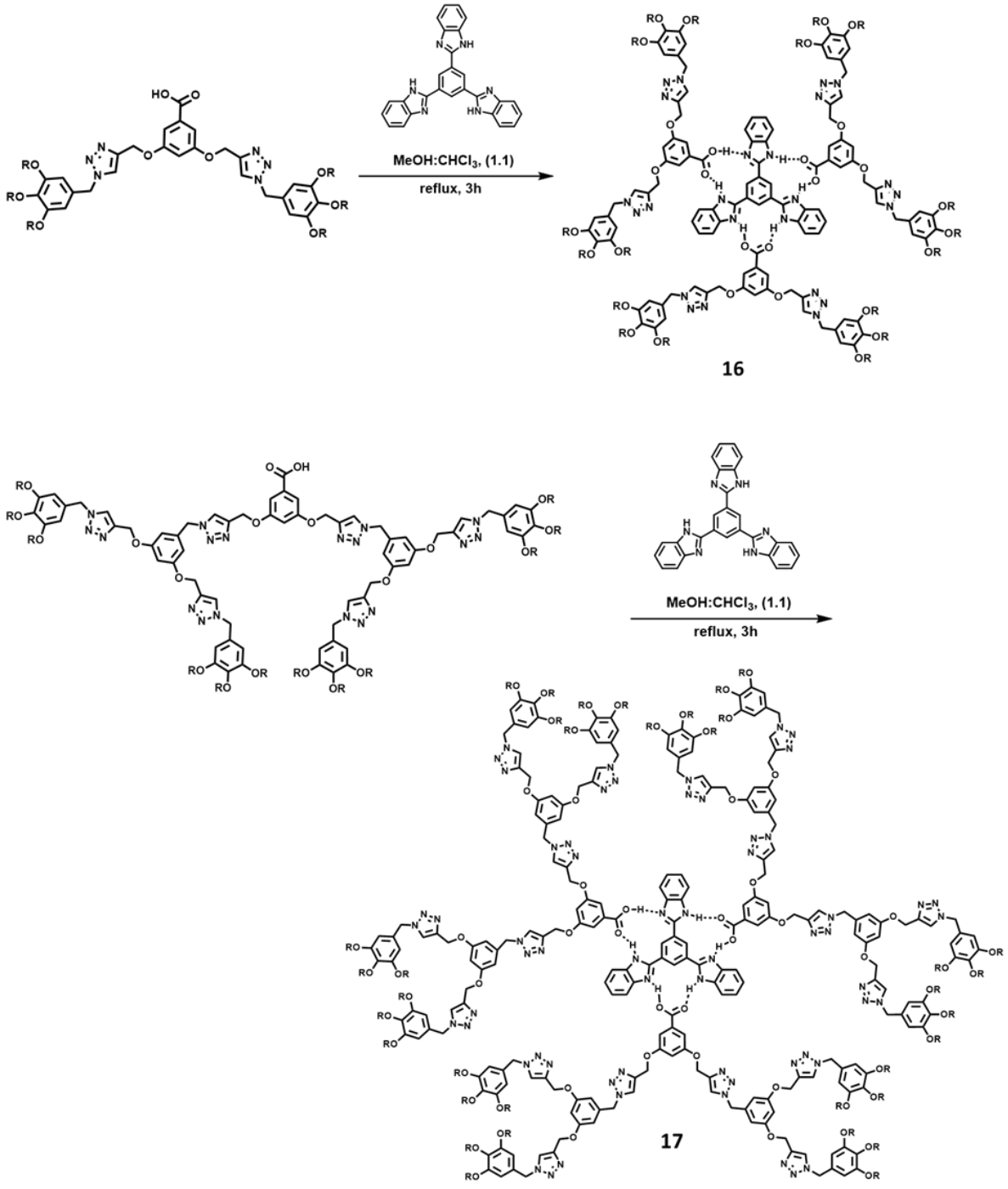

Figure 5.17: Synthetic scheme of acid-functionalized 1st and 2nd generation dendrimers and their hydrogen-bonded complexes.

5.2.2 Thermal Stability

The thermal stability of all the dendrimers and final hydrogen-bonded LC materials (**7, 9, 10, 11,** and **14 – 17**) was studied using thermogravimetric analysis. The samples were subjected to a heat scan of 10 ºC min^{-1} under a nitrogen atmosphere, recording the compound's thermal stability. They exhibit thermal stability without weight loss until 335 ºC. Upon further increasing temperature, the weight loss was observed at around 350 ºC – 475 ºC. The decomposition temperatures of all the compounds were observed at 520 ºC. The thermal stability of all the compounds is much higher than their isotropic temperature. It indicates that all compounds have excellent thermal stability. The TGA thermograms of dendrimers and hydrogen-bonded complexes are given in **Figure 5.18.**

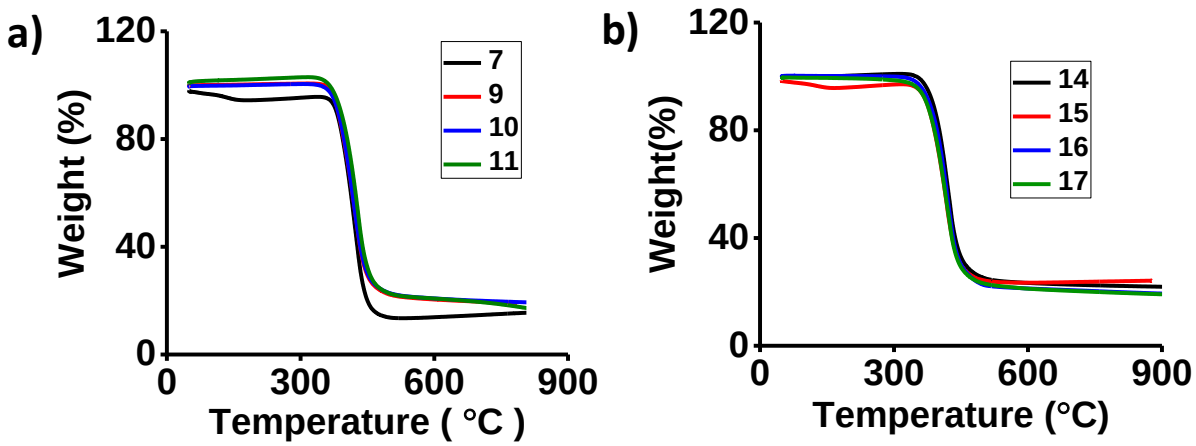

Figure 5.18: TGA thermograms of dendrimers and hydrogen-bonded complexes.

5.2.3 Mesomorphic characteristics of 7,9,10,11.

The liquid crystalline (LC) behavior of the dendrimers was investigated by polarizing optical microscopy (POM), differential scanning calorimetry (DSC), and small-angle X-ray diffraction (SAXS). All the compounds exhibited enantiotropic mesophase behavior. POM images (**Figure 5.19**) of all compounds were taken upon cooling from the isotropic phase. Compounds **7** and **9** showed the focal conic textures, which typically represent the columnar mesophase. Compounds **10** and **11** show the optically isotropic textures, which correspond to the cubic mesophase. DSC data of **7, 9, 10** and **11** show the occurrence of mesophase between a high-temperature isotropic phase and a low-temperature crystalline phase (**Figure 5.20**). The onset

temperature and enthalpy values of the phase transitions are given in (**Table 5.1**). To further confirm, the supramolecular assembly of **7, 9, 10,** and **11** small-angle x-ray scattering (SAXS). experiments were carried out using. The X-ray diffractograms of all the compounds are shown in **Figure 5.21**. Compounds **7** and **11** are found to exhibit the hexagonal columnar (Col_h) phase upon cooling from the isotropic phase, as evident from the presence of sharp diffraction peaks in the small-angle region, whose spacings (d) are in the ratio 1: $1/\sqrt{3}$: 1/2: $1/\sqrt{7}$. In the wide-angle region, the diffractograms show broad peaks at d = 4.3 - 4.50 Å, corresponding to the molten alkyl chains. The lattice parameter (a) is 38.85 Å and 42.37 Å for **7** and **11**, respectively. From the lattice parameter, the number of molecules occupying each slice of a column is estimated to be 2. The X-ray diffractograms of compound **9** at 30 ºC and compound **10** at 135 ºC show multiple peaks in the small-angle region. These peaks can be indexed on to the Pm3*n* cubic phase, and lattice parameters (a) are estimated to be 84.44 Å and 86.84 Å, respectively. For compounds **9** and **10**, the number of molecules per unit cell in the cubic lattice is 104 and 114, respectively. The d-spacings of these compounds and their Miller indices are given in **Table 5.3**, along with the lattice parameters.

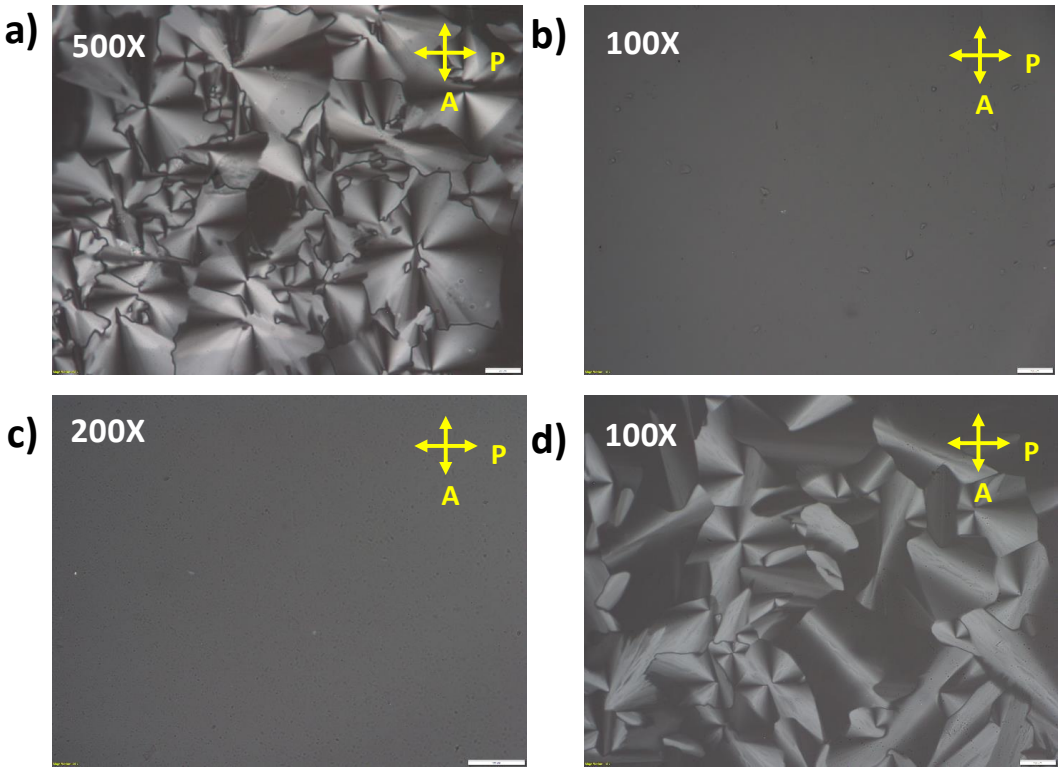

Figure 5.19: Birefringence texture observed under POM for a) Compound **7** at 95 °C b) Compound **9** at 80 °C, c) Compound **10** at 135 °C d) Compound **11** at 78 °C, at different temperatures upon cooling from the isotropic phase,

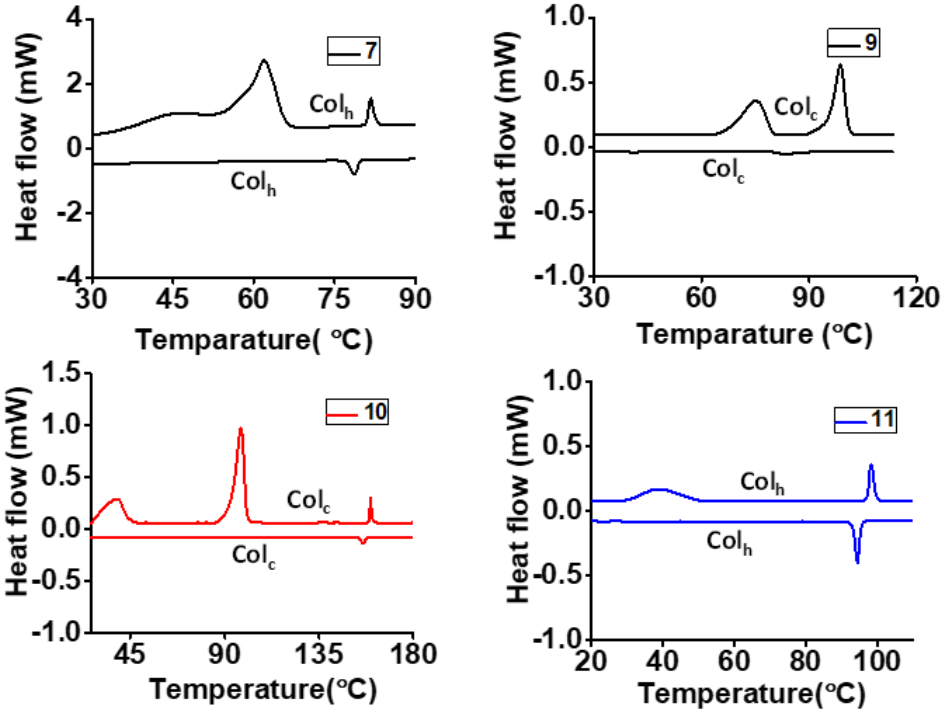

Figure 5.20: DSC thermograms obtained for the **7**, **9**, **10**, and **11** derivatives showing phase transitions during heating and cooling cycles at the scan rate of 10 °C min^{-1}.

Table 5.1: Phase transition temperatures (°C), enthalpy changes, (J/g) of dendrimers and hydrogen-bonded complexes at the time of heating and cooling obtained from DSC. Cr – Crystalline phase; Col_h – Columnar hexagonal phase; Col_c – Columnar cubic phase; I – Isotropic.

Compound	Heating	Cooling
7	Cr 61.9 (20.7) Col_h 81.7 (1.9) I	I 78.7 (1.2) Col_h
9	Cr 75.1 (10.4) Col_c 98.7 (10.9) I	I 83.1 (0.3) Col_c
10	Cr 97.7 (22.4) Col_c 159.5 (1.1) I	I 156.0 (0.6) Col_c
11	Cr 38.4 (1.4) Col_h 98.2 (1.0) I	I 94.4 (1.0) Col_h

14	Cr -10.8 (3.8) Col_h 97.8 (0.8) Col_c 193.2 (0.4) I	I 190.1 (0.3) Col_c 69.4 (1.4) Col_h -14.8 (3.4) Cr
15	Cr 60.5 (18.8) Col_c 231.2 (2.4) I	I 224.9 (0.7) Col_c
16	Cr -5.6 (4.5) Col_h 112.5 (8.7) Col_c 176.1 (0.7) I	I 168.9 (0.7) Col_c 96.8 (6.5) Col_h -11.6 (4.3) Cr
17	Cr 55.3 (4.2) Col_c 191.1 (4.4) I	I 181.3 (1.0) Col_c -20.8 (1.1) Cr

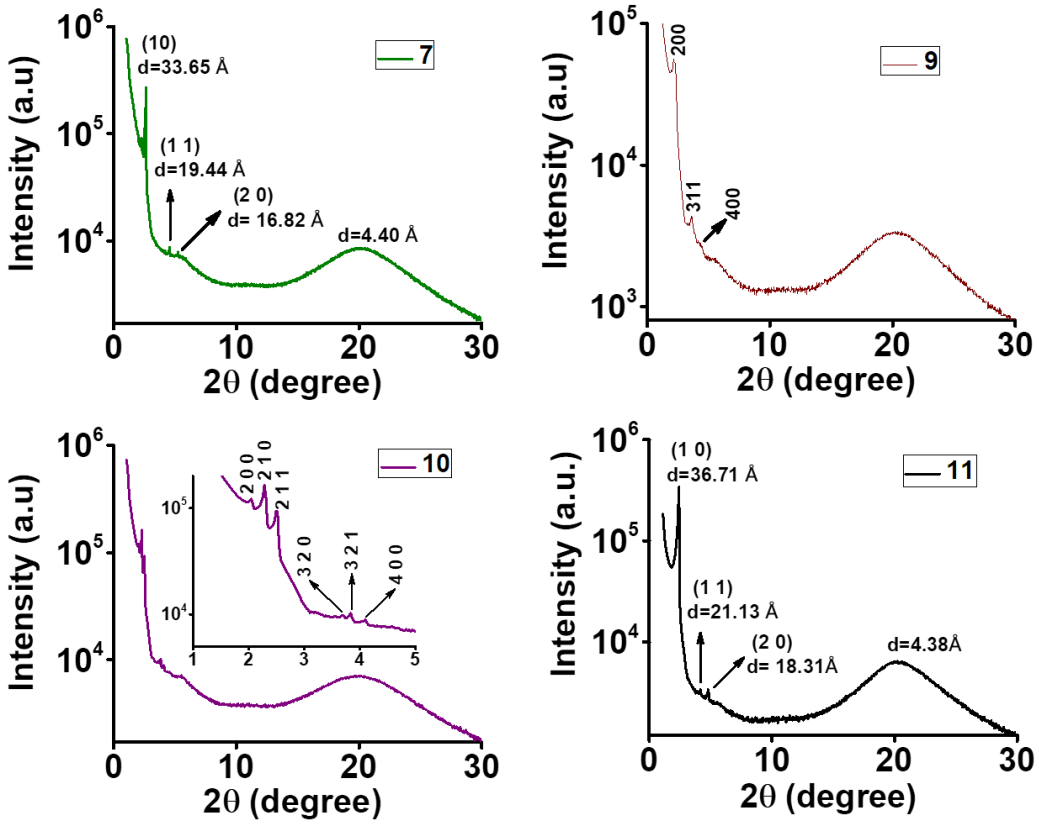

Figure 5.21: X-ray diffraction patterns of the hexagonal phase of **7** at 65 ºC, **11** at 25 ºC, and the cubic phase of **9** at 65 ºC and **10** at 135 ºC.

5.3 Detailed study of the hydrogen-bonded complexes:

Hydrogen-bonded complexes were prepared using 1:3 ratios of benzotri imidazole derivatives and 1st and 2nd generation of acid-functionalized dendrimers. Compounds **14** and **15** were prepared by dissolving the compounds **12** and **10** or **11** in a MeOH/$CHCl_3$ (1:4 v/v), stirring for two hours at room temperatures, and removing the solvents under reduced pressure.

Compounds **16** and **17** were prepared by dissolving the compounds **13** and **10** or **11** in a MeOH/$CHCl_3$ (2:3 v/v) and stirring for three hours at 60 °C, then removing the solvents to get the expected hydrogen-bonded complexes. The chemical structure of dendrimers, benzotri imidazole derivatives, H-bonded complexes, and schematic representation are shown in **Figure 5.17.** These complexes were characterized and confirmed by FTIR, NMR spectroscopic studies, and thermal analysis. These complexes show the enantiotropic liquid crystalline behavior over the wide range of temperature, implying the H-bonding strength between the compounds **12, 13,** and **10** or **11**.

5.3.1 FTIR studies of hydrogen-bonded complexes

The formation of hydrogen-bonded complexes was confirmed by using FTIR. The infrared spectra of the obtained H-bonded complex do not result from the superposition of the spectra of the pure components. The FTIR spectra of **10, 11, 12, 13,** and their H-bonded complexes **14 - 17** are given in **Figure 5.22**. The N–H stretching band of the **12** (benzotriimidazole) derivative showed at 3134 cm^{-1}. After complexation with benzotriimidazole significantly less intensive peak is observed at (3238 cm^{-1}) and also an evident change in the carbonyl stretching bands is observed between the acid and H-bonded complexes. The C=O stretching bands that appear in the acid corresponding to the dimeric form (1696 cm^{-1}). After complexation with **12** (Benzotriimidazole), C=O stretching bands, the dimeric form of the acid band is completely disappeared. The new C=O stretching band became broadened and shifted to a higher wavenumber and appeared (1639 cm^{-1}). This indicates that the formation of hydrogen bonding between **11** and **12.** A similar trend was observed in the remaining H-bonded complexes. The C=O stretching and –NH stretching frequencies of the **10-13** and all H-bonded complexes (**14 - 17**) are given in **Table 5.2**.

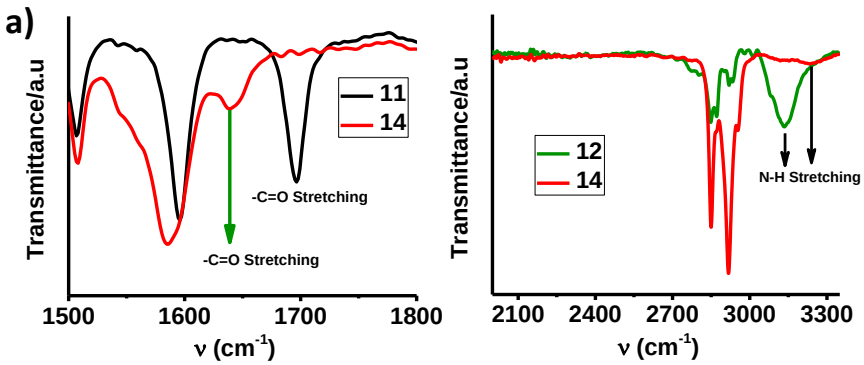

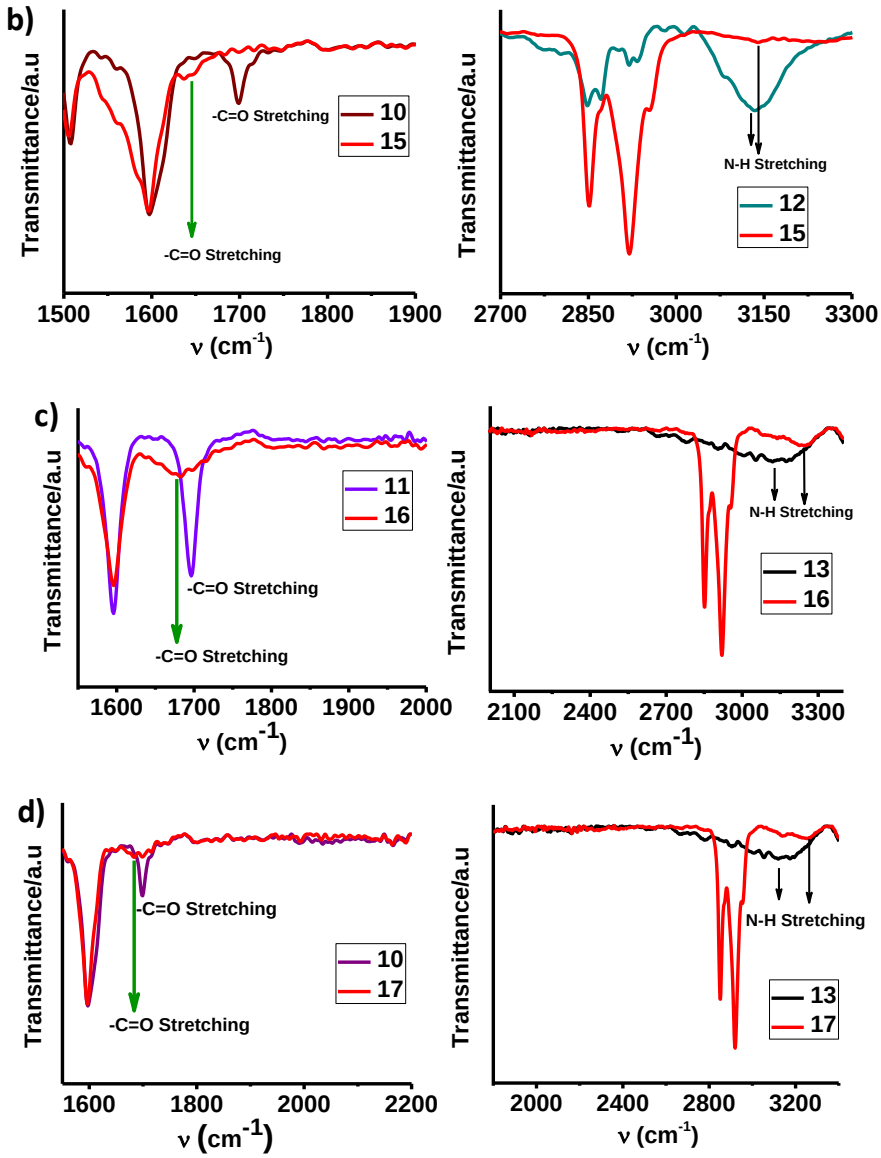

Figure 5.22: FTIR spectra: comparison in the –NH and C=O stretching region. a) pure component of **11, 12** and its H-bonded complex of **14**. b) pure component of **10, 12** and its H-bonded complex of **15**. c) pure component of **11, 13** and its H-bonded complex of **16**. d) pure component of **10, 13** and its H-bonded complex of **17**.

Table 5.2. IR stretching values of compounds **10 -17** in the region of –NH and C=O stretching region.

Compound	C=O Stretching (cm^{-1})	N-H Stretching (cm^{-1})
10	1698	--
11	1696	--
12	--	3134
13	--	3129
14	1639	3239
15	1642	3140
16	1682	3250
17	1696	3258

5.3.2 NMR studies of Hydrogen-bonded complexes

The ^{1}H NMR investigation confirmed further evidence of hydrogen bonding formation between the benotriimidazole derivatives and the 1st and 2nd generation of dendrimers. The NMR spectra of hydrogen-bonded complexes **14**, **15,** and **16, 17** were recorded in $CDCl_3$ and in 1:1 ratio of $CDCl_3$ and DMSO-d_6, respectively. The comparison NMR study of individual compounds and their H-bonded complexes of **14** and **15** are given in **Figure 5.23**. First, the proton integral peak ratio was found to be in the proportion of **12** and **11,** respectively, and these qualitative results preliminarily indicate that the complexes are indeed formed as designed. Second, we focus on the down-field shift of (Ha and Hb) protons compared to the pure benzotriimidazole derivatives because active hydrogen (e.g., N-H and COO-H) cannot be seen in the ^{1}H-NMR spectrum. This is because the proton exchange rapidly occurs between COO-H and CDCl3, while CDCl3 is used as a solvent. For the pure compound of **12**, Ha and Hb protons appear at 8.23 and 3.80 ppm, respectively. The identical protons have appeared in the H-bonded complex of **14** at 9.99 and 4.15 ppm. This clearly indicates that the formation of an H-bonded complex. A similar observation appeared in the respective H-bonded complexes of **15.** And also, identical interpretations are observed in the case of **16** and **17** with slight modifications. The comparison NMR study of individual compounds and their H-bonded complexes of **16** and **17** are given in **Figure 5.24**. The observed results are consistent and comparable with the reported literature.

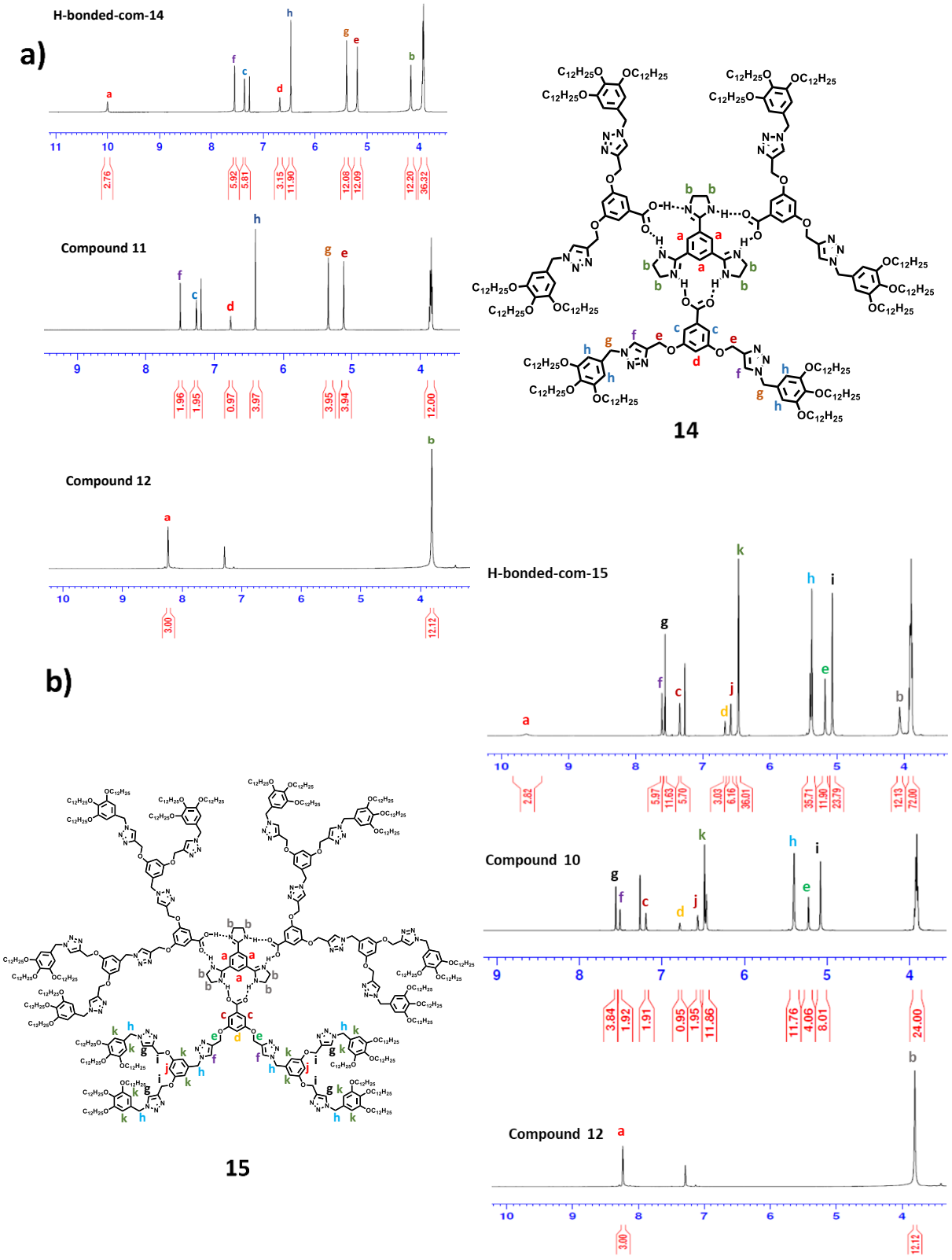

Figure 5.23: Comparative ^{1}H NMR studies of **10**, **11, 12** pure compounds, and hydrogen complex of **14** and **15** in $CDCl_3$ solution.

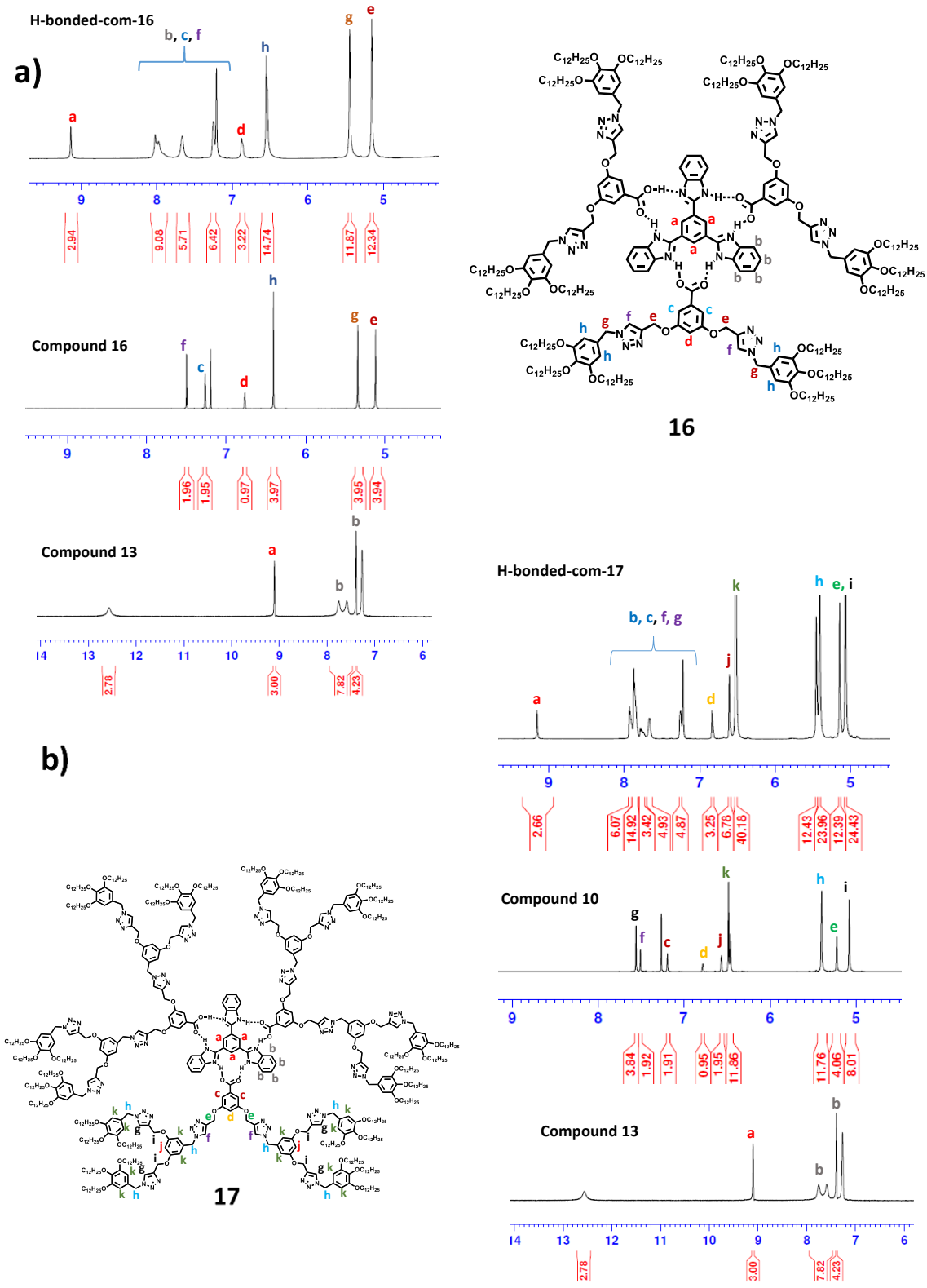

Figure 5.24. Comparative ^{1}H NMR studies of **10**, **11, 13** pure compounds, and hydrogen complex of **16** and **17** in $CDCl_3$ solution.

5.3.3 Mesomorphic characteristics of 14, 15, 16 & 17

The H-bonded supramolecular complexes with liquid crystalline properties were analyzed by using differential scanning calorimetry (DSC), polarizing optical microscopy (POM), and X-ray diffraction (XRD). Interestingly all the compounds **14 –17** were found to be mesomorphic. Compounds **14** and **16** have two mesophases: columnar hexagonal and columnar cubic. However, compounds **15** and **17** exhibits only columnar cubic mesophase. DSC was used to investigate the mesophase behavior of all H-bonded complexes. **Figure 5.25** depicts the thermograms of these compounds. Compounds **14** and **16** clearly show the three transition peaks associated with the two mesophases. These compounds exhibit the columnar hexagonal mesophase at room temperatures, and this transition appears at 97.84 ºC and 112.52 ºC, which becomes isotropic at 193.22 ºC and 176.17 ºC. On cooling from the isotropic phase, a columnar cubic phase occurs at 190.19 ºC and 168.90 ºC, respectively. Upon further cooling, columnar hexagonal mesophase appeared at 69.46 ºC and 96.82 ºC and crystallized below -10 ºC. Compounds **15** and **17** exhibit two transition peaks that correspond to the single mesophase. We also observe the broad melting temperature at 60.55 ºC and 55.37 ºC, and then it becomes isotropic at around 231.27 ºC and 198.18 ºC, respectively. Upon cooling from the isotropic phase, the columnar cubic phase appeared at 224.95 ºC and 181.38 ºC, respectively, and this phase was unaltered till room temperature. The observed phase transition temperatures and corresponding enthalpy values are given in **Table 5.1.**

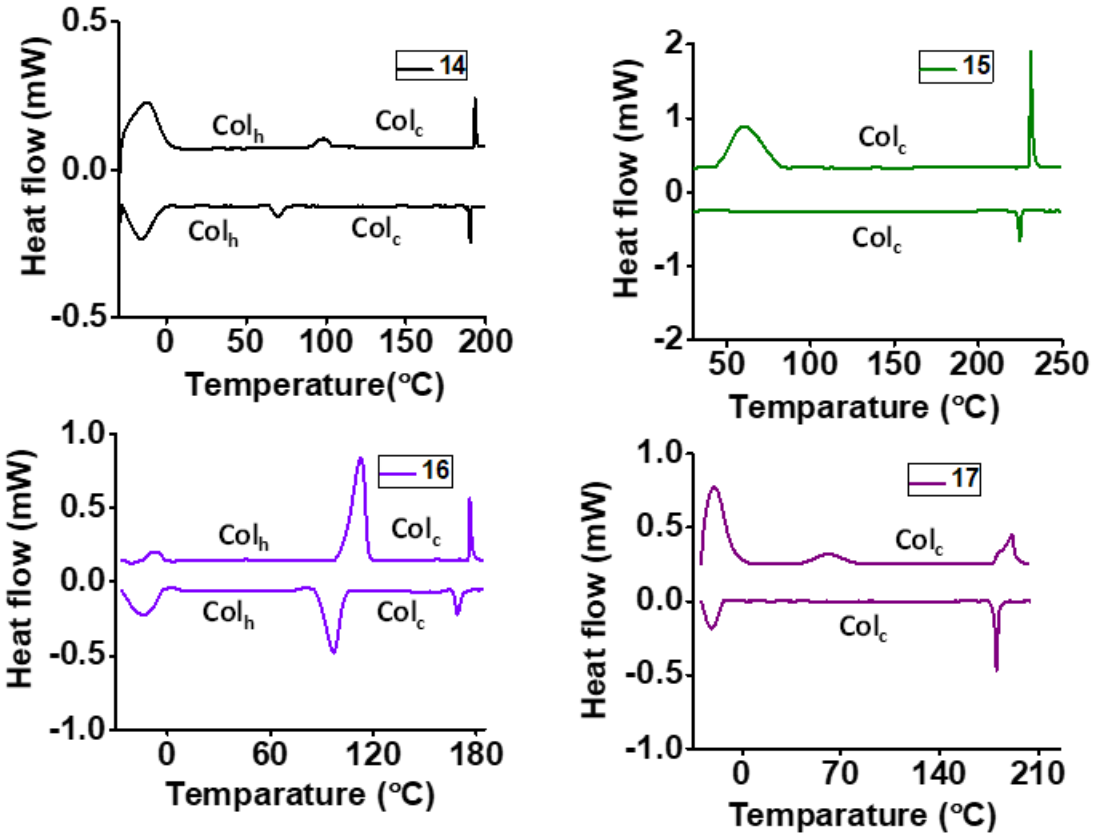

Figure 5.25: DSC thermograms obtained for the **14**, **15**, **16**, and **17** derivatives showing phase transitions during heating and cooling cycles at a scan rate of 10 ºC min^{-1}.

The transition temperatures and enthalpy values of H-bonded complexes were investigated by DSC and which was further validated by POM. The liquid crystalline texture is observed using polarised optical microscopy under cross polarisers upon cooling from the isotropic temperatures. Compound **14** exhibits two mesophases. Upon cooling, it displays the optically isotropic texture from a range of 190 ºC to 69 ºC. The same sample shows the plate-like textures at room temperature on further cooling, which corresponds to the columnar mesophase. On the other hand, compounds **16** exhibit the two mesophases. Upon cooling, it displays the optically isotropic texture from a range of 168 ºC to 96 ºC. The same sample shows the plate-like textures at room temperature on further cooling, which corresponds to the columnar mesophase. Compounds **15** and **17** only show the optically isotropic texture upon cooling from the isotropic phase. All the POM textures were given in **Figure 5.26.** These complexes were repeatedly checked under POM upon heating and cooling the samples several times even though there is

no phase segregation, which implies that the two compounds remain intact through the strong H-bonding.

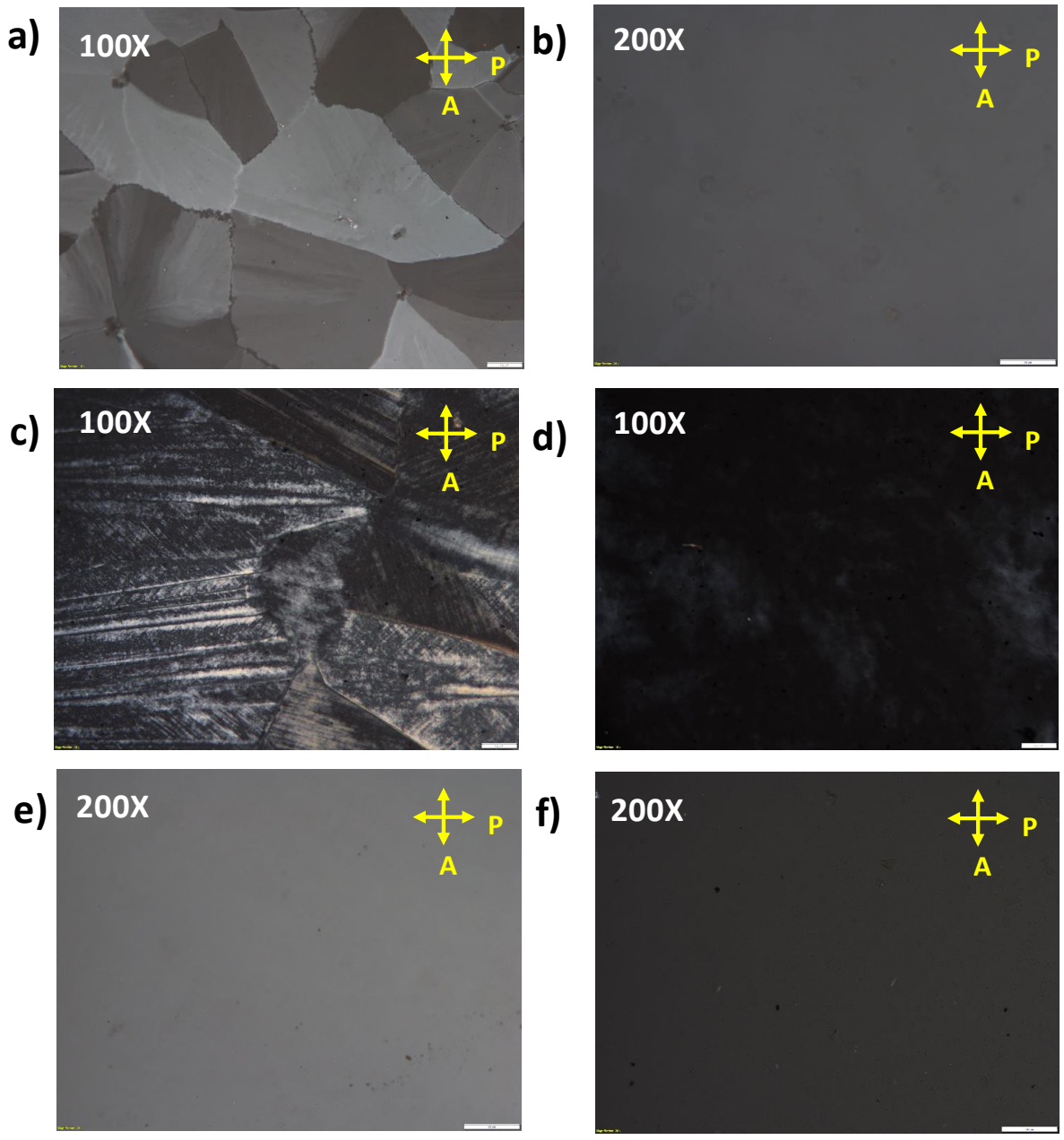

Figure 5.26. Birefringence texture observed under POM for a compound a) and b) Compound **14** at 80 °C, and 130 °C, c) and d) Compound **16** at 90°C, and 140 °C, e) Compound **15** at 140 °C, f) Compound **17** at 150 °C at different temperature upon cooling from the isotropic phase.

The liquid crystalline phase behavior of H- bonded complexes (compound **14**, **15**, **16**, and **17**) was examined using X-ray diffraction (XRD) studies on cooling from the isotropic phase. The X-ray diffraction patterns of the H-bonded complexes of **14** and **16** are given in **Figure 5.27**. DSC and POM studies indicate the formation of two different mesophases in compounds **14** and **16**. Hence X-ray diffraction studies were carried out at temperatures corresponding to the two mesophases. Compound **14** exhibits four sharp peaks at 50 ºC, and compound **16** exhibits six sharp peaks at 28 ºC in the small-angle region. These spacings are in the ratio of 1: 1/√3: 1/2: 1/√7: 1/√9: 1/√13 correspondings to the columnar hexagonal phase. The lattice parameter (a) is found to be 48.57 Å and 51.57 Å, respectively. The wide-angle region exhibits two broad peaks, one at around 4.3 Å corresponding to molten alkyl chain, along with a core-core peak at 3.44 Å and 3.57 Å, respectively for compounds **14** and **16**. All the sharp peaks in the small-angle region can be indexed on the two-dimensional hexagonal lattice. The number of molecules occupying a single slice of the column (Z) was calculated using the XRD data and is found to be very close to 1. At higher temperatures, both the compounds **14** and **16** show a few sharp peaks in the small-angle region, with their d-spacing in the ratio of 1/√4:1/√10:1/√21 and 1/√5:1/√12:1/√16:1/√18:1/√22:1/√30:1/√37:1/√50:1/√53:1/√86:1/√108 respectively, that corresponds to the (2 0 0), (3 1 0), (4 2 1) and (2 1 0), (2 2 2), (4 0 0), (4 1 1), (3 3 2), (5 2 1), (6 1 0), (5 5 0), (7 2 0), (7 6 1), (10 2 2) reflections from a cubic lattice belonging to the space group *Pm3n*. The broad peak show at 4.5 Å in the wide-angle region corresponds to the molten alkyl chains. The lattice parameters (a) of these compounds are 75.38 and 81.12. The number of molecules in the unit cell of the cubic lattice is 51 and 81. The d-spacings of these compounds and their Miller indices are given in **Table 5.3**, along with the lattice parameters.

Table 5.3: Layer spacings obtained from XRD patterns for **7, 11, 14,** and **16. Hexagonal: (**lattice area $\mathbf{S_h} = (\sqrt{3}/2)a^2$; lattice volume $\mathbf{V_h} = S_h\, h_c$ (**h_a** if **h_c** is not observed); No. of molecules per slice of column (**Z**) = $N_a\, \rho \mathbf{V_h}/M$; $\mathbf{N_a}$ = Avogadro's number; ρ = density; **a**=lattice parameter; **h_c**=core core peak; **h_a** chain peak; **M** = molecular weight). C**ubic: a**= lattice parameter; No. of molecules per unit cell in the cubic lattice (Z) = $a^3\rho N_A/M$; ρ is asuumed to be 1 gcm^{-3}).

Compounds	T (°C)	d-spacing(Å)	Phase	Parameters
7	65	33.65 (1 0), 19.44 (1 1), 16.82 (2 0) 4.41	Col_h	**a** = 38.85 Å $\mathbf{S_h}$ = 1307.44 $Å^2$ $\mathbf{V_h}$ = 5765.84$Å^3$ **Z** = 2.1
9	30	42.20 (2 0 0), 25.07 (3 1 1), 20.91 (4 0 0), 4.40	Col_C	**a** = 84.44 Å **Z** = 104.3
10	135	43.42 (2 0 0), 38.65 (2 1 0), 35.25 (2 1 1), 23.88 (3 2 0), 23.05 (3 2 1), 21.58 (4 0 0), 4.48	Col_C	**a** = 86.84 Å **Z** = 114.0
11	25	36.71 (1 0), 21.13 (1 1), 18.31 (2 0) 4.38	Col_h	**a** = 42.38 Å $\mathbf{S_h}$ = 1555.43 $Å^2$ $\mathbf{V_h}$ = 6812.81$Å^3$ **Z** = 2.4
14	50	42.07 (1 0), 24.02 (1 1), 20.88 (2 0), 15.80 (2 1), 4.40, 3.44	Col_h	**a** = 48.57 Å $\mathbf{S_h}$ = 2042.99 $Å^2$ $\mathbf{V_h}$ = 7027.89$Å^3$ **Z** = 0.8
14	110	37.69 (2 0 0), 23.73 (3 1 0), 16.50 (4 2 1), 4.51	Col_C	**a** = 75.38 Å **Z** = 50.6
15	186	46.96 (2 0 0), 41.75 (2 1 0), 38.49 (2 1 1), 25.56 (3 2 1), 23.53 (4 0 0), 4.50	Col_C	**a** = 93.93 Å **Z** = 46.8
16	28	44.67 (1 0), 25.79 (1 1), 22.49 (2 0), 16.95 (2 1), 14.89 (3 0), 12.44 (3 1), 4.33, 3.57	Col_h	**a** = 51.58 Å $\mathbf{S_h}$ = 2304.05 $Å^2$ $\mathbf{V_h}$ = 8225.48 $Å^3$ **Z** = 0.9
16	150	70.30 (2 1 0), 45.46 (2 2 2), 39.09 (4 0 0), 36.55 (4 1 1), 33.30 (3 3 2), 28.84 (5 2 1), 25.87 (6 1 0), 22.19 (5 5 0), 21.61 (7 2 0), 16.97 (7 6 1), 15.11 (10 2 2) 4.59	Col_C	**a** = 157.21Å **Z** = 447.1
17	170	64.86 (1 1 0), 46.16 (2 0 0), 41.27 (2 1 0), 37.74 (2 1 1), 32.51 (2 2 0), 29.15 (3 1 0), 26.65 (2 2 2), 25.50 (3 2 0), 24.69 (3 2 1), 23.06 (4 0 0), 18.95 (4 2 2), 18.09 (4 3 1), 17.09 (4 3 2), 4.54	Col_C	**a** = 91.73Å **Z** = 43.0

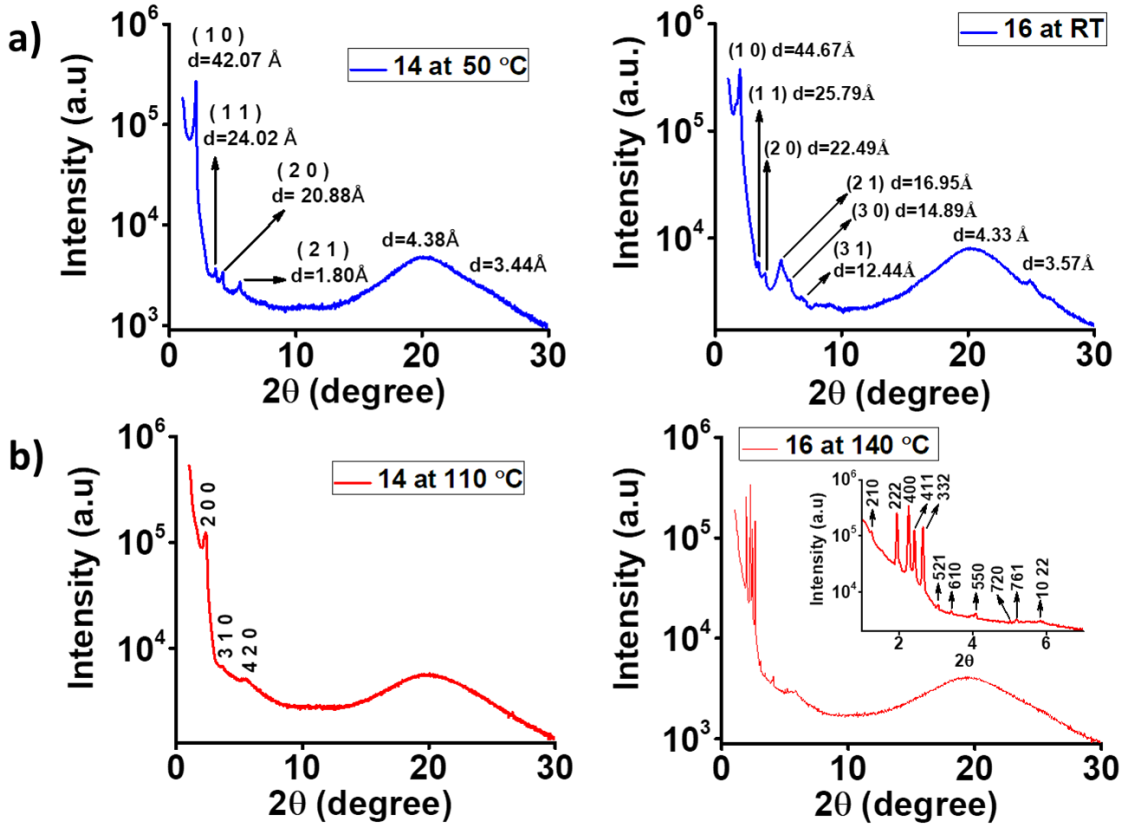

Figure 5.27: X-ray diffraction patterns of **14** and **16** obtained upon cooling from the isotropic phase showing the hexagonal columnar phase at low temperatures (a) and the cubic phase at higher temperatures (b)

For compounds **15** and **17**, the x-ray diffractograms show that the supramolecular assembly exists in the *Pm3n* cubic phase. Multiple sharp peaks are observed in the small-angle region, in the ratio of 1/√4:1/√5:1/√6:1/√14:1/√16 and 1/√2:1/√4:1/√5:1/√6:1/√8:1/√10:1/√12:1/√13:1/√14:1/√16:1/√24:1/√26:1/√29, which can be indexed on the *Pm3n* cubic lattice. The lattice parameter (a) of the cubic phase found to be 93.93 Å and 129.73 Å, respectively, for compounds **15** and **17**. In the wide-angle region,a broad peak is observed at 4.5 Å, corresponding to molten alkyl chains. The number of molecules in the unit cell of the cubic lattice is 47 and 122. The details of the indexing are given in **Table 5.3,** and the X-ray diffractograms are presented in **Figure 5.28.**

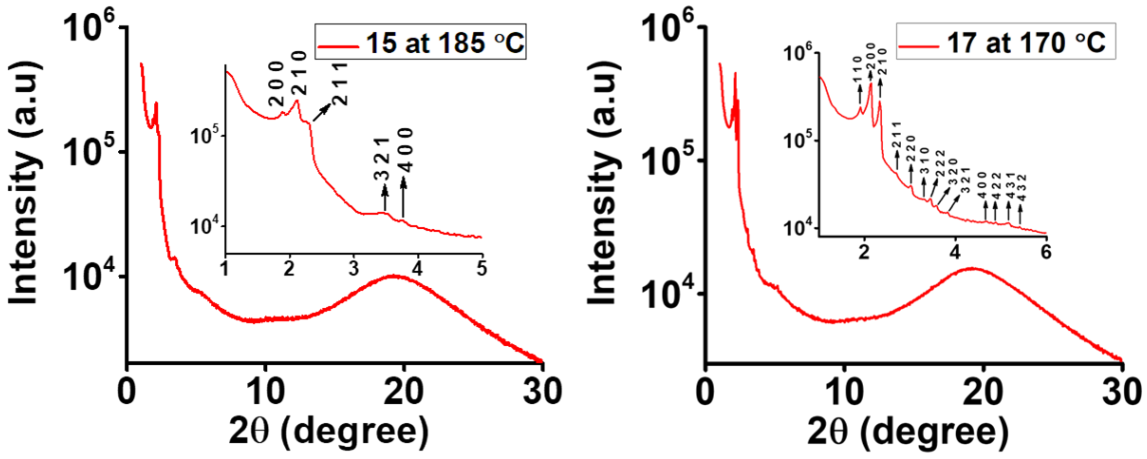

Figure 5.28: X-ray diffraction patterns of the **15** at 185 ºC and **17** at 170 ºC, in the cubic phase.

5.4 Conclusion:

In summary, we have successfully synthesized the 1st and 2nd generation dendrimers with a functional group of carboxylic acid using click chemistry and benzotriimidazole derivatives. 1st generation dendrimers contain carboxylic acid and alcohol functional groups, which exhibit the hexagonal columnar mesophase. 2nd generation dendrimers have carboxylic acid, and ester shows the columnar cubic mesophase. The mesophase behavior was confirmed by the POM, DSC, and X-ray diffractometry. The gallic acid dendrimer derivatives and benzotriimidazole derivatives were successfully designed to form hydrogen-bonded complexes. FTIR and ^{1}H NMR studies confirmed the formation of hydrogen-bonded complexes and their stability. All the H-bonded complexes exhibit mesomorphic properties. These results suggest a decisive role of mesogenic driving forces (mainly H-bonding) to help the formation of the 1:3 complex in bulk. Interestingly compounds **14** and **16** exhibit room temperature liquid crystals. It shows the columnar hexagonal mesophase at room temperatures and high temperatures columnar cubic phase. In the case of compounds **15** and **17,** it exhibits cubic mesophase. The facile formation of these dendritic hydrogen-bonded complexes using noncovalent interactions can make boundless use in the DLCs limiting due to their synthesis and solubility problem. The results and study of the hydrogen-bonded liquid crystals present here may find application in the field of switching devices, optical data storage, and optoelectronics.

5.5 Experimental section:

Materials and Methods

Referee the page number 65

5.6 Synthesis and characterization:

Compound 1: (**Figure 5.17**) To a solution of 3,5 dihydroxy benzoic acid (10.0 g, 64.88 mmol, 1eq) in methanol (200 ml) was added concentrated sulfuric acid (13.8 ml, 25.45g, 129.76 mmol, 2eq). The solution was allowed to reflux for 8h. Completion of the reaction was confirmed by TLC, and the solvent was removed using Rotavapor. After that, the crude solid was dissolved in ethyl acetate, washed with $NaHCO_3$ solution, dried over anhydrous Na_2SO_4, and evaporated the solvent to get the desired product. Yield: 92%; ^{1}H NMR (500 MHz, Methanol-d_4): δ (ppm) = 6.94 (d, *J* = 2.50 Hz, 2H), 6.50 (t, *J* = 4.50 Hz, 1H), 3.86 (s, 3H); ^{13}C NMR (125 MHz, $CDCl_3$): δ ppm = 168.93, 159.70, 133.06, 109.00, 108.45, 52.77. Elemental analysis: C, 57.14; H, 4.80 calculated (%): C, 57.64; H, 5.10(expt. %).

Compound 2: To a solution of methyl 3,5 dihydroxybenzoates (8 g, 47.57 mmol, 1eq) in acetone (150 ml), K_2CO_3 (19.72 g, 142.72 mmol, 3eq) was added. Then the reaction mixture was stirred for 30 min at room temperature under nitrogen. Propargyl bromide (80% in toluene, 20.47 ml) was added, and the reaction mixture was kept at 80 ºC for 6h. After completion of the reaction, the solvent was removed under reduced pressure and extracted with $CHCl_3$. The organic layer was dried over anhydrous Na_2SO_4. The pure product was obtained by column chromatography using petroleum ether and dichloromethane (8:2) as eluent and dried under a high vacuum to get the desired product as a white solid. Yield: 92%; ^{1}H NMR (500 MHz, $CDCl_3$): δ (ppm) = 7.29 (d, *J* = 1.0 Hz, 2H), 6.81 (s, 1H), 4.71 (d, 4H), 3.91 (s, 3H), 2.54 (s, 2H); ^{13}C NMR (125 MHz, $CDCl_3$): δ ppm = 166.46, 158.50, 132.15, 108.88, 107.51, 77.97, 76.00, 56.12, 52.37. Elemental analysis: C, 68.85; H, 4.95 calculated (%): C, 68.63; H, 4.93(expt. %).

Compound 3: In a round bottom flask, ethyl gallate (10 g, 198.17 mmol, 1 eq) was dissolved in 500 mL of DMF, K_2CO_3 (41.84 g, 302.76 mmol, 6 eq) was added to it and stirred for 15 minutes, 1-Bromododecane (50.30 g, 201.84 mmol, 4 eq) and Potassium iodide (catalytic amount) were added to it the reaction mixture was refluxed for overnight. After completion of

the reaction, it was cooled to room temperature, then the reaction mixture was poured into the ice water, and the precipitate was filtered. The crude product was purified by column chromatography using petroleum ether: dichloromethane (8:2) as eluent and dried under a high vacuum to get the desired product as a white solid. Yield: 83%; ^{1}H NMR (500 MHz, $CDCl_3$): δ (ppm) = 7.17 (s, 2H), 3.94 – 3.92 (m, 6H), 3.81 (s, 3H), 1.76 – 1.63 (m, 6H), 1.42 – 1.36 (m, 6H), 1.27 – 1.19 (m, 48H), 0.80 (t, *J* = 6.25 Hz, 9H); ^{13}C NMR (125 MHz, $CDCl_3$): δ ppm = 166.93, 152.81, 142.33, 124.65, 107.94, 73.47, 69.14, 52.08, 31.94, 30.34, 29.77, 29.74, 29.72, 29.68, 29.65, 29.58, 29.41, 29.39, 29.31, 26.09, 26.07, 22.71, 14.11. Elemental analysis: C, 76.69; H, 11.70 calculated (%): C, 76.85; H, 12.15(expt. %).

Compound 4: In a round bottom flask, compound 3 (5 g, 5.83 mmol, 1eq), was dissolved in 100 ml of dry tetrahydrofuran and cooled to 0 ºC and $LiAlH_4$ (0.331 g, 8.74 mmol, 1.5 eq), was added to the reaction mixture portion-wise and allowed to room temperature and the reaction mixture kept for overnight, after completion of the reaction, the reaction mixture was quenched. The reaction mixture was extracted with a dichloromethane organic layer, was dried over anhydrous Na_2SO_4, and the solvent was evaporated. The crude product was purified by column chromatography using petroleum ether and dichloromethane (7:3) as eluent and dried under a high vacuum to get the desired product. Yield: 97%; ^{1}H NMR (500 MHz, $CDCl_3$): δ (ppm) = 6.57 (s, 2H), 4.61 (s, 2H), 4.00 – 3.94 (m, 6H), 1.82 – 1.74 (m, 6H), 1.48 (bm, 6H), 1.28 (bm, 48H), 0.9 (t, *J* = 6.25 Hz, 9H); ^{13}C NMR (125 MHz, $CDCl_3$): δ ppm = 153.25, 137.57, 136.12, 105.36, 73.45, 69.12, 65.59, 31.95, 31.93, 30.33, 29.76, 29.75, 29.71, 29.67, 29.63, 29.44, 29.40, 29.37, 26.15, 26.12, 22.69, 14.10. Elemental analysis: C, 78.12; H, 12.20 calculated (%): C, 78.82.63; H, 12.56(expt. %).

Compound 5: To a solution of 4 (0.5 g, 0.75 mmol, 1 eq) in toluene (10 ml) 1, 8-diazabicyclo (5.4.0) undec-7-ene (DBU) (0.29 g, 1.96 mmol, 2.6 eq) and diphenyl phosphoryl azide (DPPA) (0.44 g, 1.73 mmol, 2.3 eq) were added. Then the reaction mixture was stirred at 80 ºC for 12h. After completion of the reaction, the reaction mixture was quenched with saturated NH_4Cl solution and extracted with $CHCl_3$. The organic layer was dried over anhydrous Na_2SO_4, and the solvent was removed. The crude product was purified by column chromatography using petroleum ether and dichloromethane (7:3) as eluent and dried under a high vacuum to get the desired product as a white solid. Yield: 80%; ^{1}H NMR (500 MHz, $CDCl_3$): δ (ppm) = 6.41 (s, 2H), 4.16 (s, 2H), 3.91 – 3.85 (m, 6H), 1.75 – 1.63 (m, 6H), 1.42 – 1.36 (m, 6H), 1.27 – 1.19

(m, 48H), 0.81 (t, *J* = 7.0 Hz, 9H); ^{13}C NMR (125 MHz, $CDCl_3$): δ ppm = 153.36, 138.14, 130.37, 106.61, 73.43, 69.16, 55.19, 31.95, 30.35, 29.78, 29.76, 29.72, 29.69, 29.66, 29.63, 29.44, 29.42, 29.41, 29.39, 26.14, 26.11, 22.71, 14.12. Elemental analysis: C, 75.27; H, 11.61; N, 6.12 calculated (%): C, 75.18; H, 11.93, N, 6.05 (expt. %).

Compound 6: To a solution of 2 (0.9 g, 3.68 mmol, 1 eq) and compound 5 (5.30 g, 7.73 mmol, 2.1 eq) in 150 ml of tetrahydrofuran, water (3:1 ratio). Then the reaction mixture was stirred for 15min. CuSO4 (0.0294g, 0.1842 mmol, 0.05 eq) was dissolved with the minimum amount of water and added to the reaction mixture after 5 min. Sodium ascorbate (0.0671g, 0.339, 0.092eq) was dissolved with the minimum amount of water added to the reaction mixture, and the reaction mixture was kept at room temperature for 12h. After completion of the reaction, the reaction mixture was kept at 0 ºC, diluted with water, added 26 ml of ammonia solution, stirred for 20 min, and extracted with $CHCl_3$. The organic layer was dried over anhydrous Na_2SO_4. The crude product was purified by column chromatography using petroleum ether and ethyl acetate (9:1) as eluent and dried under a high vacuum to get the desired product as a white solid. Yield: 92%; ^{1}H NMR (500 MHz, $CDCl_3$): δ (ppm) = 7.48 (s, 2H), 7.20 – 7.19 (m, 2H), 6.73 – 6.72 (m, 1H), 6.39 (s, 4H), 5.33 (s, 4H), 5.10 (s, 4H), 3.86 – 3.81 (m, 15H), 1.72 – 1.62 (m, 12H), 1.40 – 1.34 (m, 12H), 1.22 – 1.18 (m, 96H), 0.80 (t, *J* = 7.0 Hz, 18H),; ^{13}C NMR (125 MHz, $CDCl_3$): δ ppm = 166.49, 159.25, 153.62, 143.86, 138.53, 132.17, 129.20, 122.68, 108.66, 106.73, 73.47, 69.24, 62.26, 54.59, 52.29, 31.95, 31.93, 30.34, 29.76, 29.75, 29.72, 29.67, 29.65, 29.61, 29.44, 29.40, 29.38, 26.12, 26.10, 22.70, 14.11. Elemental analysis: C, 74.30; H, 10.60; N, 5.20 calculated (%): C, 74.36; H, 11.01, N, 5.15 (expt. %).

Compound 7: In a round bottom flask, compound 6 (3 g, 1.88 mmol, 1 eq), was dissolved in 100 mL of dry tetrahydrofuran and cooled to 0 ºC and $LiAlH_4$ (0.107g, 2.833 mmol, 1.5eq), was added to the reaction mixture portion wise and allowed to room temperature and the reaction mixture kept overnight, after completion of the reaction, the reaction mixture was quenched methanol. The reaction mixture was extracted with a dichloromethane organic layer, was dried over anhydrous Na_2SO_4, and the solvent was evaporated using rotavapor. The crude product was purified by column chromatography using petroleum ether and ethyl acetate (7:3) as eluent and dried under a high vacuum to get the desired product as a white solid. Yield: 95%; ^{1}H NMR (500 MHz, $CDCl_3$): δ (ppm) = 7.57 (s, 2H), 6.62 (s, 2H), 6.53 (s, 1H), 6.48 (s, 4H),

5.42 (s, 4H), 5.16 (s, 4H), 4.62 (s, 2H), 3.95 – 3.91 (m, 12H), 1.85 – 1.73 (m, 12H), 1.49 – 1.43 (m, 12H), 1.31 – 1.27 (m, 96H), 0.88 (t, *J* = 6.75 Hz, 18H); ^{13}C NMR (125 MHz, $CDCl_3$): δ ppm = 159.47, 153.60, 144.21, 143.91, 138.50, 129.23, 122.72, 106.76, 105.86, 100.94, 73.49, 69.25, 64.89, 61.97, 54.59, 31.94, 30.34, 29.77, 29.75, 29.72, 29.71, 29.68, 29.66, 29.62, 29.45, 29.41, 29.38, 26.13, 26.11, 22.71, 14.13. Elemental analysis: C, 74.86; H, 10.79; N, 5.29 calculated (%): C, 74.74; H, 11.32, N, 5.31(expt. %).

Compound 8: To a solution of 7 (7 g, 4.406 mmol, 1 eq) in toluene (100 ml) 1,8-diazabicyclo (5.4.0) undec-7-ene (DBU) (1.801 g, 11.45 mmol, 2.6 eq) and diphenyl phosphoryl azide (DPPA) (2.60 g, 1.915 mmol, 2.3 eq) were added. Then the reaction mixture was stirred at 80 ºC for 12h. After completion of the reaction, the reaction mixture was quenched with saturated NH_4Cl solution and extracted with $CHCl_3$. The organic layer was dried over anhydrous Na_2SO_4, and the solvent was removed. The crude product was purified by column chromatography using petroleum ether and ethyl acetate (8:2) as eluent and dried under a high vacuum to get the desired product as a white solid. Yield: 80%; ^{1}H NMR (500 MHz, $CDCl_3$): δ (ppm) = 7.57 (s, 2H), 6.60 (s, 1H), 6.56 (s, 2H), 6.48 (s, 4H), 5.42 (s, 4H), 5.17 (s, 4H), 4.26 (s, 2H), 3.95 – 3.91 (m, 12H), 1.82 – 1.67 (m, 12H), 1.49 – 1.43 (m, 12H), 1.31 – 1.27 (m, 96H), 0.89 (t, *J* = 6.5 Hz, 18H), ; ^{13}C NMR (125 MHz, $CDCl_3$): δ ppm = 159.66, 153.62, 144.03, 138.52, 137.79, 129.19, 122.69, 107.49, 106.75, 101.53, 73.48, 69.24, 62.12, 54.65, 54.62, 31.94, 30.33, 29.77, 29.75, 29.72, 29.67, 29.65, 29.62, 29.44, 29.41, 29.38, 26.12, 26.10, 22.71, 14.13. Elemental analysis: C, 73.70; H, 10.56; N, 7.81 calculated (%): C, 73.75; H, 10.48, N, 7.74 (expt. %).

Compound 9: To a mixture of 2 (0.5 g, 2.047 mmol, 1 eq) and compound 8 (6.93 g, 4.29 mmol, 2.1 eq) in 100 ml of tetrahydrofuran: water (3:1 ratio)was added. Then the reaction mixture was stirred for 15min. $CuSO_4$ (0.0163 g, 0.102 mmol, 0.05 eq) was dissolved with the minimum amount of water and added to the reaction mixture after 5 min. Sodium ascorbate (0.0373 g, 0.188 mmol, 0.092 eq) was dissolved with the minimum amount of water added to the reaction mixture, and the reaction mixture was kept at room temperature for 12h. After completion of the reaction, the reaction mixture was kept at 0 ºC, diluted with water, added 26 ml of ammonia solution, stirred for 20 min, and extracted with $CHCl_3$. The organic layer was dried over anhydrous Na_2SO_4. The crude product was purified by column chromatography using petroleum ether and ethyl acetate (9:1) as eluent and dried under a high vacuum to get the desired product as a white solid. Yield: 92%; ^{1}H NMR (500 MHz, $CDCl_3$): δ (ppm) = 7.59 (s,

2H), 7.55 (s, 4H), 7.26 (s, 2H), 6.80 (s, 1H), 6.59 (s, 2H), 6.48 – 6.47 (m, 12H), 5.42 – 5.39 (m, 12H), 5.16 (s, 4H), 5.08 (s, 8H), 3.93 – 3.88 (m, 24H), 3.86 (s, 3H), 1.79 – 1.69 (m, 24H), 1.61(bs, 24H) 1.46 – 1.41 (m, 24H), 1.29 – 1.25 (m, 168H), 0.87 (t, J = 6.5 Hz, 36H), ^{13}C NMR (125 MHz, $CDCl_3$): δ ppm = 166.49, 159.86, 159.21, 153.61, 143.95, 143.72, 138.52, 136.81, 132.16, 129.26, 123.07, 122.89, 108.76, 107.42, 106.91, 106.77, 101.91, 73.48, 69.26, 62.19, 61.99, 54.57, 54.09, 52.27, 31.95, 31.94, 30.35, 29.77, 29.72, 29.67, 29.66, 29.63, 29.45, 29.38, 26.12, 22.70, 14.12. . Elemental analysis: C, 73.36; H, 10.16; N, 7.26 calculated (%): C, 73.02; H, 9.66, N, 7.25 (expt. %).

General Procedure for the synthesis of 10 and 11

In a round bottom flask, 9 or 10 (1eq) was dissolved in ethanol, NaOH (1.3eq) was added, and refluxed overnight. After completion of reaction acidify (pH = 1-2) with concentrated HCl. The precipitate was observed and filtered the residue using a Buckner funnel, and the residue was dissolved in $CHCl_3$ and washed with brine solution followed by water. The reaction mixture was extracted with $CHCl_3$ organic layer was dried over anhydrous Na_2SO_4. The solvent was evaporated, and the crude product was purified by column chromatography using petroleum ether and ethyl acetate as eluent (8:2 v/v) and dried under a high vacuum to get the desired product.

Compound 10: Compound 9 (4 g, 1.152 mmol, 1 eq) and NaOH (0.059 g, 1.498 mmol, 1.3 eq) in 100 ml of ethanol Yield: 90%; ^{1}H NMR (500 MHz, $CDCl_3$): δ (ppm) = 7.55 (s, 4H), 7.50 (s, 2H), 7.19 (s, 2H), 6.78 (s, 1H), 6.56 (s, 2H), 6.48 – 6.45 (m, 12H), 5.39 (s, 12H), 5.22 (s, 4H), 5.07 (s, 8H), 3.93 – 3.89 (m, 24H), 1.79 – 1.69 (m, 24H), 1.47 – 1.42 (m, 24H), 1.25 (m, 192H), 0.87 (t, J = 6.5 Hz, 36H), ; ^{13}C NMR (125 MHz, $CDCl_3$): δ ppm = 159.86, 158.95, 153.62, 144.05, 143.62, 138.53, 136.80, 129.12, 123.02, 122..89, 108.93, 108.26, 107.40, 106.82, 101.81, 73.51, 69. 27, 62.34, 61.80, 54.67, 54.05, 31.95, 31.93, 30.34, 29.77, 29.72, 29.67, 29.66, 29.62, 29.45, 29.40, 29.38, 26.12, 26.11, 22.70, 14.13. Elemental analysis: C, 73.31; H, 10.15; N, 7.29 calculated (%): C, 72.79; H, 10.07, N, 7.07 (expt. %).

Compound 11: Compound 6 (1 g, 0.618 mmol, 1 eq) and NaOH (0.032 g, 0.804 mmol, 1.3 eq) in 100 ml of ethanol Yield: 92%; ^{1}H NMR (500 MHz, $CDCl_3$): δ (ppm) = 7.49 (s, 2H), 7.26 (s, 2H), 6.76 (bs, 1H), 6.40 (s, 4H), 5.34 (s, 4H), 5.11 (s, 4H), 3.86 – 3.82 (m, 12H), 1.72 – 1.62 (m, 12H), 1.40 – 1.34 (m, 12H), 1.24 – 1.18 (m, 96H), 0.80 (t, J = 7.0 Hz, 18H), ; ^{13}C

NMR (125 MHz, $CDCl_3$): δ ppm = 170.08, 159.23, 153.62, 143.82, 138.52, 131.86, 129.17, 122.79, 109.13, 107.39, 106.74, 73.48, 69.24, 62.17, 54.64, 31.95, 31.93, 30.34, 29.77, 29.76, 29.72, 29.67, 29.65, 29.62, 29.44, 29.41, 29.38, 26.13, 26.11, 22.70, 14.12. Elemental analysis: C, 74.20; H, 10.57; N, 5.24 calculated (%): C, 74.02; H, 10.79, N, 5.22 (expt. %).

Compound 12: Benzene-1, 3,5-tricarboxylic acid (2 g, 9.15 mmol, 1 eq), ethylenediamine (2.0 g 33.30 mmol, 3.5 eq), ethylenediamine dihydrochloride (4.42 g, 33.30 mmol, 3.5 eq), toluene-*p*-sulfonic acid (0.127 g, 0.742 mmol, 0.078 eq) and ethylene glycol (14 ml) were added and reflux for 3 h. After three hours, about half of the ethylene glycol was then slowly removed by distillation. The reaction mixture residue was dissolved in water (52ml) and conc. HCl (4ml). An addition of 50% aqueous NaOH was added until a yellow precipitate was observed. Reprecipitation was done using methanol and dried under a high vacuum to get the desired product. Yield: 40% ^{1}H NMR (500 MHz, Methanol-d_4): δ (ppm) = 8.24 (s, 3H), 3.80 (s, 12H); ^{13}C NMR (125 MHz, Methanol-d_{43}): δ ppm = 165.01, 130.91, 127.88, 49.30. Elemental analysis: C, 63.81; H, 6.43; N, 29.77 calculated (%): C, 62.91; H, 6.46, N, 29.43 (expt. %).

Compound 13: Benzene-1, 3, 5-tricarboxylic acid (2 g, 9.15 mmol, 1 eq), o-phenyl diamine (3.18 g 29.49 mmol, 3.1 eq), Phosphoric acid (H_3PO_4) 30 ml was added, the reaction mixture kept at 150 ºC for 24 h then the temperature was increased till 180 ºC kept for 18h, after the pH of the resulting mixture was adjusted to 8 – 9 with NaOH solution, then a large amount of solid precipitated. After filtration, the crude product was obtained and then further purified by recrystallization with hot methanol to give the desired product. ^{1}H NMR (500 MHz, DMSO-d_6): δ (ppm) = 13.39 (s, 3H), 9.11 (s, 3H), 7.76 (d, *J* = 7.50 Hz, 3H), 7.61 (d, *J* = 7.50 Hz, 3H), 7.28 (p, *J* = 7.25 Hz, 6H); ^{13}C NMR (125 MHz, Methanol-d_{43}): δ ppm = 150.79, 144.23, 135.78, 132.27, 125.91, 123.45, 122.49, 119.41, 112.22. Elemental analysis: C, 76.04; H, 4.25; N, 19.71 calculated (%): C, 76.41; H, 4.50, N, 18.03 (expt. %).

Hydrogen bonding complex of 14 and 15: The 1:3 LC complexes were formed by first dissolving the compound **12** and compound **10** or **11** in a MeOH / CHCl3 mixture (1:4 v/v), stirred for 2h followed by solvent removal using rotavapor dried under high vacuum to get the desired complex.

Complex 14: Compound 12 (0.010 g, 0.0354 mmol, 1 eq), compound 11 (0.170 g, 0.1062 mmol, 3 eq) MeOH / CHCl3 mixture (1:4 v/v) 5ml; ^{1}H NMR (500 MHz, $CDCl_3$): δ (ppm) =

9.99 (s, 3H), 7.55 (s, 6H), 7.36 (s, 6H), 6.67 (s, 3H), 6.46 (s, 12H), 5.39 (s, 12H), 5.18 (s, 12H), 4.15 (s, 12H), 3.93 – 3.89 (m, 36H), 1.79 – 1.69 (m, 36H), 1.45 – 1.44 (m, 36H), 1.25 (m, 294H), 0.8 (t, *J* = 6.25 Hz, 54H); ^{13}C NMR (125 MHz, $CDCl_3$): δ ppm = 172.83, 163.10, 158.98, 153.61, 144.37, 139.85, 138.51, 134.73, 129.24, 125.49, 122.65, 108.45, 106.71, 104.95, 73.48, 69.25, 62.18, 54.59, 45.57, 31.94, 31.93, 30.34, 29.76, 29.71, 29.67, 29.65, 29.63, 29.44, 29.40, 29.38, 26.13, 26.11, 22.70, 14.13. Elemental analysis: C, 73.63; H, 10.34; N, 6.60 calculated (%): C, 72.83; H, 10.55, N, 6.57 (expt. %).

Complex 15: Compound 12 (0.010 g, 0.0354 mmol, 1 eq), compound 10 (0.367g, 0.1062 mmol, 3 eq) MeOH / CHCl3 mixture (1:4 v/v) 5ml; ^{1}H NMR (500 MHz, $CDCl_3$): δ (ppm) = 9.63 (s, 3H), 7.60 (s, 6H), 7.56 (s, 12H), 7.34 (s, 6H), 6.66 (s, 3H), 6.58 (s, 6H), 6.46 (s, 36H), 5.39 – 5.37 (m, 36H), 5.17 (s, 12H), 5.06 (s, 24H), 4.06 (bs, 12H), 3.92 – 3.87 (m, 72H), 1.78 – 1.68 (m, 72H), 1.46 – 1.40 (m, 72H), 1.25 (m, 582H), 0.86 (t, *J* = 6.25 Hz, 108H); ^{13}C NMR (125 MHz, $CDCl_3$): δ ppm = 171.68, 162.19, 158.80, 157.89, 152.55, 143.37, 142.66, 138.88, 137.40, 135.90, 128.30, 124.98, 122.13, 121.94, 107.52, 106.33, 105.68, 103.98, 100.78, 72.45, 68.19, 60.98, 60.92, 53.51, 52.98, 45.11, 30.91, 29.33, 28.75, 28.70, 28.65, 28.64, 28.61, 28.43, 28.38, 28.36, 25.10, 21.68, 13.10. Elemental analysis: C, 73.05; H, 10.05; N, 7.89 calculated (%): C, 72.89; H, 9.93, N, 7.73 (expt. %).

Hydrogen bonding complex of 16 and 17: The 1:3 LC complexes were formed by first dissolving the compound **13** and compound **10** or **11** in a MeOH / CHCl3 mixture (1:4 v/v), stirred for 4h at 60 ºC followed by solvent removal using rotavapor dried under high vacuum to get the desired complex.

Complex 16: Compound 13 (0.010 g, 0.0234 mmol, 1 eq), compound 11 (0.112 g, 0.070 mmol, 3 eq) MeOH / CHCl3 mixture (1:4 v/v) 5ml; ^{1}H NMR (500 MHz, $CDCl_3$ + DMSO-d6): δ (ppm) = 9.14 (s, 3H), 8.02 – 7.97 (m, 9H), 7.66 (s, 6H), 7.25 – 7.20 (m, 6H), 6.87 (bs, 3H), 6.54 – 6.53 (m, 15H), 5.44 (s, 12H), 5.15 (s, 12H), 3.88 – 3.84 (m, 36H), 1.74 – 1.72 (m, 24H), 1.68 – 1.65 (m, 12H), 1.44 (m, 36H), 1.25 (m, 294H), 0.86 – 0.85 (m, 54H); ^{13}C NMR (125 MHz, $CDCl_3$ + DMSO-d6): δ ppm = 172.17, 164.06, 158.00, 155.66, 147.97, 142.52, 138.08, 136.87, 135.20, 128.95, 128.82, 113.45, 111.37, 111.04, 77.81, 73.59, 66.64, 58.71, 36.58, 35.06, 34.37, 34.32, 34.30, 34.10, 34.02, 30.85, 27.35, 18.99. Elemental analysis: C, 74.35; H, 10.05; N, 6.42 calculated (%): C, 74.27; H, 10.32, N, 6.10 (expt. %).

Complex 17: Compound 13 (0.010 g, 0.0234 mmol, 1 eq), compound 10 (0.243g, 0.070 mmol, 3 eq) MeOH / CHCl3 mixture (1:4 v/v) 5ml. ^{1}H NMR (500 MHz, $CDCl_3$ + DMSO-d6): δ (ppm) = 9.15 (s, 3H), 7.92 – 7.90 (m, 6H), 7.86 – 7.84 (m, 15H), 7.78 – 7.74 (m, 3H), 7.66 (bs, 5H), 7.25 – 7.24 (m, 5H), 6.83 (s, 3H), 6.60 (s, 7H), 6.52 (m, 40H), 5.45 – 5.41 (m, 36H), 5.14 – 5.07 (m, 36H), 3.89 – 3.87 (m, 72H), 1.75 – 1.67 (m, 72H), 1.43 (m, 72H), 1.25 (m, 580H), 0.88 – 0.85 (m,108H),; ^{13}C NMR (125 MHz, $CDCl_3$ + DMSO-d6): δ ppm = 172.12, 164.47, 164.01, 157.98, 148.01, 147.91, 142.52, 135.18, 128.98, 113.52, 112.21, 111.42, 111.17, 106.27, 77.80, 73.59, 66.61, 66.37, 58.69, 58.30, 36.57, 35.05, 34.39, 34.36, 34.31, 34.10, 34.01, 30.84, 27.34, 18.97. Elemental analysis: C, 73.41; H, 9.91; N, 7.78 calculated (%): C, 73.69; H, 10.21, N, 7.51 (expt. %).

5.7 NMR Spectra:

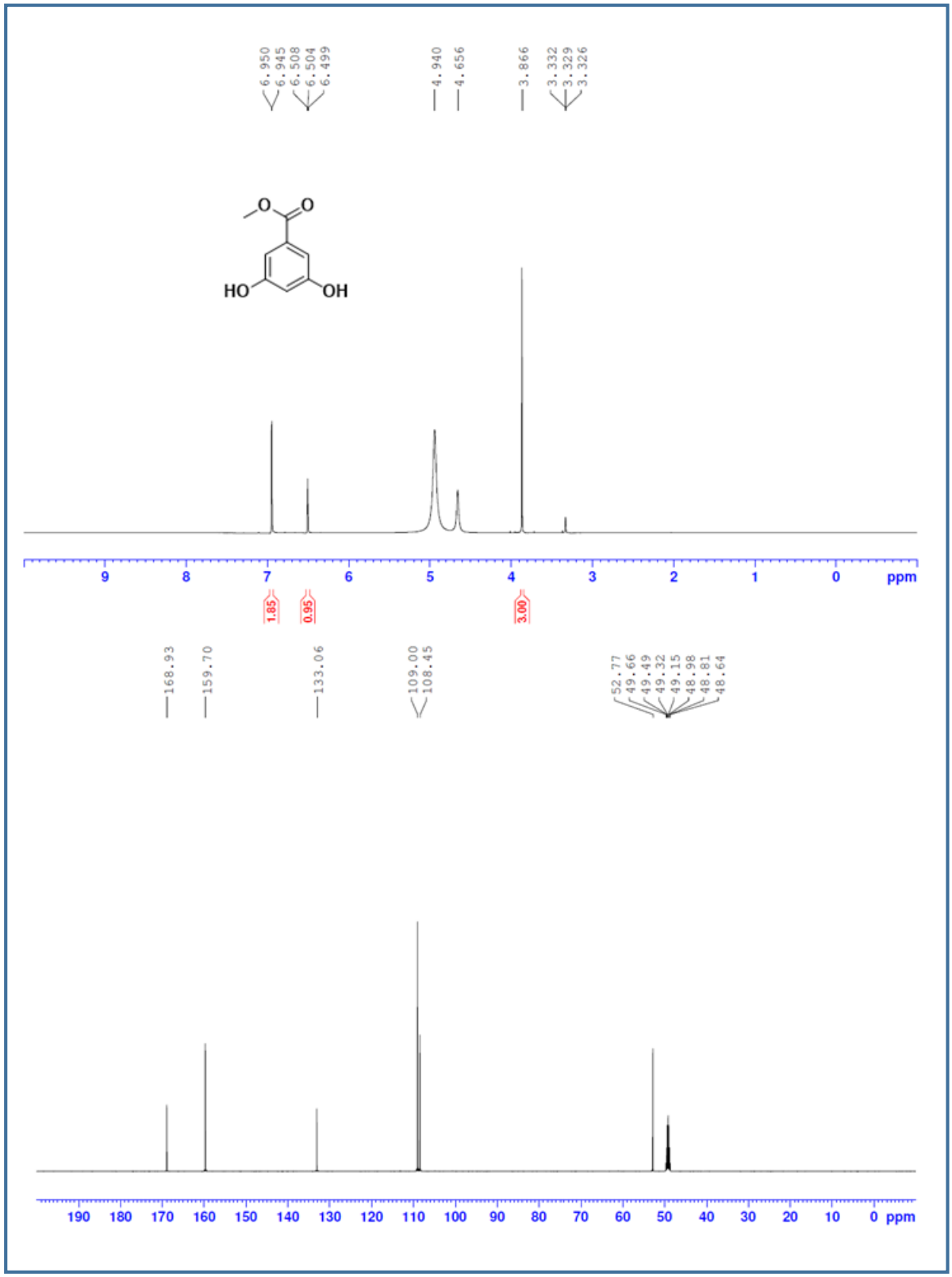

Figure 5.29: ^{1}H (top) and ^{13}C-NMR (bottom) spectra of **1**

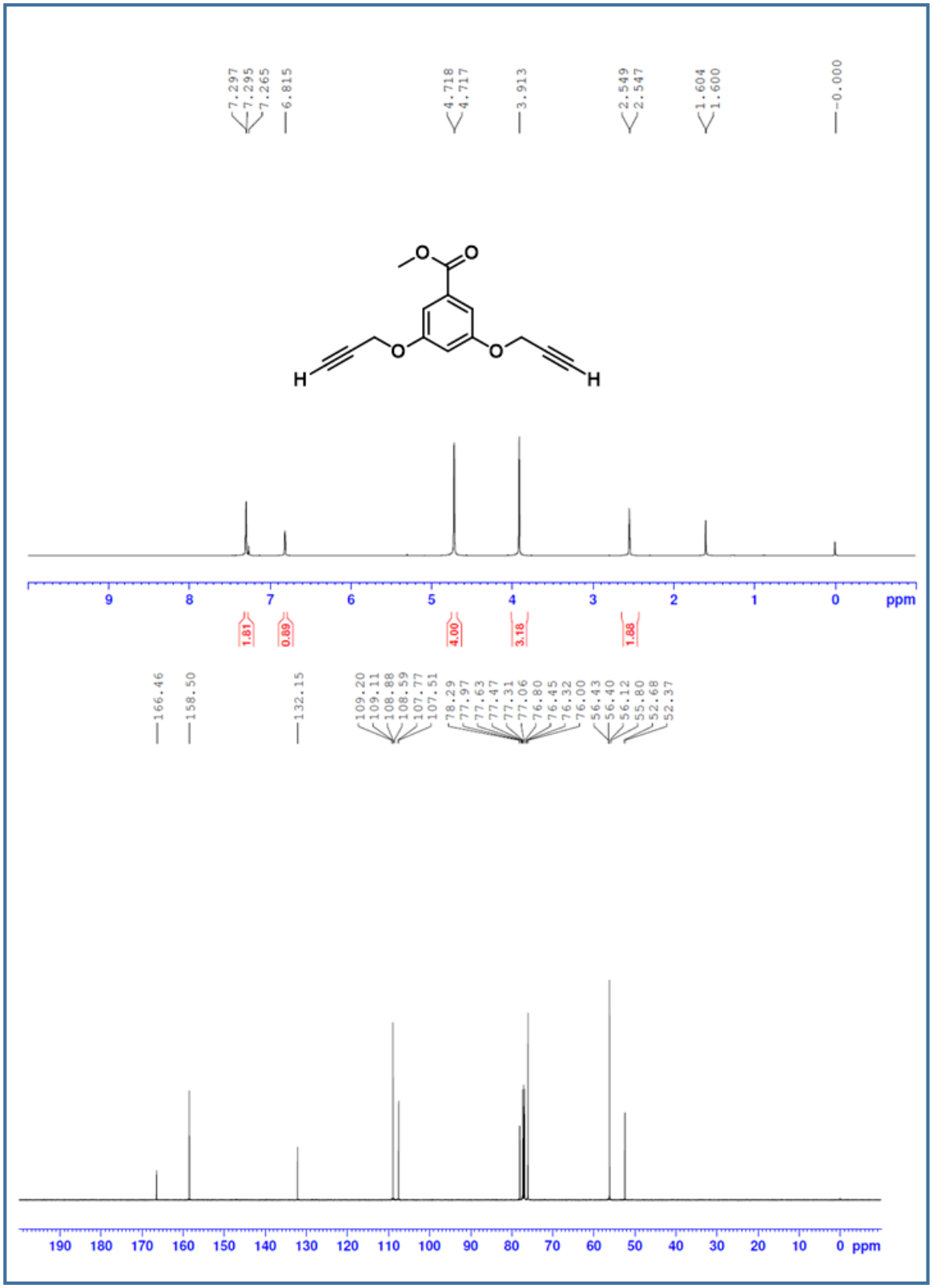

Figure 5.30: ^{1}H (top) and ^{13}C-NMR (bottom) spectra of **2**

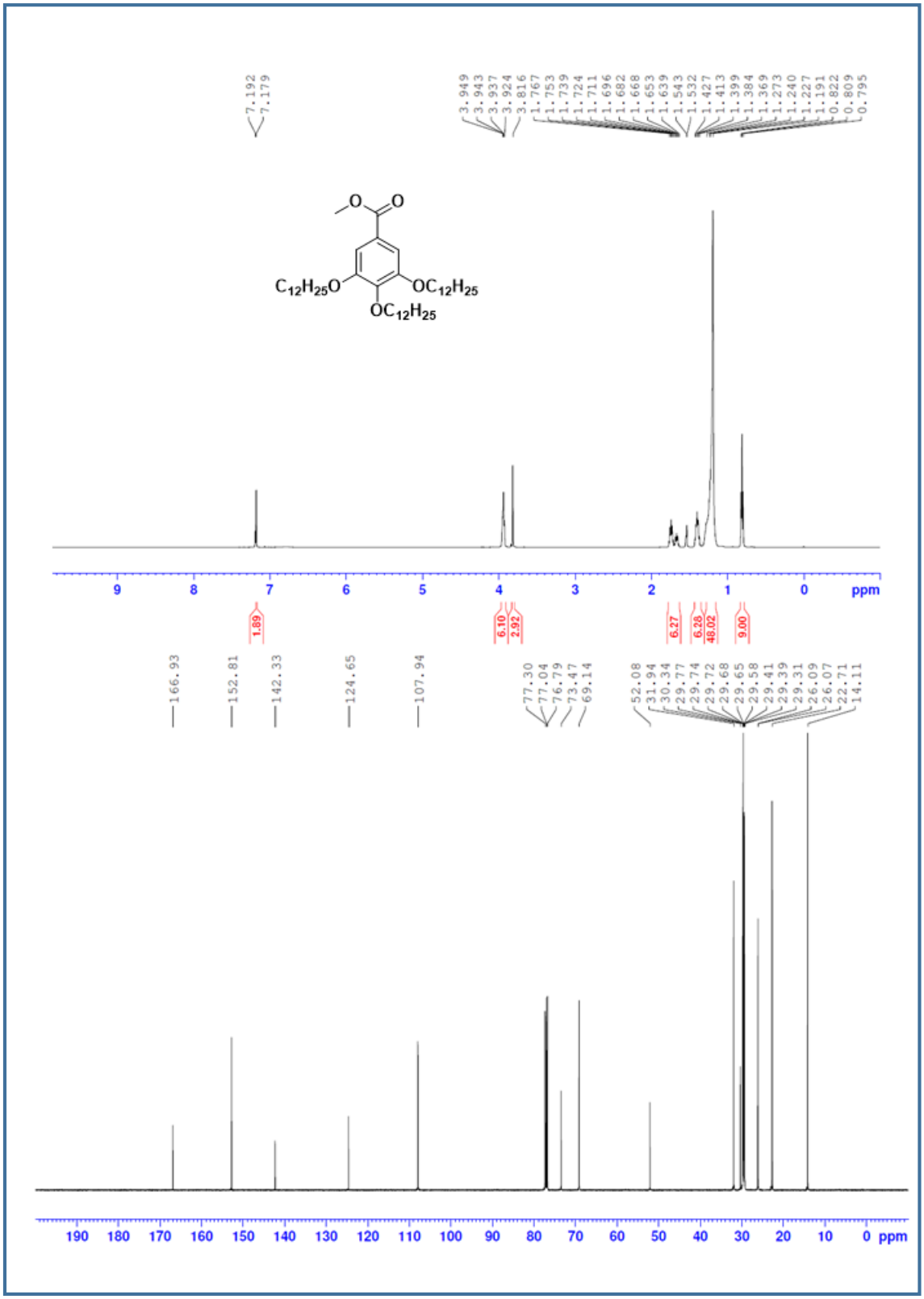

Figure 5.31: ^{1}H (top) and ^{13}C-NMR (bottom) spectra of **3**

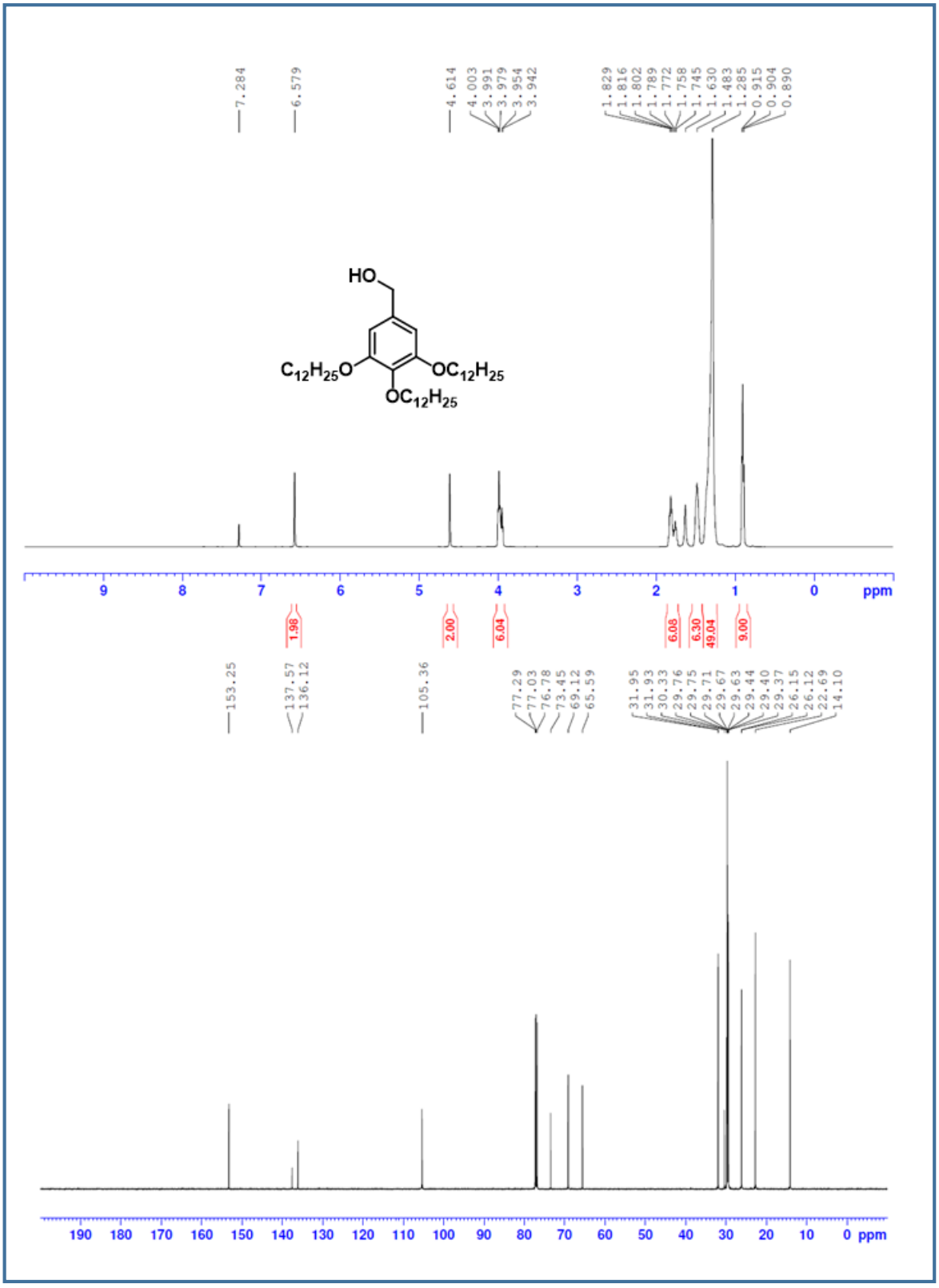

Figure 5.32: ^{1}H (top) and ^{13}C-NMR (bottom) spectra of **4**

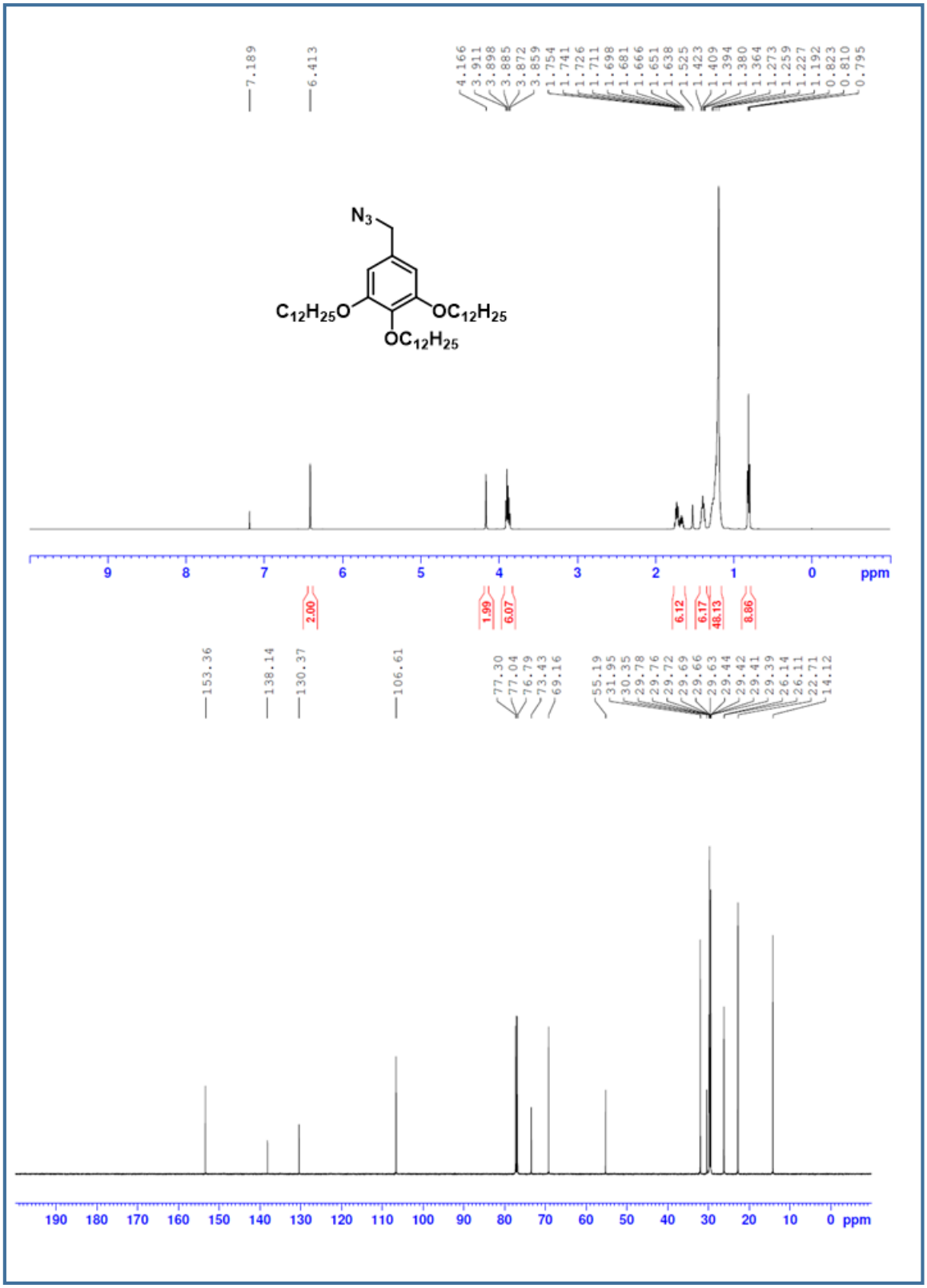

Figure 5.33: ^{1}H (top) and ^{13}C-NMR (bottom) spectra of **5**

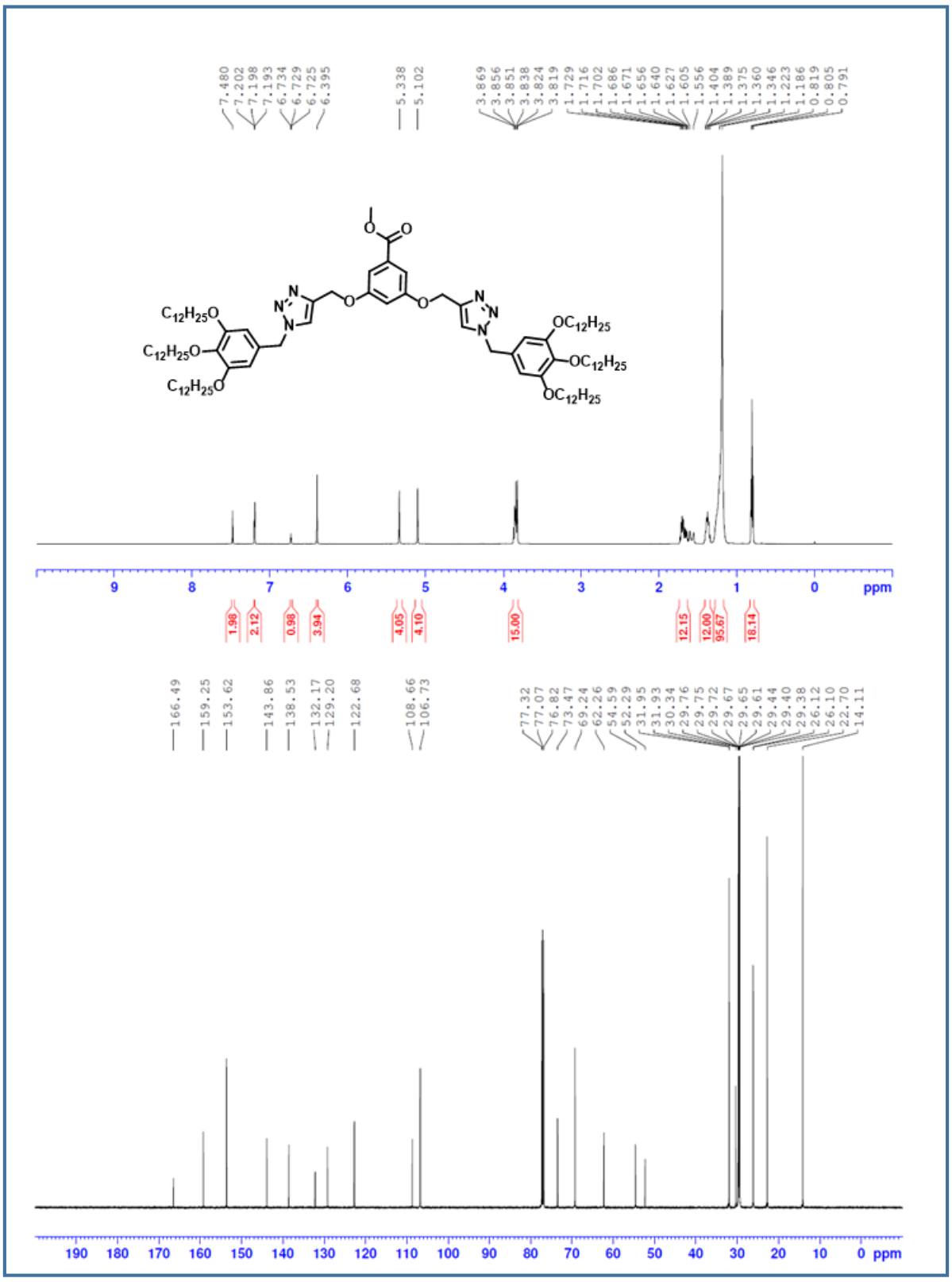

Figure 5.34: ^{1}H (top) and ^{13}C-NMR (bottom) spectra of **6**

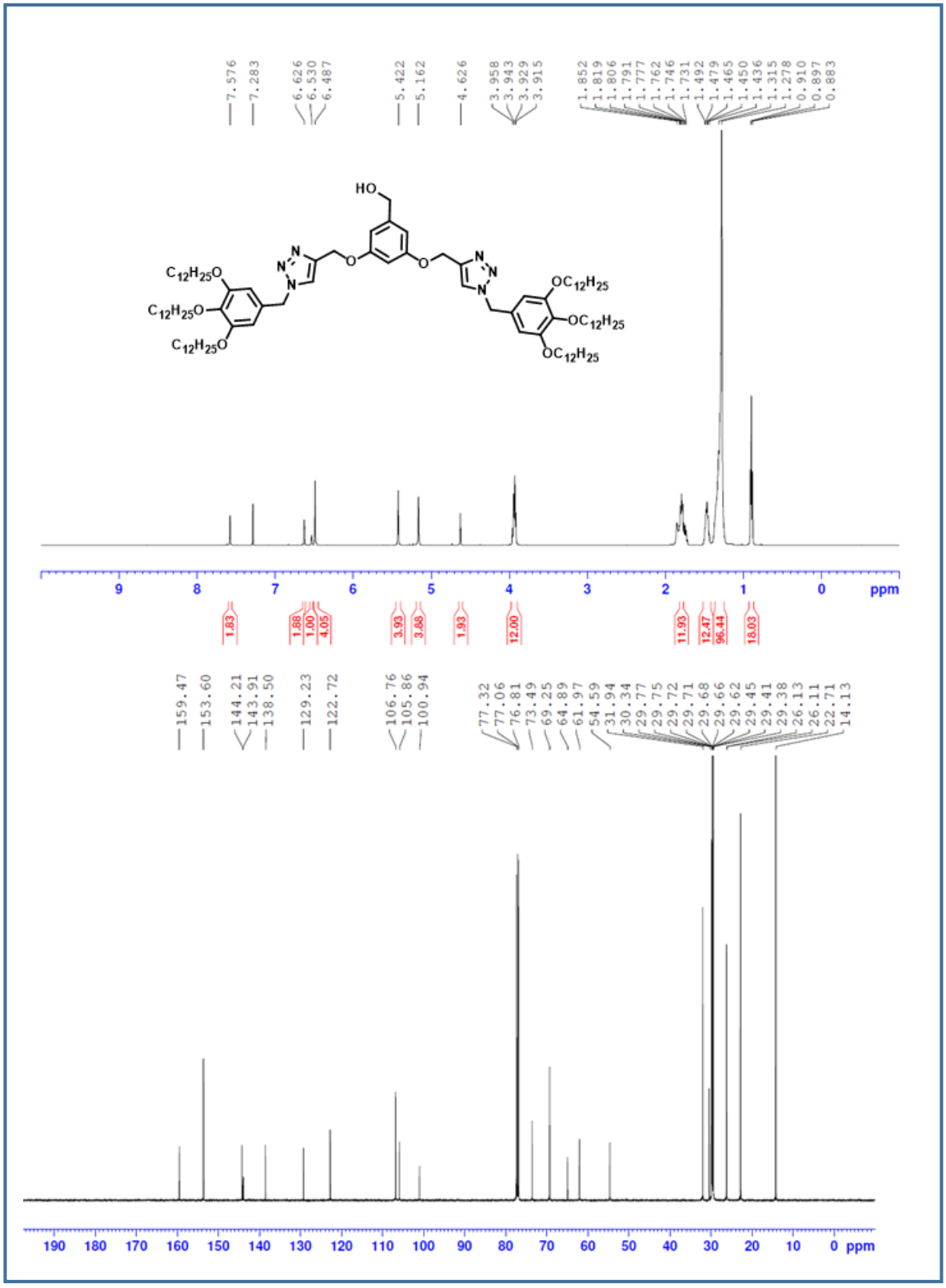

Figure 5.35: ^{1}H (top) and ^{13}C-NMR (bottom) spectra of **7**

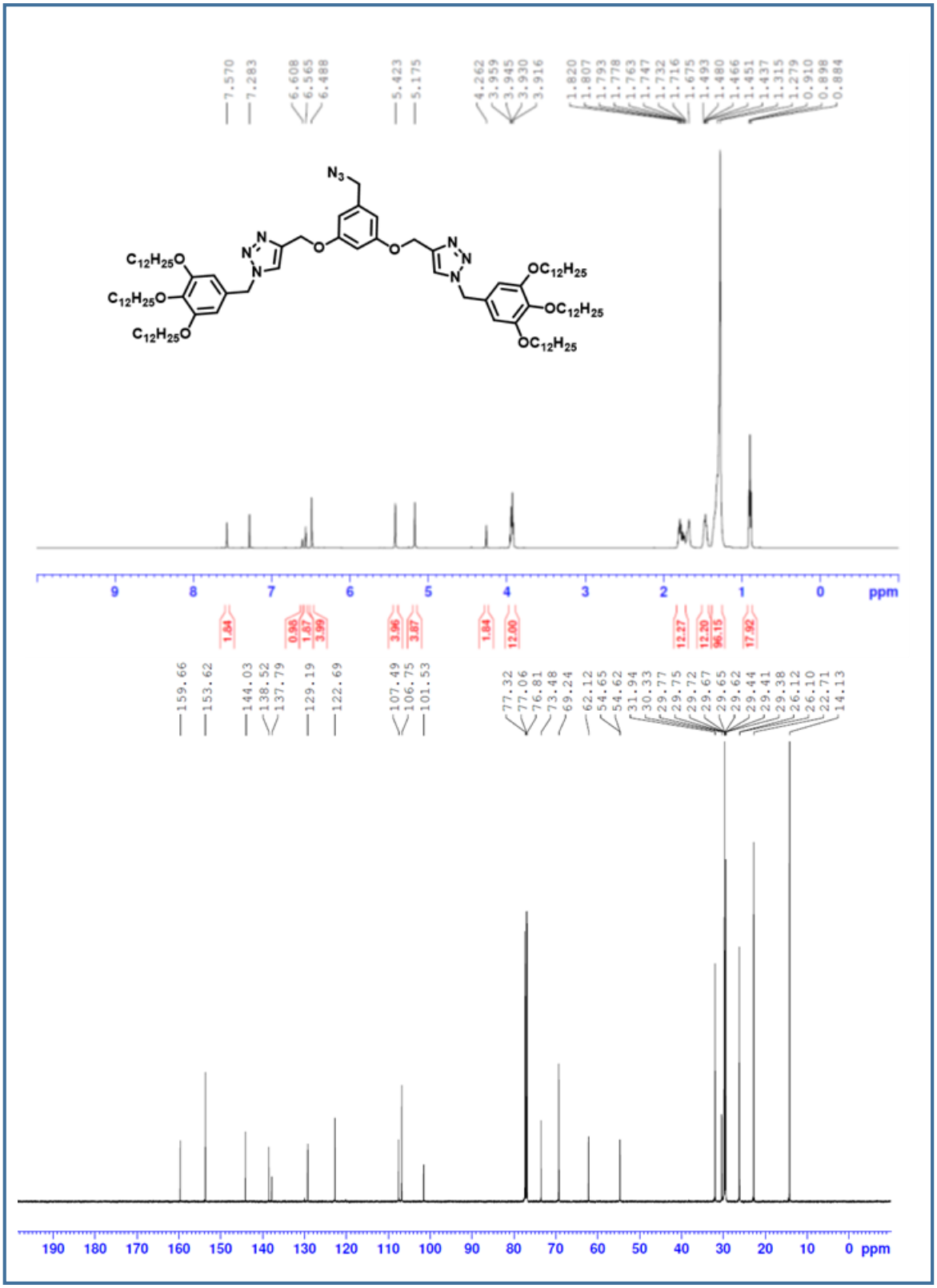

Figure 5.36: ^{1}H (top) and ^{13}C-NMR (bottom) spectra of **8**

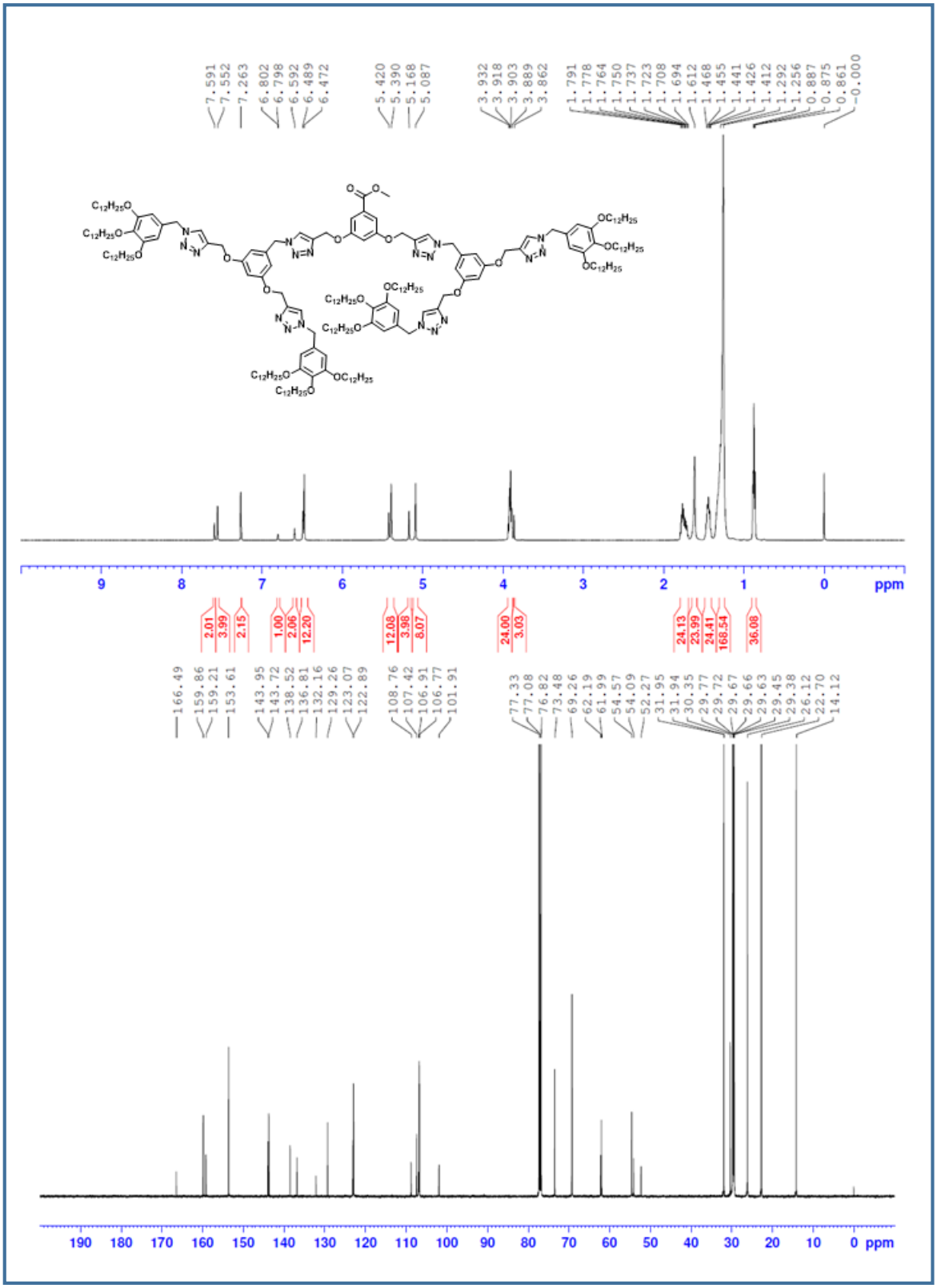

Figure 5.37: ^{1}H (top) and ^{13}C-NMR (bottom) spectra of **9**

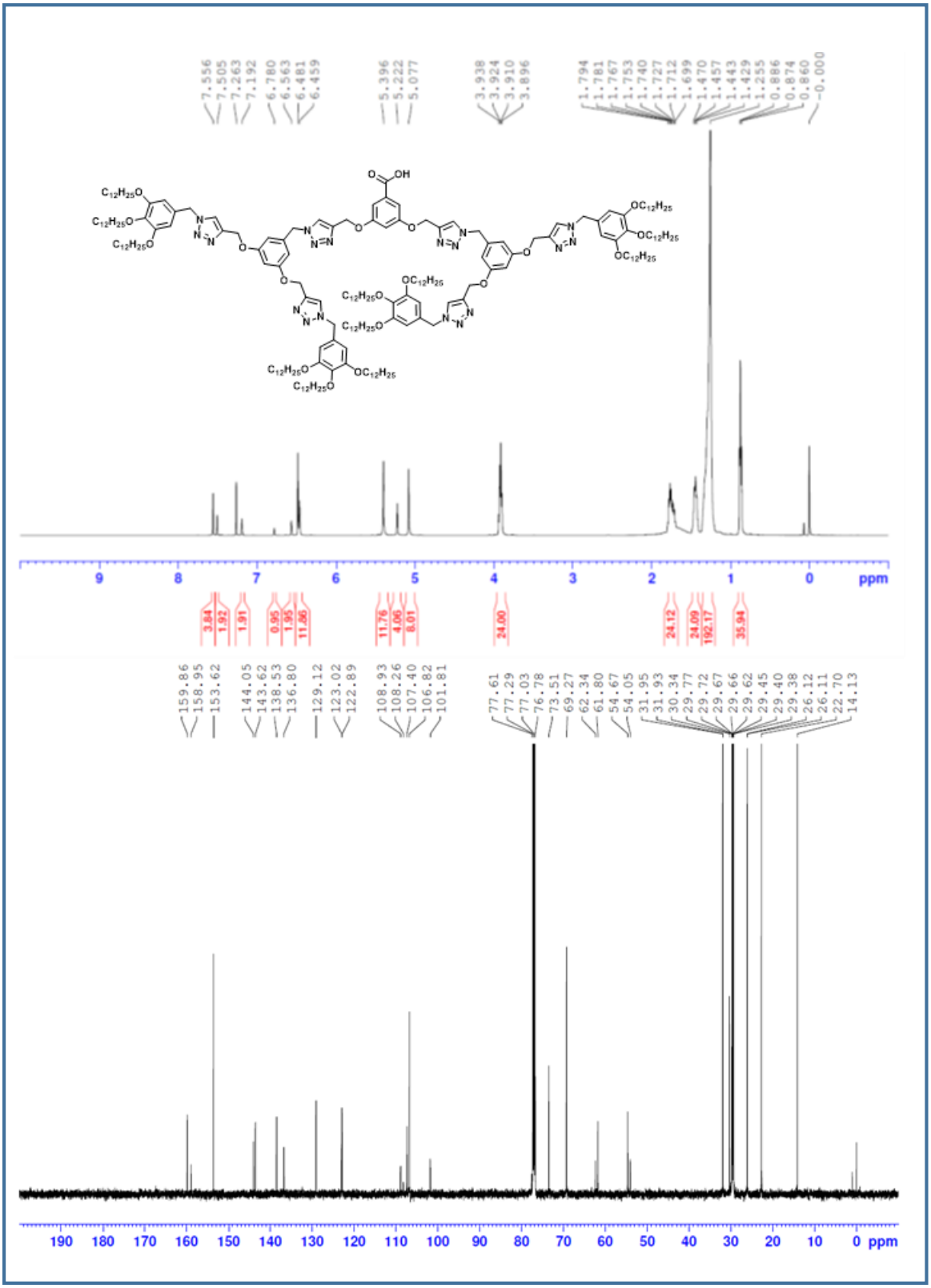

Figure 5.38: ^{1}H (top) and ^{13}C-NMR (bottom) spectra of **10**

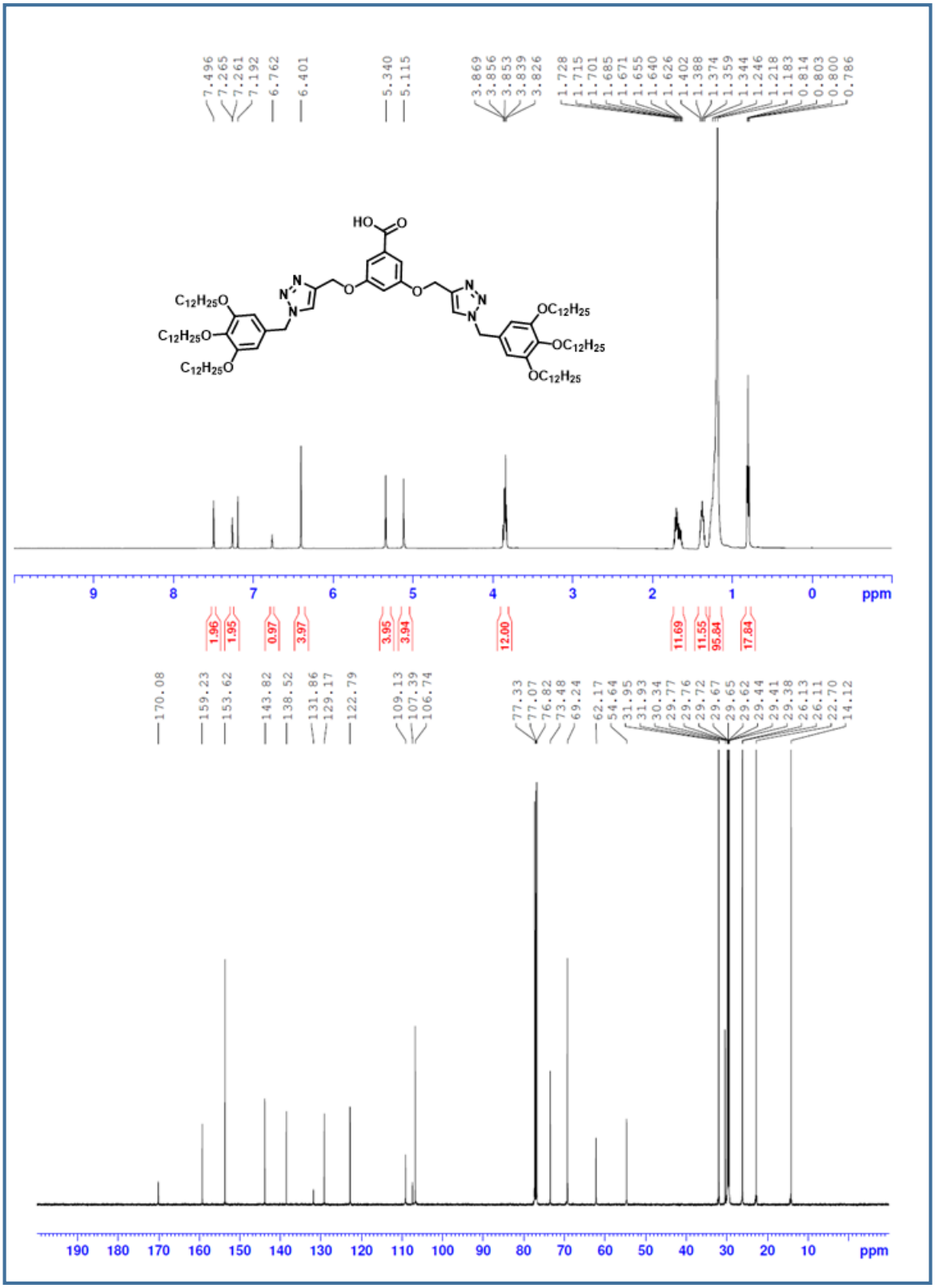

Figure 5.39: ^{1}H (top) and ^{13}C-NMR (bottom) spectra of **11**

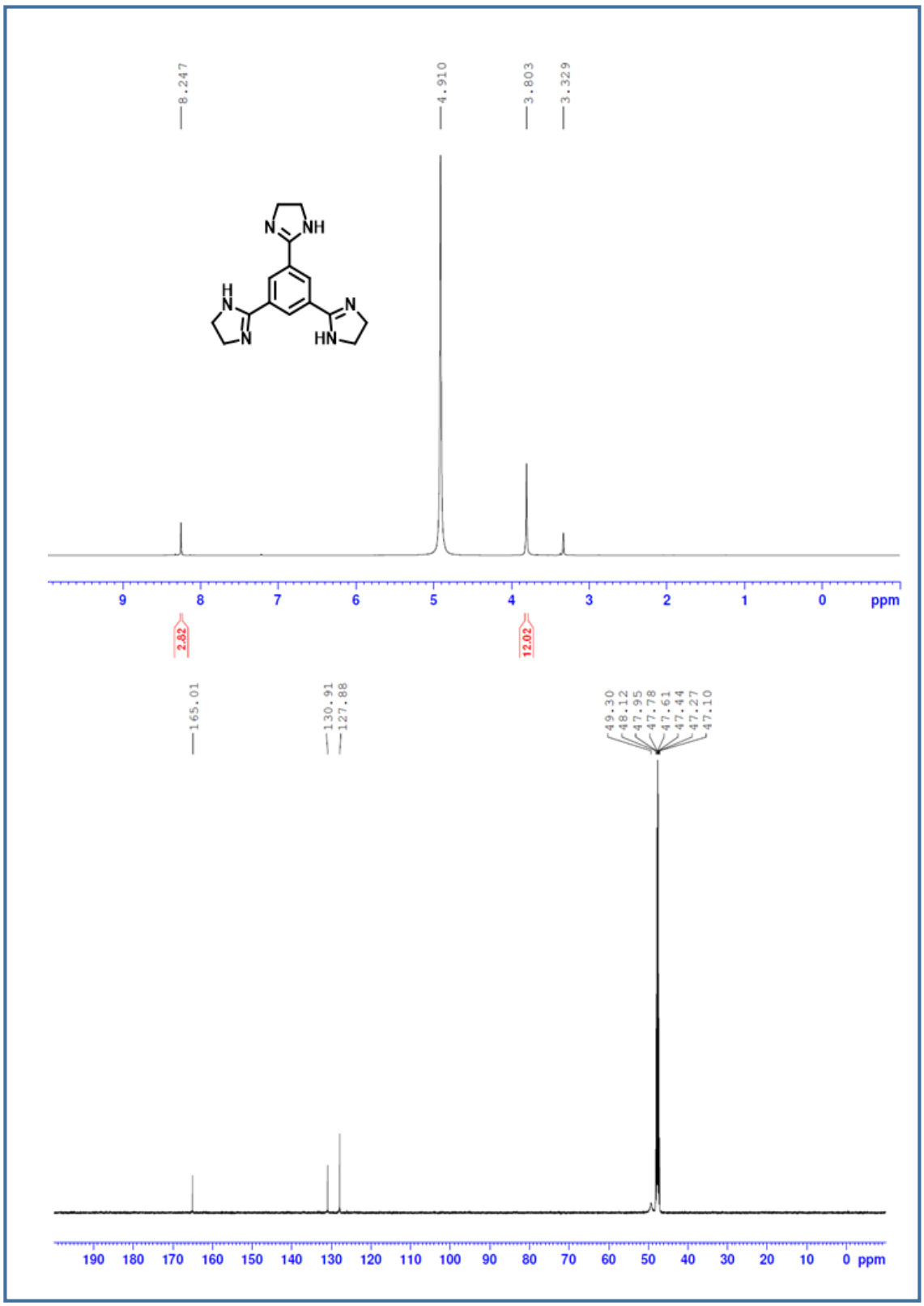

Figure 5.40: ^{1}H (top) and ^{13}C-NMR (bottom) spectra of **12**

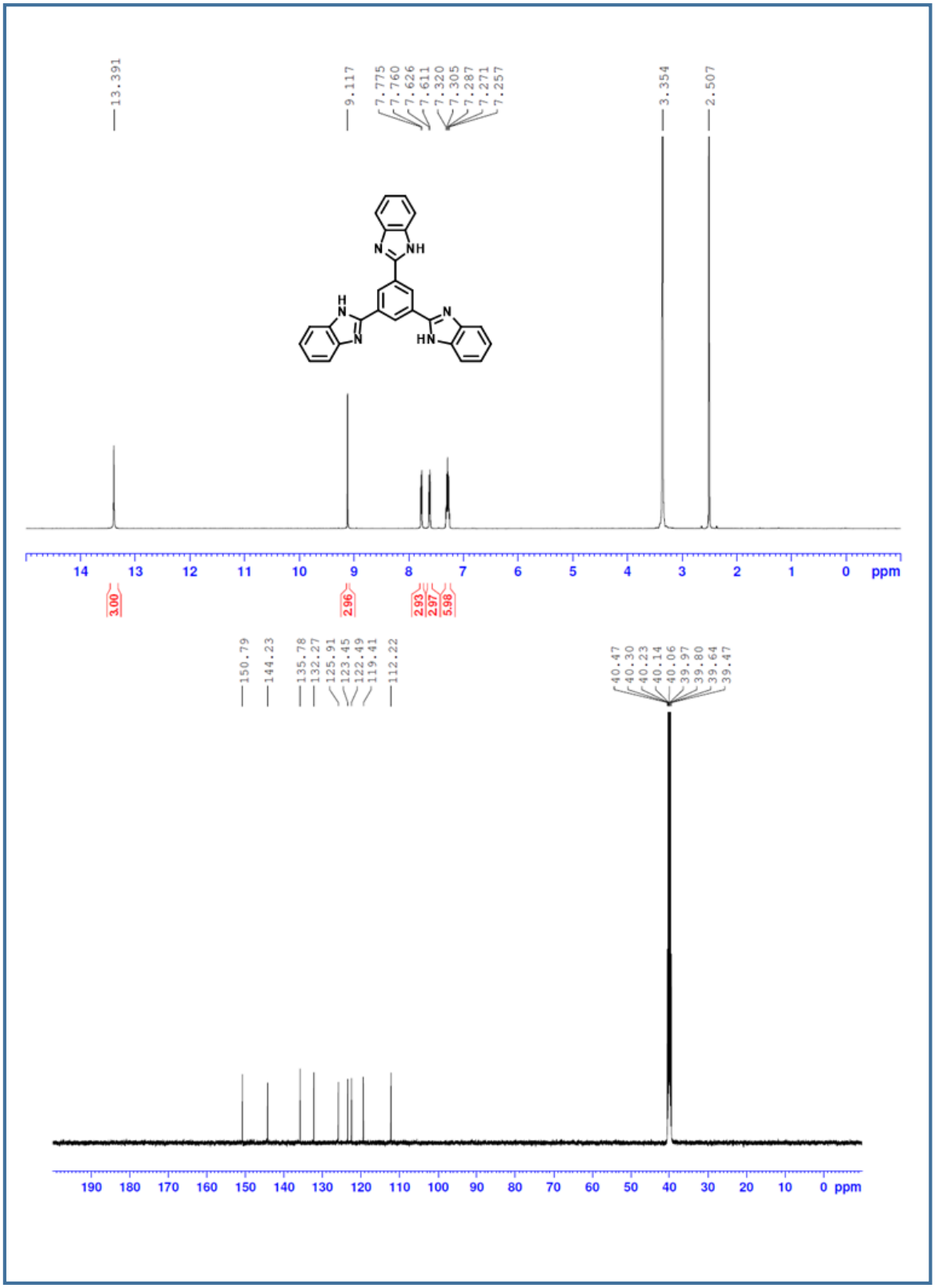

Figure 5.41: ^{1}H (top) and ^{13}C-NMR (bottom) spectra of **13**

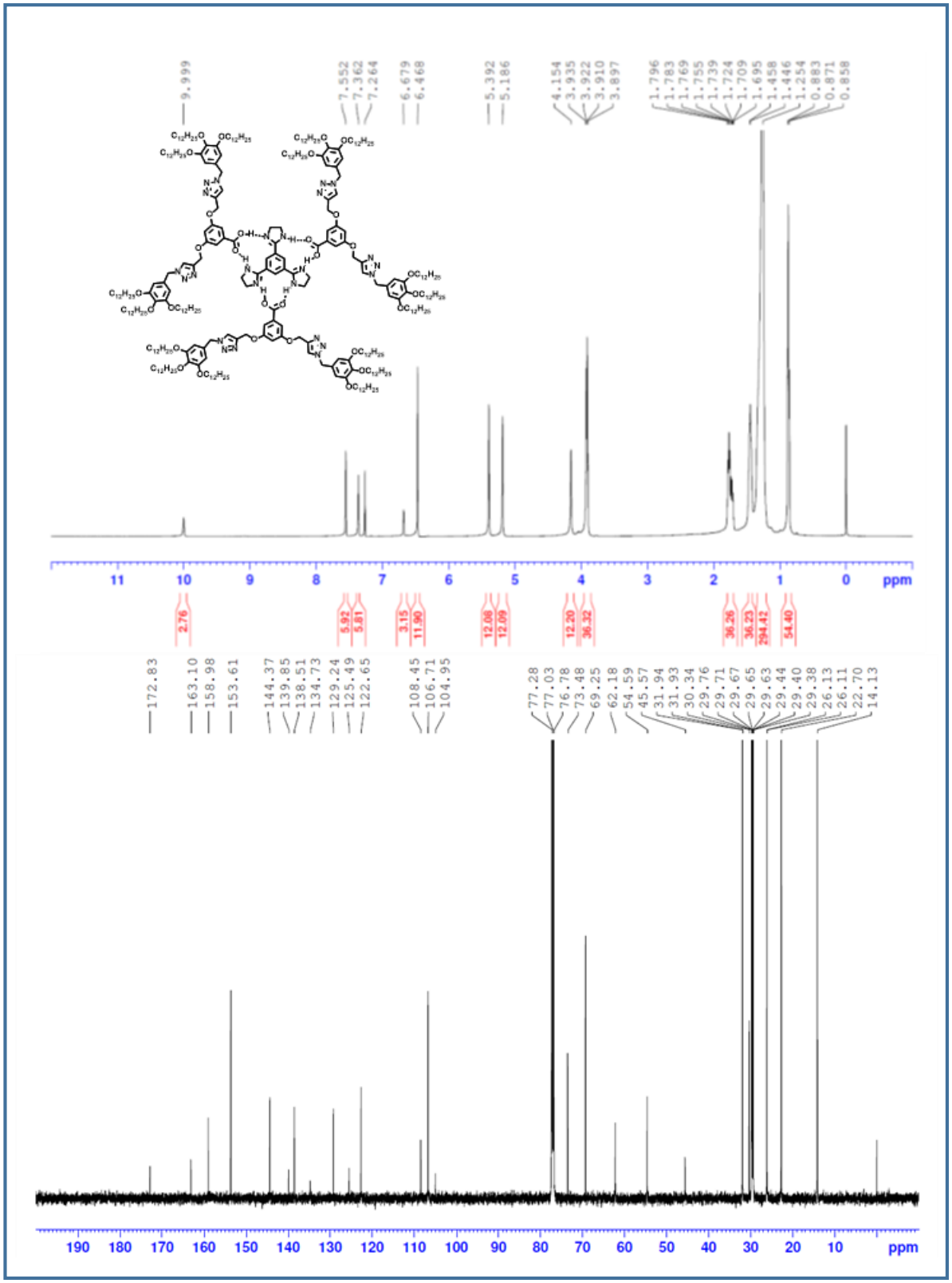

Figure 5.42: ^{1}H (top) and ^{13}C-NMR (bottom) spectra of **14**

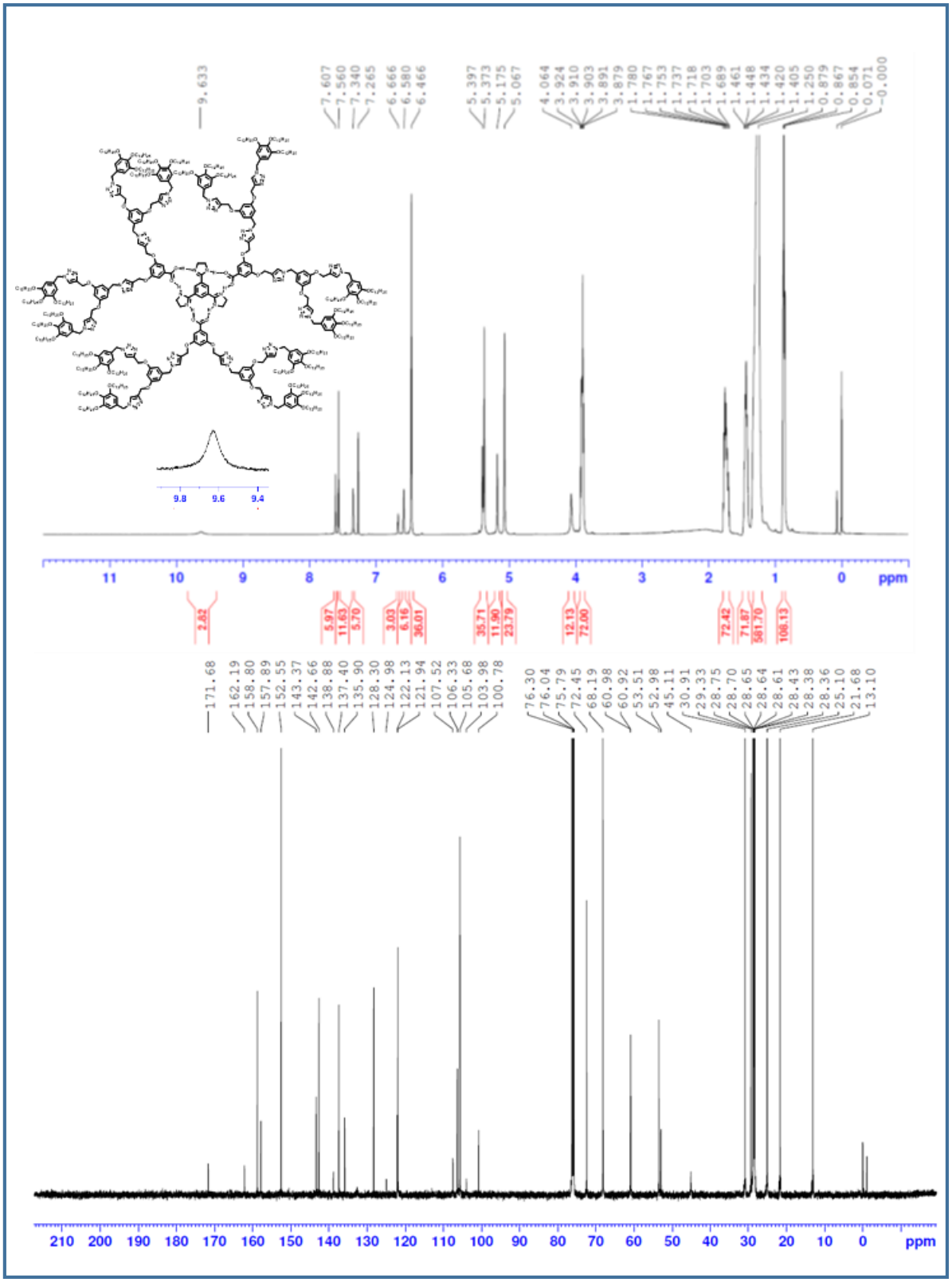

Figure 5.43: ^{1}H (top) and ^{13}C-NMR (bottom) spectra of **15**

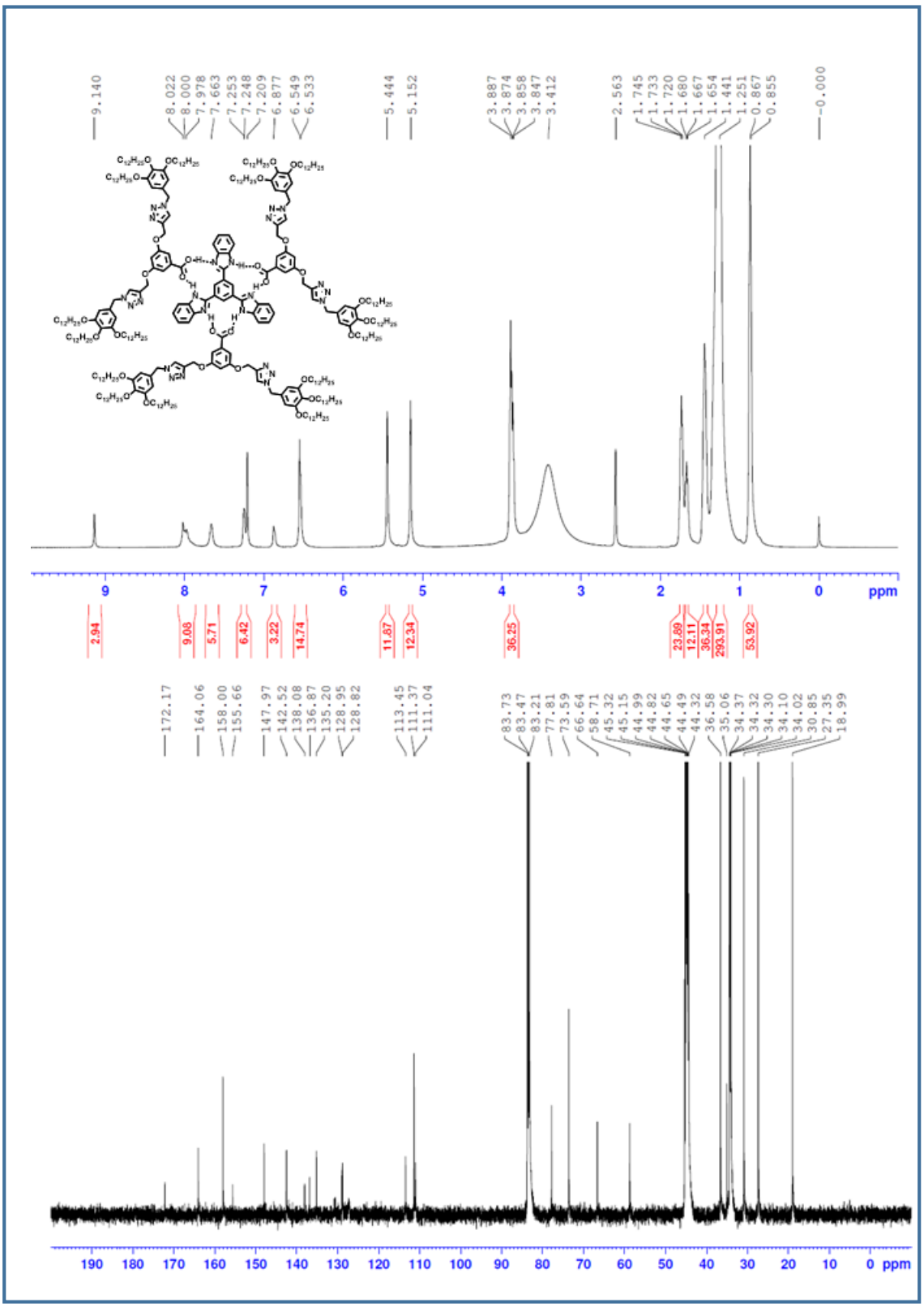

Figure 5.44: ^{1}H (top) and ^{13}C-NMR (bottom) spectra of **16**

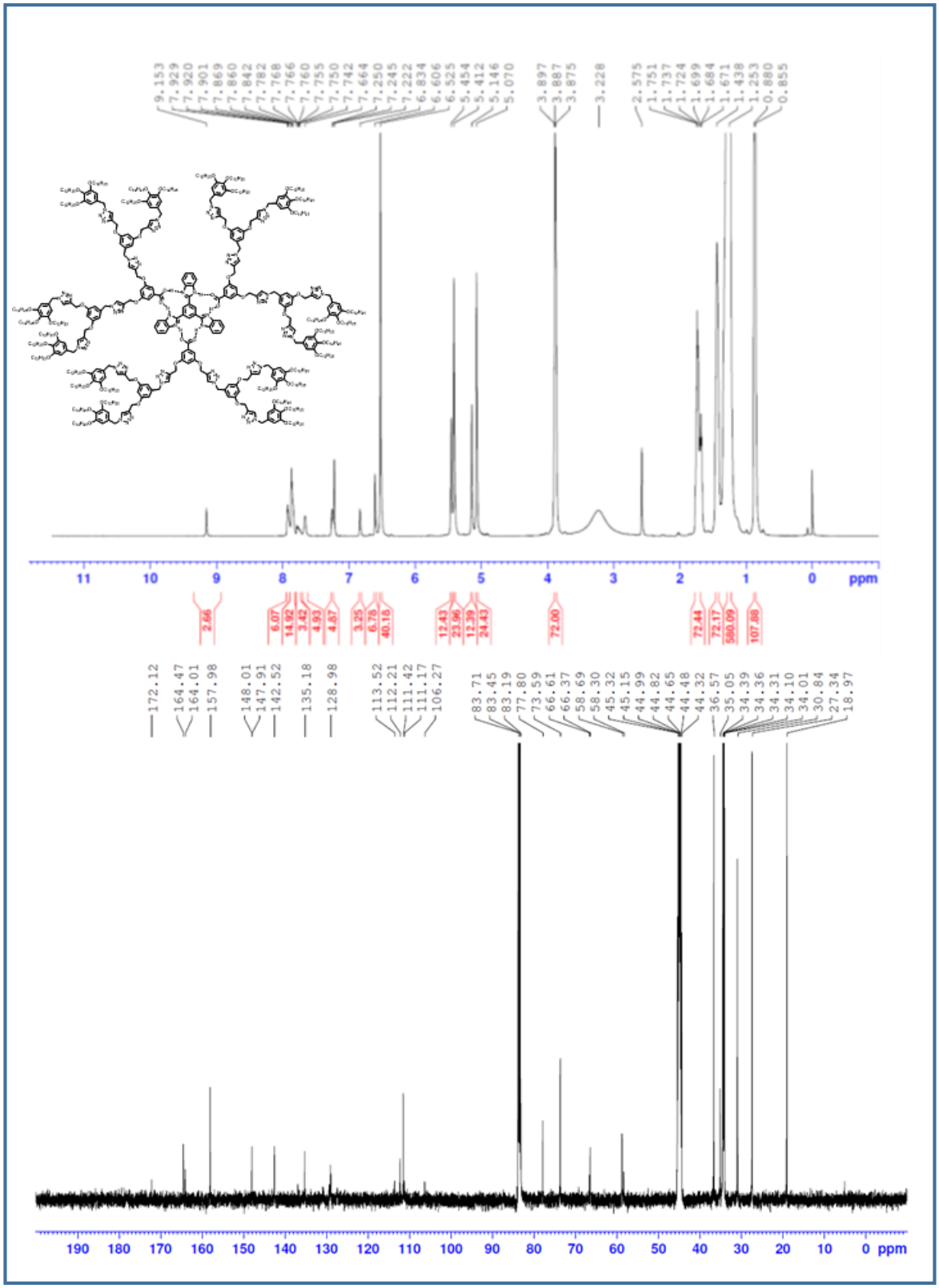

Figure 5.45: ^{1}H (top) and ^{13}C-NMR (bottom) spectra of **17**

5.8 References :

[1] U. Boas, J. B. Christensen, P. M. H. Heegaard, *J. Mater. Chem.* **2006**, *16*, 3785.

[2] W. F. Ganong, **1991**, 754.

[3] K. Autumn, Y. A. Liang, S. T. Hsieh, W. Zesch, W. P. Chan, T. W. Kenny, R. Fearing, R. J. Full, *Nature* **2000**, *405*, 681–685.

[4] D. A. Tomalia, J. M. J. Fréchet, *J. Polym. Sci. Part A Polym. Chem.* **2002**, *40*, 2719–2728.

[5] S. B. Undre, *Adv. Mater. Lett.* **2016**, *7*, 502–516.

[6] D. Astruc, E. Boisselier, C. Ornelas, *Chem. Rev.* **2010**, *110*, 1857–1959.

[7] Z. Lyu, L. Ding, A. Tintaru, L. Peng, *Acc. Chem. Res.* **2020**, *53*, 2936–2949.

[8] J. M. J. Fréchet, D. A. Tomalia, *Dendrimers and Other Dendritic Polymers*, John Wiley & Sons, Ltd, Chichester, UK, **2001**.

[9] M. Gingras, J.-M. Raimundo, Y. M. Chabre, *Angew. Chemie Int. Ed.* **2007**, *46*, 1010–1017.

[10] C. J. Hawker, J. M. J. Frechet, *J. Am. Chem. Soc.* **1990**, *112*, 7638–7647.

[11] G. R. Newkome, Z. Yao, G. R. Baker, V. K. Gupta, *J. Org. Chem.* **1985**, *50*, 2003–2004.

[12] D. A. Tomalia, H. Baker, J. Dewald, M. Hall, G. Kallos, S. Martin, J. Roeck, J. Ryder, P. Smith, *Polym. J.* **1985**, *17*, 117–132.

[13] Z. Lyu, L. Ding, A. Y.-T. Huang, C.-L. Kao, L. Peng, *Mater. Today Chem.* **2019**, *13*, 34–48.

[14] B. Donnio, D. Guillon, in *Adv. Polym. Sci.*, Springer, Berlin, Heidelberg, **2006**, pp. 45–155.

[15] M. Marcos, R. Martín-Rapún, A. Omenat, J. L. Serrano, *Chem. Soc. Rev.* **2007**, *36*, 1889.

[16] D. J. Pesak, J. S. Moore, *Angew. Chemie Int. Ed. English* **1997**, *36*, 1636–1639.

[17] J. S. Moore, *Acc. Chem. Res.* **1997**, *30*, 402–413.

[18] V. Percec, C.-H. Ahn, G. Ungar, D. J. P. Yeardley, M. Möller, S. S. Sheiko, *Nature* **1998**, *391*, 161–164.

[19] B. Donnio, *Inorganica Chim. Acta* **2014**, *409*, 53–67.

[20] D. Guillon, J.-F. Nierengarten, J.-L. Gallani, J.-F. Eckert, Y. Rio, M. del Pilar Carreon, B. Dardel, R. Deschenaux, *Macromol. Symp.* **2003**, *192*, 63–74.

[21] B. Joaquín Barberµ, A. Cristina GarcØs, N. Jayaraman, A. Omenat, J. Luis Serrano, J. Fraser Stoddart, J. L. Serrano, J. Barberµ, A. Omenat, A. C. GarcØs, *Adv. Mater* **2001**, *13*, DOI 10.1002/1521-4095.

[22] M. Lee, B.-K. Cho, W.-C. Zin, *Chem. Rev.* **2001**, *101*, 3869–3892.

[23] T. Kato, Ed. , *Liquid Crystalline Functional Assemblies and Their Supramolecular Structures*, Springer Berlin Heidelberg, Berlin, Heidelberg, **2008**.

[24] U. Boas, P. M. H. Heegaard, *Chem. Soc. Rev.* **2004**, *33*, 43.

[25] S.-E. Stiriba, H. Frey, R. Haag, *Angew. Chemie Int. Ed.* **2002**, *41*, 1329–1334.

[26] R. van Heerbeek, P. C. J. Kamer, P. W. N. M. van Leeuwen, J. N. H. Reek, *Chem. Rev.* **2002**, *102*, 3717–3756.

[27] L. J. Twyman, A. S. H. King, I. K. Martin, *Chem. Soc. Rev.* **2002**, *31*, 69–82.

[28] D. Astruc, F. Chardac, *Chem. Rev.* **2001**, *101*, 2991–3024.

[29] R. M. Crooks, M. Zhao, L. Sun, V. Chechik, L. K. Yeung, *Acc. Chem. Res.* **2001**, *34*, 181–190.

[30] J. M. J. Fréchet, *J. Polym. Sci. Part A Polym. Chem.* **2003**, *41*, 3713–3725.

[31] J. M. J. Frechet, *Proc. Natl. Acad. Sci.* **2002**, *99*, 4782–4787.

[32] V. Percec, A. E. Dulcey, V. S. K. Balagurusamy, Y. Miura, J. Smidrkal, M. Peterca, S. Nummelin, U. Edlund, S. D. Hudson, P. A. Heiney, et al., *Nature* **2004**, *430*, 764–768.

[33] M. W. P. L. Baars, E. W. Meijer, Springer, Berlin, Heidelberg, **2000**, pp. 131–182.

[34] D. A. Tomalia, I. Majoros, *J. Macromol. Sci. Part C Polym. Rev.* **2003**, *43*, 411–477.

[35] D. Guillon, R. Deschenaux, *Curr. Opin. Solid State Mater. Sci.* **2002**, *6*, 515–525.

[36] J. A. A. W. Elemans, M. J. Boerakker, S. J. Holder, A. E. Rowan, W.-D. Cho, V. Percec, R. J. M. Nolte, *Proc. Natl. Acad. Sci. U. S. A.* **2002**, *99*, 5093–8.

[37] U. Stebani, G. Lattermann, *Adv. Mater.* **1995**, *7*, 578–581.

[38] J. H. Cameron, A. Facher, G. Lattermann, S. Diele, *Adv. Mater.* **1997**, *9*, 398–403.

[39] G. Ungar, Y. Liu, X. Zeng, V. Percec, W.-D. Cho, *Science* **2003**, *299*, 1208–11.

[40] X. Zeng, G. Ungar, Y. Liu, V. Percec, A. E. Dulcey, J. K. Hobbs, *Nature* **2004**, *428*, 157–160.

[41] L. Gehringer, C. Bourgogne, D. Guillon, B. Donnio, *J. Mater. Chem.* **2005**, *15*, 1696.

[42] S.-J. Park, M.-K. Seo, in *Interface Sci. Technol.*, Elsevier, **2011**, pp. 253–331.

[43] M. H. Hey, *Mineral. Mag. J. Mineral. Soc.* **1963**, *33*, 440–440.

[44] J. H. Robertson, *Acta Crystallogr. Sect. A* **1981**, *37*, 144–144.

[45] G. W. Gray, B. Jones, *J. Chem. Soc.* **1954**, 683–686.

[46] T. Kato, J. M. J. Frechet, *J. Am. Chem. Soc.* **1989**, *111*, 8533–8534.

[47] T. Kato, J. M. J. Frechet, *Macromolecules* **1989**, *22*, 3818–3819.

[48] M.-J. Brienne, J. Gabard, J.-M. Lehn, I. Stibor, *J. Chem. Soc. Chem. Commun.* **1989**, 1868.

[49] L. Bitan-Cherbakovsky, A. Aserin, N. Garti, *Colloids Surfaces B Biointerfaces* **2014**, *122*, 30–37.

[50] K. Didehban, H. Namazi, A. A. Entezami, *Eur. Polym. J.* **2009**, *45*, 1836–1844.

[51] T. Felekis, L. Tziveleka, D. Tsiourvas, C. M. Paleos, *Macromolecules* **2005**, *38*, 1705–1710.

[52] K. Didehban, H. Namazi, A. A. Entezami, *Eur. Polym. J.* **2009**, *45*, 1836–1844.

[53] M. Lehmann, *Chem. - A Eur. J.* **2009**, *15*, 3638–3651.

[54] J. Xu, T. C. Ling, C. He, *J. Polym. Sci. Part A Polym. Chem.* **2008**, *46*, 4691–4703.

[55] A. Kraft, A. Reichert, R. Kleppinger, *Chem. Commun.* **2000**, 1015–1016.

[56] J. Uchida, T. Kato, *Liq. Cryst.* **2017**, *44*, 1–14.

[57] J. Malthête, H. T. Nguyen, C. Destrade, *Liq. Cryst.* **1993**, *13*, 171–187.

[58] H.-T. Nguyen, C. Destrade, J. Malthécte, *Adv. Mater.* **1997**, *9*, 375–388.

[59] M. Bucoş, T. Sierra, A. Golemme, R. Termine, J. Barberá, R. Giménez, J. L. Serrano, P. Romero, M. Marcos, *Chem. - A Eur. J.* **2014**, *20*, 10027–10037.

[60] S. Ishihara, Y. Furuki, J. P. Hill, K. Ariga, S. Takeoka, *J. Nanosci. Nanotechnol.* **2014**, *14*, 5130–7.

[61] S. Ishihara, Y. Furuki, S. Takeoka, *Chem. Lett.* **2007**, *36*, 282–283.

[62] Y. Tian, K. Kamata, H. Yoshida, T. Iyoda, *Chem. - A Eur. J.* **2006**, *12*, 584–591.

[63] K. Kanie, M. Nishii, T. Yasuda, T. Taki, S. Ujiie, T. Kato, *J. Mater. Chem.* **2001**, *11*, 2875–2886.

[64] T. Kato, T. Matsuoka, M. Nishii, Y. Kamikawa, K. Kanie, T. Nishimura, E. Yashima, S. Ujiie, *Angew. Chemie Int. Ed.* **2004**, *43*, 1969–1972.

[65] Y. Kamikawa, M. Nishii, T. Kato, *Chem. - A Eur. J.* **2004**, *10*, 5942–5951.

[66] K. Kanie, T. Yasuda, M. Nishii, S. Ujiie, T. Kato, *Chem. Lett.* **2001**, *30*, 480–481.

[67] Y. Kamikawa, M. Nishii, T. Kato, *Mol. Cryst. Liq. Cryst.* **2005**, *435*, 95/[755]-105/[765].

[68] J. Barberá, L. Puig, J. L. Serrano, T. Sierra, *Chem. Mater.* **2004**, *16*, 3308–3317.

[69] J.-F. Xiong, S.-H. Luo, J.-P. Huo, J.-Y. Liu, S.-X. Chen, Z.-Y. Wang, *J. Org. Chem.* **2014**, *79*, 8366–8373.

[70] J. A. M. Lugger, D. J. Mulder, S. Bhattacharjee, R. P. Sijbesma, *ACS Nano* **2018**, *12*, 6714–6724.

[71] S. Bhattacharjee, J. A. M. Lugger, R. P. Sijbesma, *Chem. Commun.* **2018**, *54*, 9521–9524.

[72] J. A. M. Lugger, R. P. Sijbesma, *ChemistryOpen* **2016**, *5*, 580–585.

[73] G. M. Bögels, J. A. M. Lugger, O. J. G. M. Goor, R. P. Sijbesma, *Adv. Funct. Mater.* **2016**, *26*, 8023–8030.

[74] N. Krishnan, M. A. H. Ameena, S. Atchimnaidu, D. Perumal, M. Golla, J. Krishna, R. Varghese, *J. Chem. Sci.* **2018**, *130*, 141.

[75] H. Yang, J.-M. Chen, J.-J. Sun, S.-P. Yang, J. Yu, H. Tan, W. Li, *Dalt. Trans.* **2009**, 2540.

[76] H. Y. Lee, J. Park, M. S. Lah, J.-I. Hong, *Chem. Commun.* **2007**, *2*, 5013.

Chapter - 6

Synthesis and mesomorphic behavior of cyanostar precursors.

Abstract

In this chapter, we summarise the synthesis of cyanostar precursors. Interestingly these precursors are found to be mesomorphic and exhibit columnar mesophase. All precursors show good thermal stability, which was confirmed using thermogravimetric analysis. Mesomorphic behavior of the compounds were characterized by different experimental techniques such as polarized optical microscopy (POM) and differential scanning calorimetry (DSC). The self-assembly of these compounds in the columnar phase was confirmed by X-ray diffraction (XRD) studies. These precursors are potential molecules to generate the novel DLCs, namely cyanostars.

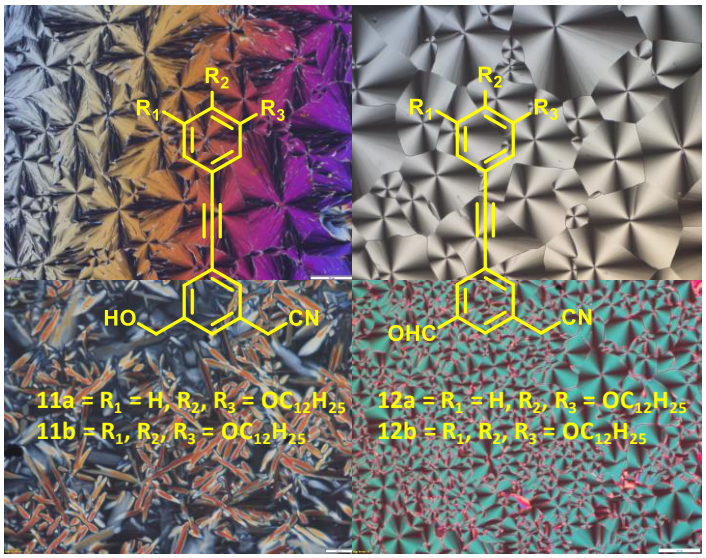

6.1 Introduction:

Macrocyclic molecules are desirable as a functional target for synthesis, molecular recognition, and hierarchical self-assembly. The macrocyclic molecules are described as molecules consisting of twelve or more membered rings. Such macrocyclic compounds are non-collapsible and geometrically distinct. These molecules are generally distinguished by the presence of repeat units and a lack of conformational flexibility. Pedersen et al incidently discovered the first macrocyclic polyethers, dibenzo [18] crown-6, along with the other homologous molecules.[1] These macrocyclic molecules are called crown ethers due to the crown-like structure of molecular models of their complexes with metal cations[2].

The groundbreaking article by Pedersen was published in 1967. Afterward, Lehn and his co-workers[3,4] synthesized a macrobicyclic polyether known as [2.2.2] cryptand. Also, his group established the encapsulation of IA and IIA group metal cations using three-dimensional receptors called cryptands[5]. The same features had been observed in macrobicyclic diamines and crown ethers[6–8]. The molecular structure of crown ether and cryptand is given in **Figure 6.1**. Prior to crown ethers and cryptands, naturally occurring cyclodextrins (CDs), macrocyclic molecules, played an essential role in developing chemistry beyond the molecules. In 1904 Schardinger characterized the three naturally occurring α, β, and γ CDs as cyclic oligosaccharides[9]. Cyclodextrins and their derivatives have been extensively explored in supramolecular chemistry for molecular recognition, host-guest interactions and commercial applications[10–12]. The chemical structures of CDs are given in **Figure 6.2.**

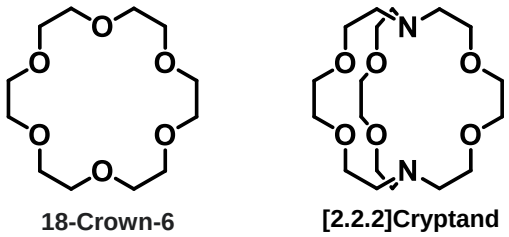

Figure 6.1: Structure of crown ether and cryptand.

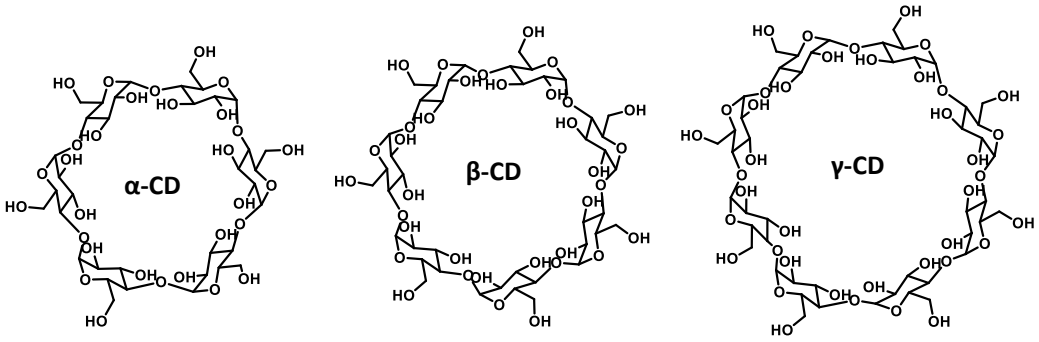

Figure 6.2: Chemical structure of the three main types of cyclodextrins.

In the last few decades, numerous artificial macromolecules like torands, calixarenes pillararenes, cyclophanes, and cucurbituril have been synthesized and studied for their excellent properties in the stream of macromolecular chemistry, especially in relation to the molecular reorganization and self-assembly process. Along with those applications, plenty of reports on cation and anion reorganization have been published in the literature[13,14]. Most of the ion-pair receptors rely on lone pair electron donors, including crown ethers[15] and π-electron donors, such as functionalized calixarenes, for cation recognition[16,17]. Therefore, macrocycles can show different affinities to various metal ions depending on cavity size and the number of electron donors.

Shape–persistent macromolecules[18] are characterized by a rigid framework that can dominate the particular conformation. These molecules can be designed for binding guest molecules or ions with specific dimensions. These macromolecules can hold the internal voids without guest molecules and build porous structures after self-assembly. Organic systems like aromatic rings and alkynyl groups have been introduced into the macrocycles to attain shape-persistent macrocycle rigidity[19]. As a result, these molecules can interact among themselves to form a layered structure using supramolecular interactions. One of the best examples for the shape–persistent macrocycles is porphyrin, which consists of four pyrrole rings connected by a methane bridge. In the literature, a lot of shape–persistent macromolecules have been reported. Researchers have managed to synthesize the numerous shape persistent macrocycles, which are explored in synthesis and self-assembly.[20–22] These are contributed to different applications such as solution-based sol-gel processing, surface-supported self-assembly, synthesis of macrocycles, preorganizations,[23] silico design,[24] catalysis,[25–27]

configurationally stable stereochemistry[28–30], and hierarchical self-assembly of multifunctional architectures.[31–36] Amar H. Flood group reported several triazolophanes, cyanostar, tricap (**Figure 6.3.)** macrocycles and their derivatives between the year 2008 to 2015. [14]

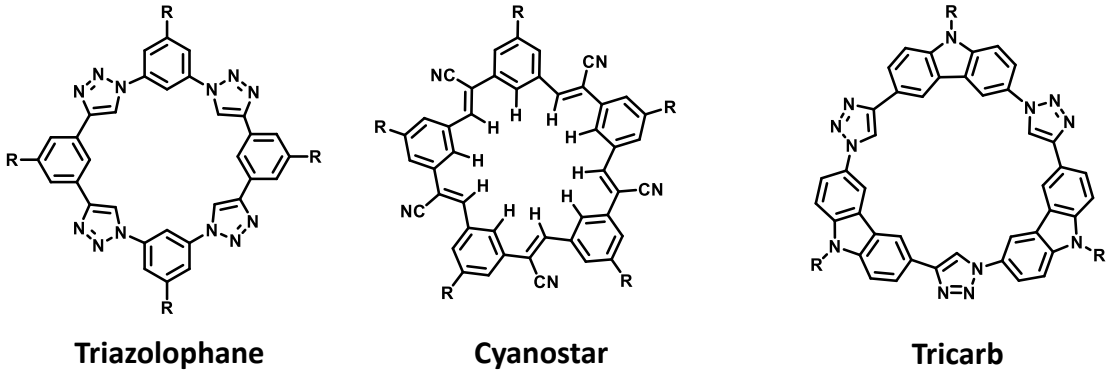

Figure 6.3: Chemical structure of the triazolophane, cyanostar, and tricarb.

Cyanostar is a remarkable molecule among those macrocycles. It is worthwhile to develop and synthesize cyanostar macrocyclic compounds, motivated by the fascinating concept of activated CH donors of triazoles, which may be employed in various applications. It is essential to know whether triazole CH donors are favored over other cyanostar CH donors. To address this problem, they recognized that any feasible polarized CH bond[37] would need to mimic the effort with which 1, 2, 3-triazoles are incorporated into preorganized receptors like triazolophanes[38,39] using click chemistry. Semin Lee has discovered another new class of molecules called tricarbazole triazolophanes (also known as tricarb). These molecules have been synthesized at one pot using click chemistry. This molecule is also used as the pocket for the anion binding, that part which is composed entirely of CH hydrogen donors. Cyanostilbenes (**Figure 6.4a**) appear as exciting molecules beyond their ability to form intermolecular CN – H hydrogen bonds in the solid state.[40] They are easy to make using Knoevenagel condensation. Furthermore, the electron-deficient π-conjugated character of cyanostilbenes led to acting as a semiconductor material[41] in the form of para-linked polymers and exploited as small molecules for aggregation-induced emission[42], raises the future potential for electronic and photochemical properties.

Here mainly, we focus on cyanostar macrocycle molecules and their derivatives. These molecules are used for the size-dependent, robust recognition of significant and weakly coordinating anions, synthesis of rotaxanes, and high fluorescent materials. Semin Lee et al. reported the synthesis of the C5-symmetric penta-t-butylpentacyanopentabenzo[25]annulene macrocycle **CS** (**Figure 6.4b**). The Knoevenagel self-condensation reaction can be used for synthesizing butylpentacyanopentabenzo[25]annulene, a macrocyclic compound. For this, meta-substituted difunctional phenylene with the functional groups of benzylic nitrile and benzaldehyde must be present in the starting material.

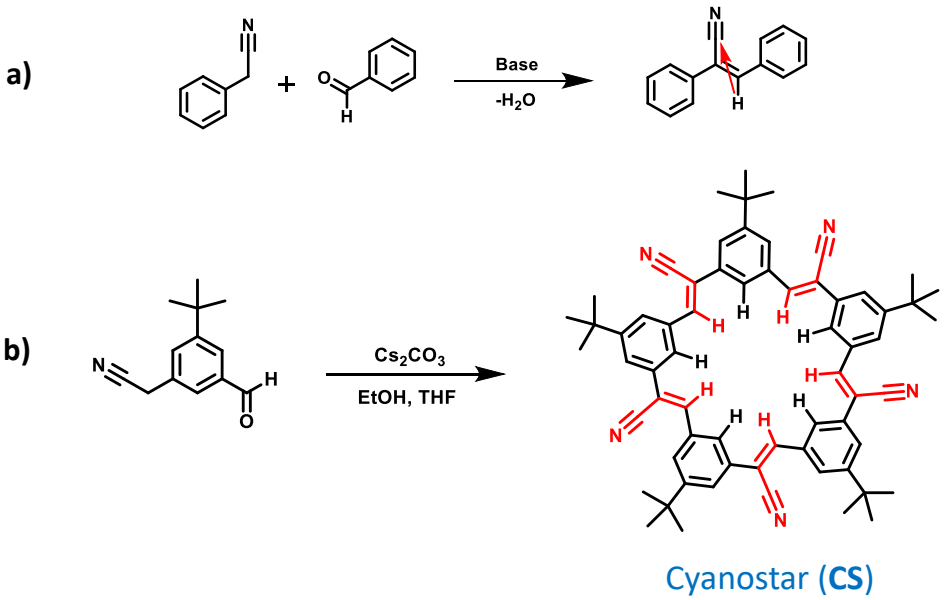

Figure 6.4: a) General preparation of cyanostilbenes using a Knoevenagel condensation b) One-pot synthesis of cyanostar.

This non-symmetric arene is commonly used to facilitate chain extension in a linear fashion all the way to the pentamer, followed by cycle formation. In contrast, the reaction between two different symmetric building blocks can only access cycles with even numbers. This macrocycle was prepared from 2-(3-(tert-butyl)-5-formylphenyl) acetonitrile, using carbonate (Cs_2CO_3) as the catalytic base (5 mol %) in ethanol/tetrahydrofuran (EtOH/THF) followed by a straightforward purification. Yielding **CS** in 81%.[43] This molecule in the solid-state existing in dimer form with the help of π- π interactions. They are constituted of chiral P and M enantiomers (**Figure 6.5**). The molecules containing the electropositive central cavity stabilize anions with CH hydrogen-bonding units activated by electron-withdrawing cyano groups. In solution, the cyanostar shows high-affinity binding as 2:1, 2:2, 3:2, 3:3, 4:3 sandwich

complexes of large anion[43–45], and they also showed the selective supramolecular recognition of anions. It offers a high conductivity that is competitive with current commercial standard electrolytes at dilute concentrations.[46]

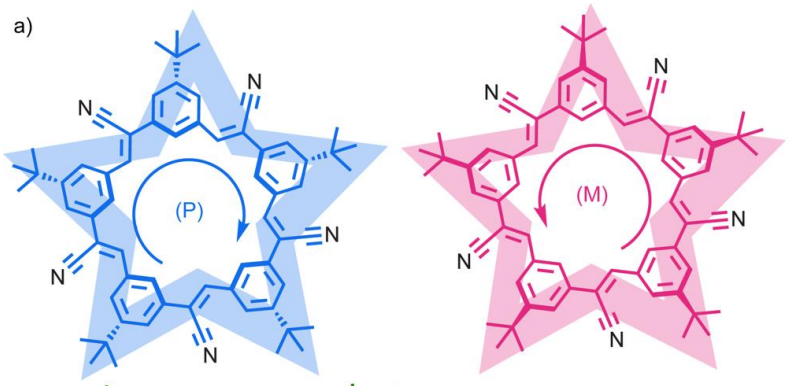

Figure 6.5: P and M enantiomers of cyanostar.

The cyanostar molecule has a size preference towards the anion recognization to form a [3] rotaxane templated around a dialkyl phosphate. Along with this, they also demonstrated a high-yielding synthesis of anion-templated [3]rotaxanes that efficiently harvest the high-fidelity pseudorotaxane species formed between two cyanostars and one dialkyl phosphate thread using click chemistry (**Figure 6.6**).[47]

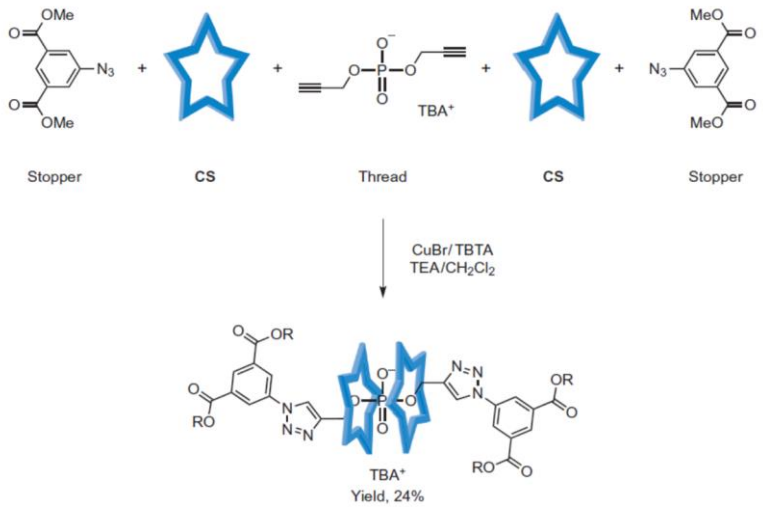

Figure 6.6: Formation of phosphate –templated [3] rotaxanes.

Brandon et al. reported the STM (scanning tunneling microscope) images, X-ray crystallographic data, and verifying anion-promoted formation of 2:1 dimers of cyanostar[48].

They have used appropriate substituents to study the cyanostars in each environment. Tert-butyl substituents of CS-1 provide steric gearing for 3D crystallization. Cyanostar CS-2 incorporates ester-terminated phenylene–acetylene arms-bearing octyl (C_8) chains, which serve as solubilizing agents during the synthesis and help to stabilize the molecules at the surface of highly oriented pyrolytic graphite (HOPG). X-ray data showed that CS-1 is coordinated with perchlorate anion. Similarly, the 2D crystallization of CS-2 showed dimer formation upon adding hexafluorophosphate anion (**Figure 6.7**).

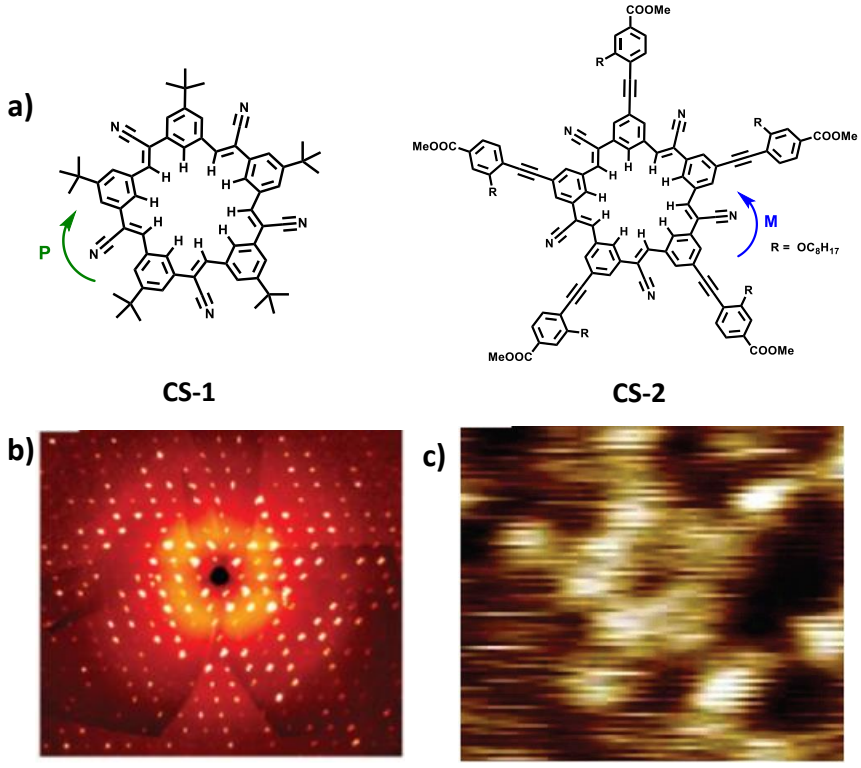

Figure 6.7: Cyanostars a) chemical structure and P and M stereoisomers of CS-1 and CS-2 b) Single-crystal diffraction (precession) of CS-1 c) STM image of CS-2 at THE TCB/HOPG interface

Wei Zhao et al. reported a new class of anion-directed supramolecular polymer[49] (**Figure 6.8**). Strong, higher-order 2:2 reorganization chemistry is used to drive the linear polymerization using difunctionalised phosphate groups employing different aliphatic chains and cyanostar. They have also reported the stoichiometry-control to specify the monomer sequence in a linear supramolecular polymer by synthesizing both a homopolymer and alternating copolymer using

glycol substituted cyanostar macrocycle and phenylene linked diphosphate monomer. The cyanostar stabilizes the homopolymer $(A)_n$ formation, and copolymer $(AB)_n$ is co-driven by cyanostar stabilized phosphate dimers and cation-stabilized phosphate dimers. Both the supramolecular polymers exhibit adhesive properties. The adhesive property of the copolymers is higher than the homopolymer[50] (**Figure 6.9**).

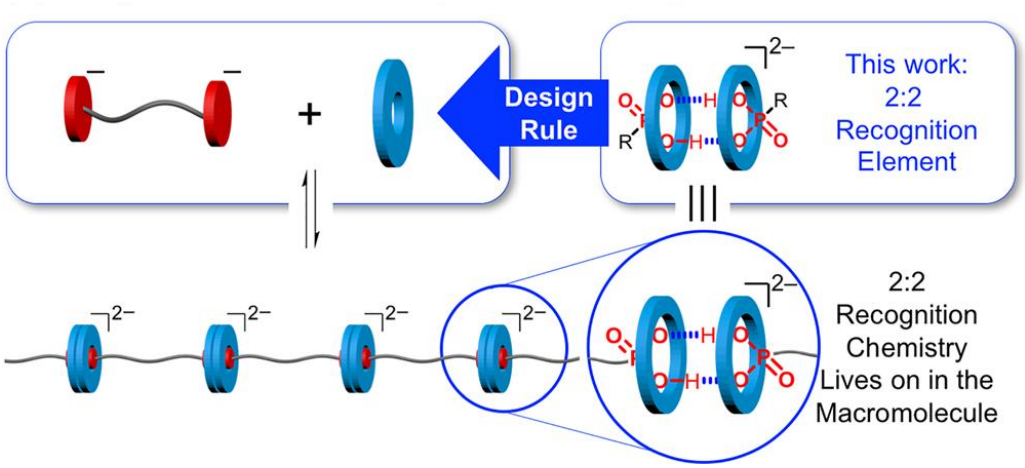

Figure 6.8: Anion-directed supramolecular polymer based on a 2:2 macrocycle: anion linkage stoichiometry.

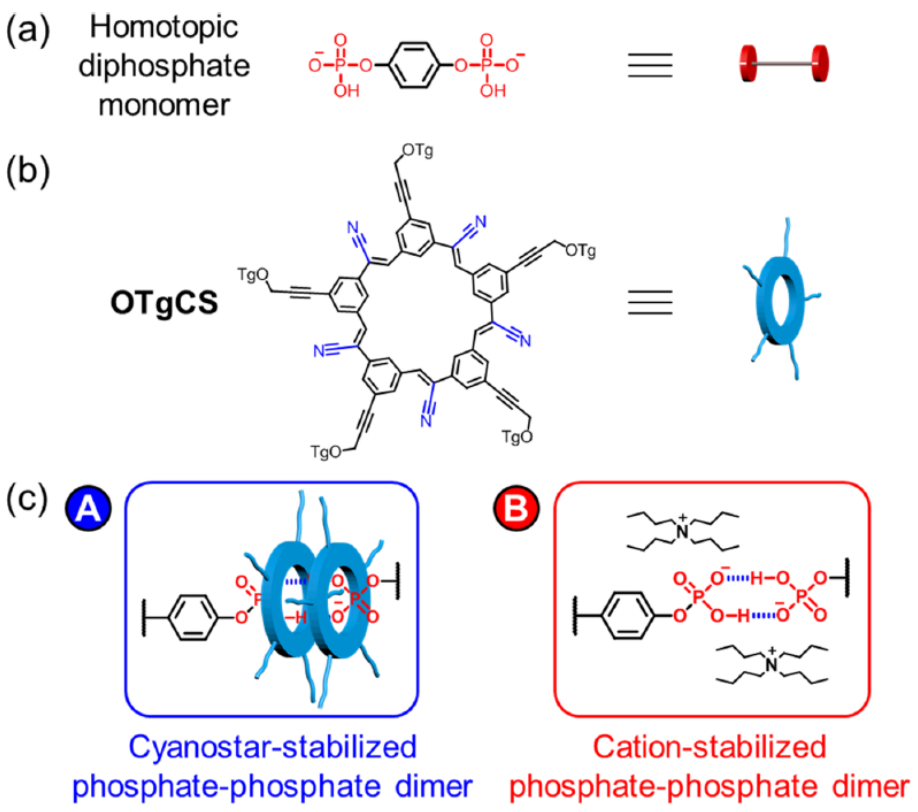

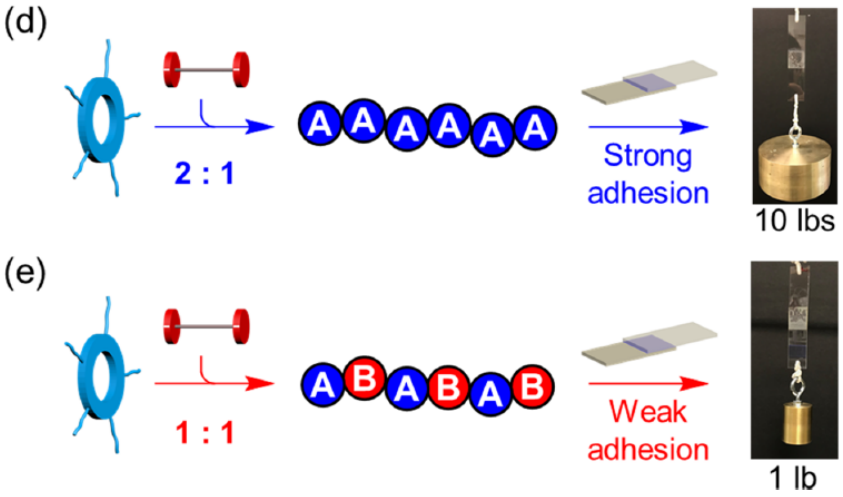

Figure 6.9: Structures of (a) the homotopic diphosphate with a rigid phenylene linker, (b) cyanostar macrocycle, OTgCS, (c) cyanostar-stabilized phosphate−phosphate dimer (A), and cation-stabilized phosphate−phosphate dimer (B). Representation of stoichiometry-controlled supramolecular polymers: (d) homopolymer (A)n shows strong adhesion, and (e) the alternating copolymer (AB)n offers weak adhesion.

Christopher R. Benson et al. studied to quantify and simulate a molecular three-body problem of threading two molecular rings onto a linear molecular thread using a molecular switch[51] (**Figure 6.10**). Here they have used tetrazine derivative as thread and as a molecular ring, cyanostar molecules. The formation of [3] pseudorotaxane, a tetrazine derivative, can capture the two molecules of cyanostar. The mechanism was studied using the analysis of cyclic voltammetry (CV) traces and Brownian dynamics simulations

Amar H. Flood and his group have developed new fluorescent materials using cyanostar molecules. Here, they studied the red-emitting oligomeric complex of large anion sandwiched by the macrocyclic cyanostar receptors, which form hierarchical assemblies with the chromogenic cation. The chromogenic trioxatriangulenium (TOTA+) cation and its co-assembly with cyanostar were used in this study (CS). The creation of 2:1 sandwich complexes with macrocycle was used to alter tetrafluoroborate (BF_4) counter anions. They have studied the optical properties of TOTA cation stacks. It clearly shows the red-shift in both solid and liquid states.[52]. The mechanism of hierarchical assembly is given in **Figure 6.11**. Also, they discovered a new class of fluorescent materials that shows the high emissive properties called SMILES (small-molecule ionic isolation lattices). This is prepared by mixing cationic dyes

with anion-binding cyanostar macrocycles and working with major commercial dyes (**Figure 6.12**)[53]. They have designed the one–step supramolecular approach to developing the nanoparticle using SMILES, which exhibits the high fluorescent properties used in bio imaging[54].

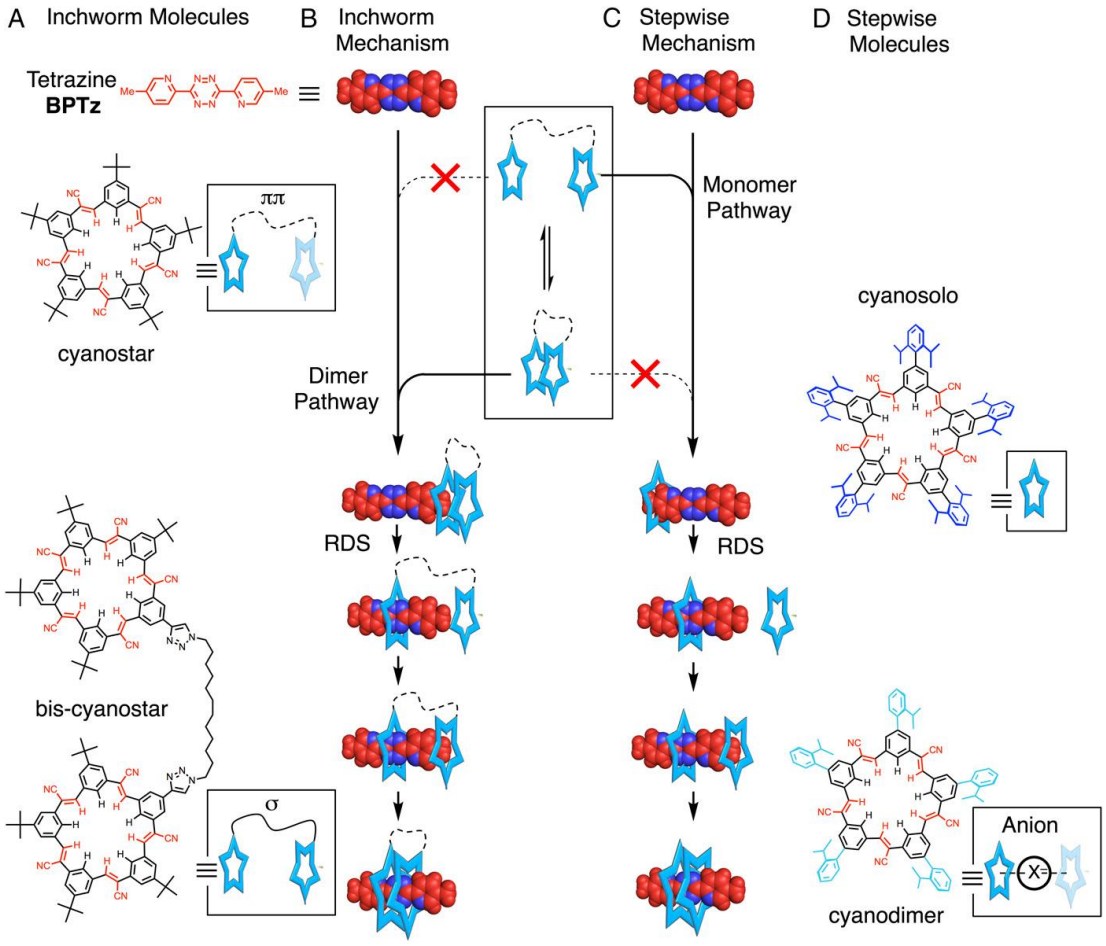

Figure 6.10: (A) Structures and cartoon representations of cyanostar ring systems (parent cyanostar and dodecyl-linked bis-cyanostar) and a tetrazine thread (colored red): 3,6-bis(5-methyl-2-pyridine)-1,2,4,5-tetrazine (BPTz). (B and C) Representations of the (B) inchworm and (C) stepwise mechanisms for threading cyanostar-based rings onto a tetrazine rod. (D) Structures and cartoon representations of cyanostar macrocycles, cyano solo, and cyanodimer thread onto a tetrazine rod stepwise. RDS indicates a rate-determining step.

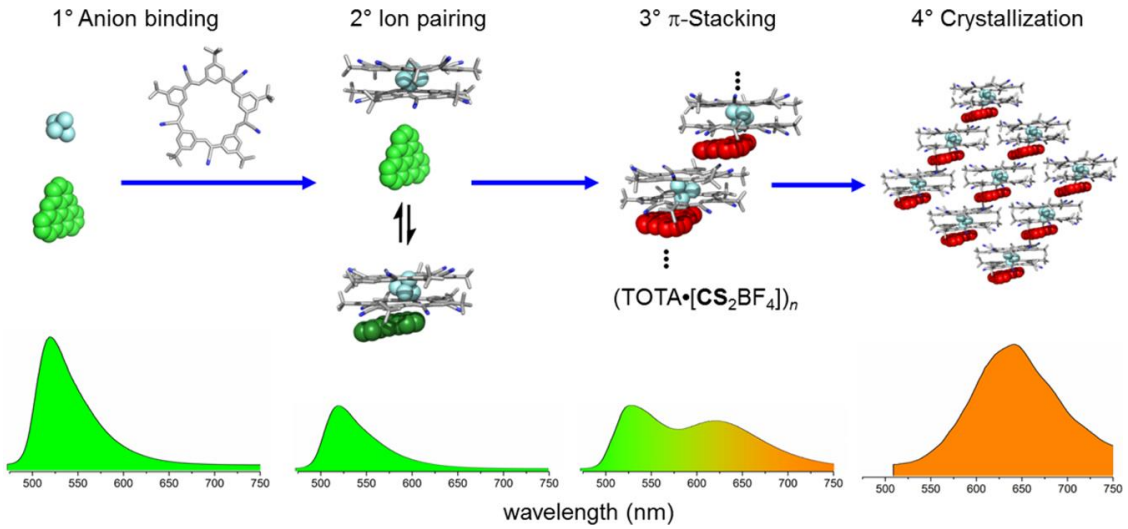

Figure 6.11: Structure−property coevolution of TOTA·BF4 with cyanostar across the hierarchy (1° → 4°) of assembled species from solution to the solid-state cocrystal of TOTA·[CS2BF4].

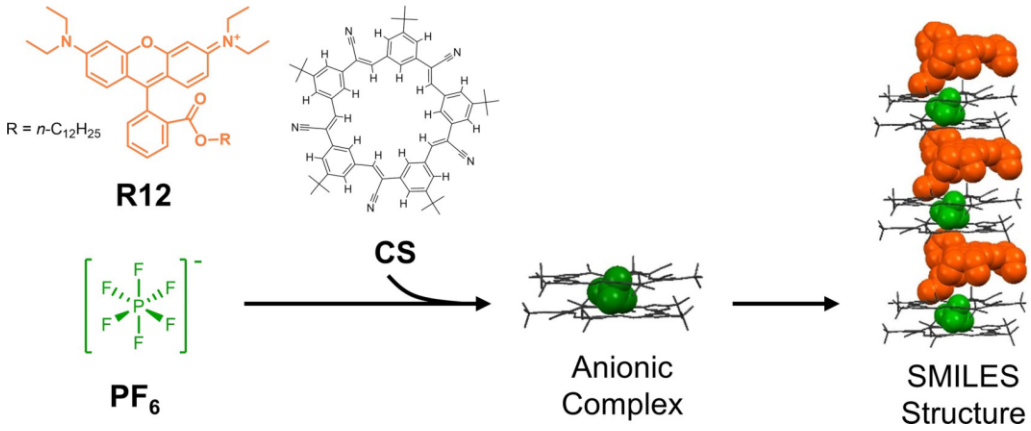

Figure 6.12: Schematic representation of the self-assembly process and the structure of small molecule ionic isolation lattices (SMILES) materials.

.

The history of the cyanostar macrocycle molecule presented above and many other articles that lack liquid-crystalline components using the cyanostar molecules prompted us to investigate this core to prepare DLCs. Discotic liquid crystals are well known in the literature. Generally, the synthesis of discotic liquid crystals is typically made of a central discotic core substituted by 3–12 saturated chains of three or more carbon atoms. These materials often have two-, three-, four-, or six-fold rotational symmetry. However, there are many exceptions, and materials with low symmetry, a nonplanar, nonaromatic core having a shorter number of chains, are also

documented. We have designed a novel molecular structure consisting of a cyanostar macrocycle as a core molecule and surrounded by 10 or 15 alkoxy chains shown in **Figure 6.13**. These molecules are also capable of forming the DLCs. Interestingly, on the synthesis process of 13**a** and **13b**, some of the intermediates compound **11a-b** and **12a-b,** which exhibits the liquid crystalline properties, are presented here.

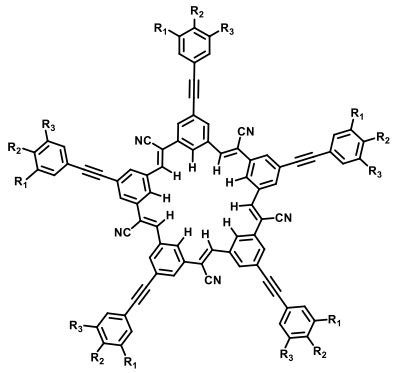

Figure 6.13: Molecular structure of cyanostar based liquid crystal.

6.2 Results and discussion:

6.2.1 Synthesis

Here we report the synthesis of novel two ring rod-shaped cyanostar precursors containing di and tri alkoxy chains. Compounds of **11a, 11b,** and **12a, 12b** were synthesized by following a route shown in **Figure 6.14.** These compounds exhibit monotropic liquid crystalline behavior. These molecules self-assemble into columnar hexagonal mesophase, as determined by x-ray diffraction studies. The mesomorphic properties of all the compounds were confirmed using a differential scanning calorimeter (DSC), polarising optical microscopy (POM), and an X-ray diffractometer.

The methyl gallate and isophthalic acid were purchased from Sigma Aldrich and used without any purifications. Compound **5** is prepared using alkylation of methyl gallate followed by reduction using $LiAlH_4$ to get compound **2**. The obtained compound **2** was converted into aldehyde using PCC and then synthesized dibromo olefin using CBr_4 and PPh_3. Further, it was converted into alkyne (Compound **5**) using TBAF. Isophthalic acid was methylated using

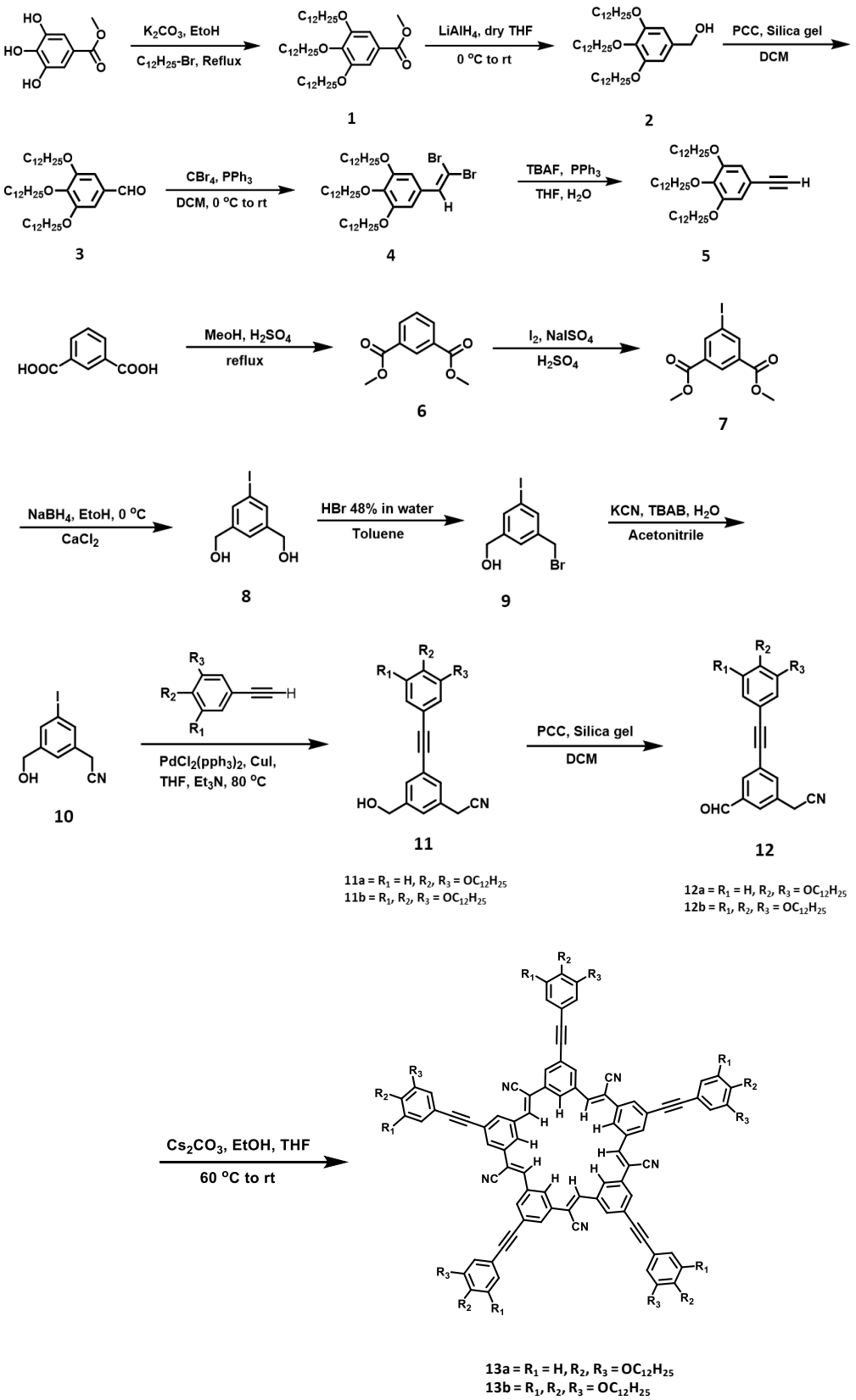

Figure 6.14: Synthesis of cyanostar precursors

H_2SO_4 and methanol, followed by iodination using I_2 and $NaISO_4$. The obtained 5-iodo isophthalate was treated $NaBH_4$ and $CaCl_2$ to get diol (**8**). Selective bromination of compound **8** using HBr 48% in water and toluene followed by cyanation with KCN to get compound **10**. Finally, the mesogenic compounds (**11a**, **11b,** and **12a**, **12b**) are obtained by Sonagashira coupling reaction with the **5** or 1,2-bis(dodecyloxy)-4-ethynylbenzene and compound **10** to get the coupled product of **11a** and **11b**. The obtained products were treated with PCC and silica gel to get **12a** and **12b**. All the compounds were purified by column chromatography on silica gel (100-200 mesh) followed by repeated crystallization using suitable analytical grade solvents. The structure of the mesogenic compounds and final compounds were confirmed using NMR and elemental analysis.

6.2.2 Thermal Stability:

The thermal stability of all mesogenic compounds is confirmed using TGA 4000 thermogravimetric analysis instrument. All the mesogenic compounds **11a**, **11b, 12a, 12b** were subjected to heat scan 10 ºC min^{-1} under a nitrogen atmosphere. Until 340 ºC, the compounds exhibit no weight loss. On further increasing the temperature, the weight loss was observed at around 390 ºC. The mesogenic compounds are completely decomposed at about 520 ºC. The TGA thermograms (**Figure 6.15**) suggest that all compounds have good thermal stability than the isotropic phase.

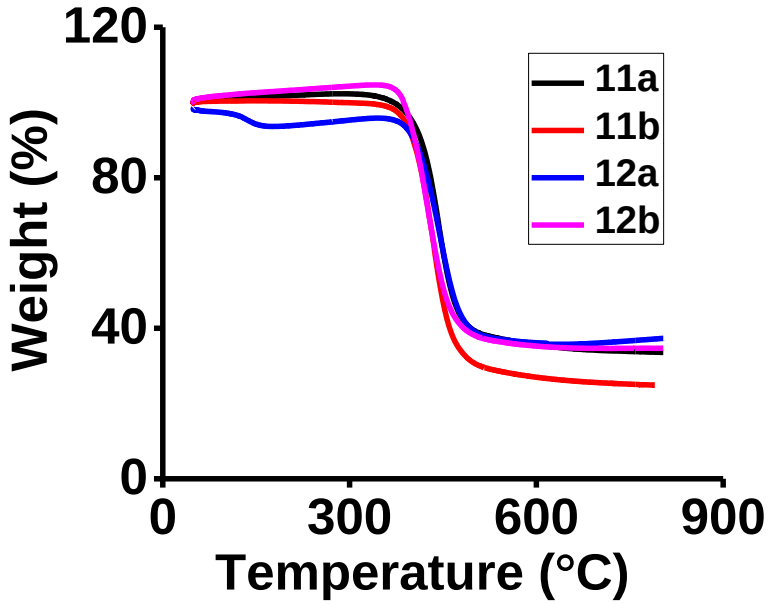

Figure 6.15. TGA spectra of **11a**, **11b**, **12a,** and **12b** show good thermal stability.

6.2.3 Mesomorphic characteristics:

The thermotropic mesomorphic properties of all the novel compounds exhibited a monotropic liquid crystalline behavior that agrees with the analysis of the textures and the thermal data recorded by POM and DSC, respectively. SAXS experiments confirmed the detailed self-assembly structures. The phase transition temperatures of all the compounds were initially determined using polarised optical microscopy. The optical textures were observed when a thin film of the sample was sandwiched between the two glass plates and cooled from the isotropic phase. We observe pseudo focal conic textures and dendritic texture of **11a**, **12a**, **11b,** and **12b** respectively, under the cross polarizers upon cooling from the isotropic phase shown in **Figure 6.16,** which agrees with columnar mesophase.

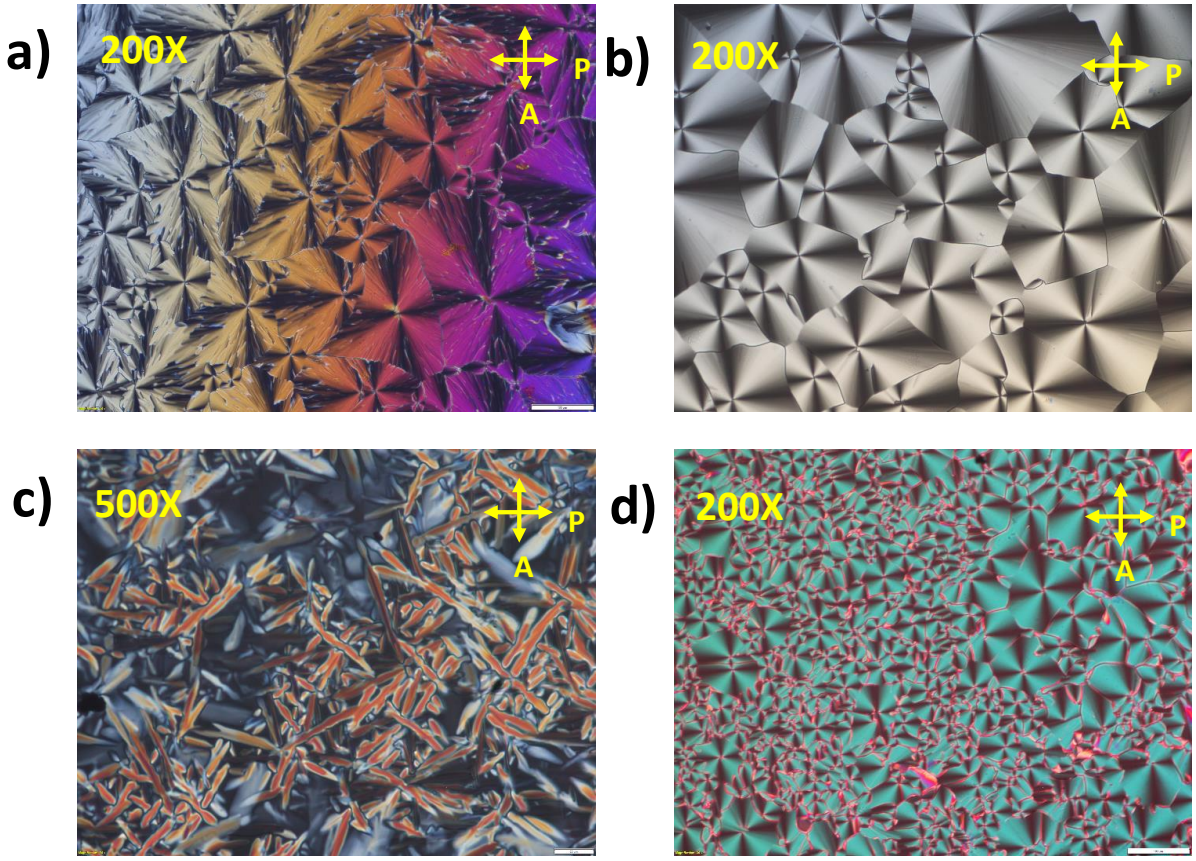

Figure 6.16. Birefringence texture of columnar mesophase observed under POM for compounds a) **11a** at 65 °C b) **12a** at 38 °C, c) **11b** at 31°C, and d) **12b** at 18.5 °C, upon cooling from the isotropic phase

The thermal transitions of all the compounds are further investigated using DSC, and thermograms are shown in **Figure 6.17**. From DSC analysis upon heating, all the compounds (**11a, 11b,** and **12a, 12b**) show only one endothermic peak from solid to isotropic liquid phase at 75.31 ºC, 43.32 ºC, 65.87 ºC, and 63.6 ºC, respectively. However, during the cooling cycle, all the compounds show two exothermic peaks below the melting point. These peaks are associated with the isotropic phase to columnar phase transitions observed at 69.32 ºC, 33.30 ºC, 47.18 ºC, and 20.81 ºC. Columnar phase to crystals phase transitions were observed at 37.37 ºC. 5.96 ºC, 24.49 ºC, and 5.14 ºC. Compared to the dialkoxy compounds, trialkoxy derivatives exhibit lower melting temperatures due to higher alkoxy chains present in the trialkoxy compounds. These properties make these compounds a low-temperature columnar phase, which can be used in electro-optical studies. The onset temperatures and corresponding enthalpy values of the phase transitions are given in (**Table 6.1**).

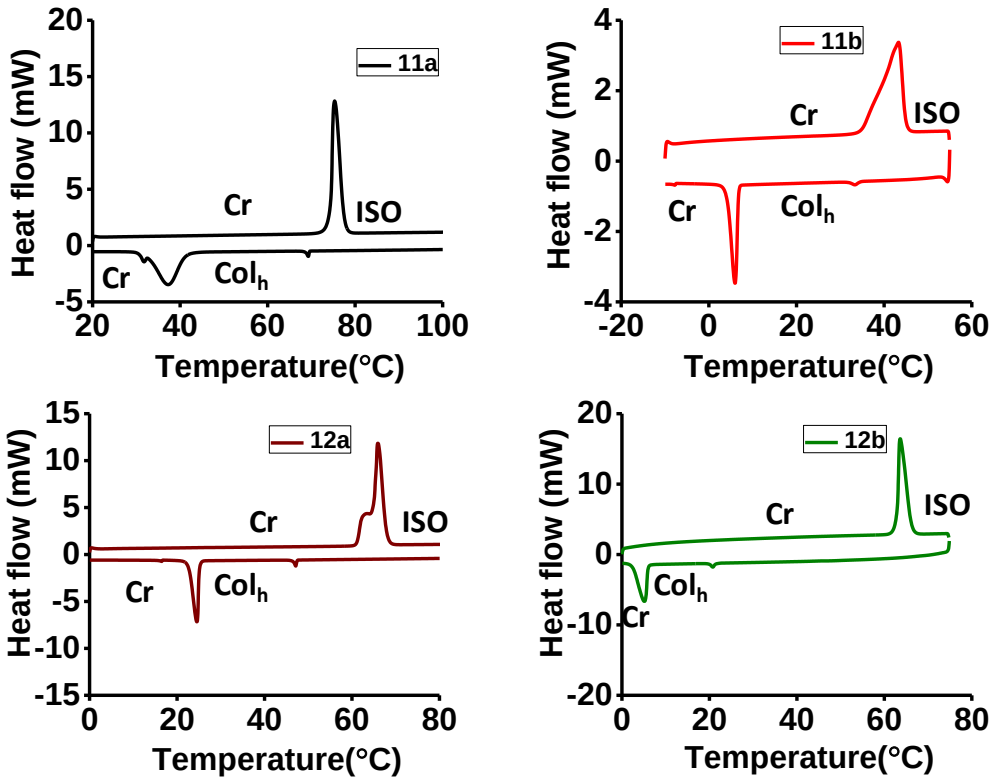

Figure 6.17. DSC thermograms obtained for the **11a, 11b, 12a,** and **12b** derivatives show phase transitions during heating and cooling cycles at a scan rate of 5 ^{o}C min^{-1}.

The supramolecular self-assembly of all the compounds was carried out using X-ray diffraction experiments. X-ray diffraction patterns of **11a, 11b,** and **12a, 12b** were recorded in the columnar mesophase 10 ^{o}C below the isotropic temperatures while cooling from the isotropic phase. A representative diffraction pattern obtained for all the compounds is given in **Figure 6.18**. The overall features observed are consistent with the structure of the Col_h phase. All the compounds exhibit three peaks at small angle regions, one very strong and two weak reflections are seen whose d-spacings are in the ratio of 1: 1/√3: 1/√4 that corresponds to the 10, 11, and 20 reflections. All the sharp peaks can be indexed in the two–dimensional hexagonal lattice, and the mesophase of these compounds can be identified as a hexagonal columnar. The wide-angle region exhibits one broad peak centered at 4.3 Å that corresponds to the liquid-like order of the aliphatic chains. The respective lattice parameters(a) of **11a**, **11b**, **12a**, and **12b** are 47.80, 42.73, 47.37, and 43.67. The d-spacings, miller indices, lattice parameters, area, and volume, are given in **Table 6.2**. By considering the X-ray data, the number of molecules per slice of the column was found to be around eight molecules for **11a** and **12a.** However**,** In the case of compound **11b** and **12b** is close to five molecules.

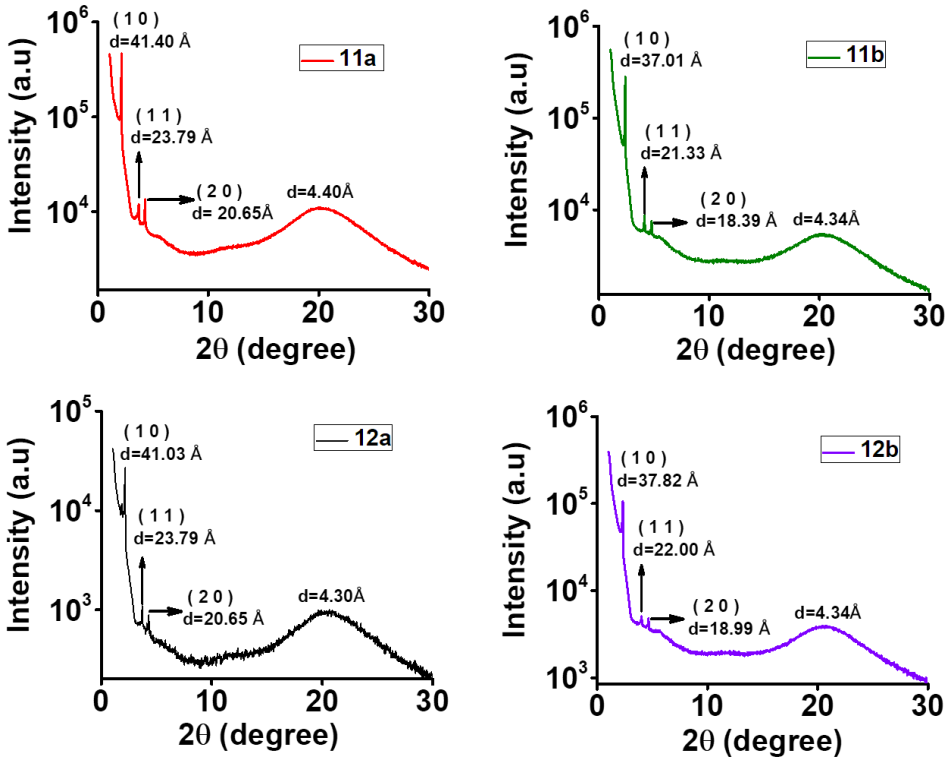

Figure 6.18. One-dimensional intensity versus 2θ profile obtained from X-ray diffraction of **11a, 11b, 12**a & **12b** at 60 ºC, 35 ºC, 40 ºC, and 20 ºC respectively upon cooling from the isotropic phase.

Table 6.1. Phase transition temperatures (ºC), enthalpy changes, and the proportional enthalpies (J/g) of **11a, 11b** and **12a,12b** at the time of heating and cooling were obtained from DSC. Cr – Crystalline phase; Col_h – Columnar hexagonal phase; I – Isotropic.

Compound	Heating	Cooling
11a	Cr 75.3 (97.66) I	I 69.3 (1.22) Col_h 37.3(65.11) Cr
11b	Cr 43.3 (81.56) I	I 33.3 (0.85) Col_h 5.9 (28.51) Cr
12a	Cr 65.8 (141.99) I	I 47.1 (1.90) Col_h 24.4 (43.82) Cr
12b	Cr 63.6 (69.65) I	I 20.8 (1.39) Col_h 5.1 (28.28) Cr

Table 6.2. Layer spacing obtained from XRD for **11a, 11b, 12a** and **12b,** Columnar Hexagonal: (**a** = lattice parameter = $\sqrt{(4/3)} \times d_{10}$; lattice area $\mathbf{S_h} = a^2\sin 60^o$; lattice volume $\mathbf{V_h} = a^2 \sin 60^o \times h_c$ ($\mathbf{h_a}$ if $\mathbf{h_c}$ is not observed); No of molecules per slice of column (**Z**) = $(\sqrt{3}\times N_a \times P \times a^2 \times h)/2M$; $\mathbf{N_a}$ = Avogadro's number; **P** = Density in Kg/m^3; **a**=lattice parameter; $\mathbf{h_c}$=core core peak ($\mathbf{h_a}$ if core-core is not observed); **M** = molecular weight in Kg/m^3).

Compounds	T (°C)	d-spacing(Å)	Phase	Parameters
11a	60	41.40 (10), 23.79 (11), 20.65 (20) 4.46	Col_h	**a** = 47.80 Å $\mathbf{S_h}$ = 1978.72 Å^2 $\mathbf{V_h}$ = 8825.123Å^3 **Z** = 8.4
11b	35	37.01 (10), 21.33 (11), 18.39 (20) 4.34	Col_h	**a** = 42.73Å $\mathbf{S_h}$ = 1581.23 Å^2 $\mathbf{V_h}$ = 6862.55Å^3 **Z** = 5.1
12a	40	41.03 (10), 23.79 (11), 20.65 (20) 4.30	Col_h	**a** = 47.37 Å $\mathbf{S_h}$ = 1943.28 Å^2 $\mathbf{V_h}$ = 8356.13Å^3 **Z** = 8.1
12b	20	37.82 (10), 22.00 (11), 18.99 (20) 4.34	Col_h	**a** = 43.67 Å $\mathbf{S_h}$ = 1651.56Å^2 $\mathbf{V_h}$ = 7167.81Å^3 **Z** = 5.4

6.2.4 Density functional theory studies:

The theoretical studies were done using the GAUSSIAN-09 program at Becke's three-parameter functional and Lee, Yang, and Parr correlation functional (B3LYP) using the 6-311G (d p) basis set. The energy-minimized structure of **11a, 11b, 12a,** and **12b** are given in **Figure 6.19**. The HOMO LUMO molecular orbitals are presented in **Figure 6.20**. The theoretical energy gap for compounds **11a**, **11b,** and **12a**, **12b** is 4.19 eV and 3.61 eV. The optical energy gap (E_g) in eV was calculated to be 3.48 and 3.22 and (according to the equation Eg = 1240/onset, where onset was resolved as the intersection of the extrapolated tangent of the most prolonged wavelength absorption peak and the x-axis).

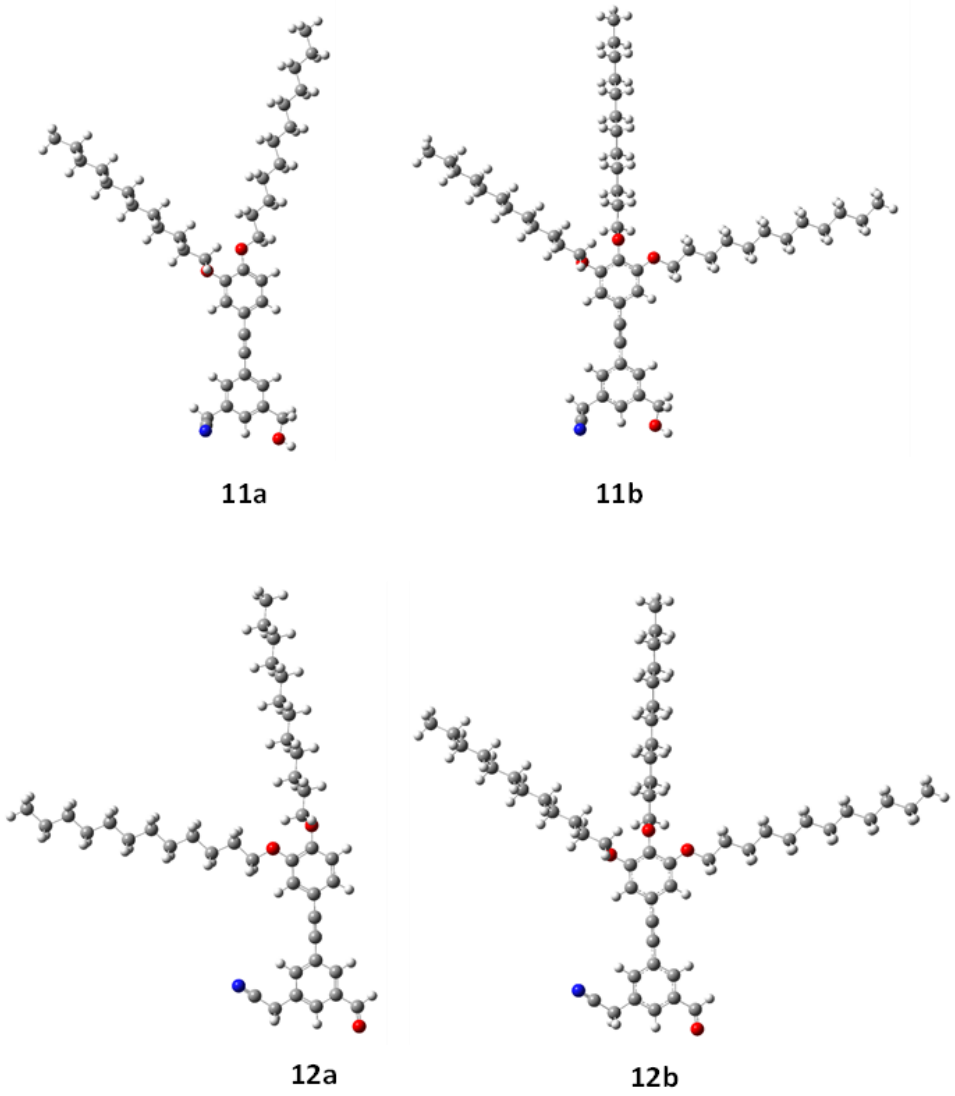

Figure 6.19. Energy minimized structure of **11a, 11b** and **12a, 12b**

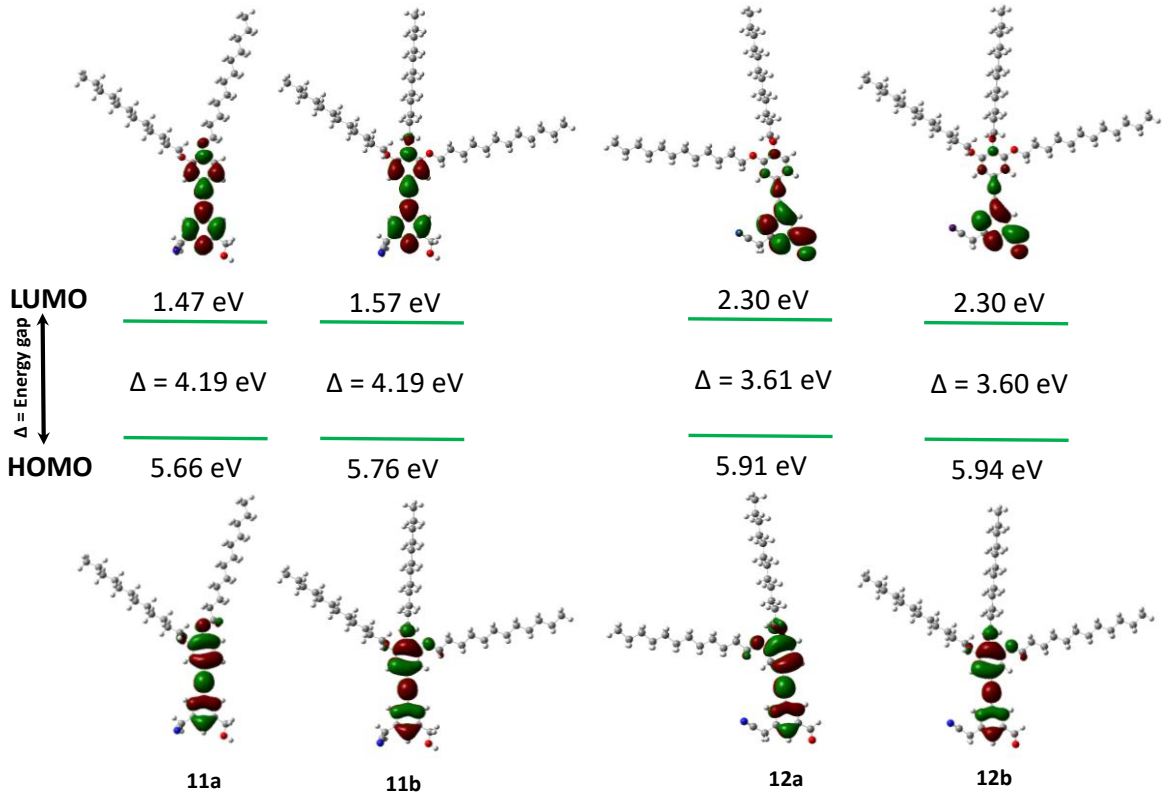

Figure 6.20. HOMO and LUMO energy level diagrams and theoretical bandgap of **11a, 11b** and **12a, 12b** calculated using **B3LYP** employing the **6-311G (dp)** basis set.

6.3 Conclusion:

In conclusion, a novel new series of dialkoxy and trialkoxy cyanostar precursors were synthesized using a Sonogashira coupling reaction followed by a PCC reaction and characterized using NMR and elemental analysis. All the molecules show excellent thermal stability and also exhibit monotropic liquid crystalline behavior. These compounds are self-assembled into the columnar hexagonal mesophase, which was confirmed by DSC, POM, SAXS. The number of molecules per slice of the column was found to be eight and five for **11a, 12a,** and **11b, 12b**, respectively. For all compounds, the mesomorphic properties are preserved upon cooling from the isotropic phase to room temperatures. The properties make these compounds a good candidate for optoelectronic properties. The synthesis of cyanostar and its derivatives for the new mesogens is in progress.

6.4 Experimental section:

Materials and Methods

Referee the page number 65

6.5 Synthesis and characterization:

Compound 1: In a round bottom flask ethyl gallate (10 g, 198.17 mmol, 1 eq), was dissolved in 500 mL of DMF, K_2CO_3 (41.84 g, 302.76 mmol, 6 eq), was added to it and stirred for 15 minutes, 1-Bromododecane (50.30 g, 201.84 mmol, 4 eq) and Potassium iodide (catalytic amount) were added to it the reaction mixture was refluxed for overnight. After completion of reaction it was cooled to room temperature, then the reaction mixture was poured into the ice water and the precipitate was filtered and the crude product was purified by column chromatography using petroleum ether: dichloromethane (8:2) as eluent and dried under high vacuum to get the desired product as white solid. ^{1}H NMR (500 MHz, $CDCl_3$): δ (ppm) = 7.17 (s, 2H), 3.94 – 3.92 (m, 6H), 3.81 (s, 3H), 1.76 – 1.63 (m, 6H), 1.42 – 1.36 (m, 6H), 1.27 – 1.19 (m, 48H), 0.80 (t, *J* = 6.25 Hz, 9H); ^{13}C NMR (125 MHz, $CDCl_3$): δ ppm = 166.93, 152.81, 142.33, 124.65, 107.94, 73.47, 69.14, 52.08, 31.94, 30.34, 29.77, 29.74, 29.72, 29.68, 29.65, 29.58, 29.41, 29.39, 29.31, 26.09, 26.07, 22.71, 14.11. Elemental analysis: C, 76.69; H, 11.70 calculated (%): C, 76.63; H, 12.12(expt. %).

Compound 2: In a round bottom flask, compound **1** (5 g, 5.83 mmol, 1eq), was dissolved in 100 ml of dry tetrahydrofuran and cooled to 0 ºC and $LiAlH_4$ (0.331 g, 8.74 mmol, 1.5 eq), was added to the reaction mixture portion-wise and allowed to room temperature and the reaction mixture kept for overnight, after completion of the reaction the reaction mixture was quenched. The reaction mixture was extracted with dichloromethane organic layer was dried over anhydrous Na_2SO_4 and the solvent was evaporated. The crude product was purified by column chromatography using petroleum ether and dichloromethane (7:3) as eluent and dried under high vacuum to get the desired product. ; ^{1}H NMR (500 MHz, $CDCl_3$): δ (ppm) = 6.57 (s, 2H), 4.61 (s, 2H), 4.00 – 3.94 (m, 6H), 1.82 – 1.74 (m, 6H), 1.48 (bm, 6H), 1.28 (bm, 48H), 0.9 (t, *J* = 6.25 Hz, 9H); ^{13}C NMR (125 MHz, $CDCl_3$): δ ppm = 153.25, 137.57, 136.12, 105.36, 73.45, 69.12, 65.59, 31.95, 31.93, 30.33, 29.76, 29.75, 29.71, 29.67, 29.63, 29.44, 29.40, 29.37,

26.15, 26.12, 22.69, 14.10. Elemental analysis: C, 78.12; H, 12.20 calculated (%): C, 78.35; H, 12.6(expt. %).

Compound 3: In a round bottom flask Compound **2** (8.3 mmol, 5.5 g) and pyridiniumchlorocromate (PCC) (12.4 mmol, 2.6 g) were taken in a 250 ml round bottom flask and 100 ml of dichloromethane (DCM) was added. After refluxing for 4 hrs the mixture was filtered and the organic layer was washed with brine, dried over anhydrous $MgSO_4$ and concentrated under reduced pressure. The resulting crude product was purified by silica gel column chromatography to obtain white solid Yield: 95%; ^{1}H NMR (500 MHz, $CDCl_3$): δ (ppm) = 9.85 (s, 1H), 7.10 (s, 2H), 4.08 – 4.04 (m, 6H), 1.86 – 1.75 (m, 6H), 1.49 – 1.48 (bm, 6H), 1.28 (bm, 48H), 0.90 (m, 9H); ^{13}C NMR (125 MHz, $CDCl_3$): δ ppm = 191.27, 153.53, 143.91, 131.45, 107.90, 73.64, 69.27, 31.92, 30.35, 29.74, 29.71, 29.69, 29.65, 29.62, 29.54, 29.38, 29.36, 29.26, 26.07, 26.03, 22.69, 14.10 Elemental analysis: C, 78.36; H, 11.93 calculated (%): C, 78.89; H, 12.40(expt. %).

Compound 4: In one neck 100 ml RBF, compound **3** (5g, 7.55 mmol, 1eq) was taken in 50 ml DCM and cooled to 0 °C. To that, CBr_4 (5.03g, 15.17 mmol, 2 eq) was added for 10 minutes and the solution was allowed to stir. After 5 minutes, PPh_3 (7.95g, 30.34 mmol, 4eq) was added and kept the solution to stir for another 2h. After completion of reaction checked by TLC. Further the evaporation of the solvent by rotavapor, make the slurry using silica-gel. The crude product was purified by column chromatography using petroleum ether and dichloromethane (9:1) as eluent and dried under high vacuum to get the desired product. Yield: 87%; ^{1}H NMR (500 MHz, $CDCl_3$): δ (ppm) = 7.36 (s, 1H), 6.76 (s, 2H), 3.98 – 3.94 (m, 6H), 1.82 – 1.70 (m, 6H), 1.46 (bm, 6H), 1.26 (bm, 64H), 0.88 (t, *J* = 6.25 Hz, 9H); ^{13}C NMR (125 MHz, $CDCl_3$): δ ppm = 152.86, 138.68, 136.80, 129.99, 107.20, 88.04, 73.42, 69.17, 31.97, 31.95, 30.34, 29.78, 29.75, 29.73, 29.69, 29.67, 29.61, 29.44, 29.40, 29.36, 26.11, 22.72, 14.13. Elemental analysis: C, 64.85; H, 9.65 calculated (%): C, 64.23; H, 9.23(expt. %).

Compound 5: In RBF, compound **4** (1.7g, 2.08 mmol, 1eq) was taken in 30 ml THF to that, PPh_3 (0.81g, 3.12 mmol, 1.5 eq) was added allowed to stir for 5min. After 5 minutes, TBAF (3.26g, 12.48 mmol, 6 eq) and then 0.5 ml of H_2O was added the reaction mixture was kept for 5h. After completion of reaction checked by TLC. The reaction mixture was quenched with water the separated organic layer Further the evaporation of the solvent by rotavapor, make the

slurry using silica-gel. The crude product was purified by column chromatography using petroleum ether as eluent and dried under high vacuum to get the desired product. Yield: 75%; ^{1}H NMR (500 MHz, $CDCl_3$): δ (ppm) = 6.68 (s, 2H), 3.94 (m, 6H), 2.99 (s, 1H), 1.81 – 1.69 (m, 6H), 1.45 – 1.42 (m, 6H), 1.29 – 1.26 (m, 48H), 0.88 (t, *J* = 6.5 Hz, 9H); ^{13}C NMR (125 MHz, $CDCl_3$): δ ppm = 152.94, 139.53, 116.42, 110.68, 84.03, 75.75, 69.13, 31.94, 30.32, 29.77, 29.75, 29.71, 29.67, 29.65, 29.60, 29.40, 29.39, 29.32, 26.10, 26.08, 22.71, 14.11. Elemental analysis: C, 80.67; H, 12.00 calculated (%): C, 81.10; H, 12.53 (expt. %).

Compound 6: In RBF, isophthalic acid **(**5g, 30.9 mmol, 1eq) was dissolved in 170 ml of methanol to that, 15 ml of H_2SO_4 was added, and the reaction mixture refluxed overnight. After completion of the reaction, half of the solvent was removed under reduced pressure using rotavapor, the reaction mixture was poured into 250 ml of ice water for 15 min. The precipitate was filtered using vacuum filtration, washed with water, and dried under a high vacuum to get the desired product. Yield: 93%; ^{1}H NMR (500 MHz, $CDCl_3$): δ (ppm) = 8.69 (s, 1H), 8.23 (d, 2H), 7.54 (t, 1H), 3.96 (m, 6H); ^{13}C NMR (125 MHz, $CDCl_3$): δ ppm = 166.20, 133.77, 130.67, 130.55, 128.60, 52.33. Elemental analysis: C, 61.75; H, 5.19 calculated (%): C, 61.83; H, 5.45 (expt. %).

Compound 7: In RBF, iodine **(**9.14g, 36.04 mmol, and 0.7eq) was added to a stirred solution of sodium periodate (4.43g, 18.02 mmol, 0.35eq) in 55ml of 96% H_2SO_4 at 36 ºC. The resulting mixture was stirred for 30 min. To this mixture compound, **6** (10.0 g, 51.49 mmol, 1eq) was added, the reaction mixture was stirred for 12h, after completion of reaction checked by TLC. The reaction mixture was poured into a 1-liter conical flask containing crushed ice and dichloromethane. The organic layer was separated, and the aqueous layer was repeatedly washed with dichloromethane then, the organic layer was washed with sodium bicarbonate solution, sodium thiosulphate solution, and brine solution respectively. The organic layer was dried over anhydrous Na_2SO_4, and the solvent was evaporated. The crude product was purified by column chromatography using petroleum ether and dichloromethane (7:3) as eluent and dried under a high vacuum to get the desired product. Yield: 60%; ^{1}H NMR (500 MHz, $CDCl_3$): δ (ppm) = 8.54 (bs, 1H), 8.46 (s, 2H), 3.87 (s, 6H); ^{13}C NMR (125 MHz, $CDCl_3$): δ ppm = 164.75, 142.42, 132.15, 129.83, 93.44, 52.65. Elemental analysis: C, 37.52; H, 2.83 calculated (%): C, 37.59; H, 2.93 (expt. %).

Compound 8: To a two-necked round-bottom flask was placed ethanol (50 ml) at 0 °C followed by sequential addition of $NaBH_4$ (0.96 g, 25.61 mmol, 4.1eq) portion-wise and compound **7** (2g, 6.24 mmol, 1eq) at the same temperature. A solution of CaCl2 (1.30g, 11.72 mmol, 2 eq) was added to this mixture in ethanol (30 mL) dropwise with stirring at 0 °C. The resulting solution was stirred at room temperature for 4 h then was quenched by adding 200 mL of 0 °C water. The mixture was concentrated under vacuum, and the residue was diluted with water (500 mL) and extracted with ethyl acetate (200 mL x 2). The combined organic layers were dried over Na_2SO_4, filtered, and the solvent was evaporated. The crude product was purified by column chromatography using petroleum ether and ethyl acetate (7:3) as eluent and dried under a high vacuum to get the desired product. Yield: 60%; ^{1}H NMR (500 MHz, DMSO-d_6): δ (ppm) = 7.54 (s, 2H), 7.26 (s, 1H), 5.27 (t, *J* = 5.50 Hz, 2H), 4.45 (d, *J* = 5.50 Hz, 4H); ^{13}C NMR (125 MHz, DMSO-d_6): δ ppm = 145.50, 133.61, 124.24, 94.86, 62.54. Elemental analysis: C, 36.39; H, 3.44 calculated (%): C, 36.17; H, 3.16 (expt. %).

Compound 9: In RBF, compound **8** (1.96g, 7.43mmol, 1eq) was taken and add 30 ml of toluene stirred at 0 °C for 15 min then 4.87 ml of (7.22 g, 89.25 mmol, 12eq) of HBr (47% v/v, aq) was added dropwise, and the reaction mixture remained at 0 ºC 2h then bring to room temperature and stirred for 3 h. After completion of reaction checked by TLC, 50 mL of water was added and extracted with chloroform (2 x 50 mL). Organic layers were dried over Na_2SO_4, filtered, and the solvent was evaporated. The crude product was purified by column chromatography using petroleum ether and ethyl acetate (8:2) as eluent and dried under a high vacuum to get the desired product. Yield: 68%; ^{1}H NMR (500 MHz, DMSO-d_6): δ (ppm) = 7.69 (s, 1H), 7.61 (s, 1H), 7.40 (s, 1H), 5.38 (bs, 1H), 4.66 (s, 2H), 4.46 (s, 2H); ^{13}C NMR (125 MHz, DMSO-d_6): δ ppm = 146.14, 140.74, 136.32, 135.23, 127.12, 94.95, 62.23, 33.57. Elemental analysis: C, 29.39; H, 2.47 calculated (%): C, 29.46; H, 2.26 (expt. %).

Compound 10: To a solution of KCN (1.39g, 21.40 mmol, 5eq) and tetra butyl ammonium bromide (0.069g, 0.21 mmol, 0.05eq) in water (5ml) was added to compound **9** (1.4g, 4.28 mmol, 1eq) was dissolved in acetonitrile (40ml). The reaction mixture was stirred at room temperature for 48 h. After completion of reaction checked by TLC, quenched with water, the reaction mixture was extracted with chloroform, the organic layer was dried over anhydrous Na_2SO_4, and the solvent was evaporated. The crude product was purified by column chromatography using petroleum ether and dichloromethane (7:3) as eluent and dried under a high vacuum to get the desired product. Yield: 97%; ^{1}H NMR (500 MHz, DMSO-d_6): δ (ppm)

= 7.64 (s, 1H), 7.59 (s, 1H), 7.33 (s, 1H), 5.37 (bs, 1H), 4.48 (s, 2H), 4.03 (s, 2H); ^{13}C NMR (125 MHz, DMSO-d_6): δ ppm = 146.39, 135.28, 134.59, 133.98, 125.89, 119.36, 95.35, 62.20, 22.21. Elemental analysis: C, 39.59; H, 2.95 calculated (%): C, 39.65; H, 2.68 (expt. %).

General Procedure for 11a &11b

Compound **10** (1eq) and **5a** or 1,2-bis(dodecyloxy)-4-ethynylbenzene (1.1eq) in dry THF and diisopropylamine degassed for 15 mins using nitrogen. To this solution $PdCl_2(PPh_3)_2$ (0.02eq) and CuI (0.017) were added. The reaction mixture was refluxed under an N_2 atmosphere overnight. After the reaction mixture was cooled to room temperature, triethylamine is removed under reduced pressure. The crude product was extracted with dichloromethane. The organic phase was dried over anhydrous Na_2SO_4, and dichloromethane was removed under reduced pressure. The crude product was purified using petroleum ether and dichloromethane as eluent by column chromatography and dried under a high vacuum to get the desired product.

Compound 11a: compound **10** (0.60g, 2.19mmol, 1eq), 1,2-bis(dodecyloxy)-4-ethynylbenzene (1.13g, 2.41mmol, 1.1eq), THF (20 ml) diisopropylamine (0.311g, 3.07 mmol, 1.4 eq), $PdCl_2(PPh_3)_2$ (0.03g, 0.042mmol, 0.02eq), CuI (0.007g, 0.037mmol, 0.017eq) Yield: 70% ; ^{1}H NMR (500 MHz, $CDCl_3$): δ (ppm) = 7.47 (s, 1H), 7.41 (s, 1H), 7.28 (s, 1H) 7.08 (d, *J* = 8.0 Hz, 1H), 7.03 (s, 1H), 6.83 (d, *J* = 8.0 Hz, 1H), 4.71 (s, 2H), 4.01 (t, *J* = 6.5 Hz, 4H), 3.75 (s, 2H) 1.82 (bs, 4H), 1.47 (bs, 4H), 1.26 (m, 32H), 0.88 (t, *J* = 6.0 Hz, 6H); ^{13}C NMR (125 MHz, $CDCl_3$): δ ppm = 149.97, 148.75, 142.21, 130.39, 129.84, 129.29, 125.67, 125.07, 124.89, 117.49, 116.62, 114.75, 113.20, 90.93, 86.75, 69.27, 69.15, 64.39, 31.93, 29.71, 29.67, 29.64, 29.63, 29.42, 29.38, 29.22, 29.18, 26.03, 26.00, 23.41, 22.70, 14.13; Elemental analysis: C, 79.95; H, 9.98; N, 2.27 calculated (%): C, 79.65; H, 10.03; N, 2.21 (expt. %)

Compound 11b: compound **10** (0.40g, 1.46mmol, 1eq), and compound **5** (1.05g, 1.61mmol, 1.1eq), THF (20 ml) diisopropylamine (0.207g, 2.07 mmol, 1.4 eq), $PdCl_2(PPh_3)_2$ (0.020g, 0.0292mmol, 0.02eq), CuI (0.0048g, 0.0253mmol, 0.017eq) Yield: 66 % ; M.P. 98 ºC; ^{1}H NMR (500 MHz, $CDCl_3$); ^{1}H NMR (500 MHz, $CDCl_3$): δ (ppm) = 7.48 (s, 1H), 7.42 (s, 1H), 7.29 (s, 1H) 6.73 (s, 2H), 4.72 (d, *J* = 4.50 Hz, 2H), 3.98 (t, *J* = 6.5 Hz, 6H), 3.75 (s, 2H) 1.83 – 1.72 (m, 6H), 1.48 – 1.44 (m, 6H), 1.34 – 1.26 (m, 48H), 0.88 (t, *J* = 6.0 Hz, 9H); ^{13}C NMR (125 MHz, $CDCl_3$): δ ppm = 153.03, 142.28, 139.29, 130.41, 129.87, 129.34, 125.84, 124.65, 117.48, 117.14, 110.15, 90.94, 87.06, 73.59, 69.15, 64.33, 31.95, 31.94, 30.32, 29.76, 29.75,

29.72, 29.67, 29.66, 29.61, 29.41, 29.38, 29.34, 26.10, 23.41, 22.71, 14.13; Elemental analysis: C, 79.55; H, 10.71; N, 1.75 calculated (%): C, 80.12; H, 10.31; N, 2.14 (expt. %)

General Procedure for 12a &12b

A mixture of PPC (1.5eq) and silica gel (5 g) was vigorously stirred for 10 min then dichloromethane was added. A solution of 11a or 11b (1eq) was dissolved in dichloromethane, added to the reaction mixture, and stirred for 1h, after completion of reaction checked by TLC. The reaction mixture was directly loaded onto a short silica gel and flushed with dichloromethane to give a white solid compound. The crude product was purified using petroleum ether and dichloromethane as eluent by column chromatography and dried under a high vacuum to get the desired product.

Compound 12a: compound **11a** (3.0g, 4.87mmol, 1eq), PCC (1.57g, 7.30mmol, 1.5eq), DCM (50 ml) silica gel (7.0 gm) Yield: 80% ; M.P. 98 ºC; ^{1}H NMR (500 MHz, $CDCl_3$): δ (ppm) = 10.01 (s, 1H), 7.96 (s, 1H), 7.76 (s, 2H) 7.11 (d, *J* = 8.0 Hz, 1H), 7.05 (s, 1H), 6.85 (d, *J* = 8.0 Hz, 1H), 4.02 (t, *J* = 6.5 Hz, 4H), 3.84 (s, 2H) 1.85 – 1.83 (m, 4H), 1.48 – 1.47 (m, 4H), 1.36 – 1.26 (m, 32H), 0.88 (t, *J* = 6.0 Hz, 6H); ^{13}C NMR (125 MHz, $CDCl_3$): δ ppm = 190.76, 150.36, 148.83, 137.17, 135.94, 132.55, 131.44, 127.39, 126.10, 125.19, 116.85, 116.69, 114.16, 113.20, 92.69, 85.58, 69.33, 69.15, 31.93, 29.71, 29.67, 29.64, 29.42, 29.37, 29.23, 29.18, 26.03, 23.31, 22.70, 14.12 Elemental analysis: C, 80.21; H, 9.96; N, 2.28 calculated (%): C, 80.40; H, 9.89; N, 2.14 (expt. %)

Compound 12b: compound **11b** (2.0g, 2.49mmol, 1eq), PCC (0.80g, 3.74mmol, 1.5eq), DCM (40 ml) silica gel (5.0 gm) Yield: 80%; M.P. 98 ºC; ^{1}H NMR (500 MHz, $CDCl_3$): ^{1}H NMR (500 MHz, $CDCl_3$): δ (ppm) = 10.01 (s, 1H), 7.97 (s, 1H), 7.77 (s, 2H) 6.75 (s, 2H), 3.99 (t, *J* = 60 Hz, 6H), 3.85 (s, 2H), 1.84 – 1.73 (m, 6H), 1.50 – 1.44 (m, 6H), 1.35 – 1.26 (m, 48H), 0.88 (t, *J* = 6.0 Hz, 9H); ^{13}C NMR (125 MHz, $CDCl_3$): δ ppm = 190.69, 153.11, 139.70, 137.18, 136.00, 132.57, 131.48, 127.62, 125.88, 116.82, 116.53, 110.27, 92.67, 85.80, 73.60, 69.20, 31.94, 30.34, 29.76, 29.71, 29.66, 29.60, 29.41, 29.38, 29.34, 26.10, 23.32, 22.70, 14.12; Elemental analysis: C, 79.75; H, 10.48; N, 1.75 calculated (%): C, 80.20; H, 11.84; N, 2.02 (expt. %)

6.6 NMR Spectra:

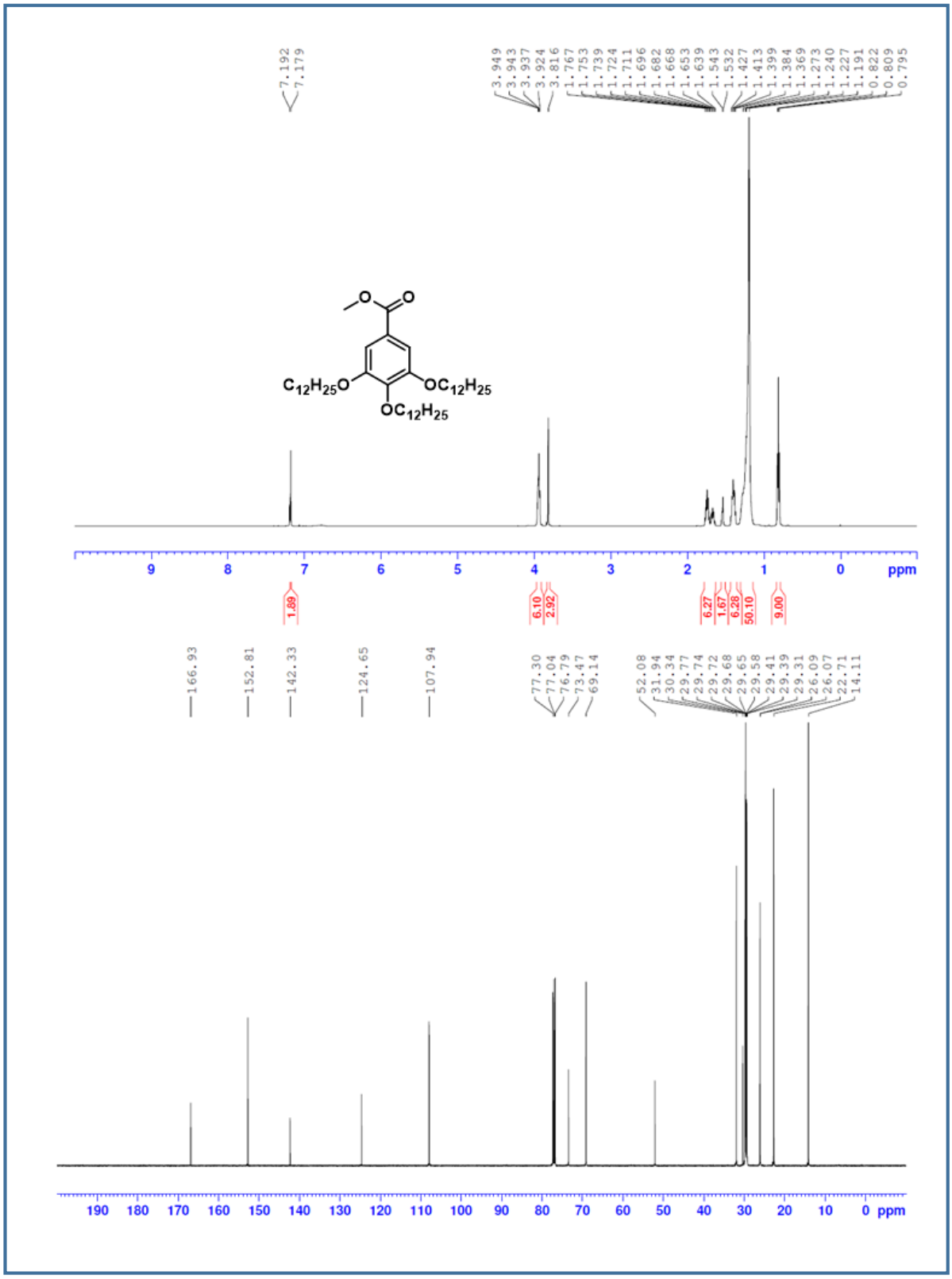

Figure 6.21: ^{1}H (top) and ^{13}C-NMR (bottom) spectra of **1**

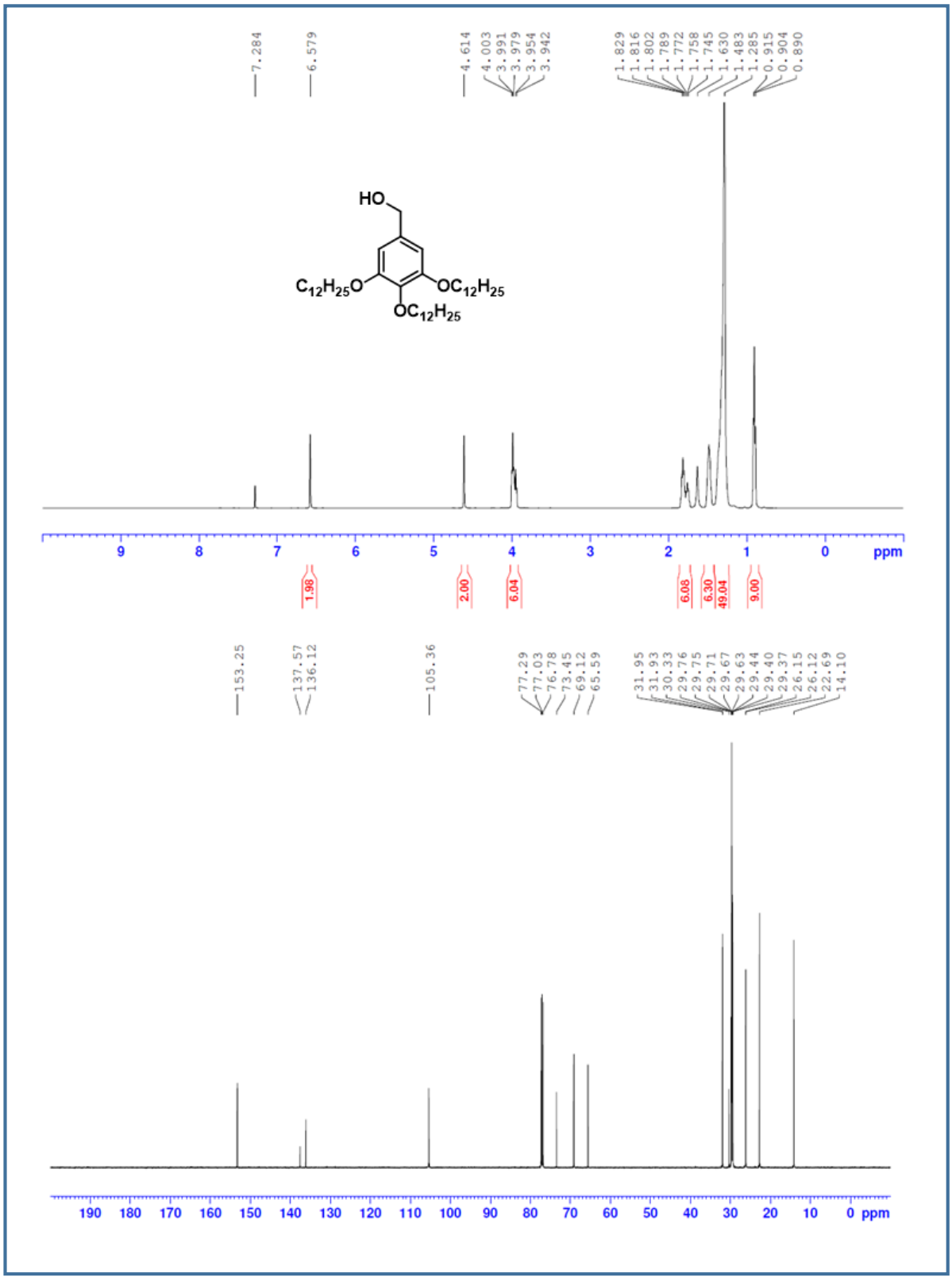

Figure 6.22: ^{1}H (top) and ^{13}C-NMR (bottom) spectra of **2**

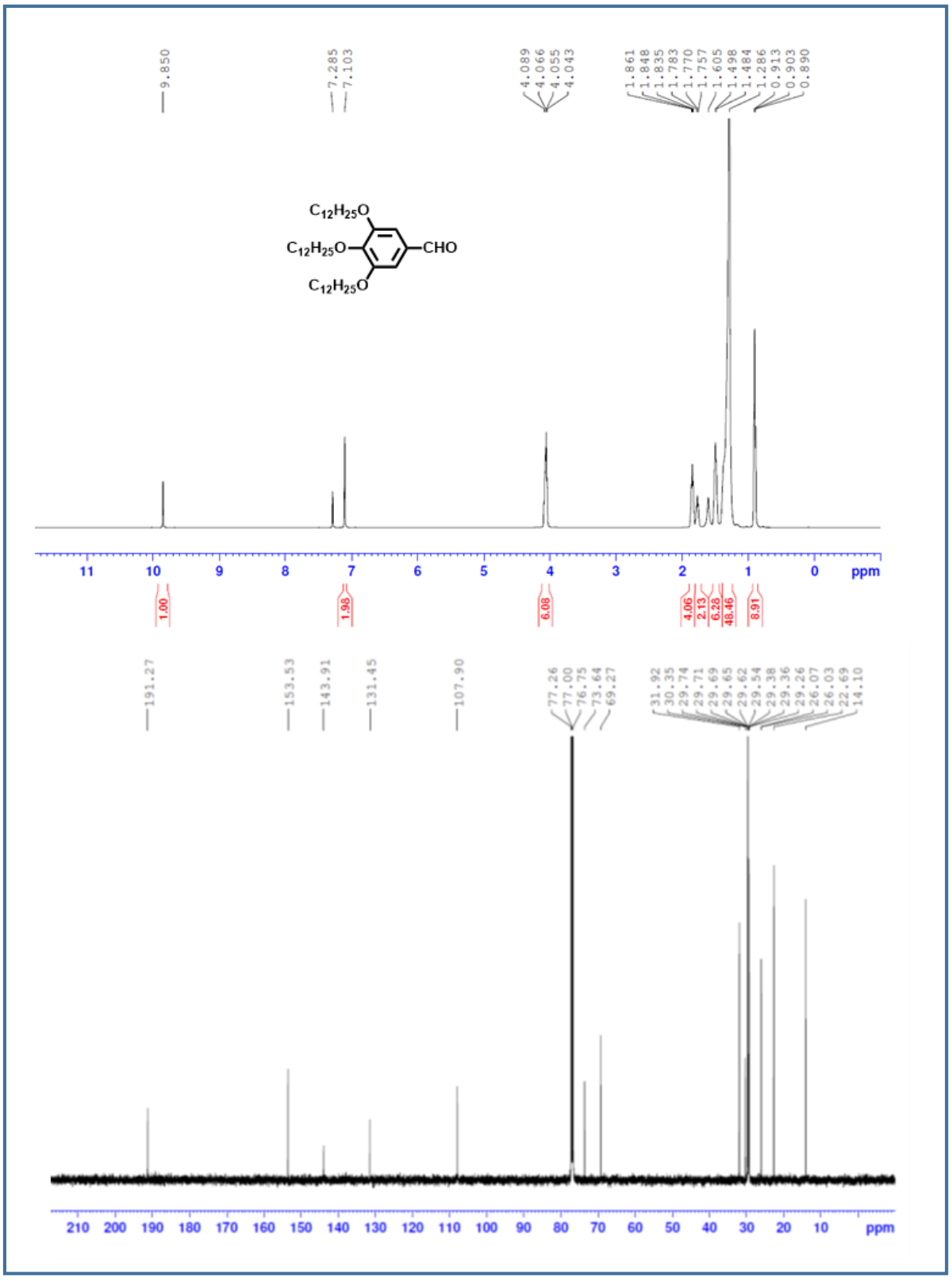

Figure 6.23: ^{1}H (top) and ^{13}C-NMR (bottom) spectra of **3**

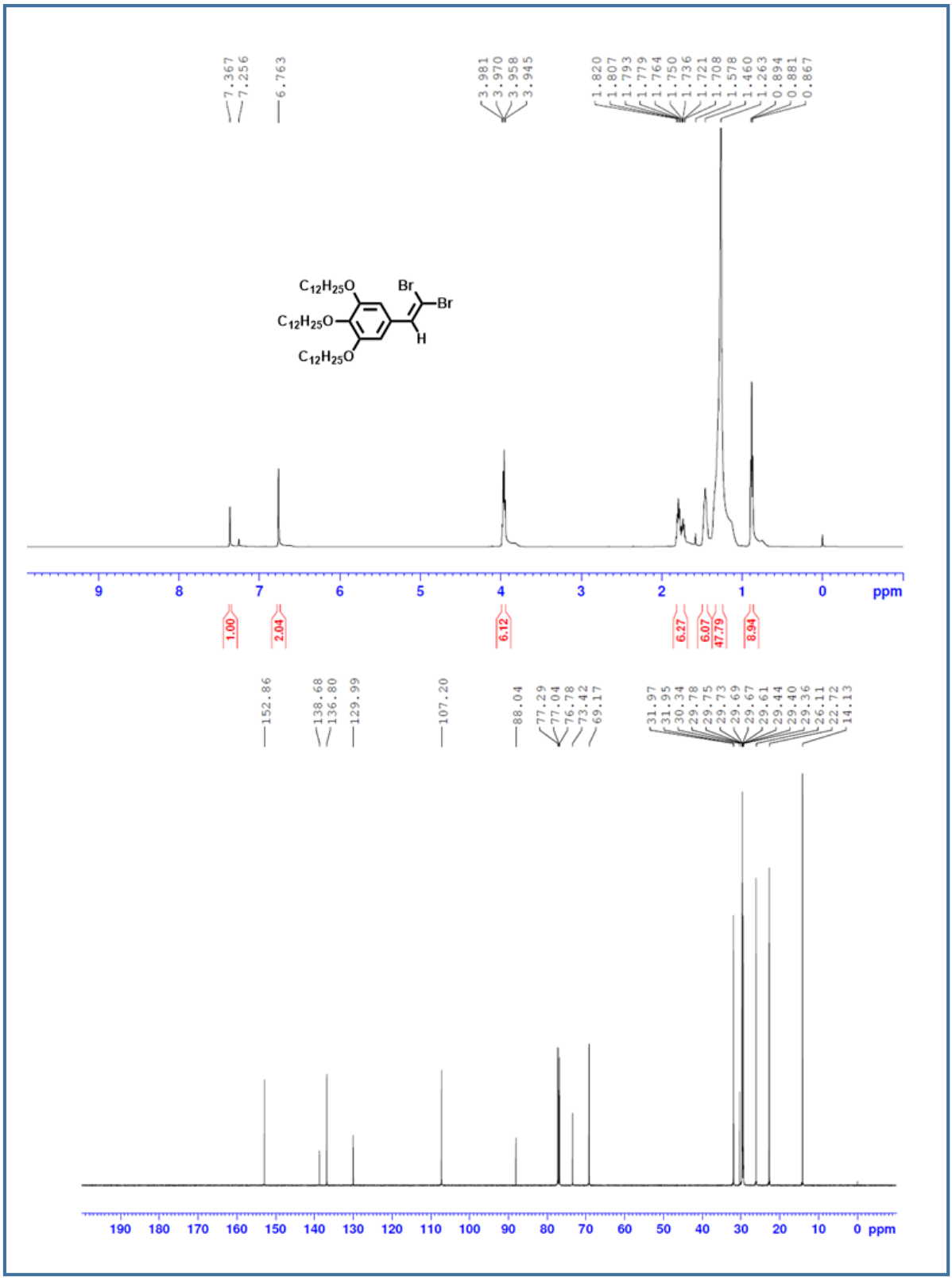

Figure 6.24: ^{1}H (top) and ^{13}C-NMR (bottom) spectra of **4**

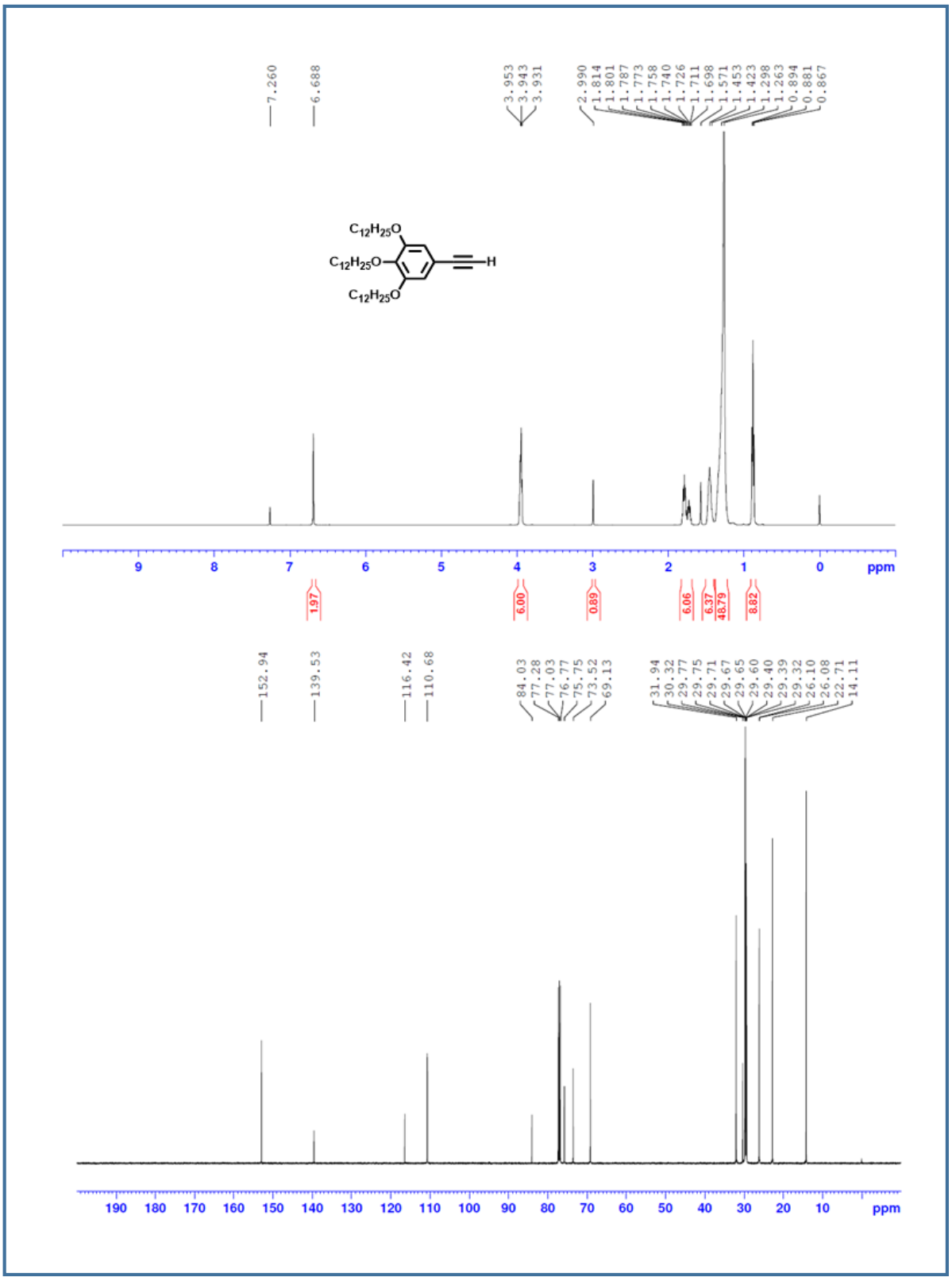

Figure 6.25: ^{1}H (top) and ^{13}C-NMR (bottom) spectra of **5**

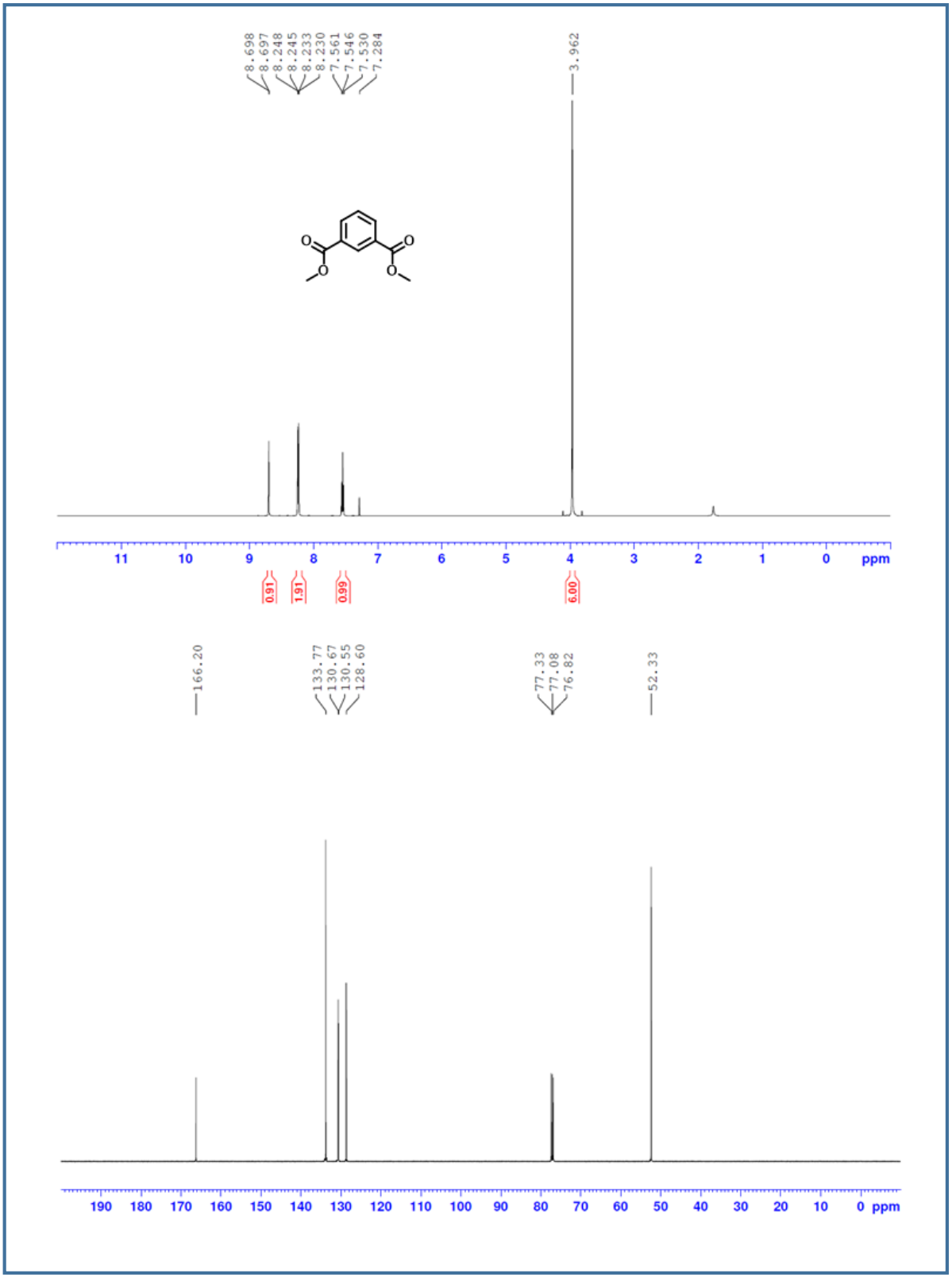

Figure 6.26: ^{1}H (top) and ^{13}C-NMR (bottom) spectra of **6**

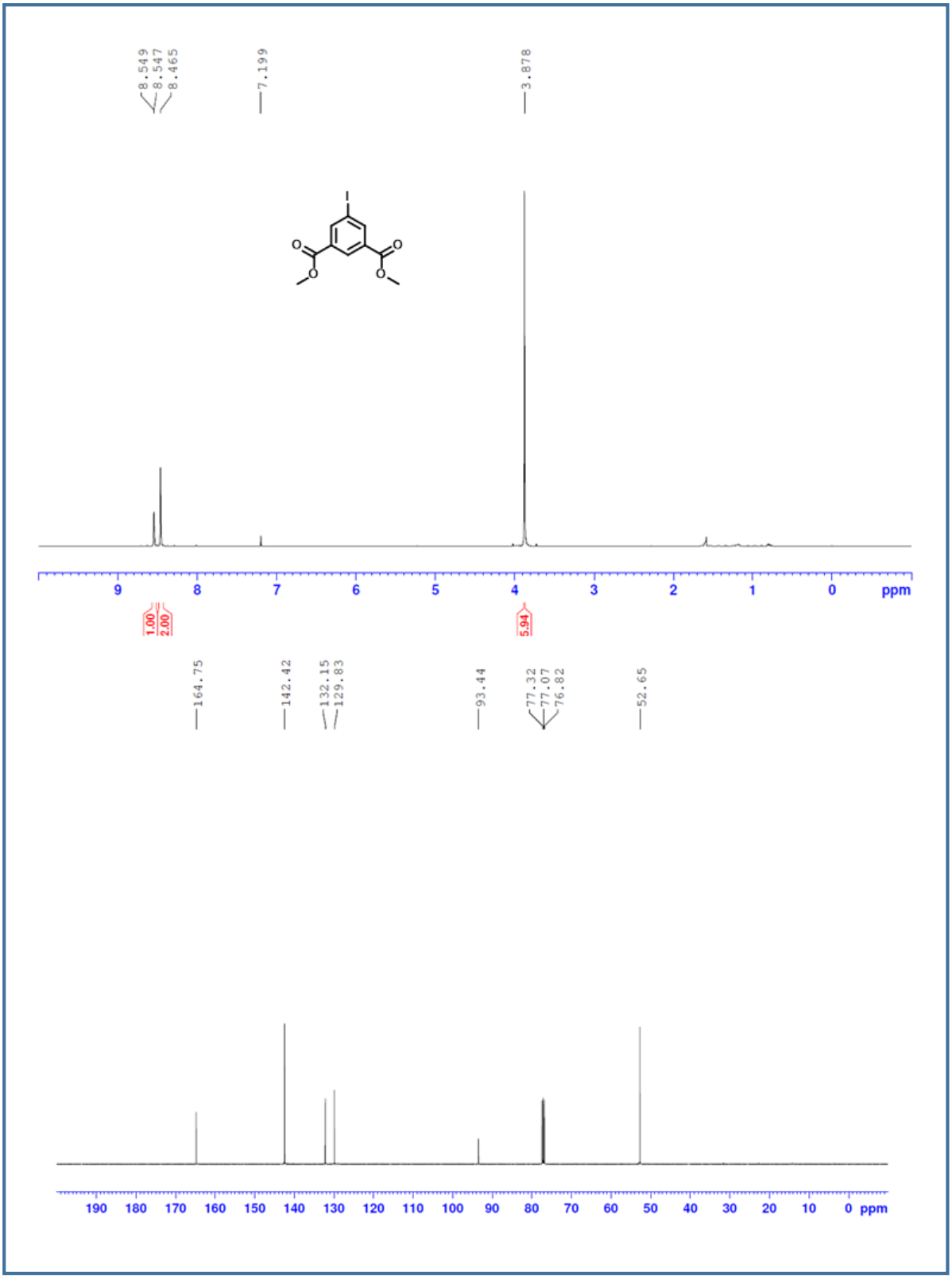

Figure 6.27: ^{1}H (top) and ^{13}C-NMR (bottom) spectra of **7**

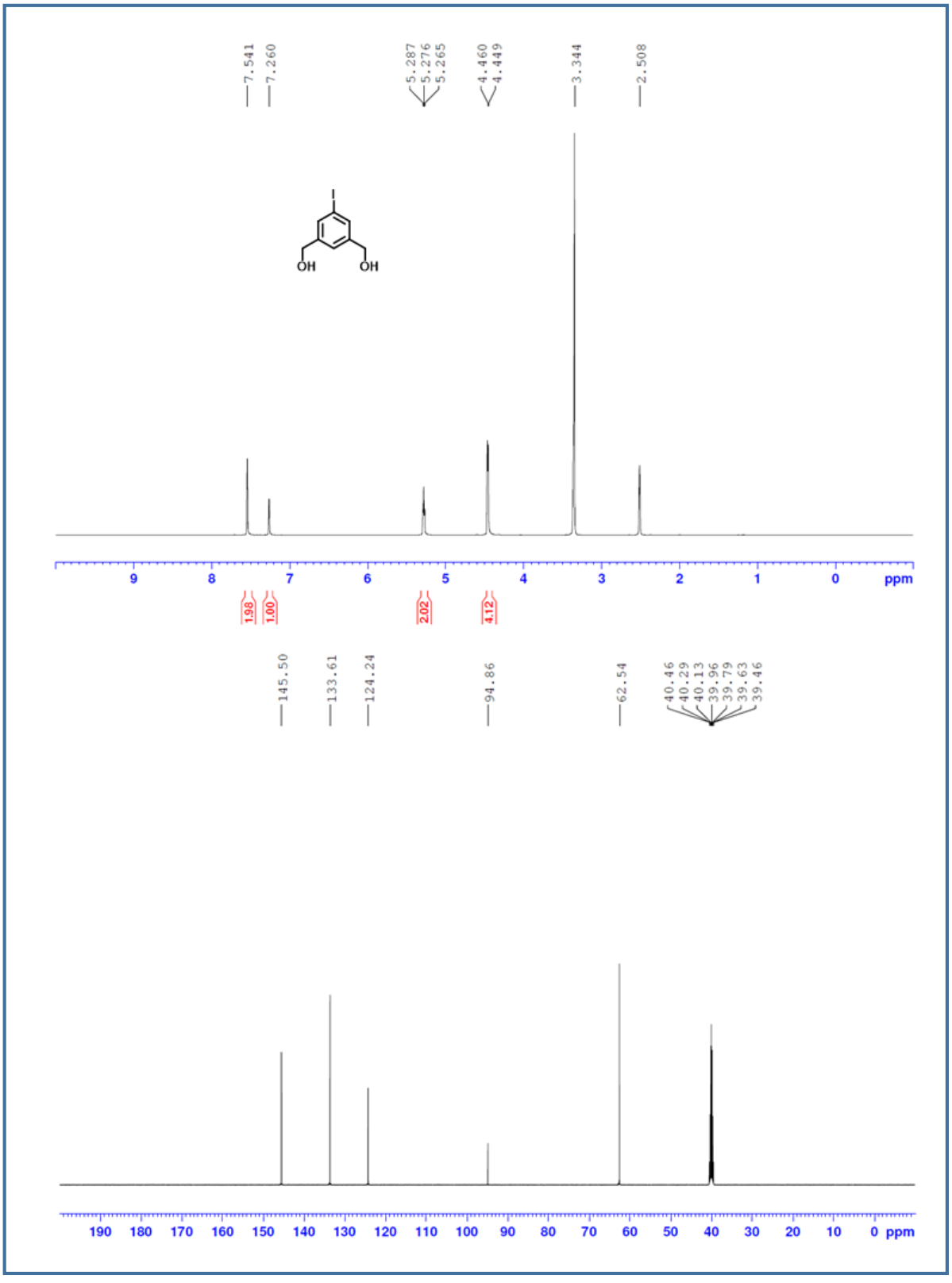

Figure 6.28: ^{1}H (top) and ^{13}C-NMR (bottom) spectra of **8**

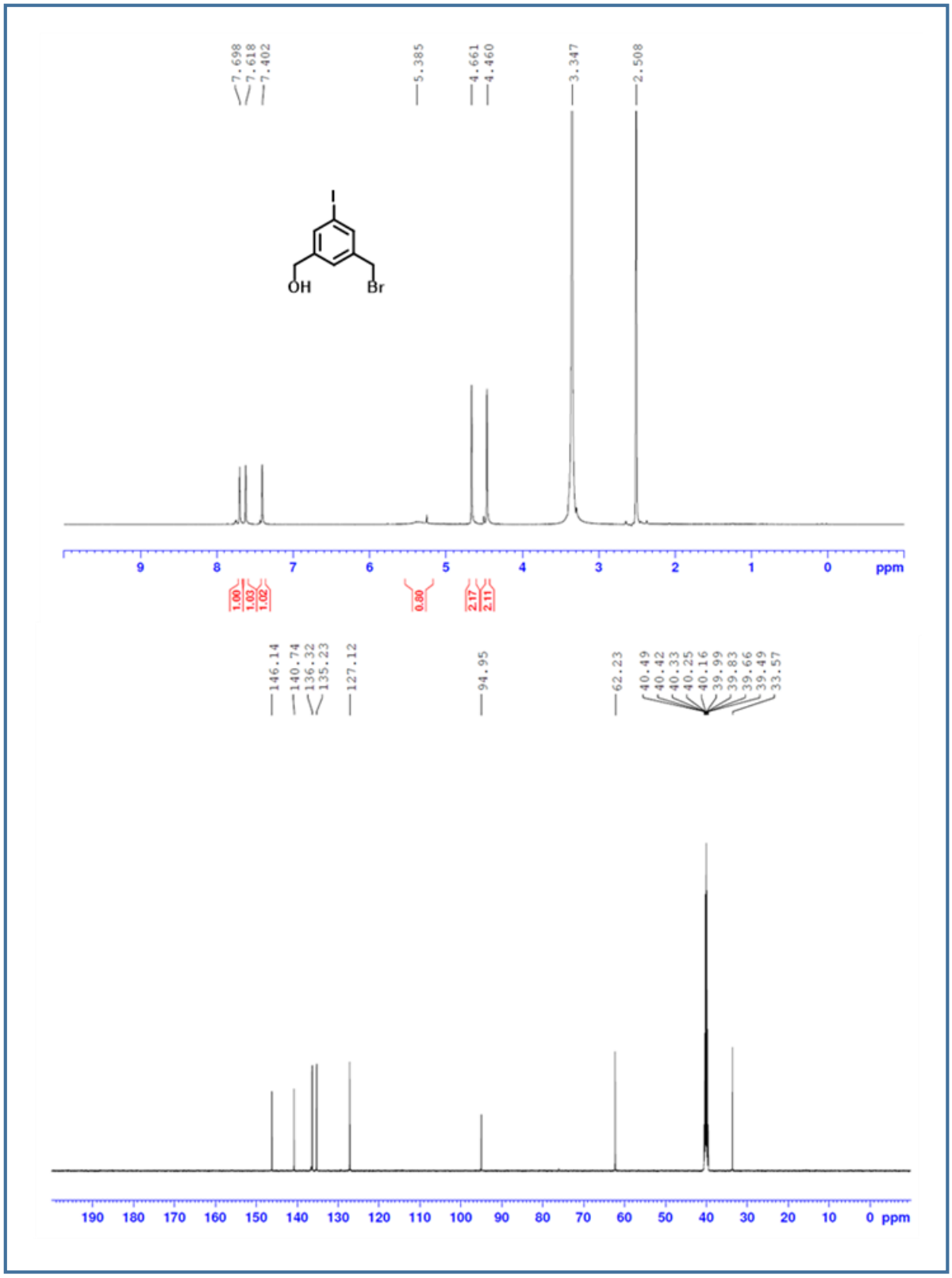

Figure 6.29: ^{1}H (top) and ^{13}C-NMR (bottom) spectra of **9**

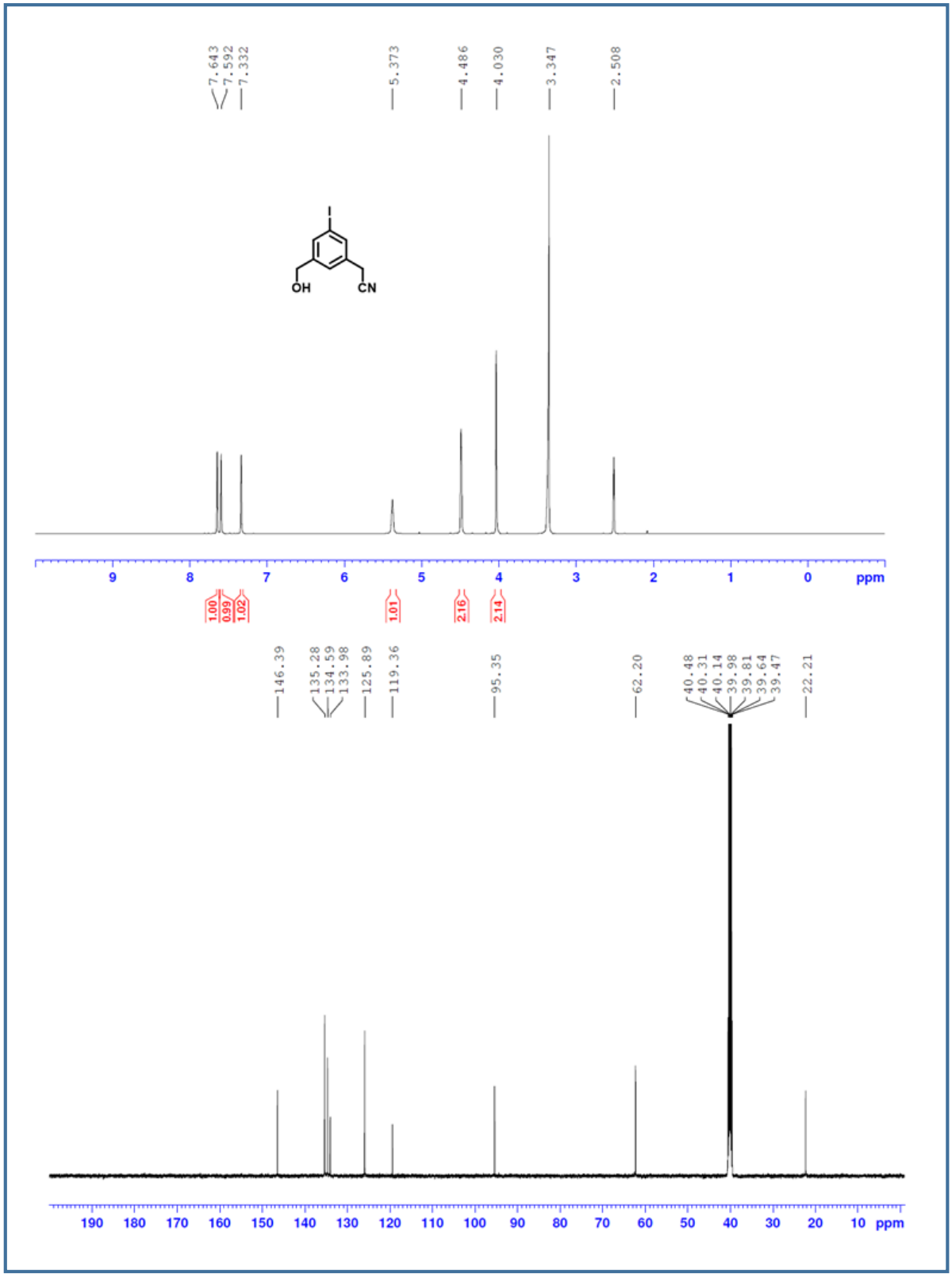

Figure 6.30: ^{1}H (top) and ^{13}C-NMR (bottom) spectra of **10**

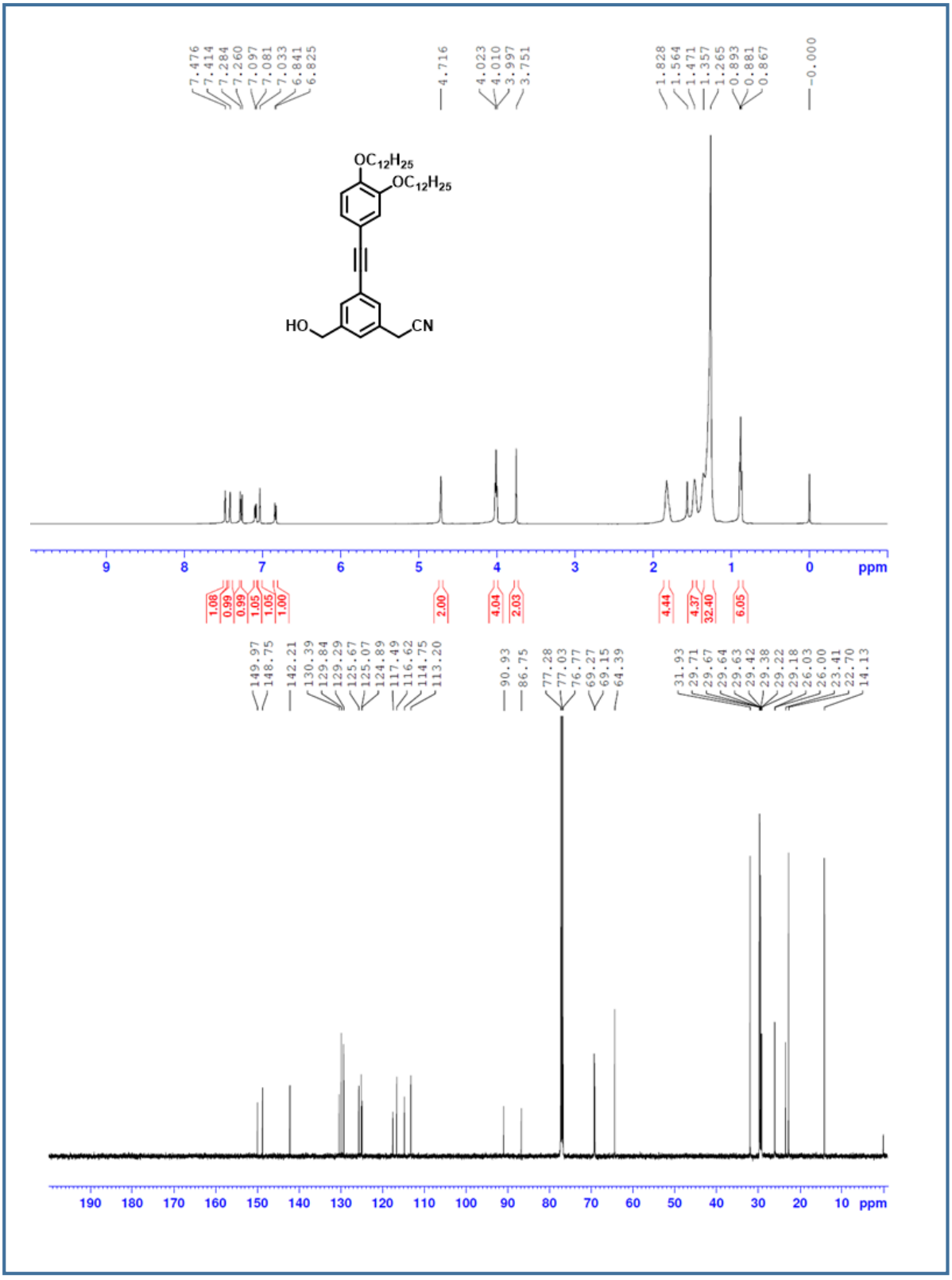

Figure 6.31: ^{1}H (top) and ^{13}C-NMR (bottom) spectra of **11a**

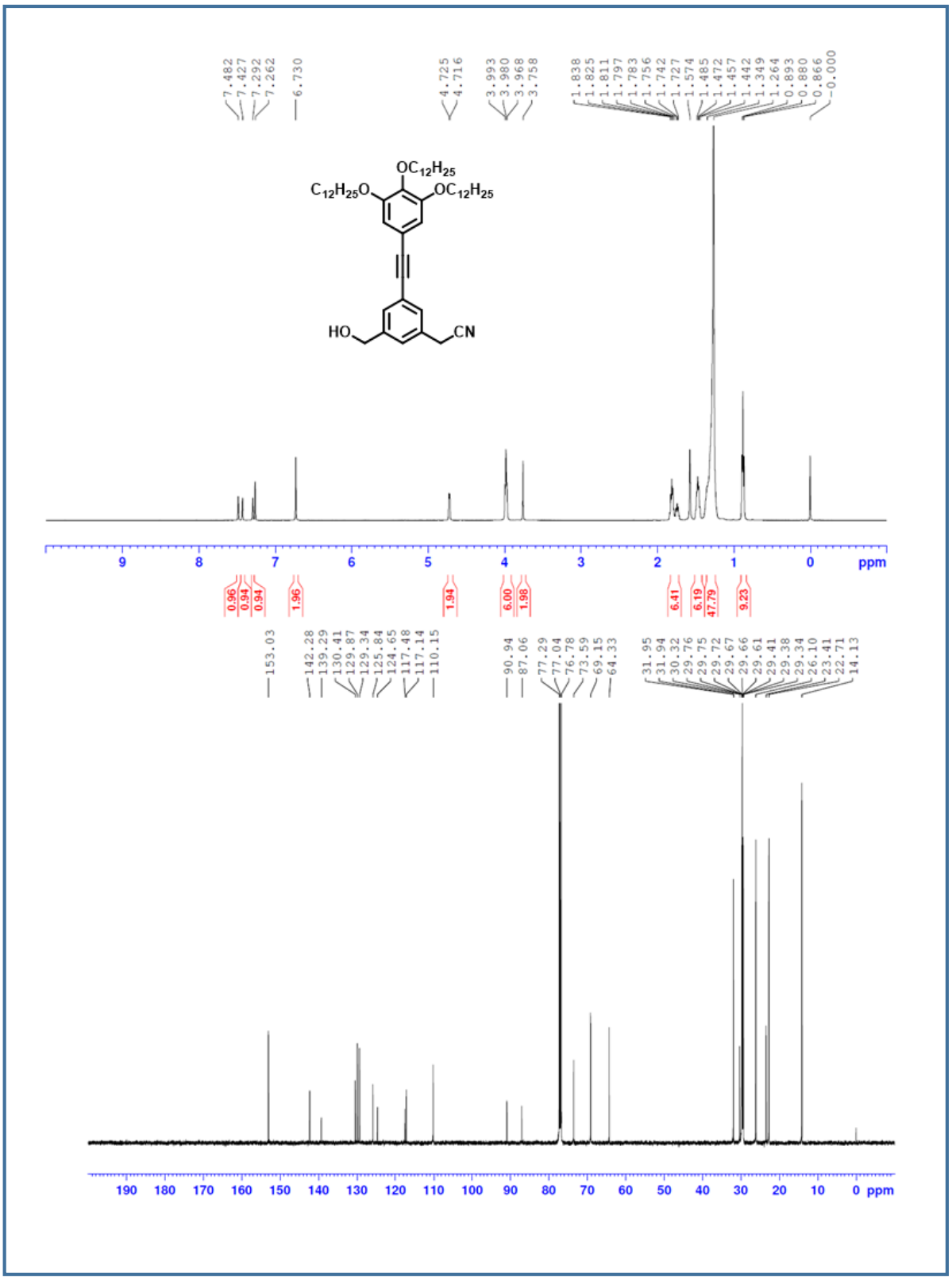

Figure 6.32: ^{1}H (top) and ^{13}C-NMR (bottom) spectra of **11b**

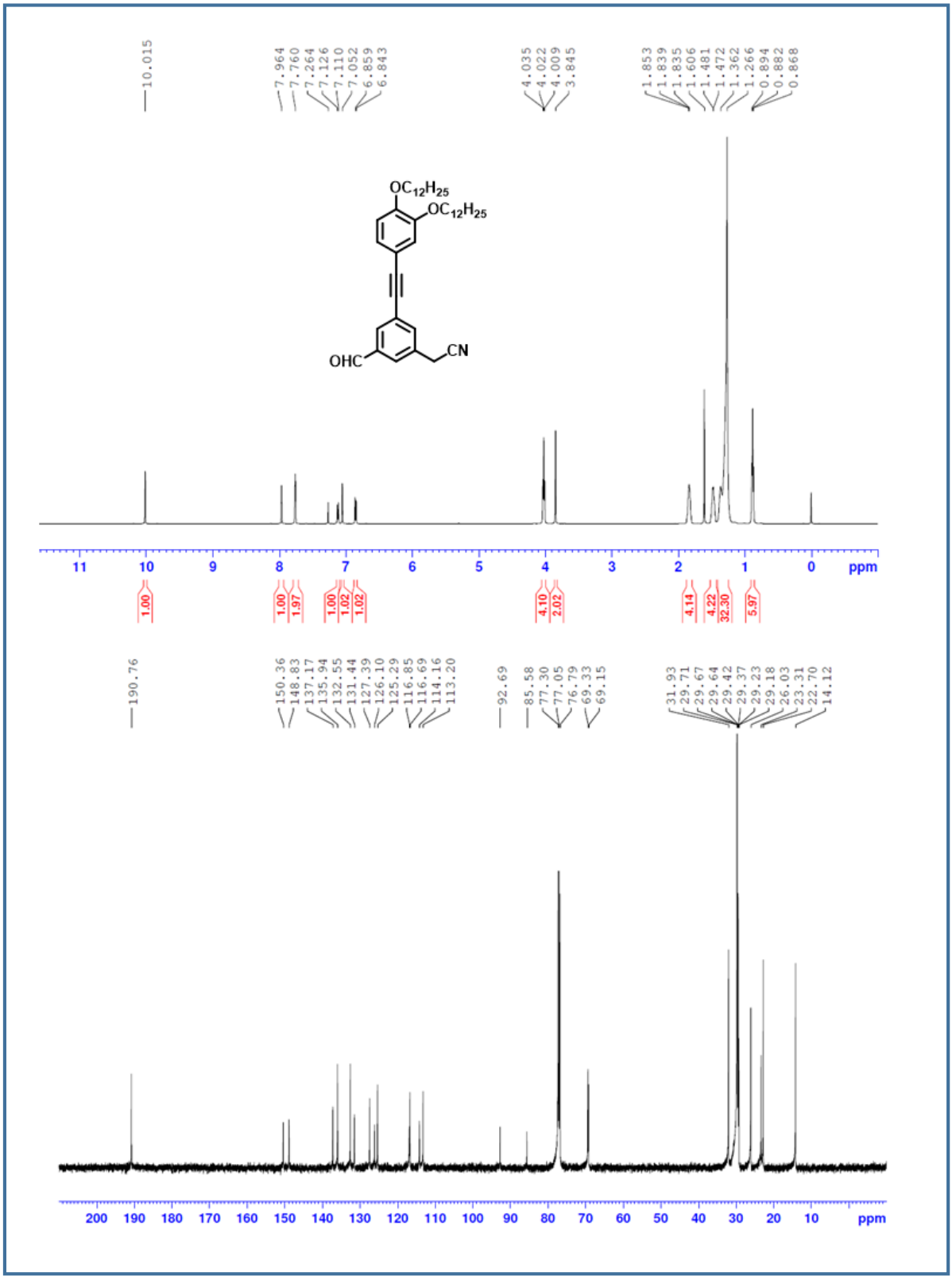

Figure 6.33: ^{1}H (top) and ^{13}C-NMR (bottom) spectra of **12a**

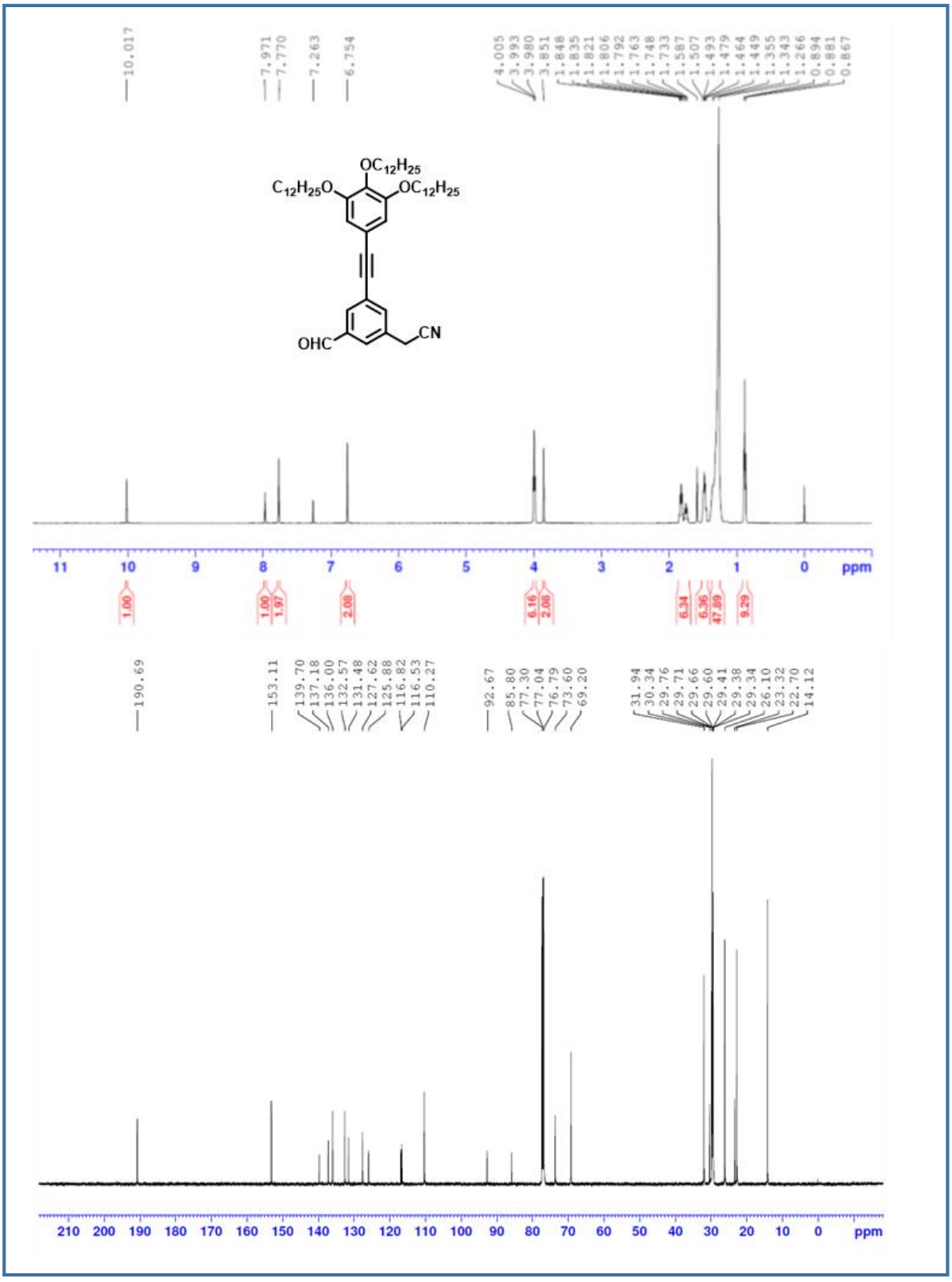

Figure 6.34: ^{1}H (top) and ^{13}C-NMR (bottom) spectra of **12b**

6.7 References:

[1] C. J. Pedersen, *J. Am. Chem. Soc.* **1967**, *89*, 2495–2496.

[2] C. J. Pedersen, in *Angew. Chemie Int. Ed. English*, **1988**, pp. 1021–1027.

[3] B. Dietrich, J. M. Lehn, J. P. Sauvage, *Tetrahedron Lett.* **1969**, *10*, 2885–2888.

[4] B. Dietrich, J. M. Lehn, J. P. Sauvage, *Tetrahedron Lett.* **1969**, *10*, 2889–2892.

[5] J.-M. Lehn, in *Alkali Met. Complexes with Org. Ligands*, Springer-Verlag, Berlin/Heidelberg, **2005**, pp. 1–69.

[6] C. H. Park, H. E. Simmons, *J. Am. Chem. Soc.* **1968**, *90*, 2429–2431.

[7] C. H. Park, H. E. Simmons, *J. Am. Chem. Soc.* **1968**, *90*, 2431–2432.

[8] C. H. Park, H. E. Simmons, *J. Am. Chem. Soc.* **1968**, *90*, 2429–2431.

[9] D. FRENCH, *Adv. Carbohydr. Chem.* **1957**, *12*, 189–260.

[10] W. Saenger, J. Jacob, K. Gessler, T. Steiner, D. Hoffmann, H. Sanbe, K. Koizumi, S. M. Smith, T. Takaha, *Chem. Rev.* **1998**, *98*, 1787–1802.

[11] J. Szejtli, *Chem. Rev.* **1998**, *98*, 1743–1754.

[12] G. Crini, *Chem. Rev.* **2014**, *114*, 10940–75.

[13] W. Zhao, A. H. Flood, N. G. White, *Chem. Soc. Rev.* **2020**, *49*, 7893–7906.

[14] A. H. Flood, *Beilstein J. Org. Chem.* **2016**, *12*, 611–627.

[15] S. A. Nepogodiev, J. F. Stoddart, *Chem. Rev.* **1998**, *98*, 1959–1976.

[16] A. Ikeda, S. Shinkai, *Chem. Rev.* **1997**, *97*, 1713–1734.

[17] J. S. Kim, D. T. Quang, *Chem. Rev.* **2007**, *107*, 3780–3799.

[18] L. Marie, E. A. Dissertation, *EFFECTS OF SECONDARY BINDING MOTIFS IN ARYLETHYNYL ANION RECEPTORS By*, University Of Oregon, **2019**.

[19] by B. Zhengyu Chen, *DISPARATE SYMMETRIES IN HEAD-TO-TAIL SCHIFF-BASE MACROCYCLES*, University Of British Columbia, **2010**.

[20] M. Iyoda, H. Shimizu, *Chem. Soc. Rev.* **2015**, *44*, 6411–6424.

[21] H.-T. Feng, Y.-X. Yuan, J.-B. Xiong, Y.-S. Zheng, B. Z. Tang, *Chem. Soc. Rev.* **2018**, *47*, 7452–7476.

[22] S. Höger, *Chem. - A Eur. J.* **2004**, *10*, 1320–1329.

[23] Y. Liu, A. Singharoy, C. G. Mayne, A. Sengupta, K. Raghavachari, K. Schulten, A. H. Flood, *J. Am. Chem. Soc.* **2016**, *138*, 4843–4851.

[24] R. O. Ramabhadran, Y. Liu, Y. Hua, M. Ciardi, A. H. Flood, K. Raghavachari, *J. Am. Chem. Soc.* **2014**, *136*, 5078–5089.

[25] Y. S. Zheng, J. Luo, *J. Incl. Phenom. Macrocycl. Chem.* **2011**, *71*, 35–56.

[26] S. Y. Li, Y. W. Xu, J. M. Liu, C. Y. Su, *Int. J. Mol. Sci.* **2011**, *12*, 429–455.

[27] L. Adriaenssens, P. Ballester, *Chem. Soc. Rev.* **2013**, *42*, 3261–3277.

[28] T. Ogoshi, T. Akutsu, D. Yamafuji, T. Aoki, T. A. Yamagishi, *Angew. Chemie - Int. Ed.* **2013**, *52*, 8111–8115.

[29] Y. Xu, M. D. Smith, M. F. Geer, P. J. Pellechia, J. C. Brown, A. C. Wibowo, L. S. Shimizu, *J. Am. Chem. Soc.* **2010**, *132*, 5334–5335.

[30] Y. Yang, M. Xue, J. F. Xiang, C. F. Chen, *J. Am. Chem. Soc.* **2009**, *131*, 12657–12663.

[31] D. Zhao, J. S. Moore, *Chem. Commun.* **2003**, *7*, 807–818.

[32] A. S. Shetty, P. R. Fischer, K. F. Stork, P. W. Bohn, J. S. Moore, *J. Am. Chem. Soc.* **1996**, *118*, 9409–9414.

[33] J. S. Moore, *Acc. Chem. Res.* **1997**, *30*, 402–413.

[34] B. Gong, Z. Shao, *Acc. Chem. Res.* **2013**, *46*, 2856–66.

[35] L. Isaacs, *Acc. Chem. Res.* **2014**, *47*, 2052–62.

[36] L. S. Shimizu, S. R. Salpage, A. A. Korous, *Acc. Chem. Res.* **2014**, *47*, 2116–2127.

[37] V. S. Bryantsev, B. P. Hay, *J. Am. Chem. Soc.* **2005**, *127*, 8282–8283.

[38] Y. Li, A. H. Flood, *Angew. Chemie Int. Ed.* **2008**, *47*, 2649–2652.

[39] J. L. Sessler, J. Cai, H. Y. Gong, X. Yang, J. F. Arambula, B. P. Hay, *J. Am. Chem. Soc.* **2010**, *132*, 14058–14060.

[40] B. Tinant, R. Touillaux, J. P. Declercq, M. van Meerssche, G. Leroy, J. Weiler, *Bull. des Sociétés Chim. Belges* **2010**, *92*, 403–404.

[41] G. Yu, A. J. Heeger, *J. Appl. Phys.* **1995**, *78*, 4510–4515.

[42] B.-K. An, S.-K. Kwon, S.-D. Jung, S. Y. Park, *J. Am. Chem. Soc.* **2002**, *124*, 14410–5.

[43] S. Lee, C.-H. Chen, A. H. Flood, *Nat. Chem.* **2013**, *5*, 704–10.

[44] W. Zhao, B. Qiao, C. Chen, A. H. Flood, *Angew. Chem. Int. Ed. Engl.* **2017**, *56*, 13083–13087.

[45] E. M. Fatila, M. Pink, E. B. Twum, J. A. Karty, A. H. Flood, *Chem. Sci.* **2018**, *9*, 2863–2872.

[46] B. Qiao, G. M. Leverick, W. Zhao, A. H. Flood, J. A. Johnson, Y. Shao-Horn, *J. Am. Chem. Soc.* **2018**, *140*, 10932–10936.

[47] B. Qiao, Y. Liu, S. Lee, M. Pink, A. H. Flood, *Chem. Commun.* **2016**, *52*, 13675–

13678.

[48] B. E. Hirsch, S. Lee, B. Qiao, C. H. Chen, K. P. McDonald, S. L. Tait, A. H. Flood, *Chem. Commun.* **2014**, *50*, 9827–9830.

[49] W. Zhao, B. Qiao, J. Tropp, M. Pink, J. D. Azoulay, A. H. Flood, *J. Am. Chem. Soc.* **2019**, *141*, 4980–4989.

[50] W. Zhao, J. Tropp, B. Qiao, M. Pink, J. D. Azoulay, A. H. Flood, *J. Am. Chem. Soc.* **2020**, *142*, 2579–2591.

[51] C. R. Benson, C. Maffeo, E. M. Fatila, Y. Liu, E. G. Sheetz, A. Aksimentiev, A. Singharoy, A. H. Flood, *Proc. Natl. Acad. Sci. U. S. A.* **2018**, *115*, 9391–9396.

[52] B. Qiao, B. E. Hirsch, S. Lee, M. Pink, C. H. Chen, B. W. Laursen, A. H. Flood, *J. Am. Chem. Soc.* **2017**, *139*, 6226–6233.

[53] C. R. Benson, L. Kacenauskaite, K. L. VanDenburgh, W. Zhao, B. Qiao, T. Sadhukhan, M. Pink, J. Chen, S. Borgi, C. H. Chen, et al., *Chem* **2020**, *6*, 1978–1997.

[54] J. Chen, S. M. A. Fateminia, L. Kacenauskaite, N. Bærentsen, S. Grønfeldt Stenspil, J. Bredehoeft, K. L. Martinez, A. H. Flood, B. W. Laursen, *Angew. Chemie - Int. Ed.* **2021**, *60*, 9450–9458.

Chapter - 7

Summary

Abstract

This chapter summarizes some of the important results and conclusions obtained from this thesis work, which deals with the "*Synthesis and characterization of new liquid crystalline compounds derived from novel aromatic ring structures*." Also, we briefly explain the divergent possibilities and scope for the future work obtained from our experimental work.

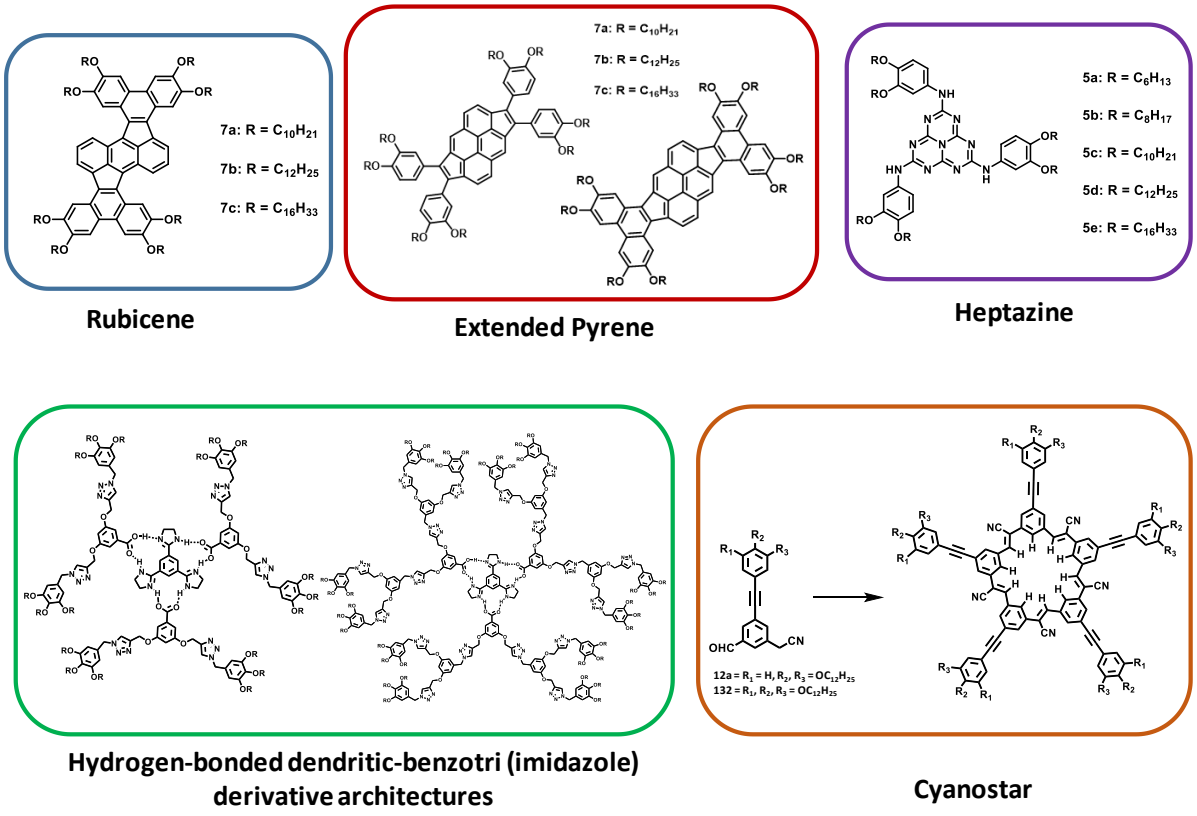

Chapter 1: ***Introduction***

This chapter begins with a brief history of liquid crystals and then moves on to a study of lyotropic and thermotropic liquid crystals, as well as their classification. A brief overview of several characterization approaches is also provided. Since this thesis focuses on discotic liquid crystals, this chapter includes a study of discotic liquid crystals and details on the columnar mesophases created by various mesogens and objective of the thesis.

Chapter 2: Rubicene, an Unusual Contorted Core for Discotic Liquid Crystals

In This chapter, we discovered that rubicene, a contorted molecule displays liquid crystalline properties upon appropriate peripheral substitution. Three new compounds have been prepared and they all show hexagonal columnar phase with a wide range of temperatures. Here our theoretical studies (Gaussian) suggested that rubicene derivatives employed twist structure where the difference in the splay angels results in a contorted arrangement. All three compounds reveal excellent thermal stability, and POM confirms the formation of the aligned structures. These aligned materials with interesting optical properties are highly attractive for various device applications such as photovoltaic solar cells, light-emitting diodes, etc. The device fabrication and studies on the liquid crystalline nature of other rubicene derivatives are under progress.

Chapter 3: ***Design and synthesis of extended pyrene-based discotic liquid crystalline materials.***

In this chapter, we summarize the new family of polycyclic aromatic hydrocarbons (PAHs) formed from pyrene core is described in this chapter. Palladium-catalyzed cyclopentannulation and Scholl reaction are used to make these compounds from 1, 6 dibromo pyrene and di-substituted arylethynylene. Enantiotropic mesomorphism is discovered in these substances. Over a wide temperature range, it exhibits the columnar hexagonal mesophase. POM, DSC, and X-ray diffraction studies have all validated the self-assembly of columnar mesophase. Molecules preferentially align homeotropically in the columnar mesophase, according to our findings. From the XRD data, the number of molecules occupying a single slice of the column was calculated and found to be close to 1 for all samples. 7a-c has a significantly larger core-

core interaction than 6a-c. Pyrene derivatives have been thoroughly investigated as new dyes and are widely used in various devices. As a result, these new self-assembling supramolecular materials could be used in a variety of optoelectronic applications.

Chapter 4: ***Columnar mesomorphism in heptazine discotics***

This chapter reports the design and synthesis of C_3- symmetry columnar liquid crystals in which the heptazine core is flanked with six alkoxy chains. These novel derivatives show two columnar mesophases that appear as a function of temperature. All the compounds exhibit columnar hexagonal phase (Col_h) at high temperatures, among which two compounds with lower alkoxy chains show a rectangular phase at lower temperatures. The lower homologs of the series were found to exhibit both rectangular and columnar hexagonal mesophase. However, there is a change in the molecular organization between the rectangular and the hexagonal mesophases, which were reflected in the difference in the number of molecules in the columnar section. In the Col_r phase, it was found to be one molecule per slice in the column, whereas in the case of Col_h phase, there are two molecules per slice in the column. The mesomorphic properties of all the compounds are confirmed by polarizing optical microscopy, differential scanning calorimetry, and X-ray diffractometry. Emission spectra of 5a-5e exhibit structured emission at lower concentrations and aggregated emission at higher concentrations.

Chapter 5: ***Supramolecular self–assembly of Hydrogen-bonded dendritic-benzotri (imidazole) derivative architectures.***

This chapter summarizes that we have successfully synthesized the 1st and 2nd generation dendrimers with a functional group of carboxylic acid using click chemistry and benzotri imidazole derivatives. 1st generation dendrimers contain carboxylic acid and alcohol functional groups, exhibiting the hexagonal columnar mesophase. Carboxylic acid and ester groups are present in second-generation dendrimers and show the columnar cubic mesophase. Hydrogen-bonded compounds were effectively constructed using gallic acid dendrimer derivatives and benzotriimadazole derivatives. The formation of hydrogen-bonded compounds and their stability were confirmed by FTIR and ^{1}H NMR investigations. All the H-bonded complexes exhibit mesomorphic properties. These results suggest a decisive role of mesogenic driving

forces (mainly H-bonding) to help the formation of the 1:3 complex in bulk. Interestingly compounds **14** and **16** exhibit room temperature liquid crystals. They shows the columnar hexagonal mesophase at room temperatures and high temperatures columnar cubic phase. In the case of compounds **15** and **17,** they exhibit cubic mesophase. The mesophase behavior was confirmed by the POM, DSC, and X-ray diffractometry. Due to their synthesis and solubility issues, the ease with which these dendritic hydrogen-bonded complexes can be formed utilizing noncovalent interactions can make their usage in DLCs limitless. The findings and research presented here on hydrogen-bonded liquid crystals could be useful in the fields of switching devices, optical data storage, and optoelectronics.

Chapter 6: ***Synthesis and mesomorphic behavior of cyanostar precursors.***

In this chapter, we summarise the synthesis of cyanostar precursors. Interestingly these precursors are found to be mesomorphic and exhibit columnar mesophase. Using a Sonogashira coupling reaction followed by a PCC reaction, a novel series of dialkoxy and trialkoxy cyanostar precursors was synthesized and characterized using NMR and elemental analyses. All precursors show good thermal stability, which was confirmed using thermogravimetric analysis. And also exhibit monotropic liquid crystalline behavior. Mesomorphic behavior of all compounds was characterized by polarized optical microscopy (POM) and differential scanning calorimetry (DSC). X-ray diffraction (XRD) studies confirmed the self-assembly of these compounds in the columnar mesophase. For 11a, 12a, and 11b, 12b, the number of molecules per slice of the column was found to be eight and five, respectively. The mesomorphic properties of all compounds are preserved when they are cooled from the isotropic phase to room temperatures. The properties make these compounds a good candidate for optoelectronic properties. These precursors are potential molecules to generate the novel DLCs, namely cyanostars, which is in progress

Chapter 7: ***Conclusion***

The topic of this thesis is the “Synthesis and characterization of new liquid crystalline compounds derived from novel aromatic ring structures.” This chapter presents some of the

key findings and conclusions. In addition, we briefly discuss the various options and scope for future study that our experimental work has shown.